

(NASA-CR-136951) PROCEEDINGS OF NUCLEAR
PROPULSION CONFERENCE (Naval Postgraduate
School) 301 p

N74-72539
THRU
N74-72572
Unclass

00/99 31131

BOOK 1

UUN

~~SECRET~~

FACILITY FORM	(ACCESSION NUMBER)	(THRU)
	301	4
	(PAGES)	(CODE)
	(NASA CR OR TMX OR AD NUMBER)	(CATEGORY)

Proceedings of

NUCLEAR PROPULSION CONFERENCE [U]

August 15-17, 1962

NAVAL POSTGRADUATE SCHOOL
MONTEREY, CALIFORNIA

CLASSIFICATION CHANGE

TO = UNCLASSIFIED

By authority of *AEC TID-1389-91 (Index)*

Changed by *C. W. [illegible]* Date *2/28/73*

LIBRARY COPY
0000000000
LANGLEY RESEARCH CENTER
L-1
LANGLEY RESEARCH CENTER
HAMPDEN SECTION

GROUP 1
Exclude from automatic downgrading

~~RESTRICTED DATA~~

This document contains restricted data as defined in the Atomic Energy Act of 1954. Its transmittal in any form or by any means without the express written approval of the AEC is prohibited.

This document contains Confidential Restricted Data relating to civilian applications of atomic energy.



United States Atomic Energy Commission
Division of Technical Information

AEC RESEARCH AND DEVELOPMENT REPORT

LEGAL NOTICE

This report was prepared as an account of Government sponsored work. Neither the United States, nor the Commission, nor any person acting on behalf of the Commission:

A. Makes any warranty or representation, expressed or implied, with respect to the accuracy, completeness, or usefulness of the information contained in this report, or that the use of any information, apparatus, method, or process disclosed in this report may not infringe privately owned rights; or

B. Assumes any liabilities with respect to the use of, or for damages resulting from the use of any information, apparatus, method, or process disclosed in this report.

As used in the above, "person acting on behalf of the Commission" includes any employee or contractor of the Commission, or employee of such contractor, to the extent that such employee or contractor of the Commission, or employee of such contractor prepares, disseminates, or provides access to, any information pursuant to his employment or contract with the Commission, or his employment with such contractor.

Printed in USA. This document consists of 2 books, total charges \$12.35. Available from the Division of Technical Extension, P. O. Box 62, Oak Ridge, Tennessee. Please direct to the same address inquiries covering the procurement of classified AEC reports.

CASE FILE COPY

[REDACTED]

TID-7653(Pt.II)

Book 1

Proceedings of
NUCLEAR PROPULSION
Conference

[U]

NAVAL POSTGRADUATE SCHOOL
August 15-17, 1962
MONTEREY, CALIFORNIA

664-4579

Sponsored by
← SPACE NUCLEAR PROPULSION OFFICE, AEC/NASA,
AMERICAN ROCKET SOCIETY
AMERICAN NUCLEAR SOCIETY
INSTITUTE OF AEROSPACE SCIENCES

GROUP 1

Excluded from automatic downgrading
and declassification

RESTRICTED DATA

This document contains restricted data as
defined in the Atomic Energy Act of 1954.
Its transmission or the disclosure of its
contents in any manner to an unauthorized
person is prohibited.

[REDACTED]

This document contains Confidential-Re-
stricted Data relating to civilian applica-
tions of atomic energy.




FOREWORD

The papers presented in this volume are the outgrowth of the first national conference on the subject of nuclear propulsion for rockets, ramjets, and space vehicles. The Nuclear Propulsion Conference itself was held at Monterey, California, at the U. S. Naval Postgraduate School, and was jointly sponsored by the American Rocket Society, the Institute of Aerospace Sciences, and the American Nuclear Society; the three largest and most vigorous technical societies concerned with nuclear propulsion.

This volume follows the typical organization of the Conference, though the order of subjects is different here than at Monterey. Included here are many of the good papers submitted, but which were not presented at the Conference because of time limitations. Those presented are grouped first in each section. There is no Index to the volume.

At the beginning of planning, late in 1960, the organizing committee felt that a serious lack of exchange of information was already confusing work in nuclear propulsion and would soon significantly hamper such work. Yet, because of the nature of the work itself, it was obvious that any technical forum supplied by the societies would fail in its goal of exchange of useful information unless the meeting aimed for discussion of work in classified areas. Thus, of necessity and by design, the meeting was organized on an entirely classified basis. It could not have been held at all without the support of the Space Nuclear Propulsion Office of the USAEC/NASA, headed by Mr. Harry B. Finger. His office undertook



the security clearance responsibility for the meeting, and enthusiastically supported the meeting in every other way possible. This Proceedings has been published under the auspices of the SNPO, and was compiled by Mr. William Hanna of that office.

We hope that the Conference served its major purpose; to acquaint the legitimately interested technical community with the real state-of-the-art in existing nuclear propulsion programs. It was noted that most of the papers came from the USAEC National Laboratories, while most of the attendees came from the nuclear and aerospace industries of the country. This is rightly so and emphasizes the premise which initially suggested the meeting: That nuclear propulsion is passing through a vigorous transition state from National Laboratory scale to industrial sized development. Surely, unless such a transition continues, and it is well along in the NERVA and RIFT programs, nuclear propulsion will not be able to fill its proper role in the era of space flight before us.

Altogether, about 215 papers were submitted. The majority of these were classified and required security documentation as well as the careful record-keeping employed to keep track of all papers. Pertinent papers were sent to each Session Chairman, who alone had the responsibility for assembling his session. We owe a debt of gratitude to these gentlemen. The major accounting and distribution job of paper handling was done by Mildred Foglesong of the Los Alamos Scientific

Laboratory. Without her constant attention, careful work, and accurate records the Conference organization could not have functioned. Millie, we thank you. And last, but of utmost importance were the pre-Conference activities of Prof. Frank E. Faulkner of the U. S. Naval Postgraduate School, and the continual efforts of the ARS Meetings Management Staff, particularly Mr. Rod Hohl, in setting up housing, registration, and other necessary arrangements.

Robert W. Bussard

Robert W. Bussard
Program Chairman
Nuclear Propulsion Conference

For the Organizing Committee:

Robert F. Trapp (ANS)
Douglas Aircraft Company

Clare Stanford (IAS)
Nuclear Division, Martin-Marietta Co.

Frank E. Rom (ARS)
Lewis Research Center, NASA

TABLE OF CONTENTS

I. KEYNOTE

CHAIRMAN: Chiao J. Wang,
Aerospace Corp.
Los Angeles, Calif.

The Rover Program
Harold B. Finger, Space Nuclear Propulsion Office,
National Aeronautics and Space Administration,
Atomic Energy Commission, Washington, D. C. [U] 1 ✓

II. REACTOR CRITICALITY-THEORY AND EXPERIMENT

CHAIRMAN: H. L. Reynolds,
Lawrence Radiation Lab,
University of Calif.,
Livermore, Calif.

Criticality and Nuclear Characteristics of the KIWI-A Series of
Nuclear Propulsion Test Reactors
J. Carlton Hoogterp and John D. Orndoff, Los Alamos Scientific
Laboratory, University of California, Los Alamos, New Mexico ... [U] 19 ✓

Neutronics of KIWI-B Nuclear Propulsion Reactors
Herbert H. Helmick and John D. Orndoff, Los Alamos Scientific
Laboratory, University of California, Los Alamos, N. M. [U] 32 ✓

Neutronic Calculations of Temperature Effects on KIWI Reactors
Eugene A. Plassmann, Los Alamos Scientific Laboratory,
University of California, Los Alamos, N. M. [U] 49 ✓

Rover Reactor Control Element Worth Calculations
Alfred W. Chermatz, Los Alamos Scientific Laboratory,
University of California, Los Alamos, N. M. [U] 56 ✓

III. RADIATION LEVELS AND ANALYSIS

CHAIRMAN: J. Warren Keller,
NASA, Washington, D.C.

The Leakage Radiation Field of a KIWI Reactor
Donald M. Peterson, Los Alamos Scientific Laboratory,
University of California, Los Alamos, N. M. [U] 66 ✓

Design Computations for a Nuclear Rocket Shadow Shield
M. A. Capo, Astronuclear Laboratory, Westinghouse Electric Corp.,
Pittsburgh, Pa. [U] 71 ✓

Calculations of Neutron Activation Dose Rates in Nuclear Rocket
Vehicles and Test Facilities
Robert M. Thornton and C. K. Butterworth, Lockheed-Georgia Co.,
Atlanta, Ga. [U] 77 ✓

Nuclear Heating of Tory II-C Hafnium Control Rods S. Kellman and A. Lorenz, University of California, Lawrence Radiation Laboratory, Livermore, Calif.	85✓
Neutron and Gamma Angular Leakage Calculation of a Kiwi-B Reactor A. D. Prescott, Marshall Space Flight Center, NASA, Huntsville, Ala.	89✓
Two Novel Radiation Calculations on Rocket Reactors R. E. Malenfant, Los Alamos Scientific Laboratory, Los Alamos, N.M.	92✓
Transport Calculations of the KIWI-B Neutron Environment D. A. McCutchan, Los Alamos Scientific Laboratory, Los Alamos, N.M.	104✓
Radiation Induced Conversion of Orthohydrogen to Parahydrogen on the RIFT Propellant Tank M. C. Johnson, The Bendix Corp., Research Laboratories Div., Southfield, Detroit, Mich.	109✓

IV. PROPULSION REACTOR CONTROL

CHAIRMAN: George K. Hess
Air Force Missile Test
Center, Patrick AFB, Fla.

Startup Studies of a Nuclear Rocket Reactor, Part 3, Startup Philosophy J. D. Balcomb, Los Alamos Scientific Laboratory, University of California, Los Alamos, N. M.	115✓
Control Systems for a Liquid-Hydrogen-Cooled KIWI-B Reactor P. J. Blake, R. J. Bohl, E. A. Brown, C. P. Milich, C.E. Stiles and B. G. Strait - Los Alamos Scientific Laboratory, University of California, Los Alamos, N. M.	120
Design and Evaluation of Electropneumatic Servo Actuators for the NERVA Engine David J. Schaffer and Alfred J. Wetzel, Research Laboratories Div., The Bendix Corp., Southfield, Mich.	128
Control and Telemetry Transducer Requirements for Nuclear Powered Vehicles Malcolm C. Johnson, Research Laboratories Div., The Bendix Corp., Southfield, Mich.	138
Prototype ROVER Actuator Nuclear Radiation Heating Analysis and Cooling System Development J. J. Edmond, Bendix Corp., Southfield, Mich.	144
KIWI-B-1A Power and Temperature Control Systems E. A. Brown, et al, N-Division, Los Alamos Scientific Laboratory, Los Alamos, N. M.	154

V. FLIGHT SAFETY OF NUCLEAR PROPULSION SYSTEMS

CHAIRMAN: Ralph Decker,
Space Nuclear Propulsion
Office, NASA-Atomic
Energy Commission,
Washington, D.C.

The Re-Entry of Nuclear Rockets into the Earth's Atmosphere Robert I. Weiner, Martin Co., Baltimore, Md.	163✓
--	------

Nuclear Rocket Destruct System Requirements Walter H. Esselman, Astronuclear Laboratory, Westinghouse Electric Corp., Pittsburgh, Pa.	[U] 177 ✓
Rover Reactor Power Transient Calculations William R. Stratton and Curtis G. Chezem, Los Alamos Scientific Laboratory, University of California, Los Alamos, N. M.	[U] 184 ✓
Nuclear Rockets-Safety Problems and Safety Programs George P. Dix, Space Nuclear Propulsion Office, NASA-Atomic Energy Commission, Washington, D. C.	[U] 192 ✓
RIFT Flight Operations James M. Rives, George C. Marshall Space Flight Center, NASA, Huntsville, Ala.	[U] 203 ✓
Transient Reactor Experiments on NERVA Fuel Elements Alvin Boltax and Max A. Vogel, Astronuclear Lab, Westinghouse Electric Corp., Pittsburgh, Pa. and Robert C. Liimatainen, Argonne National Laboratory, Argonne, Ill.	[U] 215 ✓
Effects of Liquid Propellant Explosions on Nuclear Rocket Engines E. Karl Bastress, Arthur D. Little, Inc., Cambridge, Mass.	[U] 226 ✓
The Los Alamos Scientific Laboratory Flight Safety Program L. D. P. King, Los Alamos Scientific Laboratory, University of California, Los Alamos, N. M.	[U] 236 ✓
A Destruct System for the NERVA Engine Ken N. Kreyenhagen, Warren H. Thiel and Stanley K. Yoder, Aerojet-General Corp., Azusa, Calif.	[U] 245 ✓

VI. REACTOR TEST OPERATIONS AND FACILITIES

CHAIRMAN: James W. Hadley,
Lawrence Radiation Lab,
University of California,
Livermore, Calif.

E-MAD Facility Design Concept Stanley K. Hellman, Vitro Engineering Co., New York, N. Y.	[U] 254 ✓
The KIWI-B-1A Full-Power Test Donald W. Brown, Los Alamos Scientific Laboratory, University of California, Los Alamos, N. M. and Samuel Cerni, Astronuclear Laboratory, Westinghouse Electric Corp., Pittsburgh, Pa.	[U] 264 ✓
KIWI-B-1A Temperature Reactivity Effects Howard B. Demuth, Charles E. Stiles and Joseph E. Perry, Jr. Los Alamos Scientific Laboratory, University of California, Livermore, Calif.	[U] 273 ✓
KIWI-A-Prime Disassembly Donald B. Anderson, Everett B. Ramsey and Marvin N. Swink, ACF Industries, Inc., Albuquerque, N. M. and Charles D. Montgomery, Los Alamos Scientific Laboratory, University of California, Los Alamos, N. M.	[U] 281 ✓

Design Considerations in the Development of the Liquid Hydrogen Feed System for KIWI-B

R. J. Bohl, C. P. Milich and M. Nutter, Los Alamos Scientific Laboratory, Los Alamos, N. M. 291

Tory II-C Assembly Techniques

A. W. Williams, Lawrence Radiation Laboratory, Livermore, Calif. 299

VII. REACTOR ENGINEERING DESIGN

CHAIRMAN: Walter H. Esselman,
Astronuclear Laboratory,
Westinghouse Electric
Corp., Pittsburgh, Pa.

Structural Analysis of the KIWI-B-2A Core Design

John C. Rowley and W. G. Brussalis, Los Alamos Scientific Laboratory, University of California, Los Alamos, N. M. 302

Analysis of the Specification of Temperature and Flow-Dependent Design Parameters in KIWI-B-Reactor Cores and Reflectors

J. A. McClary, Los Alamos Scientific Laboratory, University of California, Los Alamos, N. M. 310

NERVA Reactor Mechanical Design

Allen Selz and M. J. Manjoine, Astronuclear Laboratory, Westinghouse Electric Corp., Pittsburgh, Pa. 319

Tory II-C System

C. E. Walter, W. B. Myers and H. L. Reynolds, Lawrence Radiation Laboratory, University of California, Livermore, Calif. 328

Internal Support Problems in a High-Temperature Air-Cooled Reactor - Tory II-C

W. C. O'Neal, UCRL, Livermore, California 331

Pressure Requirements for the Lateral Support of a Reactor

Ethan Platt and Aubrey Miller, UCRL, Livermore, California 334

VIII. HEAT TRANSFER AND FLUID FLOW

CHAIRMAN: Armin Lietzke,
Lewis Research Center,
NASA, Cleveland, Ohio

Startup Studies of a Nuclear Rocket Reactor-Cryogenic Cooldown Experiments

G. P. Watts, Alvin R. Lyle and J. D. Balcomb, Los Alamos Scientific Laboratory, University of California, Los Alamos, N. M. 337

Decay Heat Cooling Analysis of a Nuclear Rocket Engine

Francis D. Retallick and W. L. Howarth, Astronuclear Laboratory, Westinghouse Electric Corp., Pittsburgh, Pa. 346

Experimental Heat Transfer Coefficients in a Contoured Nozzle

M. Kasahara, B. Mandell and B. L. McFarland, Aerojet-General Corp., Azusa, Calif. 355

Experimental Investigation of Jet-Driven Vortex Flows R. W. Hale and B. V. Johnson, Research Laboratories, United Aircraft Corp., East Hartford, Conn.	365
Investigation of a Unique Gaseous-Core Nuclear Rocket Concept at UAC G. H. McLafferty, Research Laboratories, United Aircraft Corp., East Hartford, Conn.	367
Theoretical Solutions for Primary and Secondary Flows in a Vortex Tube O. L. Anderson, Research Laboratories, United Aircraft Corp., East Hartford, Conn.	369

IX. MATERIALS RESEARCH I AND II

CHAIRMAN: James M. Taub,
Los Alamos Scientific
Laboratory, University
of Calif., Los Alamos, N.M.

High Temperature Testing of Mo-UO ₂ and W-UO ₂ Cermets W. H. Lenz and P. R. Munding, Los Alamos Scientific Laboratory, University of California, Los Alamos, N. M.	371
Refractory Carbides M. G. Bowman, Los Alamos Scientific Laboratory, University of California, Los Alamos, N. M.	378
High Temperature Light Weight Neutron Shielding Material for Nuclear Space Power Plants W. G. Baxter, Flight Propulsion Laboratory Dept., General Electric Co., Cincinnati, Ohio and F. H. Welch, Atomics International, Div. of North American Aviation, Canoga Park, Calif.	382
Protective Technology D. C. Winburn and R. K. Money, Los Alamos Scientific Laboratory, University of California, Los Alamos, N. M.	394
Compressive Creep of Ceramics for High Temperature Nuclear Reactors R. B. Vandervoort and W. L. Barmore, Lawrence Radiation Laboratory, University of California, Livermore, Calif.	404
The Quality of Rover Fuel Elements as Determined by Non-destructive Test Methods Gerold H. Tenney, Los Alamos Scientific Laboratory, University of California, Los Alamos, N. M.	411
The Fabrication of Fuel Elements for the KIWI-B4 Reactor William W. Martin, Donald H. Schell and Joseph W. Taylor, Los Alamos Scientific Laboratory, University of California, Los Alamos, N. M.	421
Chemical and Metallographic Evaluation of Uranium Compounds Incorporated Into Graphite Luther L. Lyon and C. Gordon Hoffman, Los Alamos Scientific Laboratory, University of California, Los Alamos, N. M.	427

BeO-Base Fuel Elements for Use in Air to 1650°C
P. P. Turner, K. M. Bohlander and E. S. Fitzsimmons,
Flight Propulsion Laboratory Dept., General Electric Co.,
Cincinnati, Ohio 436

The Fabrication of Clad Tungsten-UO₂ Fuel Plates
T. J. Schuetz, A. L. Eiss and L. Frank, Martin Co., Baltimore, Md.. 446

16. Investigation of Tungsten and Uranium Dioxide as Nuclear Rocket
Fuel Materials
Neal T. Saunders, Gordon K. Watson and Robert J. Buzzard
NASA Lewis Research Center, Cleveland, Ohio 454

The Manufacture and Properties of Graphite-Uranium Carbide Fuel
Elements
A. L. Eiss, T. J. Schuetz, L. Frank and A. R. Siegel
Martin Marietta Corp., Nuclear Division, Baltimore, Md..... 463

X. ENGINE STRUCTURES AND COMPONENT DEVELOPMENT CHAIRMAN: Stanley V. Gunn,
Rocketdyne, A Div. of
North American Aviation,
Inc., Canoga Park, Calif.

Liquid Hydrogen Pumps and Feed Systems for Nuclear Rocket Reactor
Experiments
Merle C. Huppert and Robert P. Watelet, Rocketdyne, A Div. of
North American Aviation, Inc., Canoga Park, Calif. 473

The Design of KIWI-B Type Nuclear Rocket Reactor Pressure Vessels,
with Notes to Optional Pressure Vessel Design
Joseph W. Neudecker, Los Alamos Scientific Laboratory,
University of California, Los Alamos, N. M. and
Robert Pozega, ACF Industries, Albuquerque, N. M. 490

Some Design Considerations of Cooling Systems for Nuclear Rocket
Nozzles Under Severe Thermal Conditions
John P. Sellers and Robert D. McFarland, Rocketdyne, A Div. of
North American Aviation, Inc., Canoga Park, Calif..... 502

Considerations in the Design and Choice of Material for KIWI Pressure
Vessels
R. T. Johnson, Albuquerque Div., ACS Industries, Inc.,
Albuquerque, N. M. 515

Design and Development of Columbium-1 Zirconium Reactor Pressure
Vessels
C. C. Bigelow, Pratt and Whitney Aircraft, Div. of United
Aircraft Corp., Middletown, Conn..... 524

XI. ENGINE AND VEHICLE DESIGN CHAIRMAN: William C. House,
Aerojet-General Corp.,
Azusa, Calif.

Nuclear Rocket Engine Cycle Selection
Donald F. Vanica, Aerojet-General Corp., Azusa, Calif..... 536

An Approach to Start-up Control of a Nuclear Rocket Engine Richard F. Searle and Robert D. March, Rocketdyne, A Div. of North American Aviation, Inc., Canoga Park, Calif.	546
Combined Nuclear and Chemical Propulsion Cycles Having High Specific Impulse Emmet A. Mossman and Ray L. Chapman, Martin Co., Denver, Colo.	558
Liquid Hydrogen Behavior with Heat Addition During Weightlessness Jack G. McArdle and Robert R. Nunamaker, Lewis Research Center, NASA, Cleveland, Ohio	567
Optimization of Nuclear Rocket Powerplant Parameters P. G. Johnson, G. E. Cowgill, and J. W. Miser NASA, Lewis Research Laboratory, Cleveland, Ohio	580

THE NUCLEAR ROCKET PROGRAM - 1962

Harold B. Finger*

[U]

This country has committed itself to the most difficult and dramatic technological undertaking ever attempted by man. I refer to the commitment that has been made by the President, by the Congress in supporting the President's recommendations, and by the people of the United States that we intend to explore space and apply our scientific findings and the technological developments for the benefit of all mankind. There is no question that the benefits that will result from this program will make all of mankind the winner.

As a result of the commitments made, scientific information, technological developments, and consumer application of certain space systems have been proceeding at an amazingly fast pace. Launch sites, Government laboratories, fabrication/assembly plants and tracking stations are being built; large launch vehicles are under development; manned spacecraft with all of the essential life support and guidance equipment are being developed, tens of thousands of people and thousands of industrial, Governmental, university, and non-profit institutions are involved in the over-all program. The program to land men on the moon will cost in the neighborhood of 20 billion dollars with another 15 billion over the next several years.

Obviously, such a major national commitment will go into a continuing program beyond the presently committed effort aimed at early space objectives. The achievement of even those early objectives is paced by the need to develop new system hardware which in many areas goes beyond available technology. In looking ahead at the missions and objectives we see beyond our early objectives, we are determined that we must be prepared with the technology needed to perform any desired mission in space. We never again intend to be caught in the position where there are missions we want to do, but for which the technology is unavailable. It is our anticipation of even more difficult space missions than those that have already been defined and programmed that makes the nuclear propulsion part of our program an essential portion of our over-all space effort. This importance was confirmed by the President over a year ago when he included the Rover Program as one of four areas requiring increased emphasis in our space effort. I am personally convinced that the major national effort now being devoted to space achievements will go on to the establishment of manned space laboratories, exploration bases on the moon and manned missions to the near planets. The use of nuclear energy will be required in the vehicles designed for accomplishment of these advanced missions. Our program anticipates such use, but it also recognizes that nuclear rocket systems developed for advanced missions could be used with the large chemical rockets now being developed to substantially improve the payload and energy increment capabilities of these rockets.

This discussion is limited to the nuclear rocket program; however, it is important to recognize that other nuclear systems required for advanced space missions must be pursued actively to establish the technology in these other areas, to evaluate the feasibility of these other systems, and to objectively assess them on a technical basis in comparison with the nuclear rocket system.

*Director, Nuclear Systems, National Aeronautics and Space Administration and Manager, Space Nuclear Propulsion Office (AEC-NASA), U. S. Atomic Energy Commission (Washington, D. C.)

There is no need for salesmanship in system selection for particular missions. Rather, there is a need for objective evaluation of technology and mission requirements to select systems which can perform, with greatest assurance, particular missions in a given time.

Nuclear Rocket Characteristics and Performance Potential

In the nuclear rocket system, liquid hydrogen is heated to high temperature in a nuclear reactor after having been pumped into the reactor from a large liquid hydrogen propellant tank. The specific impulses these systems can achieve, using solid core reactors, are in the range of 800 to 1000 seconds, two to three times the specific impulses of chemical combustion rocket systems. The development of the nuclear rocket involves major problems in reactor core development. These will be discussed below. In addition, other significant problems are development of liquid hydrogen cooled nuclear rocket nozzles and control system analysis and development. Hydrogen turbopump systems of large capacity will eventually be required for the nuclear rocket and, while not controlled by feasibility or lack of basic data, are a major development area.

The nuclear rocket system performance potential is indicated in the next two figures. Figure 1, familiar to many, indicates the vehicle requirements to perform a manned, Mars landing mission. Calculations indicate a nuclear rocket propelled spacecraft, weighing approximately a million pounds, assembled in an earth orbit, can accomplish this mission with a 400-day total trip time. The nuclear spacecraft would remain in Mars orbit until needed for return to earth orbit while manned landing on Mars and return to the orbiting spacecraft would use chemically propelled systems. A spacecraft weighing 10 million pounds would be required to accomplish this mission using chemically propelled systems. The performance advantages for such missions, we feel, justify our major effort in the nuclear rocket program. Accomplishment of the first such mission using nuclear rockets would pay for the development effort and the vehicle costs required to perform the mission. However, nuclear rockets developed for such advanced missions could be used with large chemical rockets, now being developed, to substantially improve the payload capability in near earth missions. This is indicated in Figure 2 which shows performance of a nuclear propelled third stage on the advanced Saturn C-5 vehicle. The Saturn C-5 vehicle, 33 feet in diameter, uses five F-1 kerosene-oxygen engines to produce a 7,500,000 lb. total first stage thrust. The hydrogen-oxygen second stage uses five J-2 200,000 lb. thrust engines. The payload presented can be placed into a lunar orbit, using these first two advanced Saturn stages and the nuclear third stage. The payload plotted as a function of the nuclear stage thrust ranges from something over 100,000 lb. to 130,000 lb. established in a lunar orbit. An all-chemical advanced Saturn, using four stages, could deliver approximately 55,000 lb. to 65,000 lb. into this same lunar orbit. Incorporation of the nuclear third stage substantially increases the payload capability of the advanced Saturn vehicle.

The lunar orbit payload is shown because lunar orbit rendezvous has been selected as the technique to accomplish the manned, lunar landing. A single advanced Saturn would be used during the initial landing mission to place the Earth return vehicle and lunar landing bug in an orbit around the Moon. The bug would land on the Moon and the men would then return to the orbiting return vehicle, rendezvous with that vehicle, and return to Earth. Approximately doubling the lunar orbit payload through the use of nuclear systems indicates the potential of a direct flight mission using a vehicle such as the one shown here. We anticipate that after the initial Moon landings, nuclear stages will be used to perform lunar operation missions. The lunar orbit payload is also of interest because of the potential advantages of a nuclear system as a

reusable ferry between earth and lunar orbit. The nuclear vehicle, initially established in an earth orbit would transport passengers, equipment and supplies to a lunar orbit. Transfer from lunar orbit to Moon's surface would be accomplished by another vehicle. Return payloads would be taken back to earth orbit by the nuclear vehicle. The system would then be refueled in the earth orbit and reused.

This is obviously an advanced mission in that frequent nuclear stage reuse and restart are required. Even the first lunar orbit mission indicated requires nuclear stage reuse. At least two re-firings are required in the postulated mission trajectory. The system is first restarted in the earth parking orbit to achieve the lunar intercept trajectory and the second re-firing is needed to establish the system in a lunar orbit. Almost every mission we postulate requires restart of the nuclear stage. Restart is, therefore, an important reactor development program requirement.

The first nuclear engine, NERVA, will operate at a thrust at the low end of the curve of Figure 2 corresponding to about 100,000 lb. lunar orbit payload. It is conceivable that we will go to somewhat higher powers, as development proceeds, if the increased payload justifies such power increases. We anticipate that there will be major useful NERVA engine applications in missions related to lunar operations.

These two figures have indicated performance potential we foresee in nuclear systems. I have not indicated a need for extremely high power stages, although such a need, we are convinced, does exist. High power 10,000 to 20,000 megawatt stages producing 500,000 lb. to 1,000,000 lb. thrust would be required for second stage applications with the NOVA type large chemical booster vehicles.

AEC - NASA Nuclear Rocket Program

As you know, the development of nuclear rocket propulsion is being conducted jointly by NASA and AEC through the Space Nuclear Propulsion Office (SNPO). The SNPO, organized in August, 1960, is responsible for managing all aspects of the propulsion effort. This effort constitutes a large program, larger than anyone would have hoped for, or expected only two years ago. But this is a logical program with restrictions to assure satisfactory components before proceeding with complicated systems. In addition, this is not a program to develop a single article, but rather to develop a whole technology that will permit real exploration and exploitation of space.

The major elements of the AEC-NASA nuclear rocket program are as follows. The KIWI reactor testing will define a basic reactor configuration which will be applied in the NERVA engine and engineered for flight applications in the NERVA engine development. The NERVA engine, in turn, will be flight tested in the RIFT stage which is intended to evaluate the flight operating problems of nuclear rockets. The RIFT stage will be designed to consider eventual application in useful space missions. In addition, we have our advanced technology program and the major facilities required to perform all aspects of this effort. These are the essential ingredients of the joint nuclear rocket program.

I would like to review each of these major areas to show how the program fits together, the status of each major program element and our plans for overall system and technology development.

Reactor Development

There is no question that the major problem area is in the reactor. The KIWI reactor project, conducted by the Los Alamos Scientific Laboratory, includes design, fabrication, and test of reactors to define a basic rocket reactor core configuration. The major reactor development problems, we anticipate, are high temperature fuel element materials, uniform radial core temperature, core structure support, fast startup with combined power and flow control, and last but not least, restart capability with the companion problem of controlled shutdown to maintain core integrity. Since these items are self explanatory, I will proceed to describe the reactor program being conducted to solve these problems.

The KIWI project began in 1955. The first three reactors tested in this program were the KIWI-A reactors in Figure 3. The tests, started in 1959, were conducted after extensive laboratory design analysis, materials investigations, neutronic investigations, as well as fabrication development work. The three KIWI-A reactor tests confirmed the design of these reactors, provided materials information and some controls information. These were strictly research devices not applicable to a flight system and for this reason the active core volume was minimized. A central heavy-water island was incorporated in the system, and water was used to cool critical non-nuclear components of the system, such as the converging nozzle.

The KIWI-A reactor characteristics are compared in the table below with the KIWI-B reactor characteristics.

KIWI REACTOR CHARACTERISTICS

	<u>KIWI - A</u>	<u>KIWI - B</u>
Power	100 MW	1,000 MW
Pressure Vessel O. D.	73 IN.	51 IN.
Power Density	4.25 MW/FT ³	34.5 MW/FT ³
Reflector	Graphite	Beryllium
Coolant-Propellant	H ₂ Gas	H ₂ Liquid
Hydrogen Flow Rate	7 LB/SEC.	70 LB/SEC.
Exit Gas Temperature	3460°F	3600°F
Control System	Center-Island Axial Rod	Rotating Reflector Segment

The KIWI-B design is intended to evolve into the flight type system required for the NERVA engine. The KIWI-B will have a tenfold increase in power level over the KIWI-A, while reducing the outer core diameter. The core power density is increased approximately eight fold and the pressure vessel O.D. is reduced to 51 inches. Much of this size reduction results from replacing the thick graphite reflector with beryllium. Hydrogen flow is increased and hopefully core exit temperature as well. In addition, the central-island axial-rod control system was changed to the reflector control.

The KIWI-B1A, first of the KIWI-B series, was tested in December 1961 and a photograph is shown in Figure 4. The reactor has a cleaner configuration than the KIWI-A. Since liquid hydrogen was not yet available in the test cell, the reactor power level was limited to approximately 300 megawatts due to the lower heat removal capability of the gaseous hydrogen cooled nozzle. The December test was terminated after 30 seconds of the planned five minutes run because of a hydrogen leak in the pressure vessel-nozzle flange seal. The data obtained were encouraging, having indicated satisfactory fuel element operation and

suitability of the reflector control system. The first liquid hydrogen tests with the KIWI-B reactor were completed in July with a uranium-238 loaded reactor, referred to as the cold flow reactor. In these devices, the system startup relies upon the nozzle-reflector-core heat capacity to vaporize the liquid hydrogen propellant prior to entering the core. Therefore the first ten seconds of reactor startup can be investigated using a non-critical reactor system. The purpose of the July tests were therefore to evaluate this initial startup period, to determine the control system requiring hot operation startup and to check out the facility. Both test operations provided the data required for the first hot reactor operation with liquid hydrogen.

The KIWI-B1B was used for the first hot reactor run with liquid hydrogen. During the September 1, 1962, test, reactor power exceeded 900 megawatts and exit gas temperature was increased at a rate of $70^{\circ}\text{R}/\text{sec}$. At approximately 700 megawatts, the core suffered damage and fuel element modules were ejected from the nozzle at intervals. The reactor power continued to increase until fuel loss forced the level down as the control drum limits had been reached.

Early in the start cycle, hydrogen pressure fluctuations were observed at the pump outlet, however these fluctuations had ceased about ten seconds before damage was noted. We believe these pressure variations resulted from an unchilled bypass line at the pump outlet; however, pressure data indicated that the fluctuations were well attenuated at the core inlet.

The results of the test indicate reactor startup with liquid hydrogen is feasible and reactor power is stabilized by core hydrogen flow. The core damage in the test confirmed our prior judgment not to select the KIWI-B1 design as a candidate for NERVA application.

As indicated above, one of the major reactor problems is development of a suitable core structural support. The fuel element work has been most promising, but the method of retaining these elements within the core has not been selected or proven by test. Several different reactor designs have therefore been defined, aimed primarily at determining a satisfactory core support for the KIWI reactor and one which may then be developed for core support in the NERVA flight system.

Graphite is an extremely good high temperature material. It is not as strong at low temperature as at high temperature and, in addition, it is stronger in compression than in tension. The basic difference among our varying designs, therefore, results from the fact that although the first design has the fuel modules and structure in tension, it is our intent in later designs to put the structure, as much as possible, under compressive load.

The KIWI-B reactors that have been run to date utilized the KIWI-B1 core design shown in Figure 5. This figure shows the reflector section with rotating control drums, the outer pressure shell, the core, and the core support plate. Core configuration detail is shown in the lower right sketch. It is an unfueled graphite module containing fueled cylindrical fuel elements, each of which has seven holes. A similar fuel module configuration was used in two of the KIWI-A tests; however, the fuel elements in those tests were four hole fuel elements. The modules are nested to form the reactor core and each is supported from the top support plate by a hollow threaded bolt through which hydrogen may pass into the central fuel element. The pressure drop resulting from the flow of hydrogen through the fuel elements imposes a tensile stress in the module and in the KIWI-A tests. Certain of these modules cracked and in one test three were discharged through the nozzle. Although we have attempted to alleviate the problem by keying the modules together at the core discharge end, the basic reason for module failure has not been uncovered in laboratory tests. Primarily for this

reason, we are not depending on the KIWI-B1 design. However, retest of the KIWI-B1 was planned because the hardware was available and we believe that liquid hydrogen startup information obtained from this design is applicable to startup of the other designs.

The next three reactors to be discussed, KIWI-B2, KIWI-B4 and KIWI-B6, are designed to place most of the core graphite components under compressive load. The KIWI-B2 reactor shown in Figure 6 uses a modular core structure similar to the KIWI-B1. However, rather than depending upon the cold end support shown for the KIWI-B1, a solid graphite block is used at the discharge of the reactor to support the unfueled modules. The fuel elements themselves pass through holes bored in the graphite support block. Design problems include maintaining the geometric stability of the graphite block and limiting thermal stresses at the block edges to acceptable values. This is, however, one of the designs that we plan to test early next year.

At the present time, the KIWI-B4 design, shown in Figure 7, is the prime candidate for adaptation to NERVA requirements. It involves a compressive graphite system and a different fuel element configuration. The KIWI-B4 has a homogeneous, fully loaded core rather than the heterogeneous system of the B1 and the B2. Six hexagonal fuel elements are clustered about an unloaded graphite rod as shown at the top right of the figure. These are held together by a cluster retaining plate and suspended from the top support plate of the reactor by a bolt which passes through the fuel element cluster to graphite support blocks at the bottom of the core. The pressure load from the flow through the reactor puts a tensile load on this steel support rod, but the fuel element cluster is in compression, bearing against bottom support blocks. Hydrogen cools the central support rod and a pyrolytic graphite tube, surrounding the rod, insulates it from the fuel elements. The greater fueled graphite volume in this core design gives us, we believe, higher power potential than that required for NERVA. Part of this potential may be used to attain higher NERVA system temperatures than indicated earlier, since impulse has a greater effect than power level on performance in most of our missions. The final reactor design, now being prepared, is the KIWI-B6 reactor and is shown in Figure 8. Comparatively new to the program, the design is made feasible by the development of pyrolytic graphite components which provide good insulating properties. A hydrogen cooled fabricated support plate will be used in this design to support the reactor core. Hydrogen from the nozzle coolant tubes will cool the plate and will then flow to reflector inlet channels. One KIWI-B6 design problem is the transition of core flow passages into the limited number of pass-throughs in the hydrogen cooled bottom support plate. For this reason, 19 fuel elements are included in the fuel cluster. This design has not progressed much further than the conceptual design phase and is the responsibility of Los Alamos. However, it will be worked on jointly by Los Alamos, Aerojet and Westinghouse.

KIWI project accomplishments include:

- a. satisfactory fuel element developed,
- b. uniform reactor core radial temperature demonstrated,
- c. combined power and flow control using gaseous hydrogen demonstrated,
- d. startup data obtained with liquid hydrogen in hot reactor test,
- e. high heat flux nozzle proof tested,
- f. hydrogen turbopump for Test Cell A acceptance tested and operated on cold flow reactor test, and
- g. three KIWI-B core structural support designs completed and reactors fabricated.

We believe that we have gone a long way toward developing a satisfactory fuel element. We have not yet operated at the powers or the durations that we intend, nor have we restarted the system at desired power and temperature. However, all laboratory tests indicate the fuel element should operate satisfactorily for a limited number of restarts at KIWI and NERVA design temperature and power density. Core temperature distribution has proven to be remarkably uniform, an important requirement for these high temperature systems. We have obtained, as I indicated, startup data with liquid hydrogen during both cold flow and hot reactor operations. The KIWI-B nozzle has been proof tested with a hydrogen-oxygen combustion chamber and has operated satisfactorily during the KIWI-B1B test. It is extremely important to recognize that much has been accomplished in the KIWI project. Many problems were encountered; many have been solved; others still exist to be solved, but we are confident that these too will be solved. Several designs are being worked on and out of these at least one will have sufficient design margin to provide a satisfactory reactor for the KIWI - NERVA system.

NERVA Project

Even after accomplishing the objectives of the KIWI program to define a basic reactor core configuration to be used in the NERVA engine, considerable engineering work will be required to provide a reactor suitable for the flight loads that will be experienced during flight operation of the NERVA engine. Although it had been our intent to demonstrate the suitability of a reactor design, delays that have been encountered in obtaining necessary reactor data have led to a different approach. We have tentatively selected KIWI-B4 as the most promising reactor for application in NERVA. We have instructed our contractors, Aerojet and Westinghouse, to proceed with design and fabrication of NERVA reactors, based on this B4 design, suitable for meeting the flight loads to be experienced in NERVA. In addition, our contractors are proceeding with design evaluation of KIWI-B6 for possible application in NERVA. We have greater overlapping and anticipation of results than we had planned in order to keep the program moving on as rapid a pace as is practicable. This does involve greater risk of funding and manpower use and from that point of view involves a greater gamble than we had originally proposed. The engineering development will have to be conducted by Westinghouse as the principal Aerojet subcontractor. This engineering development is due to the higher loads to be experienced by the NERVA engine reactor as compared to KIWI reactors design loads.

Some of the modifications required to meet these load specifications are shown in Figure 9 which is a drawing of the NRX-A, the designation for the NERVA version of the KIWI-B4 reactor. Lateral support must be provided to the reactor because side loads will be imposed during the handling and launch phase of the flight operation prior to reactor startup. The lateral support system is shown as a series of 3x3 pyrolytic graphite blocks which are spring loaded against the core to retain it as a fairly rigid package. Lateral support design is complicated by deflections on the fuel element clusters due to the side loads. These deflections cause shifting of one fuel element cluster against the next and excessive friction between these clusters would cause binding and prevent freedom of expansion, leading to possible fracture.

A shield contained within the pressure shell will be required in the flight system to attenuate radiation energy leaking from the core by an order of magnitude to reduce propellant heating in the tank. This shield will be evaluated first during the KIWI-B5 reactor tests. KIWI-B5 is a KIWI-B4 reactor with a shield.

Extensive system design and analysis and component research and development for the NERVA engine system will be in process during the KIWI-B and NRX reactor

testing. Based on work done to date, estimated performance characteristics of this engine are presented below.

Estimated Nuclear Engine Performance Characteristics
(Hot Bleed Cycle)

Thrust	LBS	54,600
Pressure, Chamber (Nozzle Inlet)	PSIA	550
Nozzle Expansion Ratio		40:1
Specific Impulse, Steady State	SEC	780
Flow Rate, Propellant	LB/SEC	70
Temperature, Core Exit Gas	°F	3,630
Weight, Engine Dry	LBS	13,750

You will note that the engine weight is high, but the high specific impulse compared to chemical combustion systems more than compensates for the comparatively high engine weight in the lunar and planetary missions which we intend for the nuclear rocket.

A full scale mockup of the NERVA engine is shown in Figure 10. Here you see the reactor, reactor control drums actuators, liquid hydrogen cooled nozzle, the thrust structure, and the large spheres which accumulate high pressure gas during operating cycles to provide pneumatic gas for actuator power during engine restart operations. The over-all engine stands approximately 25 to 28 feet tall. The tank shutoff valve and the gimbal bearing are located in the inlet duct within the upper thrust structure. The turbopump system is located in the duct region downstream from the gimbal. The gas used to drive the turbine is exhausted through the roll control nozzles.

Although we have authorized our industrial contractors to proceed with NRX-A reactor fabrication, a basic guide line in the program still requires that successful reactor operation with liquid hydrogen be achieved prior to the initiation of the major non-nuclear hardware procurement and development on both the engine and the RIFT vehicle. Nevertheless, through analysis and tests, very important fabrication and operating data have been obtained on the NERVA nozzle, methods for bleeding gas for turbine drive fluid, engine control, turbopump operation, and development of temperature, pressure and flow sensors for the control system. Work will be continued on non-nuclear component areas considered to be major problems in the nuclear rocket system. It is intended that sufficient component and radiation effects information be available before assembly of the first engine to give the greatest possible assurance that the first engine will operate satisfactorily and that the difficulties encountered will result from those component matching and integration problems which cannot be satisfactorily evaluated with prior tests and analyses. The difficulties of conducting nuclear rocket engine system tests require that careful experiments and analyses be conducted prior to such tests to insure the greatest probability of success. A trial and error process in this area will not provide a developed engine in the time that we have allocated for the program.

RIFT Project

We have already initiated efforts required to develop the RIFT stage which will be used to flight test the NERVA engine. Lockheed has been selected for that contract work. The principal objective of the RIFT Project is to flight test the NERVA engine and obtain information on the operation of a nuclear rocket system in the space flight environment. In addition, it is intended that these RIFT tests provide data necessary for the development of an operational stage.

They, therefore, constitute the first flights in the development of an operational vehicle. For that reason, the RIFT stage has been designed, primarily, for the flight test objective in mind, but it is geometrically configured with consideration of optimum escape payload when used as a third stage on the advanced Saturn vehicle. The RIFT project does involve certain unique problems in cryogenic systems, radiation effects, nuclear hazards, weight distribution and start, restart and cool down operations.

Although chemical combustion systems also use cryogenic fluids, the nuclear rocket does involve new cryogenic problems. For example, the RIFT stage will involve the design, fabrication and operation of the largest liquid hydrogen propellant tank planned on any of our vehicles. Nuclear rocket operation is complicated by the radiation effects imposed on the components of this system. Where hydraulic actuators have worked effectively in all other chemical systems, electropneumatic systems will be required in the nuclear rocket, and most of the electronic gear, cable, and other components for the system will have to be evaluated under radiation environment conditions. In addition, the nuclear hazards of operating the RIFT project and the effect of follow-on operational use on the RIFT program safety design will be considered. The weight distribution is different, largely because of the massive weight of the nuclear engine. The startup, restart, shutdown and cool down of this system provides unique control requirements on the vehicle and also unique trajectory and guidance requirements.

A drawing of the RIFT stage is shown in Figure 11. The stage will stand approximately 86 feet tall. The nose cone that will be included in the flight test system will add an additional 54 feet to this height. The diameter of the stage is 33 feet, which is the same as the diameter of the first two stages of the advanced Saturn. The total stage weight is 200,000 pounds, with a hydrogen propellant capacity of 156,000 pounds. The configuration of the entire RIFT vehicle is shown in Figure 12. The total height of the vehicle will be 364 feet. The first stage will be the S-1C stage, which I discussed above, and which has a take-off thrust of 7-1/2 million pounds. A water filled dummy stage will be used in place of the S-2 stage in order to provide reasonable acceleration to the RIFT stage.

It is now planned that four flights will be conducted with the RIFT stage. The first flight will be a cold flow test and will involve operation of the engine in the manner similar to that conducted for the KIWI test this past July. The first flight will, therefore, evaluate the initial startup of the nuclear system, but it will be conducted with the reactor fueled with uranium 238 so that there are no criticality or safety operating problems associated with that first flight. Such a flight is also required in order to checkout the dynamics of the entire booster vehicle system and the telemetry system.

The second flight trajectory, with one nuclear thrust period, is depicted in the next two figures. Figure 13 shows the trajectory plot in relation to surrounding land masses. The take off will, of course, be in Canaveral. The first stage after cutoff will impact in the ocean approximately 450 nautical miles from Canaveral and impact of the RIFT stage will occur approximately 2,400 nautical miles downstream in the Atlantic Ocean. The altitude and range coordinates of the second flight trajectory are shown in Figure 14. The first stage, S-1C booster, will cutoff at approximately 60 nautical miles and will impact, as I indicated above, about 450 nautical miles from the launch point. The second, or nuclear stage, will be brought up to full power after this cutoff and will operate for approximately 12 to 1300 seconds, cutting off at 1500 miles range with impact at the 2400 miles range. The total flight time will be 2000 seconds.

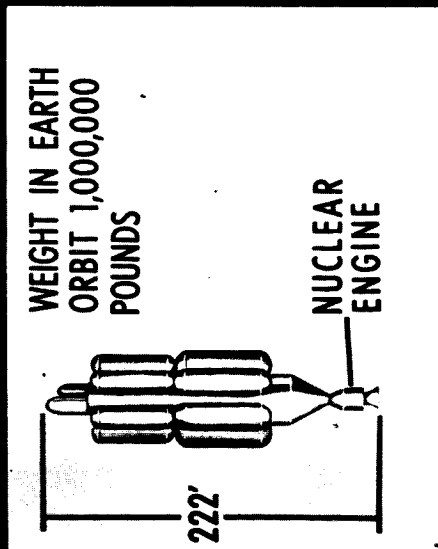
I have indicated here our plans for the second flight involving a single operating period. Consideration is now being given to multiple operating periods for the third and fourth flight. I should point out that these multiple

operating period flights have not yet been definitely established, especially in view of the fact that the reactor operation with restart has not yet been evaluated. The data obtained during the reactor operation will significantly affect the kind of flight mode we establish for this system.

It is important to recognize that we have limited the RIFT project to these first four flights and fully expect that beyond this time we will continue with the flight testing of the vehicle. At that time, however, we expect that the program will no longer be the Reactor-In-Flight-Test program, but will become the program aimed at the development of an operational vehicle.

I have just described the AEC-NASA Nuclear Rocket Program and where we are in 1962. The program began in a Laboratory seven years ago. Now, with our major contractors selected, we have large scale industrial participation. We have a total program consisting of reactor, engine, and stage development efforts to demonstrate the practicability of nuclear flight. We also have advanced research and technology efforts to provide techniques needed to perform useful missions with nuclear rockets. We have progressed to full scale reactor testing at approximately design power level. The testing pace will increase since our second test cell is almost available, the KIWI reactor pipeline has reactors available for testing and NERVA reactor tests are scheduled to begin within a year. We have achieved several important technological milestones. We feel that we have the fuel element required for the first engine program and we have shown that rocket reactors can be started and operated using liquid hydrogen coolant without significant control problems. Many difficult problems remain before a nuclear rocket engine is developed, but we will be ready when the need arises for nuclear rockets to propel sustained lunar exploration missions and manned flights to the near planets.

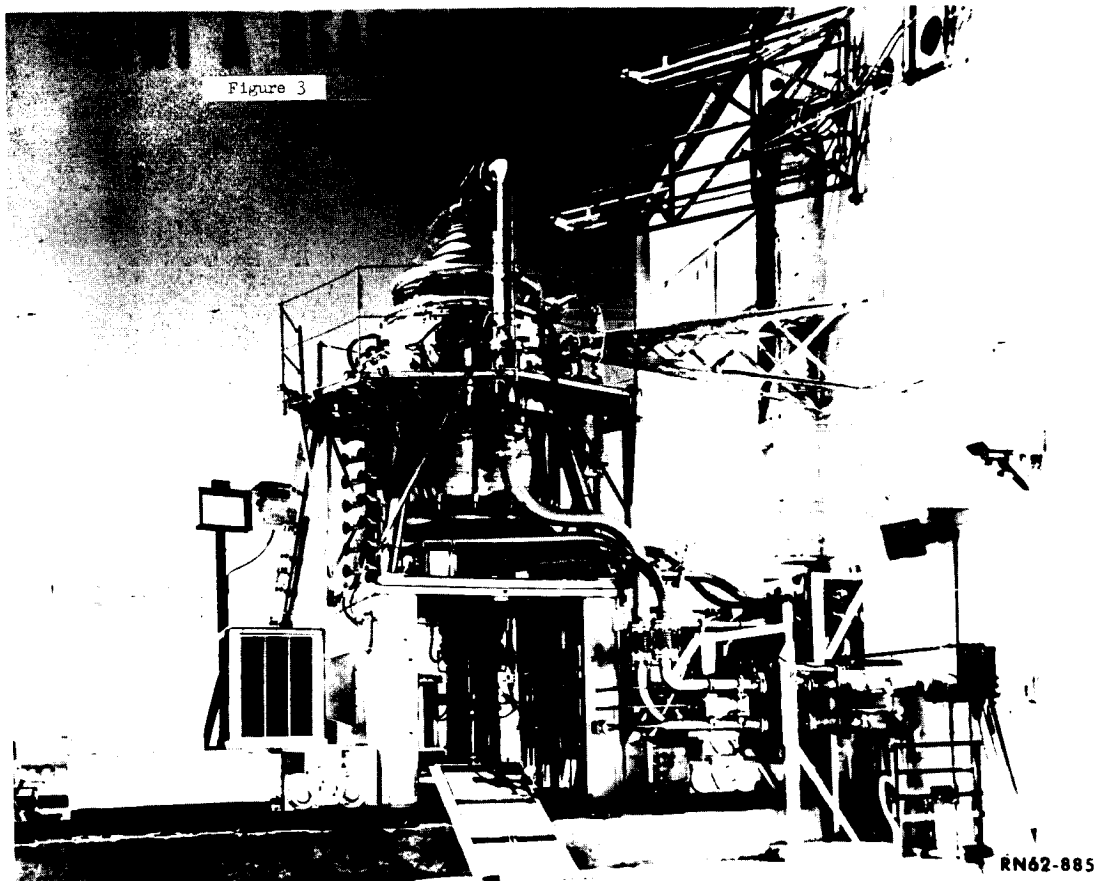
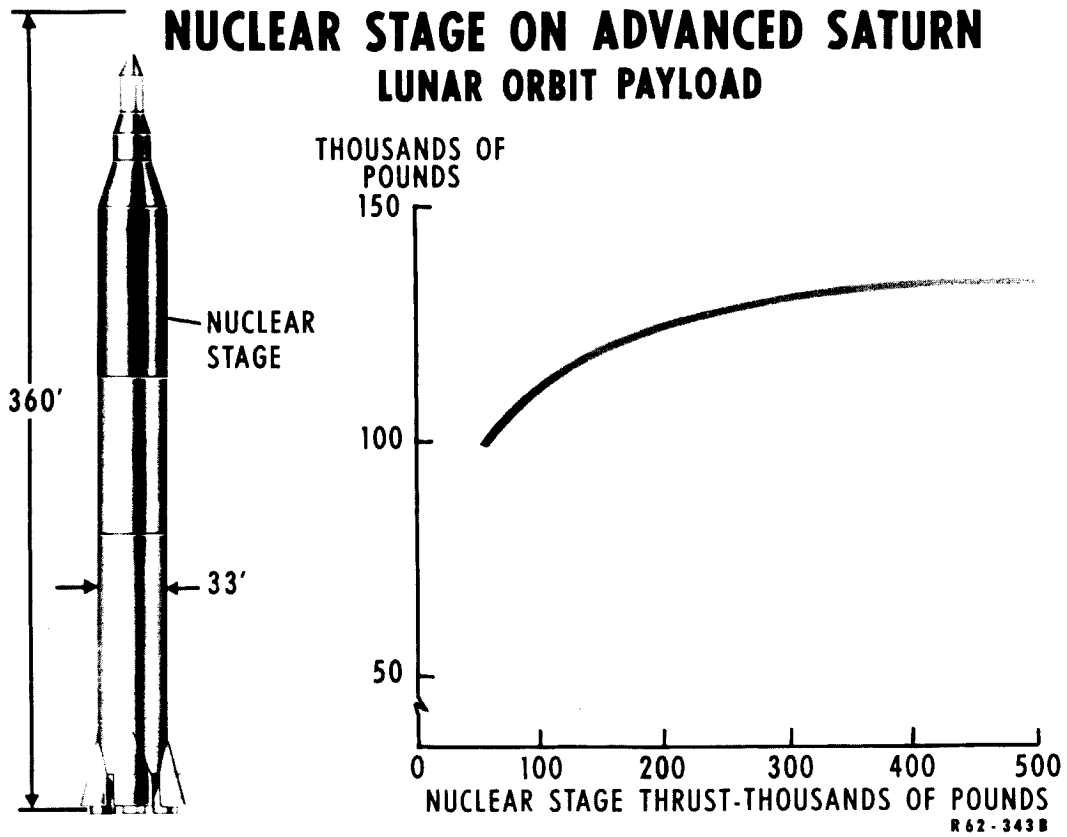
MARS LANDING MISSION NUCLEAR ROCKET

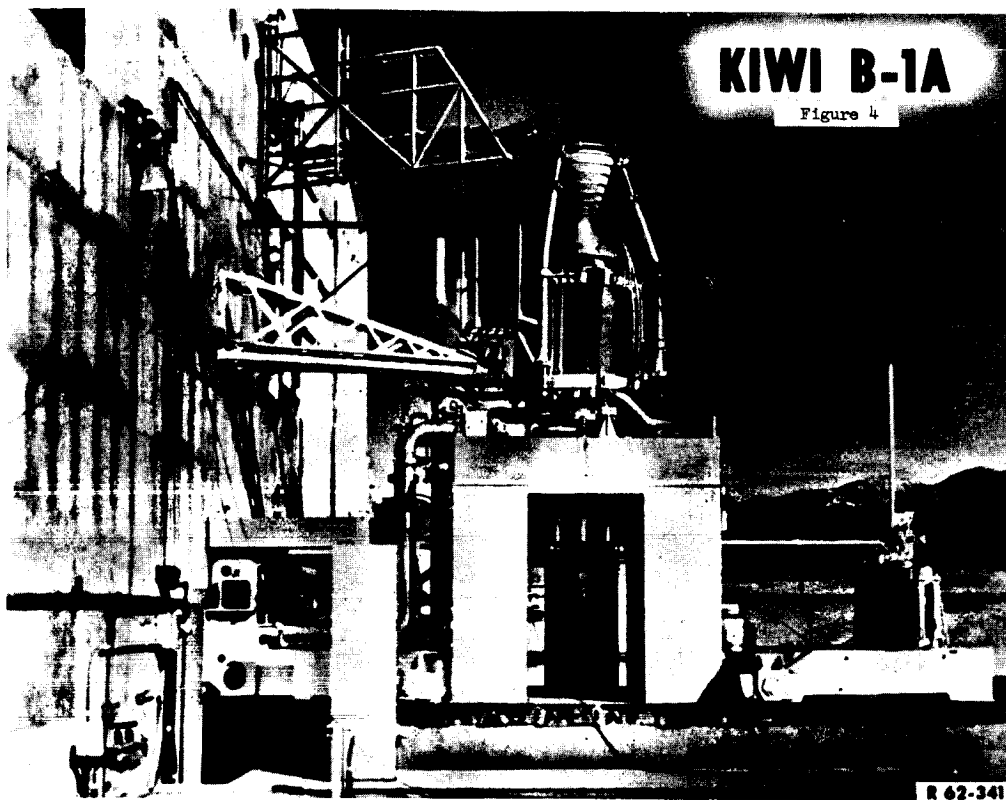


R 62-338

Figure 1

NUCLEAR STAGE ON ADVANCED SATURN LUNAR ORBIT PAYLOAD





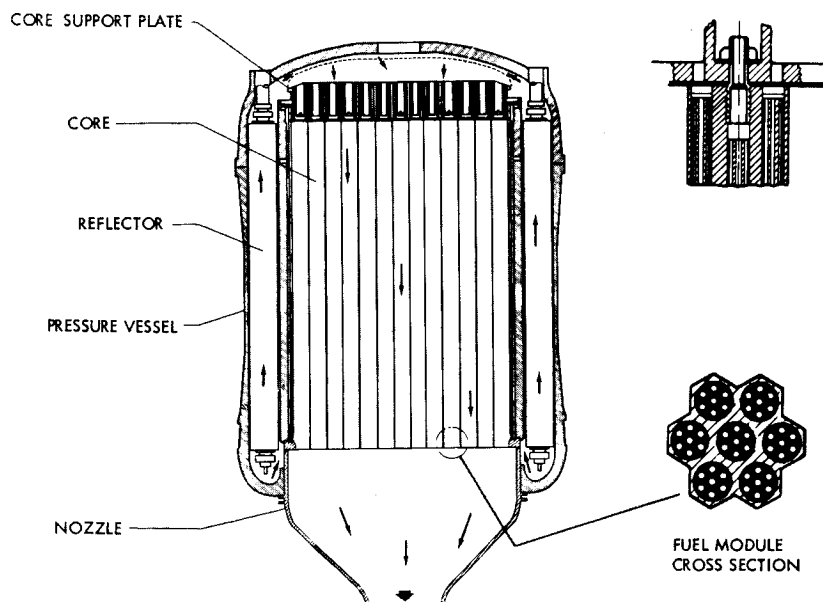
KIWI B-1A

Figure 4

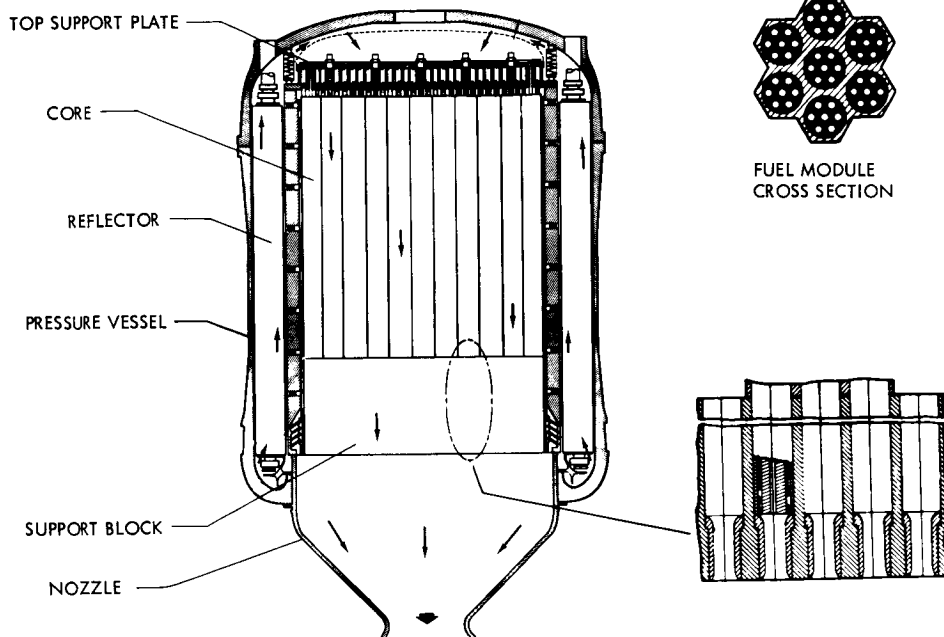
R 62-341

KIWI B1

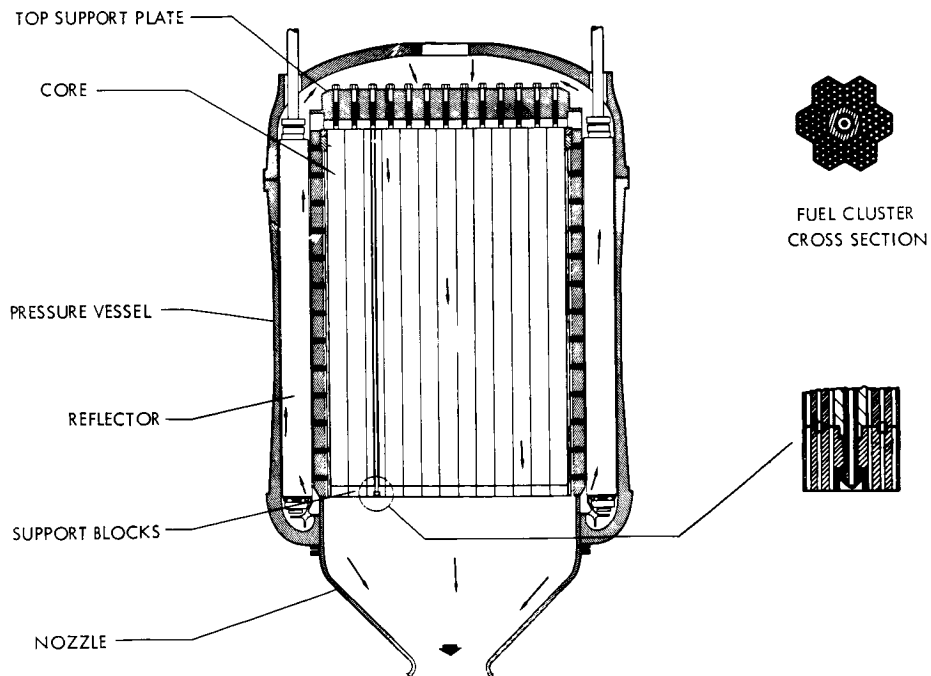
Figure 5



KIWI B-2
Figure 6

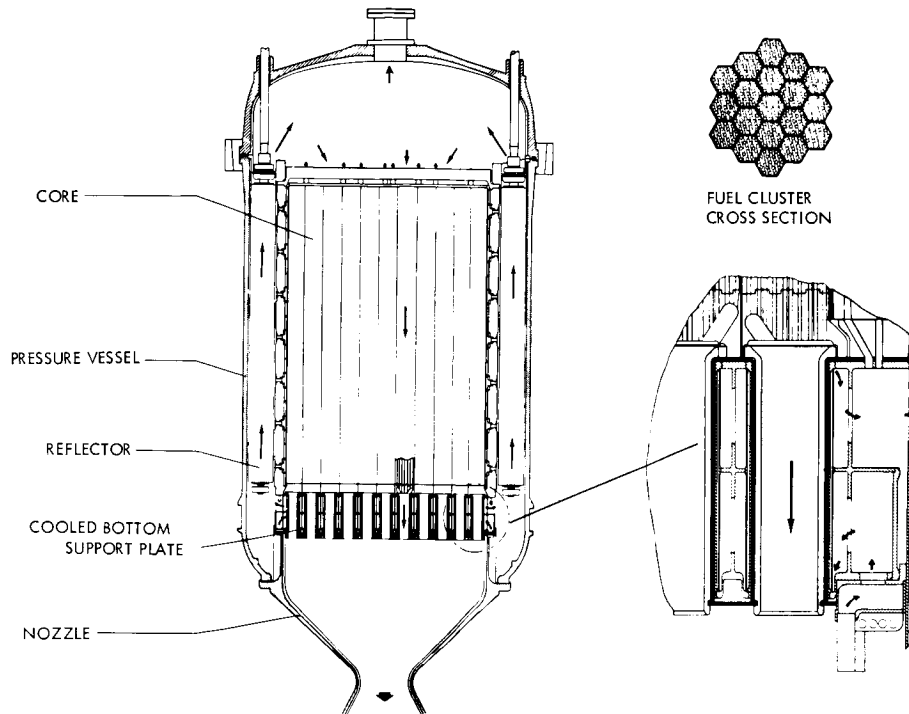


KIWI B-4
Figure 7



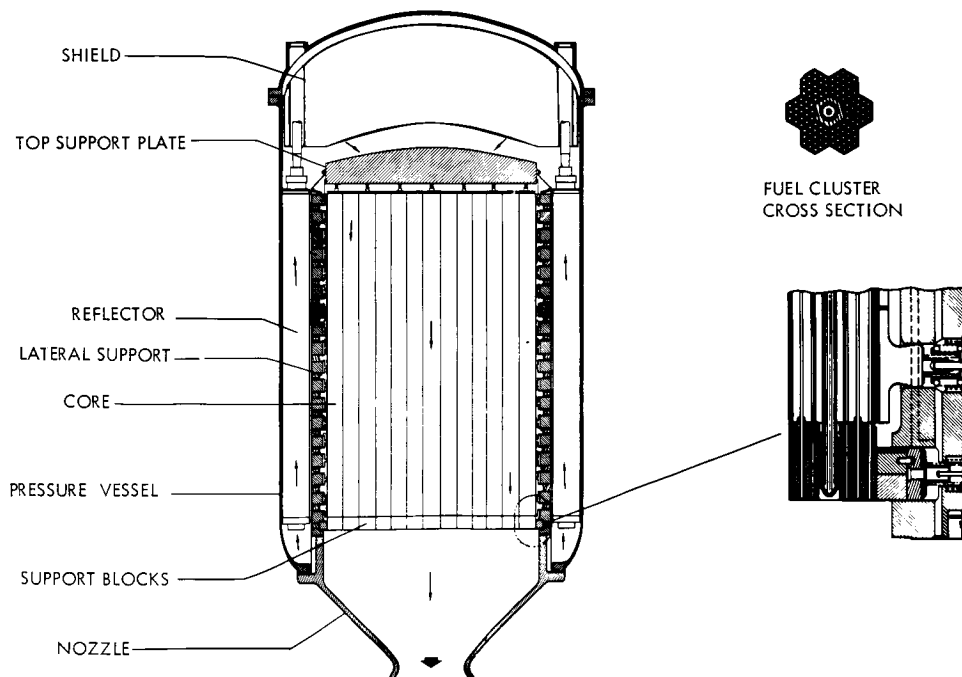
KIWI B-6

Figure 3



REACTOR ASSEMBLY NRX-A

Figure 3



NERVA MOCKUP

Figure 10



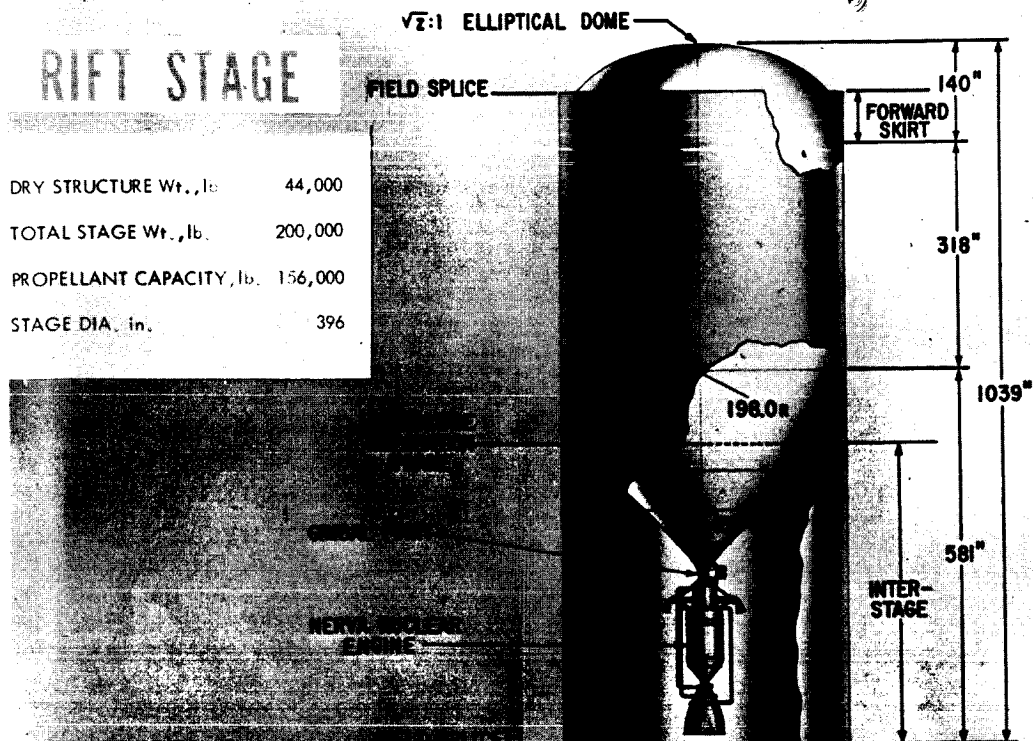


Figure 11

RM62-884

C-5 RIFT

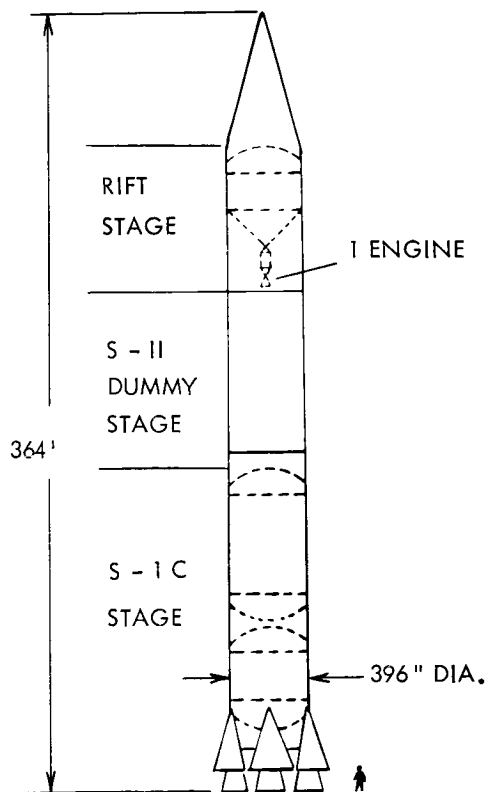
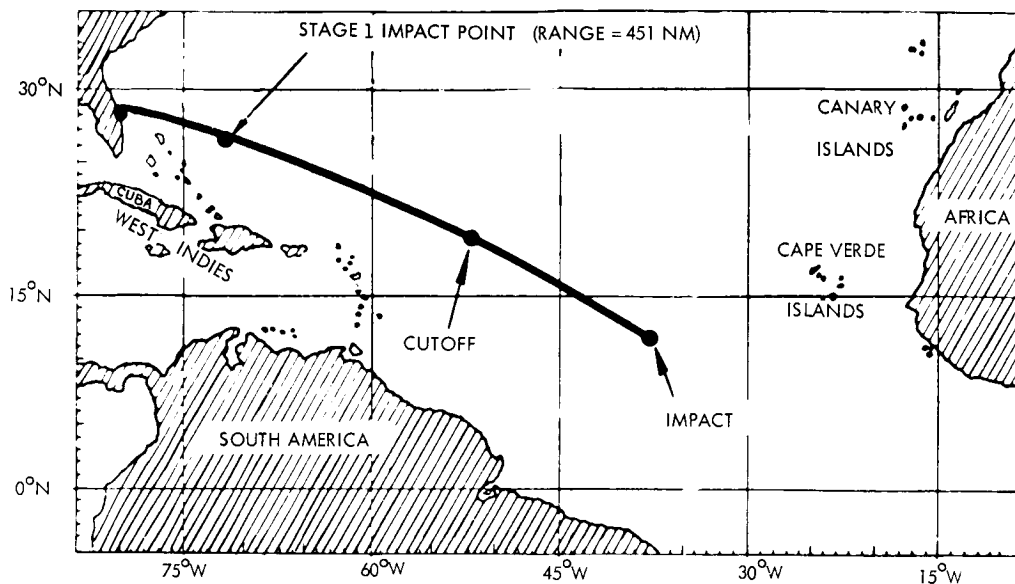


Figure 12

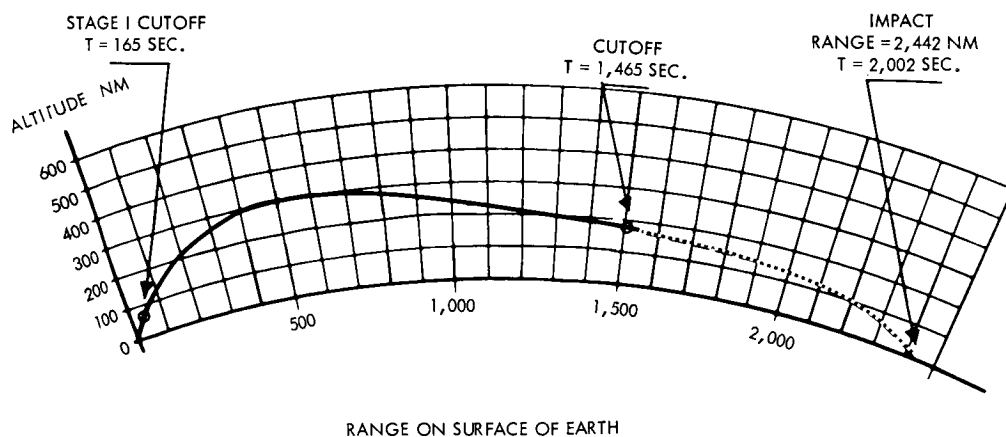
C-5 RIFT TRAJECTORY IN GEOGRAPHIC COORDINATES ONE OPERATING PERIOD



LAUNCH AZIMUTH = 100°

Figure 13

C-5 RIFT-TRAJECTORY GEOMETRY ONE OPERATING PERIOD



LAUNCH AZIMUTH = 100°

Figure 14

X 66 50278

CRITICALITY AND NUCLEAR CHARACTERISTICS OF THE
KIWI-A SERIES OF NUCLEAR PROPULSION TEST REACTORS

J. C. Hoogterp
J. D. Orndoff
Los Alamos Scientific Laboratory
University of California
Los Alamos, New Mexico

[U]

I. Kiwi-A Reactor Objectives.

The "A" series of three Kiwi nuclear propulsion test reactors for experiments at the Nevada Test Site contained a uranium (93.2% U^{235}) loaded graphite core, a graphite reflector and a D_2O island. Boral rods in the D_2O served as control. The core heat exchange medium was gaseous hydrogen.

The aim of the test reactor was to provide as inexpensively as possible, a temperature and environment suitable for core material testing, (instead of simulating a flyable reactor). Secondary goals were to check computed temperature effects on neutronics and to gain experience in reactor testing. The purpose of the D_2O island within the core was to reduce fuel volume and simplify control.

In the interest of early results, compromise test conditions were set at a power density of 12 Mw/ft^3 , with maximum power at 100 Mw , and exit gas temperatures in the neighborhood of 2000°C .

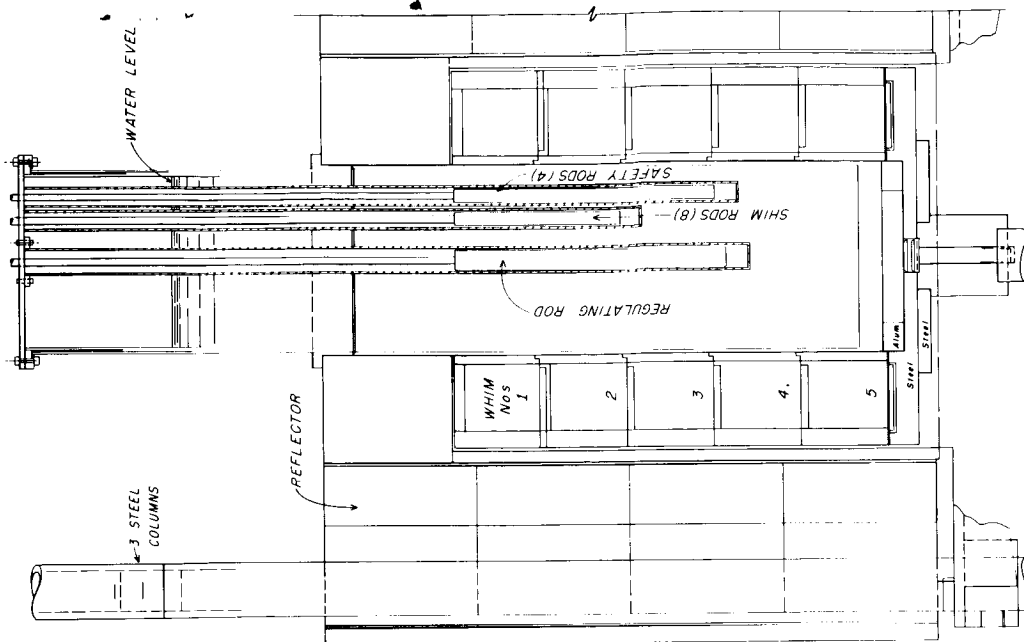
II. Mockup Studies.

At the beginning of the Rover Program, in 1954, basic critical information was needed for dimensioning preliminary reactor designs. So the earliest critical assemblies at the LASL Pajarito Site constituted a survey of the dependence of critical size on parameters such as fuel loading, core density, island size and reflector. When approximate design conditions were established, there followed crude simulations of vessel walls, insulating layers and controls. These assemblies were set up in the "Honeycomb" machine (Figure 1), which sacrificed geometric perfection for flexibility and had fuel regions made up of long sandwiches of graphite plates and enriched-uranium foils.

As design progressed to the point that more detailed neutronic information was required, measurements shifted to a "ZEPO" mockup (Figure 2) with a precise but inflexible geometry. Here the emphasis was on detailed fuel loading for favorable power distribution (allowing for computed differences at operating temperatures), and establishing a control and safety system with suitable characteristics.



Figure 1. "Honeycomb" Machine.



Longitudinal cross section of Zepo-A.

Figure 2. "Zepo" Machine.

In Zepo-A, the mockup of Kiwi-A, structures were realistic, except that uranium foil and graphite plates first simulated all the loaded graphite fuel (Figure 3). Later, reactor fuel plates were substituted in portions of the assembly. Zepo-A' mocked up the Kiwi-A', -A3 modular core design with fuel-rods appropriately distributed in a graphite matrix (Figure 4).

The 18 different critical configurations assembled on Honeycomb are described in Table I. The first seven of these assemblies were slanted toward variation in carbon: U^{235} ratios. The next three rather clean systems were designed as checks for computations. Assemblies 11, 12 and 13 gave critical data on cores of near minimum volume. The balance of the Honeycomb assemblies approached the realistic reactor design.

Kiwi-A design was based on Honeycomb Assembly A-18, with Zepo-A establishing the final fuel loadings and control properties.

In Kiwi-A, fuel loadings were adjusted radially to compensate for most of the flux peaking near the D_2O island and graphite reflector. As established by U^{235} activation measurements in Zepo-A and computed effects of temperature change, fuel-plate loadings in this reactor ranged from 60 to 300 mg U^{235}/cm^3 .

For Kiwi-A' and -A3, flow-channel sizes were varied radially so that only 3 loading gradations were required for a nearly flat radial temperature profile under operating conditions.

Table III gives fuel loadings for these reactors, and Figure 5 shows typical application of corrections to convert a Zepo power distribution to that expected for the hot reactor.

III. Features of The Test Reactors.

General design features of the three reactors is typified by the schematic of Kiwi-A in Figure 6. Identical pressure shells were water cooled. Reflectors were 14" thick graphite annuli with ~ 5% of the volume occupied by coolant channels for a bypass stream of hydrogen. Graphite wool served as thermal insulation between the core and island and core and reflector. The double-walled island container was cooled by rapidly circulating D_2O .

The boron control and safety rods moved lengthwise within the D_2O island. The controls consisted of six ganged rods (shims) and a vernier rod. Four additional safety rods were adequate to maintain the reactor subcritical for any positioning of the control rods. Figure 7 summarizes integral control rod calibrations for the three reactors.

The core of the Kiwi-A', -A3 reactors (Figure 8) consisted of 126 modules which were 45" long and supported at the cold end of the reactor by tie rods. Each module contained 7 stacks of fuel elements. For these reactors, the island, core and reflector liners were coated with a thermal insulating paint.

IV. Reactor Test Results.

Each test reactor was assembled at Los Alamos and operated

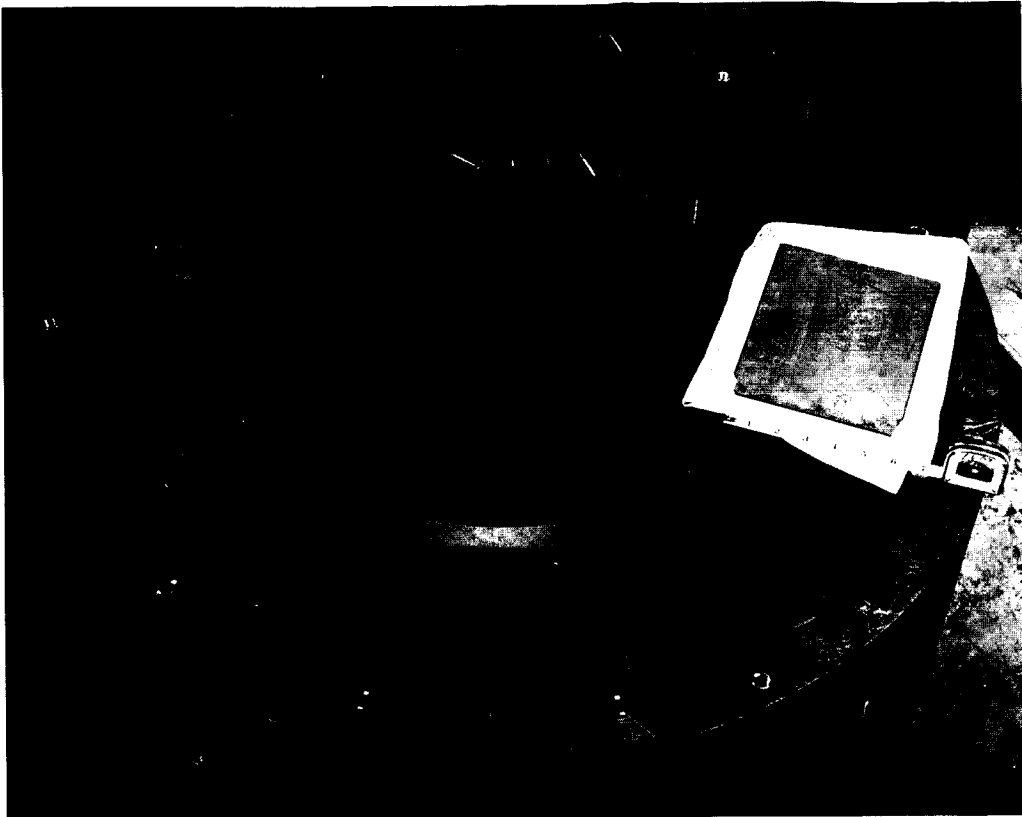


Figure 3. Zepo mockup of Kiwi-A "Whim".

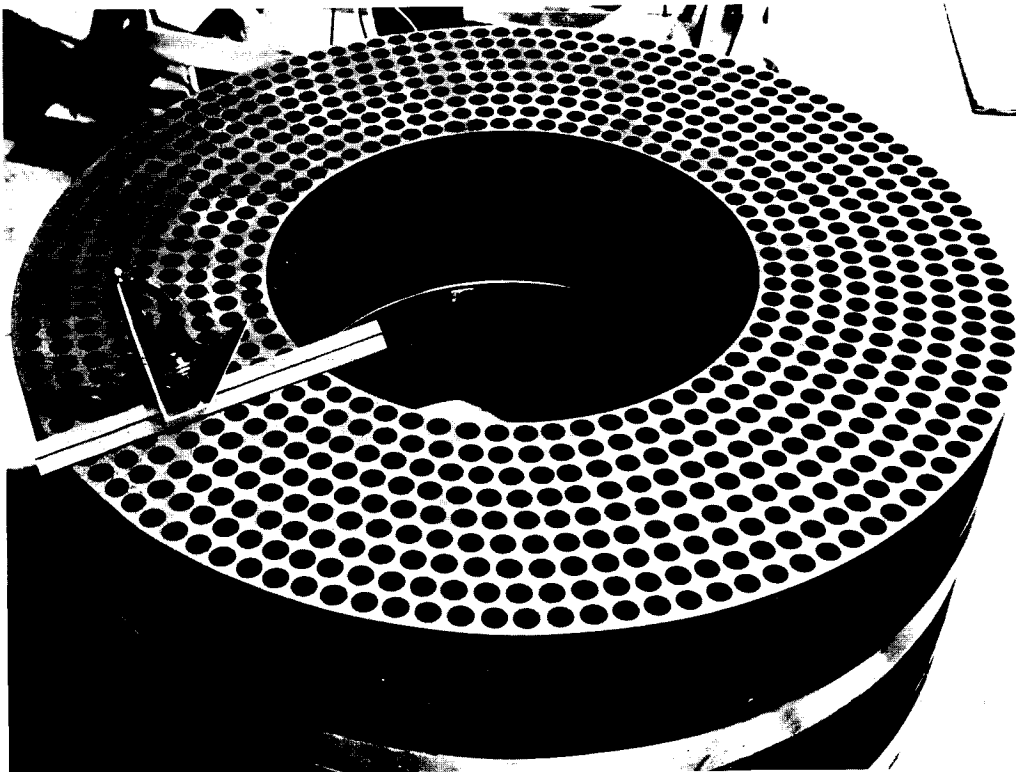


Figure 4. Zepo donut mock-up of Kiwi-A'-A3 Module geometry.

Table I. Honeycomb Critical Conditions.

Core Conditions (dimensions in inches)

Assembly	kg U-235	C/U-235	Annular Fuel Thickness	Fuel Length	Graphite Density in Fuel	Island		Region Between Island and Core	
						Material	Radius	6061 Al	Graphite
A-2	11.8	521	6.30	32	1.47	Be	7.76		
A-6	11.8	521	6.30	30	1.47	Be	7.76		
A-7	16.5	371	6.30	30	1.47	Be	7.76		
A-8	12.4	371	5.02	30	1.47	Be	7.76		
A-9	16.3	170	3.39	30	1.42	Be	7.76		
A-10	13.1	170	3.73	30	1.42	D ₂ O	5.08		
A-11	10.0	357	5.37	30	1.42	D ₂ O	5.08		
A-12	7.5	357	3.27	30	1.42	D ₂ O	7.76		
A-13	8.3	170	1.87	30	1.42	D ₂ O	7.76	0.27	0.26
A-14	13.3	254	3.82	30	1.42	D ₂ O	7.76	0.57	0.76
A-15	21.5	254	5.23	30	1.42	D ₂ O	7.76	0.27	0.76
A-16	25.8	254	6.06	30	1.42	D ₂ O	7.76	0.57	0.76
A-18	25.8	graded	6.06	30	1.42	D ₂ O	7.76	0.57	0.76

Reflector Conditions (dimensions in inches)

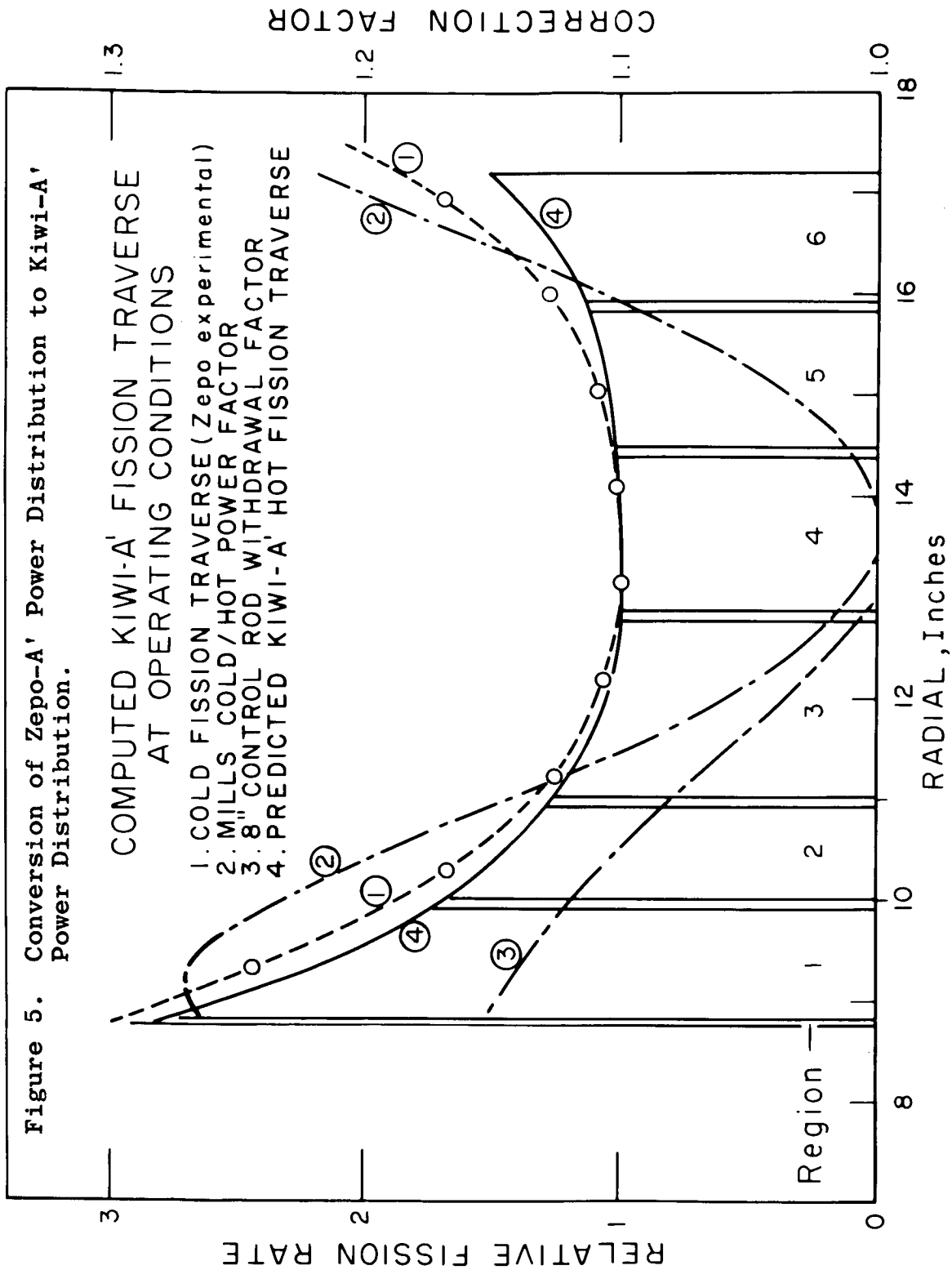
Assembly	Graphite Density		End Reflector Dimensions		Annular Sections of Cylindrical Reflector			
	Reflector	Cylindrical Reflector	A	B	1	2	3	4
A-2	1.55	1.55	8 C	4 Be (island) 4 C (core)	3.61 C	4.07 Be	10.95 C	
A-6	1.55	1.55	4 Be + 4 C	8 C	14.98 C			
A-7	1.55	1.55	4 Be + 4 C	8 C	12.00 C			
A-8	1.55	1.55	4 Be + 4 C	8 C on island	16.24 C			
A-9	1.55	1.50	4 Be + 4 C	8 C	18.8 C			
A-10	1.55	1.54	4 Be + 4 C	8 C	21.1 C			
A-11	1.55	1.54	4 Be + 4 C	8 C	19.5 C			
A-12	1.55	1.54	4 Be + 4 C	8 C	18.9 C			
A-13	1.55	1.54	4 Be + 4 C	8 C	20.3 C			
A-14	1.55	1.50	4 Be + 4 C	8 C	1.6 C	0.25 gap	16.8 C	
A-15 ^a	1.55	1.54	4 Be	8 C	0.8 C	0.26 gap	16.0 C	
A-16 ^b	1.55	1.54	4 Be	8 C	0.7 C	0.28 gap	16.7 C	
A-18 ^c	1.55	1.54	12 C	8 C	0.7 C	0.28 gap	16.7 C	

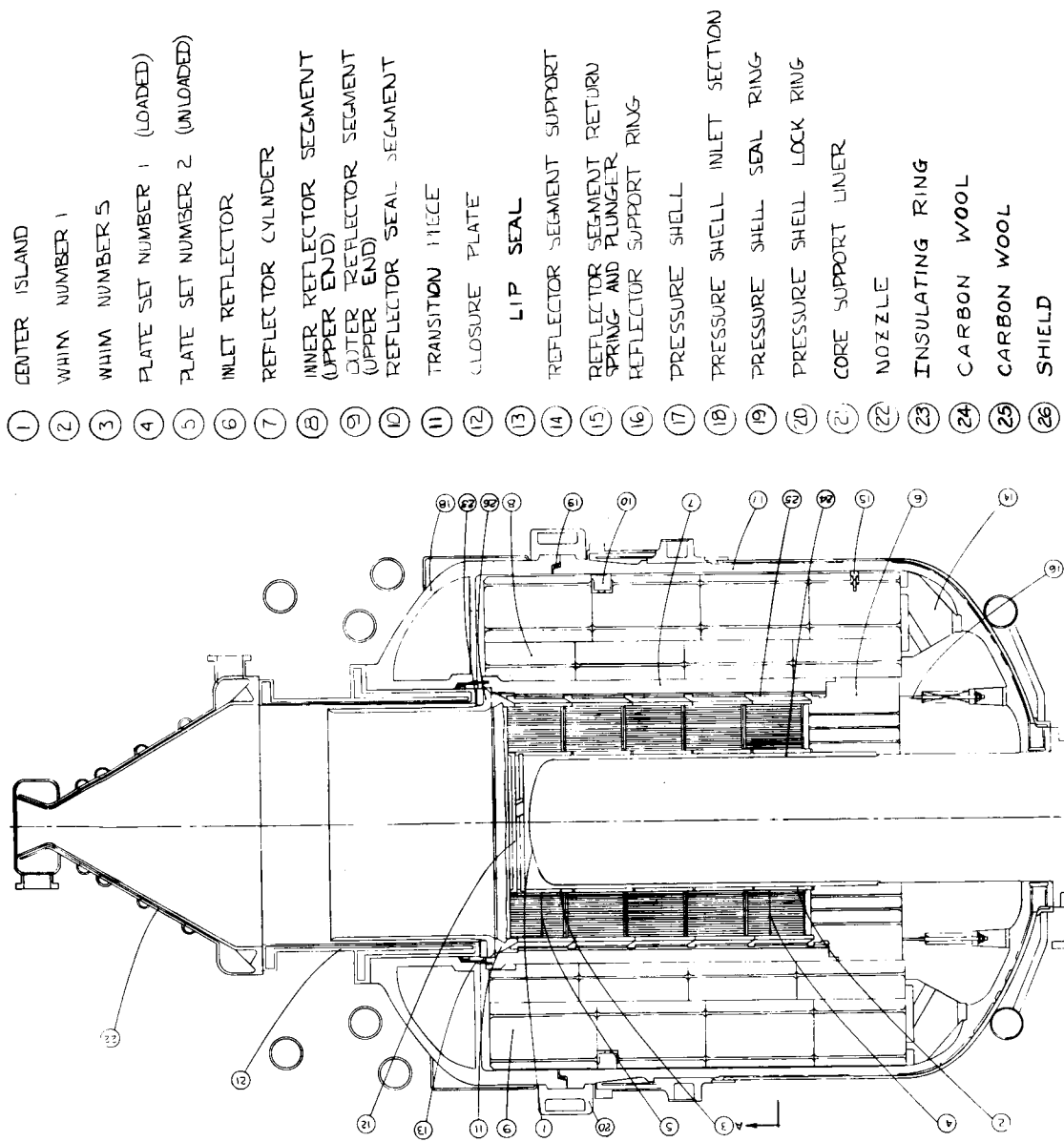
Average Al(1100F) density due to matrix 0.165 gm/cm³.
Effective D₂O density 1.01.
Effective Be density 1.66.

^a 3 x 3 x 16" axial cavity in end B of D₂O island (decreased reactivity ~ 15%).

^b Above axial cavity with #2 of B-plastic rod inserted.

^c Above axial cavity with #3 of B-plastic rod inserted.





- ① CENTER ISLAND
- ② WIM NUMBER 1
- ③ WIM NUMBER 5
- ④ PLATE SET NUMBER 1 (LOADED)
- ⑤ PLATE SET NUMBER 2 (UNLOADED)
- ⑥ INLET REFLECTOR
- ⑦ REFLECTOR CYLINDER
- ⑧ INNER REFLECTOR SEGMENT (UPPER END)
- ⑨ OUTER REFLECTOR SEGMENT (UPPER END)
- ⑩ REFLECTOR SEAL SEGMENT
- ⑪ TRANSITION PIECE
- ⑫ CLOSURE PLATE
- ⑬ LIP SEAL
- ⑭ REFLECTOR SEGMENT SUPPORT
- ⑮ REFLECTOR SEGMENT RETURN SPRING AND PLUNGER
- ⑯ REFLECTOR SUPPORT RING
- ⑰ PRESSURE SHELL
- ⑱ PRESSURE SHELL INLET SECTION
- ⑲ PRESSURE SHELL SEAL RING
- ⑳ PRESSURE SHELL LOCK RING
- ㉑ CORE SUPPORT LINER
- ㉒ NOZZLE
- ㉓ INSULATING RING
- ㉔ CARBON WOOL
- ㉕ CARBON WOOL
- ㉖ SHIELD

Figure 6. Kiwi-A Design Features.

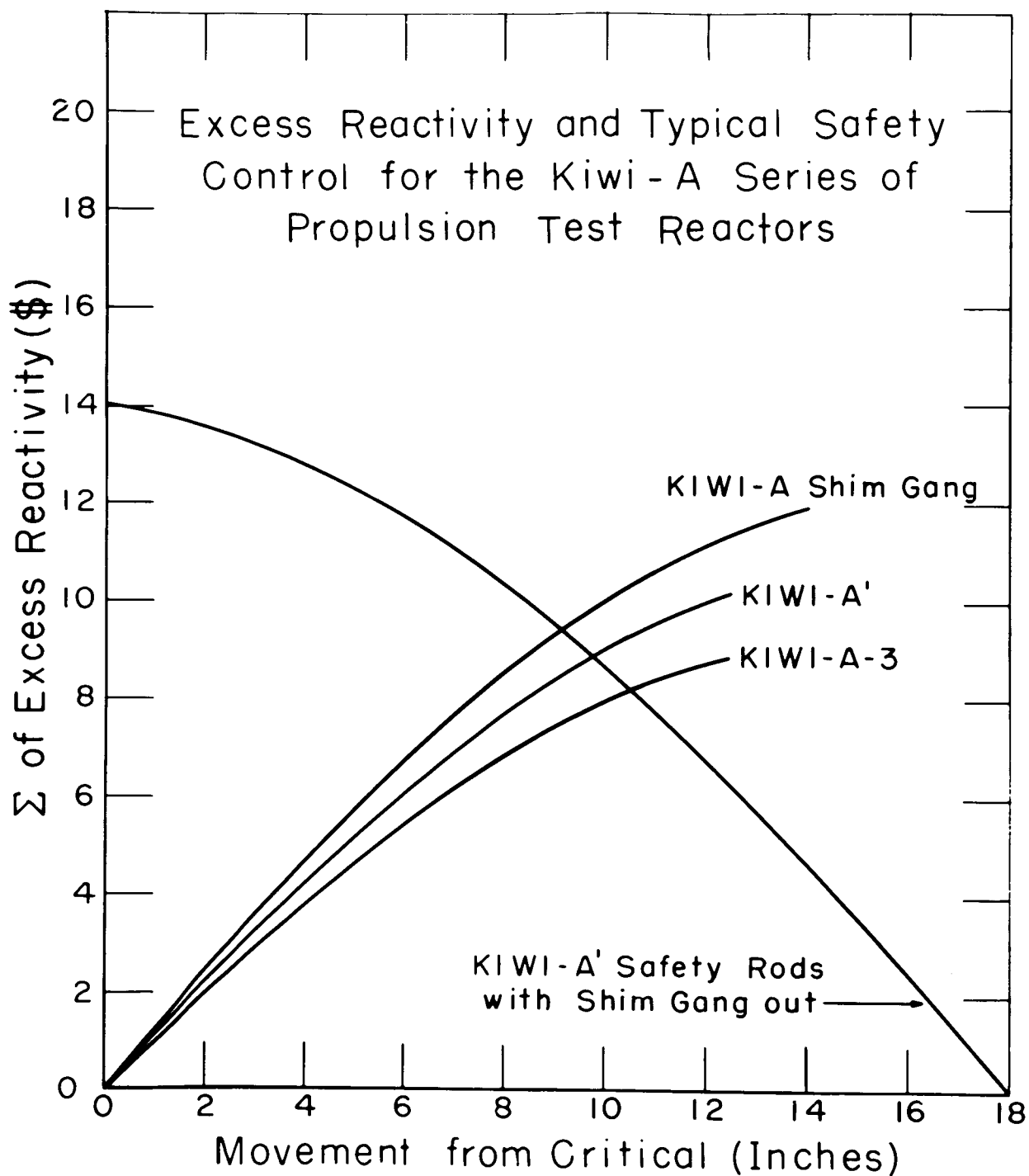


Figure 7. Integrated Values of Kiwi Control.

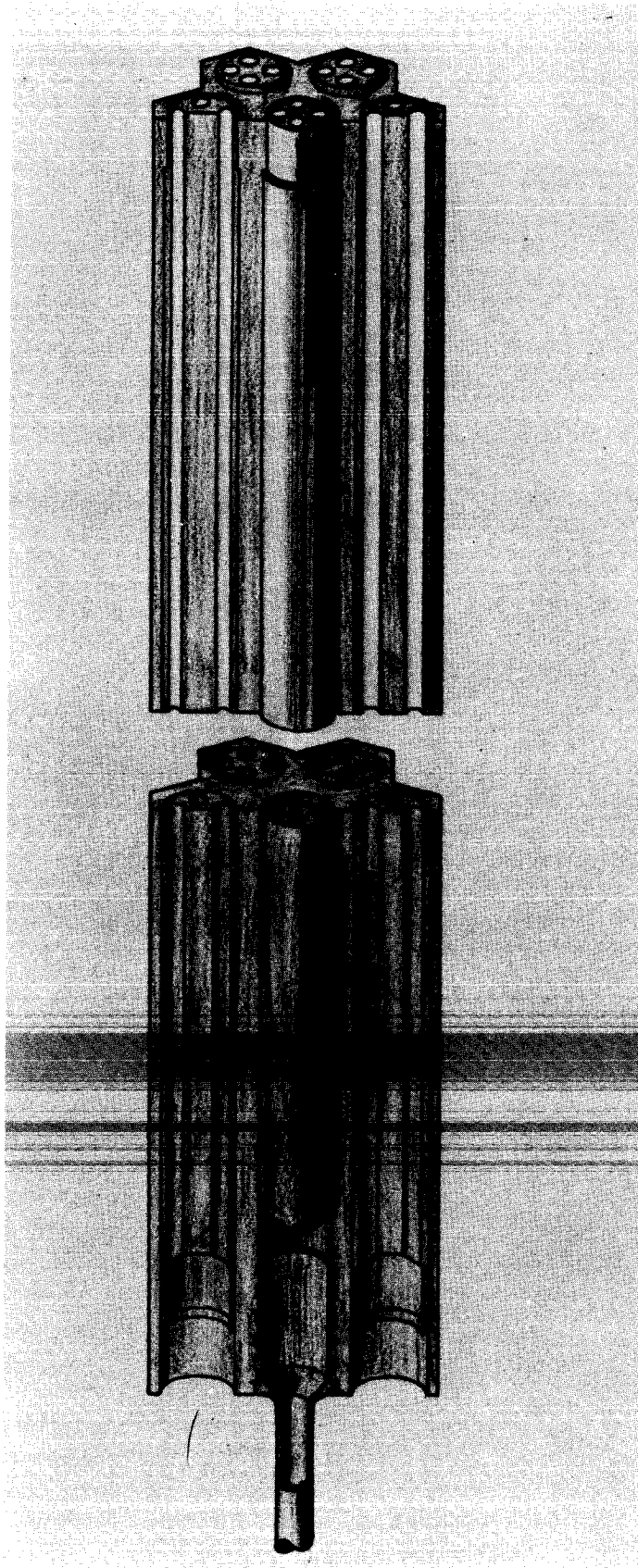
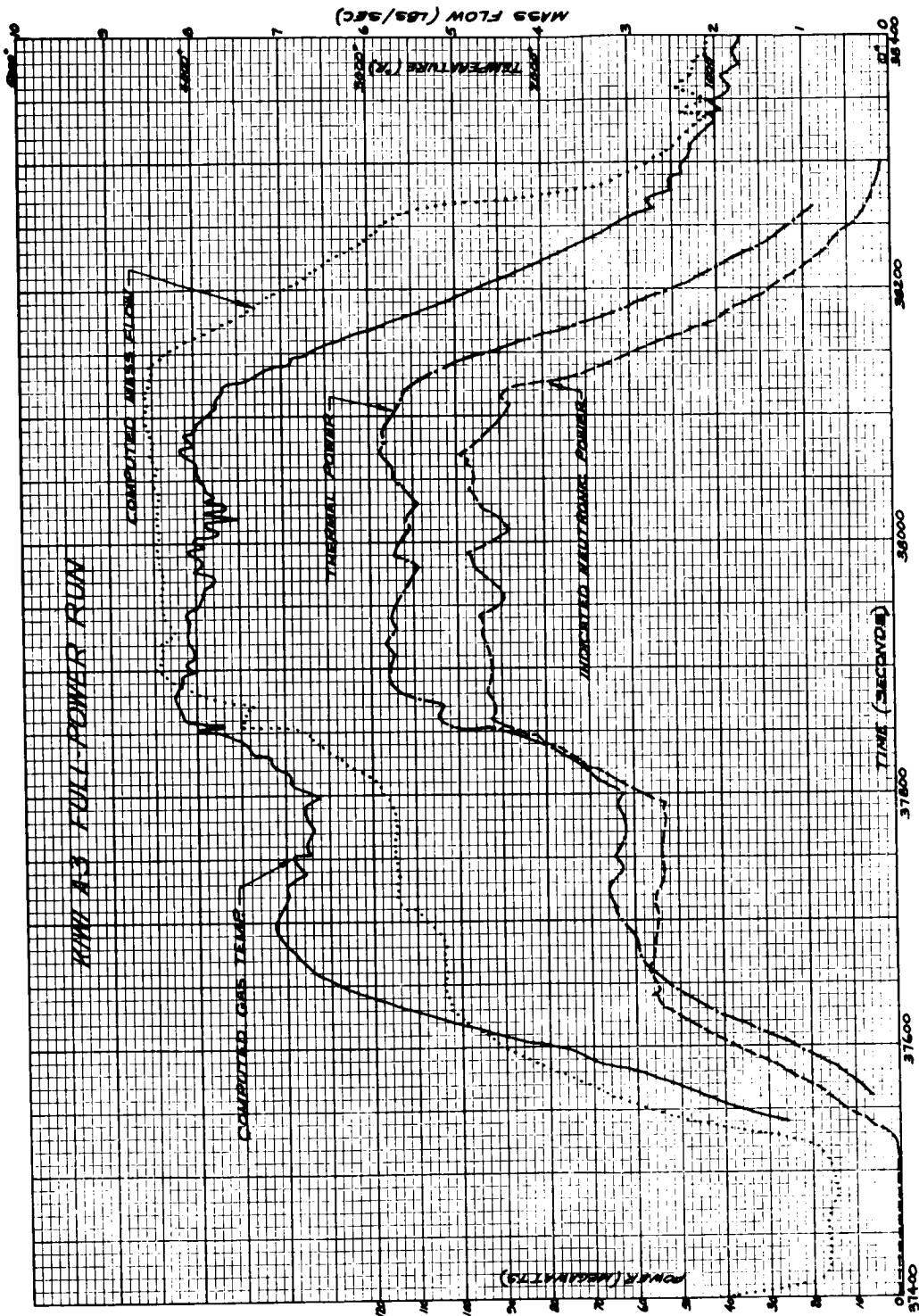


Figure 8. Kiwi-A',-A3 Fuel and Module Design.



Results of Kiwi-A-3 full-power run

Figure 9. Kiwi-A3 Full Power Run.

Table II: Expected Cold Kiwi-A Excess Reactivity (from ZA-6) and Utilization of Reactivity by the Hot Kiwi-A

Zepo Feature	Reactivity Gain in Kiwi-A	Predicted Required Excess Reactivity for Kiwi-A
ZA-6	11.2\$	Thermal base shift 7.0\$
D20 Purity	1.7	Expansion effects 3.0
ΔA1 around island	0.3	Resonance broadening 0.5
Expansion gaps	- 0.3	
Instrumentation	- 0.5	
Exchange of shim rod for oscillator rod	0.5	
Graphite and miscellaneous differences	small	
	<u>12.9\$</u>	

Table III: Specifications of the Kiwi-A' Fuel Element Loadings Determined by Zepo A'

Region	Radii (in.)	Fuel Element Flow Channel Diameter (in.)	Relative Fission Density Required*	Predicted Fission Density For Uniformly Loaded Core	Estimated fuel Element Loading mg/cm ³ U	Kiwi A' Fuel Element Loading mg/cm ³ U
1	8.80- 9.90	0.178	1.64	2.16	84	79
2	10.00-10.92	0.178	1.52	1.45	115	116
3	11.02-12.76	0.161	1.16	1.09	117	116
4	12.86-14.38	0.151	1.00	1.00	110	116
5	14.48-15.82	0.161	1.12	1.06	116	116
6	15.92-17.20	0.178	1.60	1.30	135	132

* Axial integral over loaded fuel.

at low power to confirm proper control characteristics and the desired power distribution.

The reactor power was calibrated as follows. Just before disassembly of the reactor, the fuel was activated by low-level operation. Afterward, γ -counts of fuel elements established the relative fissions distribution throughout the core. Radiochemical analysis of several elements placed this distribution on an absolute scale, so that the total number of fissions in the core was obtained and related to the response of auxiliary radiochemical samples. Similar samples then could carry this power calibration over to NTS instrumentation.

At NTS three sets of counters with overlapping ranges carried the low-level power calibration to the required 100Mw operating range. Enriched uranium fission chambers were used from zero to about 10 watts of reactor power, compensated ion chambers covered the intermediate range, and uncompensated ion chambers about 400 feet from the reactor registered from $\sim 10^4$ watts to full power.

As an illustration, Figure 9 combines records of control rod position, reactivity (reconstructed), and power for the Kiwi-A' high-temperature run. Conditions at full power, i.e. power values, hydrogen flow rate, and exit gas temperature, are summarized in Table IV for the three A-type reactors.

In Table V are values of available and utilized excess reactivities, plus a breakdown of the latter for the three power runs.

Kiwi-A had the mishap of losing the island closure plate and the graphite wool around the island during the high power run. Kiwi-A' lost segments of three modules and all the fuel elements in these modules. Modules in Kiwi-A3 were cracked but the reactor held together for the duration of its test.

Erosion in fuel plates of Kiwi-A was severe in the hottest section of the reactor. This plate erosion cost $\sim 4.00\$$ in reactivity. Niobium coating of the flow channels in the Kiwi-A'-A3 reactors reduced fuel erosion to a negligible amount.

Table IV
Results of the "A" Series Tests

	<u>Kiwi-A</u>	<u>Kiwi-A'</u>	<u>Kiwi-A-3</u>
Date	7/16/59	7/8/60	10/19/60
Duration at full power, seconds	301	346	259
Thermal power, average Mw	74	90.3	114
Thermal power, peak Mw	77	105.	118
Exit gas temperature, Av °C	1543	1960	1949
Gas flow rate, pounds/second	7.1	6.7	8.5

Table V
Available and Utilized Reactivity for
"A" Series Test Reactors (\$)

	<u>Kiwi-A</u>	<u>Kiwi-A'</u>	<u>Kiwi-A3</u>
Available Control Excess Reactivity from cold critical (Estimated)	10.6	10.2	8.85
Reactivity contributed by Hydrogen Propellant	0.1	0.2	0.2
Total Utilized Reactivity as indi- cated by Control withdrawal	7.2	7.5	7.7
Reactivity utilized by Reactor Temperature Coefficient	1.4	6.2	6.2
Reactivity Utilized by Reactor parts losses	1.2	0.6	---
Reactivity Utilized by Reactor Core Corrosion	4.0	Negligible	---
Residual Reactivity Difference Post run cold minus Pre Run Cold	5.7	1.00	1.3

X 66 50279

NEUTRONICS OF KIWI-B NUCLEAR PROPULSION REACTORS

H. H. Helmick and J. D. Orndoff
Los Alamos Scientific Laboratory
University of California
Los Alamos, New Mexico

The Kiwi-B series of Rover reactors, the second phase of the Kiwi program, is aimed at developing a reactor design suitable for flight application. The initial design of the Kiwi-B series called for a beryllium-reflected graphite-moderated core, rather than the graphite reflected graphite-moderated core containing a D₂O island, as in the Kiwi-A reactors. Stages in the neutronic studies for the design of Kiwi-B type propulsion reactors consist of: (a) preliminary critical mockups in the Honeycomb assembly machine to establish gross features; (b) refined mockup studies with Zepo (zero power) assemblies to determine control characteristics and suitable U loading distributions; and (c) cold critical measurements on the reactor itself to confirm its characteristics, particularly to provide improved power distribution estimates for specification of flow-passage orifices.

The Honeycomb assembly machine, in which critical surveys were conducted consists of a matrix of 3" square aluminum tubes which assemble into a 6' cube. The fuel region of the mockups was made up of .002" and .005" enriched uranium (oralloy) foils placed between 0.28" thick graphite plates and inserted in the 3" x 3" aluminum Honeycomb tubes. Two of the fuel tubes were movable and served as vernier control rods while safetys were provided by four more retractible fuel tubes. Poison materials located at the graphite-beryllium interface in the assemblies mocked up control vanes in the proposed reactors. Figure 1 is a summary of the effectiveness of various control materials in a typical Kiwi mockup assembly. Figure 2 shows the reactivity contribution of hydrogen distributed uniformly over the cross section of the core as a function of distance from the unreflected end.

Based on the data obtained from Honeycomb measurements, a uranium-loaded graphite core 35" in diameter and 52" long was established for the Kiwi-B series of reactors, with void fraction and uranium loading as variables. The universal reflector system to be used with a variety of core designs was a beryllium cylinder of annular thickness 4-1/2" containing 12 rotatable control drums with boral inserts. The initial design (Kiwi-B-1A) had cylindrical fuel elements within unloaded graphite "modules" which fitted together in a hexagonal-based matrix. Later designs aimed at eliminating the support modules to give a core made up completely of hexagonal fuel elements. Maximum uranium loadings of 0.4 gm/cc result in non-thermal reactors with consequent low neutronic

temperature coefficients of reactivity.

In the second reactor mockup series, Zepo assemblies provide close neutronic simulation of the eventual reactor. The Zepo core, raised by a hydraulic lift into a beryllium mockup reflector assembly (Figure 3), consisted of a graphite cylinder which contained 1159 three-quarter inch diameter holes arranged in a hex pattern identical to the Kiwi-B-1A design. Fuel was in the form of .003" uranium-foil hole liners, and graphite rods were inserted in the holes to provide the desired average density. The 12 rotatable Kiwi-B control rods were mocked up by boron strips (53" long x 3.3" wide) installed in the Be reflector. An actual reactor reflector with control cylinders was installed later (Figure 4).

Table I gives the characteristics common to the first ten mockups, and Table II is a summary of critical data for these variations. Each of the mockups from ZB-6 through ZB-10 has two values for uranium density and C to U ratio. The first value listed applies to the 204 outermost fuel rod holes, and the second value is for the remainder of the core. The percent "Effective Kiwi-B void," is corrected for minor geometric differences between Zepo and Kiwi cores. Reactivity contributions of uranium and graphite as functions of radius are shown in Figure 5.

Fission distributions along radii directed either toward or between control rods shown in Figure 6 indicate the effect of controls on the local fission power. Data have been converted to hot reactor conditions, and the value listed for a control rod, is the amount of poison that the rod contributes to the system.

The photograph, Figure 7, shows equipment for measuring radial fission distributions. An array of ten fission counters is installed on the core and is remotely positioned axially so that a complete core flux map can be made in a relatively short time.

The effectiveness of several materials installed on the rotatable Be control drums is shown in Table III. "Reactivity contribution" refers to the effect of rotating a control drum from full "out" to full "in" when 120° of its surface is covered with the material specified.

Table III
Control Rod Material Effectiveness

<u>Material</u>	<u>Surface Density (gm/cm²)</u>	<u>Thickness (in.)</u>	<u>Reactivity Contribution (dollars)</u>
Gd	.102	.005	-0.43
Gd	.204	.010	-0.47
Cd	.322	.015	-0.45
Cd	.665	.031	-0.46
Boral	.063 (B ¹⁰)	.047	-0.72

The final stage in the checkout of the Kiwi-B design was a cold critical check of the actual B-1A reactor. The primary

purpose was to provide a checkout of the system prior to shipment to the Nevada Test Site; however, a number of additional measurements were made because of the high desirability of obtaining such information at this time.

Multiplication measurements throughout the various stages of assembling the reactor provided a safety guide for the succeeding Nevada assembly. The first stages were building up the core (Figure 8) and surrounding it by the graphite reflector cylinder. Then Cd "safing" strips were attached to the exterior of the reflector cylinder, after which the pressure shell with Be reflector and control rods was installed around the Cd clad core. The completed reactor assembly is shown in Figure 9.

A delayed critical configuration for the cold, dry reactor was obtained with the twelve control rods 123° from their full "in" position. The differential and integral control rod worth of a typical rod is shown in Figure 10.

Values of Rossi- α , the neutron chain decay constant, with the reactor near critical gave a prompt neutron mean lifetime of 43 μ sec.

The radial fission distribution was obtained by gamma counting .006" diameter uranium wires which were distributed through the core resulting in the normalized radial fissioning flux distribution shown in Figure 11. Upon applying cold/hot correction factors and multiplying by the fuel element loadings, the predicted "hot" fission density curve of Figure 12 was produced.

Power was calibrated by numerically integrating the product of uranium weight and cold radial flux distribution over the entire core, and normalizing to results of radiochemical analyses of the center fuel element and several neighboring uranium monitor wires. With the above information, radiochemical analyses of similar wires in the reactor during a low power run in Nevada, provided the basis for calibration of the neutronic instrumentation at the test site.

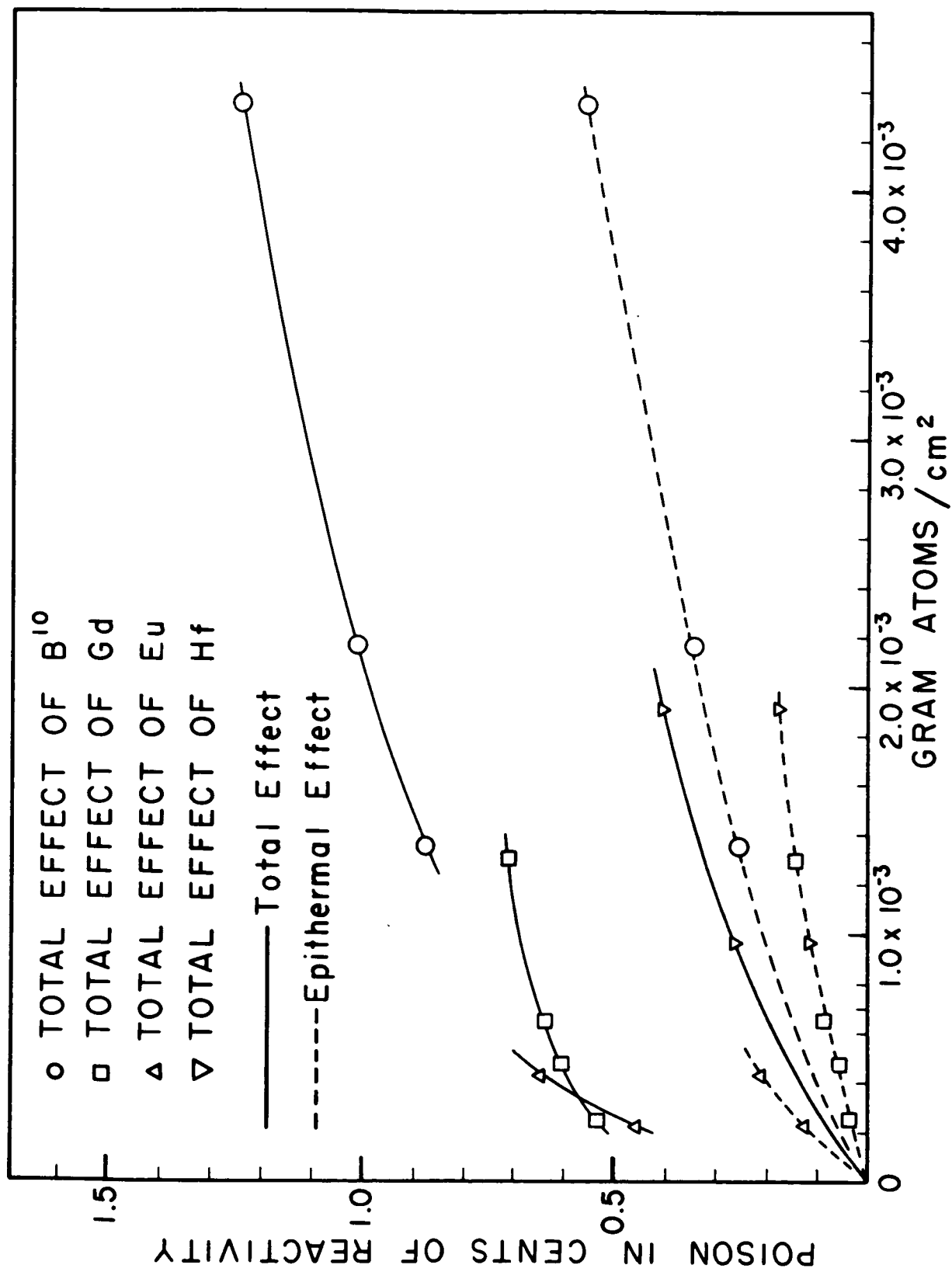


Figure 1. Effectiveness of control materials in Honeycomb

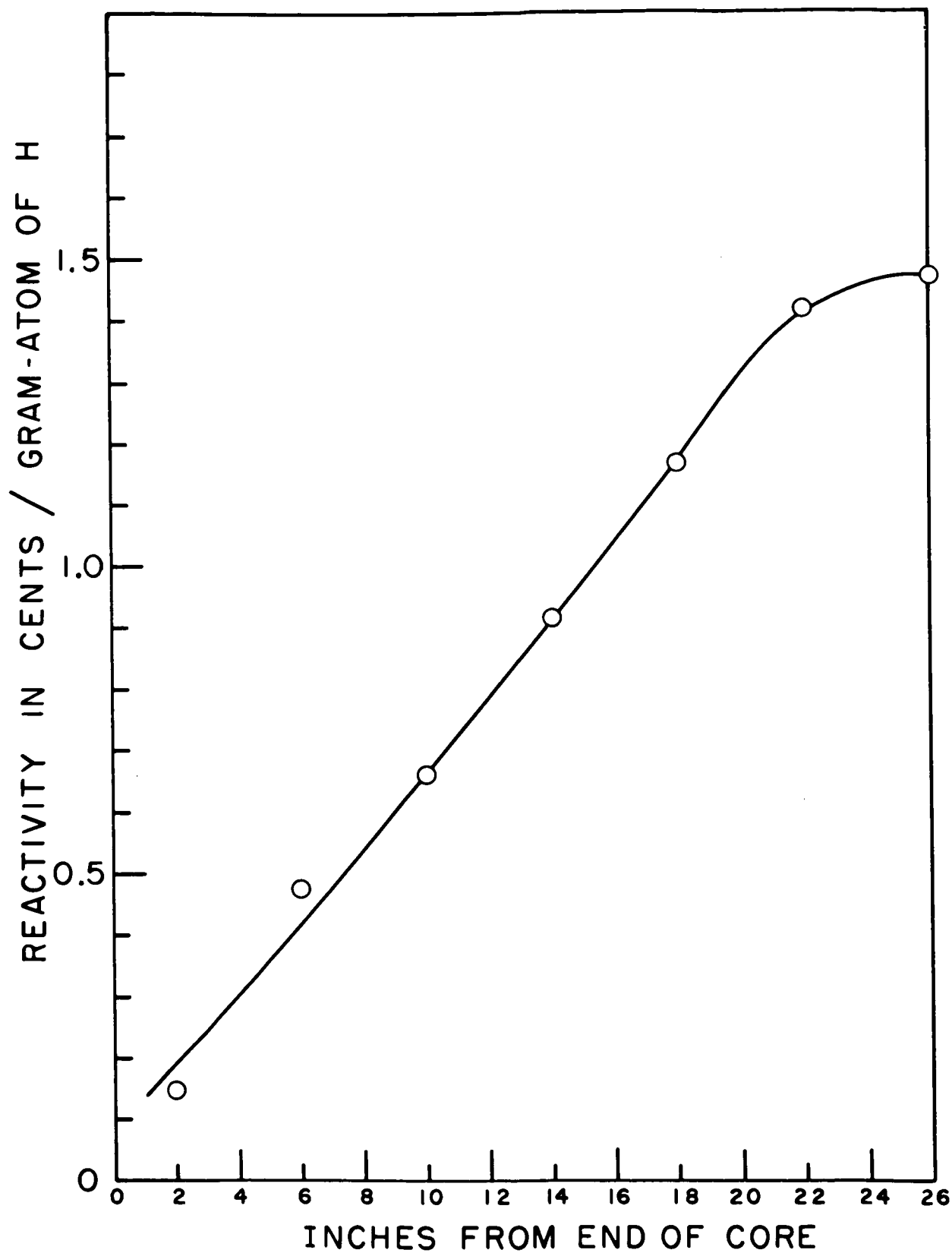


Figure 2. Reactivity contribution of hydrogen distributed uniformly over the cross section of the core.

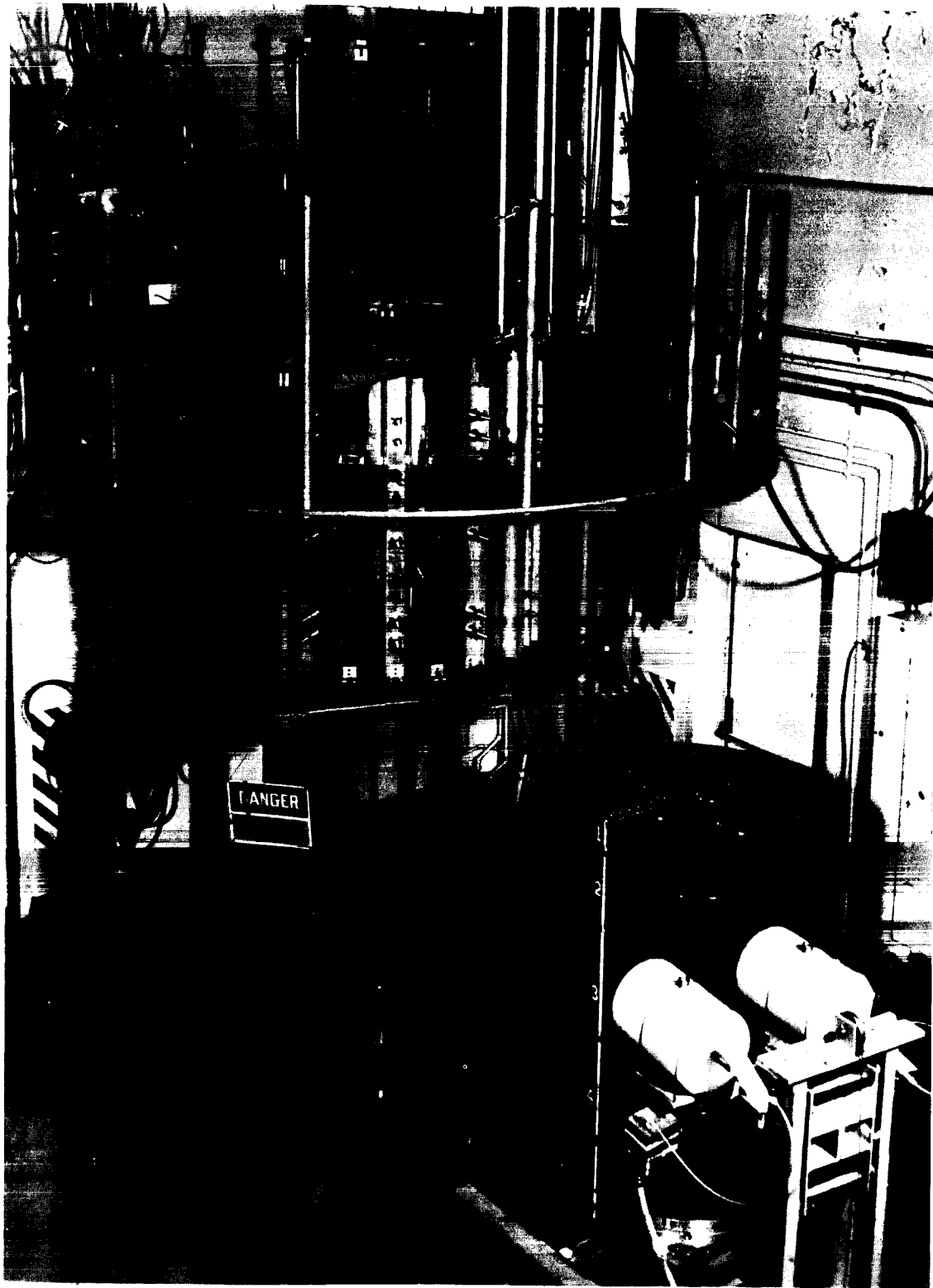


Figure 3. Zepo critical assembly machine

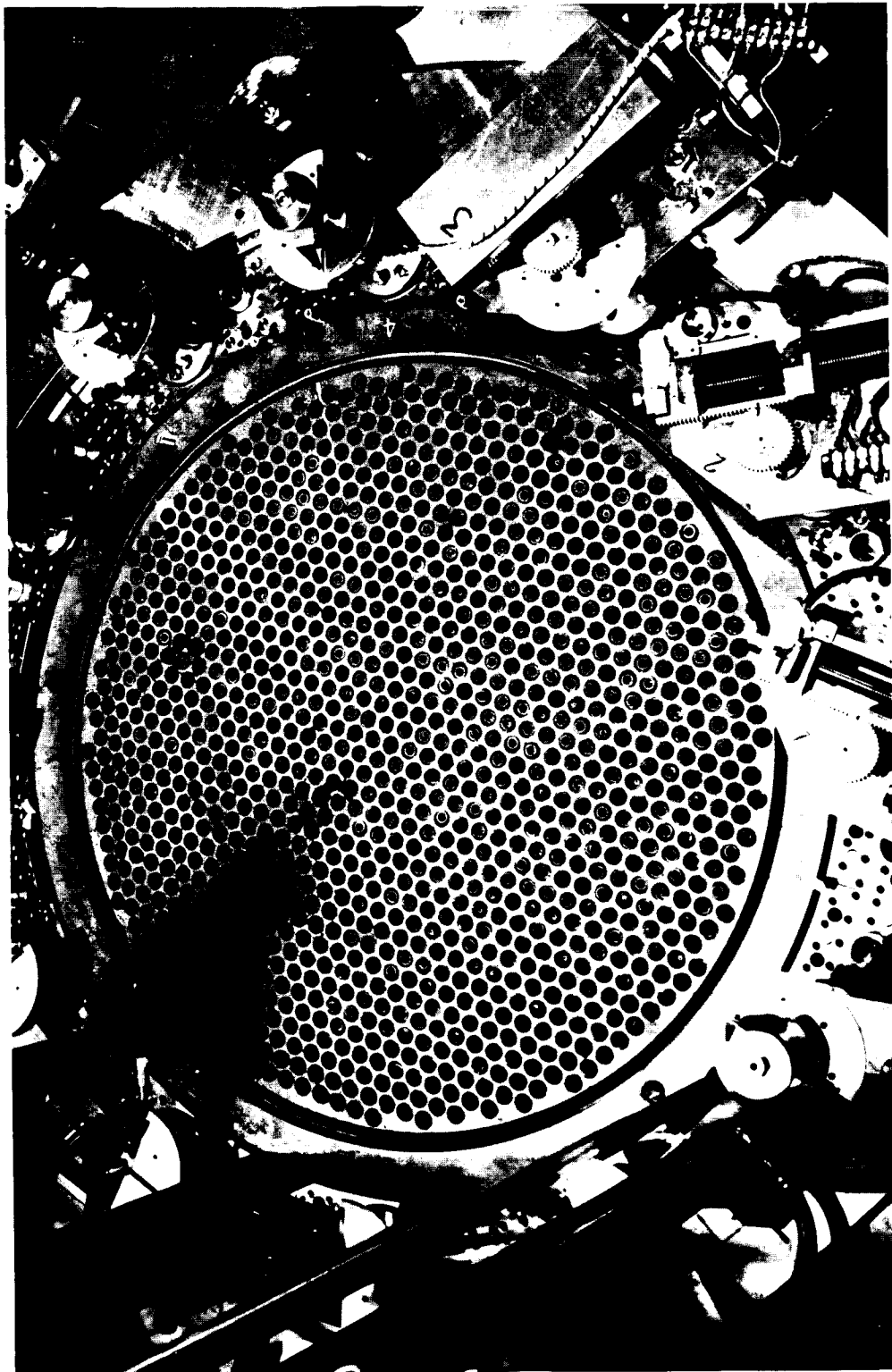


Figure 4. Actual reactor reflector with control rods installed
on Zepo

Table I. Common characteristics of the first ten Zepo mockups
GROSS FEATURES OF ZEPO MOCKUPS OF KIWI-B-1A

<u>Region</u>	<u>Radii (in)</u>	<u>Material</u>	<u>Density(gm/cc)</u>
	0		
Fuel		Oy	0.074, 0.113
		C	
		Nb	
	17.5		
Gap		Void	
	18.0		
Reflector		C	1.84
	19 875		
Reflector		Be & Gaps	1.62
	24.6		
Core Length	52.75 in		
Peripheral Reflector Length	52.0 in		
End Reflector 4-1/2" thick Al plate 70% void placed 1/2" away from core inlet.			
Control Rod Mockup 3.3" x 53" x .100" boral, surface density .126 gm/cm ² normal boron.			

Table II. Critical data obtained from Zepo mockup

SUMMARY OF CRITICAL DATA FOR ZEP0 MOCKUPS OF KIW1-B-1A										CONTROL ROD MOCKUP	
	Oy(kg)	$\rho_{Oy}(cm/cc)$	$\rho_c(gm/cc)$	C/U	Nb(kg)	$\rho_{Nb}(gm/cc)$	Effective Kiw1-B Void (%)	Excess Reactivity (\$)	No of Rods	Poison Per Rod (\$)	
ZB - 1	93.79	0.113	1.27	221	0.0	0.0	31.5	0.4	0	- -	
ZB - 3	93.79	0.113	1.38	239	0.0	0.0	24.8	4.1	7	- 0.51	
ZB - 4	93.79	0.113	1.45	251	40.6	0.049	20.5	4.2	7	- 0.51	
ZB - 5	93.79	0.113	1.45	251	49.0	0.089† 0.049**	20.5	4.8	7 1	- 0.51 - 0.62	
ZB - 6	87.56	0.074* 0.113**	1.45	383* 251**	49.0	0.089† 0.049**	20.5	4.1	5 3	- 0.55 - 0.30	
ZB - 8	87.56	"	1.44	380* 249**	60.3	0.089† 0.067**	21.2	2.8	9	- 0.31	
ZB - 10	87.56	"	1.46	387* 254**	60.3	0.089† 0.067**	19.6	4.2	12	- 0.31	

* 204 Peripheral Fuel Rods

** Remainder of Core

† 90° Segment of Core

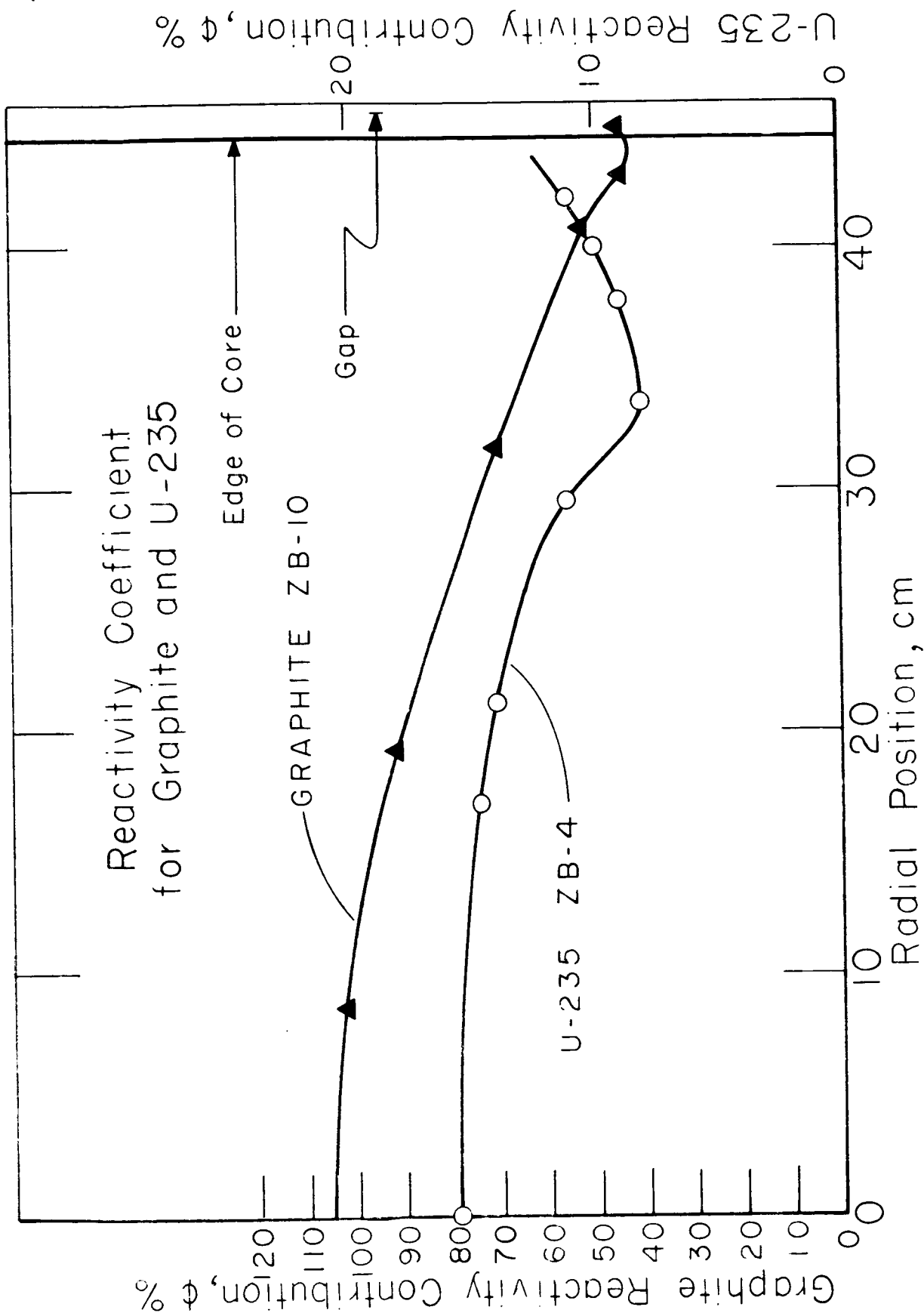


Figure 5. Contribution of uranium and graphite as a function of radial location in Zepo mockups

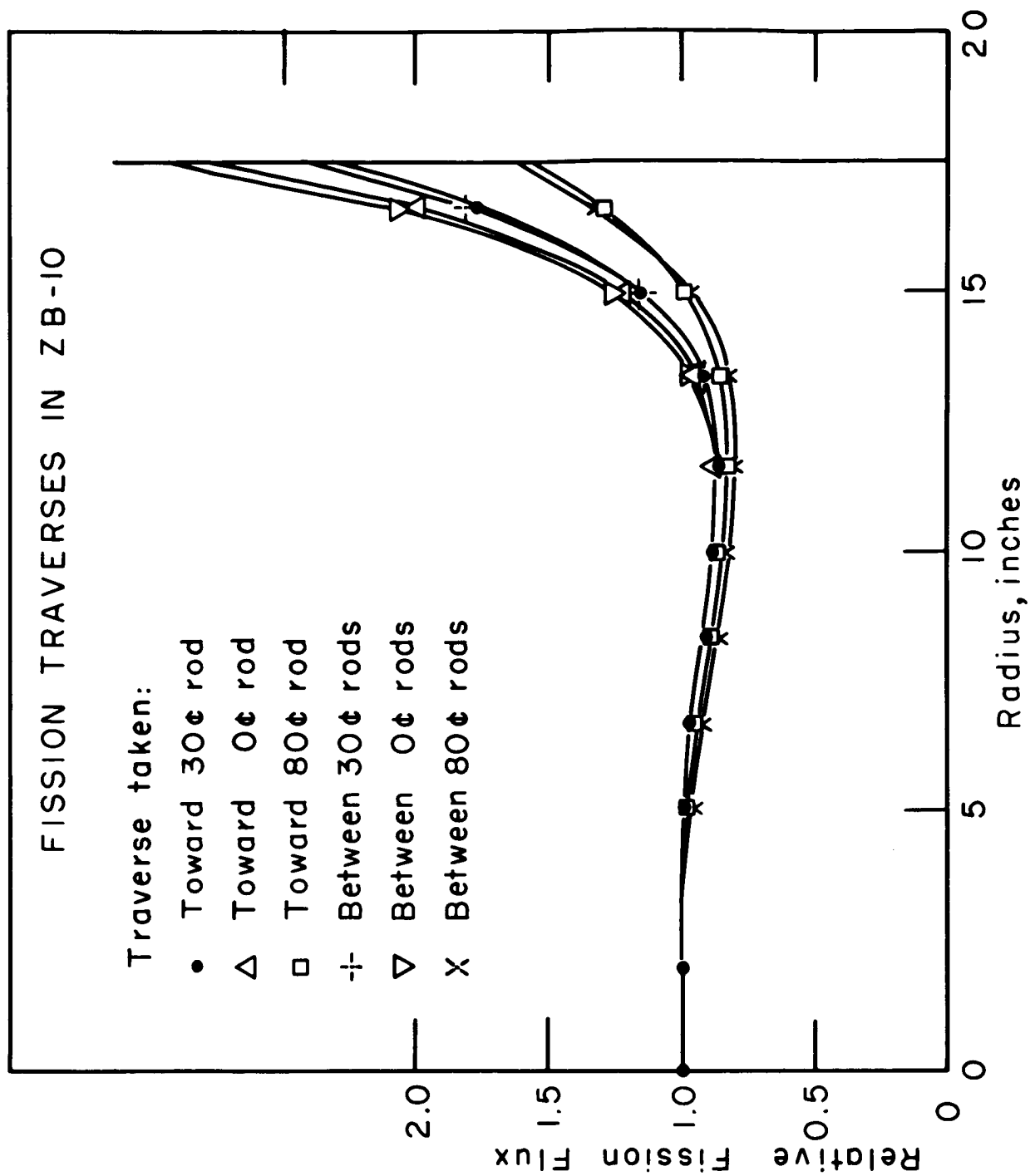


Figure 6. Effect of controls on local fission power

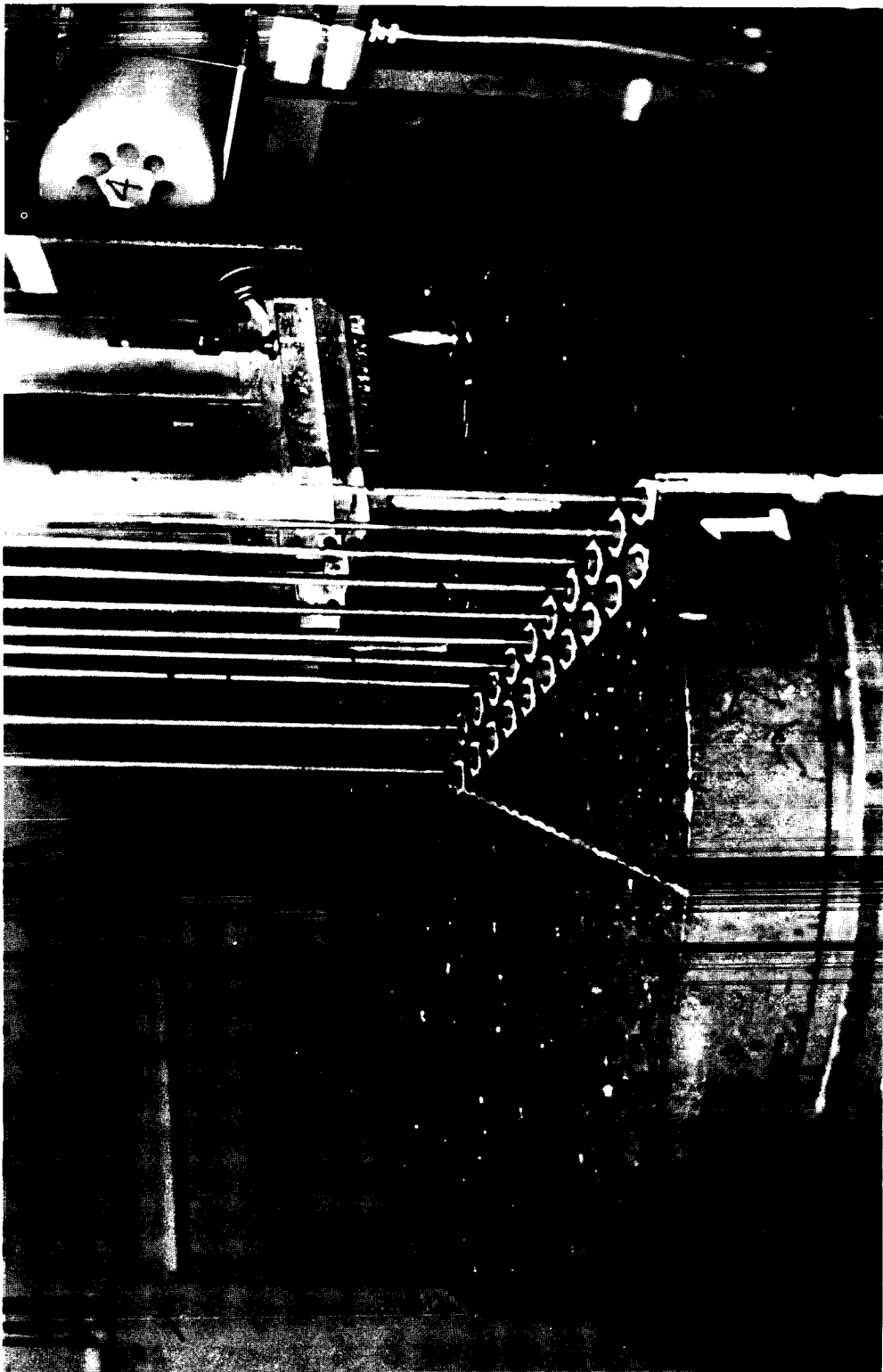


Figure 7. Ten fission counters used to measure fission distributions in the Zepo core

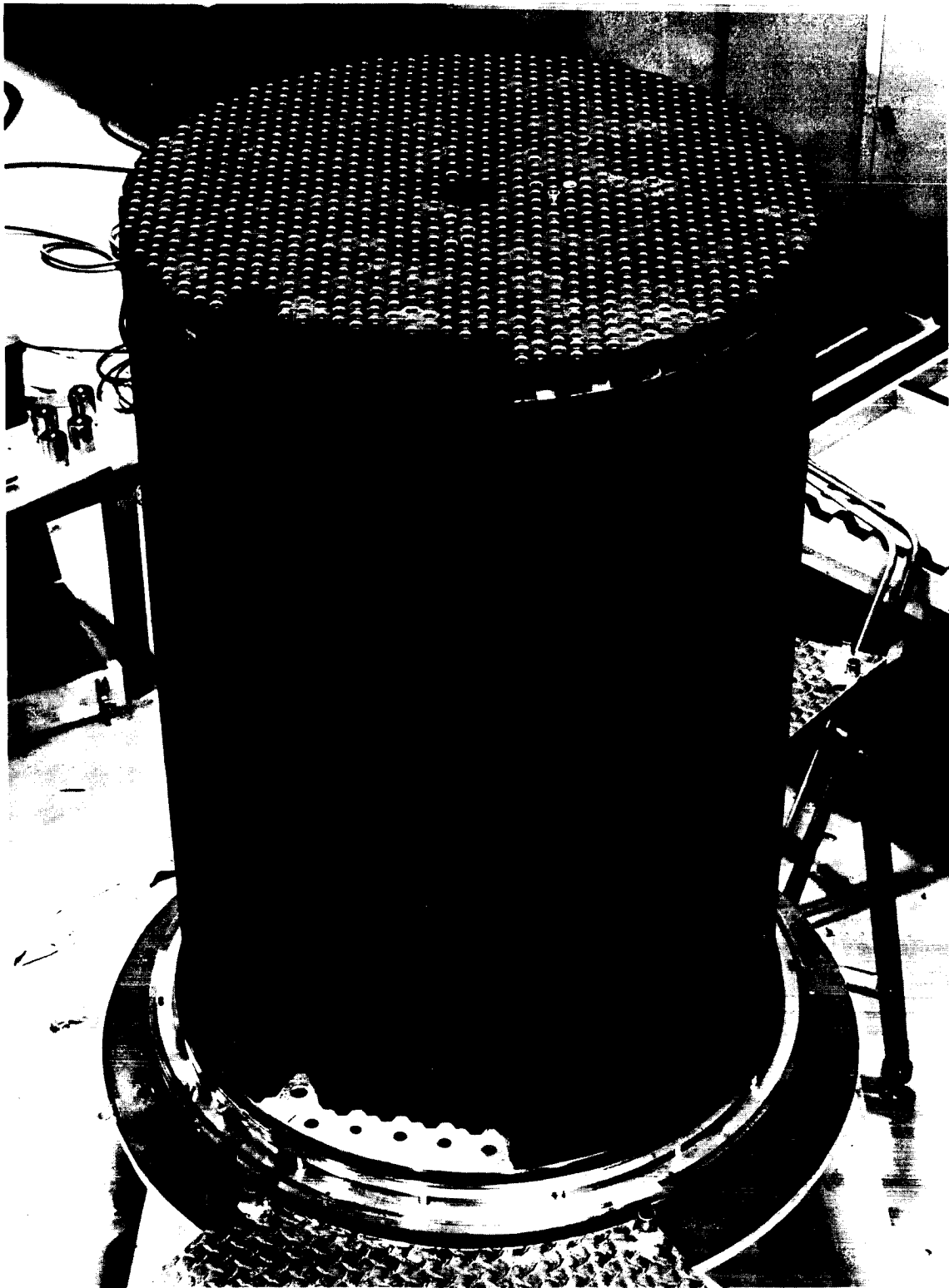


Figure 8. The nearly completed Kiwi-B-1A core

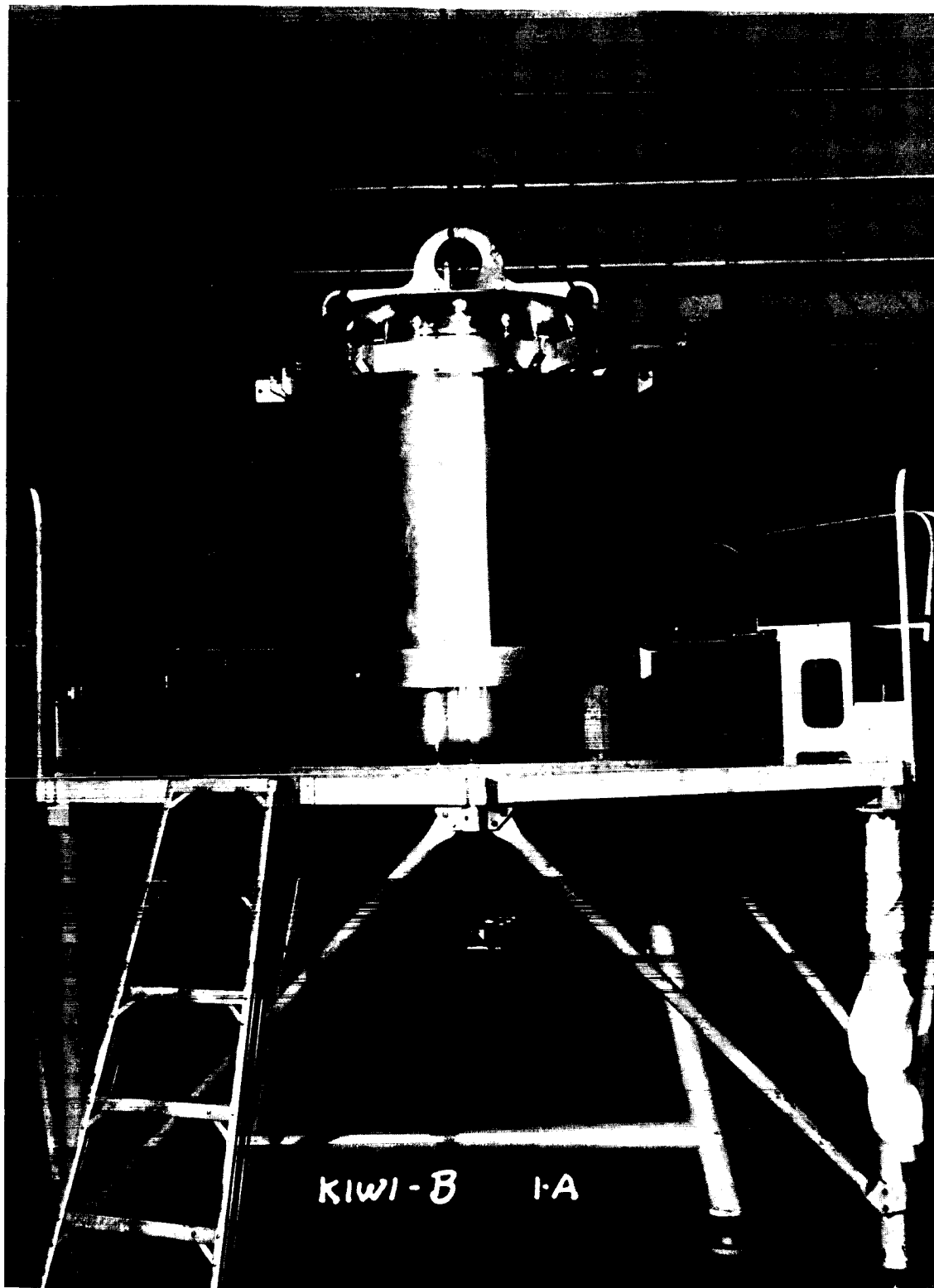


Figure 9. The complete Kiwi-B-1A reactor assembly

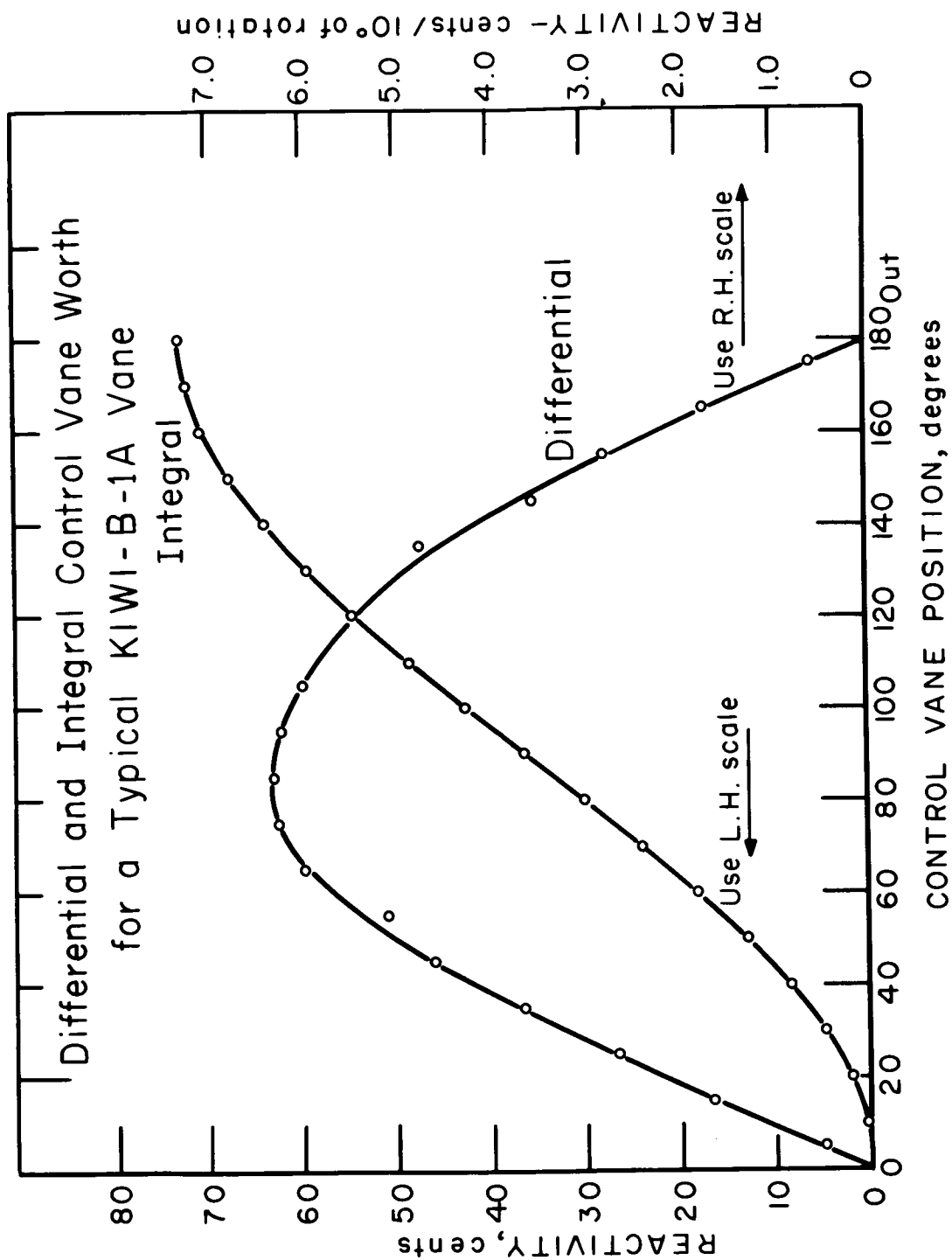


Figure 10. Kiwi-B-1A control rod calibration

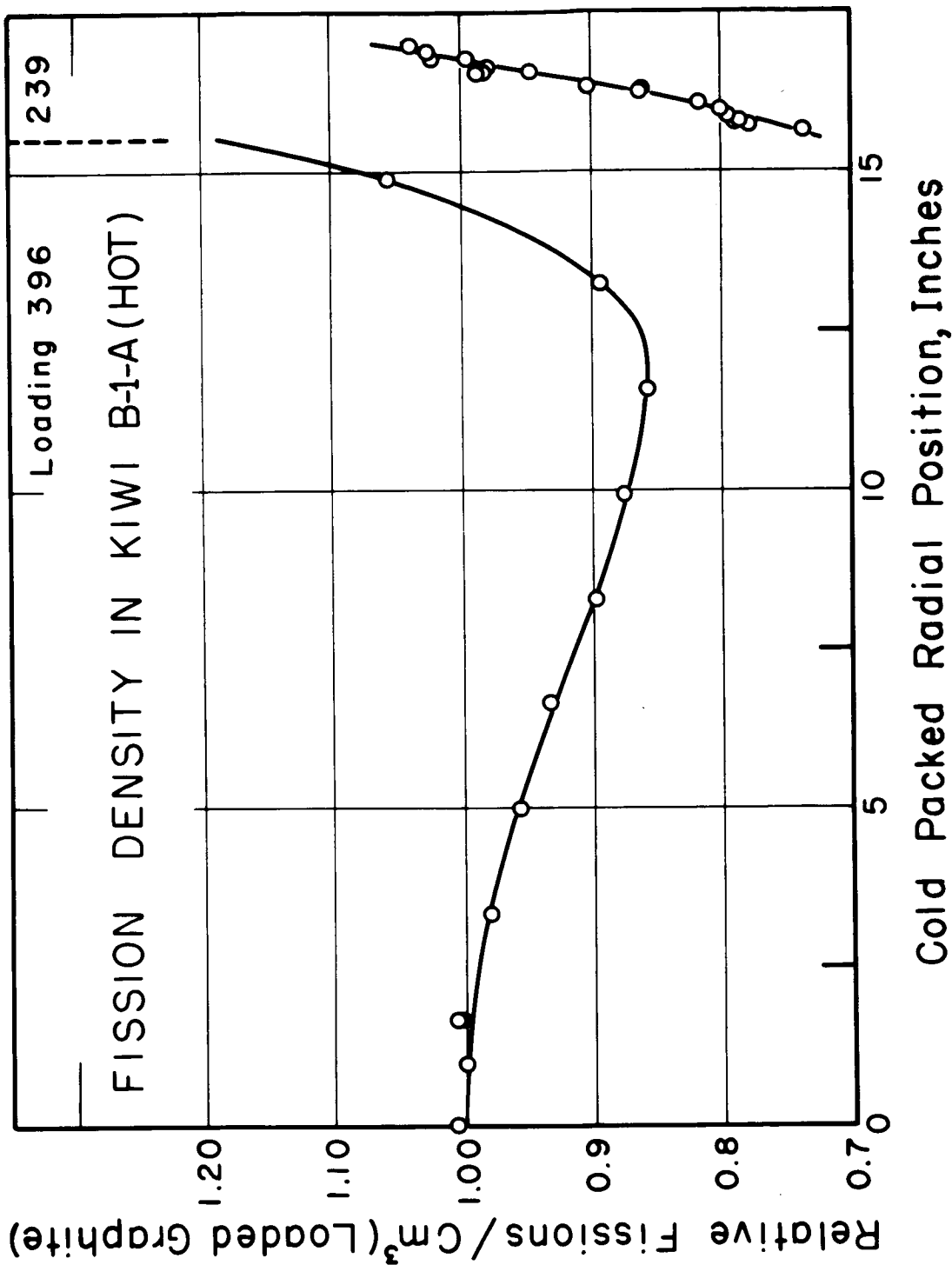


Figure 12. Predicted "hot" fission density for Kiwi-B-1A

X 66 50280

NEUTRONIC CALCULATIONS OF TEMPERATURE
EFFECTS ON KIWI REACTORS

Eugene A. Plassmann
Los Alamos Scientific Laboratory
University of California
Los Alamos, New Mexico

[U]

ABSTRACT

50280

The one-dimensional DSN neutronic code has been successfully used to reproduce the radial fission distribution measured in zero power critical mockup experiments of Kiwi reactors. The calculations were then extended to predict the change in fissioning rate produced at Kiwi operating conditions. The neutronic temperature coefficient for these reactors is also predicted.

Conf. R.D. Author

Machine calculations on the neutronic behavior of Kiwi reactors have, in general, been done in close cooperation with the experimental program. That is, experimental measurements, obtained with critical assembly mockups of Kiwi configurations, were used as the starting point for the calculational series, and these in turn, could be used to predict and perhaps even guide future experiments.

One of the basic requirements in the design of a Kiwi reactor is a fairly uniform radial power distribution, so that the core structure will not be subjected to undue thermal stresses. Thus one must be able to predict the distribution of fission density within the core of the reactor at its operating temperature. Since critical assembly experiments are generally limited to room temperature operation, one must resort to calculational procedures in the prediction of these high temperature effects. Such temperature dependent neutronic calculations have been done using the one-dimensional DSN code¹ developed at Los Alamos. This code is capable of solving a variety of neutron transport problems using the IBM types 704 and 7090 computers. In general, the calculation will compute the neutron and fission distributions in the reactor and can be used to predict the neutronic temperature coefficient of reactivity.

In all the temperature related calculations, twenty-four energy group cross-sections^{2,3} for all the reactor materials were used. These are especially suitable for this type of calculation since the energy region below 1.125 electron volts is subdivided into eleven of the groups. It is in this energy range where most of the change associated with the expected reactor temperatures would take place. Up-scattering cross sections were included in the uranium, carbon, and beryllium sets. Only

		UNIFORM LOADED LASHUP REFLECTOR		0.66 Oy ZONE LASHUP REFLECTOR		0.66 Oy ZONE NEW REFLECTOR PRESSURE SHELL	
		Cm Radius	gm/cm ³	Cm Radius	gm/cm ³	Cm Radius	gm/cm ³
CORE	Central	0	0.121 Oy 1.462 C 0.0783 Nb	38.997	0.0799 Oy		
	Depleted Oy		0.121 Oy 1.462 C 0.0783 Nb				
	No Oy	43.073	1.818 C				
		44.450					
REFLECTOR (and void) CYLINDER			1.472 C				13.23 C
REFLECTOR	(Boron Sheath)	50.482	1.655 Be			51.118	1.721
		56.198 56.298	(Adjustable)				
		63.182				62.548 64.113	2.432 A
PRESSURE SHELL (and void)							
K _{eff} (No B in Reflector) (Between control rods) (Toward control rods)		1.0616 1.0533		1.0493 1.0245		1.0377 1.0245	

Table I. Data for DSN calculations on ZEPO-B-1.

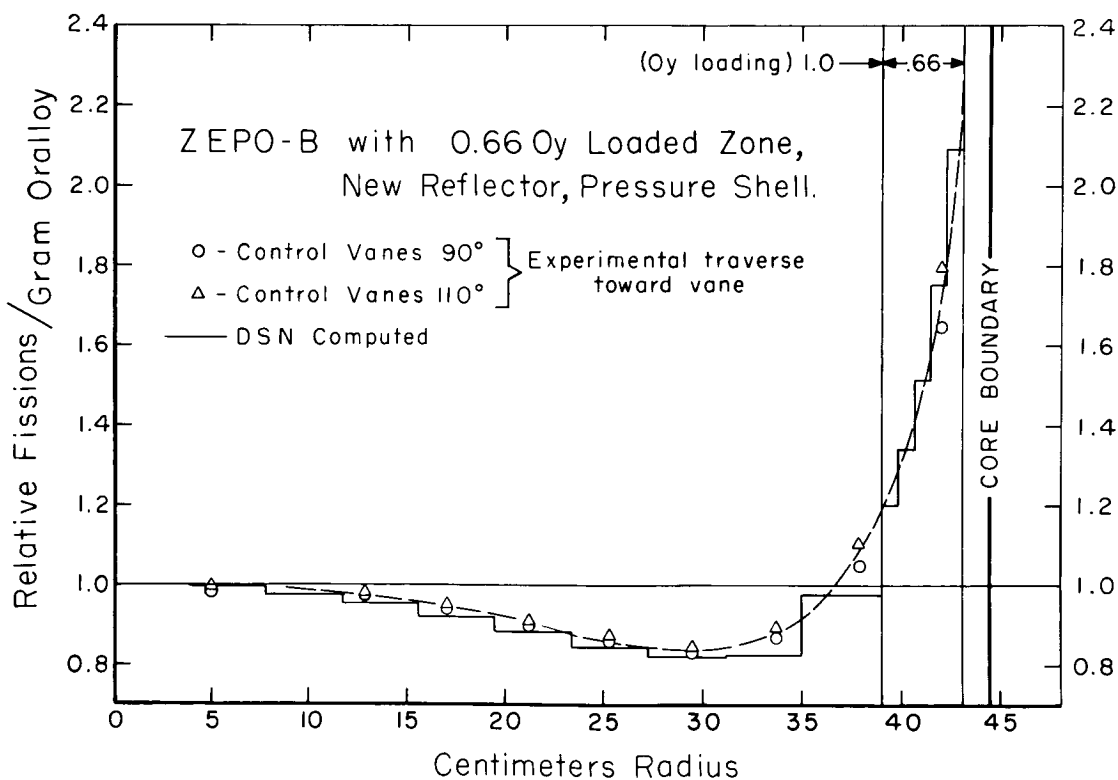


Figure 1. Comparison of DSN calculations with experimentally measured fission distribution of ZEPO-B-1.

radial calculations were made, and axial leakage, suitable for a reactor length of 132 cm (plus extrapolation lengths), was represented by a buckling approximation.

Kiwi-B-1A

At the time that this series of calculations was started, experimentation had reached the stage of a fairly detailed zero-power critical mockup, which is called ZEPO⁴, of the Kiwi-B-1A reactor. Thus, experimentally measured radial fission traverses were available, and the first problem was to reproduce these on the computer. The core, reflector cylinder, reflector, and pressure shell were divided into radial zones in the usual manner so that the reactor materials at their proper densities could be represented in the code.

Radial dimensions and material densities associated with the ZEPO mockup of Kiwi-B-1A are listed in Table I. The first ZEPO assembly was quite rough. It had a uniformly loaded core with 19.6% void, and the reflector was made up of slabs and blocks of beryllium with an overall void of about 10%. In this ZEPO, the twelve rotating control rods were mocked up as strips of boral inserted between the beryllium slabs. In the calculation, the control rods were represented by a 0.1 cm thick sheath of boron imbedded in the middle of the beryllium reflector. Using the density of boron in this sheath as the variable parameter, a set of calculations was performed to match the experimentally measured fission distribution.

As is indicated in Table I, the calculations followed several stages in the experimental development of the ZEPO machine. Entries in the table show only the changes which were made from the preceding set-up. In the second column, the or alloy density was decreased at the outside of the core. This was done because there is a sharp increase in fission rate at the outer boundary of the core caused by the return of thermal neutrons from the beryllium reflector. A reduction of the or alloy density in this region, coupled with changes in the proposed hydrogen propellant flow rate would produce a sufficiently uniform radial core temperature.

The next column in the table, represents the ZEPO after the real reflector with its twelve rotating control rods was received and the pressure shell was mocked up. The variable void in the reflector was set at 7%.

As previously discussed, the calculations reproduced the experimentally measured fission traverses by varying the boron density in the 0.1 cm sheath in the reflector. It was found that 3×10^{20} atoms/cm³ was needed for a good match when looking at a traverse between control rods, and 10×10^{20} atoms/cm³ when looking toward a control rod. The reproduction numbers calculated for these various cases are given at the bottom of the table. Since the purpose of the calculation is primarily to obtain a correct fission distribution, a computed k_{eff} differing from unity by several percent is quite satisfactory. Of significance, however, is the change in k_{eff} in going from one calculation to the next.

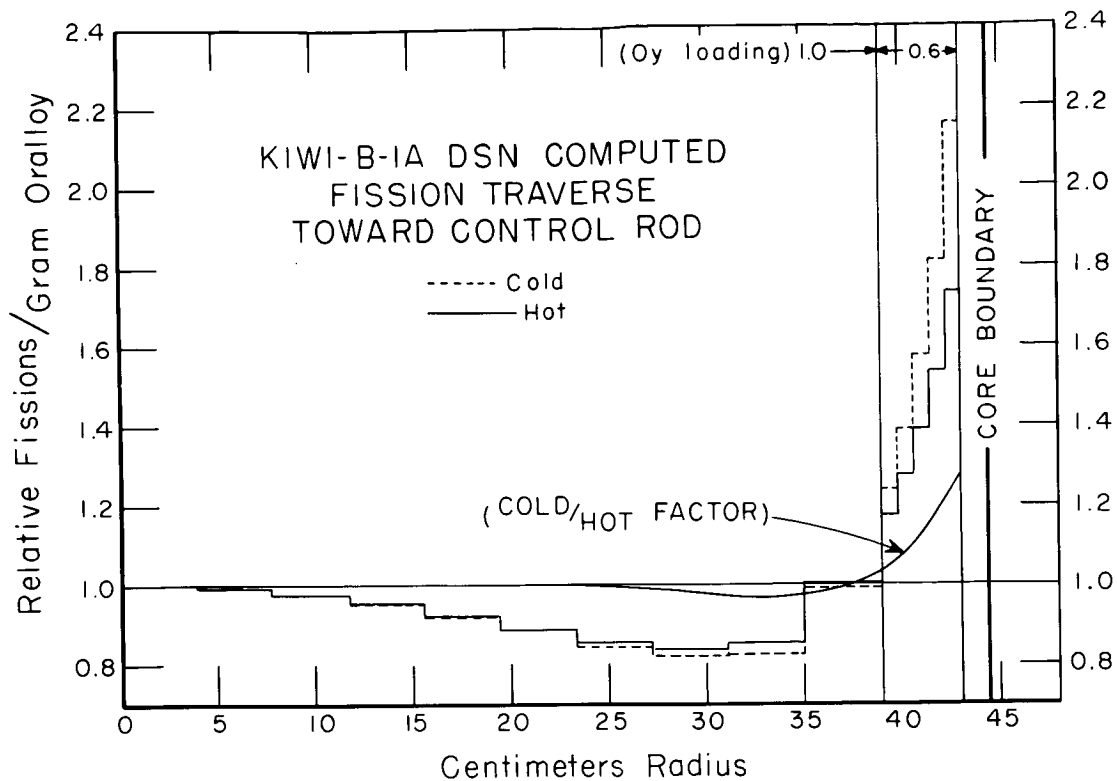


Figure 2. DSN computed radial fission distribution for Kiwi-B-1A.

DATA FOR DSN CALCULATIONS ON KIWI-B-I-A						
		Cm Radius	gm/cm ³	Temperature °C		
CORE	Central Depleted Oy No Oy	0	0.125 Oy 1.468 C 0.0866 Nb	17	2000	2000
		38.997	0.0750 Oy 1.468 C 0.0866 Nb			
		43.073	1.818 C			
		44.450				
REFLECTOR CYLINDER (and void)		51.118	1.400 C	17	890	340
REFLECTOR	Boron (Sheath)	56.198	1.721 Be	17	17	175
		56.298	(Adjustable B)			
PRESSURE SHELL (and void)		62.548		17	17	17
		64.113	2.432 Al			
K _{eff} (Between control rods) (Toward control rods)				1.0449 1.0317	1.0408 1.0280	1.0421 1.0299

Table II. Data for DSN calculation on Kiwi-B-1A.

An example of the success achieved in matching the experimental fission distribution is shown in Figure 1. This represents the final ZEPO case in Table I, where the proper reflector and pressure shell were installed. The dashed curve is the experimental traverse shown as an average of two critical configurations. In the final reactor, the control rods should be about halfway out, so this curve is a good representation of the desired conditions. The solid line histogram then shows the DSN computed fissions per gram of oralloy averaged in each of the core intervals. The results are normalized to unity at the center of the reactor.

Having thus gained confidence that reliable fission distributions could be calculated, the dimensions and material densities of the actual Kiwi-B-1A test reactor were substituted into the calculation. These are listed in Table II, and show small changes from the final ZEPO set-up. In this way, a predicted cold fission distribution was obtained. The cross sections were then modified to the temperatures indicated in the table, first to a preliminary guess, and then to a more refined prediction, to compute the expected hot fission distributions. The results are plotted in Figure 2. The fission rate decreases at the core boundary as the temperature is increased.

Also plotted is the cold to hot fission ratio which increases at the edge of the loaded core to about 30% more than its value at the center of the core.

After the Kiwi-B-1A reactor had been assembled at Los Alamos, and the actual fission distribution measured at delayed critical, this fission ratio was used to help decide the dimensions of orificing plugs needed to produce a flat radial temperature profile for the test at Nevada.

The calculated k_{eff} values show a change of -0.00028 indicating a decrease of about 35 cents in reactivity in going to the operating temperature. This, of course, does not include the effect of core expansion which would contribute an additional loss in reactivity.

Kiwi-B-4A

For calculational purposes, Kiwi-B-4A is essentially the same as the B-1A reactor except in core composition. This new reactor has about 12% less graphite and twice as much oralloy. Stainless steel which is present in the core, although included in the calculations, does not contribute markedly to either reactivity or fission distribution.

ZEPO type experiments were performed to determine an oralloy loading scheme to eliminate the fission spike in the peripheral elements. DSN calculations again closely followed the experimental development. As before, the experimental fission distributions were matched in the calculations by adjusting the boron density in the 0.1 cm sheath representing the control rods. For this case, it was found that 20×10^{20} atoms/cm³ produced the best fit.

Figure 3 gives an example of the match obtained for one of

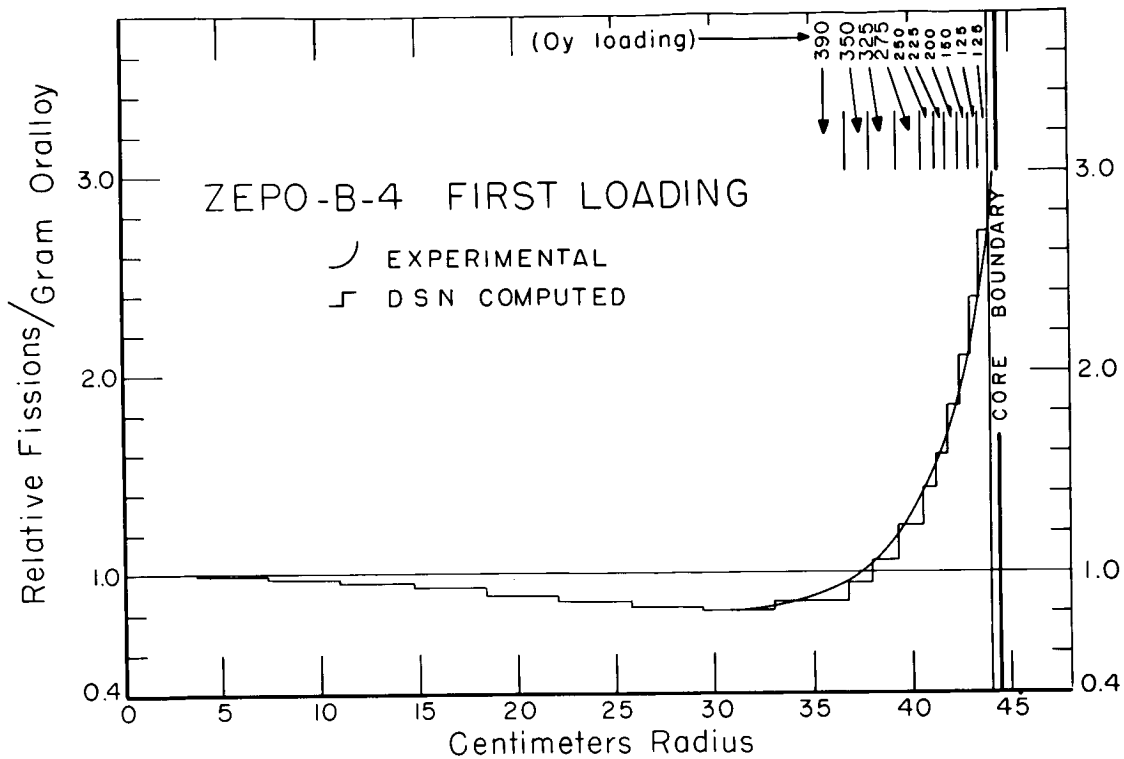


Figure 3. Comparison of DSN calculation with experimentally measured fission distribution of ZEPO-B-4.

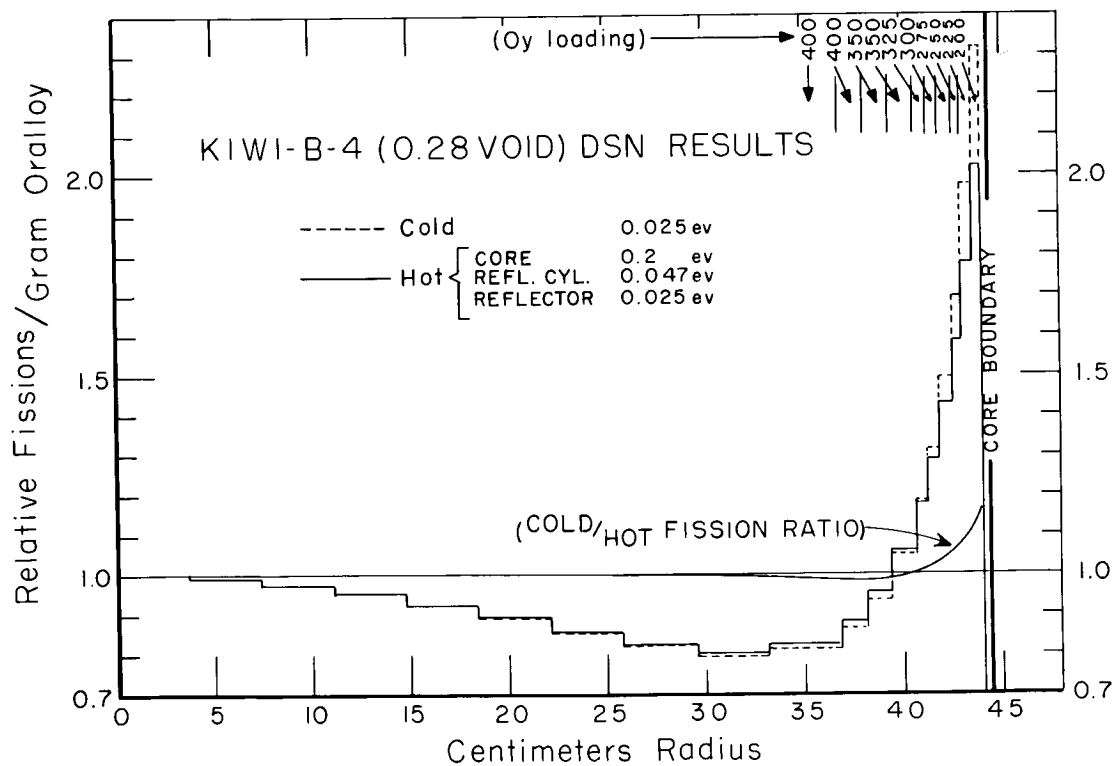


Figure 4. DSN computed radial fission traverse for Kiwi-B-4A.

the early loading schemes. Here the fuel element or alloy loading was varied in ten radial zones from 390 gm/cm³ at the center to 125 gm/cm³ at the periphery of the core. The solid curve shows the experimental traverse as an average of measurements toward and between control rods. The histogram is the calculated distribution normalized to one at the center of the core.

Having thus found the proper boron sheath density, the Kiwi-B-4A design dimensions and material densities were substituted into the calculation to obtain cold and hot fission distributions. These are shown in Figure 4 for a later version of the or alloy loading scheme. In going to operating temperature, the fission density again decreases at the core periphery, however not as much as in Kiwi-B-1A, because the average neutron energy is now higher into the epithermal region. The cold to hot fission ratio at the outside of the core is now about 18% higher than the center value.

The reproduction numbers produced by these calculations show that the neutronic temperature coefficient of reactivity for Kiwi-B-4A is very small and probably positive.

References

1. B. Carlson, C. Lee, J. Worlton, The DSN and TDC neutronic transport codes, Los Alamos Scientific Laboratory Report LAMS-2346 (1960)
2. C. B. Mills, F. W. Brinkley, Physics of intermediate reactors, Los Alamos Scientific Laboratory Report LAMS-2288 (1959)
3. C. B. Mills, private communication
4. H. H. Helmick and J. D. Orndoff, Neutronics of Kiwi-B nuclear propulsion reactors, Proceedings this meeting

X 66 50281

ROVER REACTOR CONTROL ELEMENT WORTH CALCULATIONS

Albert W. Chermatz
University of California
Los Alamos Scientific Laboratory
Los Alamos, New Mexico

50281

Summary

Calculations were performed to determine reactivity worth of control elements in reactors suitable for rocket propulsion. The resulting approximate values were used to evaluate the feasibility of alternate control methods, for an estimate of actuator requirements, and for analyses of control system behavior resulting from individual rod motion.

Configurations considered included reactors with absorbing rods located within the reactor core, as well as those using rotating control vanes located within an external reflector, and rotating vanes in both the reflector and a central moderating island. Calculations were performed to determine means of reducing power peaking at the core - reflector interface. A brief survey was also performed to determine an approximate upper limit on reactor power level beyond which control by neutron absorption in the reflector alone is no longer feasible.

Conf. R.D. Author

Code and Cross Sections

Use was made of the discrete S_p approach to the numerical solution to the neutron transport equation (DSN) in one dimensional form, for solution on IBM 704 and 7090 computers. Cross sections used included 13, 16, 18, and 24 neutron energy groups.

Reactor Type I - DUMBO

The Dumbo system was a heterogeneous, thermal reactor consisting of separate fuel-moderator modules on a 12 cm triangular spacing (Fig. 1A). Each module consisted of a central void into which hydrogen flowed after passing radially first through a zirconium hydride moderator annulus and then through a fuel-loaded molybdenum annulus. Control rods were placed in the interstice formed by three nearly-touching modules. This geometry was converted to a form suitable for the one dimensional transport code, as shown in Fig. 1B. The separation of the control rod from the first neutron-emitting (ZrH₂) surface was made on the assumption that, given isotopic neutron emission from the

* Work performed under AEC Contract W-7405-ENG. 36.

surface, the probability of neutrons seeing the absorbing rod was identical for both the actual reactor and the one dimensional model. Cell calculations were performed to obtain appropriate cross sections for the homogeneous core.

Table I lists poison rod configurations and calculated central control rod worth, as well as experimental worth measured on the DUMBO ZEPO, where available. In this and following tables, calculated control element worth is given to two significant figures for comparison purposes within a set of calculations, and not with an expectation of absolute two place accuracy.

Reactor Type II - Kiwi-B

A. Central Rod Worth

Calculations of reactivity worth of centrally located cylindrical rods were performed on various reactor models. An early reactor type which was converted to DSN calculational form for rod worth, and later, for reflector neutron-absorbing curtain calculations, is shown in Fig. 2. Figure 2A shows a typical module, while Fig. 2B shows a loaded section in greater detail with its share of the surrounding unloaded region. Fig. 2C indicates a typical model used in cell calculations to determine flux depressions within the loaded portion and flux-averaged modified cross sections to be used in the homogeneous core part of the overall reactor model. Table II lists the results of central rod worth calculations.

B. Reflector Control Vanes

Relative worth of rotating control drums within the reflector was determined by solving for system reactivity with neutron absorbing curtains representing a "poison in" or a "poison out" position, placed in either of two positions with the reflector, the former 0.5" from the inner reflector surface and the latter 0.5" from the outer reflector. Using the one dimensional code a change in reactivity worth of the entire poison curtain was obtained for the two extreme positions, yielding a reactivity worth per unit surface area of absorbing curtain. Considering the curved geometry of individual poison segments and examining flux shapes in the reflector regions, the integrated worth of a given vane (full out to full in motion) could be simulated with sufficient accuracy for the required purposes by representing the true vane surface area by that of a larger vane. The control vane arc length (one-third of the periphery associated with a given control vane) was considered to be one-third of 2π times (the true vane radius plus about 1 1/2 cm), where the added constant is in the order of a thermal neutron mean free path in the beryllium of interest. The ratio of this fictitious area to that of the calculational model's curtain area, times the total curtain worth, was then called the worth of an individual control vane. Table III indicates some calculated values for typical curtains and vanes, as well as clean reactor reactivity vs. reflector thickness.

C. Power Peaking at Core Edge

For a uniformly loaded core, fission density is found to increase quite rapidly near the core edge because of a return of low energy neutrons from the reflector. One method of reducing the magnitude of this peaking is to place a selective neutron absorber (e.g., a cadmium sheath) between the core and the reflector to absorb low energy neutrons returning toward the core while permitting high energy neutrons to pass from the core to the reflector. A disadvantage is the reduction in control vane worth, since the control vane is operating partly on low energy neutrons. Table IV summarizes results of calcu-

lations. Measurements of the effect of adding a four mil Cd screen at the inner edge of the Be reflector of a faster spectrum reactor, which were made on the Honeycomb critical assembly machine, resulted in a $\approx 6\%$ reactivity decrease, and a decrease in peaking from about 1.6 times core average to 1.0 times average, analogous to the changes listed in Table IV.

Kiwi-B-4

Table V describes a Kiwi-B-4 model, used for rod worth and reflector control vane studies, and a comparison of calculated and measured results.

8000 and 20,000 MW Reactors

Calculations were performed to determine approximate reactivity worth of rotating control vanes located in the reflectors of reactors resulting from conceptual design studies. Tables VI and VII list results and reactor descriptions.

Vane Worth vs. Power Level

Vane worth, observed as a function of reactor power level for certain detailed reactor designs (Table VIII), shows no significant change over the power range considered, as well as an approximately constant Eu_2O_3 to B^{10} relative worth.

40,000 MW Reactors

Simplified models of 40,000 MW reactors were examined in order to obtain a measure of the feasibility of reflector control of large reactors. Instead of 150 MW/cubic foot of active core as in the 20,000 MW design, 175 was used, yielding a 228 ft³ core volume requirement. The effects of changing reactor length (5, 6, and 7 ft), core void fraction (30 and 40%), and reflector thickness (6 and 8") were studied (Table IX). The lack of power peaking at the core edge indicated thicker reflectors could be considered; this led to higher vane worths ($\approx 1\%$ for 12" reflectors on some models).

Because of decreasing reflector control worth for thin reflector models, a reactor model was investigated in which a central Be island was emplaced. Table X indicates a significant increase in total curtain worth, but also reveals a large interdependence of the two control regions.

Full power hydrogen reactivity worth may be estimated as being in the order of + 20\$, subject to many initial assumptions. Temperature reactivity effect (room temperature to 3000 R average core temperature) has been calculated at $\approx -20\%$. The uniform addition to the core of Gd (≈ 1 to 3×10^{16} a/cc) results in a decrease to ≈ -5 to 10% , for the 40 KMW 30% void 8" reflector, and the 40 KMW island models, although fuel loading must be increased (Table XI). Beyond this, the complex interrelation of reactor type (core void, length, reflector thickness and operating (H_2) conditions) with temperature and hydrogen reactivities, has not been investigated.

Acknowledgement

The author wishes to express his appreciation to the many members of the Pajarito Critical Assembly Group (N-2) of the Laboratory, (in particular to H. H. Helmick), for their cooperation in obtaining experimental verification of calculational results, and to G. E. Hansen (N-2) and R. S. Cooper of the Theoretical Division for many fruitful discussions.

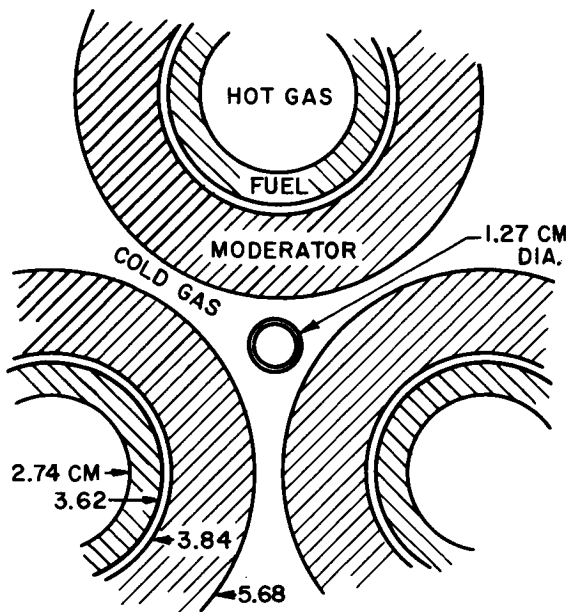


FIG. 1A. DUMBO REACTOR-CONTROL ROD GEOMETRY.

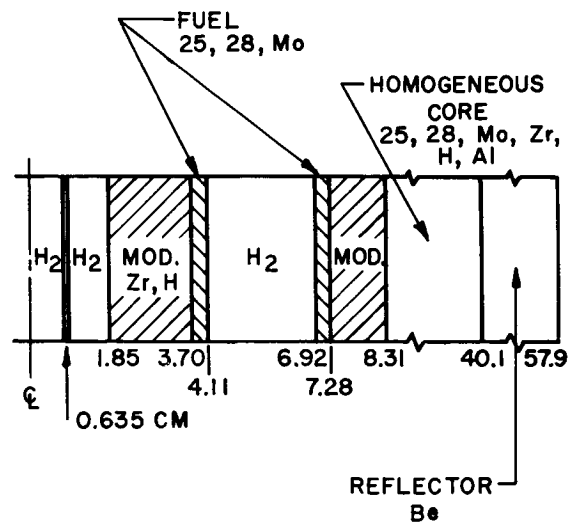


FIG. 1B. ONE DIMENSIONAL MODEL.

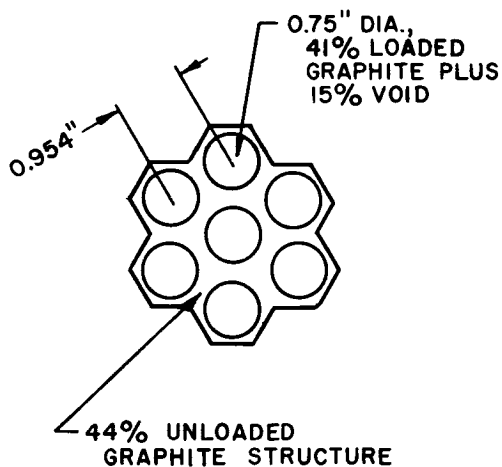


FIG. 2A. ONE KIWI-B CORE MODULE.

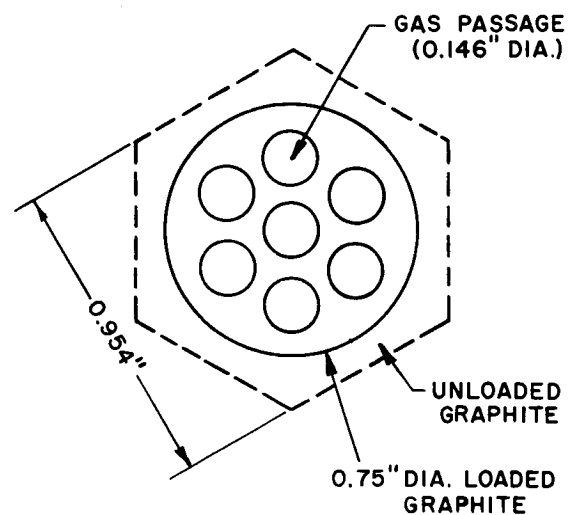


FIG. 2B. ONE LOADED SECTION WITHIN THE MODULE.

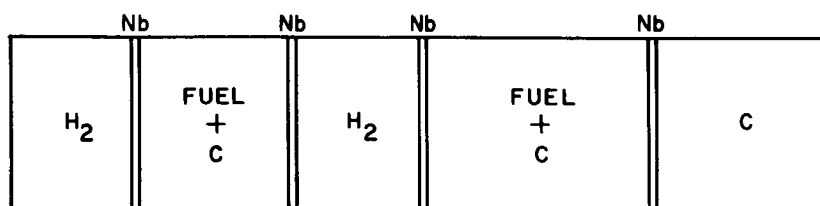


FIG. 2C. CELL CALCULATION MODEL.

Table I - Dumbo Central Control Rod Worth

<u>Absorber</u>	<u>Rod O.D.</u>	<u>Absorber Thickness</u>	<u>Rod Worth</u>	
			<u>Calculated</u>	<u>Measured (ZEPO)</u>
Cd	0.5 inch	17 mils	\$0.35	\$0.37
Gd	0.5	3	.39	---
B ¹⁰	0.595	2	.57	.67

Table II - Kiwi-B Central Control Rod Worth

<u>Absorber</u>	<u>Rod O.D.</u>	<u>Absorber Thickness</u>	<u>Rod Worth, Calculated</u>
B ¹⁰	0.5 inch	2 mils	\$0.38
"	2.36	2	1.2
Eu ₂ O ₃ - Gd ₂ O ₃	0.5	9 + 1	0.41
"	2.36	4 + 1	0.87
"	2.36	9 + 1	1.6
Hf	0.5	solid	0.52

Reactor Description:

Core - 36 inch O.D., 15% void, 400 mgU/ccC
Gap - 0.3 inch C wool
Reflector cylinder - 2.0 inch C
Reflector - 5.0 inch Be, 10% void

Table III

<u>Kiwi-B B¹⁰ Curtain Worth</u>				
<u>Absorber Thickness</u>	<u>Reflector Thickness</u>	<u>Worth Relative to Clean Reactor</u>	<u>Worth Relative to "Curtain Out"</u>	<u>Vane Worth</u>
6 mils	4.0 inch	\$15.2	---	<\$0.54
0.4	4.5	10.8	---	< 0.44
4	4.5	16.6	---	< 0.67
6	4.5	17.5	\$16.2	< 0.71 (0.66)
6	5.0	19.8	18.5	< 0.86 (0.81)

<u>Kiwi-B Reactivity vs. Reflector Thickness</u>			
<u>Reflector Thickness</u>	<u>Reflector Void Fraction</u>	<u>Beryllium Density</u>	<u>Reactivity</u>
4.5 inch	0.10	1.234 a/cm ²	\$1.9
4.5	0.175	1.138	0 (Reference)
4.5	0.25	1.031	-2.6
5.0	0.175	1.265	2.3
4.5	0.175	1.138	0 (Reference)
4.0	0.175	1.012	-2.5

Reactor Description:

Core - 52 inch L x 35.5 inch O.D., 20% void, 41% loaded at 250 mgU/ccC
 Gap - 0.25 inch C wool
 Reflector cylinder - 2 inch C
 Gap - 0.25 inch
 Reflector - 4, 4½, or 5 inches Be

<u>Kiwi-B-1B Vane Worth</u>				
<u>Absorber</u>	<u>Reflector</u>	<u>Calculated Worth Curtain</u>	<u>Measured Worth Vane</u>	<u>Measured Worth (Reactor at Kiva)</u>
10 mils B ¹⁰	4.5 in. Be	\$18.2	\$0.77	\$0.78

Table IV - Poisoned Reflector in Kiwi-B

<u>Absorber</u>	<u>Centerline F_0</u>	<u>Edge F_0</u>	$\Delta\rho$	Boral
	<u>Average F_0</u>	<u>Average F_0</u>	<u>from Clean</u>	<u>Vane Curtain</u> <u>$\Delta\rho$ from Cd</u>
None	1.13	1.91	---	---
1 mil Cd	1.28	1.17	\$ 8.2	---
2 mils Cd	1.30	1.04	9.7	---
1 mil Cd (+ 6 mils B^{10} vane curtain)	1.47	0.71	17.6	\$9.4
2 mils Cd (+ 6 mils B^{10} vane curtain)	1.48	0.69	17.8	8.1

Reactor Description:

Core - 52 inch L x 35 inch O.D., 20% void, 36% loaded to 250 mgU/ccC
 Gap - 0.5 inch C wool
 Reflector cylinder - 2 inch C
 Gap - 0.125 inch
 Reflector - 4.5 inch Be, 17.5% void

Table V - Kiwi-B-4 - Central Rod and Reflector Vane WorthI. Central Rod

<u>Absorber</u>	<u>Rod O.D.</u>	<u>Rod Worth</u>	
		<u>Calculated</u>	<u>Measured (ZEPO)</u>
$B^{10}C$	0.125 inch	6.1¢	4¢ (Average of 28 close rods)

II. Reflector

<u>Absorber</u>	<u>Absorber Thickness</u>	<u>Vane Worth</u>	
		<u>Calculated</u>	<u>Measured (ZEPO)</u>
B^{10}	10 mils	\$0.55	\$0.67
Eu_2O_3	5	---	.41
"	10	---	.50
"	12.5	.42	---
"	15	---	.53
"	20	.47	---

Reactor Description:

Core - 52 inch L x 35.1 inch O.D., 28% void
 Reflector cylinder - 1.8 inch C, 10% void
 Reflector - 4.5 inch Be, 12% void
 Core loading: 400 mgU/ccC to r = 15 inches, then 348 to r = 15.75,
 304 to r = 16.5, 264 to r = 17, and 220 to r = 17.25.

Table VI - 8,000 MW Reactor Control Vane Worth

	<u>Reflector Thickness</u>	<u>Absorber</u>	<u>Absorber Thickness</u>	<u>Total Curtain Worth</u>	<u>Vane Worth</u>
4.1 inch	1.03×10^{24} a Be/cm ²	Eu ₂ O ₃	30 mils	\$ 6.24	\$0.17
6.0	1.51	Eu ₂ O ₃	10	12.2	.45
6.0	1.51	Eu ₂ O ₃	30	14.1	.52
6.0	1.51	B ¹⁰	10	15.9	.59
7.5	1.89	Eu ₂ O ₃	30	23.9	1.1

Reactor Description:

Core - 52 inches L x 55 inch O.D., \approx 35% void

Reflector cylinder - 1.9 inch C plus Al

Reflector - Be, 20% void

The only variation among reflector thickness models is number density of 25 and 28 in the core.

Table VII - 20,000 MW Reactor Control Vane Worth

<u>Absorber</u>	<u>Absorber Thickness</u>	<u>Total Curtain Worth</u>	<u>Vane Worth</u>
B ¹⁰	6 mils	\$14.7	\$0.43
Eu ₂ O ₃	10	12.0	.35
"	30	14.6	.42
Eu ₂ O ₃ + Gd ₂ O ₃	9 + 1	12.0	.35
"	27 + 3	15.8	.46

Reactor Description:

Core - 60 inches L x 69.5 inch O.D., 34% void, four radial loading variations (\approx 60 mgU/ccC)

Reflector cylinder - 1 inch C, 10% void

Reflector - 6 inches Be, 20% void

Table VIII - Vane Worth as a Function of Reactor Power Level

<u>P_R</u>	<u>Boron-ten Thickness</u>	<u>Worth</u>	<u>Europium Oxide Thickness</u>	<u>Worth</u>	<u>Relative Worth</u>	<u>Measured or Calculated</u>
4,000 MW			5 mils	\$0.41	---	Zepo
	10 mils	\$0.67	10	.50	0.75	Zepo
			15	.53	---	Zepo
	10	.55	12.5	.42	\approx .76	DSN
			20	.47	---	DSN
8,000	10	.59	10	.45	.76	DSN
			30	.52	---	DSN
20,000	10	.49	10	.35	.71	DSN
			30	.42	---	DSN

Table IX - 40,000 MW Reactor Control Vane Worth

<u>Core</u> <u>L X D (in.)</u>	<u>Core</u> <u>Void</u>	<u>Thickness</u> <u>Reflector</u>	<u>Eu₂O₃</u>	<u>Curtain</u> <u>Worth</u>	<u>Vane</u> <u>Worth</u>
60 x 91	30%	6 inch	20 mils	\$ 4.4	\$0.10
	30	8	20	7.4	.22
	30	8	50	8.1	.24
	40	6	20	8.0	.18
	40	8	20	11.6	.35
72 x 83.5	30	8	20	10.6	.35
84 x 77.5	30	8	20	16.2	.56

Table X - 40,000 MW Reactor With Central Island

<u>Reflector</u> <u>Poison</u>	<u>Island</u> <u>Poison</u>	<u>Reactivity</u> <u>Change</u>
Out (Min. Poison)	Out-->In	\$ 9.5
In (Max. Poison)	Out-->In	17
In-->Out	In (Min. Poison)	11
In-->Out	Out (Max. Poison)	18

Reactor Description:

Island - 8 inch radius, 20% void Be
 Core - 46.5 inch outside radius, 35% void
 Reflector cylinder - 1 inch C
 Reflector - 6 inches Be, 20% void
 Absorber - 20 mils Eu₂O₃

Table XI - 40,000 MW Reactors' Temperature Reactivity Effect

A. 40 KMW REACTOR W/ISLAND

<u>Gd Loading</u>	<u>Δk, RT to 3000 R</u>	<u>Δk Loss at RT Due to Gd</u>	<u>Remarks</u>
None	-\$21	\$ 0	Reference
10^{16} a/cc	- 18	4.8	Subcritical at RT
3×10^{16}	- 10	15	Subcritical at RT
None	- 14	0	Higher fuel loading, Reference
10^{16}	- 12	4.1	Higher fuel loading
3×10^{16}	- 7	9.5	Higher fuel loading, Subcritical at RT
Island - 8 inch radius, 20% void Be			
Core - 38.5 inch thick, 35% void			
Reflector - 1 inch C plus 6 inch 20% void Be			

B. 40 KMW REACTOR W/O ISLAND

<u>Gd Loading</u>	<u>Δk, RT to 3000 R</u>	<u>Δk Loss at RT Due to Gd</u>	<u>Remarks</u>
None	-\$19	\$ 0	Reference
10^{16}	- 17	5.5	Subcritical at RT
3×10^{16}	- 8.8	16	Subcritical at RT
None	- 16	0	Higher fuel loading, Reference
10^{16}	- 13	4.1	Higher fuel loading
3×10^{16}	- 7.1	12	Higher fuel loading, Subcritical at RT
Core - 45.7 inch radius, 30% void			
Reflector - 1 inch C plus 8 inch 20% void Be			

X 66 50282

LEAKAGE RADIATION FIELDS FROM THE KIWI-B-1A

[U]

D. M. Peterson
Los Alamos Scientific Laboratory
University of California
Los Alamos, New Mexico

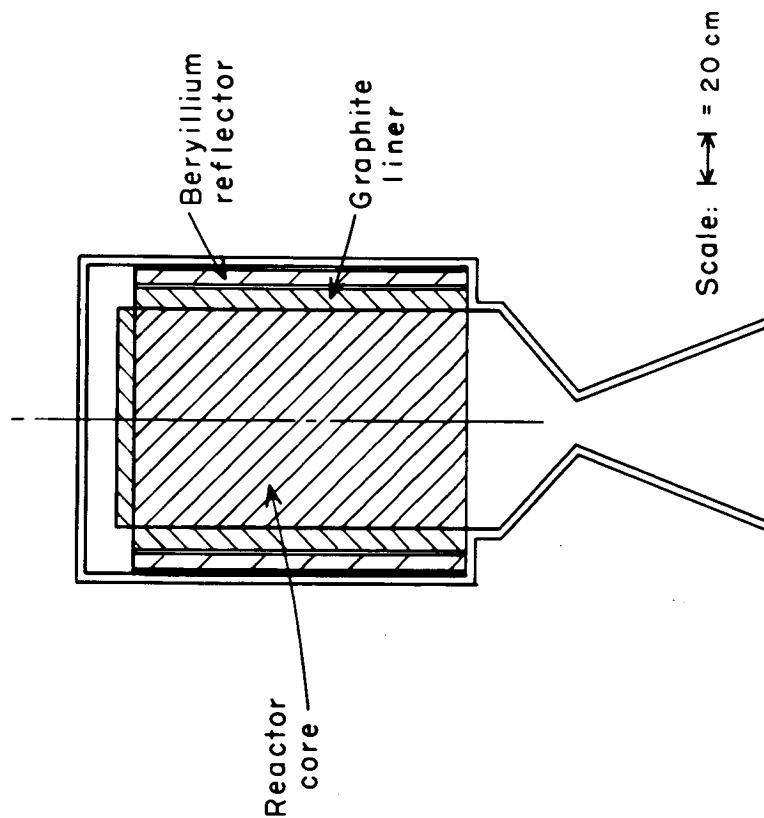
The leakage radiation fields from a simple model of the Kiwi-B-1A reactor system have been computed using the QAD program originally developed by R. E. Malenfant of LASL. Some predicted shapes for these radiation patterns are given here, and one particular calculation is compared to experiment to permit some discussion of the agreement attained.

The QAD program utilizes a distributed point source, line-of-sight calculation. That is, this program considers the source region as a set of small volumes, with a point source in each volume and calculates the contribution of each of these sources at a particular detector considering only the effects of those materials on a line-of-sight between the point source and the detector. Gamma source spectra, material attenuation factors, and buildup coefficients may be arbitrary. Neutron sources presently must be given the Watt fission spectrum and the neutron attenuation factors employed are based upon moments method data. At each detector point, the QAD program will provide an arrival number spectrum or energy spectrum as well as dose and heat generation rates from both gamma radiation and fast neutrons.

The geometry used in these calculations (which is shown in Figure 1) was assumed to be in free space, that is no air scattering or other external scattering was considered. The system consisted of a central cylindric core, a graphite liner, a beryllium reflector, an aluminum core support plate, an aluminum pressure vessel, and a nickel nozzle.

The reactor source was simulated by 750 source points, the source intensities being chosen to correspond to a flat radial power distribution, and a cosine longitudinal power distribution. A nineteen line source spectrum was used for the gammas; a fission spectrum source was used for the neutrons. The calculation required 6-10 seconds per detector point.

Some gamma isodose patterns are shown in Figure 2. These were computed for a reactor power of 1000 MW. The high dose rate regions exhibit irregularities which may be roughly correlated with the effective penetration lengths for radiation emanating from the central portion of the reactor. As the distance from the reactor center increases, these irregularities become less pronounced, and the radiation patterns tend toward isotropicity;



SCHEMATIC DIAGRAM OF KIW-B-1A
AS USED FOR THE CALCULATIONS

Figure 1

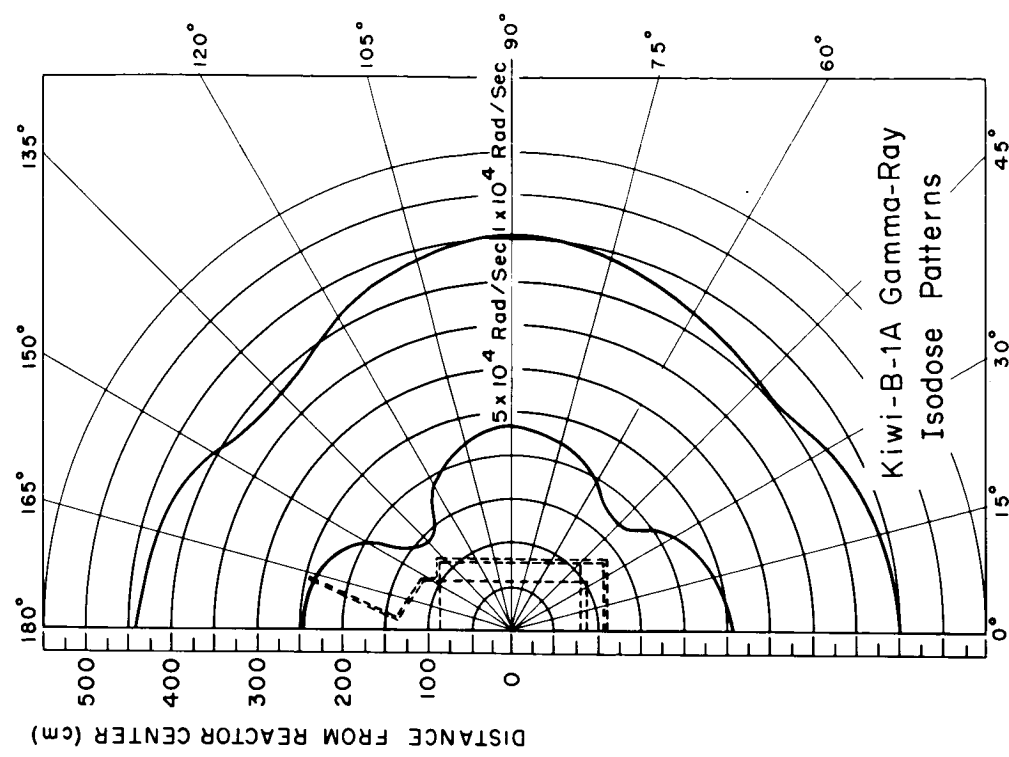


Figure 2

this is nearly achieved at 4 meters.

In order to provide a better comparison between the analytic method and experiment, the total gamma ray dose and the activation to be expected in sulfur (from fast neutron flux above 2.2 mev) were also computed for various points along a meridian ring geometry located 127 cm from the center of the reactor core. There were some fourteen experimental setups, stationed ten degrees apart, on this ring. The calculated data were normalized to correspond to 2.95×10^{18} fissions, which is believed to be the correct source strength for the particular run to which comparison was made.

The calculated and experimentally determined gamma ray doses for this case are shown in Figure 3, on which there is also a phantom view of the reactor and meridian ring geometry superimposed for purposes of orientation.

Since the analytic dose predictions did not take into account radiation which was scattered from the massive test stand shield - the 19" thick object which is outlined below the reactor - it is not surprising that the analytic results are lower than the measured doses at the bottom or inlet end of the system. Otherwise the agreement between the two sets of results is very good, both in shape and magnitude.

Except for those effects near the inlet end previously attributed to external scattering, the largest percentage deviations between the experimental and analytic results occur in that portion of the figure above 120°. In this region, the geometry used for the calculated models was oversimplified in comparison to the rather irregular and complex arrangement of the actual system. Better agreement might have been obtained if the calculational geometry had been a more precise representation of the system, but it is felt that an adequate representation was obtained with the simple model chosen.

For the remainder of the system, the analytic and experimental results appear to agree to within five percent. However, the experimental results were probably enhanced a few percent by radiation delivered after shutdown, but prior to the recovery of the dosimeters. Thus, it is probable that the calculations are over-predicting the doses by approximately 10% in the area of best agreement - i.e., that part of the calculational geometry which best approximates the actual system. Small as this difference is, the agreement in the shape of the data is probably better - i.e., if the calculated curve had been renormalized for a best fit to the data in the upper two-thirds of the figure, few deviations would be greater than five percent.

A comparison of some tentative neutron flux calculations and experimentally determined neutron fluxes are shown in Figure 4. The analytic data have been normalized to the experiment at the 92° position in order to compare the shapes of the two sets of data.

This figure shows that the fast neutron experimental and normalized analytic data are in reasonable agreement. The absolute agreement is not as good as for the gamma ray data; the unscaled

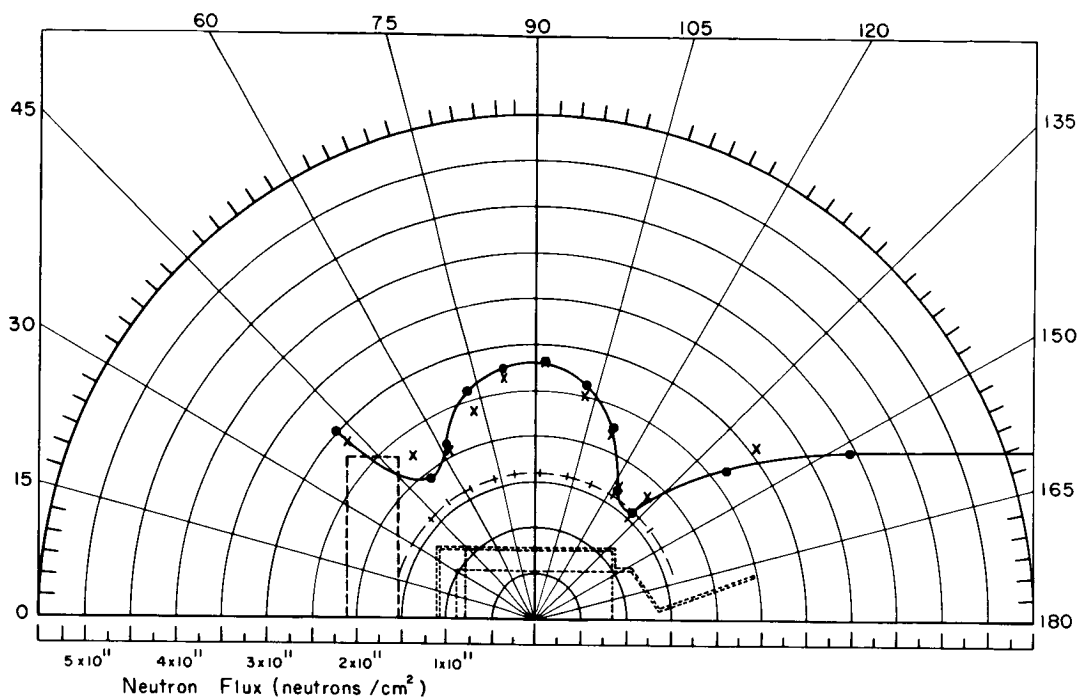


Figure 4

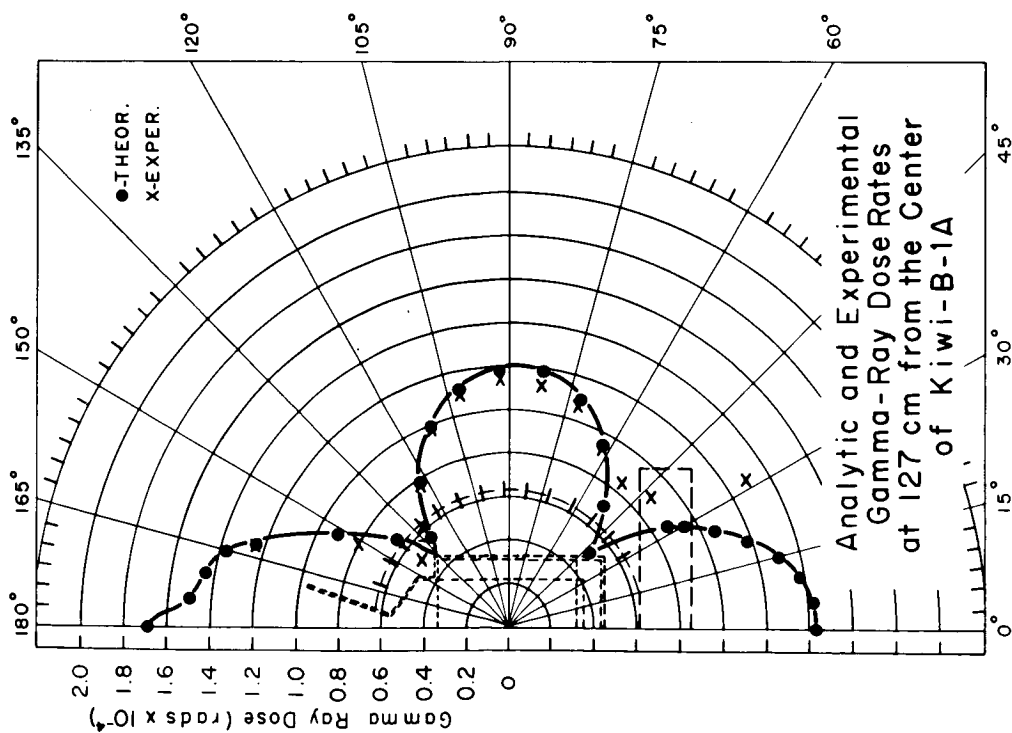


Figure 3

analytic data are about a factor-of-two higher than experiment. It may ultimately be possible to obtain better absolute agreement between such calculations and experiment, but it is too early to tell, since there are fundamental differences between these geometries and the situations for which the moments method data were developed.

These attempts to calculate neutron fluxes by the moments method have just recently been undertaken in the hope of generating a neutron program which can perform calculations with the same ease, speed and reliability now inherent in the QAD gamma program. With growing experimental and theoretical experience available as a normalizing guide, via measured doses and Monte Carlo calculations, it should be possible to realize these aims regardless of the absolute accuracy ultimately obtainable.

This program can be used to compute radiation fields for systems with more complex physical configurations than can be readily handled by Monte Carlo and S_n type programs, though the QAD results are not as detailed as those of Monte Carlo or S_n . Thus, QAD is not considered as a replacement for these other approaches, rather it is a supplement which is used both to perform initial survey type calculations for new systems and to apply Monte Carlo and S_n results to the complex portions of more thoroughly studied systems by normalizing to such results at suitably chosen points.

X 6 6 5 0 2 8 3

DESIGN COMPUTATIONS FOR A NUCLEAR ROCKET SHADOW SHIELD

BY

Mary Ann Capo

Westinghouse Electric Corporation
Astronuclear Laboratory

Pittsburgh, Pennsylvania

[U]

The objective of this study was to design a shield for use in the NERVA nuclear rocket engine system. The primary purpose of the shield is to reduce the radiation heating of the liquid hydrogen in the propellant tank to a tolerable level in order to minimize the vehicle system weight. Experimental data are not yet available that define the propellant flow in the tank so as to correlate propellant temperature rise with tank heat input. Therefore, it was assumed that a shield would be required which reduces the total tank heat input by 90%.

Before designing the shield, it was necessary to define the magnitude and distribution of heat deposited in an unshielded tank. Three processes of heat deposition in liquid hydrogen were considered: core gamma ray interactions, fast neutron elastic scattering, and the capture gamma reaction with the emission of a 2.23 Mev gamma ray.

Illustrated in Figure 1 is a scaled drawing of the unshielded propellant tank with the reactor core, reflector and core top support plate in position. This configuration illustrates a 37.5° angle tank. If one visualizes the lower section of the tank as the frustrum of a cone, the apex of which is located at the center of the reactor, the major base of the cone is equal to the tank diameter (30 feet); and the minor base is located 8.5 feet above the core center. The tank angle, θ , is then half the angle of the cone.

Throughout this study it was assumed that a KIWI B-1 type core would be used for the NERVA mission generating 1120 MW of thermal power and operating for 20 minutes. The radial power distribution within the reactor was considered flat, while the axial power distribution was assumed to be a skewed cosine distribution.

Tank heat input data were calculated for three different tank angles of 25° , 30° and 37.5° . Gamma energy fluxes were obtained along the plane area subtending the tank from the center of the core using Program 14-0. This program evaluates point-to-point attenuation kernels and integrates over the cylindrical source volume in performing reactor-shield penetration calculations. Neutron energy fluxes were obtained by normalizing multigroup one dimensional diffusion data to the fast neutron data computed by Program 14-0. The total heat input to each tank was obtained by integrating the normal component of the total energy flux over the plane area. The normal component was obtained by multiplying the flux by the $\cos \alpha$ determined by the R, Z location of each detector.

Results are shown in Table I for three tank angles.

TABLE I
HEAT INPUT DATA FOR THREE TANK ANGLES

Heat Input, MW	Tank Angle		
	25°	30°	37.5°
Core Gamma	0.33	0.46	0.66
Neutron	0.07	0.095	0.13
Capture Gamma	0.24	0.33	0.45
TOTAL	0.64	0.885	1.24

This analysis assumes that all of the incident energy flux is absorbed in the tank, that all the neutrons that reach the tank will be thermalized and produce a 2.23 Mev gamma ray, and that all the secondary gamma rays are subsequently absorbed. Studies are now in progress to determine the per cent of gamma rays that might escape the tank, and to determine a better distribution and effect of the capture gamma rays.

The above data indicate that 52% of the total heat is due to core gammas, 11% to neutron kinetic heating and 37% is due to capture gammas.

Since the shield specification is a 90% reduction in total tank heating, the following equation can be established:

$$P = 0.52 F_{\gamma} + 0.48 F_n$$

where

P	=	fraction of unshielded propellant heating
F_{γ}	=	ratio of shielded to unshielded heating due to core gamma rays
F_n	=	ratio of shielded to unshielded heating due to neutrons

If the fraction 0.52 and 0.48 should change drastically due to a more refined analysis of the tank heating problem, then the shield, of course, would also change. However, there was an immediate need for determining a basic criteria for the shield design. The above equation was therefore selected as a basis for the shield design.

With various thicknesses of shield materials positioned above the core top support plate, Program 14-0 was used to calculate gamma ray and neutron dose rates at a detector point located on the core midplane at the bottom of the tank. The shield extended radially to the outer edge of the core.

The parametric data thus generated consist of the attenuation factor for each shield material for neutrons and gamma rays as a function of shield material thickness.

Several values of the fraction P , defined above, were selected for the parametric study; namely, 0.2, 0.1, 0.07 and 0.04 which correspond to 80, 90, 93 and 96% center line attenuation. From the parametric attenuation data, values of the unshielded to shielded ratios for neutrons and gammas were determined for each material and were combined to obtain the values F_{γ} and F_n also defined above. Since, for configurations consisting of two materials, several shields could be selected that would result in a specific center line atten-

uation, the problem remained to determine the minimum weight shield for a given attenuation factor.

Presented in Table II are the weight calculations for a 96% center line attenuation shield consisting of Li H and steel.

TABLE II
WEIGHT CALCULATIONS FOR A 96% CENTER LINE ATTENUATION SHIELD

	Shield No. 1	Shield No. 2	Shield No. 3	Shield No. 4
Steel, cm	9	8.6	8	7.2
Li H, cm	15	17	20	25
Total, cm	26.7	28.4	31.1	35.8
% Steel	33.7	30.2	25.7	20.1
ΔL	14	15.7	18.4	23.1
Shield Weight (gm/cm ²)	82.4	80.7	78.1	75.4
Engine Weight (gm/cm ²)	9.1	10.3	12.0	15.1
Total Weight (gm/cm ²)	91.5	91.0	90.1	90.5

The four cases represent four different shield configurations consisting of Li H and steel. Notice that the total thickness does not equal the steel plus lithium hydride thickness. This is due to a 10% void fraction included to account for necessary coolant channels. The per cent of steel in the shield mixture is tabulated. The ΔL represents the increased pressure vessel and interstage vehicle length required for each particular shield. It was assumed that a 5-inch (12.7 cm) plenum above the reactor would be needed regardless of whether or not a shield was present. Thus, ΔL = the shield length minus 12.7 cm. The shield weight for each case is given. The engine weight = ΔL times the engine density of 0.653 gram/cm³. This density was derived from an aluminum pressure vessel weight of 17.4 lb/in, and an interstage sleeve weight and engine connection weight of 16 lb/in based on previous RIFT studies. An effective interstage weight factor for the nuclear stage of 1/2.7 was assumed. This weight trade-off factor is necessary since the interstage sleeve would not be carried for a full mission as would the shield. The total weight shown here is then equal to the shield weight plus the engine weight.

The total weight can then be plotted as a function of the per cent of steel in the shield material mixture to determine where the minimum shield weight occurs. The per cent steel at which the minimum weight occurs varies depending upon the desired attenuation factor. The minimum weight for a 96% center line attenuation shield occurs at about 27% steel, and for a 90% center line attenuation shield at about 17.5% steel. Given the total weight and per cent steel at which the minimum shield weight occurs, the shield weight and subsequently the shield thickness can easily be determined.

This same type of analysis was carried out for several material configurations. Results are shown below in Table III.

TABLE III
VARIOUS MINIMUM WEIGHT SHIELDS - 90% CENTER LINE ATTENUATION

Shield Material	Total Thickness, cm	Shield Weight (Gram/cm ²)	Total Weight (Gram/cm ²)
Li H - U	23.9	43.6	50.9
Li H - Steel	26.0	50.8	59.5
Be - Steel	26.0	51.2	59.9
L H ₂ - U	42.1	41.5	60.7
BeO	25.0	63.0	71.1
L H ₂ - Steel	37.4	56.7	72.8
Graphite - Boron	40.0	61.2	78.9
Be - Boron	38.1	63.4	79.9

The total shield thickness is given, as well as the shield weight and corresponding total weight which includes the engine weight. The Li H - Uranium shield appeared interesting from a weight viewpoint. However, uranium is toxic and required special handling facilities. In addition, both the lithium hydride and uranium would have to be placed within a containing material which would increase the weight. The container material itself should be included as a gamma shielding. Thus, the shield design would require an iterative design process where the mechanical designers would include canning and structure material, and the configuration reanalyzed to determine how much the shielding could be reduced. This appeared prohibitive from a time standpoint. The configuration of Li H - Steel was selected for the first NERVA shield design since it appeared more practical because of manufacturing technology and adaptability to the heated bleed engine cycle. In the heated bleed cycle it is advantageous to extract heat from the shield. The Li is an excellent heat source due to the n, α reaction. The steel container for the Li H was included as a gamma shield. The next configuration worthy of investigation appears to be a beryllium-steel shield. It shows evidence of promise but more extensive calculations will be required to determine its value. The other configurations were either incompatible with the heated bleed cycle or resulted in heavier weights.

With the selection of the lithium hydride-steel shield, the problem remained to determine the thickness of shielding and the radius of the shield required to reduce the total tank heating by 90%. Two different shield radii were investigated; these two radii correspond to the outer radius of the core and the outer radius of the reflector.

A parametric family of curves was generated, shown in Figure 2, illustrating shield weight as a function of propellant heating. These data were obtained by calculating the total heating in the tank with shield thicknesses corresponding to 80, 90, 93 and 96% center line attenuation for the two different shield radii. Only two tank angles are shown here for simplicity. The zero weight corresponds to the unshielded condition. For a 25° angle tank it can be seen that either shield effects a 90% reduction in total tank heating. The weights of these two shields are approximately 1400 and 1800 pounds. The lighter of the two shields is that which extends to the reflector outer radius. For the 37.5° angle, where the shield radius equals the core radius, no amount of shielding effects a 90% reduction. With the shield extended to the outer radius of the reflector, a 2100 pound shield is applicable. This shield represents approximately a 96% center line reduction.

It then seemed expeditious to shape the shield to effect a weight savings. An iterative process was followed in shaping the shield for each tank angle pursued in this analysis. The final shaped shield weighed 1660 pounds for a 37.5° tank angle compared to about 2100 pounds for the unshaped case. This shield consists of the original cylinder covering the entire reflector diameter but with a diagonal slice removed at the corners. This diagonal slice begins at the core outer radius and projects to zero thickness of the reflector outer radius.

The Li H - Steel shield is now being built by Westinghouse Astronuclear Laboratory for delivery to Los Alamos Scientific Laboratory for a series of tests with the KIWI B-4 reactor core as the source.

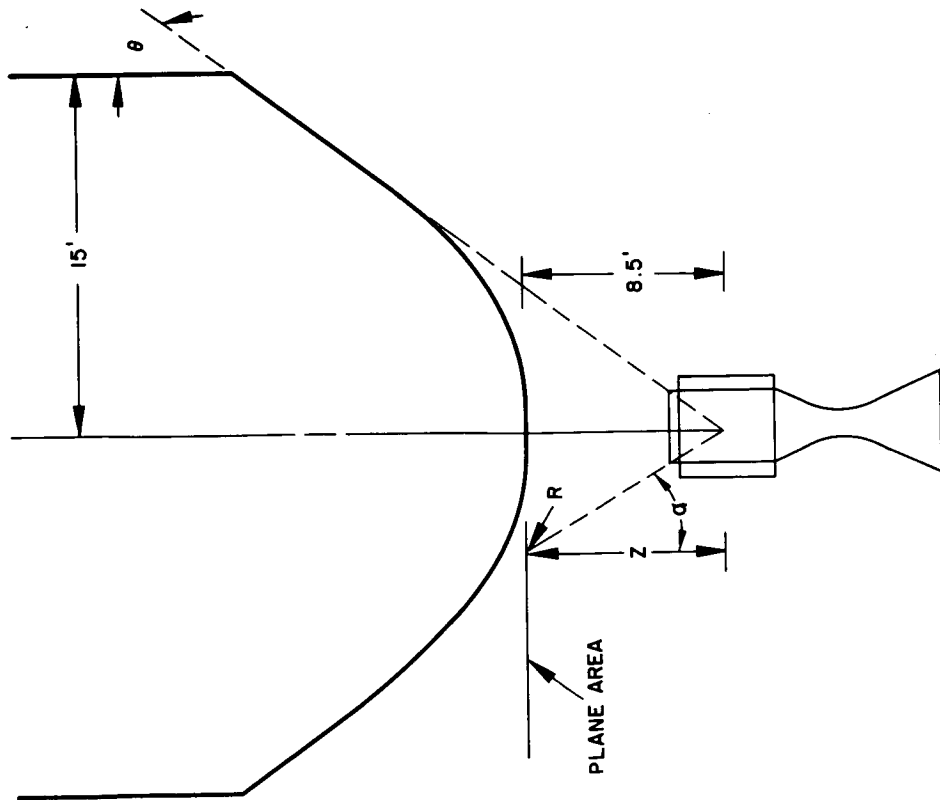


FIGURE 1
SKETCH OF LH₂ TANK GEOMETRY

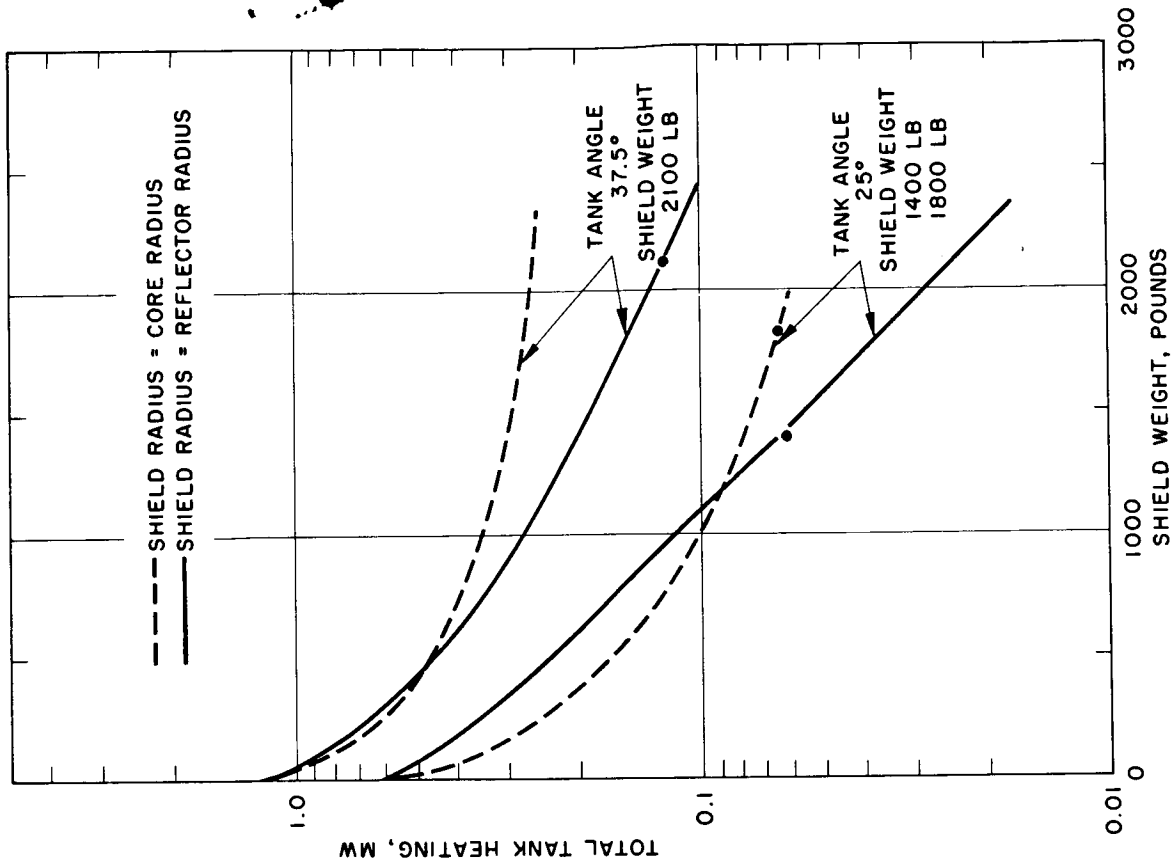


FIGURE 2
SHIELD WEIGHT VERSUS TANK HEATING

X 6 6 5 0 2 8 4

CALCULATIONS OF NEUTRON ACTIVATION DOSE RATES IN NUCLEAR ROCKET VEHICLES AND TEST FACILITIES

Robert M. Thornton and C. K. Butterworth
Lockheed-Georgia Company

[U]

INTRODUCTION

Static testing of nuclear rockets will result in neutron activation of the engine, the stage and any other materials and structures that are exposed to the neutron leakage during a test. The magnitude of the gamma dose rates from activation must be considered in planning the test program, designing the test facilities and determining the feasibility of re-use of components in the test program.

We have performed calculations of the activation characteristics of alloys for RIFT applications, dose rates from the RIFT stage, the NERVA engine, and several versions of a static test stand. The current Lockheed RIFT stage design has been used and the structural design of the NERVA engine has been obtained from Aerojet reports. In calculating the neutron leakage of the NERVA engine, a KIWI B-1 core configuration with a 2200 pound reactor shield was used, assuming an 1120 MW power.

COMPUTER PROGRAM

The calculations have been carried out with an IBM-7090 computer program. The component to be investigated is divided into a large number of modules, each of which is subsequently considered as a point source of decay radiation. Input information to the program consists of:

- coordinates of each module centroid
- weight and types of alloys in each module
- fast and thermal neutron fluxes at the module centroid
- coordinates of the points at which the dose rates are desired

The program has built into it:

- alloy compositions
- thermal and fast neutron reaction rates per unit neutron flux
- isotope decay constants
- flux-to-dose-rate conversion factors

The dose rate contribution from each module is determined at the point of interest, accounting for spherical divergence, and the sum of all contributions is computed. The

program considers a total of 52 fast and thermal neutron reactions on 20 elements. For thermal neutron reactions the 2200 m/sec cross sections have been used and, for fast neutron reactions, effective cross sections measured in a U235 fission spectrum have been used. In determining the flux-to-dose-rate conversion factors, the decay scheme of each isotope has been considered.

As a check on the accuracy of the program calculations, a problem was set up to duplicate the experimental conditions under which an alloy irradiation was carried out at the General Dynamics-Fort Worth reactor facility. In this experiment, a number of alloys were irradiated and the gamma dose rates were measured as a function of decay time.

Figure 1 shows typical results of the comparison between measured and calculated values, where dose rates per unit weight are given vs. decay time. The curves represent measured values and the points are calculated.

The agreement for aluminum alloys, as typified by 1100 Al is excellent in both half-life and magnitude. The titanium alloys, as typified by RS-140 titanium showed good agreement, as did the high temperature alloys typified by Inconel-X. The 4340 steel calculations show a departure from the measured values in half life. The cause for this departure has not been isolated as yet, but the comparison is still within the desired accuracy of the program calculations.

RESULTS OF CALCULATIONS

The calculations of the activation of the NERVA engine, the RIFT stage and the static test stand have been made using flux profiles calculated with the GE 04-4 shielding program. In addition, Monte Carlo calculations were performed to estimate the thermal to fast flux ratio within the shadow of a 2200 pound NERVA shield.

ALLOY ACTIVATION CHARACTERISTICS

Calculations of the dose rate at one foot from one pound of an alloy have been performed for all alloys that have been considered for use in the RIFT program. The exposure location considered was along the conical portion of the stage propellant tank where the incident neutron flux is almost uniform, and engine operation of 1300 seconds at 1120 MW was assumed.

Figure 2 shows results for this location. Shown here is $R/HR-LB$ vs. decay time, and this offers a means of comparison of all alloys on a common basis. The relative ranking of the alloys is clearly a function of the decay time. The aluminum alloys, typified by 5456 Al, are relatively high in activity at short decay times, due to 2.6-hour Mn56. From 10 hours to about 1 week the dose rate is due to 15-hour Na24, produced mainly by (n,α) reaction on Al-27. The long-lived activities, which become controlling at about 1 week, are due to the $Zn64(n,\gamma)Zn65$ reaction and fast reactions on iron and titanium. The curve shown here is representative of most aluminum alloys considered, except 7075 and 7079 which are about an order of magnitude higher at long decay times due to their higher zinc contents. The activity of the titanium alloy A110AT is relatively low at short decay times, but is much higher than the aluminum alloys at long decay times. The activity at short decay times is due to the $Al27(n,\alpha)Na24$ reaction and (n,p) reactions on Ti46, Ti47 and Ti48. The activity at long decay times is due entirely to the same (n,p) reactions.

The AZ31B magnesium decay over the first week is due to 15-hour Na24, formed by Na23(n, γ)Na24 and Mg24(n,p)Na24 reactions.

The Inconel-X activity is about the same as the Mg and Al activities at short decay times, and initially decays with the 2.6 hr. half life of Mn56, formed by the Mn55(n, γ)Mn56 reactions. The 71-day half life activity from the Ni58(n,p)Co58 reaction becomes controlling at about 20 hours, and continues to govern the decay out to 10,000 hours.

STAGE ACTIVATION CHARACTERISTICS

Figure 3 shows typical results of the calculation of dose rates from the stage as a function of decay time following a 1300 second test at 1120 MW. The vehicle was divided into 1050 modules for this calculation. The point for which these dose rates are given is indicated on the figure. This point is considered to be representative of the points to which workers would need access in the stage disassembly and rework process after the hot engine has been removed. These dose rates show a rapid decay in the first week after a test, where longer-lived activities become controlling. Dose rates at this point are below 2.5 mr/hr at about 75 hours after a test.

The major contributor to the dose rates at short times is the propellant tank bottom which is composed of about 3000 pounds of 5456 Al. At long decay times the controlling activity is that from the two attitude control rocket packages, each of which is composed of 25 pounds of tantalum-tungsten, 55 pounds of stainless steel and 70 pounds of aluminum.

Figure 4 shows the buildup in the dose rate at one week after shutdown from the stage-less engine as a function of the number of tests. Two curves are shown - one for one month test spacing and one for two month spacing. For the one-month spacing the buildup approaches a maximum of a factor of about 2, and for the two month spacing a factor of about 1.5.

NERVA ENGINE ACTIVATION

For calculations of the dose rates from the NERVA engine, the engine was divided into 184 modules. Figure 5 shows gamma dose rates at the midplane of the NERVA engine at a distance of 2 feet from the pressure vessel for a 1300 second test at 1120 MW. The upper curve shows the dose rates from core fission products. This curve was calculated with the GE 04-4 shielding program and the Lockheed Perkins-King fission product program. Dose rates from the activation of the NERVA engine-less the core are shown in the lower curve. The decay is rapid in the first 100 hours where long half-lived activities become controlling. The activation dose rates at this point do not drop below laboratory tolerance, even out to 10,000 hours.

Comparison of the two curves shows that the activation dose rates are negligible as long as the core is still in the engine.

STATIC TEST STAND

Close attention must be given to activation in the design of the static test stand. Many tests must be performed on each stand and access is required to the test stand area shortly after removal of a tested stage in order to prepare for the next test. Therefore, the test stand must be designed to minimize activation dose rates shortly after a test and also to minimize the buildup in activity due to repeated tests.

We have analyzed several test stand concepts, one of which is shown in Figure 6. The essential features of this concept are:

- the stage is permanently attached to a dolly throughout its whole test lifetime
- the dolly with stage is transported to the test area on a trackway
- a split shield of water-filled stainless steel tanks is placed around the engine at the stage diameter in order to attenuate the leakage flux and thus minimize activation of the dolly and the surround test stand structure
- at the completion of a test, the split shield halves, which are the greatest source of activation, are moved away from the test stand area

Figure 7 shows the activation dose rates after a 1300 second test at a point on the concrete pad. The controlling activity is that from the split shield halves assumed to be moved back 200 feet. These dose rates do not include any contribution from fission products deposited in the exhaust duct. While a shield can be placed over the exhaust duct inlet before personnel enter the area, there still might be an appreciable dose rate contribution through this shield at points near the exhaust duct.

Figure 8 shows the buildup in the dose rate at one week after a test as a function of the number of tests. For a 1 month test spacing, the buildup approaches a maximum of a factor of about 4, and the 2 month spacing a factor of 2.

It was assumed for the purpose of computing the activation, that the split shield reduced both the thermal and fast fluxes by a factor of 10^6 . The dose rates from the dolly at points under and around the dolly range from 10^3 to 10^6 less than those from the stage alone.

FUTURE PLANS

All calculations to date have been for a completely transparent system, i.e., no self-shielding of the activation gamma radiation by large components has been accounted for. The resulting dose rates, therefore, are upper limits for the assumed fluxes. The departure of the dose rates from the stage-less engine from this upper limit should not be too great because of the thin skin structure of most of the vehicle and its components. However, the dose rates from the engine will depart considerably from these upper limits. We are currently preparing to use the activation program in conjunction with the GE14-1 shielding program to account for self-shielding.

Another area we are now studying is the effect on the dose rates of the difference between the NERVA neutron spectrum and the model used in these calculations.

COMPARISON OF CALCULATIONS AND MEASUREMENTS

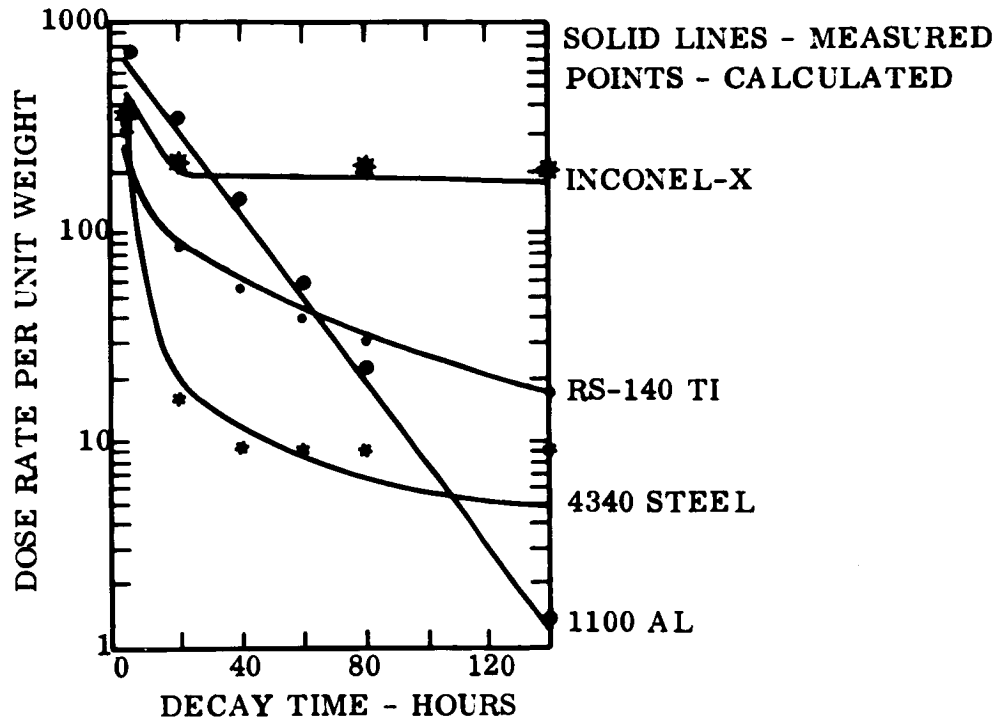


Fig. 1

ALLOY ACTIVATION - TANK BOTTOM 1300 SEC TEST

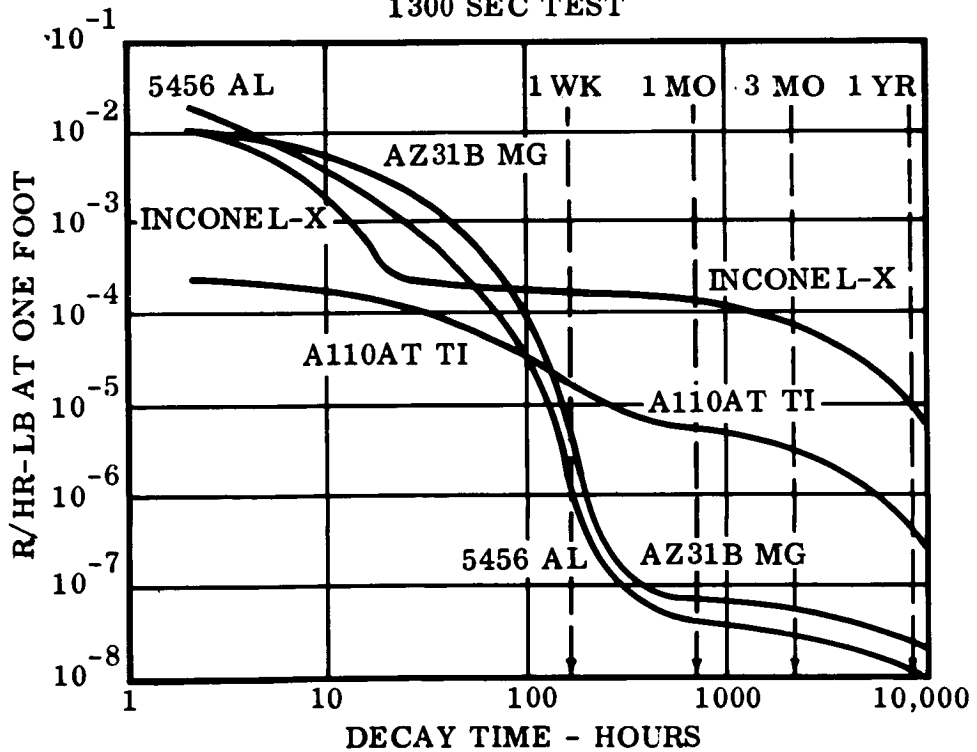


Fig. 2

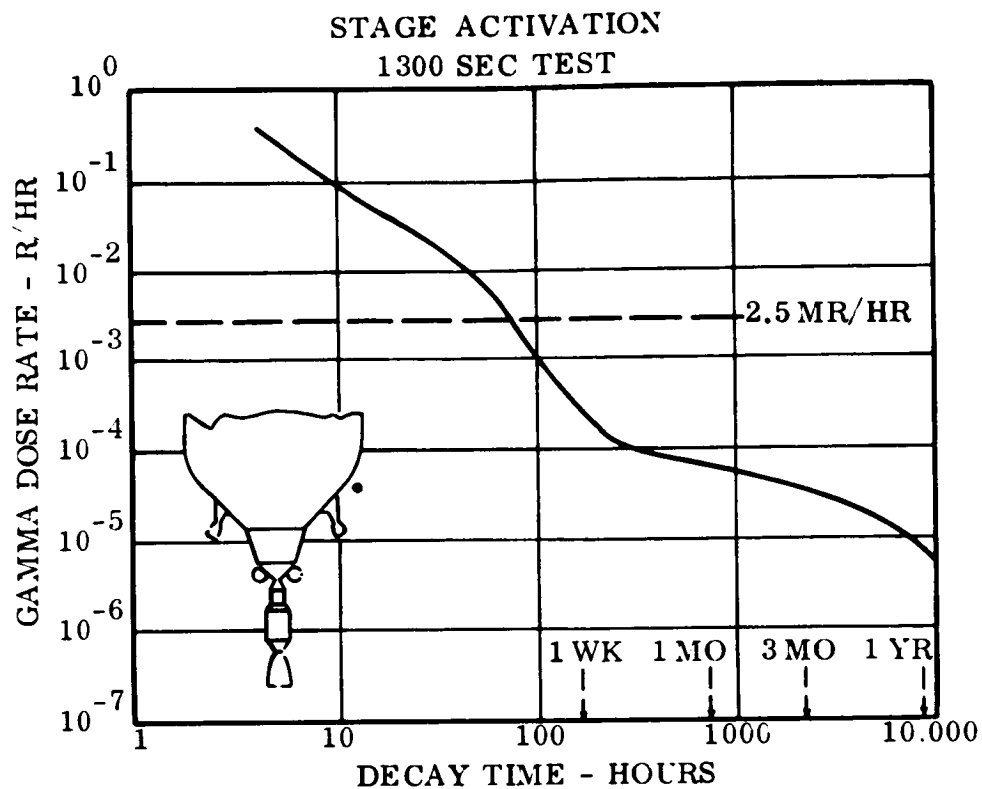


Fig. 3

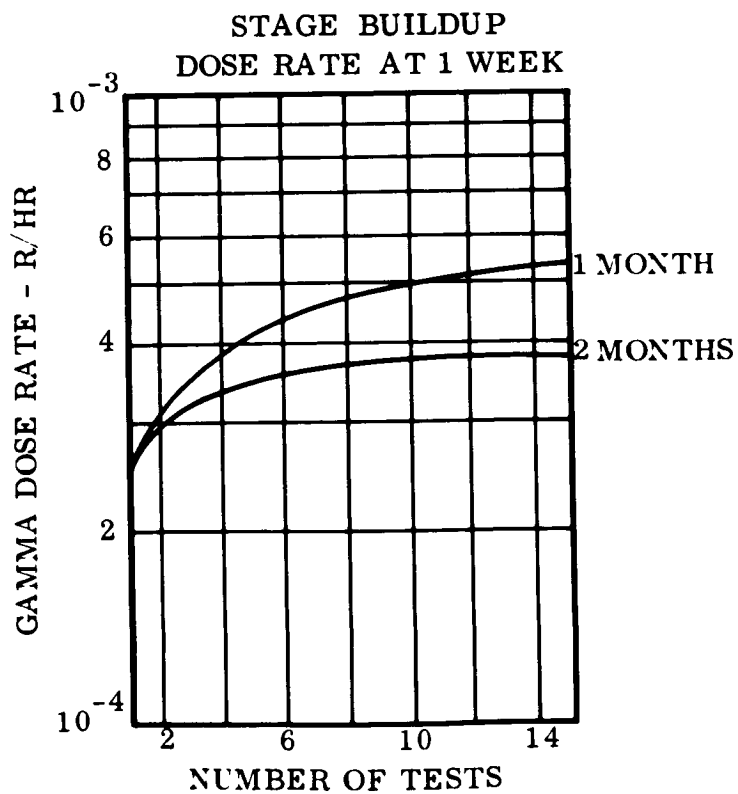


Fig. 4

NERVA ACTIVATION AND FISSION PRODUCT DOSE RATES 1300 SEC TEST

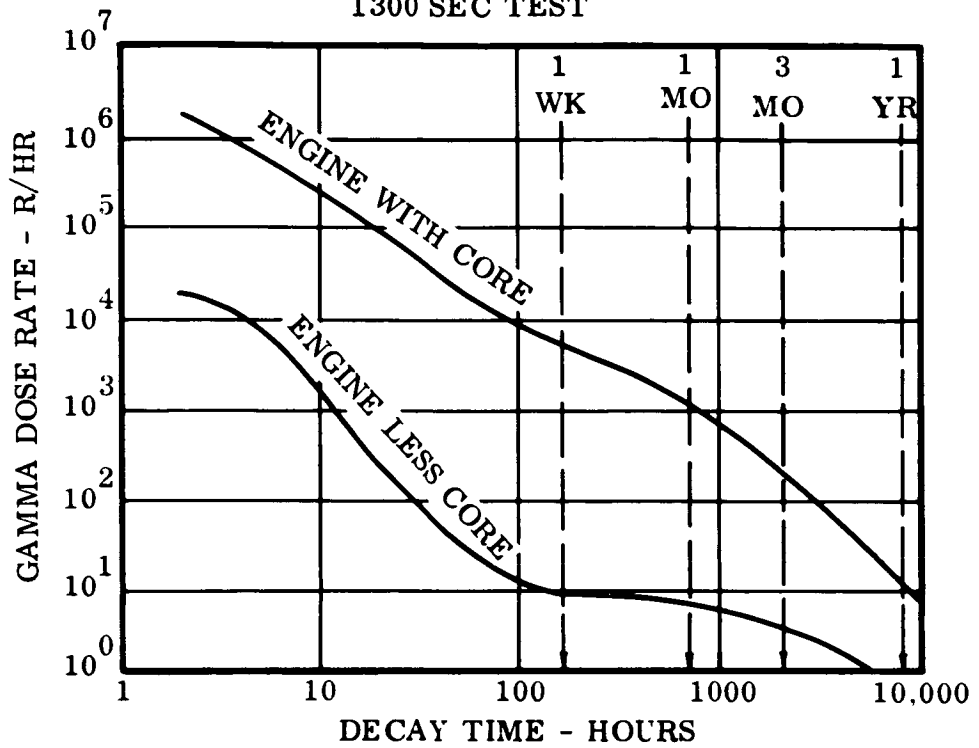


Fig. 5

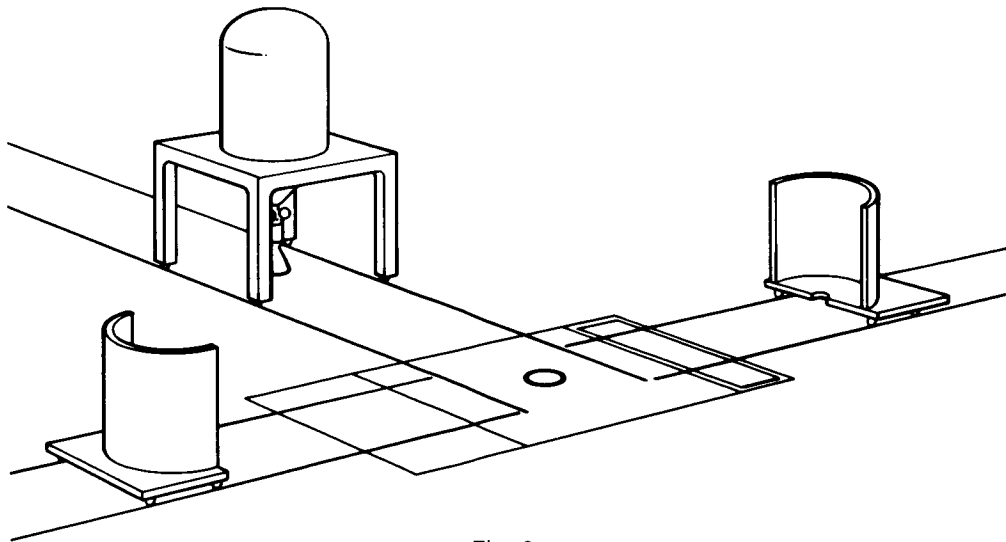
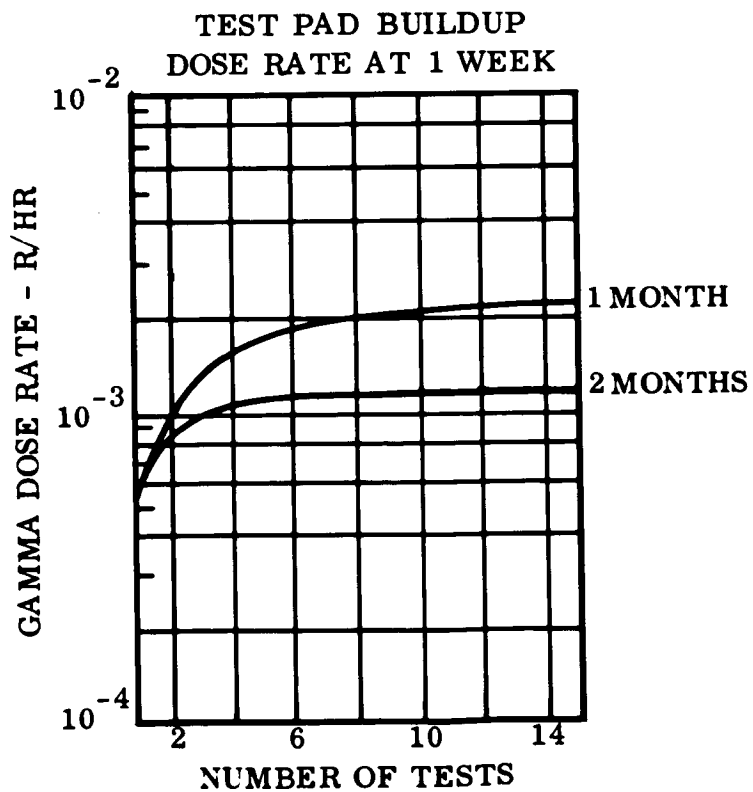
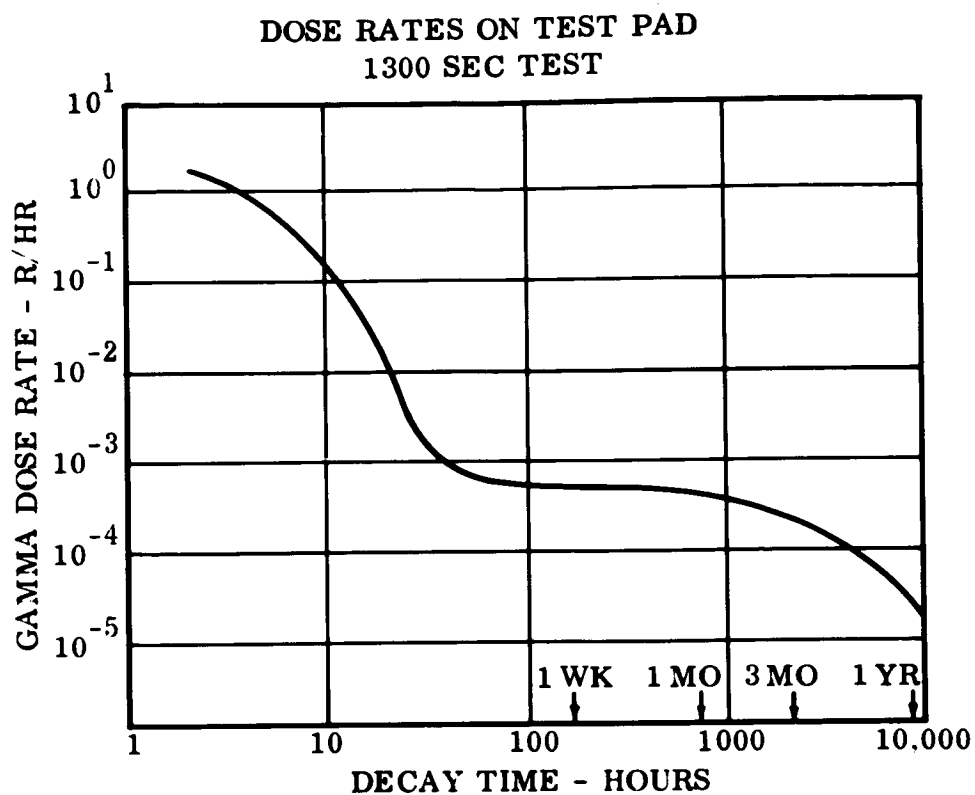


Fig. 6



NUCLEAR HEATING OF TORY II-C HAFNIUM CONTROL RODS

S. Kellman and A. Lorenz

Lawrence Radiation Laboratory, University of California
Livermore, California

[U]

A. Introduction

A nuclear heating analysis of the control rod assembly within the TORY II-C core was made to determine its power density at full power conditions. The use of hafnium as control poison and the selection of an asterisk rod geometry made a detailed study of the (n, γ) heating necessary. Because of the complexity of the heating process, a gamma-ray Monte Carlo code was developed for use in this analysis.

B. Analysis

A drawing of the control rod assembly, in Figure 1.a, shows the hafnium rod surrounded by a René-41 control tie-rod that is separated from the fuel by one layer of unfueled BeO tubes. Gamma-ray interactions are the major sources of nuclear heating in unfueled regions of reactors. The gammas arise from three principal processes: prompt fission, fission product decay and radiative neutron capture. In the present analysis of control rod heating, three "sources" have been considered: gammas from prompt fission, fission product decay and radiative capture originating in the core medium; radiative capture gamma rays originating in the hafnium rod; and radiative capture gamma rays in the René-41 control tie rod. These sources are referred to below as "external", "internal" and "tie-rod" respectively. The spectral distribution of each source was constructed from the latest experimental data available and expressed in terms of 30 energy groups, ranging from 0.01 to 10.0 Mev.

The gamma energy distribution in the control rod assembly was determined by means of a Monte Carlo code developed specifically for this analysis. The YOGI-R gamma-ray Monte Carlo code, written in FORTRAN for the IBM 7090, computes the fraction of gamma source energy deposited in the components of a system described by a cell; the sides of the cell are parallel to the three coordinate axes of a Cartesian coordinate system. A system of infinite extent in the Z direction is considered; in the X and Y directions, the cell is bounded by planes at which reflection is required. YOGI-R is equipped to handle a system of 50 zones, composed of 10 different materials. Absorption is tallied by zone and by energy group in which it occurs. An average incident energy "flux" is obtained by dividing the energy absorbed in a given group in a given zone by the appropriate macroscopic absorption cross section.

A series of problems were run for each of the three source zones considered. In order to determine the effect that each of the components surrounding the control rod has on the heating value, problems were run in which each component was added successively to the cell. In the more exact models, it was necessary to describe the rod by a cruciform because of the limitation on the number of zones handled by the YOGI code (see Figs. 1-b and 1-c).

Within the statistical accuracy of the Monte Carlo results, which ranged between 5% and 10%, the following properties were found to have little or no effect on the energy distribution analysis:

- 1) presence of the air gap between rod and fueled moderator regions,
- 2) presence of the unfueled BeO region surrounding the control tie-rod,
- 3) variations of the uranium loading in the fueled moderator,
- 4) presence of tie-rods in the vicinity of the considered assembly.

It should be noted that both the asterisk and cruciform descriptions of the control rod were found to absorb comparable energy fractions. The control tie-rod had an approximate 10% shielding effect on the external heating of the control rod.

The final results of this study, incorporating all corrections outlined above, are:

Source	Area in Cell (in ²)	Fraction of Source Energy Deposited in		
		Rod	Unfueled BeO	Hastelloy Tie Rod
External	7.29	0.089	0.061	0.019
Internal	0.0586	0.257	0.075	0.034
Tie Rod	0.0296	0.154	0.089	0.057

In this model the rod was represented by a cruciform having $1/8'' \times 1/2''$ blades; the BeO:U²³⁵ atom ratio in the moderator region was assumed to be 423:1.

C. Results

The average heating density of a component in Mw/ft³ per Mw/ft³ of local power density in the moderator region was obtained by multiplying the fraction of source energy; deposited in the component by the factor, $(E_\gamma/A_c)/(E_m/A_m)$; E_γ is the source energy available per fission in the source region considered, E_m the total energy produced per fission in the moderator (i. e. 191.5 Mev), A_c the area of the heated component in the cell, and A_m the area of the source region in the cell. Final heating power density values are given in Mw/ft³ in solid, hot component material normalized to Mw/ft³ of average core power density. Normalization is based on the active hot core volume of 53.42 ft³. The anticipated power of the TORY II-C reactor is 510 Mw; the corresponding average core power density will be 9.55 Mw/ft³.

The contributions from the three sources to the total heating density of a shim rod (i. e. one at R = 8.92''), averaged over the total insertion length of 40'' is:

	\bar{H} (Mw/ft ³ per Mw/ft ³)
External gamma source	0.93
Internal (n, γ) source	1.16
External (n, γ) source (from René-41 tie rod)	0.14
Total average heating density	<u>2.23</u>

The compound error in the nuclear heating calculations is approximately $\pm 20\%$. The statistical uncertainty of the Monte Carlo problems was less than $\pm 10\%$; additional errors arising from the uncertainties existing in the input quantities for both gamma and neutron heating, are approximately $\pm 10\%$.

The axial distribution of the total heating density was compiled from the individual contributions described above, each modified by its proper axial dependence, and is given in Figure 2.

Independent heat transfer calculations showed that for the conditions treated, the hafnium control rod attains peak temperatures of approximately 1600°F.

The foregoing analysis treated fully inserted rods (i. e. 40" into reactor). However, the expected mode of high power operation is one in which the shim rods will project approximately fifteen inches into the reactor. This corresponds to $\Delta k_{\text{rods}} = -0.03$. Therefore the peak power density will, in normal TORY II-C operation, exist at the rod tips and should be approximately 2.2 (Mw/ft³ of solid hafnium)/(Mw/ft³ of average core power density). The comprehensive treatment reviewed above allows one to estimate the hazardous condition which might arise if a single shim rod were fully inserted at high power levels.

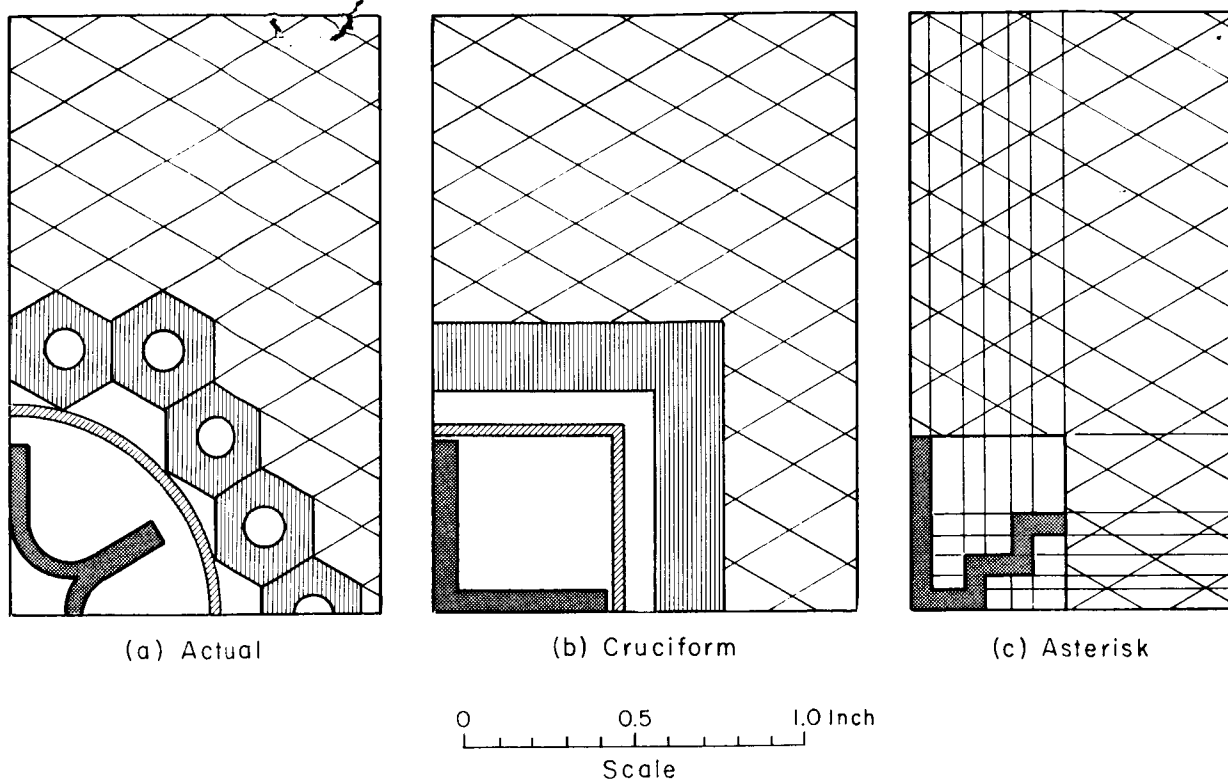


Fig. 1. Drawings of control rod assembly: (a) actual assembly; (b) cruciform description used for YOGI code; (c) asterisk description.

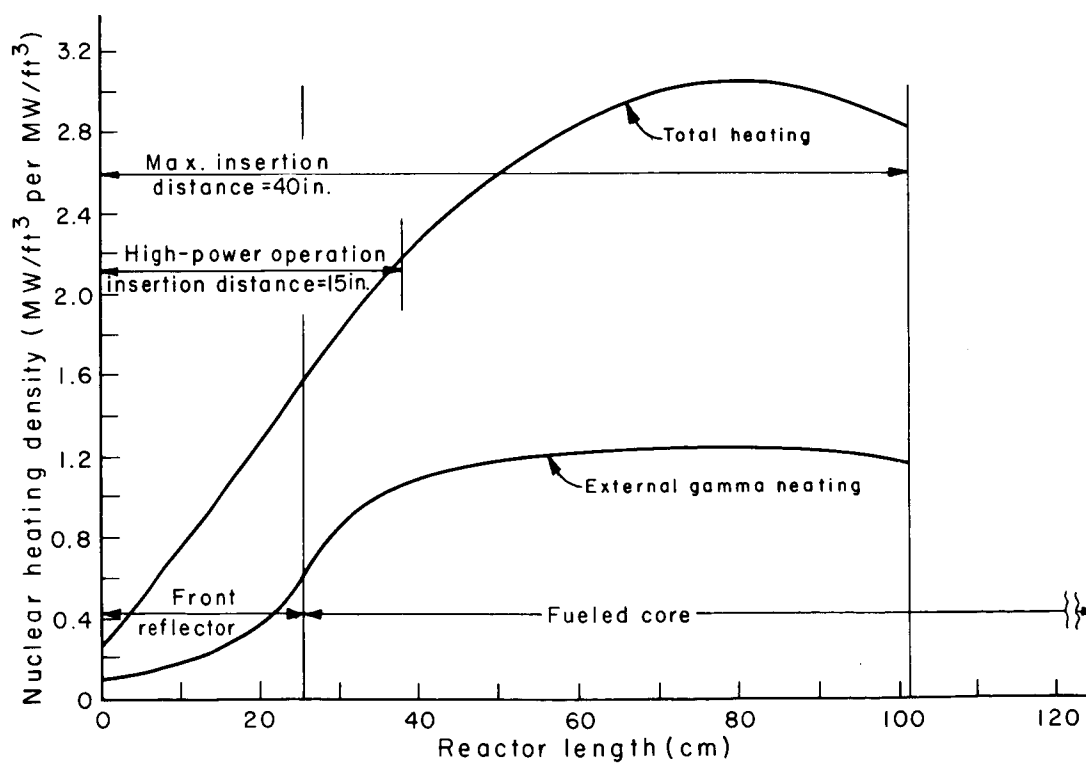


Fig. 2. Nuclear heating of Tory II-C hafnium control rod as a function of axial position.

X 66 50286

NEUTRON AND GAMMA ANGULAR LEAKAGE CALCULATION OF A KIWI-B REACTOR

[U]

By Arthur D. Prescott
Research Projects Division
George C. Marshall Space Flight Center

The reactor gamma number flux density and the reactor neutron (prompt neutron) number flux density are machine calculated for a full power operation of a 1000 MW KIWI-B1 reactor as a function of angular position around the unshielded reactor at 1.5 meters and 4.5 meters from the fission center of the core, using moments method differential energy spectra data. The reactor core is divided into 216 volume elements; and the neutron number flux density, gamma number flux density, neutron dose rate, and gamma dose rate are calculated using a Convair-Ft. Worth code known as D-53. This code uses the infinite media neutron and gamma moments method data generated by Nuclear Development Associates [2, 3].

The calculated gamma flux densities are compared with Monte Carlo leakage calculations of the magnitude of the gamma current densities carried out by Dr. Glen Graves of Los Alamos Scientific Laboratory [1]. The gamma source spectrum consists of prompt fission gammas, U^{235} capture gammas, and short period delayed gammas, and is identical with the Monte Carlo source spectrum. The gamma differential number spectra (or flux density) agree remarkably well with the Monte Carlo histograms of the magnitude of the gamma current density (Figures 2, 3, 4, 5). By definition the magnitude of the gamma current density is less than or equal to the gamma flux density at a non-reflecting boundary, and agreement is even better than indicated. The moments method calculations overestimate the low energy portion of the leakage spectra, as is to be expected.

The D-53 calculated gamma energy leakages are within 13% of the corresponding Monte Carlo calculations out the top and the side of the reactor (Figures 6 and 7). Agreement is better out the top of the reactor than out the side, or nozzle end of the reactor. Apparently there are two reasons for this disagreement. For the detector points at 180° many of the path lengths are oblique to the nozzle. The moments method data is more applicable when the source-detector line is perpendicular to the surface of a medium bounded in one dimension, i.e. the method underestimates the emerging integrated energy flux density at oblique incidence. At 90° , this effect is counter-balanced by the fact that the infinite media moments method data includes back scattering beyond the detector. This contribution becomes more important at large penetration depths, especially in low Z materials; and thus, at perpendicular incidence, the infinite media data, upon application to finite media, overestimates the emerging integrated energy flux density. The

average path length from the source points near the core surface through the Be and C reflectors is greater than the average path length from the source points near the top of the core through the aluminum support plate. The neutron and gamma leakage curves are four leaf clover shaped, shifted in the tank direction due to the off-center fission distribution, becoming more nearly circular at 4.5 meters. The gamma dose rate is roughly independent of angular position at 4.5 meters and is approximately 3×10^7 r/hr (Figures 8 and 9).

The neutron number spectra at 0° and 180° are similar in shape indicating that the aluminum support plate and pressure shell do not harden the spectrum to any extent. Comparing the neutron number spectra with Watt's fission spectrum, very rough fast neutron shielding calculations at 0° could be made assuming the leakage spectrum to be a fission spectrum (Figures 10, 11). The reactor leakage is highly peaked along the reactor-tank centerline due to the absence of top or bottom reflectors. The 4.5" of Be and 2" of carbon wrapped around the side of the core is a much better shield than the 6" of aluminum support plate above the core. Reactor neutron leakages of 2.5×10^{13} n/cm²-sec and 1.5×10^{12} n/cm²-sec were calculated out the top of the reactor at 1.5 meters and 4.5 meters respectively (Figures 12 and 13). The corresponding calculated neutron dose rates were 2×10^9 rem/hr and 1.50×10^8 rem/hr, respectively (Figures 14 and 15). However, the neutron leakage calculations are over-conservative probably within a factor of 2.

Changing the radial power distribution to a flat distribution reduced the fission intensity near the surface of the core thus reducing the neutron number leakage and gamma energy leakage by a maximum of 16%. Total 7090 machine time for the D-53 calculations was 30 minutes compared to approximately 18 hours for the Monte Carlo gamma calculations.

REFERENCES

1. Graves, Glen A.: "Leakage Spectra of a Typical 1000 MW Reactor," Private communication.
2. Goldstein, H.: "Calculations of the Penetrations of Gamma Rays," NYO-3075, June 1954.
3. Aronson, R., et al: "Penetration of Neutrons from Point Isotropic Mono-energetic Sources in Water," NYO-6269, December 1954.

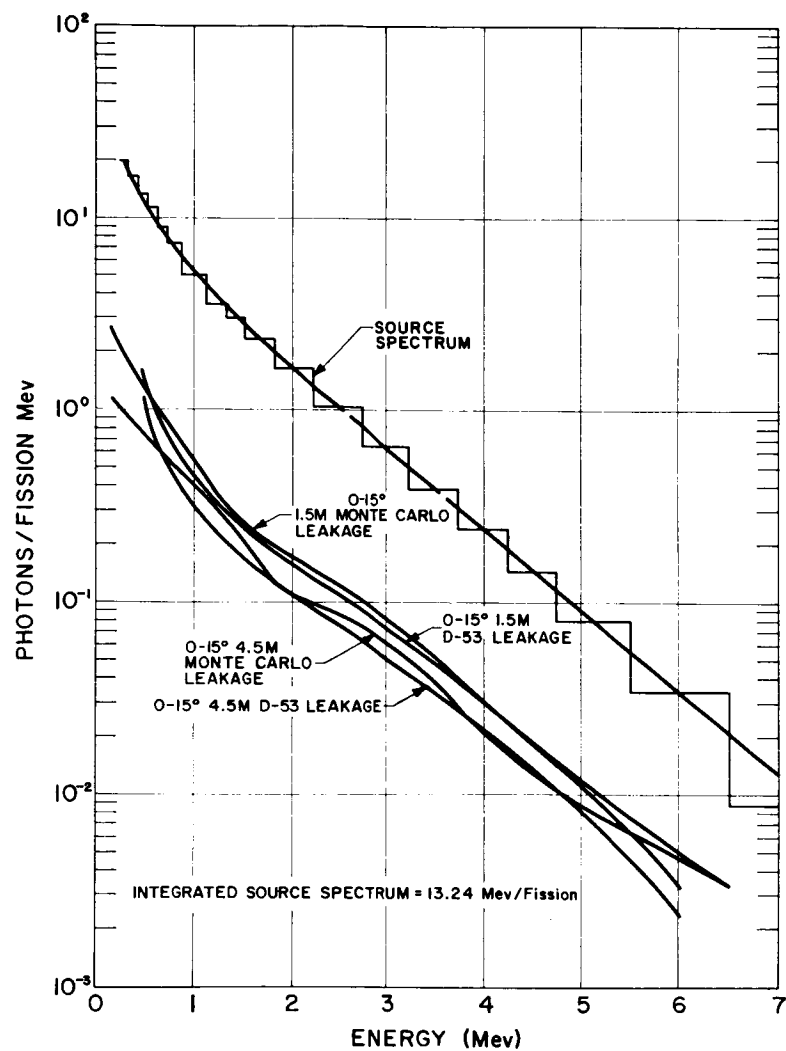


FIGURE 1. REACTOR GAMMA SOURCE SPECTRUM OF THE KIWI-B1
COMPARED WITH LEAKAGE SPECTRA

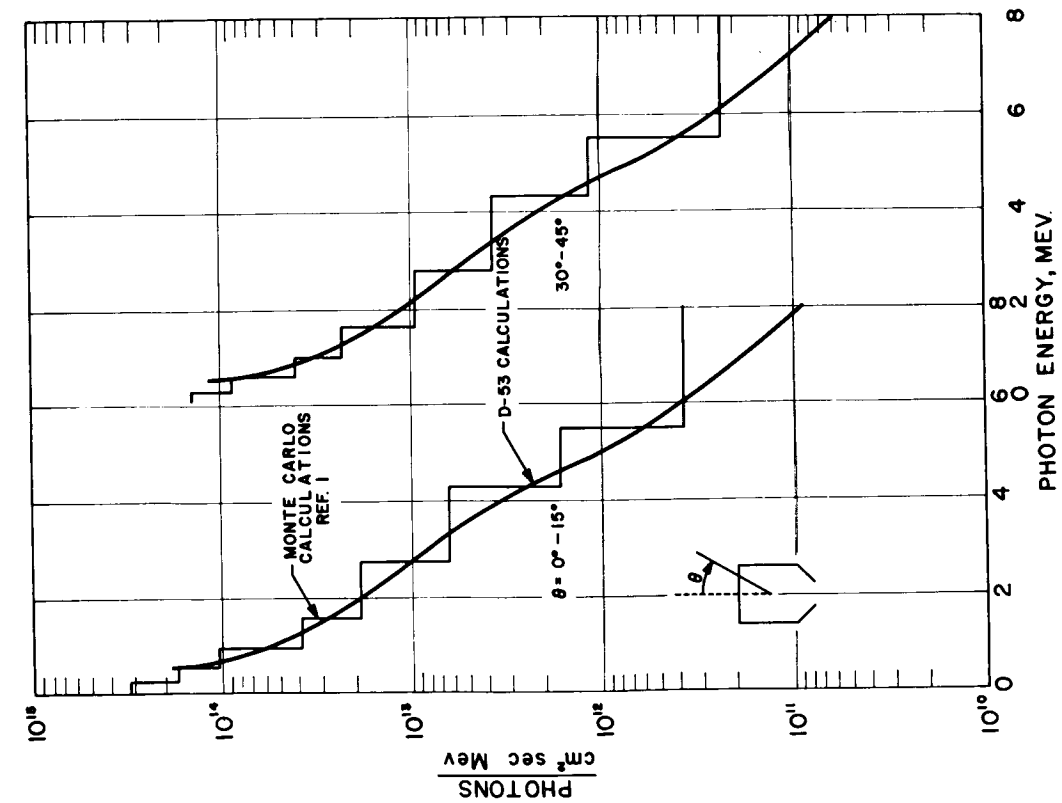


FIGURE 2. COMPARISON OF REACTOR GAMMA NUMBER SPECTRA AT 1.5 METERS FROM THE FISSION CENTER OF THE CORE

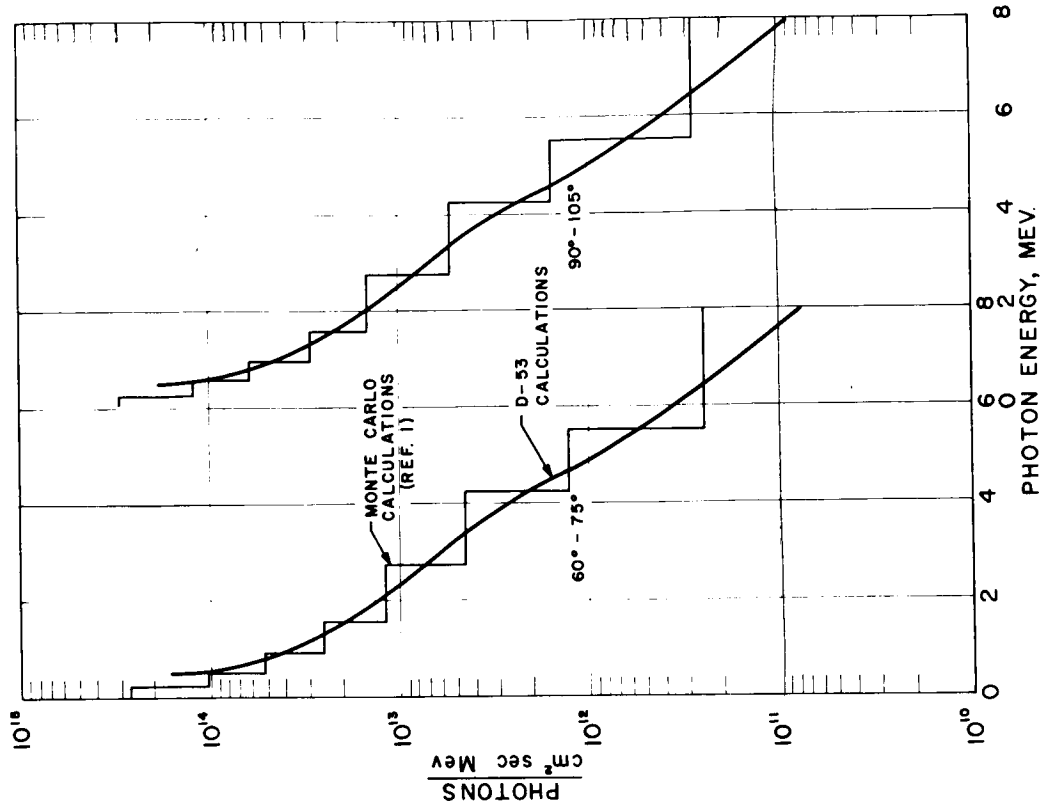


FIGURE 3. COMPARISON OF REACTOR GAMMA NUMBER SPECTRA AT 1.5 METERS FROM THE FISSION CENTER OF THE CORE

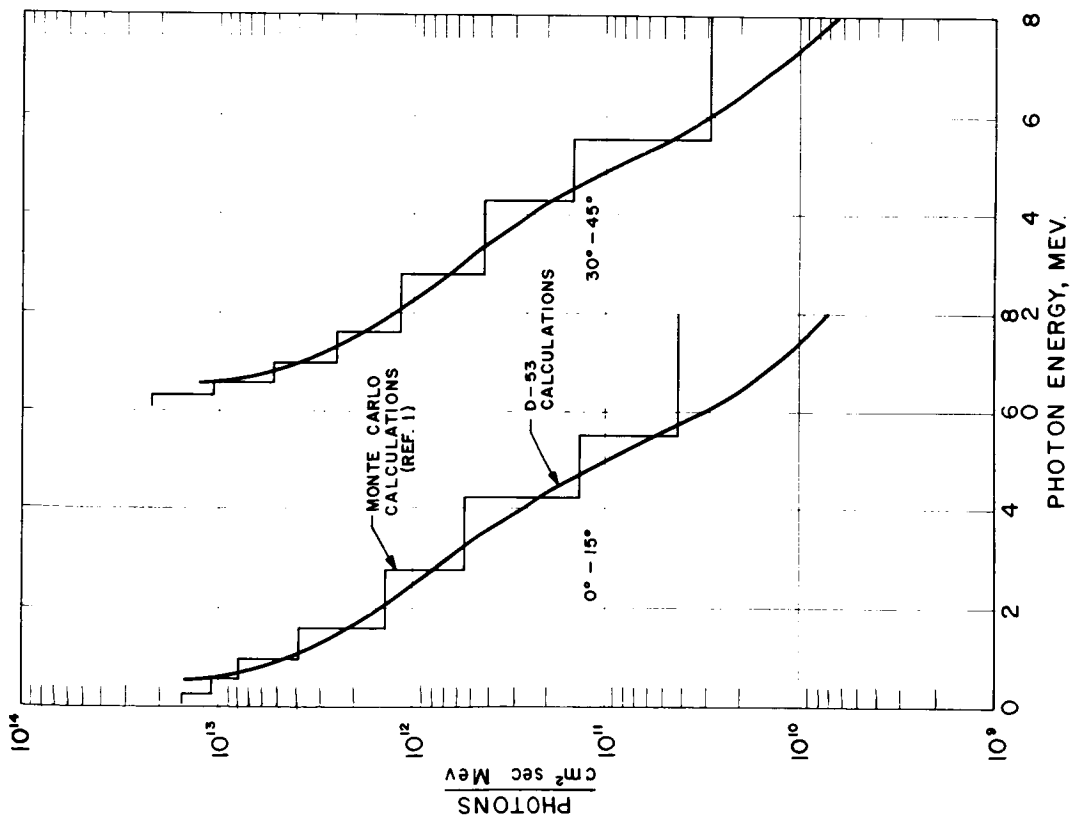


FIGURE 4. COMPARISON OF REACTOR GAMMA NUMBER SPECTRA AT 4.5 METERS FROM THE FISSION CENTER OF THE CORE

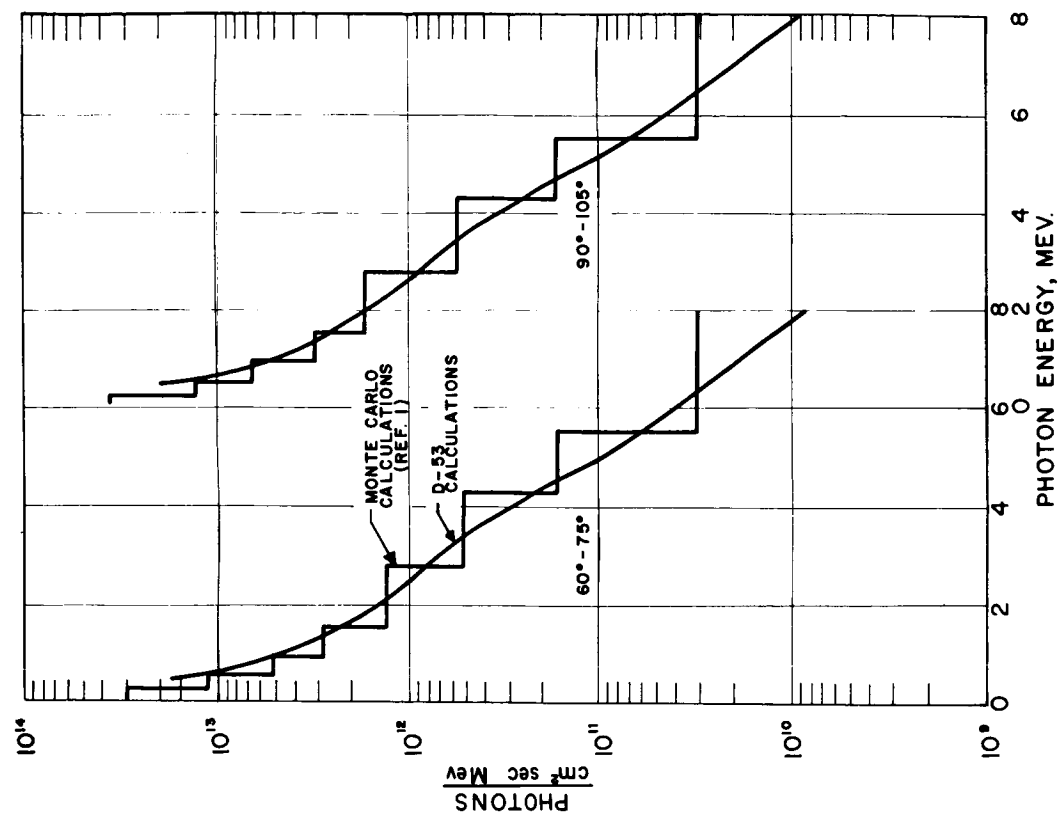


FIGURE 5. COMPARISON OF REACTOR GAMMA NUMBER SPECTRA AT 4.5 METERS FROM THE FISSION CENTER OF THE CORE

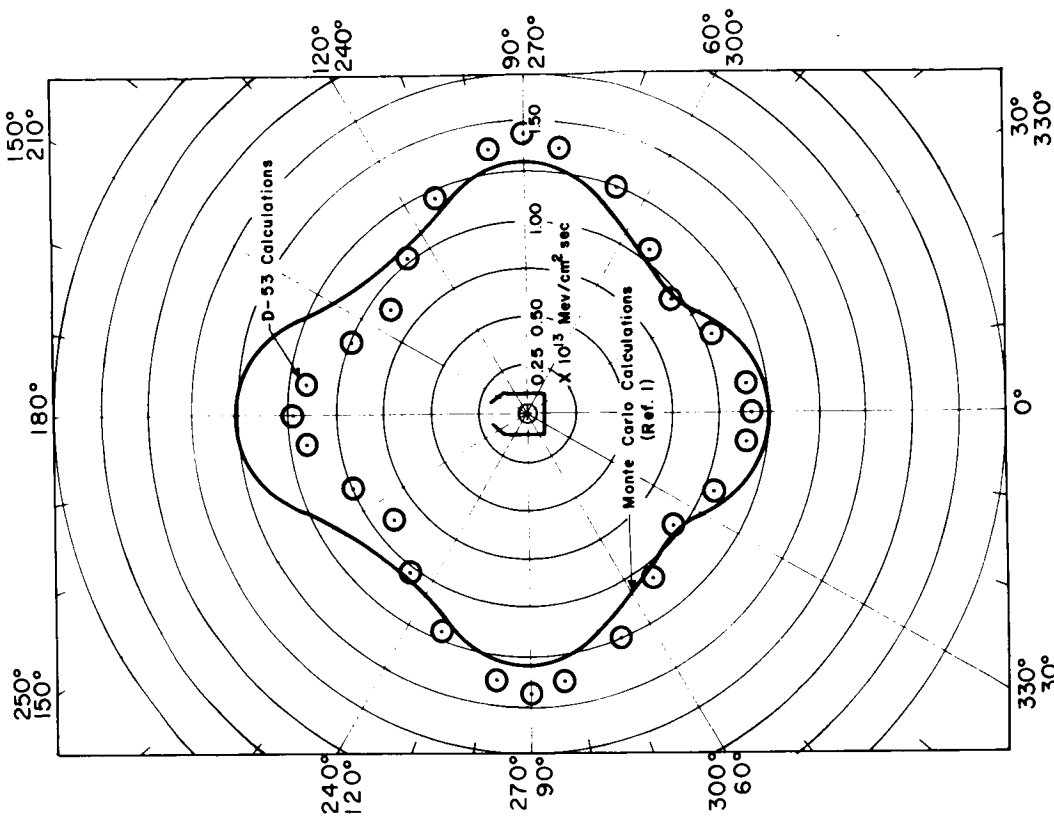


FIGURE 6. REACTOR GAMMA LEAKAGE (INTEGRATED DIFFERENTIAL ENERGY SPECTRUM, 0.5 \pm 8.0 MEV) 1.5 METERS FROM FISSION CENTER OF THE CORE VS ϕ

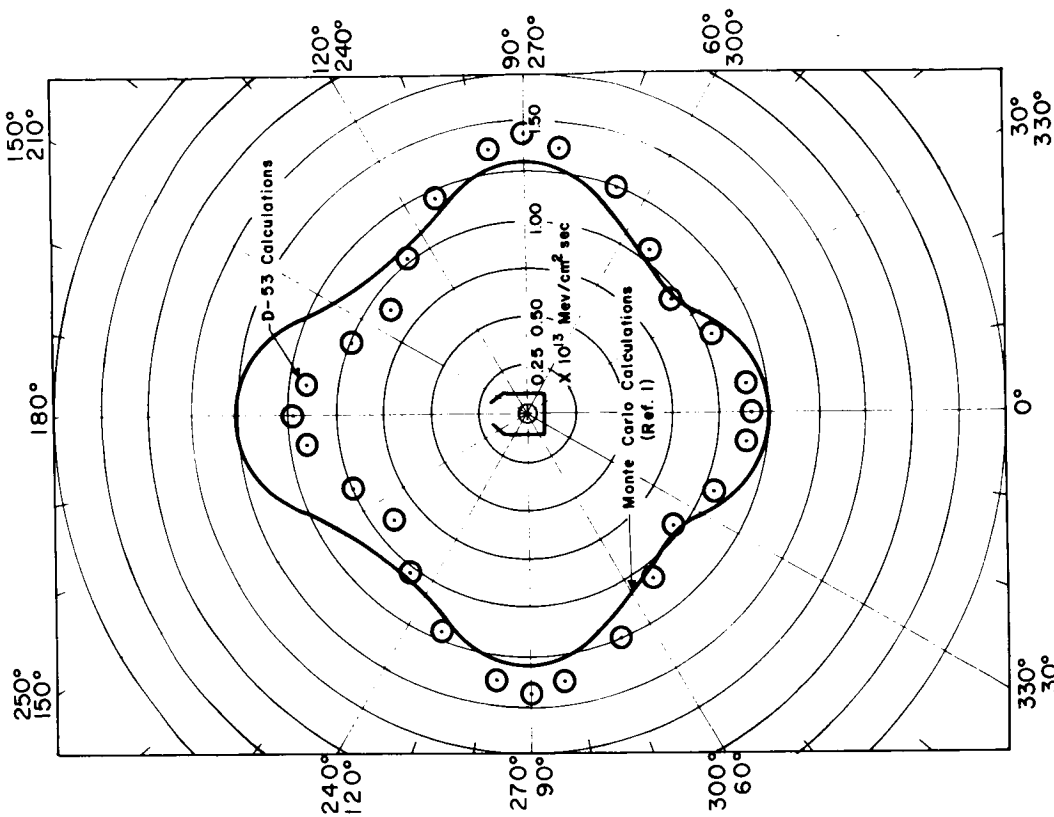


FIGURE 7. REACTOR GAMMA LEAKAGE (INTEGRATED DIFFERENTIAL ENERGY SPECTRUM, 0.5 \pm 8.0 MEV) 4.5 METERS FROM FISSION CENTER VS ϕ

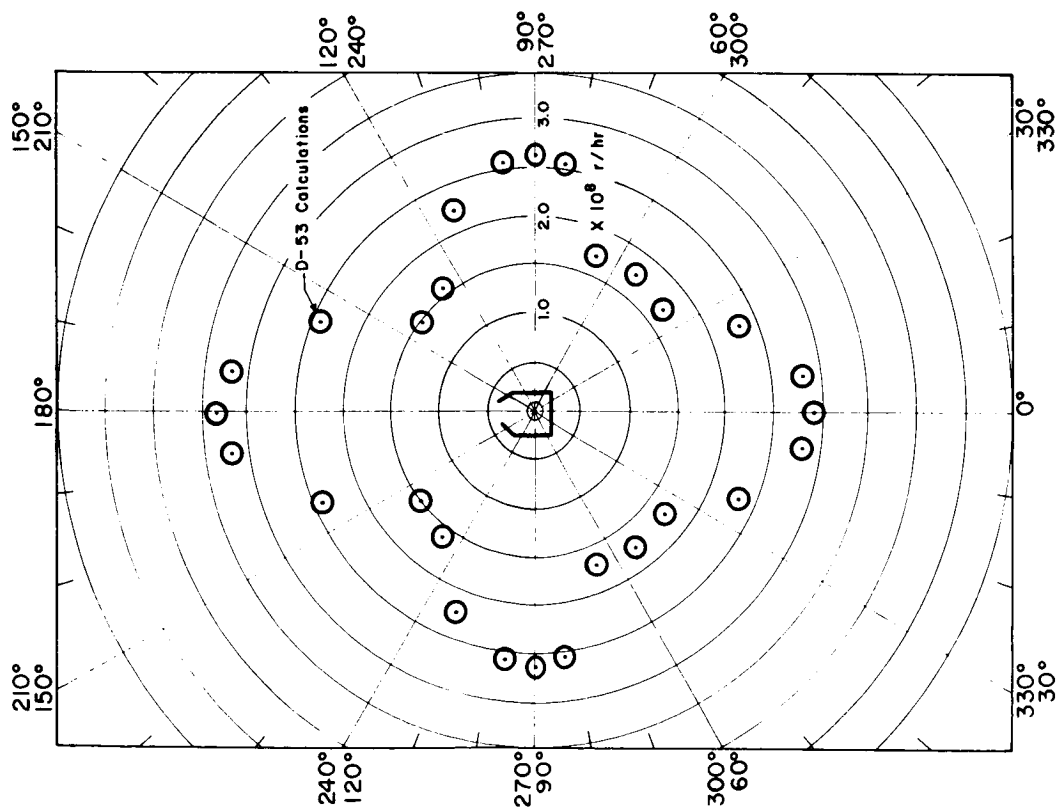


FIGURE 8. REACTOR GAMMA DOSE RATE 1.5 METERS FROM THE FISSION CENTER VS ϕ

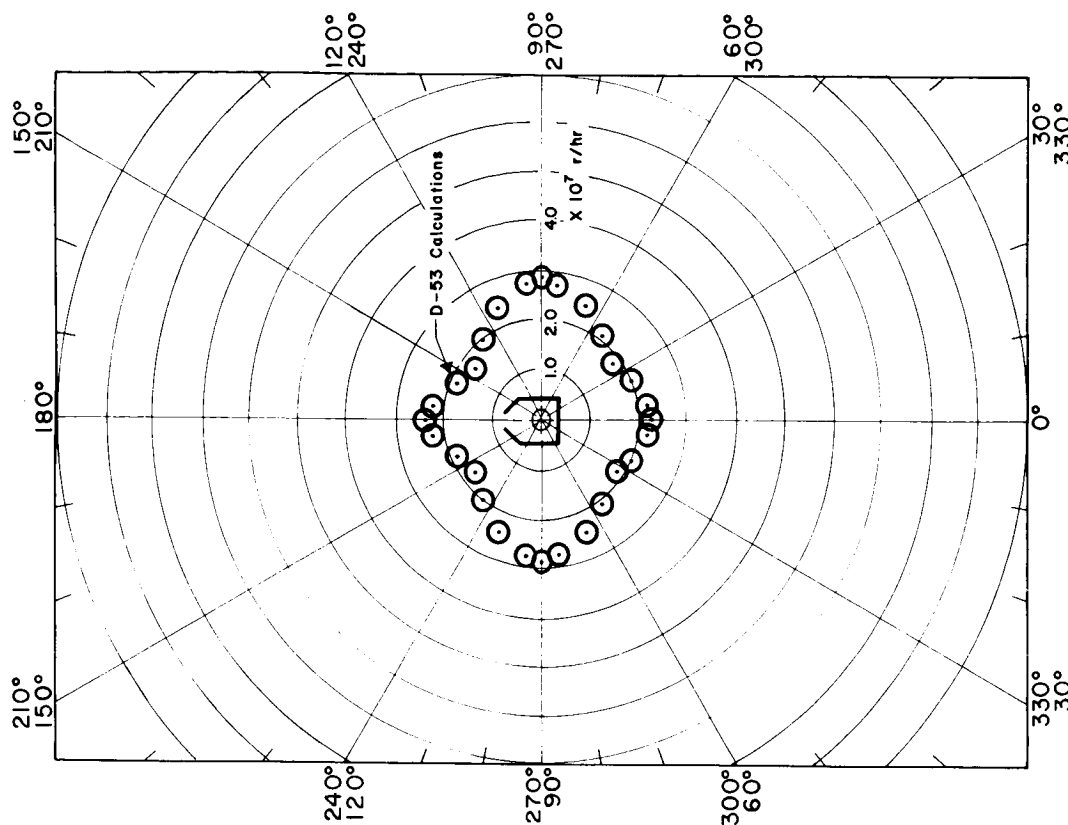


FIGURE 9. REACTOR GAMMA DOSE RATE 4.5 METERS FROM THE FISSION CENTER VS ϕ

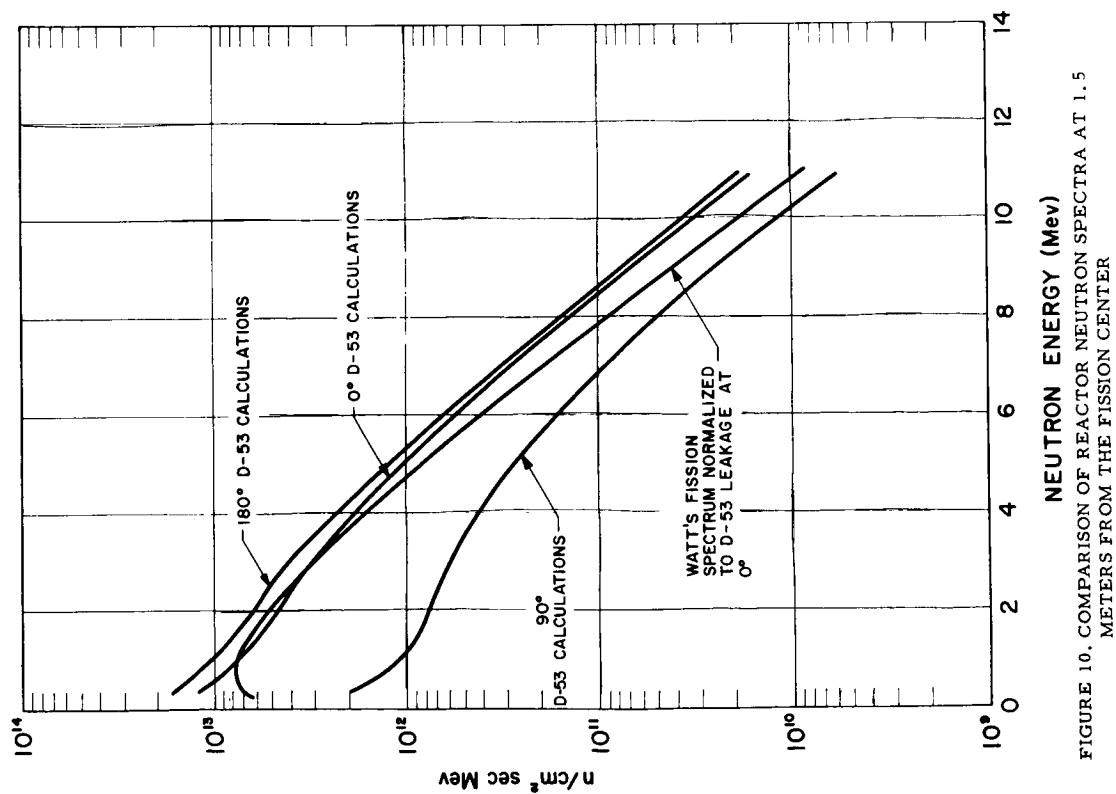


FIGURE 10. COMPARISON OF REACTOR NEUTRON SPECTRA AT 1.5 METERS FROM THE FISSION CENTER

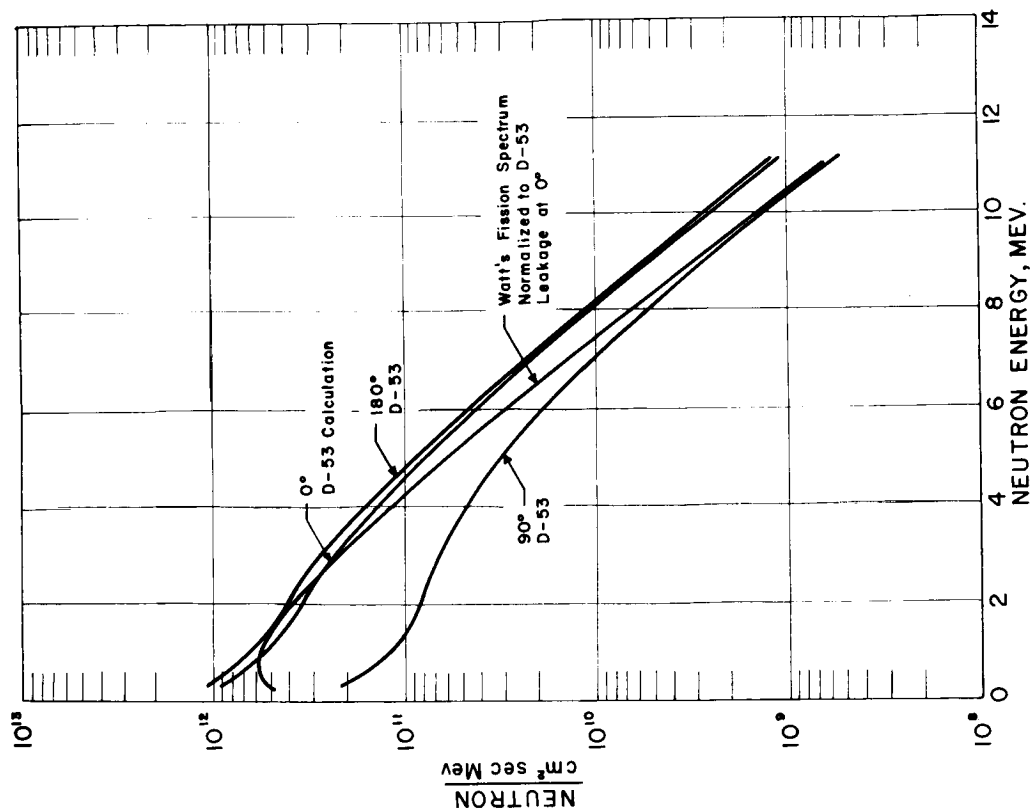


FIGURE 11. COMPARISON OF REACTOR NEUTRON NUMBER SPECTRA AT 4.5 METERS FROM THE FISSION CENTER

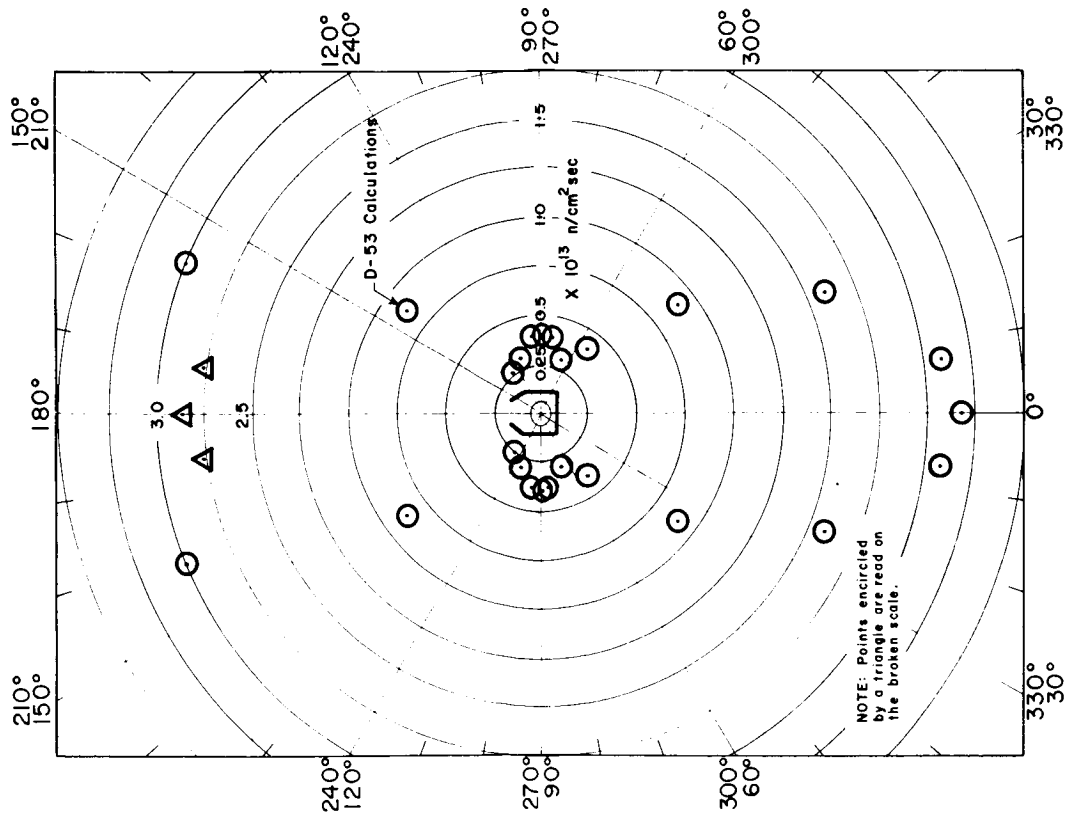


FIGURE 12. REACTOR NEUTRON LEAKAGE (INTEGRATED DIFFERENTIAL NUMBER SPECTRUM, 0.33 to 10.9 MEV) 1.5 METERS FROM THE FISSION CENTER VS θ

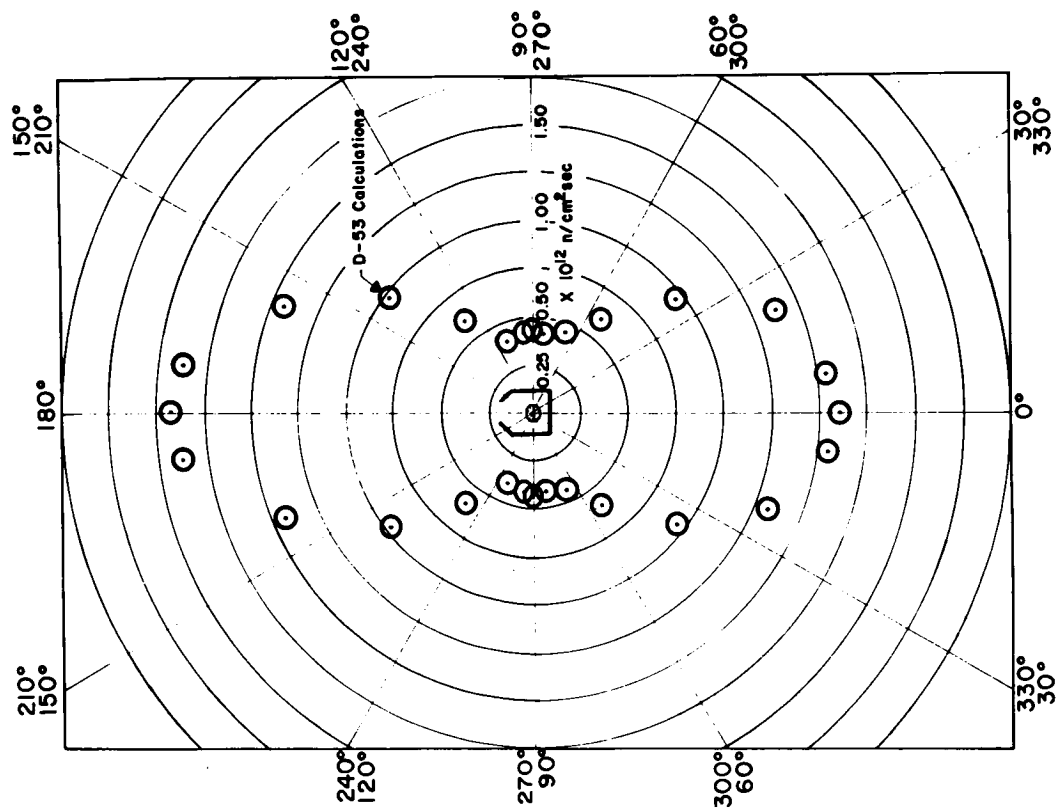


FIGURE 13. REACTOR NEUTRON LEAKAGE (INTEGRATED DIFFERENTIAL NUMBER SPECTRUM, 0.33 to 10.9 MEV) 4.5 METERS FROM THE FISSION CENTER VS θ

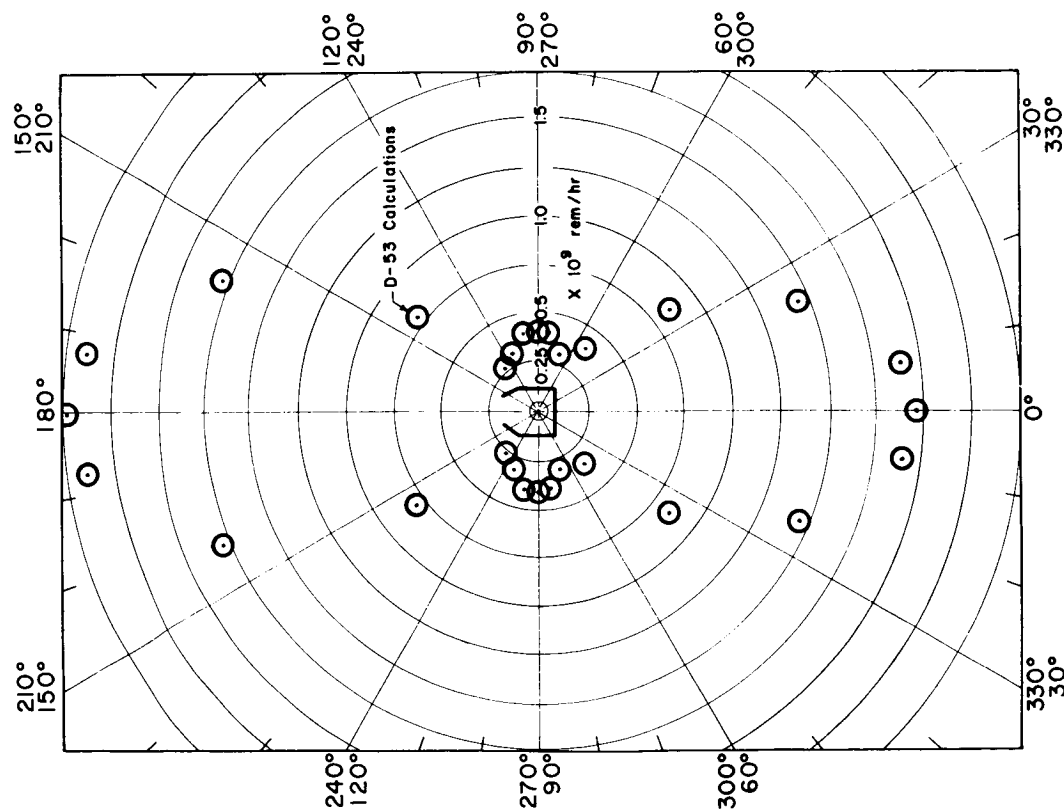


FIGURE 14. REACTOR NEUTRON DOSE RATE 1.5 METERS FROM THE FISSION CENTER VS θ

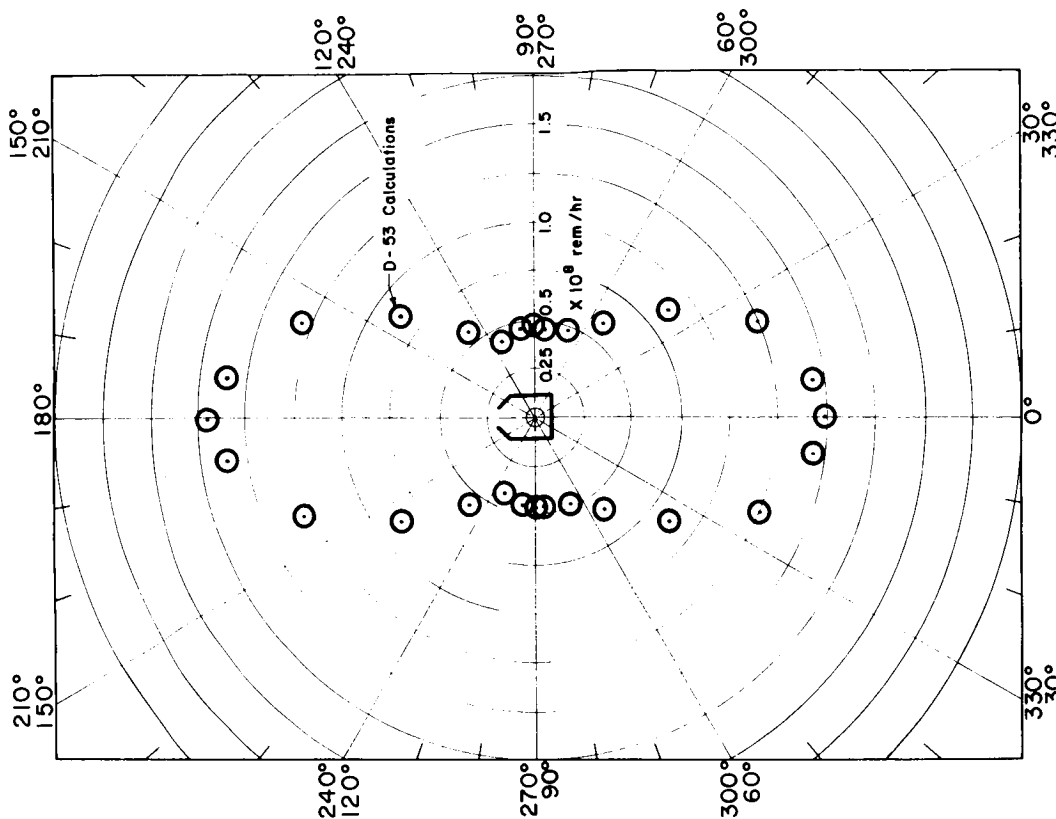


FIGURE 15. REACTOR NEUTRON DOSE RATE 4.5 METERS FROM THE FISSION CENTER VS θ

X 66 50287

NOVEL RADIATION CALCULATIONS ON ROCKET REACTORS

R. E. Malenfant
Los Alamos Scientific Laboratory
University of California
Los Alamos, New Mexico

[U]

Large numbers of localized and detailed calculations must be made on a system as complex as a flying reactor. It has been found that many of those associated with radiation can be readily handled with a general-geometry point-kernel computer program, QAD, even though the program was not specifically developed for such particularized calculations. Two examples which fall into this category are given here along with the method of approach and results.

Possible alleviation of local energy deposition in control materials prompted comparison of a material emitting gamma radiation upon neutron absorption with one which emits particles. Specifically, 20% (vol) Eu_2O_3 - 80% (vol) Al was compared with B_4C - Al as the control material. It was shown that the choice of a material such as the latter, which deposits its capture energy over a large volume, could result in reduction in the local energy deposition by a factor of ~ 20 .

Both calculations were performed by estimating the absorptions in the control material from DSN neutron transport calculations and determining the energy deposition from the reaction products. As indicated by the geometry of Figure 1, the Kiwi-B control rods consist of 12 beryllium cylinders, each of which has a 120° sector covered with a thin vane of the control material. (A 50 mils thickness of boral is presently employed). A cross-section of one rod and its immediate environment of the beryllium reflector is depicted in Figure 2.

Determination of the energy deposition from the B^{10} (n, α) reaction assumes that both reaction particles (α and Li^7) deposit all of their kinetic energy (2.3 mev) in the vane and that the energy deposited from the 0.5 mev decay gamma from excited Li^7 is negligible. For 1000 Mw reactor operation, the maximum energy deposited from reaction products occurs near the reactor midplane and amounts to ~ 840 watts/gm of vane material while an additional 15 watts/gm arises from core gammas and neutrons for a total of 855 watts/gm.

Gamma energy deposition from Eu_2O_3 was determined by mocking up one rod in the geometry of Figure 2 for a calculation with QAD. Several hundred source points emitting 6 gamma groups were used to represent the capture source in the vane. Results indicated 30 watts/gm deposited by reaction gammas and 15 watts/gm from core

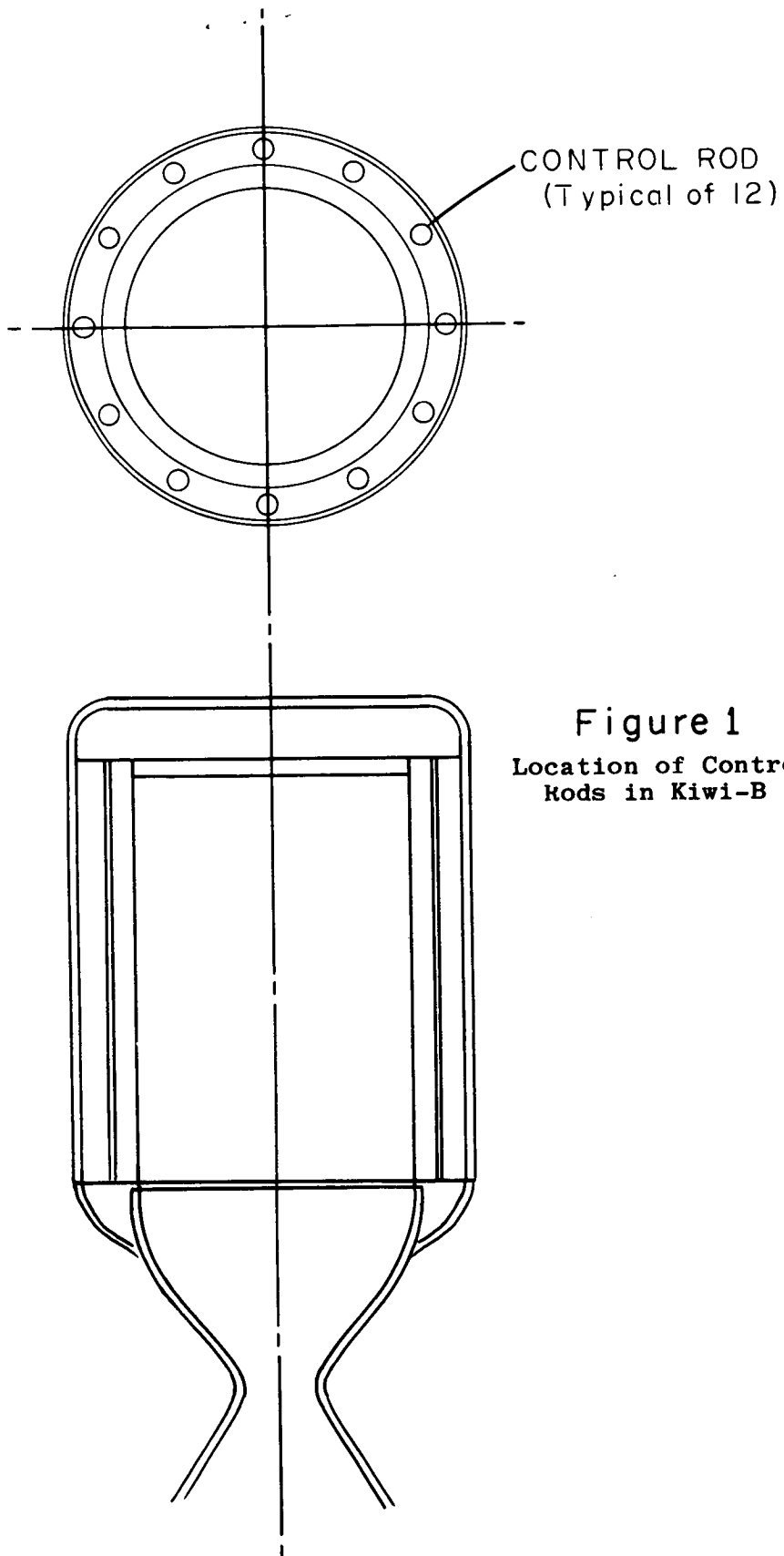
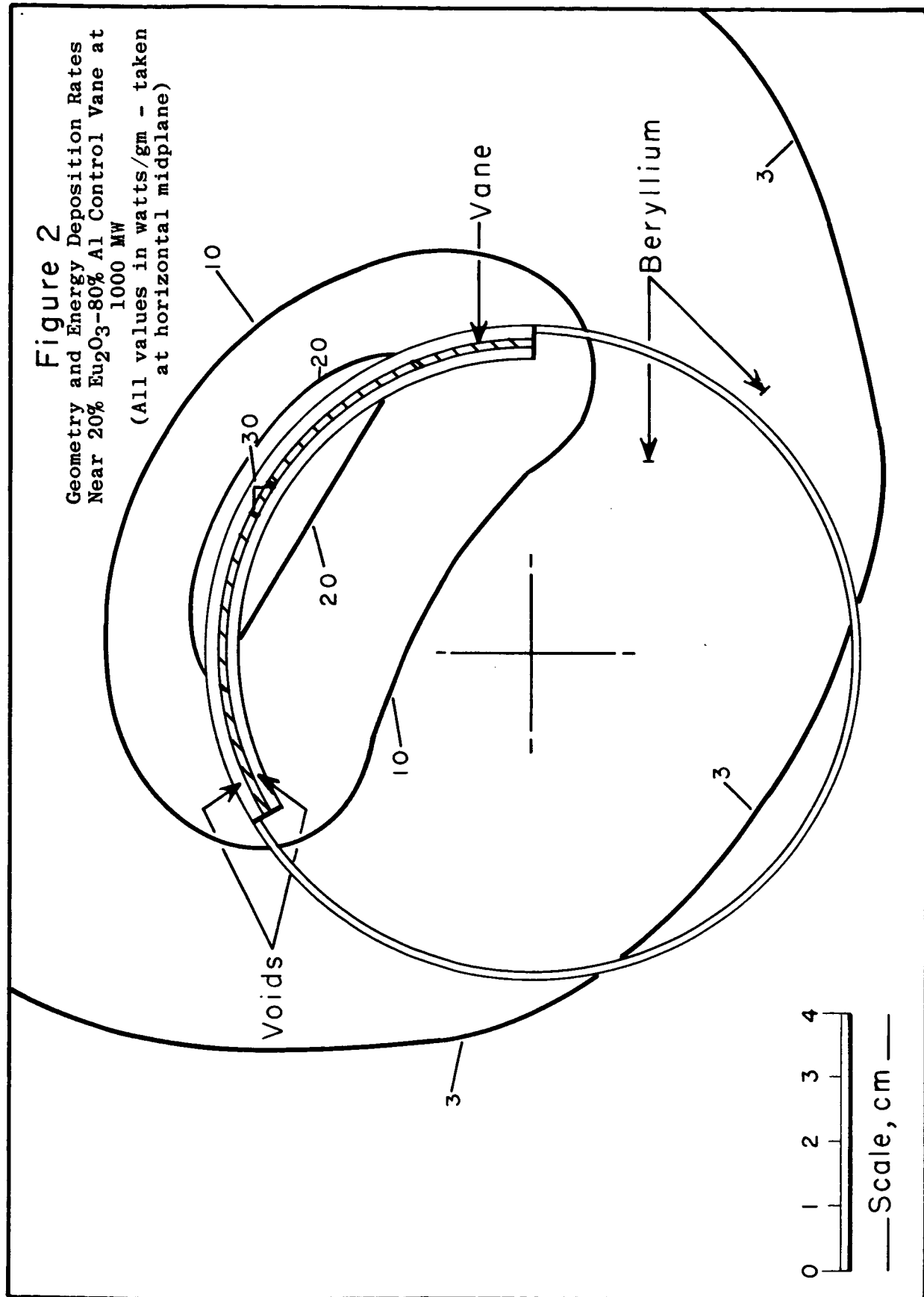


Figure 1
Location of Control
Rods in Kiwi-B

Figure 2

Geometry and Energy Deposition Rates
Near 20% Eu_2O_3 -80% Al Control Vane at
1000 MW

(All values in watts/gm - taken
at horizontal midplane)



gammas and neutrons, for a total of 45 watts/gm. The calculation was sufficiently refined to permit a very good determination of the energy deposition contours, which are indicated on Figure 2.

The postulated total neutron absorptions and vane thicknesses for these two representative vane-heating calculations were identical (0.23 n/fission and 50 mil thick vanes). While neutron absorptions would be expected to be constant for equivalent control rod worth, vane thicknesses would be expected to change upon changing the poison material, depending on the effective absorption cross section of the material used. Because of this, these results are reported in watts per gram in order to apply to any reasonable thickness of europium vane which might be considered.

Another calculation was made to estimate the photoneutron production rate in the beryllium reflector of a Kiwi reactor both during operation and post shutdown. Results were expected to be of importance for estimating post shutdown core heating due to photoneutron induced fissions.

The calculations were made by representing the geometry of Kiwi-B in a realistic manner through QAD. After determination of specific neutron formation rates as a function of position and energy dependent photon flux, totals were determined by integrating over the volume of the beryllium reflector. Using hundreds of source points, a 19 line gamma spectrum, and the energy dependent γ, n , cross sections of Jakobsen, (1) it took only 10 seconds per detector point to obtain the neutron production density. Results indicated a total of 4×10^{12} n/sec - Mw during reactor operation and values as indicated in Figure 3 after shut down.

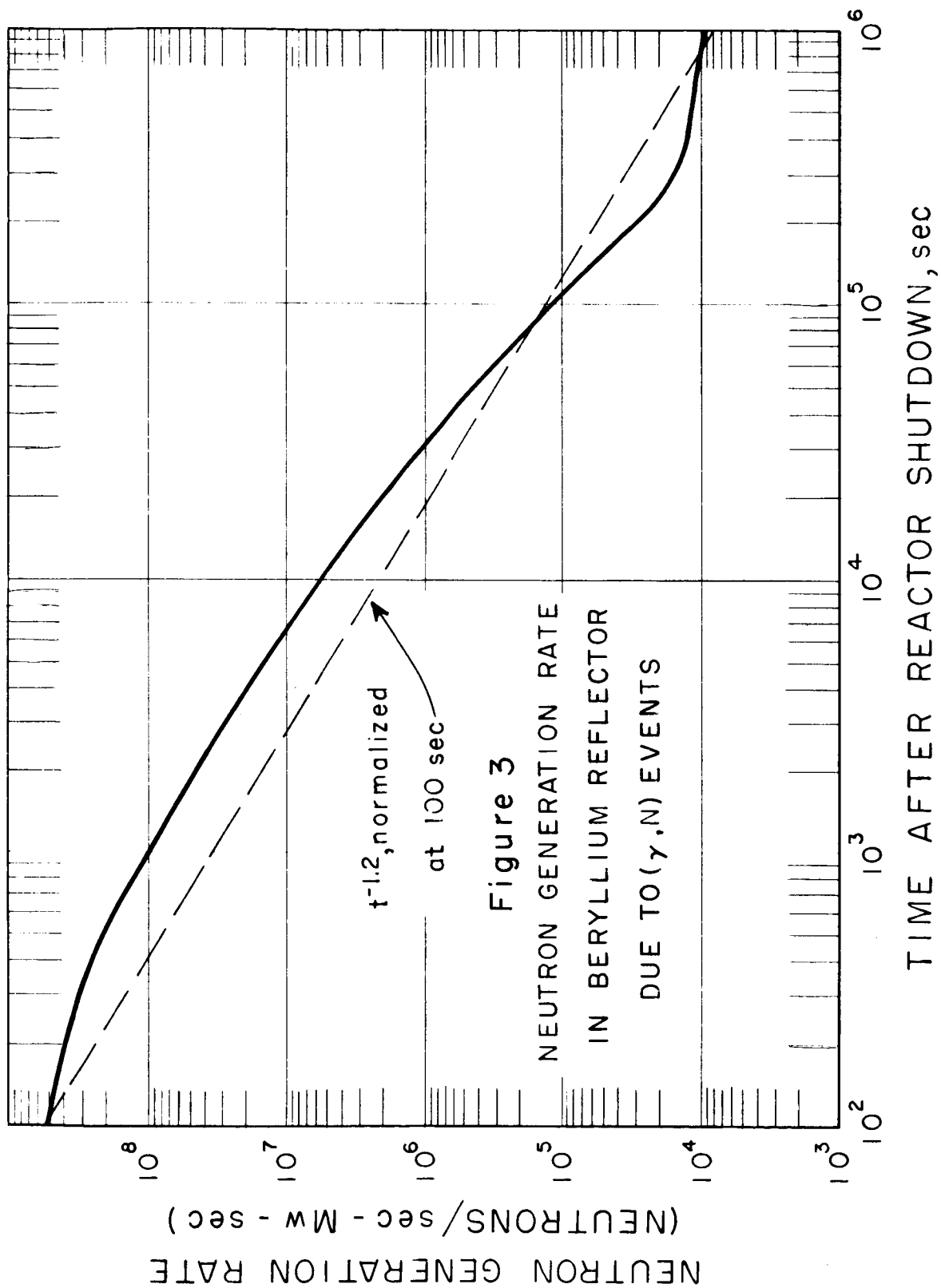
Although scandium and some other minor contaminants of beryllium become activated during reactor operation, their decay gammas are generally too low in energy to produce photoneutrons. As a result, photoneutrons will not be present after separating the reactor core and reflector, and will pose no hazards to reflector reuse.

It has been determined from this calculation that core heating from photoneutron induced fissions should always be unimportant ($< 1\%$) in comparison with concurrent core gamma heating, but the possible influence of the photoneutron production on reactor kinetics remains to be evaluated.

Many different calculations have been made with QAD during its one year existence. Others not mentioned have included estimates of control rod actuator heating for several actuator geometries and locations, radiation around an assembled beryllium reflector after removal from the reactor, radiation heating in and around the core, and many others. (2) All of these calculations, as well as those presented here, were performed readily and accurately with what has been proven an extremely useful flexible program.

(1) Jakobsen, Physical Review, 123: 229 (July, 1961)

(2) Cf. Paper by D. M. Peterson, "The Leakage Radiation Field of Kiwi Reactors", also submitted to this meeting.



X 66 50288

TRANSPORT CALCULATIONS OF THE
KIWI-B NEUTRON ENVIRONMENT

D. A. McCutchan

[U]

Los Alamos Scientific Laboratory
University of California
Los Alamos, New Mexico

Several one dimensional transport theory calculations have been made for Kiwi-B-1, using the DSN code. Some results are given here concerning the reactor's overall neutron economy, interior flux, and leakage currents.

The 24 group cross-sections published by Mills⁽¹⁾ are those which have been most widely used in Kiwi calculations. These cross section groups are particularly effective in coping with various thermal conditions, since there are ten energy groups below 0.4 ev and there is provision for scattering to 4 groups above and to 5 groups below an initial energy. The set is less refined in the high energy region, possessing only two groups above 1.4 mev. To gain more information about the high energy reactor spectrum, these two groups have been replaced for the present, by five new groups developed by Gordon Hansen of LASL. The data reported here are all based on this revised 27 group cross-section set, though there is no intention to use it continuously in future Kiwi calculations.

Neutron Balance

Table I below gives some information on the neutron balance in a Kiwi-B-1 in a cold, dry critical condition.

Table I
Neutron Balance in Kiwi-B-1

<u>Element</u>	<u>Captures per fission</u>
U ²³⁵	1.406
U ²³⁸	.035
C	.003
Nb	.083
B	.225
Al (pressure shell)	.003
Be	.005
axial leakage	.309
radial leakage	.395
	<u>2.45₄</u>

The negative absorption cross section in beryllium refers to

the difference between the production of neutrons by the $(n,2n)$ reaction and the loss of neutrons through (n,α) and (n,γ) reactions. The numbers in Table I are useful only as a guide: in particular, exact values of absorptions in Nb, Al, and B may vary from those shown. Here the control vanes were represented by an annular sheath with a boron loading chosen to reproduce an experimental fission distribution. Though this magnitude is probably correct, the actual boron absorption varies with control drum orientation. The foregoing calculation represented the reactor as an infinite cylinder in which fictitious absorbers of cross section DB^2 were introduced to simulate leakage in the axial direction. While appropriate group values of the diffusion coefficient D were chosen for the different reactor regions, a constant geometric buckling B^2 was used, based on a 2.4 cm extrapolation distance.

Interior Flux

The central flux in Kiwi-B-1, also obtained from the infinite cylinder problem, appears in Table II. The absolute value of the fission density at the core center which was used for problem normalization is based on a power level of 1000 megawatts (3.3×10^{19} fissions/sec) and an experimental value of 1.6 for the ratio of central to average power densities. These densities are approximately 59 and 37 megawatts per ft³ respectively.

Table II
Central Flux in Kiwi-B-1 at 1000 Megawatt Power

Group	Lower Energy	Flux n/cm ² -sec
1	6.0 mev	8.39 (13)
2	4.2	2.32 (14)
3	3.0	4.00 (14)
4	2.1	8.69 (14)
5	1.4	1.30 (15)
6	.9	1.49 (15)
7	.4	2.61 (15)
8	.1	3.82 (15)
9	17 kev	3.85 (15)
10	3	3.24 (15)
11	.454	3.15 (15)
12	61.4 ev	2.31 (15)
13	22.6	7.80 (14)
14	8.32	5.03 (14)
15	3.06	3.84 (14)
16	1.13	3.17 (14)
17	.414	3.10 (14)
18	.322	4.15 (13)
19	.251	3.02 (13)
20	.197	2.42 (13)
21	.152	1.54 (13)
22	.092	1.94 (13)
23	.056	7.91 (12)
24	.034	2.75 (12)
25	.025	6.43 (11)
26	.021	2.33 (11)
27	.013	4.24 (11)

In this table, the numbers in parentheses denote the multiplicative power of ten. The summed internal flux is 2.58×10^{16} neutrons/cm²-sec.

Leakage Currents

Table III shows the total radial leakage from Kiwi-B-1 at 1000 megawatts power, as obtained from the infinite cylinder problem. A preliminary comparison between the calculated S/U^{238} threshold detector ratio, Kiwi-B-1A measurements at the Nevada test site shows agreement to about 10%. In addition the activation of a $S^{32}(n,p)$ detector on the outer surface of the Kiwi-B-2 reflector* at midplane was found experimentally at Pajarito Site to be 1.15×10^{-9} /fission per gram of S^{32} . If we divide the calculated radial leakage of Table III by the radial surface area of the reflector, multiply by $\pi/2$, and interpret the result as an isotropic flux, the calculated $S^{32}(n,p)$ activation integral is 1.14×10^{-9} /fission - gm. As the experimental values at this location vary by about five percent, this close agreement is in part fortuitous.

The average energy of the neutrons in the radial leakage is $\sim .26$ mev. The average current density adjacent to the side pressure shell is $\sim 2.5 \times 10^{14}$ neutrons/cm²-sec.

Although axial leakage from the core may be approximated by the product of the diffusion coefficient and a geometric buckling, the axial core leakage spectrum given in Table III was obtained explicitly from a DSN analysis of a bare slab of core composition. In that calculation, radial leakage was accounted for by introducing a fictitious absorption defined by the ratio of radial leakage to core flux in a cylindrical geometry problem. (In the thermal groups the sign of the absorption was negative because of thermalization by the reflector. Since the reflected neutrons were introduced uniformly throughout the core by this artifice, rather than at the periphery, the calculated thermal leakage from the core may be too high). The core leakage shown in Table III corresponds to the Kiwi-B-1 without end reflector or shield. Upon dividing these values by the core end area, one obtains an average leakage current density of $\sim 6.6 \times 10^{14}$ neutrons/cm²-sec. This value would be most applicable near the reactor axis. The average energy of these neutrons is $\sim .73$ mev.

Comparison of these axial leakage values to $S^{32}(n,p)$ activation experiments with Kiwi-B-2 has been made. The calculated S^{32} activation at the core end surface was 7.11×10^{-9} per fission per gram of S^{32} ; the observed activation on centerline was 8.4×10^{-9} /fission-gm. Activation at three radial positions indicate an average of about 78% of this figure, or 6.6×10^{-9} /fission-gm.

The axial neutron leakage spectrum from the core was also determined experimentally using the method of proton recoils in nuclear photographic emulsions. The system was collimated to

* Kiwi-B-2 and Kiwi-B-1 are essentially identical neutronicallly, though they differ in their mechanical details.

confine observations to the core spectrum. Preliminary analysis of about 800 tracks confirms the spectrum predicted by a slab DSN problem (Table III) using the 27 group cross section set. The plate analysis is being continued to obtain better statistics in the high energy tail of the spectrum.

Table III also indicates the summed leakage from one end (only) of the graphite and the beryllium reflector cylinders, as found from an infinite cylinder DSN result. These numbers are the product of a volume integrated group flux and a DB_Z^2 term. (The DB_Z^2 term was derived from an appropriate group diffusion coefficient and a constant axial buckling corresponding to a 2.4 cm extrapolation distance). The average current density across the end area of these reflector cylinders is $\sim 1.7 \times 10^{14}$ neutrons/cm²-sec; the average neutron energy is $\sim .52$ mev.

When all the leakages cited are totalled, one finds that an unshielded reactor leaks $\sim .7$ neutron per fission; the average energy of all the leakage neutrons is $\sim .44$ mev; and the total power carried from a 1000 MW-reactor by neutrons is ~ 1.6 megawatts.

While propulsion reactors of this specific power offer a new magnitude of internal flux (e.g., 2.6×10^{16} neutrons/cm²-sec), it is interesting to note that the rather high current densities at the pressure shell do not really pose external radiation problems of an unknown order, since more difficult radiation environments may be found inside various existing test reactors.

Table III

Neutron Leakage from Kiwi-B-1 at 1000 MW.

Group	E lower	Leakage from One End n/sec		Radial Leakage n/sec
		Core	Reflector	
1	6.0 mev	3.28 (16)	1.03 (16)	4.25 (16)
2	4.2	7.41 (16)	1.76 (16)	6.87 (16)
3	3.0	1.00 (17)	1.75 (16)	5.11 (16)
4	2.1	2.26 (17)	4.88 (16)	2.48 (17)
5	1.4	3.03 (17)	6.99 (16)	5.23 (17)
6	.9	3.04 (17)	5.93 (16)	4.08 (17)
7	.4	4.46 (17)	8.35 (16)	5.93 (17)
8	.1	5.51 (17)	1.09 (17)	9.16 (17)
9	17.0 kev	4.78 (17)	1.02 (17)	8.87 (17)
10	3.0	3.79 (17)	9.25 (16)	9.76 (17)
11	.454	3.68 (17)	9.42 (16)	8.52 (17)
12	61.44 ev	2.70 (17)	8.66 (16)	9.10 (17)
13	22.60	8.95 (16)	4.55 (16)	6.36 (17)
14	8.315	5.90 (16)	4.17 (16)	6.49 (17)
15	3.059	4.81 (16)	3.81 (16)	6.46 (17)
16	1.1256	4.20 (16)	3.49 (16)	6.28 (17)
17	.4141	3.99 (16)	5.07 (16)	9.21 (17)
18	.3224	5.55 (15)	8.71 (15)	1.76 (17)
19	.2511	4.06 (15)	8.78 (15)	1.80 (17)
20	.1965	3.47 (15)	1.01 (16)	2.12 (17)
21	.1523	2.41 (15)	1.01 (16)	2.19 (17)
22	.0924	3.58 (15)	2.56 (16)	5.74 (17)
23	.0560	1.85 (15)	2.68 (16)	6.14 (17)
24	.0340	8.10 (14)	2.17 (16)	5.04 (17)
25	.0252	2.28 (14)	9.25 (15)	2.16 (17)
26	.0206	8.85 (13)	4.71 (15)	1.09 (17)
27	.0125	1.70 (13)	1.52 (16)	3.08 (17)
		3.83 (18)	1.14 (18)	1.31 (19)

X 66 50289

RADIATION INDUCED CONVERSION OF ORTHOHYDROGEN TO PARAHYDROGEN ON THE RIFT PROPELLANT TANK

M. C. Johnson
The Bendix Corporation
Research Laboratories Division
Southfield (Detroit), Michigan



INTRODUCTION

The hydrogen molecule exists in either of two states, orthohydrogen or parahydrogen. The equilibrium concentration of each of these states depends upon the temperature. However, the transition from one state to the other is strongly forbidden quantum mechanically, so that there is a considerable time lag between a change in temperature and the establishment of the new ortho-para equilibrium ratio. The importance of this process lies in the fact that the conversion of orthohydrogen to parahydrogen is exothermic, producing more heat than the heat of vaporization. If this conversion occurs in a propellant tank, it represents an additional source of heat which may become a problem.

DISCUSSION

The distinction between the two states of hydrogen is in the directions of the electron spin vectors. The lower energy configuration, in which the two spins are in opposite directions, is parahydrogen; and the higher energy configuration, with the spins parallel, is orthohydrogen. Considering a single unperturbed molecule, the half life of the conversion is 300 years. But due to perturbations in the liquid state, the conversion reaction proceeds much more quickly, obeying the following equation:

$$-\frac{dx}{dt} = kx^2 \quad (1)$$

or

$$\frac{1}{x} - \frac{1}{x_0} = k(\Delta t)$$

where: x = fraction above equilibrium at time t
 k = constant experimentally determined to be
 1.14×10^{-2} per hour
 x_0 = original fraction above equilibrium

As equilibrium is approached, the rate of conversion becomes very slow. At room temperatures (approximately 300°K), the equilibrium ratio of orthohydrogen to parahydrogen is 3 to 1. At the temperature of liquid hydrogen, about 20°K, the ratio is 99.79 percent parahydrogen to 0.21 percent orthohydrogen. Since the conversion rate is so slow, hydrogen can be liquified from room

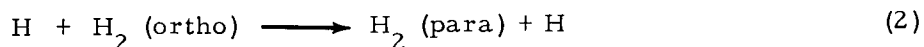
temperature and remain in its 75 to 25 ortho-to-para condition. However, conversion heating would completely vaporize this hydrogen within 48 hours.

Therefore, catalysts are used in the liquefaction process which greatly increase the conversion rate, so that the heat of conversion is removed during processing. Bulk liquid hydrogen generally is 95 percent parahydrogen. Conversion of the remaining 4.79 percent orthohydrogen does not add significantly to the evaporation rate, and the cost of converting the last few percent rises disproportionately.

If the liquid hydrogen is used in a nonnuclear environment, there should be no problems. The conversion will take place over a long period of time and will probably provide a small thermal input relative to other heat sources. However, an experiment by Capron published in 1935⁽¹⁾ indicates that ionizing radiation will induce the conversion. Eyring, Hirshfelder, and Taylor⁽²⁾ published a theoretical treatment of Capron's experiment, deriving results which agreed quantitatively with the measured data. This theory has been extrapolated to liquid hydrogen in order to predict the possible effect of the NERVA reactor radiation on the hydrogen in the propellant tank.

There are two interesting possibilities. One is that the conversion will take place almost instantaneously while the tank is still full. In this case, the relief valve would have to vent a large amount of gaseous hydrogen very quickly or the tank would burst in spite of supercooling. The other effect is less spectacular but could be serious. The hydrogen might vaporize to such an extent that there would not be sufficient fuel to complete the mission. If the radiation-induced conversion rate is sufficiently slow, other sources of heat will completely mask the heat of conversion.

The calculation of heating rate is based on conversion due to bond breakage and to atomic hydrogen interaction. In the first case, approximately one to six molecular bonds are broken per ion pair. For every 1000 free atoms formed, on the average 48 which were originally ortho will recombine as para in liquid 95 percent parahydrogen. The other interaction is the exchange reaction,



All of the free hydrogen is assumed to be lost by recombination.

The calculation proceeded as follows: Typical numbers for the radiation at the bottom of the tank are 10^{11} n/cm²-sec with an average energy of 1 Mev and 2×10^{12} Mev/cm²-sec gamma radiation with an average energy of 2 Mev. The number of ion pairs per cubic centimeter can be determined assuming one pair is formed for every 33 ev of energy deposited. Since the number of free hydrogen atoms formed per ion pair is not well determined, the calculation was split at this point in an attempt to bracket the actual conversion rate with worst and best cases. One set of curves was generated assuming one free hydrogen atom per ion pair and a reaction rate of 10^5 cm³/mole-sec, while the other assumed 6 free hydrogen atoms per ion pair and a reaction rate of 10^7 cm³/mole-sec.

The average concentration of free hydrogen can be found from the formula in Reference (3):

$$C_H = \left(\frac{I}{K_o C_{H_2}} \right)^{1/2} \quad (3)$$

where: C_H = free hydrogen atom concentration in moles/cm³
 I = rate of formation of free hydrogen, moles/cm³-sec
 C_{H_2} = concentration of molecular hydrogen, moles/cm³
 K_o = recombination coefficient = 10^{16} cm⁶/moles²-sec

The constant K_o was measured in gaseous hydrogen at standard temperature and pressure. It is not known whether it is different in liquid hydrogen. Knowing the reaction rate, it is possible to calculate the time required to obtain conversion to a fraction x above equilibrium.

$$\Delta t = \frac{1}{\frac{I}{C_{H_2}} + K_1 C_H} \ln \frac{x}{x_o} \quad (4)$$

where: x = unconverted fraction above equilibrium
 x_o = original unconverted fraction, in this case 0.05
 Δt = time
 K_1 = rate of the exchange reaction, 10^5 or 10^7 cm³/mole-sec depending on the assumption.

The constant K_1 is known to be temperature-dependent, decreasing by a factor of 10^3 between 600 and 300°K. At 300°K it was evaluated to be 8.5×10^7 , but sufficient information prevented an actual calculation at 20°K in the liquid state. This is the reason for the assumption of the two different rates as worst and best cases. Since conversion of 1 cm³ of orthohydrogen to parahydrogen releases 8.9 calories, the heat deposition per cubic centimeter versus time can be plotted directly from Equation (4). This is shown in Figures 1 and 2 as compared to the heat deposition rate due to natural conversion and to nuclear heating.

CONCLUSIONS

The heating is increased over that due to natural conversion; but nuclear heating is much more significant than the conversion heating, even assuming the high reaction rate. Unless there are changes in the values of the reaction rates and recombination rates in going from gaseous to liquid hydrogen of magnitudes much greater than seems reasonable at the present time, the contribution of ortho-para conversion heating is not significant compared to nuclear heating. It is concluded that this will not be a problem.

REFERENCES

- (1) Ann. Soc. Sci. Bruzelles, 55, 222 (1935).
- (2) Eyring, Hirshfelder, and Taylor, "The Treatment of Chemical Reactions Produced by Ionization Processes," J. Chem. Phys., 4, 479 (1936).
- (3) Hirshfelder, Eyring, and Topley, "Reactions Involving Hydrogen Molecules and Atoms," J. Chem. Phys., 4, 170 (1936).

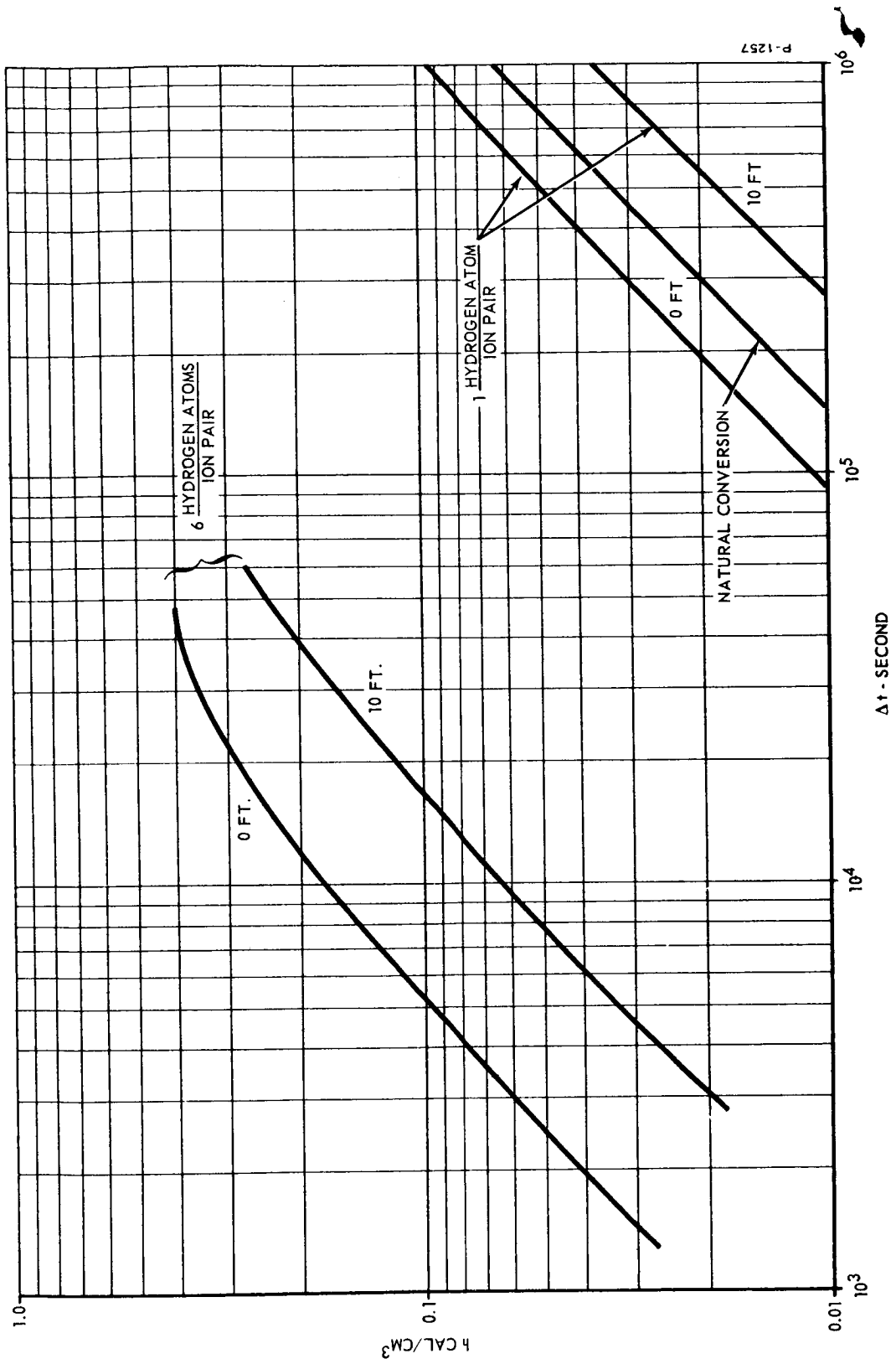


Figure 1 - Radiation Induced Conversion Heating Compared to Natural Conversion

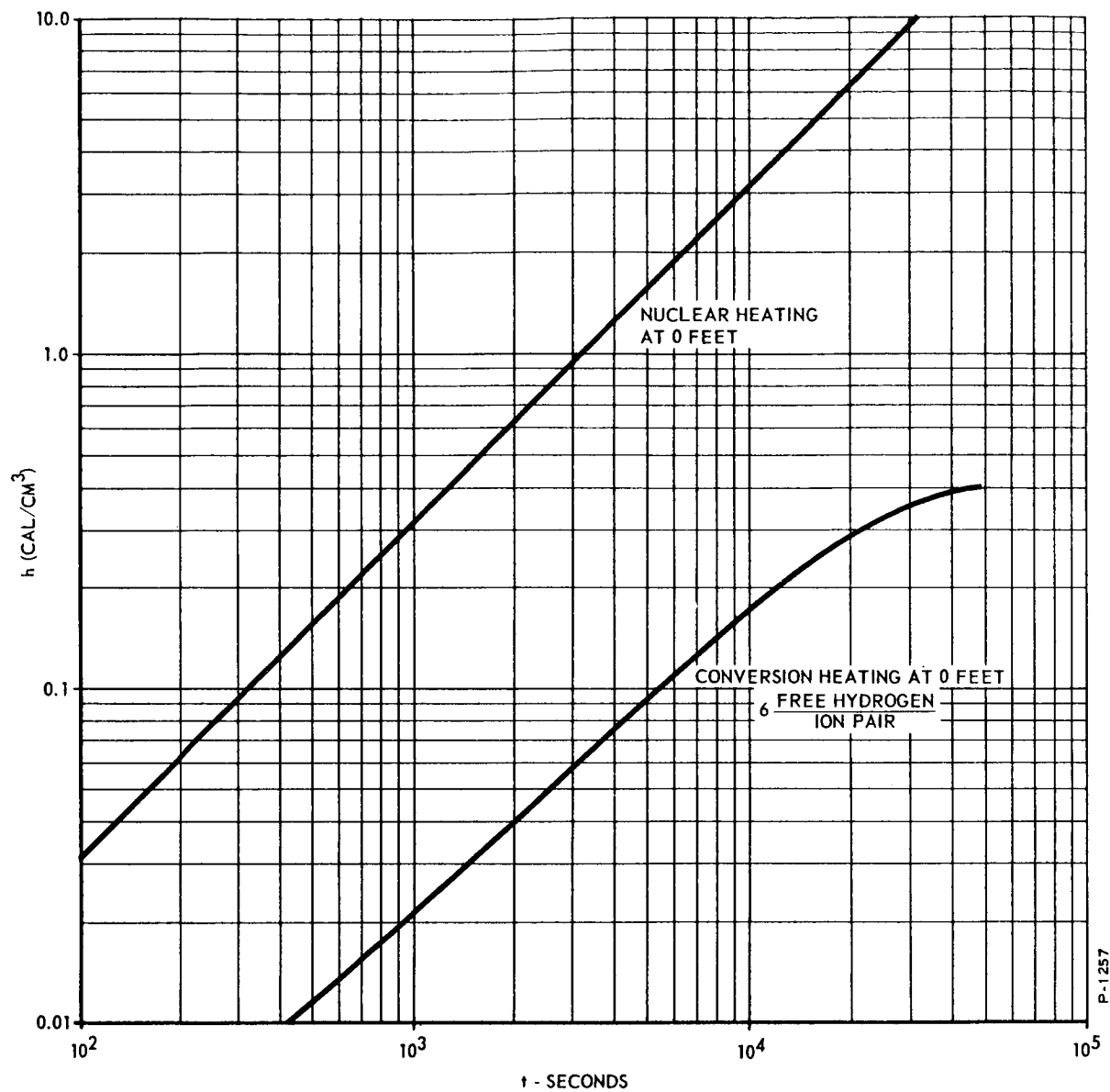


Figure 2 - Nuclear Heating Compared to Conversion Heating

X 66 50290

STARTUP STUDIES OF A NUCLEAR ROCKET REACTOR

Part 3 STARTUP PHILOSOPHY*

[U]

J. Douglas Balcomb
Los Alamos Scientific Laboratory

I. INTRODUCTION

The startup of nuclear propulsion reactors on liquid hydrogen has been a subject which has caused a great deal of apprehension since the inception of the Rover program. The fear arises because a small amount of hydrogen in the reactor core greatly enhances the efficiency of the neutron chain reaction. Figure 1 shows the core axial distribution of hydrogen reactivity worth in Kiwi-B. We estimate that if the core were filled with liquid hydrogen, the increase in criticality would be 30-40 dollars ($k \approx 1.3$). For small amounts of hydrogen evenly distributed through the core, the reactivity increase is about 4.2 dollars per pound. This hydrogen reactivity is a negative feedback, self-control mechanism which seems to be stable and well behaved. The fear is that violent local fluctuations in the boiling of the liquid hydrogen in the reflector will cause blobs of liquid to enter the core and cause extreme power excursions or reactor power control problems.

To decrease the probability of blobs of liquid entering the core we have imposed the ground rule that the average fluid temperature in the core inlet plenum shall be maintained greater than 90° R.

The choice of 90° R as a lower limit is based on the properties of hydrogen. Below the critical temperature, 59.3° R, hydrogen can exist as a two-phase equilibrium mixture. Between 59.3° R and about 90° R, hydrogen heat transfer continues to exhibit a two-phase nature. That is, there is a distinct separation of dense and light hydrogen. This region we call the pseudo-two-phase region. Since the object is to avoid congregation of dense hydrogen in the core inlet plenum, 90° R is chosen as the minimum allowable temperature. Above 90° R, hydrogen seems to maintain a single phase nature.

Other restrictions may limit the possible range of startup profiles. Los Alamos Scientific Laboratory is currently testing the Kiwi-B series of reactors at the Nevada Test Site. For these tests, hydrogen will be supplied to the reactor by an axial flow turbopump (NFS-1) developed by Rocketdyne. The flow facility for these tests allows the hydrogen either to be bypassed around the reactor or to be throttled by a valve in the line to the reactor. In this way the startup pressure-flow rate relationship does not need to correspond to the operation region of the turbopump. However, for flying reactors, it will probably not be

* Work performed under AEC Contract W-7405-ENG. 36.

possible to bypass flow. This paper includes the case in which flow cannot be bypassed, thus, the ground rule is adopted that the reactor inlet pressure and flow rate relationship shall be confined to the turbopump operating region. Figure 2 shows the NFS-1 "pump map" showing the operating regions.

During the initial portion of the startup the main hydrogen heating in the reflector is due to the initial stored heat content of the reflector which we presume is at ambient temperature. Thus, in order to maintain the temperature at the core inlet plenum as high as possible, it is advantageous to make the startup as short as possible and to maintain flow rates as low as possible.

A third constraint on the startup profile is imposed by the permissible thermal stress in the reactor core. This limits the maximum rate of rise of core temperature and thus determines the minimum startup time. The maximum startup rate is not known at this time; it may be that this information can only be obtained from reactor tests. For the meantime, startup rates in the range of 25° R/sec to 100° R/sec are being considered.

II. STARTUP SEQUENCING

Figure 3 shows a typical reactor system startup sequence. A typical startup sequence might be divided into three phases as follows:

Phase I. Duration - 10 to 20 seconds. The purpose of this phase is to provide the proper initial conditions for Phase II. The power at the end of Phase I is to be of the order of 100 MW so that the reactor core temperature will be rising at about 100° R per second. To accomplish this, power is brought up from a low value on a constant period. Periods which are considered are in the range 1 - 5 seconds. Flow is started at the end of Phase I so that the nozzle cooling passages and inlet piping are chilled down, flow is stabilized, and the pump is running. A net result of Phase I is that the reactor core is heated to 700 - 1000° R, but the reflector is still near ambient temperature.

Phase II. Duration - 10 to 20 seconds. The purpose of this phase is to get quickly through the hazardous part of the startup. Once the core and outlet gas temperatures reach about 2500° R there is no longer danger of temperatures in the core inlet plenum dropping below 90° R. The minimum duration of Phase II is limited by permissible core thermal stresses. We have taken 100° R/sec as the rate of change of outlet gas temperature permitted during Phase II. Thus, core outlet gas temperature is programmed linearly from about 900° R to 2500° R in Phase II. The flow rate profile is the parameter which is varied to delineate between startup types. Power is programmed consistent with the desired flow rate and core outlet gas temperature profile.

Phase III. Duration - greater than 10 seconds. The danger of blobs of hydrogen entering the core is past and so this phase is very arbitrary. It can be prolonged, a half-power hold can be inserted, or the startup can be terminated without going to full power.

III. DISCUSSION OF THE CONSTRAINTS

A typical plot of the temperature in the core inlet plenum during a startup will show a decrease, a minimum, and a slow rise to about 200° R at full power. This temperature is maintained greater than 90° R by the stored heat content of the reflector, by the heat generated in the reflector, and by the heating in the nozzle. The reflector heat content alone (initial temperature = 540° R) is sufficient to maintain temperatures in the core inlet plenum greater than 90° R for an integrated hydrogen flow of about 170 pounds. One desires to keep the total hydrogen used during Phase II to a minimum in order to conserve this

stored heat; this is done by minimizing both the flow rate and the duration. On the other hand, some minimum flow rate must be maintained in order to avoid the stall region of the pump; this minimum flow increases as the core temperature increases. A logical way to program flow during Phase II is to demand, at each point in time, the minimum flow rate at which the pump can safely operate.

It is not clear at this time that pump operation needs to be confined to the normal operating region. Operation in the soft stall regime may be permissible. It has been experimentally demonstrated that such operation does not injure the pump, but does degrade pump efficiency.

The second half of the startup is not nearly as critical as the first half. This is because the power generation in the reflector region becomes sufficient to maintain the temperature in the core inlet plenum above 90° R. Figure 4 shows steady state core inlet temperature as a function of flow rate for core exit gas temperatures of 2000° R and 2500° R. We have selected 2500° R as a conservative definition of the transition from the intermediate to the final phase of the startup.

IV. RESULTS OF PARTICULAR STARTUP STUDIES

We have studied several startups by means of the HEX digital code. Three of these studies are reported here in order to present a range of numerical examples. The studies presume that Phase I of the startup is completed leaving the core at an average temperature of 950° R and the nozzle and piping chilled. The flow profiles during Phase II are shown in Fig. 5. Startup A is chosen to barely avoid stall in the manner described above. Startup B is chosen to keep temperatures in the core inlet plenum high by keeping flow rate low without regard to the pump. Startup C is chosen to keep the pump well away from stall without regard to the temperature in the core inlet plenum. The power profiles are shown in Fig. 6. The calculation is terminated at 16 seconds, the time when the outlet gas temperature reaches 2500° R.

The most important results are shown in Figs. 7 and 8. Figure 7 shows the temperature in the core inlet plenum vs. time. All three startups satisfy Ground Rule No. 1, however, Startup C is very marginal. Figure 8 shows the path of the three startups on a plot of pump discharge pressure vs. flow rate. Also plotted are dotted lines defining the pump operating regions for a 75 psia pump supply pressure. Startup A narrowly avoids stall, Startup B goes well into stall, and Startup C clearly avoids stall.

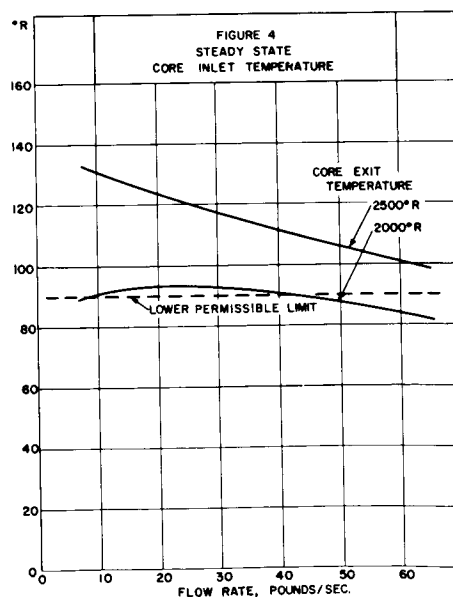
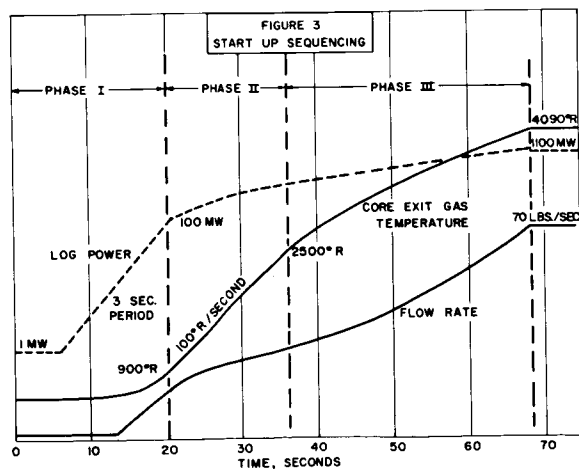
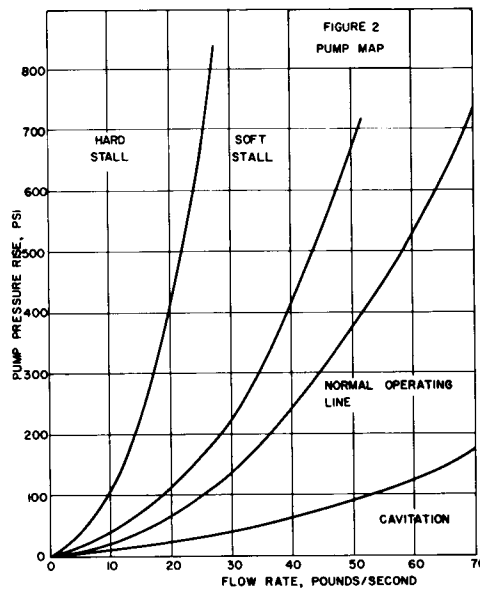
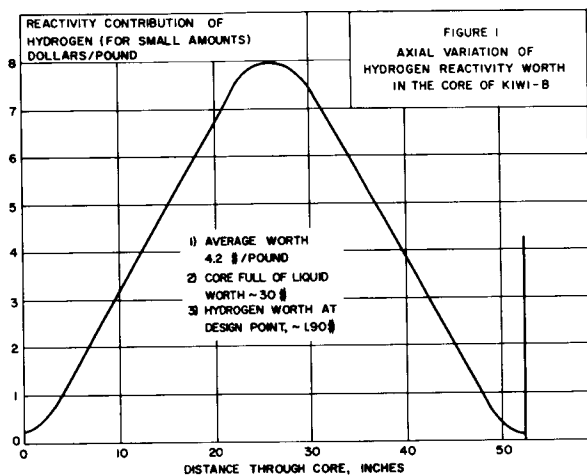
V. CLOSING COMMENT

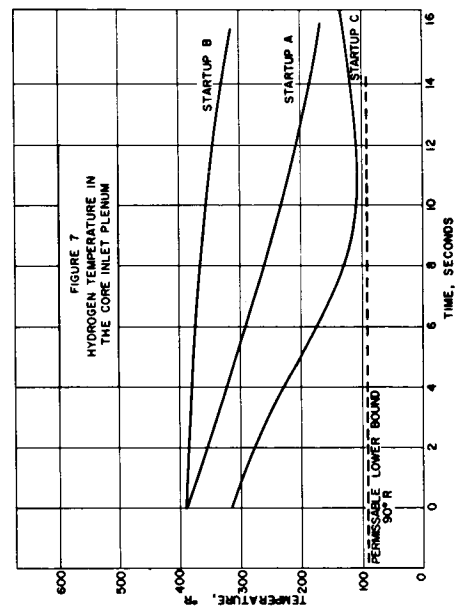
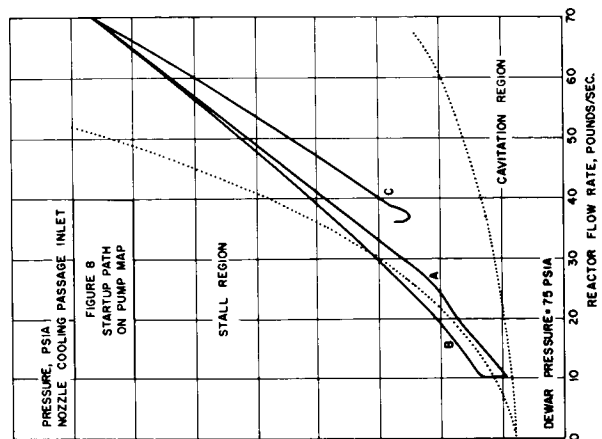
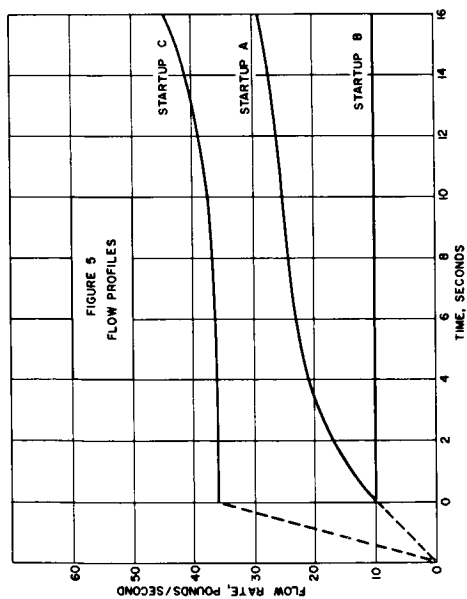
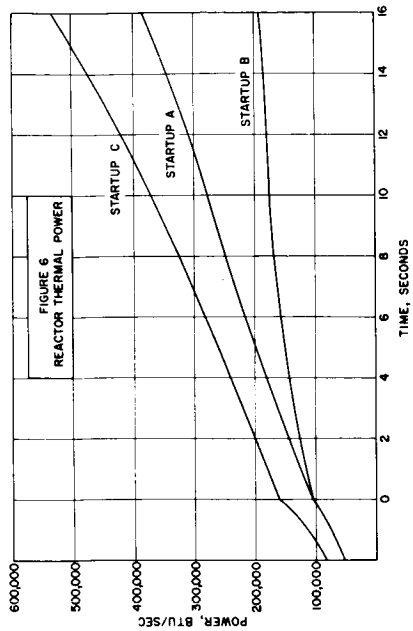
Kiwi-B-1B, the first rocket reactor to be started on liquid hydrogen was tested on September 1, 1962. Reactor core damage occurred as the reactor approached full power. However, the critical portion of startup, from ambient to about 2500° R exit gas temperature, went approximately as predicted by the HEX calculations. The minimum core inlet gas temperature was 160° R. No abnormalities were noted which could be attributed to fluctuations in propellant reactivity. We conclude from this that 160° R is well within the permissible range of core inlet temperatures.

The results obtained from the Kiwi-B-1B test after the core damage note above had occurred are inconclusive. However, they are very encouraging. During this time there were large gaps in the core and holes in the nozzle. Conditions are not sufficiently well known to make accurate heat transfer calculations. During this period the observed temperature in the core inlet plenum fell to about 60° R (The measurement is not accurate at low temperature.). Flow rate was varied over the range from 70 to 20 pounds per second; the pressure in the core

inlet plenum varied over the range 390 psia to 55 psia. The reactor was near critical this entire time, and the measured reactor power was observed to be stable and free of fluctuations that would be expected from unsteady flow. It appears that stable reactor operation may be possible for conditions in the core inlet plenum below 90° R, perhaps even for two phase conditions. If this is true, it will modify future startup philosophy considerably.

A startup philosophy is evolving in the Rover program. This paper has presented some thoughts current today. The picture is certain to change as experiments are performed and as new ground rules are laid down.





66 50291

CONTROL SYSTEMS FOR A LIQUID-HYDROGEN-COOLED KIWI-B REACTOR*

[U]

P. J. Blake,⁺ R. J. Bohl, E. A. Brown, C. P. Milich,
M. J. Nutter, C. E. Stiles and B. G. Strait

Los Alamos Scientific Laboratory

INTRODUCTION

Kiwi-B-1B, the first nuclear propulsion reactor to be cooled by liquid hydrogen, was run on September 1, 1962. This test was highly successful in that it proved that a Kiwi-B reactor can be started up and run in a predictable, well-behaved manner with liquid hydrogen coolant.

The Kiwi-B-1B controls analysis done by the Los Alamos Scientific Laboratory was complicated by the uncertainties associated with heat transfer calculations in two-phase hydrogen, and by the reactivity effects of dense hydrogen in a reactor core. Hydrogen acts as a moderator, thus increasing reactivity. Conceptually, the hydrogen could add several times more reactivity than the control rods were worth. If this were allowed to happen, a nuclear accident would have followed. A secondary concern was the unknown character of the random noise which could have been introduced by slugs and droplets of liquid hydrogen passing through the core.

The systems developed to control the operation of Kiwi-B-1B and a brief summary of the hot run will be described in this paper. It was necessary to make certain simplifying assumptions and to restrict the mathematical treatment to simply a presentation of the applicable transfer functions in order to keep the paper within the specified length. More complete descriptions of most of the systems have been printed^{1,3}. The most notable assumption was that the interaction of flow rate with power and exit gas temperature was negligible. Other assumptions will be pointed out in the descriptions of the various systems. Analog and digital computer data, which have none of the assumptions mentioned in this paper, indicate that the assumptions are valid for the frequency range of interest in studying the stability of the systems.

A simplified block diagram of the Kiwi-B-1B control systems is shown in Fig. 1. The primary controlled variables were the logarithm of power, exit gas temperature, and mass flow rate. The log power and turbopump speed control systems operated as sub-loops in the temperature and flow rate systems, respectively.

During hot runs the speed demand voltage was developed by the flow rate controller. The log power demand was the sum of two voltages - one from the master programmer and a second vernier correction from the temperature controller. The master programs for log power and flow rate were designed to keep the exit gas

* Work performed under the auspices of USAEC and NASA under Contracts W-7405-ENG. 36 and SNP-1.

+ On loan to Los Alamos Scientific Laboratory from Westinghouse Astronuclear Laboratory, Pittsburgh, Pennsylvania.

temperature at the desired value within the limits of accuracy of the system calibrations. This arrangement permitted the operators to open the temperature control loop if a malfunction occurred. The run could then be continued on log power and flow rate control with reduced temperature accuracy.

POWER CONTROL

Kiwi-B-1B power was regulated with a five-decade log power control system. Power was varied by positioning 12 rotary control rods located in a beryllium reflector which surrounded the core. The rods were beryllium cylinders with boron sheaths covering 120° of the cylinders. The core reactivity could be increased approximately \$9 by rotating the boron from positions toward the core to positions directly away from the core. All of the rods received a common positional command voltage from the power controller.

Referring to Fig. 1, the log power system transfer functions for small perturbations were as follows:

$$G_1(s) = \frac{\delta E_p(s)}{\delta E_1(s)} = \frac{6.67 \left(\frac{s^2}{31.42} + \frac{2(0.6)s}{31.4} + 1 \right)}{s \left(\frac{s}{376} + 1 \right)} \quad \frac{\text{Volts}}{\text{Volt}}$$

$$G_2(s) = \frac{\delta \theta(s)}{\delta E_2(s)} = 1.8 \frac{\delta \theta(s)}{\delta \theta_d(s)} \quad \frac{\text{Degrees}}{\text{Volt}}$$

$$G_3(s) = \frac{\delta(\delta K_r)(s)}{\delta \theta(s)} = 0.0006 \sin \theta \quad \text{degrees}^{-1}$$

Assuming that temperature and propellant reactivity effects are negligible in the frequency range of interest, the neutronics transfer function at infinite period was:

$$G_4(s) = \frac{\delta Q(s)}{\delta(\delta K_r)(s)} = \frac{135Q_0 \left(\frac{s}{0.1} + 1 \right)}{s \left(\frac{s}{150} + 1 \right)} \quad \text{KW}$$

$$G_5(s) = \frac{\delta E_3(s)}{\delta Q(s)} = \frac{8.67}{Q_0} \quad \frac{\text{Volts}}{\text{KW}}$$

The open loop transfer function for $\theta = 90^\circ$ and an infinite period was:

$$G_Q(s) = \frac{8.43 \left(\frac{s}{0.1} + 1 \right) \left(\frac{s^2}{31.42} + \frac{2(0.6)s}{31.4} + 1 \right)}{s^2 \left(\frac{s}{150} + 1 \right) \left(\frac{s}{376} + 1 \right)} \cdot \frac{\delta \theta(s)}{\delta \theta_d(s)}$$

Nichols' plots of the log power system open loop characteristics for the two extremes of reactor period considered are shown in Fig. 2. The effect of sustained period on the reactor transfer function has been described²; therefore, it will not be given further treatment in this paper. Changing the average control rod position from 90° to either 15° or 165° lowers the open loop gain approximately 12 db.

TEMPERATURE CONTROL

Kiwi-B-1B core exit gas temperature was controlled automatically with the system shown in Fig. 1. The gas temperature was measured with 3 tungsten/tungsten-rhenium thermocouples⁴. The temperature error voltage was developed by comparing the temperature demand voltage to the amplified average of the three

thermocouple voltages. A reject circuit was included which would automatically reject any thermocouple which differed from the average by more than 400° R. The controller regulated temperature by applying appropriate corrections to the programmer log power demand voltage. The temperature controller was clamped so that it could not change the power by more than + 15% or - 50% of the demanded power.

The linearized transfer functions for the temperature control system are given below. Bode plots of the open loop characteristics for two operating points are shown in Fig. 3.

$$G_6(s) = \frac{\delta E_5(s)}{\delta E_4(s)} = \frac{0.1 \left(\frac{s}{0.14} + 1 \right)}{s \left(\frac{s}{100} + 1 \right)} \quad \frac{\text{Volts}}{\text{Volt}}$$

$$G_7(s) = \frac{\delta Q(s)}{\delta E_5} = \frac{Q_0}{8.67} \frac{\delta [\text{Log } Q(s)]}{\delta [\text{Log } Q_d(s)]} \quad \frac{\text{KW}}{\text{Volt}}$$

$$G_8(s) = \frac{\delta T_{ce}(s)}{\delta Q(s)} = \frac{\left(\frac{s}{1.3} + 1 \right)}{4.08 W_0 \left(\frac{280s}{W_0} + 1 \right) \left(\frac{s}{2} + 1 \right)} \quad \frac{^\circ\text{R}}{\text{KW}}$$

$$G_9(s) = \frac{\delta E_6(s)}{\delta T_{ce}(s)} = \frac{1}{50 \left(\frac{3.5s}{\sqrt{W}} + 1 \right)} \quad \frac{\text{Volts}}{^\circ\text{R}}$$

The open loop transfer function of the temperature system was:

$$G_T(s) = \frac{Q_0 \left(\frac{s}{0.14} + 1 \right) \left(\frac{s}{1.3} + 1 \right)}{s(1.77)(10)^4 W_0 \left(\frac{280s}{W} + 1 \right) \left(\frac{s}{2} + 1 \right) \left(\frac{3.5s}{\sqrt{W}} + 1 \right)}$$

TURBOPUMP SPEED CONTROL

The liquid hydrogen which cooled Kiwi-B-1B was pumped through the reactor by a turbine-driven pump. The turbopump speed was varied by positioning a linear valve located between the turbine inlet nozzle and a gaseous hydrogen tank farm. The speed control system shown in Fig. 1 was used to regulate speed to the value required to maintain the desired reactor flow rate.

The equations which represent the characteristics of the speed control loop elements are as follows:

$$G_{10}(s) = \frac{\delta E_8(s)}{\delta E_7(s)} = \frac{11 \left(\frac{s}{8} + 1 \right) \left(\frac{s}{40} + 1 \right)}{s \left(\frac{s}{80} + 1 \right) \left(\frac{s}{100} + 1 \right)} \quad \frac{\text{Volts}}{\text{Volt}}$$

$$G_{11}(s) = \frac{\delta W_t(s)}{\delta E_8(s)} = \frac{1.22(10)^{-4} P_s}{\left(\frac{s}{63} + 1 \right) \left(\frac{s^2}{282^2} + \frac{2(0.5)s}{282} + 1 \right)} \quad \frac{\text{lb/sec}}{\text{Volt}}$$

The equation which describes the pump torque is $L_p = K_1 N^2 + K_2 NW + K_3 W^2$; however, this equation can be approximated by $L_p = K_4 N_0^2$ if the pump operating

point is kept on a constant specific speed line. If we assume that $L_p = 2.03(10)^{-5} N_o^2$, then

$$G_{12}(s) = \frac{\delta N(s)}{\delta W_t(s)} = \frac{2050 - 0.0185 N_o}{[4.06(10)^{-5} N_o + 0.0185 W_{to}] \left[\frac{4.51s}{1.22(10)^{-3} N_o + 0.555 W_{to} + 1} \right]}$$

$$G_{12}(s) = \frac{\delta N(s)}{\delta W_t(s)} \quad \frac{\text{RPM}}{\text{lb/sec}}$$

At $N_o = 23,500$ RPM and $W_{to} = 6.9$ lb/sec:

$$G_{12}(s) = \frac{1.5(10)^3}{\left(\frac{s}{7.2} + 1\right)}$$

$$G_{13}(s) = \frac{\delta E_s(s)}{\delta N(s)} = 3.33(10)^{-3} \quad \frac{\text{Volts}}{\text{RPM}}$$

The speed control system open loop transfer function at $P_s = 3300$ psi and full flow was:

$$G_N(s) = \frac{22.1 \left(\frac{s}{8} + 1\right) \left(\frac{s}{40} + 1\right)}{s \left(\frac{s}{7.2} + 1\right) \left(\frac{s}{63} + 1\right) \left(\frac{s}{80} + 1\right) \left(\frac{s}{100} + 1\right) \left(\frac{s^2}{282^2} + \frac{2(0.5)s}{282} + 1\right)}$$

A Nichols' plot of the open loop characteristics of the speed control system at full flow rate is shown in Fig. 4. Reducing the speed increases the bandwidth slightly and decreases the stability margin.

FLOW RATE CONTROL

The liquid hydrogen used to cool Kiwi-B-1B was stored in two 28,000-gallon dewars. During reactor runs the dewars were pressurized to 60 psig with gaseous hydrogen to provide suction pressure for the coolant pump. The reactor liquid hydrogen flow rate was measured with a venturi located a few feet downstream from the pump. The flow rate control system shown in Fig. 1 varied the turbo-pump speed to keep the venturi flow rate equal to the programmed flow rate demand. The reactor flow rate differed somewhat from the venturi flow rate at appreciable frequencies due to the effects of the 8-inch diameter, 100-foot long pipe line between the venturi and the reactor.

Referring to Fig. 1, the flow rate control system transfer functions were as follows:

$$G_{14}(s) = \frac{\delta E_{Nd}(s)}{\delta E_{10}(s)} = \frac{2 \left(\frac{s}{20} + 1\right)}{s \left(\frac{s}{4} + 1\right)} \quad \frac{\text{Volts}}{\text{Volt}}$$

$$G_{15}(s) = \frac{\delta N(s)}{\delta E_{Nd}(s)} = 400 \frac{\delta N(s)}{\delta N_d(s)} \quad \frac{\text{RPM}}{\text{Volt}}$$

At full power and full flow:

$$G_{16}(s) = \frac{\delta W_v(s)}{\delta N(s)} = 3(10)^{-3} \quad \frac{\text{lb/sec}}{\text{RPM}}$$

$$G_{17}(S) = \frac{\delta E_{12}(S)}{\delta W_v(S)} = 1 \quad \frac{\text{Volt}}{\text{lb/sec}}$$

The flow rate system open loop transfer function at full power and full flow was:

$$G_1(S) = \frac{2.4\left(\frac{S}{20} + 1\right)}{S\left(\frac{S}{4} + 1\right)} \cdot \frac{\delta N(S)}{\delta N_d(S)}$$

A Nichols' plot of the open loop transfer function is shown in Fig. 5. The rather conservative design indicated by this figure was chosen to increase the ability of the system to operate stably under the influence of relatively large disturbances. Such disturbances were observed on several occasions while testing the flow facility prior to the Kiwi-B-1B run. Two primary causes of the disturbances were the action of the specific speed control system and the abrupt transition from film to nucleate boiling in pipe lines which had not been thoroughly chilled prior to starting the turbopump. The specific speed control system was an auxiliary servo system which bypassed liquid hydrogen from the pump discharge line to atmosphere to keep the pump out of stall.

HOT RUN SUMMARY

There were two principal objectives of the Kiwi-B-1B full power run. The first was to prove that a Kiwi-B reactor can be started up and run with liquid hydrogen coolant. The second was to see if the reactor and test facility would operate satisfactorily under full flow and full power conditions. The successful completion of both these objectives was needed prior to the full power, relatively long duration run planned for Kiwi-B-4A. Kiwi-B-4A will be the first of several reactors having fuel elements similar to those planned for the Nerva reactors.

The planned startup for Kiwi-B-1B was to change from a holding level of 1 MW and 2 lb/sec to 1110 MW, 70 lb/sec, and 4100° R at a rate of 100°/sec. After a hold of 30 seconds the operating level was to be reduced to 690 MW, 56 lb/sec, and 3280° R for a second hold of approximately 2 minutes duration. Pipeline and temperature control system dynamic measurements were planned for this hold. The shutdown included a hold at 31 MW and 20 lb/sec to study the effects of allowing the core inlet coolant to approach liquid hydrogen temperatures.

A preliminary analysis of the run data indicates that the startup on liquid hydrogen was highly successful. The nuclear power and thermodynamic processes inside the reactor followed well-behaved patterns essentially as predicted. Random reactivity noise caused by liquid hydrogen slugs passing through the reactor was negligible; however, one reactivity transient was observed following what could have been the formation of a gas bubble in the pipeline leading to the reactor. This transient lasted for approximately 100 ms., resulting in a maximum corrective rod velocity of 16°/sec and a minimum reactor period of approximately 1 second. Reactor power rose momentarily to a value about 40% above the demanded power.

The run profile was changed rather drastically after the startup because eleven fuel modules departed from the core over a period of approximately 100 seconds. During most of this time the power, flow rate, and exit gas temperature demands were left at the full power hold. After 6 modules had left, reactivity was so decreased by the loss of carbon and uranium that the control rods went full out in an attempt to maintain reactor power. The maximum rod velocity during this process was approximately 36°/sec. After the control rods reached their full out positions, reactor power and exit gas temperature were controlled entirely

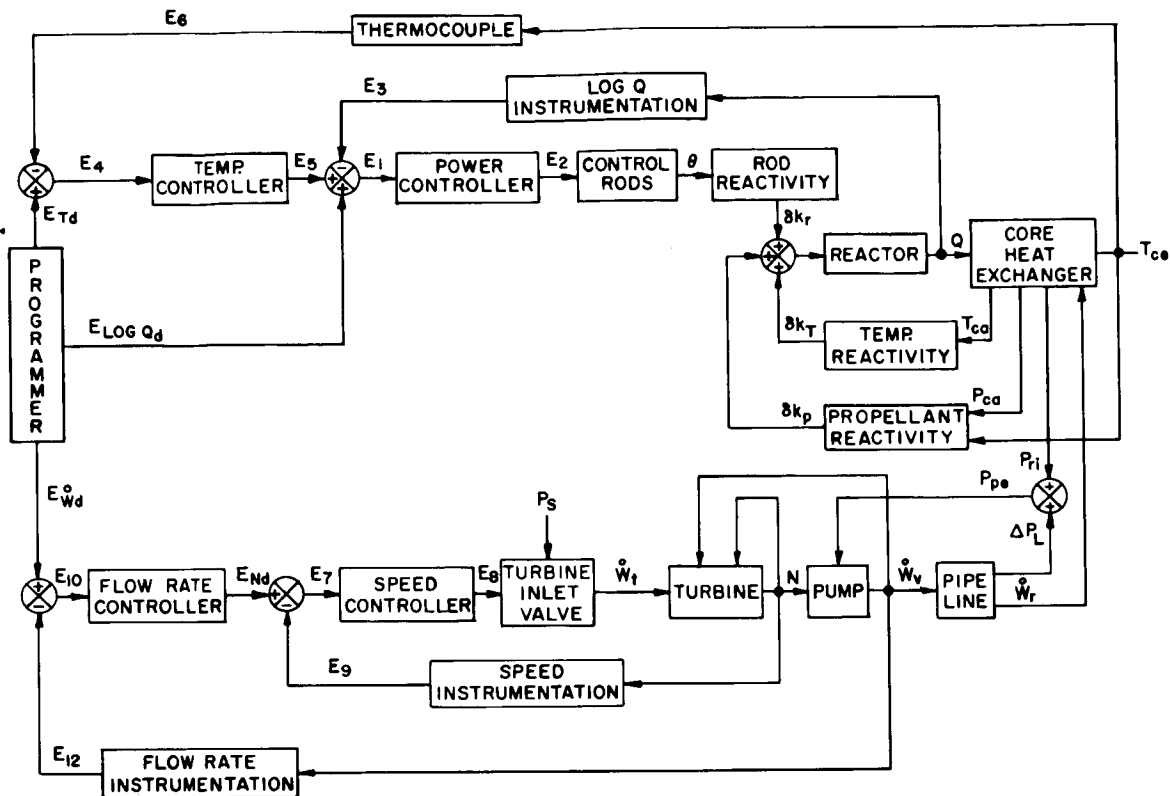
by the natural balance between positive propellant reactivity and negative core temperature reactivity. After each subsequent module departure power quickly dipped approximately 20%, then slowly recovered part way as the core cooled and hydrogen density and reactivity increased in the core. This operation was smooth and very similar to analog computer predictions.

As the flow rate was decreased during shutdown, power fell and the hydrogen in the core inlet plenum got steadily colder. It is not clear yet whether liquid hydrogen actually entered the core, though the hydrogen must have been very dense.

The power instrumentation calibration was in error such that actual power was some 25% lower than indicated power. This caused temperatures to be low throughout the run. The temperature controller was in the +15% power correction clamp during the entire run; therefore, no dynamic data were obtained for this system. The flow rate and turbopump speed control systems operated well despite large pipeline flow and pressure oscillations during most of the startup. The pipeline oscillations are believed due to an interaction between the specific speed control system and pipe lines which had not been sufficiently cooled down prior to the run.

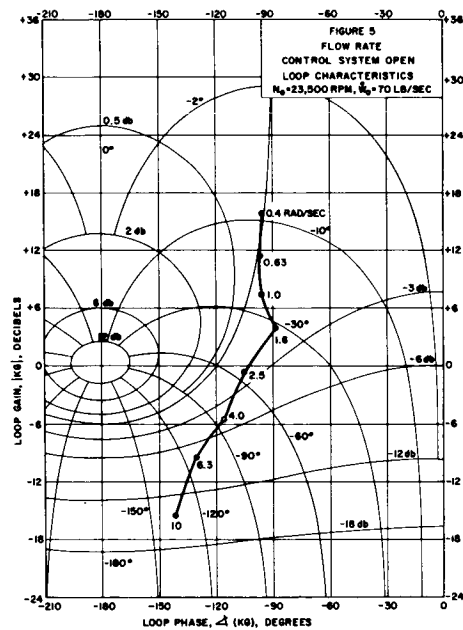
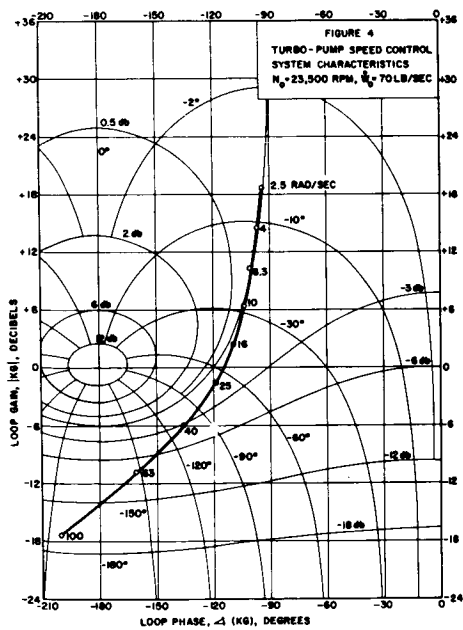
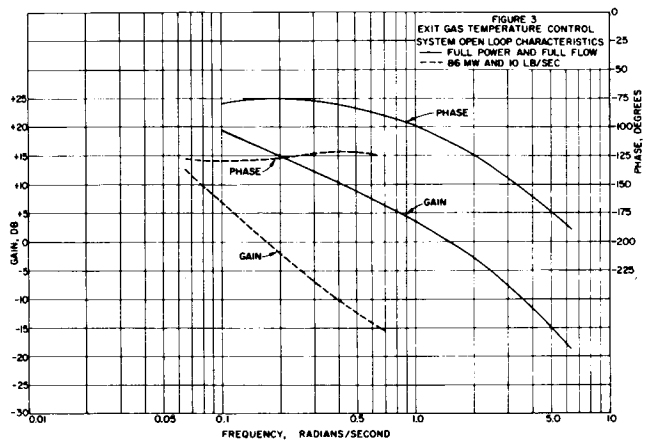
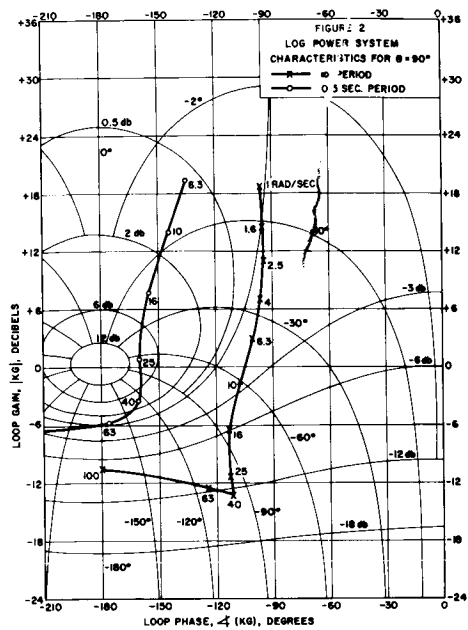
REFERENCES

1. E. A. Brown, "Logarithmic Power Control in Kiwi-A Reactors", I.R.E. Trans. on Nuclear Science, Vol. NS-9, No. 1, Jan. 1962.
2. S. Singer, "The Period Equilibrium Effect in Reactor Dynamics", Los Alamos Scientific Laboratory Report LA-2654, Jan. 1962.
3. E. A. Brown, H. B. Demuth, P. B. Erickson, R. R. Mohler, S. J. Singer, and C. E. Stiles, "Kiwi-B-1A Power and Temperature Control Systems", Proceedings of the Nuclear Propulsion Conference, Monterey, August 1962.
4. A. R. Driesner, C. P. Kempter, C. E. Landahl, C. A. Linder, and T. E. Springer, "High Temperature Thermocouples in the Rover Program", I.R.E. Trans. on Nuclear Science, Vol. NS-9, No. 1, Jan. 1962.



- θ = AVERAGE POSITION OF THE CONTROL RODS (DEGREES)
 δk_r = CONTROL ROD REACTIVITY (ABSOLUTE UNITS)
 δk_T = CORE TEMPERATURE REACTIVITY (ABSOLUTE UNITS)
 δk_p = PROPELLANT REACTIVITY (ABSOLUTE UNITS)
 Q = REACTOR POWER (KW)
 T_{ce} = CORE EXIT GAS TEMPERATURE ($^{\circ}R$)
 T_{ca} = AVERAGE CORE STRUCTURE TEMPERATURE ($^{\circ}R$)
 P_{ca} = AVERAGE CORE PRESSURE (PSIA)
 P_{ri} = REACTOR INLET PRESSURE (PSIA)
 P_{pe} = TURBO-PUMP EXIT PRESSURE (PSIA)
 ΔP_L = PRESSURE DROP IN PIPE LINE (PSIA)
 E = VOLTAGE
 \dot{W}_t = TURBINE FLOW RATE (LB_m/SEC)
 \dot{W}_v = VENTURI FLOW RATE (LB_m/SEC)
 \dot{W}_r = REACTOR FLOW RATE (LB_m/SEC)
 N = TURBO-PUMP SPEED (RPM)
 SUBSCRIPT o = QUIESCENT VALUE

FIG. 1 CONTROL SYSTEMS BLOCK DIAGRAM



DESIGN AND EVALUATION OF ELECTROPNEUMATIC
SERVO ACTUATORS FOR THE NERVA ENGINE¹

D. J. Schaffer² and A. J. Wetzel³

The Bendix Corporation

ABSTRACT

This paper discusses the type of control actuators being developed by The Bendix Corporation for use in the environments of the NERVA engine. Included are slides showing the major work functions and the approach to the design and analysis of sub-systems to accomplish these functions. The factors affecting the design approach as well as basic sizing criteria are reviewed. Slides and data showing the status of development tests on components and materials for applicability to the temperature, nuclear, and working fluid environment are presented. Analytical and test data are compared to indicate the validity of the mathematical models used to evaluate performance.

The material presented herein is only a summary, and this information is amplified upon oral presentation using the slides shown.

INTRODUCTION

The need for controls which must operate in extreme environments and in the high intensity radiation fields of a nuclear rocket engine led to sponsorship of a program for development of electropneumatic controls by the Los Alamos Scientific Laboratory. The technologies established under this program have been extended and are being applied to engine controls for the NERVA engine. Figure 1 shows schematically the relationships of the controls to the engine functions. Cryogenic temperatures and high neutron and gamma flux levels preclude the use of conventional hydraulic servo systems; availability of power and operating fluid from the engine pumping system enhance the use of a pneumatic system.

¹Presented at Joint ARS/ANS/IAS Nuclear Propulsion Conference, Monterey, California, August 15-17, 1962.

²Supervisor, Nuclear Propulsion Controls Group, Mechanical Development Department, Research Laboratories Division, Southfield(Detroit)Michigan.

³Project Engineer, Propulsion Controls, Products Aerospace Division, South Bend, Indiana.

The basic configuration, applicable to many engine work functions, consists of a high speed rotary element in combination with a speed reducing transmission for either rotary or linear output motion. A high speed motor with small volumes under compression minimizes compressibility effects of the operating fluid and results in satisfactory performance when using supply pressure either as low as 100 psi or in excess of 1000 psi. The indicated success of dry film lubricants would appear to permit operation with gas at cryogenic temperatures and eliminates the need for external lubrication systems.

TYPICAL PNEUMATIC POSITION SERVO SUBSYSTEM

A functional block diagram of a rotary position actuator (Figure 2) and corresponding simplified computer model (Figure 3) may be used to illustrate typical components and their individual performance characteristics.

The computer model typifies the Bendix rotary actuator design approach. The particular gain settings and loop compensation may be optimized for each actuation system. Typical component characteristics are discussed in later paragraphs.

Four types of servo amplifiers have been designed, fabricated and tested with pneumatic servos; all have resulted in satisfactory performance. These are (1) Magnetic Amplifiers (2) Transistor Amplifiers (3) Combination Magnetic and Transistor Amplifiers (hybrid) (4) Ceramic Vacuum Tube Amplifiers. A mag-amp design, which is probably the best compromise for radiation tolerance, performance, and reliability, has been used in the analytical and test comparisons made in this paper. A typical transfer function and dynamic characteristics of the amplifier for one actuator are shown on Figure 4.

The torque motor travel is made proportional by the use of a spring tube in which the rigid output member is centered. The spring tube also acts as a pressure seal. Polarizing flux for moderate to very low temperature environments is supplied by permanent magnets. For extremely high temperature, in another application where 1200° F operation is required, electromagnetic polarization is used. The frequency response to voltage and the steady state characteristics of an early design PM torque motor are shown on Figure 5.

The servo valve for this application is a two stage, four landed, closed center, area control valve. The spool valve operating as the second stage uses position feedback with one-to-one motion ratio to the pilot stage. Stable operation is obtained by means of controlled volumes of "damping tanks" at each end of the spool. These tanks, along with an entry bleed, are sized as a function of ram volume/area ratio, the average pressure level, steady state servo flow and servo medium. All other parameters remaining constant, the damping volume is proportional to the gas constant. Dynamic performance of the valve and torque motor combination is shown in Figure 6.

Typical torque-speed characteristics of the servo motor (shown on Figure 7) are necessary for the nonlinear computer performance evaluation. The map shown in Figure 7(a) is the idealized torque developed from the motor and 7(b) reflects the friction torque characteristic of the motor. A three-gear motor is used and various flow porting schemes are incorporated to obtain optimized

performance characteristics.

It can be shown that to obtain optimum sizing with respect to gas consumption and motor size, notwithstanding other requirements, the power section of the actuator may be sized to meet frequency response requirements; that is, the motor and transmission are sized to provide power saturation at the specified amplitude and frequency. This method of component selection will result in the typical generalized characteristics shown on Figures 8 and 9. Compromises are sometimes necessary since optimum power matching for response to sinusoidal inputs may not result in desired slew rates or acceleration potentials.

Actuation gas consumption may be small in comparison with engine requirements, nevertheless an understanding of motor leakage and its effect on motor performance is necessary. Gas consumption is dependent upon motor speed and system leakage; in addition, porting schemes used to achieve optimum dynamic motor-valve performance may have a bearing on gas consumption.

Figure 10 indicates schematically the valve and motor leakage paths as shown on the circuit in Figure 11. The calculation of leakage areas was verified by stalled and free running motor tests on a typical design motor. Flow-torque studies of the motor with various porting schemes have been made. Typical pressure-torque characteristics with the ported and unported motor are shown in Figures 12 and 13. The observed improvement in gain obtained with the ported motor is caused by the increased separation of the pressure curves.

A complete nonlinear simulation study of the steady state and dynamic characteristics of the actuator was performed on an analog computer. Again referring to Figure 3, two function generators, (Figure 7) were used to express the steady state servo motor performance and since this mapping function permits the simulation of nonlinear effects, the correlation of analytical and experimental tests was very good. A photograph of the generator is shown in Figure 14.

One principle problem that exists from a test correlation standpoint is the proper simulation of the load friction. Steady state performance and dynamic stability or bandpass are not seriously affected, but the character of the slow ramp response is affected by the load friction simulation. After considerable effort good correlation with test results was obtained. Figure 15 shows the correlation of computer to actual hardware test results. A major result of this work is the establishment of confidence in the analytical techniques developed for pneumatic systems.

COMPONENT DESIGN AND TEST RESULTS AT CRYOGENIC TEMPERATURES

The most significant problem area with respect to actuators for the NERVA engine is operation at cryogenic temperatures with either no lubrication or with solid film lubricants. An extensive component test program has been established on NERVA and some of the results and critical design problems are reported in this paper.

Tests on the servo motor, consisting of the torque motor, servo valve and gear motor, have been performed in a gaseous nitrogen environment at -240°F . While the servo motor functioned properly at low temperatures and no seizures or failures occurred, both dynamic and static friction increased slightly. The speed-current gain change was very close to that predicted analytically from the Gas Laws due to lower supply gas temperature and the bandpass was reduced from 12 to 8.5 cps as shown on Figure 16. The small, non-predicted change is attributed to the combined effects of leakage, friction and gain change of the servo valve. Since these are the results of the first tests at low temperature they are felt generally to be satisfactory. Evaluation of the components is continuing and recommendations for design changes are being made.

Rotary-to-rotary and rotary-to-linear transmissions are undergoing tests. Ball-lead screws of different materials in combination with either no lubricant or dry film lubricants have been tested at -360°F . In one application satisfactory operation was achieved without lubricant; torque efficiency of another unit fell off due to accumulation of lubricant on the balls. At this date no significant life test data can be reported. Figure 17 shows the rotary-to-linear transmission in the test fixture adaptable for cold temperature evaluation.

The balls and retainers of ball bearings appear to present the greatest problem and new lubricants are being investigated. For rotary-to-rotary high reduction transmissions, Bendix is developing the Nutator Drive. This device is shown in schematic and assembly form in Figure 18. In view of the bearing problem, a significant advantage of the Nutator Drive design is the reduction in total number of parts (e.g., 5 bearings instead of 18 for a planetary drive of equal ratio) as well as theoretically higher load carrying capabilities. Satisfactory results have been achieved during initial room temperature and cold temperature operation; life tests are now in progress.

In general, the problems associated with pneumatics have been minor -- most problems being of a mechanical nature. Also tests on amplifiers and transducers at low temperatures have been very satisfactory. The potentiometers used are of the conductive plastic type and there is negligible change in output as temperatures are varied from 400°F to -300°F . The servo amplifier as previously described is either a three or four stage mag-amp, depending upon the application. Although, at this writing, the environmental specifications for the electrical equipment have not been defined, study and preliminary tests of radiation hardened amplifiers have been made and are still in progress. Components, insulation, and encapsulating materials were chosen on the basis of a literature survey and from results achieved in actual reactor tests. Limited vibration tests showed excellent results. Performance at a temperature range of $+300^{\circ}\text{F}$ to -300°F has been very good.

Figure 19 is a photograph of a control drum actuator fabricated and tested during the NERVA Phase I period. Figure 20 is a photograph of the Bendix Model ND-D1 control designed, fabricated and tested for the Westinghouse Astronuclear Laboratories under the NERVA program. Figure 21 shows a layout of the TPCV actuator currently being fabricated for developments tests. This unit includes the high pressure dynamic seal and the features necessary to

facilitate the remote handling problem.

Figure 22 shows a design of the NERVA 5-HP Gimbal Actuator including sizing to meet the projected reliability goals.

CONCLUSION

Electropneumatic actuators which will meet the performance and environmental requirements of the NERVA engine appear to be both feasible and practical, however, continued development work is necessary to establish reliability under low temperature operating conditions. Analytical techniques have been developed to the point where fair correlation between test and analysis is obtained for the pneumatic systems described. Some of the observed phenomena is still inexplicable, however, refinements in mathematical models as well as better test procedures should resolve these differences.

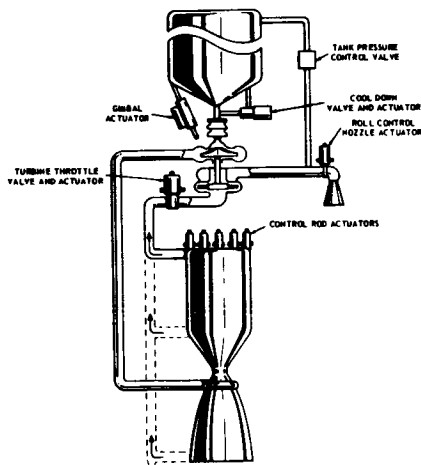


Figure 1 - Schematic of Engine and Major Engine Controls

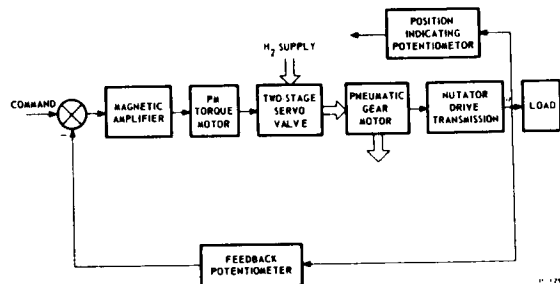


Figure 2 - Functional Block Diagram Bendix Rotary Pneumatic Actuator for NERVA Application

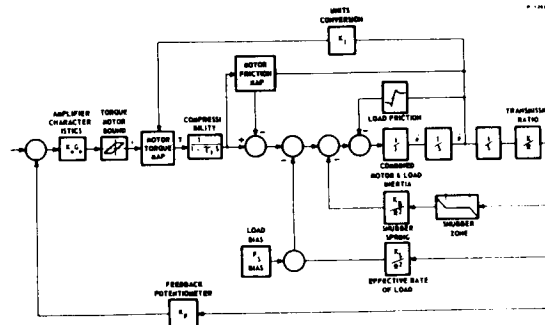


Figure 3 - Simplified Computer Model Bendix Pneumatic Actuator

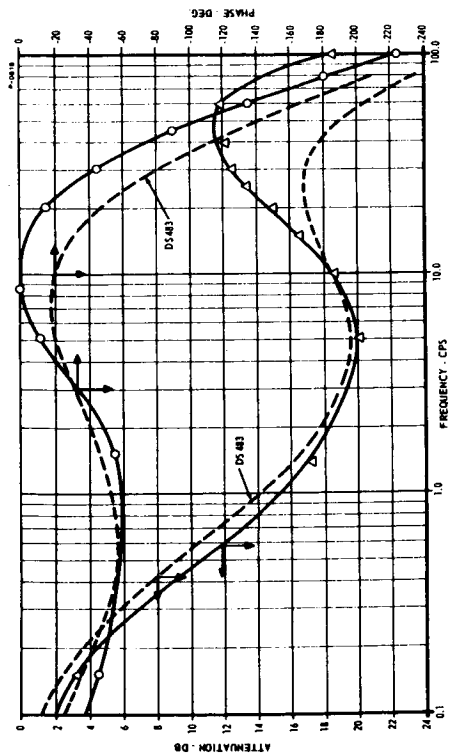


Figure 4 - Servo Amplifier Response - Control Rod Actuator

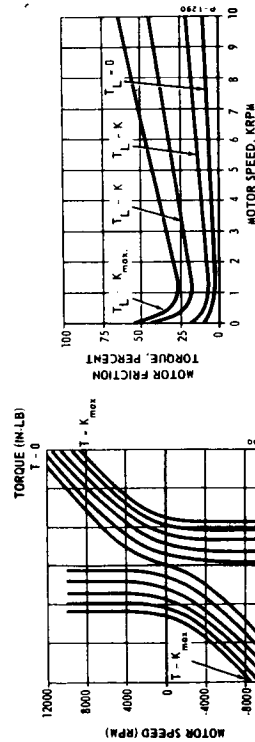


Figure 7(a) - Idealized Torque-Gear Motor

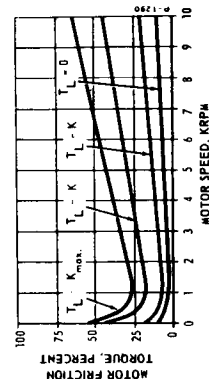


Figure 7(b) - Friction Torque-Gear Motor

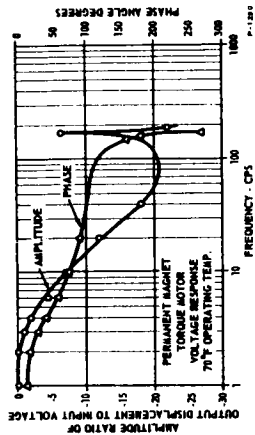


Figure 5 - Voltage Frequency Response

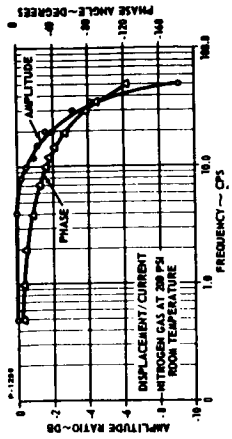


Figure 6 - Frequency Response P_M Torque Motor-Servo Valve

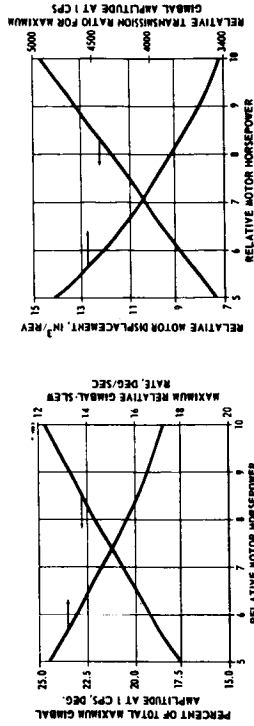


Figure 8 - Gimbal Actuator Sizing Characteristics

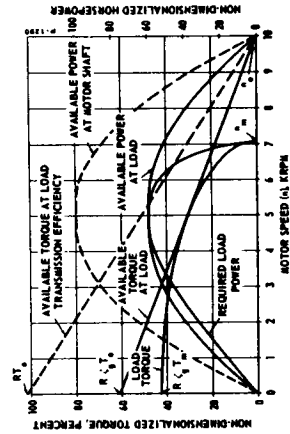


Figure 9 - Load Profiles - Gimbal Actuator

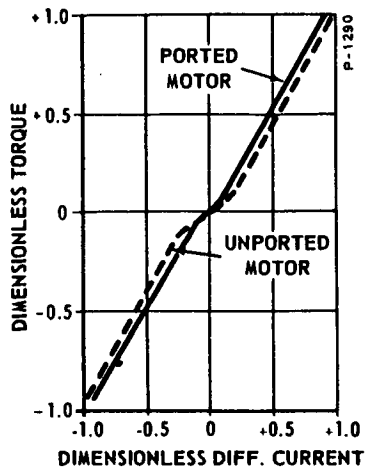


Figure 13 - Servomotor Torque Gain Characteristic Stalled Motor

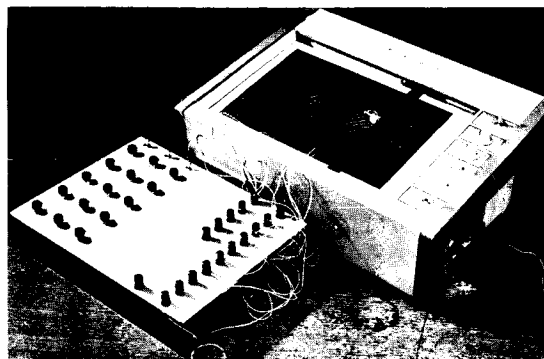


Figure 14 - Mapping Function Generator

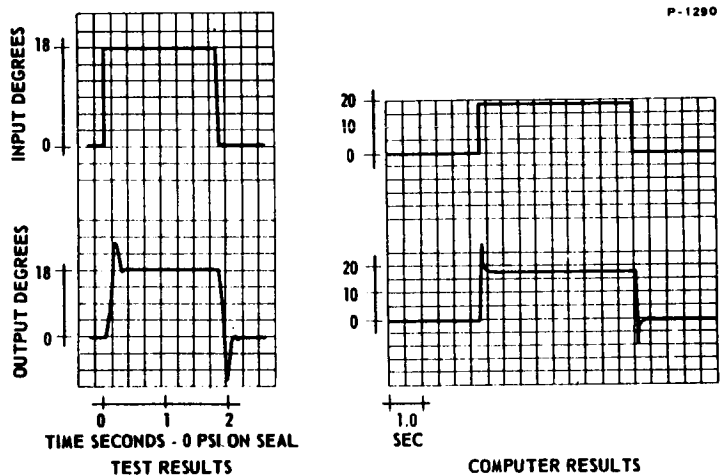


Figure 15 - Reactor Control-Step Response

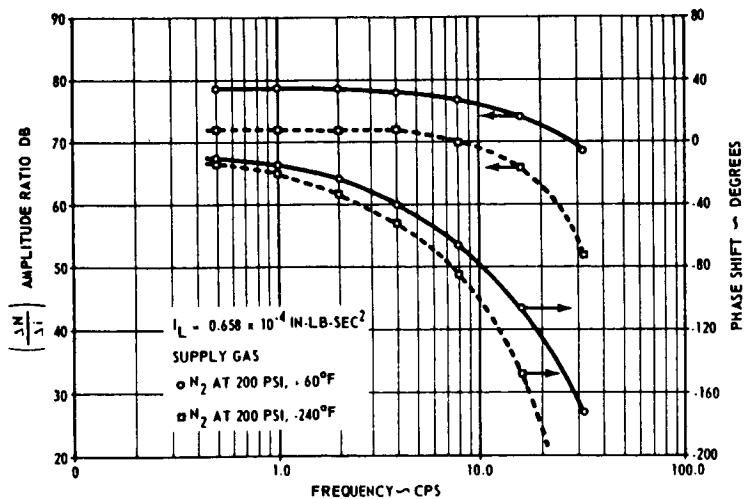


Figure 16 - Frequency Response NT-1 Servomotor

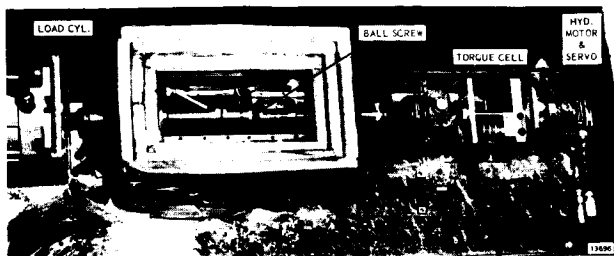


Figure 17 - Fixture - Rotary to Linear - Drive End

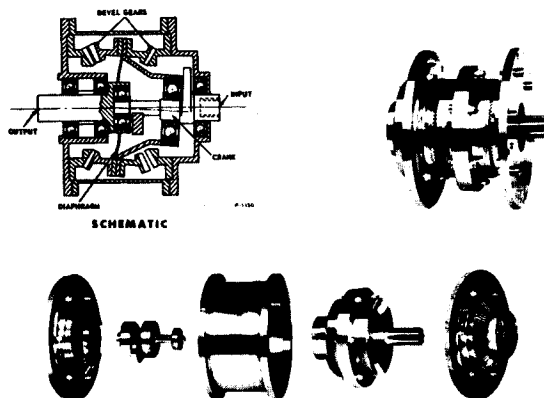


Figure 18 - Nutator Transmission

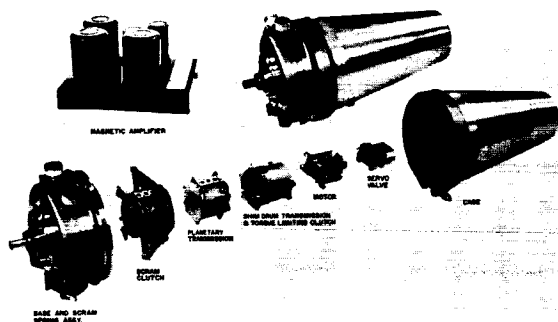


Figure 19 - Rotary Servo Actuator and Components

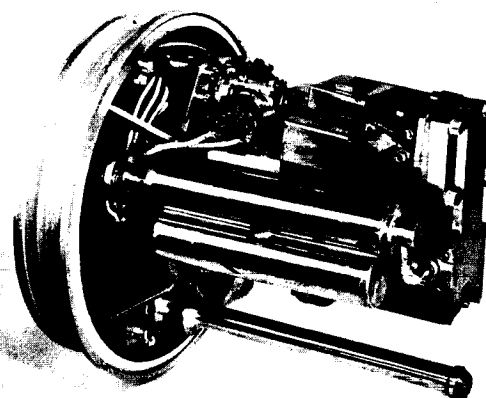


Figure 20 - ND-D1 Control Drum Actuator

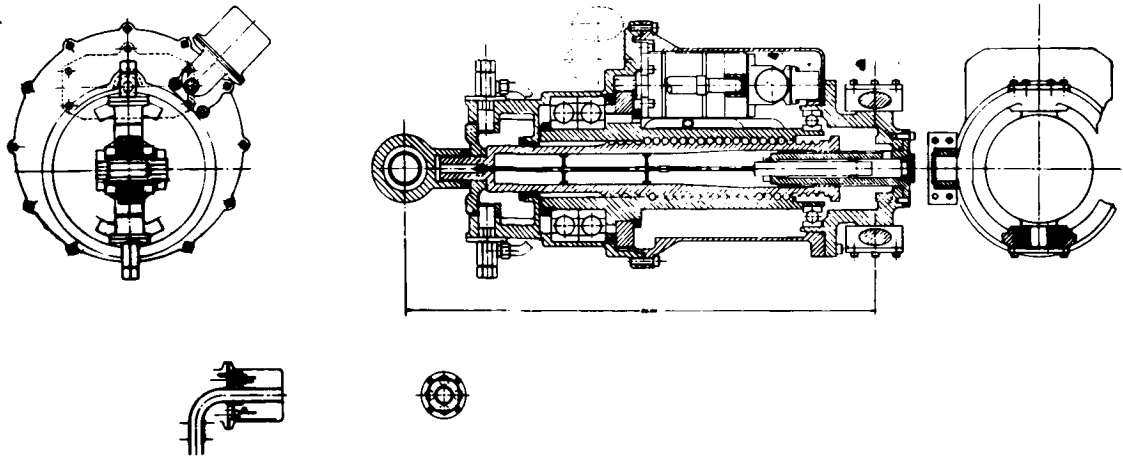


Figure 21 - Model NT-B1 Turbine Power Control
Valve Actuator

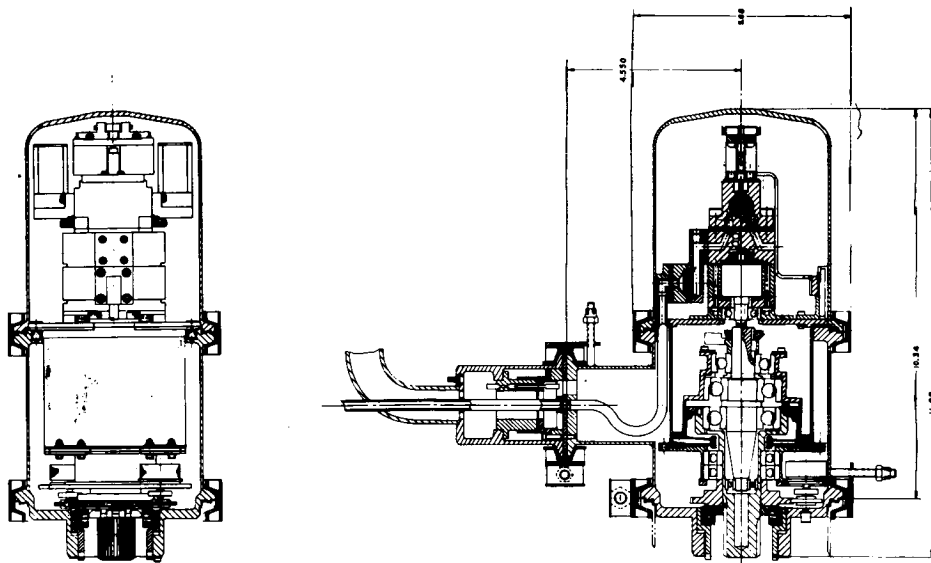


Figure 22 - NERVA Actuator - Thrust Vector Control

66 50293

CONTROL AND TELEMETRY TRANSDUCER REQUIREMENTS
FOR
NUCLEAR POWERED VEHICLES*

by M. C. Johnson
The Bendix Corporation

The development of new vehicles and new propulsion techniques results in the need to measure some parameters to accuracies, magnitudes, or in environments that have not previously been encountered. The nuclear powered vehicle programs exemplify this. For example, measurements of pressures and temperatures in a space vehicle environment which includes high level neutron and gamma radiation, are new requirements demanding advancement in the state-of-the-art.

Since there is sometimes a lack of good communication between those engaged in producing transducers for vehicle applications and those developing the vehicles, a survey has been made to determine what transducers will be required, what is available or under development, and in what areas development work should begin to insure that a transducer will be available to meet a new requirement.

In the following discussion, some of the major problem areas in Rover, SLAM, and SNAP vehicles are discussed and some potential solutions are mentioned.

A typical nuclear rocket configuration is shown in Figure 1. The difficult environments here are the nuclear radiation and the liquid hydrogen at 20°K. Some areas contain hydrogen at extremely high temperatures, and there is fairly severe vibration throughout the vehicle.

Table 1 lists the measurements on the nuclear rocket vehicle which exceed the present telemetry transducer state of the art. With two exceptions the problems are those of a combined low temperature and radiation environment. The primary reason for this is the fact that test data in this environment are so sparse that it is not known whether available transducers will survive and operate in it. Some tests on standard pressure transducers in liquid hydrogen were performed by the National Bureau of Standards at Boulder, Colorado. They found hysteresis in a potentiometric type, but some strain gauge pressure transducers operated quite well although rated to only -65°F. A great deal of combined environment testing at cryogenic temperatures will be required to determine which transducers will operate reliably in these locations on the nuclear rocket.

* The information in this paper is based on work performed by the Bendix Corporation, Research Laboratories Division, for the Aeronautical Systems Division under Contract AF 33(616)-8077, Project No. 4107, Task No. 410719-4.

The two measurements required in extremely high temperature environments cannot possibly be made in that environment by any pressure or vibration transducer that will be available in the foreseeable future. Environmental control is imperative and in these cases can be achieved by cooling with the cold gaseous hydrogen which is readily available. There is a possibility of thermal shock at startup, so even this may be a low temperature problem area.

Liquid level transducers can be constructed which will operate without deterioration in the propellant tank environment; but boiling, zero g, and ionization in the liquid hydrogen can introduce errors. Temperature measurements also can be made in all the environments to be encountered, but a general improvement in characteristics is required for better accuracy and reliability. Mass flow transducers having rotating parts have a reliability problem. They have been known to explode when a slug of gas passed through the turbine due to runaway.

The SLAM vehicle is outlined in Figure 2. In contrast to Rover this vehicle is characterized by an over-all temperature level as high as 1200°F (Table 2). There is also a high vibration level and, for the longer mission times, an extremely high total radiation dose. In these cases the radiation dose will be a minor problem compared to temperature. High temperature materials and construction techniques are inherently radiation-resistant. Lifetime will be fairly short, in the range of 10 to 30 hours. Cooling with 1200°F ram air can be done for measurements other than those directly on or in the reactor. These measurements do not appear feasible, barring some break-through in high-temperature strain and vibration measurement technology. The measurements at 1200°F are close to present capabilities. Displacement transducers based on the differential transformer principle are now available for operation at 1300°F. Application of these techniques to pressure transducers should not be too difficult. Work has been done on high-temperature alloys for strain and vibration transducers at 1600°F. These are not commercially available items, and more work needs to be done before useful measurements can be made at these temperatures. A 1000°F ion chamber has been produced. A great deal of other work has been going on to develop radiation detectors for use within reactors at temperatures approaching 1000°C. The techniques developed should be applicable to telemetry detectors also. Temperature transducers will operate in all environments, but drift and vibration may be problems.

Figure 3 is a sketch of SNAP-8. SNAP-10A is similar in outline but does not have the mercury turbine loop. Instead, electrical power is generated by means of thermoelectric cells. The problem areas listed in Table 3 are for both SNAP-8 and SNAP-10A. The lower temperature measurements are for SNAP-10A.

The measurement problems on the SNAP are quite serious, the major difficulty being the requirement for reliable operation over 10,000 hours in the high temperature vacuum or NaK environment. Pressure measurements have been made in NaK at 1400°F, but the transducers used were unsuited to a space vehicle, and reliability and life were far less than required. Radiation will not be a problem, in all likelihood; but no test data are available for

reliability of these types of components exposed to a very long-term radiation dose. Remote location and shielding are possible to ease the requirements. For example, the pressure transducers could be brought down to the lower temperature environment below the shield by using a few feet of tubing.

In general, environmental modification is undesirable for transducers in all of these vehicles because of the size and weight penalty involved. In some cases it must be done; for example, the pressure transducer on the nuclear rocket exit plenum, because the measurement is necessary and the environment is intolerable. In others, it is relatively easy, such as relocation of the SNAP pressure transducers below the shield. In most cases, however, these difficult measurements will not be made unless a transducer is developed which will withstand the environment and operate satisfactorily.

To summarize, the conclusions of the survey are:

- (1) Many of the new requirements can be met by substitution of inorganics for radiation-sensitive materials in the construction of the transducer.
- (2) There is a need for testing of transducers in combined cryogenic-radiation-vibration environments.
- (3) The high-temperature limit of most transducer types should be extended up into the 1500°F range.
- (4) Reliability data for long-time operation in high temperature and combined high-temperature-radiation environments are needed.
- (5) The desirability of high-level dc outputs indicates that the temperature capability of potentiometers should be extended above 1000°F and down into the cryogenic region.
- (6) Most transducers will be subjected to heating by gamma radiation, and adequate cooling or heat paths must be provided.
- (7) Cables and connectors are a major problem area in the combined temperature, radiation and vibration environment.

REFERENCE

Bendix Research Laboratories Division Report No. 2084,
"Transducers for Nuclear Vehicles," 24 January 1962.

Table 1 - Rover Measurement Problem Areas

TYPE	OPERATING TEMPERATURE (°F)	RADIATION DOSE (n/cm ²)	AMBIENT MEDIUM	RANGE	COMMENTS
ROTARY DISPLACEMENT	-240	1×10^{17}	AIR VACUUM AND GASEOUS H ₂	0 - 180°	_____
ROTARY DISPLACEMENT	-300	1×10^{16}	AIR AND VACUUM	-5° TO +5°	_____
LINEAR DISPLACEMENT	-420	5×10^{15}	AIR AND VACUUM	0 TO 2.5 INCHES	_____
PRESSURE	COOLED, MAY BE -400 AT STARTUP	7×10^{17}	AIR, VACUUM AND L H ₂	0-550 PSIA	FLUID AT 4400°F UNCOOLED
PRESSURE	-310 FLUID TEMPERATURE	3.6×10^{16}	AIR OR VACUUM	0-650 PSIA	FLUID IS GASEOUS H ₂
PRESSURE	-260 FLUID TEMPERATURE	7×10^{15}	AIR OR VACUUM	90-650 PSIA	FLUID IS GASEOUS H ₂
STRAIN	-300	7×10^{17}	AIR OR VACUUM	_____	STATIC AND DYNAMIC
STRAIN	-420	6×10^{13}	AIR, VACUUM OR L H ₂	_____	STATIC AND DYNAMIC
TORQUE	-420	1×10^{16}	AIR OR VACUUM	_____	STATIC
VIBRATION	-410	3×10^{16}	AIR OR VACUUM	_____	OUTPUT PROBLEM
VIBRATION	-410	5×10^{13}	AIR AND VACUUM	_____	OUTPUT PROBLEM
VIBRATION	4540	7×10^{18}	GASEOUS H ₂	_____	_____
MASS FLOW	-407	1×10^{16}	L H ₂	6 TO 100 LBS/SEC	_____

LIQUID LEVEL - MAY BE RADIATION INDUCED ERRORS IN THE LH₂

STRAIN - BONDING MAY BE THE MOST SEVERE PROBLEM

TEMPERATURE - GENERAL ADVANCEMENT REQUIRED, PROBLEMS OF DRIFT, UNIFORMITY, RELIABILITY, AND SIGNAL

Table 2 - SLAM Measurement Problem Areas

TYPE	OPERATING TEMPERATURE (°F)	RADIATION DOSE (n/cm ²)	AMBIENT MEDIUM	RANGE	COMMENTS
LINEAR DISPLACEMENT	2000	2×10^{18}	AIR	20 INCHES	—
PRESSURE	2250	2×10^{18}	AIR	TO 226 PSIA	FLUID IS AIR
PRESSURE	1560	2×10^{17}	AIR	0 TO 2.7 PSIA	FLUID IS AIR
PRESSURE	1200	1×10^{18}	AIR	0 TO 350 PSIG	FLUID IS AIR
DYNAMIC STRAIN	2600	3×10^{19}	AIR	—	INTENSE VIBRATION
VIBRATION	2600	3×10^{19}	AIR	—	—
NUCLEAR	1200	2×10^{17}	AIR	TO 6×10^{12} nV	NEUTRON RADIATION
NUCLEAR	1200	2×10^{17}	AIR	2×10^6 ERGS/GM C-SEC	GAMMA RADIATION

P-1257

TEMPERATURE - GENERAL DRIFT AND SIGNAL LEVEL PROBLEMS

Table 3 - SNAP Measurement Problem Areas

TYPE	OPERATING TEMPERATURE (°F)	RADIATION DOSE (n/cm ²)	AMBIENT MEDIUM	RANGE	COMMENTS
ROTARY DISPLACEMENT	1300	1×10^{20}	VACUUM	0 - 180°	1 YR OPERATION
ROTARY DISPLACEMENT	1000	1×10^{19}	VACUUM	0 - 180°	1 YR OPERATION
PRESSURE	1300 FLUID TEMPERATURE	9×10^{18}	VACUUM	0 - 31 PSIA	NaK FLUID
PRESSURE	1100 FLUID TEMPERATURE	9×10^{18}	VACUUM	0 - 31 PSIA	NaK FLUID
PRESSURE	900 FLUID TEMPERATURE	1×10^{18}	VACUUM	0 - 40 PSIA	NaK FLUID
PRESSURE	800 FLUID TEMPERATURE	1×10^{18}	VACUUM	0 - 40 PSIA	NaK FLUID
STATIC AND DYNAMIC STRAIN	1450	4×10^{20}	NaK	—	ON FUEL ELEMENT
DYNAMIC STRAIN	1000	3×10^{19}	NaK	—	ON FUEL ELEMENT

P-1257

TEMPERATURE - SERIOUS DRIFT PROBLEM
 ALL TYPES - SERIOUS RELIABILITY PROBLEM FOR 1 YR OPERATION

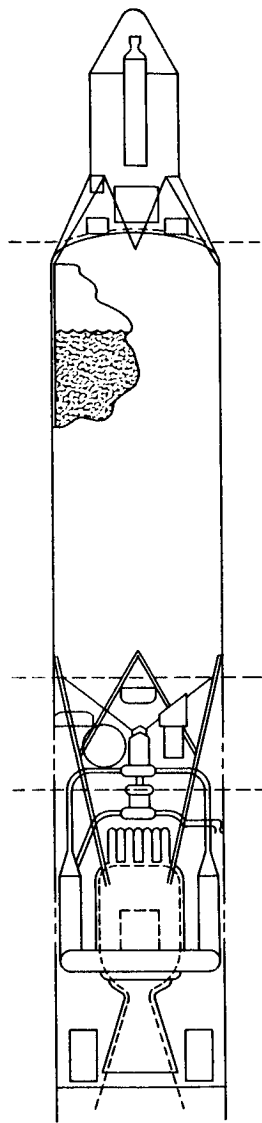


Figure 1 - Conceptual Nuclear Rocket

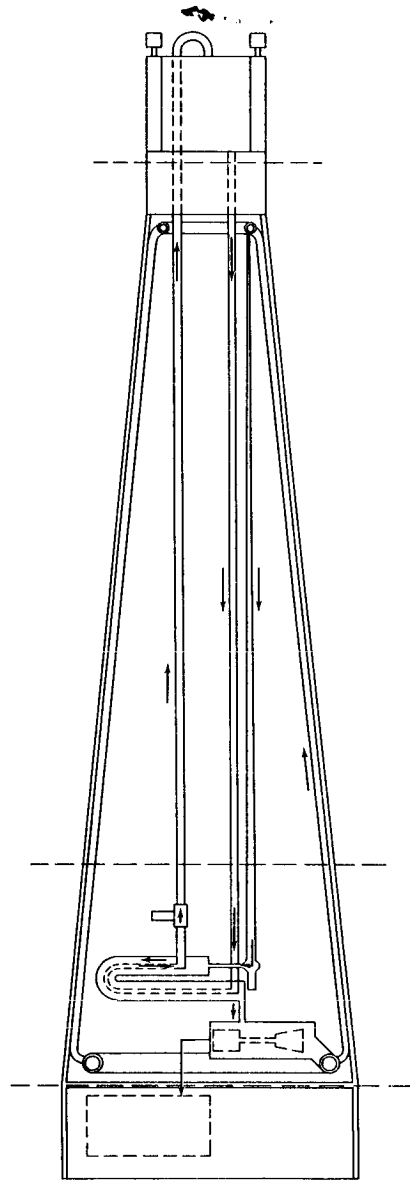


Figure 3 - SNAP Vehicle

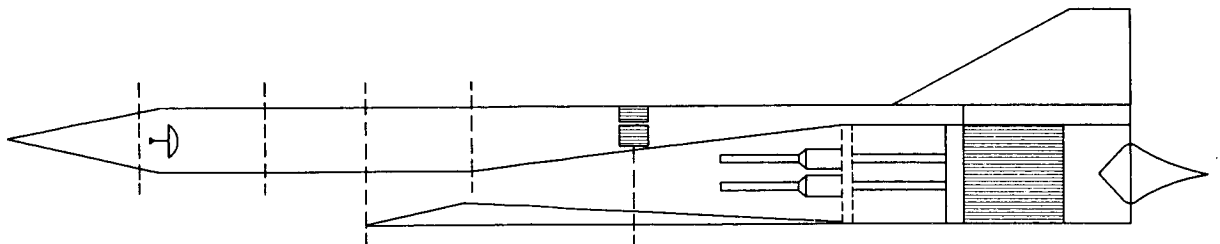


Figure 2 - Conceptual Nuclear Ramjet

SUMMARY OF NUCLEAR RADIATION HEATING ANALYSIS AND
COOLING SYSTEM DESIGN OF A KIWI-B PROTOTYPE
ROTARY ELECTROPNEUMATIC CONTROL ACTUATOR [U]

By
James J. Edmond,

66 50294

FOREWORD

This paper reports work conducted at the Research Laboratories Division of The Bendix Corporation, sponsored by the Los Alamos Scientific Laboratory under Atomic Energy Commission Contract AT (29-2)-705.

The author also wishes to acknowledge the contribution of Mr. C. W. Hamilton* and Mr. B. G. Southward of Bendix Research Laboratories Division, on gamma heating and neutron heating portions of this paper.

Superscript numbers in parentheses indicate references listed at the end of the paper.

INTRODUCTION

The prototype electropneumatic actuators developed to position the reactor control drums in Kiwi-B are mounted on the pressure vessel and exposed to leakage radiations from the core. On Kiwi-B the anticipated radiation intensity in this region at 1000 Mw reactor power will produce an estimated adiabatic temperature rate in steel of about 7°F per second. A cooling method more effective than conduction or thermal radiation is required to maintain equilibrium actuator temperatures within tolerable limits during tests at full reactor power. Forced gas convection using a portion of the hydrogen propellant was a logical choice as the basic heat transfer mechanism of the cooling system.

The radiation heating rates in the actuator were determined from the anticipated radiation environment, upon which heat transfer analyses were conducted leading to the design, construction, and laboratory testing of the convective cooling system.

DESCRIPTION OF RADIATION ENVIRONMENT

Data on the anticipated Kiwi-B leakage fluxes in the vicinity of the actuator location were supplied by the Los Alamos Scientific Laboratory. The radiation is assumed to be directed essentially outward from a spherical surface defined by a 1.5 meter radius from the center of the core between the conical coordinates superimposed on Figure 1. The calculated spectra of the gamma and neutron energies at the 1.5 m coordinate surface are given in Figure 2. The total gamma flux through the surface is about 1.5×10^{14} Mev/cm²-sec, peaked at 2 Mev, with a neutron leakage of about one neutron per fission, or approximately 10^{14} neutrons/sec-cm² at full reactor power.

*Presently (1962) with Los Alamos Scientific Laboratory,
Los Alamos, New Mexico.

DETERMINATION OF HEATING RATES

To enable a reasonably economical calculation program, a simplified model of the flux and actuator geometries was chosen as shown in Figure 3. The flux was approximated by a collimated beam intercepting the vertical axis of a variable-mass-density model of the actuator at an average angle of 22°. These approximations ignored statistical deviations of the angle of the incident flux vector, effects of scattering, and geometric attenuation of incident flux intensity with distance from the source.

GAMMA HEATING

A series of iso- μx lines, or "lines of constant shielding" were drawn connecting points within the actuator model shielded by the same mass density along straight lines at the 22 degree angular inclination with the model center-line (Figure 4). For the gamma radiation, these lines were then transformed into contours of constant energy deposition rate per unit mass by application of the equation

$$\frac{d^2 E}{dt dm} = \sum_{i=1}^N A_n B_n \mu_n e^{-\mu_{(on)} x}, \quad (1)$$

where

- n = identifies the gamma ray energy group $E_1, E_2 \dots E_N$
- μ_n = energy absorption coefficient⁽¹⁾ for this group
- $\mu_{(on)}$ = total energy absorption coefficient⁽²⁾ for the mean energy of this group
- A_n = power carried by the n^{th} group of gamma rays
- B_n = energy absorption buildup factor⁽¹⁾ for n^{th} energy group
- x = shielding distance from surface along a 22° inclination line.

The computation was performed digitally for the eight energy groups noted on Figure 2a for increments of one-half inch penetration, which generated a profile of gamma energy deposition in the model based on the assumptions made. The maximum gamma heating in the first half inch of the base of the actuator is estimated at approximately 640 watts per pound (steel).

NEUTRON HEATING

Neutron energy deposition in the actuator was calculated by assuming a most probable energy loss per collision of 3.4 per cent (one-half the maximum loss of 6.8 per cent) with a most probable elastic scattering angle of approximately 90 degrees. The 1.44 Mev gamma occurring from inelastic scattering of neutrons by chromium was not considered. However, a portion of neutron attributable heating due to high energy gammas from the thermal neutron capture was considered to occur in the base regions of the actuator. About 85 per cent of the high energy portion of the neutron spectrum undergoes first collisions; within the 8 cm diameter of the reference cylinder, the number of collisions per neutron was considered to be 18 for those energies

below 100 ev, diminishing to 4 collisions for those energies above 100 kev. The bare and reflected sphere neutron spectra were mixed to represent the direct and reflected neutron distribution, and the energy deposition (H) attributable from neutron collisions per energy group was calculated from

$$H_i = \sum_{j=1}^n \left[\Sigma_i^s (0.034)(1-0.034)^j E_i N(E_i) \right] + \Sigma_i^c N(E_i) E_\gamma$$

such that

$$\sum_{i=1}^m H_i = \sum_{i=1}^m \left\{ \sum_{j=1}^n \left[\Sigma_i^s (0.034)(1 - 0.034)^j E_i N(E_i) \right] + \Sigma_i^c N(E_i) E_\gamma \right\} \quad (2)$$

where

Σ_i^s = macroscopic scattering cross section of i^{th} neutron group, cm^2/g

Σ_i^c = macroscopic capture cross section of i^{th} neutron group, cm^2/g

E_i = initial energy of neutrons in the i^{th} neutron group

E_γ = energy of gamma photon from neutron interaction other than elastic scattering

= 10 Mev (capture)

$N(E_i)$ = number of neutrons/ cm^2 sec in the i^{th} energy group

n = number of scatterings = $8 \text{ cm}/\lambda_i f$

λ_i = mean distance traveled per collision, an inverse function of neutron energy

$$f = \sqrt{\lambda_x^2 + \lambda_y^2 + \lambda_z^2} / 6\lambda = \sqrt{4 \lambda_x^2} / 6\lambda$$

The neutron heating rate is estimated at about 60 watts per pound in the base assembly and about 26 watts per pound in the rest of the actuator, roughly an order of magnitude below the gamma heating rates.

HEATING RATE DISTRIBUTION

The total estimated maximum radiation heating rate in the actuator base is about 700 watts per pound (iron), which was conservatively assumed to occur within the first half-inch of actuator material along the 22 degree average slant path. The geometric concept of iso- μx lines in the initial mathematical model was then applied to a similar plot across an actual cross section of the actuator, as shown in the view of Figure 5. Transverse sections were then developed across certain massive portions of the actuator as shown.

The transverse plots show crescent shaped areas of variable heat generation, differing by as much as a factor of three across a given section, resulting from the extensive approximations used. No further approximations regarding smoothing effects were introduced and heat transfer analyses upon

the transverse sections were made to determine the tolerability of thermal effects which would result from assuming the existences of the heating gradients indicated.

INVESTIGATION OF VARIABLE TRANSVERSE HEATING RATES

The reference actuator design is not particularly susceptible to performance decrements, such as increased friction or binding caused by unrestrained thermal bowing of the cantilevered assembly under moderate transverse temperature gradients, but may become a problem for transverse temperature differences on the order of 150°F.

The heating gradient problem was studied by an electrical resistive-surface analog method. The effects of various heat transfer coefficients and coolant flow rates were investigated, with the simulation indicating that transverse temperature gradients would not be excessive for axial coolant flows and would tend to be overcome by circumferential cooling flows introduced on the hot side of the components. The fairly uniform surface temperatures were interpreted to indicate that uniform average values of heating rates could be used for the convective heat transfer calculations, varying in steps according to the axial location of the individual components.

DESIGN OF COOLING SYSTEM

Nominal design values were chosen of 300°F for the maximum actuator operating temperature and 70°F for the coolant inlet temperature. A nominal value of 0.06 lb/sec coolant flow rate per actuator was chosen, to represent a reasonable balance between coolant temperature rise and realistic heat transfer coefficients versus the desire to minimize the potential nonpropulsive expenditure of hydrogen. Standard empirical convective heat transfer correlations (3), (4), (5) of the form

$$N_{Nu} + K N_R^m N_{Pr}^n \quad (3)$$

where

N_{Nu} = Nusselt Number

N_R = Reynold's Number

N_{Pr} = Prandtl Number

K, m, n = empirical coefficients referring to the local flow process,

were applied to work out the design of the coolant channels and the local coolant flow rates required.

Many components of the reference actuator have complex inner geometries, with central rotating portions thermally isolated from housings and external structure by bearings. As a result, cooling only the exterior housing surfaces of such parts would not be particularly effective. Many of these components have narrow gaps between rotating parts and other interior surfaces, and fairly minor modifications (a practical requirement) could effect high-velocity flows of coolant gas through these spaces. Baffles and other secondary devices provided high local gas velocities over or through

parts to be cooled. Often coolant was introduced into the interiors of complex components through hollowed shafts or through their bearings from sealed coolant inlet chambers. For more massive components, such as the gear motor, servovalve, and base of the actuator, external thin metal shrouds were designed to provide narrow coolant flow spaces between the shroud and surface of the component. Metered flows of cooling gas were introduced into these passages, designed to direct the coolant over the surfaces are required. Such shrouds provide high local heat transfer coefficients by high local gas flow rates per unit flow area with a minimum total flow rate of coolant, and the carefully defined flow geometries allow more confident application of standard empirical flow correlations.

The various cooling passages in the actuator constitute a complex system of series-parallel flow paths between the coolant source and final exhaust. To keep macroscopic distribution of flow to individual components independent of local back-pressure effects in the actuator, coolant supply gas is metered into individual sealed channel entrances by orifices operated far above the critical pressure ratio.

A cross section of an early version of the actuator showing the cooling system and flow distribution is shown in Figure 6. For initial Kiwi-B tests, coolant gas was brought to the actuator from a separate high-pressure line, was passed through a filter in the base and distributed to the various components by an internal manifold. The exhaust gases were collected inside the actuator cover and exited through a discharge port in the base.

COOLING SYSTEM TESTS

The heat transfer performance of the cooling system was evaluated by a series of laboratory tests. The provision of a steady-state heat transfer condition in a device as complex as the actuator in the laboratory by non-nuclear methods is impractical, but transient heat transfer conditions (the basis of the test method employed) are readily produced. Hot gas is applied to the cooling system of an instrumented actuator to raise the actuator to an elevated temperature; a cooling transient is then induced by applying a large step change downward in the cooling gas inlet temperature. Thermocouples attached to various surfaces of the actuator record the resulting temperature decays.

Certain actuator parts, e.g., shafts, gears, housing, and the base assembly, have negligible internal thermal resistance; * when such parts at an elevated temperature are subjected to a sudden cooling environment, the rate of change of surface temperature approximately equals the rate of change of the average temperature of the part, and the instantaneous surface heat flux at anytime τ is

* Characterized by $N_{Bi} < 0.5$; $N_{Bi} = \frac{\Delta}{h(s/k)}$, where h is the local surface heat transfer coefficient to the external environment and (s/k) is the ratio of the dimension of the part in direction of heat flow with respect to its thermal conductivity.

$$\left. \frac{dQ_s}{d\tau} \right]_{\tau} \cong W C \left. \frac{dT_s}{d\tau} \right]_{\tau} \quad (4)$$

where

W = weight of the part

C = thermal capacity of the part (specific heat)

$\left. \frac{dT_s}{d\tau} \right]_{\tau}$ = Instantaneous rate of change of surface temperature at time τ .

The effectiveness of the cooling system for cooling these parts was thus evaluated by comparing the (negative) rate of adiabatic temperature rise $(dT/d\tau)_a$ for the anticipated local average heating rate \bar{q} , defined as

$$\left. \frac{dT}{d\tau} \right]_a = \frac{\bar{q}}{C}, \quad (5)$$

with the cooling test temperature decay curves. The point on the experimentally derived cooling curve at which the instantaneous slope is equal to the inverse heating slope represents the condition at which the surface heat flux equals the magnitude of the anticipated heat deposition. The value (ordinate) of the environmental temperature difference at this point was thus taken as an indication of the equilibrium surface-temperature excess which would exist for heat transfer from that part under the anticipated heating rate for that flow condition.

The simple evaluation method of Equations (4) and (5) cannot be applied to actuator components which have appreciable internal thermal resistance, e.g., the clutch, motor and servovalve. Upon sudden cooling, the rate of surface temperature change of these parts does not closely represent their rate of average temperature change, and Equation (4) is no longer a reasonable approximation.

Estimations of cooling system effectiveness of these parts from the transient surface temperature data therefore include compensation for internal conduction effects. The evaluation method used entailed the use of Groeber's figures, ⁽³⁾ in which the external heat transfer coefficient h was estimated graphically from a combination of the test data and geometric and materials properties of the device. The equilibrium temperature excess $\bar{\theta}_s$ at the anticipated heating rate is then determined from the weight W and surface area A by

$$\bar{\theta}_s = \frac{\bar{q}W}{hA}. \quad (6)$$

The foregoing methods were used to evaluate data from three heat transfer tests. The first two tests were run with nitrogen to evaluate the uniformity of cooling throughout the actuator with the actuator inoperative. The third test was conducted with hydrogen coolant and with the actuator in operation. The over-all initial temperature difference of the third transient test was about 400°F, with maximum initial rates up to 10°F/sec. The

recorded cyclic output waveform of the actuator showed no perceptible changes throughout the test (Figure 7).

CONCLUSIONS

Anticipated temperatures at heat transfer equilibrium within the actuator at various locations for the calculated heating rates and the design coolant flow rate are shown in Figure 8. These temperatures are extrapolated from the results of the cooling system evaluation tests and are given for two conditions of coolant inlet temperature, $+70^{\circ}\text{F}$ and -220°F .

On an absolute temperature basis, the (indicated) equilibrium surface temperatures for 70°F inlet temperature are within $+8$ percent and -11 percent of the nominally chosen 300°F (760°R) maximum surface temperature, for the design conditions of 70°F hydrogen inlet temperature and 0.06 lbs/sec. flow rate (750 psi inlet pressure). As noted, the operation of the actuator remained unchanged throughout the maximum period of heat transfer.

The actuator is presently undergoing tests to establish its performance at temperatures in the vicinity of -300°F . Coolant temperatures this low also represent a considerably greater heat transfer potential, from which further increases in allowable heating rate would tend to become limited more by internal temperature-difference problems than by a maximum allowable surface temperature rise.

Certain margins of safety are present in the over-all design of the actuator and present design of the cooling system should the heating environment be higher than predicted. The individual actuator components are designed for operation up to 600°F , and the cooling system has been proof-tested for operation at pressures up to 1000 psi. The factors indicate a margin of about 2.8 times the anticipated heating rate for average actuator temperature not to exceed 600°F using room temperature hydrogen coolant at 1000 psi inlet pressure.

REFERENCES

- (1) H. Goldstein and J. E. Wilkins, "Calculations of the Penetration of Gamma Rays," AEC Report No. NYO-3074, Contract AT-30-(1)-862, Nuclear Development Associates; June 30, 1954.
- (2) T. Rockwell, "Reactor Shielding Design Manual," D. Van Nostrand, Princeton, N.J., p 44; 1956.
- (3) M. Jakob, "Heat Transfer," Wiley and Sons, N.Y., pp. 274-278; 1949.
- (4) W. H. McAdams, "Heat Transmission," McGraw Hill, N.Y.; 1954.
- (5) W. H. Geidt, "Principles of Engineering Heat Transfer," D. Van Nostrand, N.Y.; 1957.

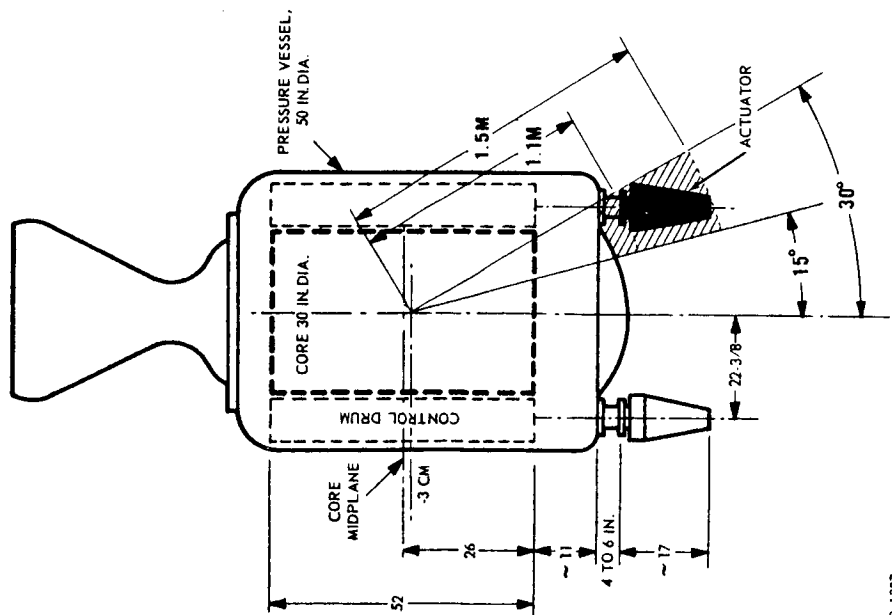


Figure 1 - Location of Rotary Control Drum Actuator on Kiwi-B and Flux Coordinates

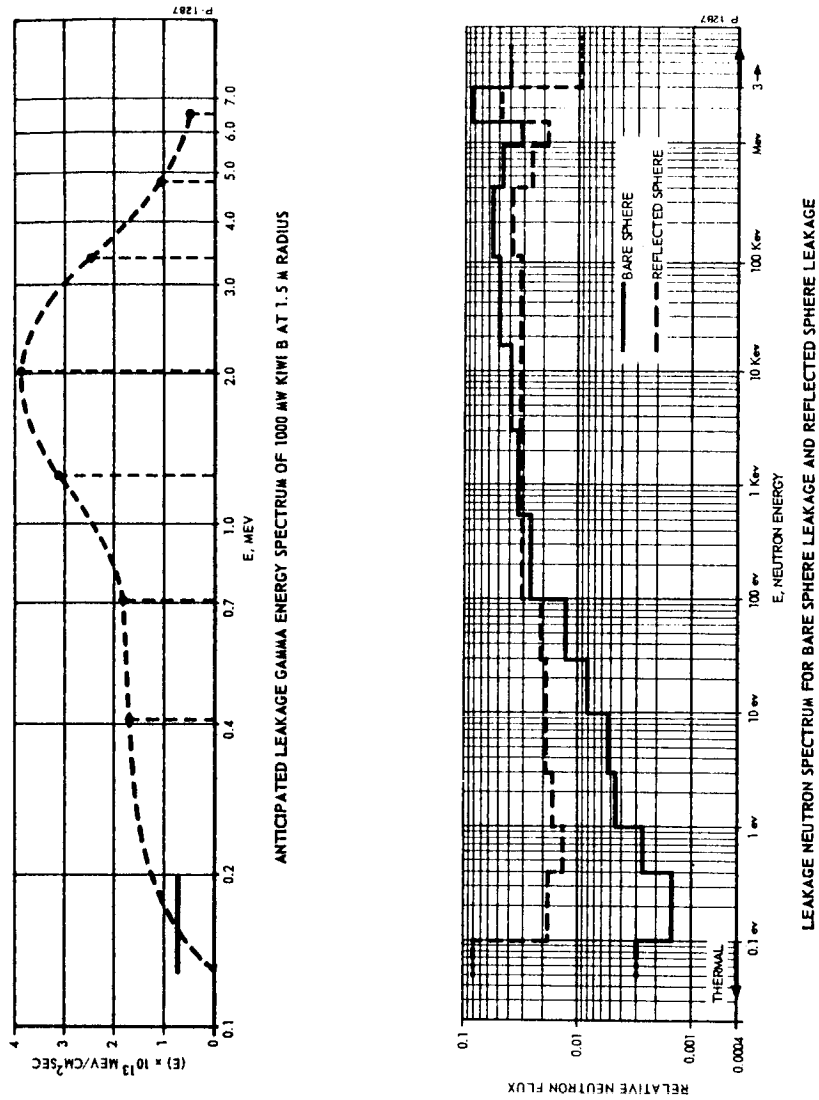


Figure 2 - Anticipated Gamma and Neutron Leakage Spectrum

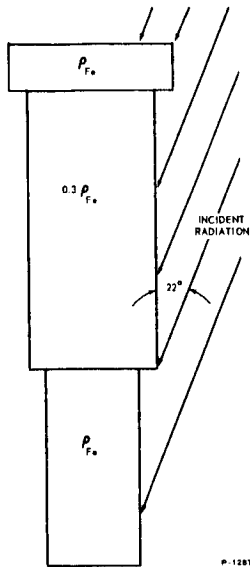


Figure 3 - Simplified Actuator and Flux Geometry Model

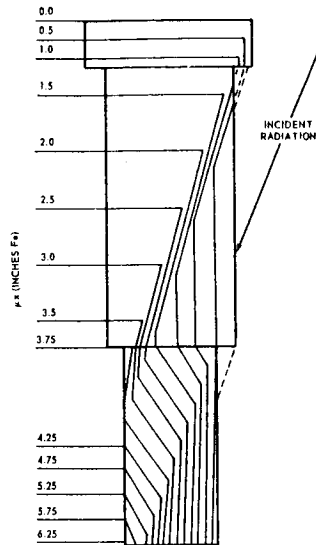


Figure 4 - Iso- μx Lines for Simplified Variable Density Model

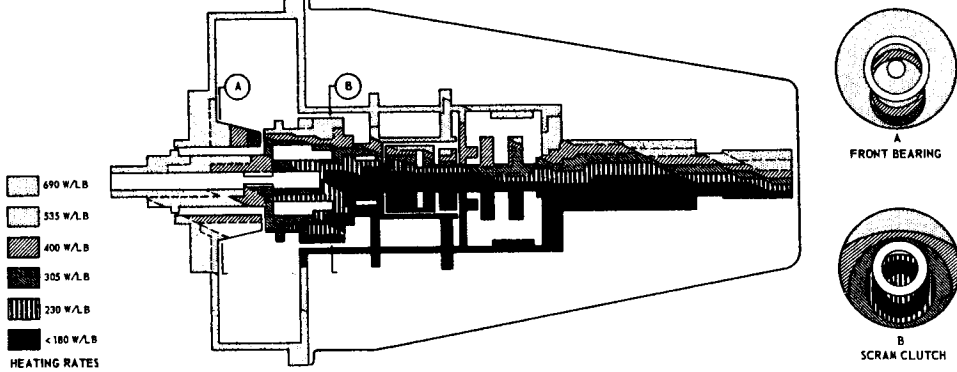


Figure 5 - Heating Rate Distribution in Actuator Based on 22° Collimated Flux Approximation

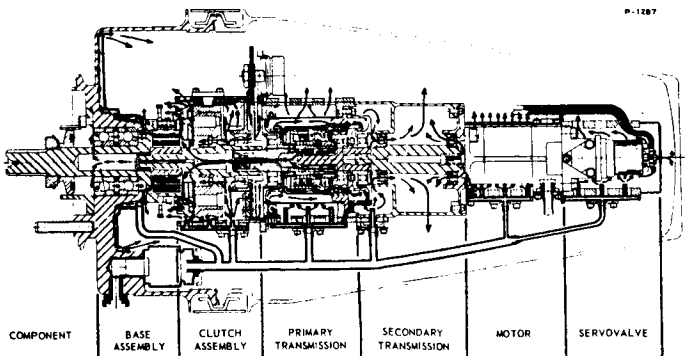


Figure 6 - Typical Coolant Distribution, Prototype Regulating Version of Control Drum Actuator (Model A-1)

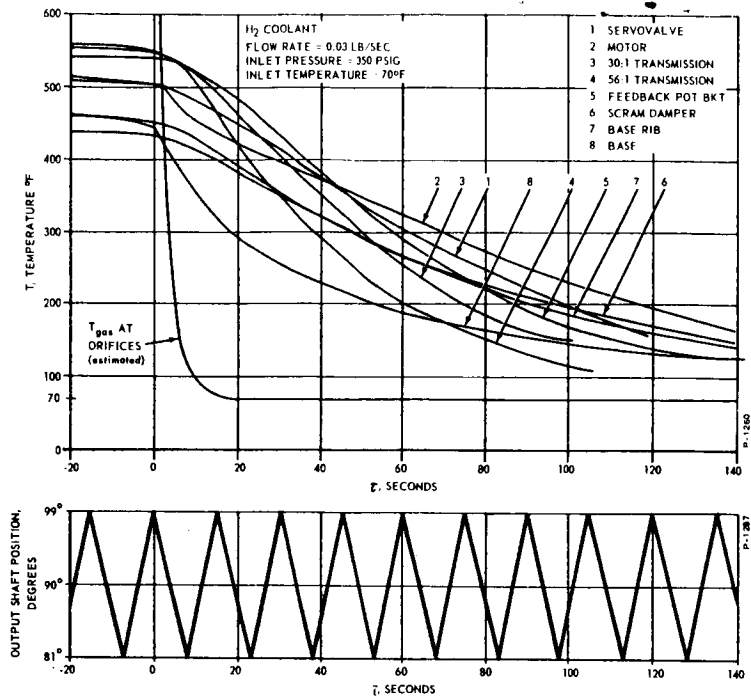


Figure 7 - Transient Heat Transfer Test Data of Operating Prototype Actuator

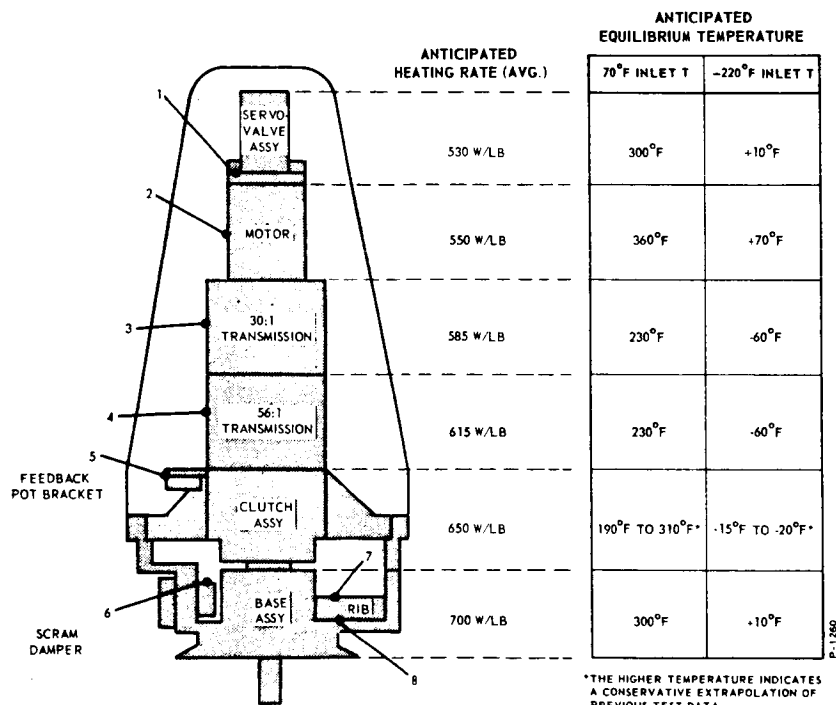


Figure 8 - Anticipated Actuator Equilibrium Temperatures for Calculated Heating Environment and Design Coolant Flow Rate

KIWI-B-1A POWER AND TEMPERATURE CONTROL SYSTEMS*

[U]

E. A. Brown, H. B. Demuth, P. B. Erickson,
R. R. Mohler, S. J. Singer and C. E. Stiles

University of California
Los Alamos Scientific Laboratory
Los Alamos, New Mexico

X 66 50295

INTRODUCTION

Kiwi-B-1A was the first of a series of reactors intended to culminate in a core design suitable for the Nerva Program. The Kiwi-B-1 core was designed for operation with liquid hydrogen propellant at a power of 1093 MW, a flow rate of 70 lbs/sec, and an exit gas temperature of 4090° R.

Early in the Kiwi-B-1A project it was realized that liquid hydrogen flow facilities would not be ready in time to test the reactor; therefore, it was decided to run Kiwi-B-1A on gaseous hydrogen at a power of 269 MW and a flow rate of 20 lbs/sec. The primary objectives of the test were to measure core temperature and flux distributions, to test the reactor structural integrity, to measure the core temperature reactivity, and to test the exit gas temperature control system.

The variables which were regulated by automatic control systems in Kiwi-B-1A were flow rate, core exit gas temperature, and the logarithm of power. A simplified block diagram of these systems is shown in Fig. 1. The demand voltages for the controlled variables were generated in a drum programmer. The log power control system maintained the reactor power at the demanded value by positioning 12 rotary control rods in a beryllium reflector which surrounded the core. The rods were beryllium cylinders with boral sheaths covering 120° of the cylinders. The core reactivity could be increased approximately \$9 by rotating the boral from positions toward the core to positions directly away from the core. The flow rate control system adjusted flow to the desired value by positioning a valve in the propellant feed line. The exit gas temperature control system adjusted temperature to the programmed value by applying appropriate corrections to the programmer log power demand voltage.

The exit gas temperature control system was the major new reactor control development for Kiwi-B-1A. The log power and flow rate systems were very similar to those reported^{1,2} for earlier Rover reactors; therefore, the linearized analysis portion of this paper will be devoted to the temperature control system. This paper also describes the log power and temperature system responses to startup programs and to disturbances of reactivity, log power demand, and temperature demand. In addition, the programming techniques and the performance of the reactor and its control systems during critical tests are presented.

TEMPERATURE CONTROL

The use of an exit gas temperature control system on Kiwi-B-1A was made possible by the development of a suitable thermocouple³. The core heat exchanger time constant of 14 seconds at full flow imposed a high gain requirement on the temperature controller, but this was not considered to be prohibitive.

* Work performed under AEC Contract W-7405-ENG.36.

The lack of experience with reactor automatic temperature controls plus the absence of a convincing amount of thermocouple reliability data dictated the use of a conservative system design to make the reactor less vulnerable to the effects of malfunctions in the temperature control system. Some of those features were:

1. The average of three thermocouples was used as the measure of exit gas temperature. A sample and reject circuit was used to reject any thermocouple which had an indication differing from the average by more than 400° R.
2. Power and flow rate were programmed to yield the desired temperature within the limits of accuracy of the systems. The output of the temperature controller acted as a vernier correction to the log power demand voltage to keep the demanded and measured temperatures equal. If the temperature control system malfunctioned, it could be de-energized and the run continued on log power and flow rate control.
3. The output voltage from the temperature controller was clamped so that it could not demand a power increase of more than 10% of the actual power.

Referring to Fig. 1, the transfer functions of the temperature control system for small perturbations were as follows:

$$G_1(s) = \frac{\delta E_2(s)}{\delta E_1(s)} = \frac{0.135 (s/0.022 + 1)}{s (s/110 + 1)} \quad \frac{\text{Volts}}{\text{Volts}}$$

$$G_2(s) = \frac{\delta P(s)}{\delta E_2(s)} = \frac{P_d}{9.2} \frac{\delta \log P(s)}{\delta \log P_d(s)} \quad \frac{\text{KW}}{\text{Volt}}$$

$$G_3(s) = \frac{\delta T_{eg}(s)}{\delta P(s)} = \frac{1}{3.88 \dot{W} (\frac{280}{\dot{W}} s + 1)} \quad \frac{^\circ\text{R}}{\text{KW}}$$

$$G_4(s) = \frac{\delta E_3(s)}{\delta T_{eg}(s)} = \frac{1}{50 (\frac{3.5}{\sqrt{\dot{W}}} s + 1)} \quad \frac{\text{Volts}}{^\circ\text{R}}$$

$$G_5(s) = \frac{\delta E_4(s)}{\delta E_3(s)} = \frac{(s/1.28 + 1)}{(s/67 + 1)} \quad \frac{\text{Volts}}{\text{Volts}}$$

The temperature open loop transfer function was:

$$G(s) = \frac{7.57(10)^{-5} P_d}{\dot{W}} \frac{(s/0.022 + 1)(s/1.28 + 1)}{s (\frac{280}{\dot{W}} s + 1) (\frac{3.5}{\sqrt{\dot{W}}} s + 1) (\frac{s}{111} + 1) (\frac{s}{67} + 1)} \cdot \frac{\delta \log P(s)}{\delta \log P_d(s)} \quad (1)$$

The characteristics of the log power control system are shown in Fig. 2. Combining data from Fig. 2 with the remaining terms of equation (1), the open temperature loop characteristics for full power and full flow are shown in Fig. 3. This figure indicates a gain margin of 14 db, a phase margin of 66°, and an open loop gain of one at 0.55 cps.

DYNAMIC PERFORMANCE

The general method of attack in studying the Kiwi-B-1A control systems was to simulate them on digital and analog computers. The digital computer and hand analyses were used for linearized work in the frequency domain. The analog simulation contained most of the system non-linearities, including an actual

rod positioning servo. The analog computer was used primarily for controller synthesis and time-domain studies. Some of these studies are discussed in the following paragraphs.

During the early Kiwi-B-1A control synthesis work it was found that the temperature control system would become unstable following temperature demand step changes of 150°R or larger. A recording of this phenomenon is shown in Fig. 4. This difficulty was caused by the large transient error voltage at the temperature controller output resulting from the relatively high controller gain at high frequencies. This large voltage was transmitted through the log power controller, driving the control rods into velocity saturation. The rods were velocity limited to $45^{\circ}/\text{sec}$ for nuclear safety reasons. The non-linear effect of the rod velocity limiting was sufficient to cause an increasing amplitude oscillation in the system. The addition of the temperature controller output voltage clamp discussed earlier limited this voltage sufficiently to make it impossible for the temperature controller to drive the rods into velocity saturation in the power increasing direction. Since this clamp was effective in stabilizing the system for positive step changes of temperature demand, an additional clamp was provided to avoid this difficulty for negative-going temperature demand steps. A voltage clamp equivalent to a 50% power decrease clamp was found to be satisfactory. The response of the system to temperature demand steps of 250°R after the clamps were added is shown in Fig. 5.

The system response to a positive step reactivity disturbance of $\$1.40$ is shown in Fig. 6. The power increased 130% during this transient, but the exit gas temperature increased only 75°R , and the system recovered satisfactorily. The analog simulation would not recover from a step reactivity disturbance of $\$1.50$.

The responses to small and large step changes of log power demand are shown in Fig. 7 and Fig. 8, respectively. The ability of the temperature control system to correct the power to regulate the temperature following a step change in log power demand is shown in Fig. 7. The step disturbance shown in Fig. 8 amounts to a 150% power change, which is beyond the range of the temperature controller clamp. As can be seen, the power did not return to the pre-disturbance value in this case.

A portion of the simulated Kiwi-B-1A hot run is shown in Fig. 9. The exit gas temperature demand was changed from 2000°R to 3600°R at a rate of $25^{\circ}/\text{sec}$. At the same time, power demand was increased from 10 to 180 MW, and flow rate from 2 to 16 lbs/sec. The maximum temperature error during the run was 40°R . The effect of the temperature controller clamp is evident on the power and temperature controller output curves between 5 and 23 seconds.

PROGRAMMING TECHNIQUES

The exit gas temperature, power, and flow rate programs designed for Kiwi-B-1A are shown in Fig. 9. There are three holds. The first hold was included to expand the core thermally at low flow rates to avoid possible displacement of internal reactor parts. The second hold was put in to obtain high-temperature data from the core thermocouples at a temperature below their burn-out value. The third hold, at full power and flow, was included to test the integrity of the core, reflector, control vanes, etc. at high temperatures. The rapid power increases at the end of each hold were designed to establish a desired rate of change of temperature in the core and/or the exit gas. The magnitude of the power "step" was approximately proportional to the product of the core mass heat capacity and the desired rate of change of temperature. Appropriate step power decreases were injected at the beginning of each hold to reduce the rate

of change of temperature to zero for the hold. The exit gas temperature demand step decrease of 100° R late in the program was put in to obtain information about the dynamic performance of the control system.

The programs in Fig. 10 were derived from a combination of hand calculations and analog computer studies. A first approximation to the programs was obtained by hand using a one-lump heat exchanger model with variable specific heats for graphite and hydrogen. The first approximation was improved through trial and error procedures with a relatively sophisticated analog computer model of the system.

The three-input system with appropriate programmed demands offers the following advantages over programming only exit gas temperature and flow rate:

1. Correct demands to the 3 inputs establish steady state exit gas temperatures and core temperatures very quickly and thereby help obtain better test data.
2. It is possible to operate without the temperature loop, if necessary.
3. The right log power demand signal helps keep E_g small, and makes the temperature loop more effective by keeping the controller out of its voltage clamps.
4. A programmed log power demand in the presence of a ramp exit temperature demand helps minimize the exit gas temperature error.

CONTROL SYSTEM PERFORMANCE

The log power and temperature control systems performed well in many cold critical tests prior to the full power run. In such tests, of course, the temperature control system was closed through a heat exchanger simulator.

In Experimental Plan 6A, the final full power run, all control systems behaved well until the end of the first hold. The temperature loop was not particularly effective up to this time because it was in saturation at one limit and then the other. This behavior was expected because of the extremely large system time constants at low flows, and the relatively narrow limits on the temperature controller output voltage.

As the programmer started from the first hold, one of the exit gas temperature thermocouples became noisy. Unfortunately, the thermocouple selector circuit did not reject the offending device immediately. In the heat of the moment, the power excursions resulting from the noise were attributed to a temperature control system instability. Consequently, the temperature loop was opened and the rest of the experiment was carried out without it. Ironically, the selector circuit rejected the noisy thermocouple seconds after the loop was opened. The rejected thermocouple soon lost its noisy characteristic and gave good data for the rest of the run.

Once the temperature loop was opened, the accuracy of the exit gas temperature depended on the accuracy of the log power instrumentation calibration. Although the log power control system worked well during the rest of the experiment, the log power calibration was off, and the exit gas temperature at the second and third holds was low. It was so low, in fact, that the temperature loop, with its +10% available power correction, could not have given a correct exit gas temperature without a manual power correction from the operator.

Aside from the exception noted above, the control systems worked well. Unfortunately, the opening of the temperature loop and the early termination of the experiment due to a nozzle fire did not allow the 100° R exit gas temperature

step to be inserted as had been hoped. Thus, a recording of the temperature loop step response was not obtained.

CONCLUSIONS

The general control system with three programmed inputs worked well, and will be used in the next reactor test.

The temperature control system performed satisfactorily before the thermocouple noise was encountered. Future temperature control systems should be made resistant to noise. In particular, they should be made compatible with appropriate thermocouple selection circuits in resisting noise. The exit gas temperature control system should have a wider effective control range in the next test so as to be able to compensate for inaccurate neutronic calibrations more effectively.

The Kiwi-B-1A log power control system as such worked well, but neutronic instrumentation inaccuracies led to low exit gas temperatures at the two high holds. The necessity for an accurate power measuring system will be relieved considerably if a reliable exit gas temperature control system with sufficient unclamped range is developed in the future.

REFERENCES

1. E. A. Brown, "Logarithmic Power Control in Kiwi-A Reactors," I.R.E. Trans. on Nuclear Science, Vol. NS-9, No. 1, Jan. 1962.
2. S. S. Singer, "Automatic Control Systems for the Kiwi-B Reactor Test," A.R.S. Paper 2118-61.
3. A. R. Driesner, C. P. Kempter, C. E. Landahl, C. A. Linder, and T. E. Springer, "High Temperature Thermocouples in the Rover Program," I.R.E. Trans. on Nuclear Science, Vol. NS-9, No. 1, Jan. 1962.

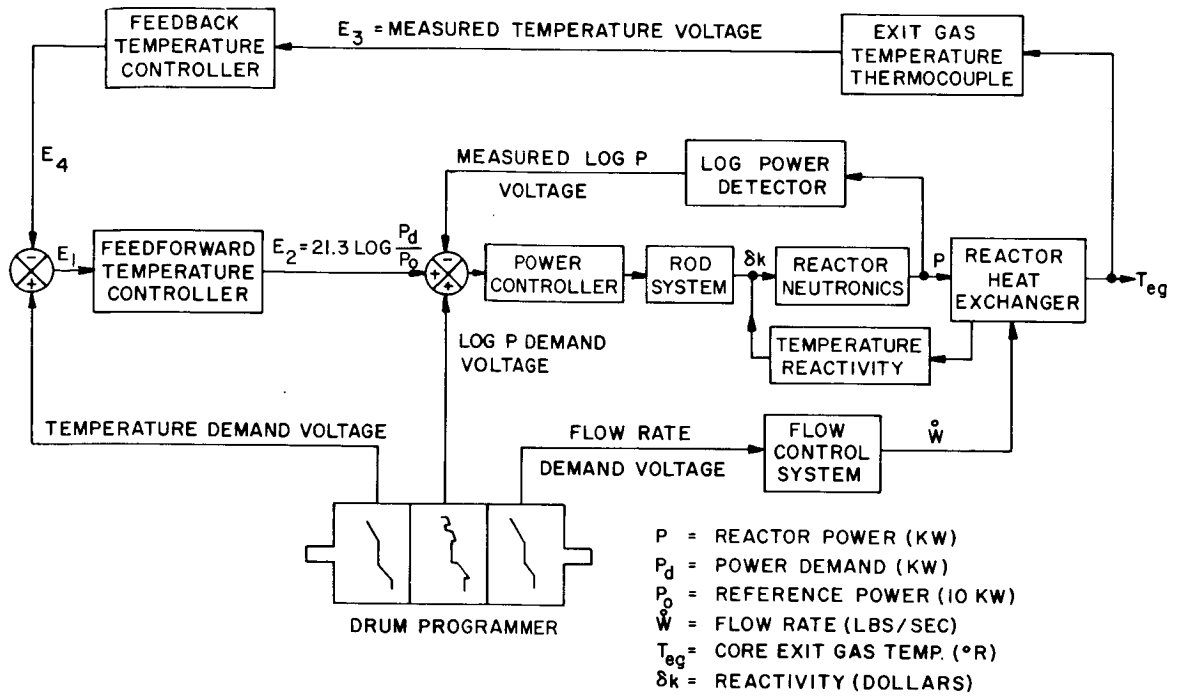
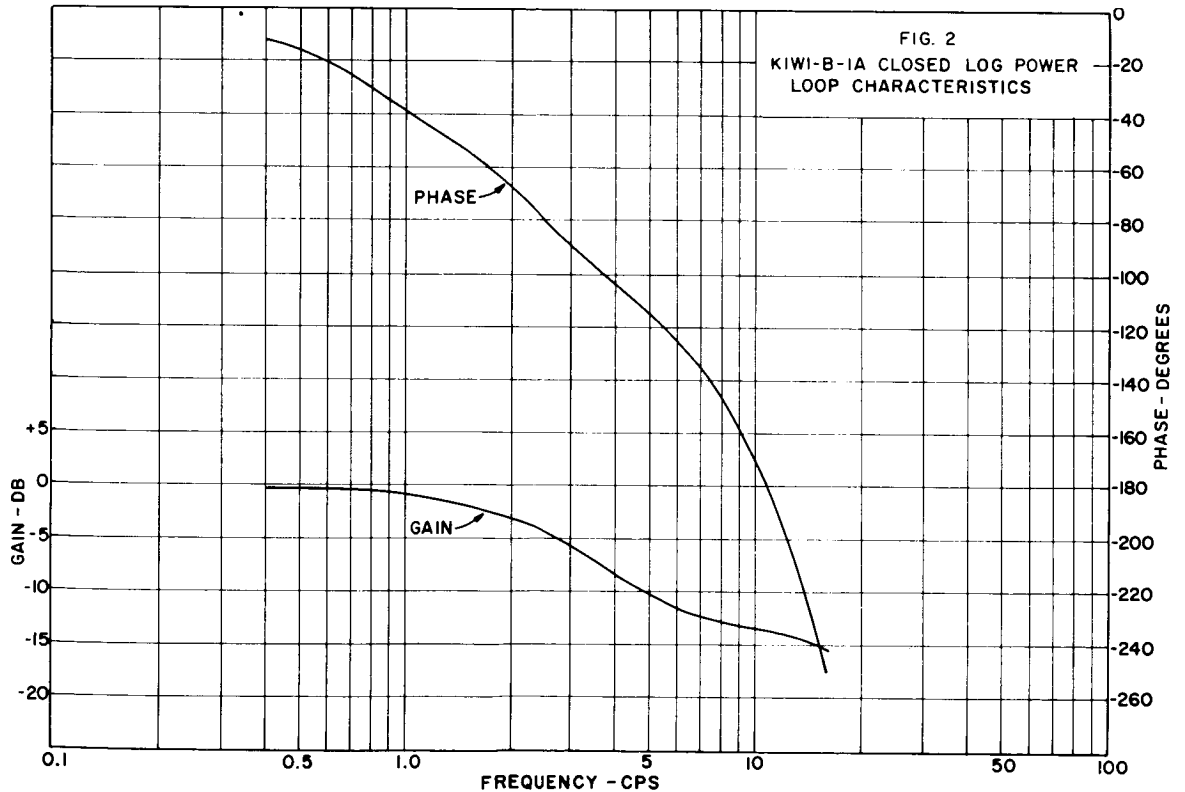
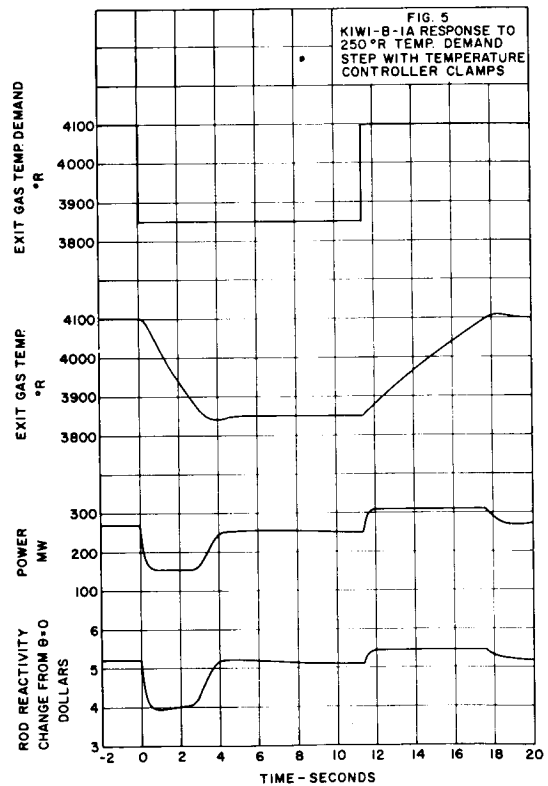
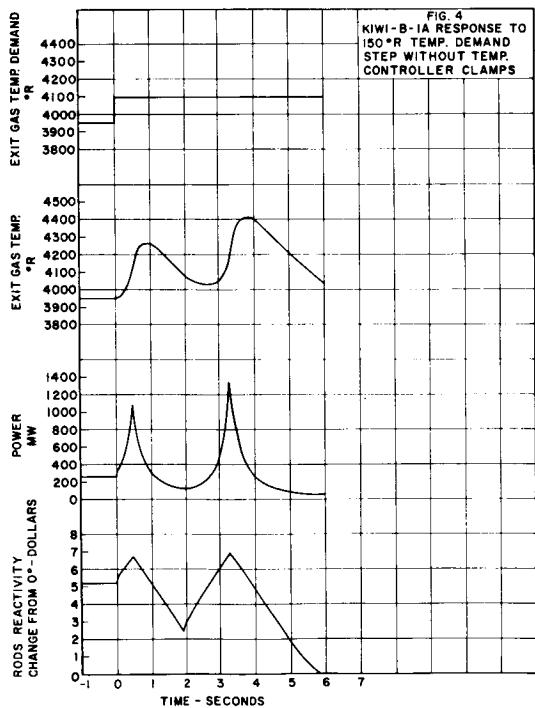
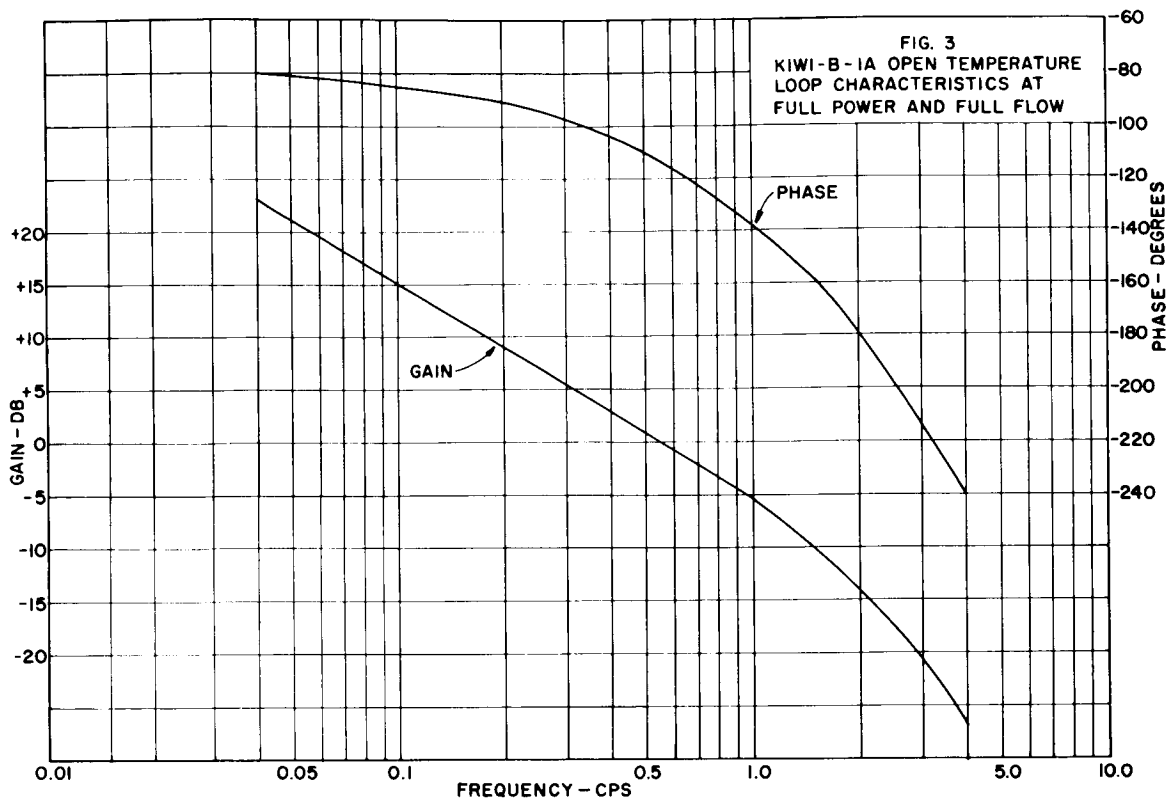
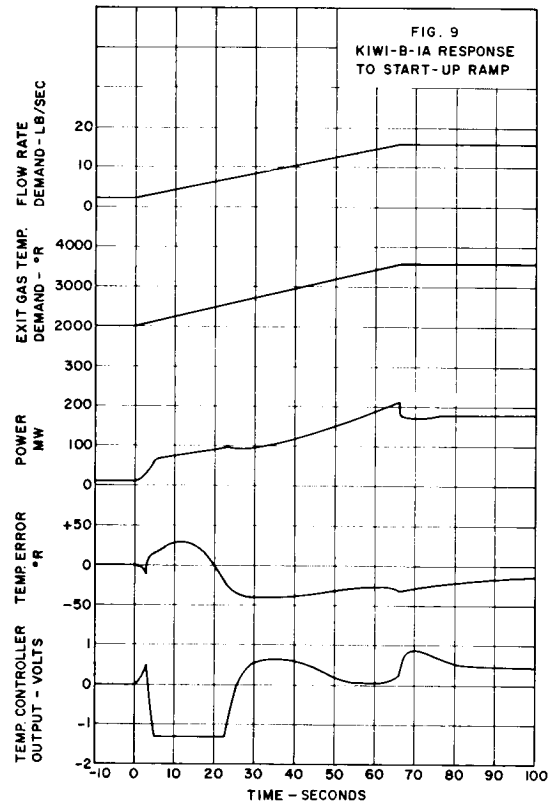
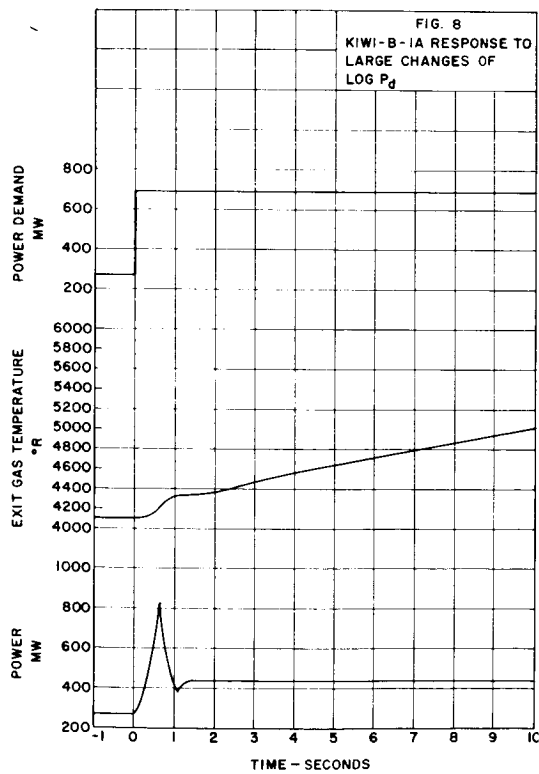
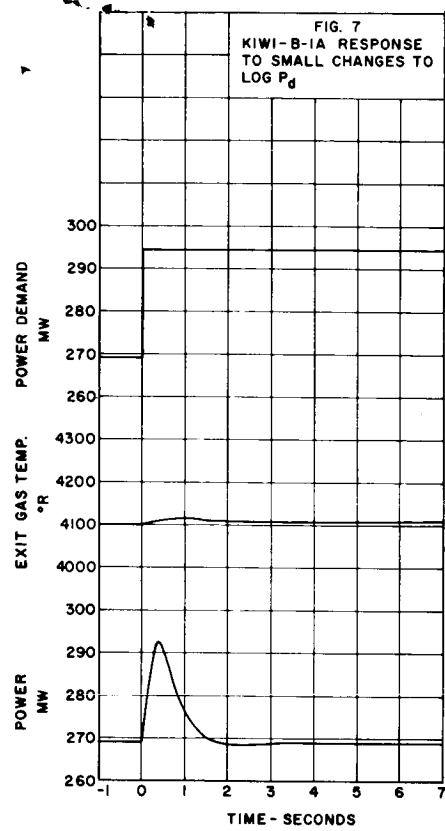
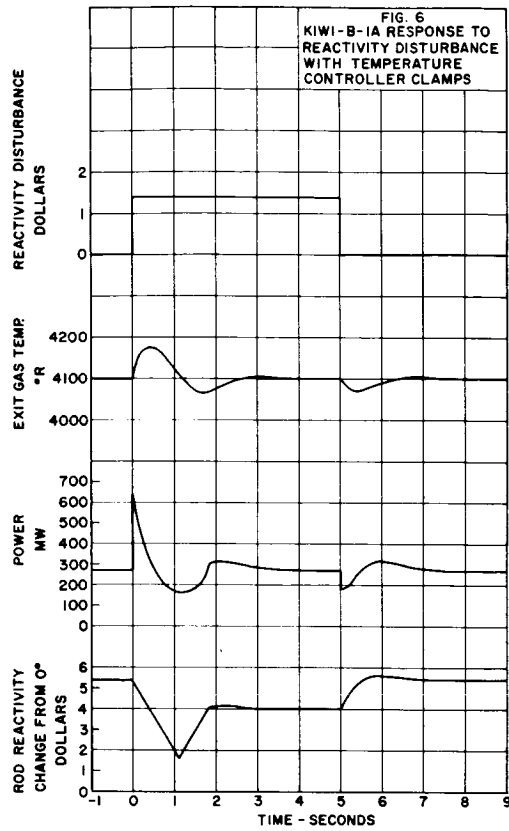


FIG. 1

KIWI-B-1A PROGRAMMER AND AUTOMATIC CONTROL SYSTEMS







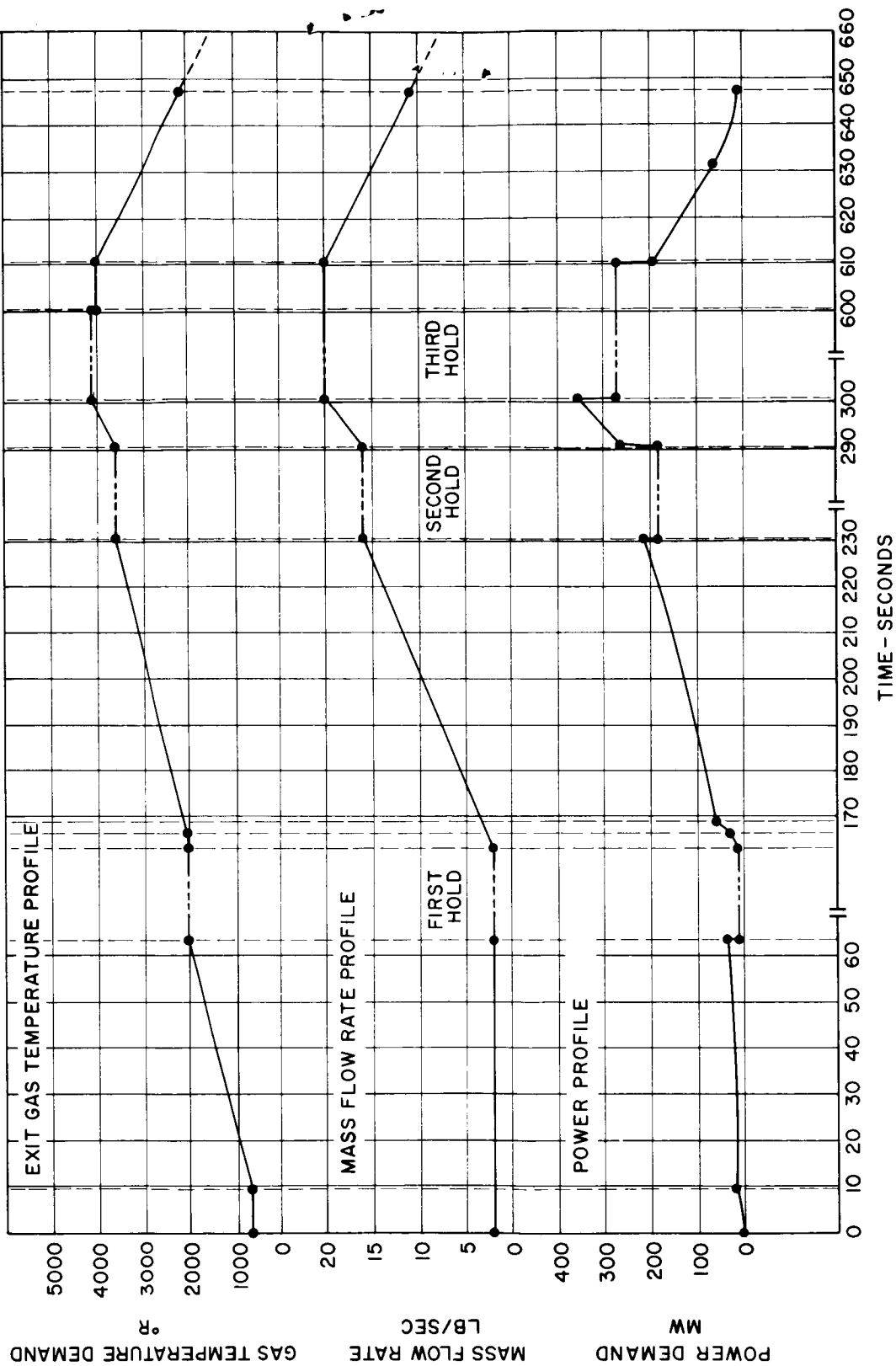


FIG. 10
PROGRAMMED DEMANDS FOR KIWI-B-1A

RE-ENTRY OF NUCLEAR ROCKETS INTO EARTH'S ATMOSPHERE [U]

R. I. Weiner

Martin Company - Nuclear Division

50296

ABSTRACT--This paper presents the techniques and results of a study of nuclear rocket re-entry into the earth's atmosphere due to orbital and suborbital aborts. Two cases are analyzed; an explosive destruct system is assumed to have fractured the core into a subcritical assembly, and the initial size of particles that could be reduced to 25 microns at 100,000 feet by passive aerothermochemical means is determined. Both continuum flow and free molecule flow estimates were made and it was found that the initial sizes of debris at destruction would have to be between 1/24 and 1/16 inch in diameter to satisfy the boundary conditions imposed on the solution.

The second case considered the possibility of destruct system failure and the re-entry of the intact engine from orbital and suborbital aborts. It was determined that the engine will re-enter intact from any aborts below 400,000 feet and for any aborts above this altitude, engine afterheat not aeroheating is the primary mode of engine structural failure. In addition, not enough energy or exposure time is available in any of the ballistic or orbital injection mission aborts studied to appreciably destroy the engine fuel elements or reflectors that fall free after a pressure vessel meltdown.

Conf. R.D. — Author

INTRODUCTION--A nuclear reactor re-entering the earth's atmosphere due to a vehicle system abort poses a major operational safety problem. Consequently, methods of disposing of this reactor that do not compromise the nuclear rocket propulsion system performance and yet ensure the greatest possible reliability must be evaluated.

One method is an explosive destruct system activated by an abort that physically breaks up the reactor core. This destroys the critical geometry, but the highly radioactive debris will continue to re-enter. This investigation is concerned with the amount of destruction which can be achieved passively by re-entry heating and oxidation, on the debris and intact engine if the destruct system fails to operate.

To achieve these ends, five specific objectives have to be met; they are: (1) identify the important physical phenomena which control debris burnup; (2) develop an analytical model that would approximate all reactor debris throughout the majority of the re-entry regime; (3) derive a unified aerothermochemical analysis which would predict the order of magnitude of the sizes of all reactor debris that could be destroyed by these re-entry phenomena; and (4) approximate behavior of an undestroyed re-entering complete engine.

PHILOSOPHY OF SOLUTION--The derivation of a precise theory to describe the aerothermochemical phenomena that occur during re-entry of reactor debris is a task that utilizes information from the very limits of our physical environment. Since an exact solution based on known physical constants is impossible, due to limited experimental information dealing with the early portions of the re-entry environment, an approximate solution was proposed.

The problem was approached from the standpoint of determining a re-entry corridor or band within which fuel graphite debris could be rendered harmless. The band limits were taken as those created by assuming the most optimistic and pessimistic atmospheric and materials characteristics. This band is a function of debris geometry, dynamics, velocity, re-entry angle, mass and material.

The results of the analysis should then yield the upper and lower size limits of the loaded graphite debris which could be destroyed in any particular type re-entry.

GENERAL ANALYTICAL SOLUTION--The objective of past re-entry studies was to preserve the re-entry body, and analyses of these bodies assume a constant mass throughout re-entry. Here the inverse problem must be considered and this analysis differs in that it considers large mass changes in the body. Consequently, for each step change in altitude a corresponding change in mass of the re-entering debris occurs. This has a significant effect on their velocity profiles by changing drag on the body. A step-by-step solution of the problem as shown in Fig. 1 was followed.

BOUNDARY CONDITIONS

Analytical Model--The possible sizes and shapes of debris that would result from the explosive destruction of a nuclear rocket engine are infinitely variable. Therefore, to avoid analysis on many geometries a conservative geometry was chosen (i.e., if this particular geometry was destroyed all other debris of different shapes will definitely be destroyed). Hence, the analysis need be performed on only one model. A spherical geometry meets this requirement since it has the smallest surface area-to-volume ratio of any geometry.

Concept of Debris Destruction--One of the most important boundary conditions affecting the solution is developing those conditions which constitute destruction of reactor debris.

The criterion chosen was that all debris must be reduced to sizes below 25 microns in diameter by the time they reach 100,000 feet or, effectively, they are aerosols. This criterion was based on early AEC requirements for SNAP re-entries. Future review of this boundary condition is suggested since it may impose too severe a restriction on the destruct system, the object being to determine whether larger sizes than aerosols can be tolerated as safe. However, this boundary condition was retained in this analysis as certainly being conservative.

MECHANISM OF ENERGY INPUT AND MASS LOSS FROM REACTOR DEBRIS--There are three significant mechanisms which make up the total energy inventory of a typical piece of reactor fuel element during its re-entry. They are: (1) latent particle energy at initiation of re-entry heating due to fission product decay heating; (2) aerodynamic heating during the re-entry; and (3) chemical heat-input from surface combustion of graphite debris and effects of the resulting mass transfer.

Latent Energy of Debris--If it is assumed that the nuclear stage is fragmented in orbit, the debris might contain significant latent energy at the altitude where aerodynamic heating begins. Consequently, this heat must be included as part of the total heat inventory available to act on the particle. The energy balance that exists when the particle falls from orbit to the sensible atmosphere, where free molecule flow begins, can be represented for fuel element debris as:

$$WC_p \frac{dT}{dt} = \sum_{i=0}^n \alpha_i e^{b_i t} - SG \epsilon T^4$$

where the first term represents the heat generated in a particle of the core by fission product decay and the second represents the mechanism of energy loss by radiation as the particle falls toward the atmosphere. The solution of this equation shown in Fig. 2 yields temperature as a function of time for any initial conditions of temperature and particle size. Interpretation of Fig. 2 shows that thermal radiation is the controlling factor and the contribution of decay heat to the potential energy of the particle at the inception of re-entry is negligible. Therefore particle initial temperature, which is indicative of its initial position in the core, initial mass and its re-entry angle, indicative of total time from abort to re-entry, are the controlling factors in this case.

Simple Aerodynamic Heating--As the first step in determining the primary mode of debris destruction, the total heat transferred to a typical graphite re-entry model, from aerodynamic inputs only, was computed using the basic analysis of Refs. 1 and 2. It was found that even when cold wall heat rates were assumed (i.e., no radiation heat losses) giving highly optimistic values of total heat input during re-entry, burnup is far from being achieved, as sublimation temperatures of graphite debris can never be reached. (Note: 12,500 Btu/lb maximum available and 28,000 Btu/lb is required.) Therefore the only mode of complete passive destruction is thermochemical and appears as a result of surface combustion during re-entry.

The only real value of the basic aeroheating is found in the early stages of re-entry where it rapidly raises the particle surface temperatures to the point where chemical reactions with oxygen begin.

Surface Combustion and Mass Transfer of Graphite--Having determined the primary mode of reactor fuel element debris destruction to be oxidation during re-entry, a meaningful analytical model to which the various theories of graphite oxidation can be applied must be set up.

Due to the low volume fraction of uranium in a typical fuel element, it was determined that if a suitable analytical description of pure graphite oxidation during re-entry can be derived, only small changes in its coefficients and basic form would be necessary to extend it to the fueled case. This results because the effects of impurities and radiation on the graphite manifest themselves by lowering the activation energy and increasing the active oxidation sites of the graphite surface. In any case, the real fueled and irradiated debris should demonstrate only slightly higher mass loss rates than the pure graphite. Consequently, the assumption of the pure graphite re-entry was felt to give conservative results.

RE-ENTRY REGIMES--Any particle re-entering the earth's atmosphere may pass through three distinct regimes which affect the aerothermochemical phenomena acting on the particle. When the particle first re-enters the atmosphere, it is in the region of free molecule flow, characterized by the diameter of the particle being much less than the mean free path between molecules. As the re-entering body descends lower into the atmosphere, the molecular mean free path decreases and the flow eventually may become of the continuum type where the characteristic diameter of the body is much larger than the mean free path between molecules. Reference 1 summarizes these phenomena and indicates that small particles may well be in free molecule flow throughout their entire re-entry down to 100,000 feet.

GENERAL ANALYSIS FOR PURE GRAPHITE--FREE MOLECULE FLOW ESTIMATES--Supplementing the definition of free molecule flow by assuming that above a certain altitude, intermolecular collisions are infrequent compared with collisions of molecules with the re-entering particles, an analytical model of the body and flow interactions can be shown in Fig. 3. Since each molecule that collides with the re-entering particle suffers a minimum of energy loss due to other molecular collisions in the vicinity of the body, the transfer of momentum and energy from the atmosphere to the particle is particularly efficient in free molecule flow. Therefore, for a given atmospheric density, the effects of drag (momentum transfer) and aerodynamic heating (energy transfer) as well as any chemical reactions which might occur (mass transfer) are more pronounced than in other flow regimes (Refs. 1 and 3).

In addition, a re-entering body gives rise to a flow of nonuniform density, that is, the mean free paths of molecules near the body where the density is higher may be appreciably smaller than the free stream mean free paths of atmospheric molecules at the same altitude (Ref. 4). Therefore, the criterion for the existence of free molecule flow was based on the mean free path of molecules in the immediate vicinity of the body.

The mechanism of graphite oxidation in free molecule flow is not well known and the calculation of oxidation rates must be best estimates. The major obstacles are the unknown nature of the accommodation of free molecules on a graphite surface and the unknown ratio of the products of combustion. The former affects the probability of a chemical reaction between an incident oxygen molecule and the surface, and the latter determines whether oxygen molecules and atoms will react and form CO_2 , CO or some fraction of both.

This reaction is also temperature dependent with carbon and in the range of temperatures a typical particle undergoes during re-entry (300 to 3000° R) for a 1/32-inch particle, the reaction goes from almost all CO_2 at 1000° R to all CO above 2000° R (Ref. 5).

Since typical temperature profiles show temperatures above 1000° R during most of the re-entry (Fig. 4), the free molecule case was idealized by assuming only the CO reaction prevalent. An analysis, based on the assumption of free molecule flow over the entire re-entry trajectory, would be expected to give an estimate of the maximum size fragment that could burn completely in the atmosphere under the most ideal conditions.

Heat Transfer Analysis--Heat transferred to a high velocity sphere in free molecule flow by direct energy exchange and exothermic chemical reactions on its surface is given by:

$$E = (\text{KE} + \text{PE})_g + E_{\text{CHEM}} - E_{\text{RAD}} \quad (\text{Ref. 1})$$

where only a portion of the chemical energy serves to heat the particle. The remainder is carried away by the products of combustion. It was also determined that the liberated chemical energy is much smaller than the energy input to the particle due to the direct kinetic energy exchange in free molecule flow.

Mass Transfer Analysis--In free molecule flow, the stream of oxygen molecules flowing toward the surface of the graphite sphere is not as impeded by the presence of combustion products or other air molecules as in continuum flow because of the absence of a definite boundary layer. Therefore, graphite oxidation in the presence of free molecule flow is controlled by the rate of the chemical reaction itself, whereas in continuum flow, the controlling element is the diffusion of the oxygen to the surface and the counter diffusion

of the products of combustion away from the surface through the boundary layer (Ref. 5). In free molecule flow, mass is lost according to:

$$\frac{dm}{dt} = V S (\delta) \rho (p)$$

where

ρ = density of oxygen molecule and atom concentrations

p = probability of reaction

$$= e \left(\frac{-E}{[KE + PE]_g} \right)$$

and

E = surface activation energy of graphite = 44,000 gm/cal/mole based on Hottels work (Ref. 6)

and δ is determined by the relative quantities of carbon monoxide and carbon dioxide produced at the surface.

Analytical Model Continuum Flow--If it is assumed that the particle is always in continuum flow, with its inefficient heat and mass transfer mechanisms, an overly conservative answer results which represents that size for which any smaller particle than that calculated will definitely burn completely in the atmosphere. Figure 5 represents the analytical model used in the analysis of the continuum flow case.

Continuum Flow Estimates--A preliminary evaluation of available graphite oxidation theories, carried out by the Martin Company, resulted in the use of Scalas results for continuum flow applications (Ref. 5). The results of his work, using a large range of commercial graphites, are summarized and indicate that although flight speed (stagnation enthalpy) and surface temperature (shifting chemical equilibrium) effects do exist in a hypersonic environment, the most important single independent variable is stagnation pressure, or, effectively, altitude.

Since the equations hold only at the stagnation point, a method was devised to determine mass loss at points away from stagnation and the dependence of the mass flux parameter on particle dynamics (Ref. 1). A total average mass loss from the particles can then be determined throughout its re-entry. This was computed, in preliminary Martin investigations for rotating spheres, as being approximately 13% of the stagnation point value, i. e., the whole rotating sphere will lose mass at an average rate, 87% less than in the stagnation regime of a stable sphere.

RESULTS--The difference in the two methods of solution is presented in Fig. 6 which shows the curves derived from the analysis of both continuum and free molecule flow regimes. The range of particle sizes which can be destroyed is shown to be between 4/1000 and 5/1000 of a foot in diameter or between approximately 1/24 and 1/16 inch; for the most optimistic re-entry conditions considered, $\phi = -1^\circ$ giving maximum exposure time and 25,000 fps.

Therefore a rather narrow band of maximum sizes which can be destroyed is produced due to the choice of conservative or optimistic assumptions governing the methods of solution. The effects of flow transition from free molecule to continuum flow were also studied and are shown for a typical size close to the burnup band where burnup is slow enough so transition will occur. The

effects of initial diameter and re-entry angle on burnup size were also computed and are summarized in Ref. 1. In general, they show that re-entry angles between one and eight degrees give maximum assurance of destruction. No burnup occurs outside this band.

RE-ENTRY OF INTACT ENGINE--Destruct system failure is an ever present reality; therefore re-entry of the intact engine was studied to predict the resultant hazards (Ref. 1).

Figure 7 shows the zone of pressure vessel meltdown for a series of orbital injection aborts. Pressure vessel meltdown of the hot engine is primarily caused by afterheat with aerodynamic heating serving only to increase the meltdown altitude. Though the fuel elements and reflector segments of the hot engine will be released at relatively high altitudes following orbital injection aborts, there is insufficient aerodynamic heat or oxidation to destroy them prior to impact. The orbital injection aborts occurring before or just after nuclear stage startup do not result in the melting of the pressure vessel of the cold engine, and the engine will impact in an intact condition.

CONCLUSIONS--The following general conclusions can be drawn from this study: (1) during re-entries contemplated for the studied RIFT missions, reactor debris will not be destroyed by aeroheating alone; (2) the most important phenomena affecting debris burnup during re-entry is oxidation mass loss; (3) the sizes of particles which will burn up are predominately in free molecule flow throughout their entire re-entry; (4) continuum flow estimates of the maximum size particle which can be destroyed will give conservative answers; (5) particle burn-up range is between 1/24 and 1/16 inch for graphite; (6) if the destruct system does not operate, the engine will re-enter intact from any aborts below 400,000 feet in both the orbital injection and ballistic missions studied for RIFT; (7) for any aborts above this altitude, engine afterheat, not aeroheating, is the primary mode of engine structural failure; (8) not enough energy or exposure time is available in any of the ballistic or orbital injection mission aborts studied to appreciably destroy the engine fuel elements or reflectors falling free during re-entry.

RECOMMENDATIONS--It is doubtful whether an explosive destruct system alone could succeed in breaking the reactor into pieces small enough to be passively destroyed. It is recommended that other methods such as oxidizer injection, fuel element additives and/or planned excursions be investigated to supplement any explosive destruct system.

NOMENCLATURE

g--gravitational constant (ft/sec ²)	V--(particle) velocity (fps)
W--weight (lb)	u--streamline velocity (fps)
C _p --specific heat (Btu/lb-°R)	δ--ratio of products of combustion (CO/CO ₂)
T--temperature (°R)	ρ--density (lb/ft ³)
t--time (sec)	p--probability of reaction
m--mass (slugs/ft ³)	E--activation energy (gm-cal/mole)
α--energy production at time t	S--surface area (ft ²)
b--radioactive decay constant	R--radius (ft)
σ--Stephan-Boltzmann constant	x--direction along streamline
ε--surface emissivity	

ϕ --re-entry angle (deg)

J--778 (ft-lb/Btu)

\dot{m} --mass loss rate (lb/ft²-sec)

KE--kinetic energy of particle = $\frac{V^2}{2gJ}$
(Btu/lb)

PE--potential energy of gas = RT_g (Btu/lb)

Subscripts

i ith species

S stagnation

g gas

e entry

w wall

∞ free stream

ℓ boundary layer interface

B body

REFERENCES

1. "Final Report Nuclear Rocket Safety Study," Martin Company, Nuclear Division Report MND-2517, August 1961, SRD.
2. Fay, J. A. and Riddell, F. R., "Theory of Stagnation Point Heat Transfer in Dissociated Air," J.A.S., Vol. 25, pp 73, February 1958.
3. Gilbert, L. M. and Scala, S. M., "Free Molecule Heat Transfer in the Ionosphere," General Electric MSVD Report R-61SD076, March 1961.
4. Probstein, R. F., "Shock Wave and Flow Field Development in Hypersonic Re-Entry," ARS Semi-Annual Meeting, May 1960.
5. Scala, S., "A Survey and Study of Hypersonic Ablation," General Electric MSVD Report R59SD438, September 1959.
6. Hottel, H. C., Davis, H. and Tu, C. M., Ind. Engr. Chem., Vol. 26, p 749 to 757, 1934.

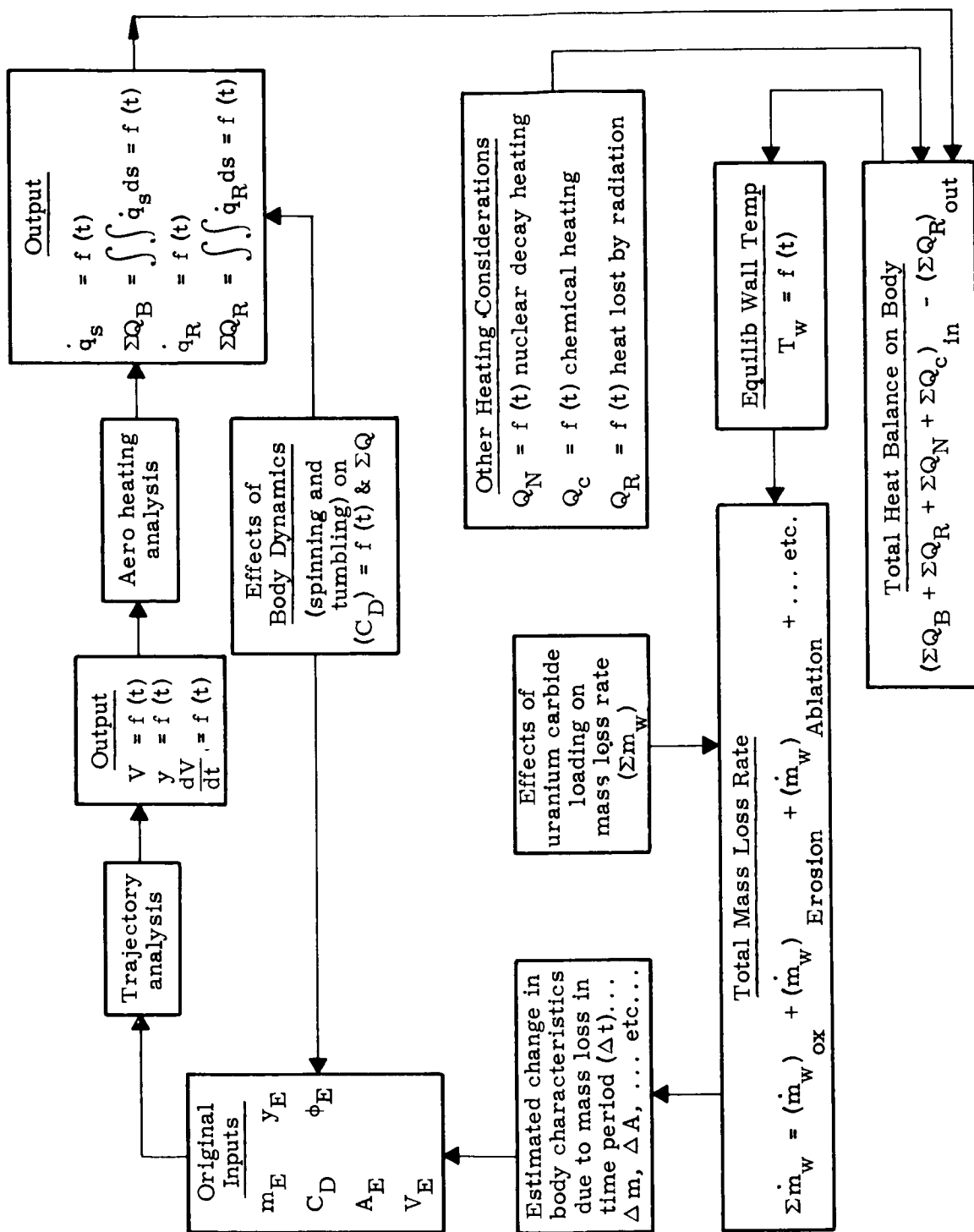


Fig. 1. Formulation of the General Solution for Re-entry Phenomena Simulation

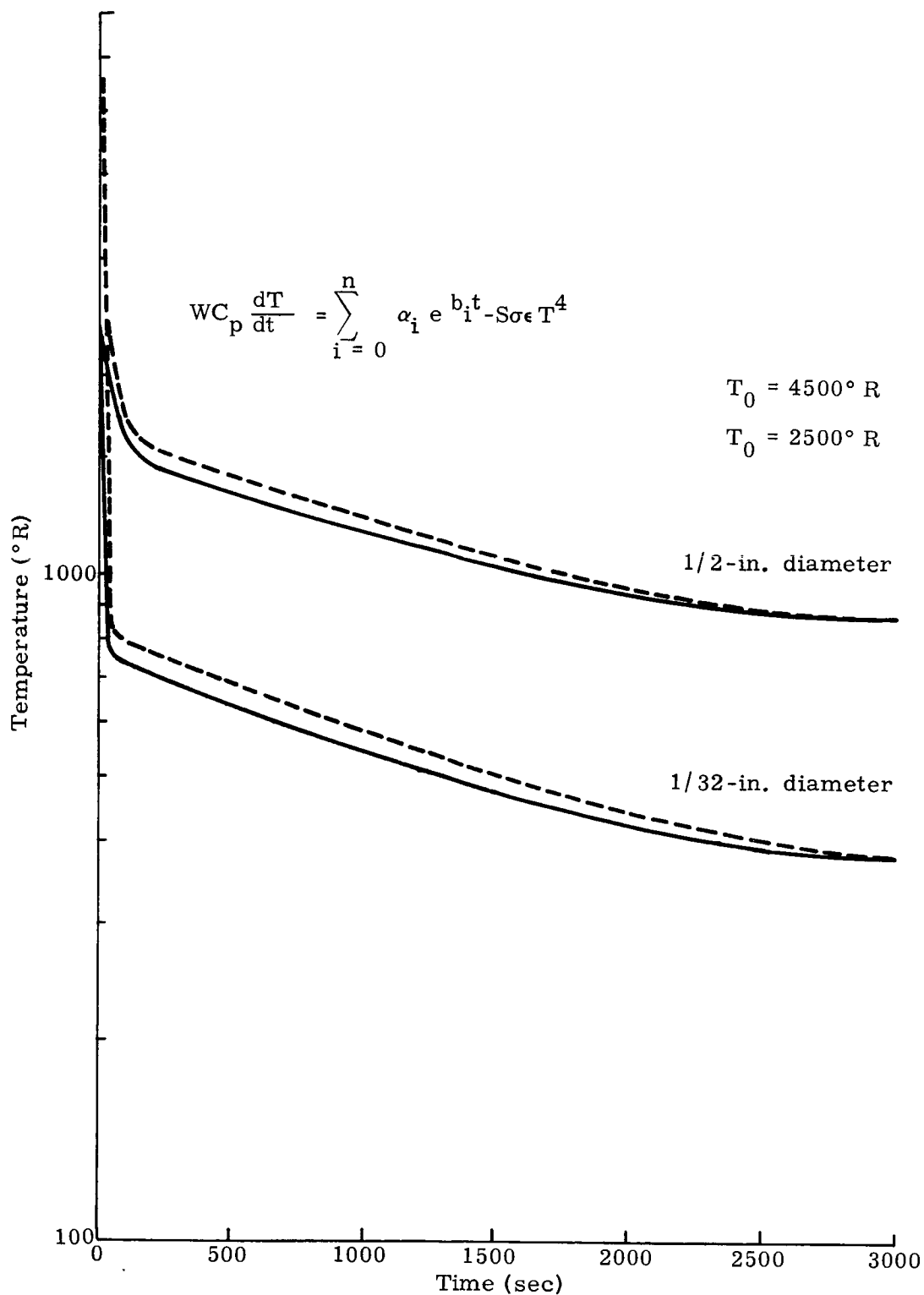


Fig. 2. Estimated Temperature History of Various Graphite Spheres Simulating Reactor Debris with Initial Temperature of 4500° and 2500° R

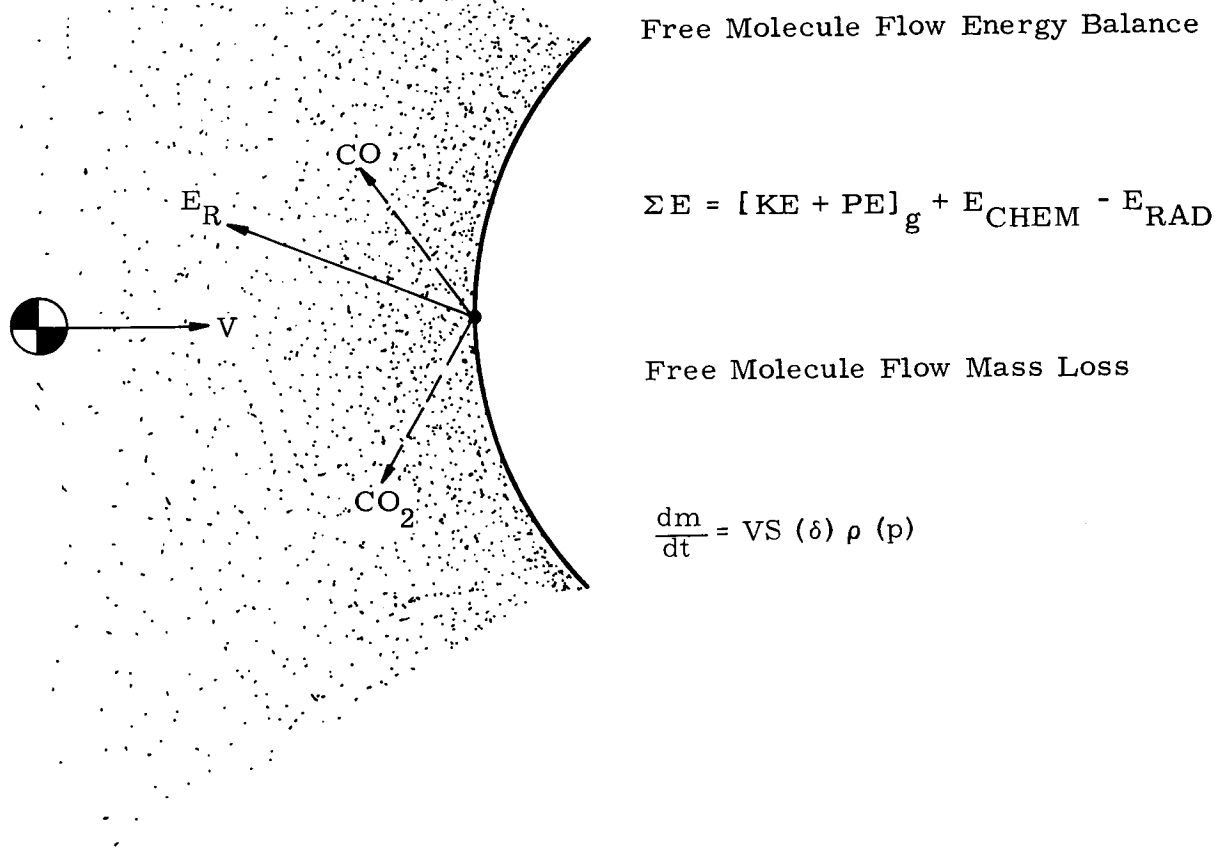


Fig. 3. Analytical Model--Free Molecule Flow

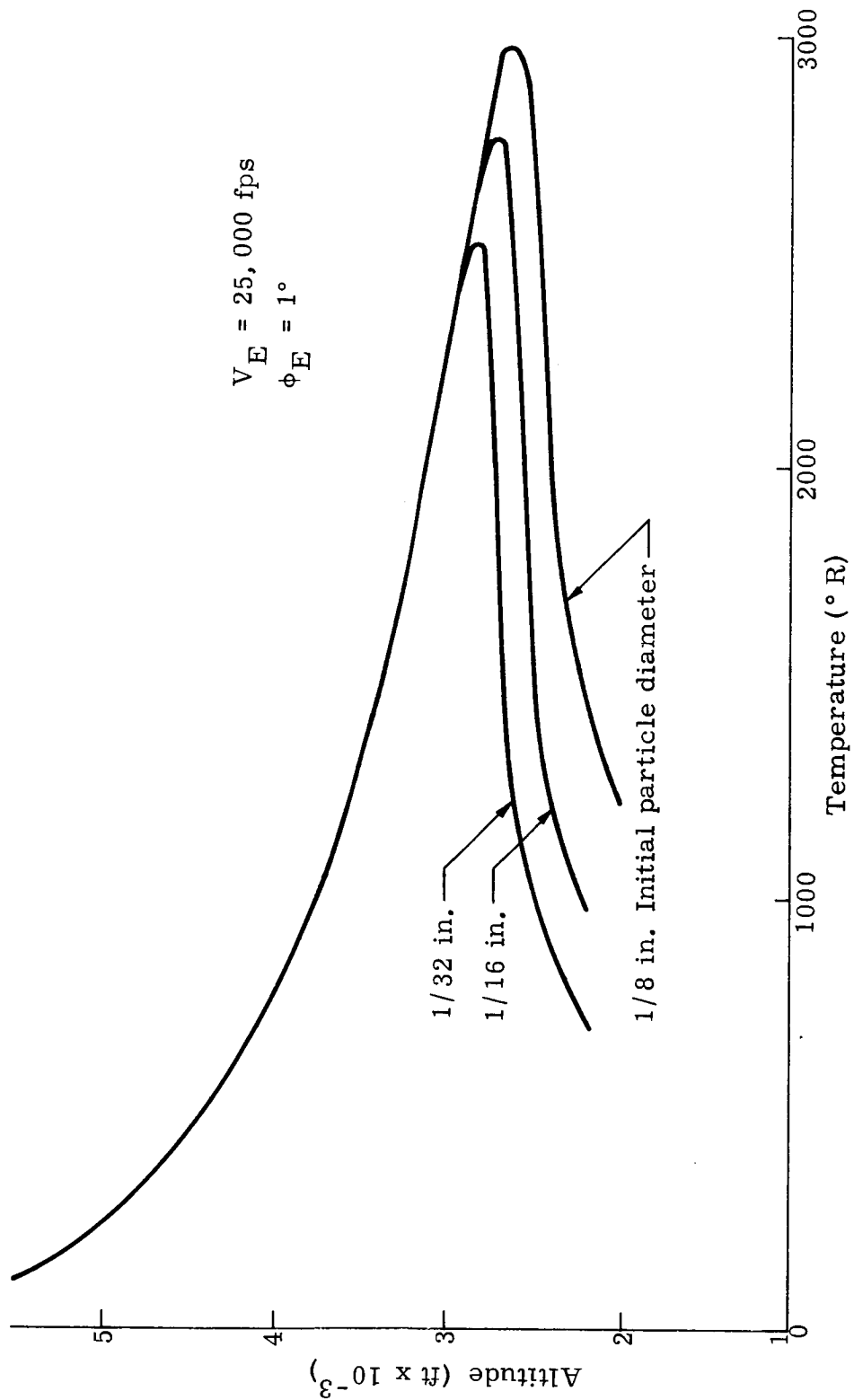


Fig. 4. Particle Temperature Histories -- Free Molecule Flow

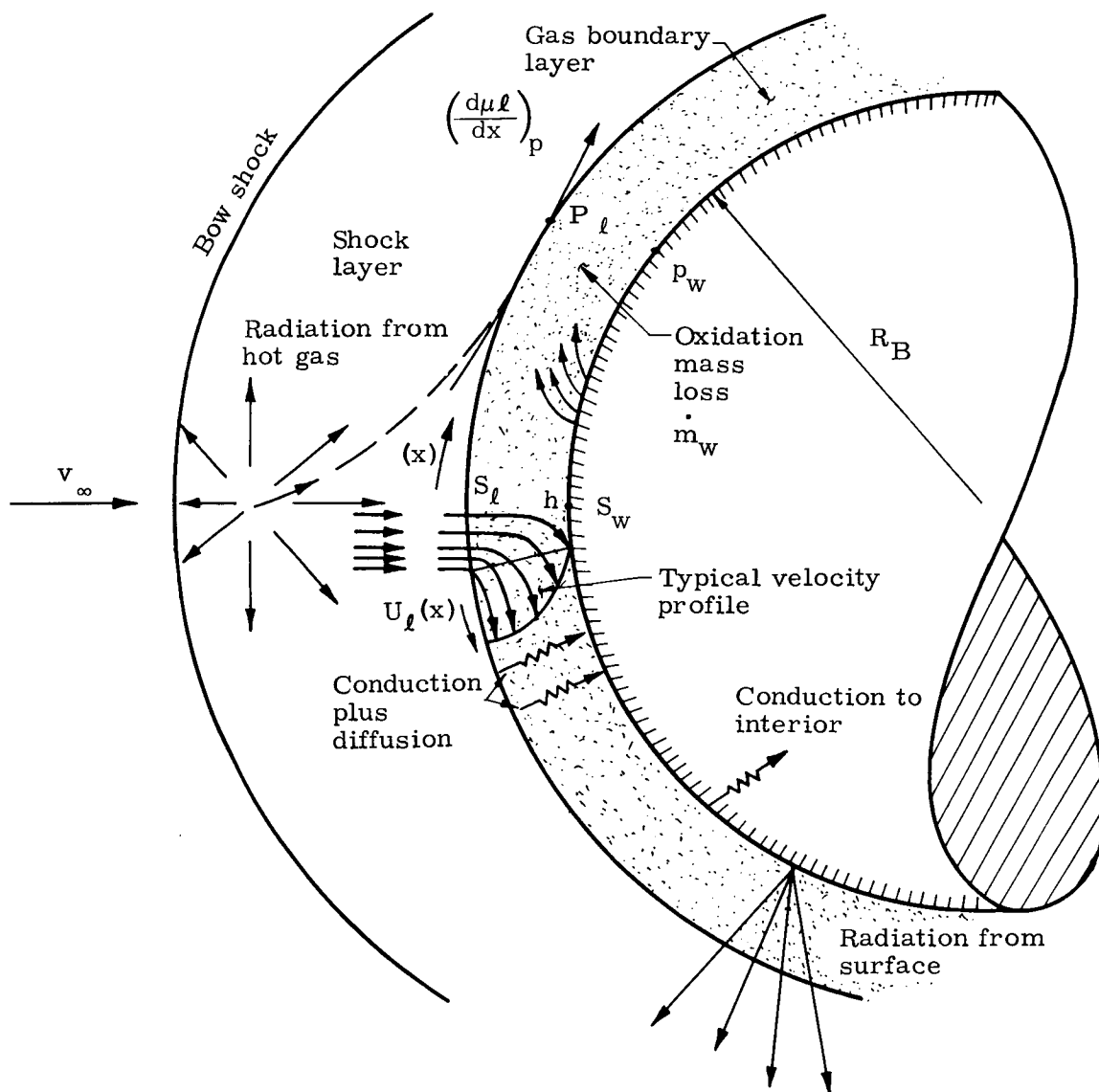


Fig. 5. Analytical Model--Hypersonic Continuum Flow Over Blunt Nosed Body

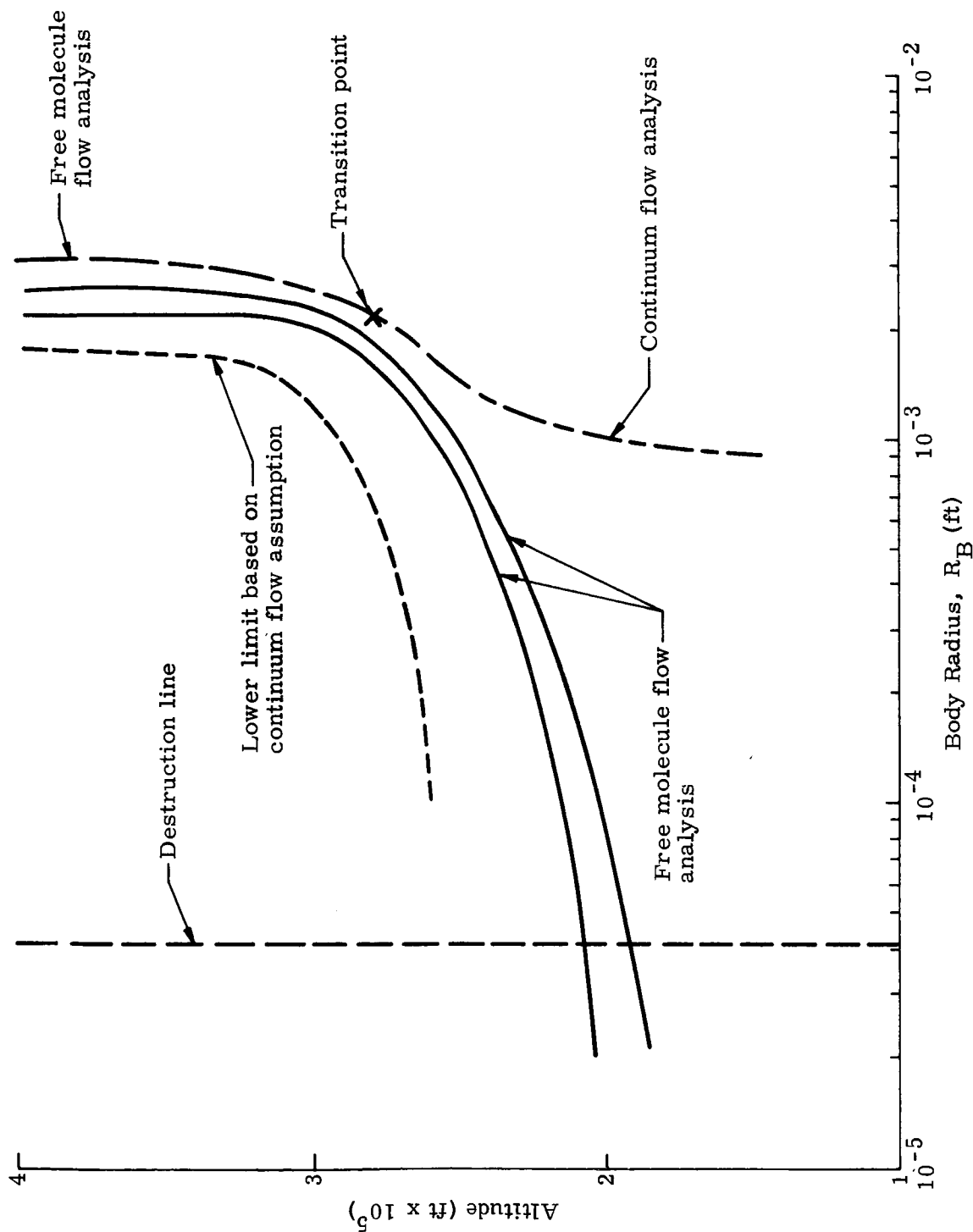


Fig. 6. Comparison of Various Methods of Solution on the Determination of Maximum Particle Sizes Which Can Be Destroyed

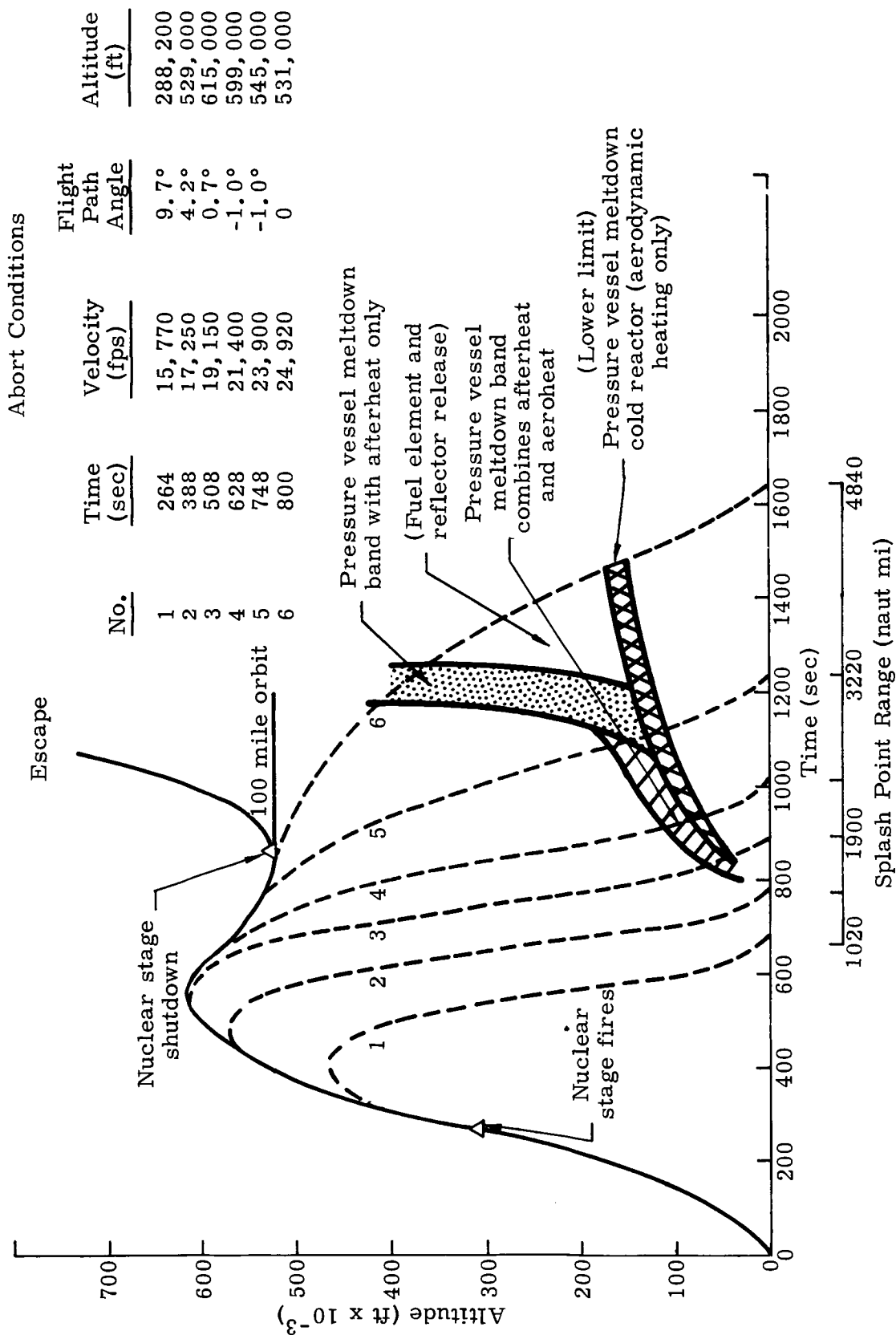


Fig. 7. Orbital Injection Mission Aborts--Zone of Pressure Vessel Meltdown

X 6 6 5 0 2 9 7

NUCLEAR ROCKET DESTRUCT SYSTEM REQUIREMENTS

BY

W. H. ESSELMAN

WESTINGHOUSE ELECTRIC CORPORATION

ASTRONUCLEAR LABORATORY

[U]

An important aspect in assuring the flight safety of nuclear rocket engine systems is establishing the criteria for the design of the destruct system. These requirements can be divided into those applicable prior to engine operation and those following operation. The first, called anti-criticality destruct, would perform the function of subdividing the reactor into subcritical parts in the event of an incident prior to nuclear engine operation. Since the most severe condition occurs when pieces of the reactor fall in water, this system need only break the core into parts which will assure subcriticality when immersed in water.

A preliminary evaluation would indicate that the reactor should be subdivided into integral parts which will remain subcritical when flooded and reflected by water. For example, a spherical geometry of perhaps 50 cm in diameter with water filling the coolant channel voids could be assumed. Such a model is unrealistic since destruction of the reactor will result in individual pieces of fuel elements being dispersed into the water as illustrated in Figure 1. These fuel element arrays must be subcritical as they descend through the water and settle on the bottom. The chemical action of the water must also be considered. At this stage of the development it must be assumed that the fuel element will disintegrate. More optimum mixtures of water and uranium could occur and finally a layer of fueled graphite particles could exist. To account for these cases, a philosophy has been tentatively adopted to disperse the fuel elements such that the pieces cannot combine in critical geometries.

Calculations⁽¹⁾ were made to establish the ratios of water to graphite fuel mixtures which will result in the minimum critical mass. This analysis was performed for five different loadings of the reactor fuel from .500 to .03 gm/cm³. The corresponding carbon to uranium ratio ranged from 1270 to 77.5. The model used was a sphere with uniform dispersion of graphite fuel and water. This sphere was reflected with eight inches of water. It was shown that a water reflected sphere of fueled graphite and water has a minimum critical mass of .89 Kg for a carbon to uranium ratio of 74.47 and .93 Kg for a carbon to uranium ratio of 157.04. These ratios cover the range which could occur with the Nerva design. To allow some margin a tentative criteria has been proposed that the fuel in one area of the water be limited to 750 grams. Figure 1 indicates this condition and shows the fuel dispersed with an optimum U²³⁵/H₂ ratio. Such a mixture can be allowed to fall into a 27" cylinder of water. When the particles reach the bottom, they could result in a uniform U²³⁵ layer of .2g/cm² which is about 1/2 that which would cause criticality of a slab of this type. Areas of this type could be adjacent to each other without risking criticality. Preliminary investigations indicate that this criteria can be achieved in a practical system without excessive difficulty.

Following engine operation, the requirements of the destruct system are vastly altered and more difficult to achieve. The purpose of the post-operative destruct system is to dispose of reactor parts so that no excessive radioactivity returns to a populated area

of the earth. To focus the discussion on a particular case, a model for discussion is postulated. This model consists of a reactor engine in orbit at an altitude of 1.8×10^6 ft. following 30 minutes of operation at 1120 megawatts. Thirty seconds following such operation, the reactor will contain 2.31×10^{10} curies of activity. It is postulated that at this time the engine is broken into small particles by some form of destruct system. The question to be answered concerns the tolerable size of these particles.

A severe condition would be an immediate re-entry of the particles following this operation. It is estimated that a re-entry angle of 5° could result from the destruct system action or other system malfunction. It is believed these initial conditions could be somewhat pessimistic, however, a discussion of this case gives an order of magnitude appreciation of the problem.

To establish the history of reactor fragments during the re-entry period, a combined analytical and experimental program was undertaken. The range of initial particle size chosen for investigation was from about 1/8 in. down to 1/64 in. diameter. These particles will experience loss of mass due to oxidation and sublimation during the re-entry into the earth's atmosphere. It is assumed that the loss of fission products will be proportional to the loss in mass. This is a conservative initial assumption in that some benefits will be obtained by the diffusion of fission products during this operation. From 1×10^5 ft. down to the earth, no additional mass losses occurred; but radioactive decay results in reduction in dose rate expected from the fragments.

The theoretical approach which was used involves the incorporation of one of the existing oxidation theories⁽²⁾ into a digital computer program. This program calculates the fate of re-entry particle based upon various initial velocities and angles of re-entry. The analysis includes the effects of aerodynamic heating, radiation from the particle and decay heat from fission products. Concurrent with the development of this program, a series of experiments were performed using an arc plasma wind tunnel in which specimens of graphite and fuel graphite were exposed to simulated re-entry conditions. The re-entry conditions for a particle at a particular altitude and velocity were simulated by proper adjustment of gas stagnation enthalpy and pressure in the experimental equipment. Mass losses due to oxidation were measured for various particle sizes at various exposure times.

The results of the theoretical analysis and the experimental data were compared to determine the degree of validity of the theory. The first phase of experimental work dealt primarily with unfueled material (pure graphite) which was chosen because the available theory applied only to this material. The subsequent phases of the work were performed with fueled material. Table I shows a comparison of the experimental mass loss rates for graphite samples and fueled graphite samples under three test point conditions. The sample material contained 400 mg/cc of uranium. It was initially hoped by many people that fueled graphite material would have a much greater rate of mass loss than graphite samples. It can be seen that the difference between the two materials is not great. Table II compares the predicted mass loss rates with the experimental results. It is also seen that the theory agrees with the experimental figures within a factor of 2 or 3.

Using the above analytical model and initial conditions, the fate of various sized particles was calculated during the re-entry. Figure 2 shows the velocities of a 1/8 in., 1/16 in. and 1/32 in. particle versus altitude. These curves are all shown for 5° re-entry angle. It is seen that small particles reach low velocities at relatively high altitudes. Figure 3 is a typical particle size reduction curve run in the computer program for a 1/24" particle. It was assumed that size reduction ceased at a surface temperature of 1000°R since oxidation is negligible below this temperature. Figure 4 is a similar typical curve

- depicting percent mass loss as a function of altitude for 1/24" and 1/32" particles. It is seen that mass loss becomes negligible between 200,000 to 250,000 ft. where the particle velocity has been reduced to below 1000 fps.

A summary of the conditions of the particles as they approach the earth is shown in Table III which indicates the final particle diameters obtained from the re-entry computer program. It is shown, for example, that a 1/8 in. particle loses 42% of its mass while 1/64 in. particle will lose 96%. The settling time to earth which is shown in this table is a combination of re-entry time plus the time for the particle to drift from 10^5 ft. to land. This time to drift to land for different particle sizes is given in Figure 5.

The last two columns in Table III are the key ones which can be used to evaluate how large an initial particle size must be established as a destruct system criteria. If one considers a particle of initial size of 1/24 in. diameter, it is seen that when it hits the earth, it is .026 in. in diameter. Such a particle would contain .03 curies of activity, and the dose rate at 1 ft. would be .159 r per hour. A particle of 1/32 in. initial diameter would contain .0038 curies, and the dose rate at 1 ft. would be .018 r per hour. Activities of the latter level are in a reasonable range. It is further indicated that if the initial particle size diameter is as small as 1/64 in., a notable degradation in activity would result.

For practical reasons, it is desirable to be able to tolerate as high a value of initial particle size as possible and, therefore, a number of effects are being investigated. It has been shown that some reduction in particle activity will be obtained by the diffusion of fission products from the fuel pieces during the heating cycle of the fuel, during decay heating, and during re-entry. Estimates are presently being made of the benefit that can be derived from this source. A second benefit may be derived from more definitive establishment of the validity of the re-entry calculations and the experimental plasmajet results versus the calculated values.

It is not anticipated that either of these effects will result in an order of magnitude reduction of activity of the returning pieces. When combined, however, a factor of ten may be realizable and a consequent easing of the destruct criteria could result.

- (1) W. R. Stratton, "Critical Dimensions of U(93.5) - Graphite - Water Spheres, Cylinders, and Slabs.
- (2) S. M. Scala, "A Study of Hypersonic Ablation", General Electric Missile and Space Vehicle Department - T.I.S. Document No. R595D438 (September, 1959).

ACKNOWLEDGMENT

The author is grateful to the members of the Flight Safety Group of the Westinghouse Astronuclear Laboratory for their individual contributions to the program which forms the basis for this paper.

TABLE I

Comparison of Experimental Reaction Rates of Fuel Graphite and Graphite.

Simulated Conditions		Mass Loss Rate x. Radius ^{1/2}	
Velocity (ft/sec)	Altitude (ft)	Fueled (lb/ft ^{3/2} -sec)	Unfueled
17,250	215,000	$2.6 \pm 0.3 \times 10^{-4}$	$2.5 \pm 0.6 \times 10^{-4}$
22,500	240,000	$2.8 \pm 0.3 \times 10^{-4}$	$1.9 \pm 0.3 \times 10^{-4}$
25,000	280,000	$1.8 \pm 0.2 \times 10^{-4}$	$1.5 \pm 0.2 \times 10^{-4}$

TABLE II

Experimental and Predicted Reaction Rates for Fueled Graphite Under Simulated Re-Entry Conditions.

SIMULATED CONDITIONS		MASS LOSS RATE x. RADIUS ^{1/2}	
VELOCITY (FT/SEC)	ALTITUDE (FT)	EXPERIMENTAL **	PREDICTED
17,250	215,000	$2.6 \pm 0.3 \times 10^{-4}$	1.4×10^{-4}
22,500	240,000	$2.8 \pm 0.3 \times 10^{-4}$	1.1×10^{-4}
25,000	280,000	$1.8 \pm 0.2 \times 10^{-4}$	0.5×10^{-4}
		**(LB/FT ^{3/2} -SEC)	

TABLE III

Mass Loss and Radioactivity History of Core Fragments.

INITIAL PARTICLE SIZE (DIA.)	INITIAL PARTICLE VOLUME (IN ³)	FINAL PARTICLE SIZE (DIA.)	FINAL PARTICLE VOLUME (IN ³)	INITIAL RADIOACTIVITY CONTENT	MASS LOSS (%)	SETTLING TIME TO EARTH*	RADIOACTIVITY CONTENT ON EARTH	DOSE RATE AT 1 FOOT
1/8 .125"	1.02×10^{-3}	.1042 IN.	6.16×10^{-4}	7.32×10^2 CURIES	42.37	3.1×10^3 SEC	5.08 CURIES	24.4 R/HR
1/16 .0625"	1.28×10^{-4}	4.632×10^{-2} IN.	5.19×10^{-5}	92.2 CURIES	59.55	4.84×10^3 SEC	2.84×10^{-1} CURIES	1.36 R/HR
1/24 .04167"	3.79×10^{-5}	2.568×10^{-2} IN.	3.72×10^{-5}	26.2 CURIES	76.64	6.94×10^3 SEC	3.32×10^{-2} CURIES	159 R/HR
1/32 .03125"	1.60×10^{-5}	1.52×10^{-2} IN.	1.84×10^{-5}	11.5 CURIES	88.48	1.16×10^4 SEC	3.81×10^{-3} CURIES	.018 R/HR
1/64 .015625"	1.99×10^{-6}	5.26×10^{-4} IN.	7.67×10^{-11}	1.43 CURIES	96.20	2.41×10^6 SEC	4.35×10^{-7} CURIES	< .01 MR/HR

*INCLUDES TIME DURING ABLATION

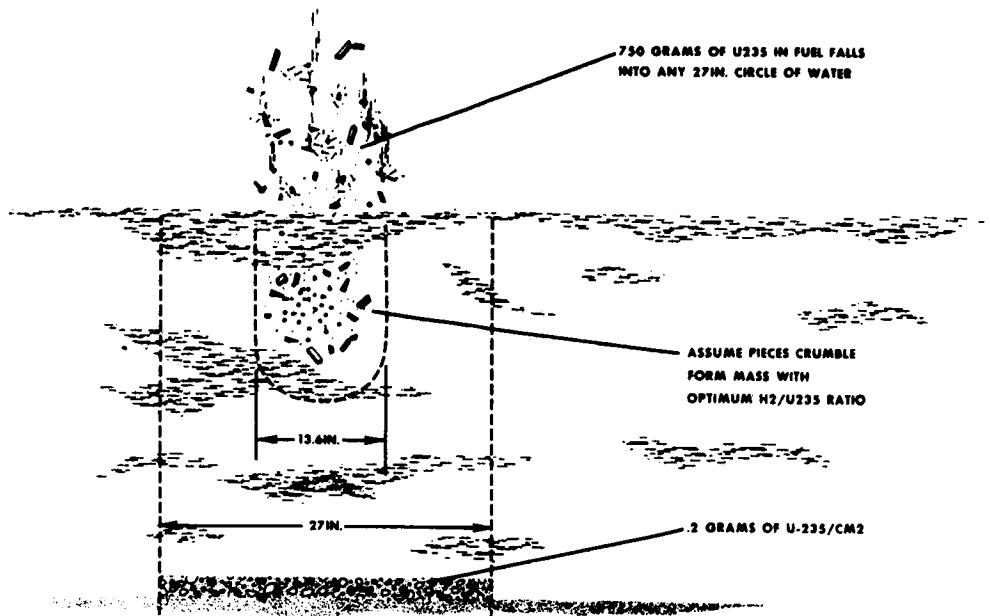


FIGURE 1
Model of Core Parts Falling in Water.

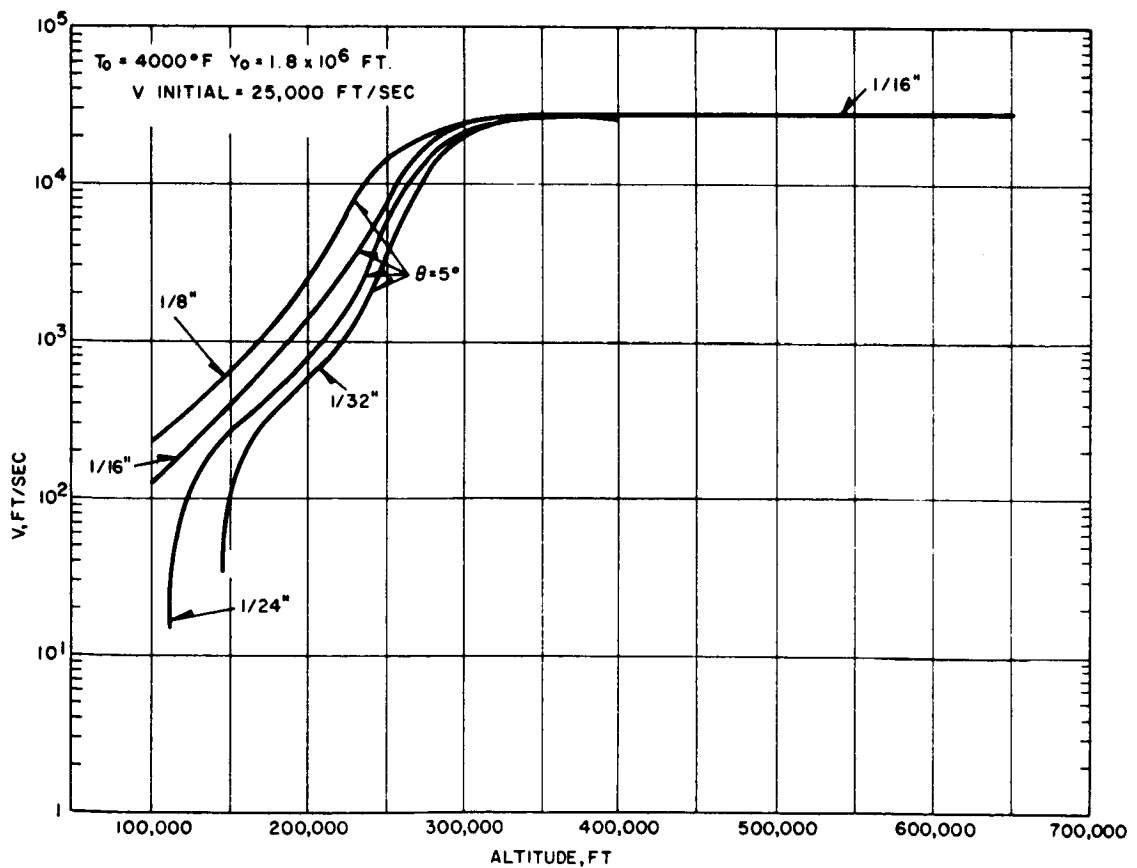


FIGURE 2
Particle Velocity as a Function of Altitude.

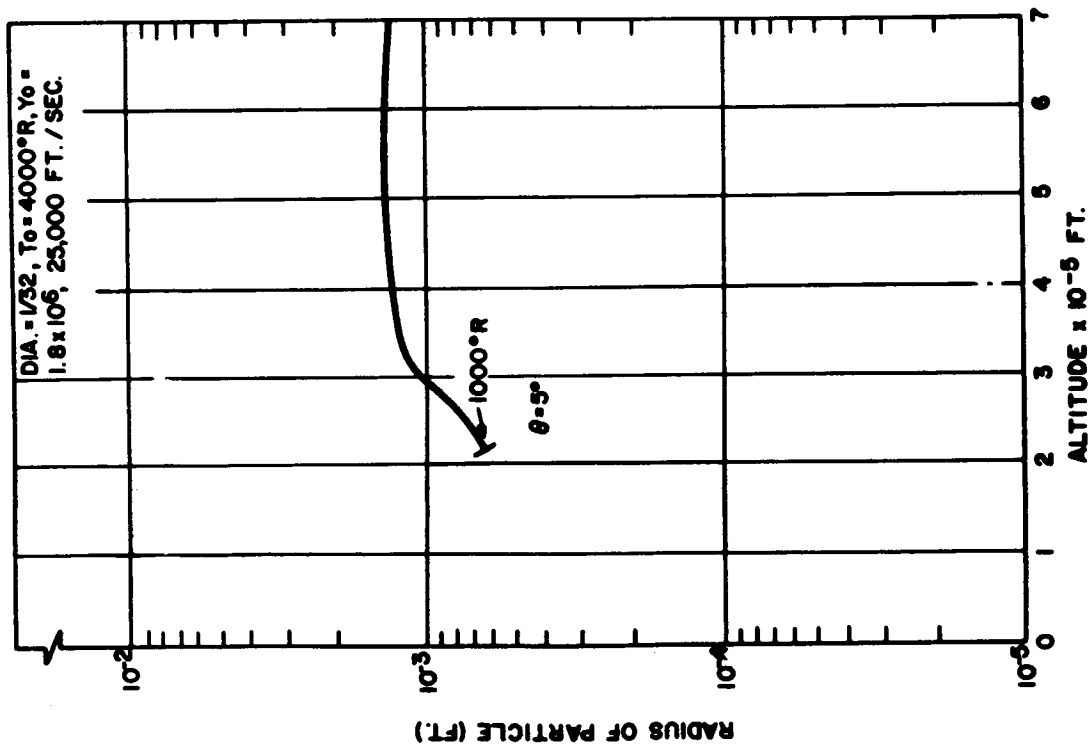


FIGURE 3

Particle Radius as a Function of Altitude.

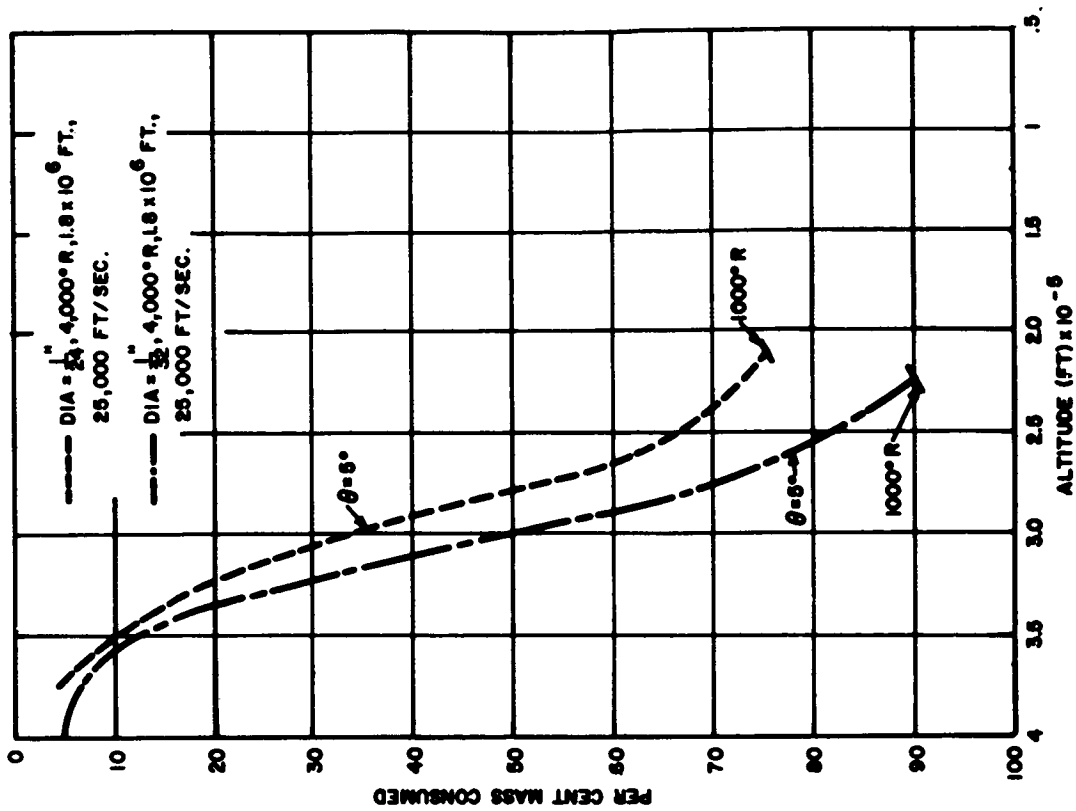


FIGURE 4

Percent Mass Consumed as a Function of Altitude.

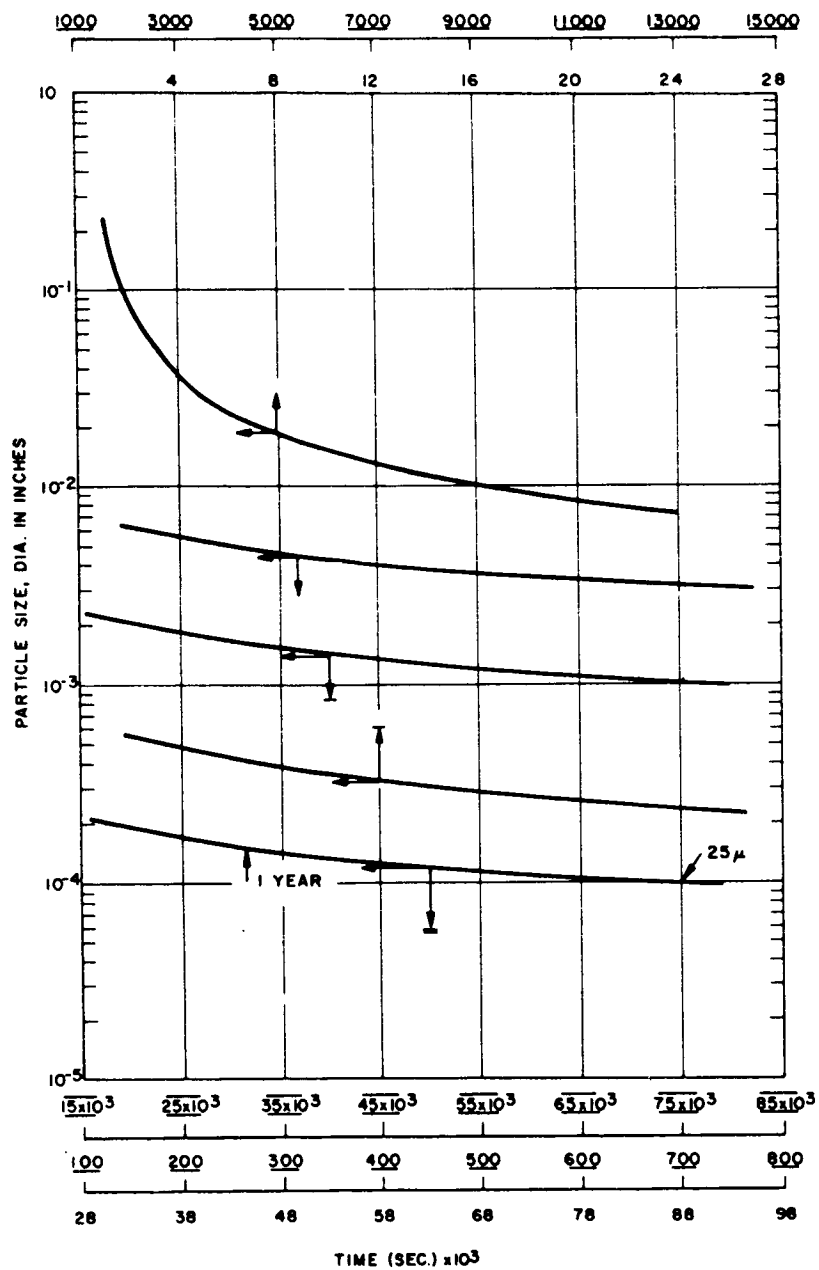


FIGURE 5
Particle Size as a Function of Time for a Particle to Settle.

66 50298

ROVER REACTOR POWER TRANSIENT CALCULATIONS

[U]

W. R. Stratton and C. G. Chezem
Los Alamos Scientific Laboratory
University of California
Los Alamos, New Mexico

ABSTRACT

50298

Two of the codes currently in use for analyzing nuclear power excursions in Kiwi-B-4 type reactors are discussed. These are the Los Alamos RTS and RAC codes. The RTS code allows an exact treatment of delayed neutron effects but is space independent. The RAC code provides for detailed treatment of materials (thermal expansion, phase change, etc.) and some geometries, but contains only a very simple neutronic scheme. Accidents severe enough to create about 2×10^{20} fissions will vaporize some graphite and create a small explosion. Control rod created excursions do not reach this magnitude, but conceptual water immersion accidents could be as large as 3×10^{20} fissions.

Codes and Surveys

CONF.R.D.

Author ↑

Rover reactor power transient calculations have been performed with the aid of two digital computer codes. These are the RTS code (G. R. Keepin, Nuclear Sci. & Eng. 8, 670 (1960)) and the RAC code (C. G. Chezem).

RTS Code

The RTS code integrates the reactor kinetic equations with no approximations beyond the usual space-independent and one-velocity assumptions involving the introduction of an effective delayed neutron fraction and an effective prompt neutron generation time. For Kiwi-B-4 reactors the delayed fraction, β , and prompt generation time, ℓ , are 7.3×10^{-3} and 2.5×10^{-5} sec, respectively. Input to the RTS code may include a completely arbitrary reactivity function and a constant or time varying energy coefficient of reactivity such that

$$\delta k(t) = \delta k_0(t) - bE^f(t) \quad (1)$$

In equation 1, $\delta k_0(t)$ is the imposed reactivity function, E^f is the fission energy density at time t and b is a negative energy coefficient of reactivity appropriate to a Kiwi-B-4. To obtain results pertinent to any given reactor additional assumptions must be formulated about the spatial flux densities, constancy of the reactivity coefficients over the range of interest and the physical state of the reactor core material during the transient. This code is most useful and important in the reactiv-

ity regions between delayed critical and prompt critical and somewhat above prompt critical.

RAC Code

The RAC code is relatively new and is a first attempt to describe in some detail the dynamic behavior of a Rover reactor during a power transient. For calculational purposes the core is imagined to be homogeneous (solid core of density ~ 1.57) and divided into an arbitrary number (usually ~ 16) of squat, adjacent cylinders with a flux (or fission) density assigned to each such region. This arbitrary distribution can be forced to simulate, for example, a control rod transient with a normal cosine type flux or a water penetration type transient with a very peaked flux at the end of the core subjected to flooding. Given an assumption on the imposed reactivity function (step or ramp), the code then cyclically generates fission energy in each region (or mass point) increasing temperatures and internal pressures as demanded by heat capacities and an assumed graphite equation of state. Also, during each time cycle, each mass point is allowed to perform thermodynamic work on its neighbors through the common interface and thus relieve internal pressures (thermal expansion) and in extreme cases physically to set the core mass into motion. The fundamental equation for each region is

$$\frac{dE(T, \rho)}{dt} = \frac{dE^f}{dt} + P \frac{dv}{dt} \quad (2)$$

and for each interface is

$$\frac{d^2 R}{dt^2} = \frac{1}{\rho} \frac{\partial P}{\partial R} \quad (3)$$

where $E(T, \rho)$ is the internal energy assumed to be a function only of density and temperature, E^f is the fission energy, P is the pressure, $v = 1/\rho$ is the specific volume and R is the interface coordinate. Reactivity is decreased as the core expands; the amount of the change is proportional to the change in length.

Assumptions about the graphite equation of state are of most importance in this code. The low-temperature function is a linear combination of temperature and density change of the form

$$P(\rho, T) = C_1(T - T_0) + C_2 \frac{(\rho - \rho_0)}{\rho} \quad (4)$$

where the C_i are adjustable constants related to graphite thermal expansion and compressibility. Negative pressures are allowed to simulate tensions, but a maximum allowable tension is defined beyond which a rupture is assumed and the pressure in the given region is no longer allowed to assume negative values. At low temperatures this "breaking tension" is -300 atm but above $\sim 3600^\circ\text{K}$ its magnitude decreases and is zero at and above the triple point (3960°K). Above 3600°K , the graphite vapor pressure becomes significant and at about 3960°K , the graphite triple point, the equilibrium vapor pressure is 100 atmospheres. One form of the graphite P-T diagram for this temperature range is illustrated in Figure 1. Credence in this figure is limited,

but the triple point pressure seems to be better established than is the temperature. The code allows for the production of graphite gas (latent heat of sublimation, L , equal to 172 Kcal/mole), but for temperatures at or below 3960°K, the vapor pressures are not allowed to exceed a limiting function of the form

$$P = C_3 e^{-\frac{C_4}{RT}} \quad (5)$$

The limiting values of equation 5 do not apply to equation 4. If temperatures exceed 3960°K, a second limiting function similar to equation 5 is used, but in this temperature regime another heat sink is possible - the conversion of solid to liquid, for which the latent heat is estimated to be 11 Kcal/mole. It is assumed that equation 4 is descriptive of the liquid as well as the solid state, except that tensions are disallowed.

To gain an understanding of characteristics and general behavior, some results taken from a series of problems with appropriate constants for a Kiwi-B-4 are illustrated in Figures 2, 3, 4, and 5. These problems were initiated by use of a step increase of reactivity - a scheme that reasonably approximates very fast control rod motions, abrupt changes of reflection, moderation, etc. The fission energy release for a wide range of initial reactivities (relative to prompt critical) is illustrated in Figure 2. The initial prompt α (reciprocal period) for any reactivity may be obtained from

$$\alpha = \frac{\delta k_p \beta}{\ell} \quad (6)$$

where δk_p is the reactivity in dollars relative to prompt critical. Temperature coefficients of reactivity equivalent to 0.60 and 1.20 dollars/1000°C have been used for this survey.

For initial reactivities somewhat less than ~1.5 dollars over prompt critical the fission yield is nearly proportional to the excess reactivity - the core expansion is in near-equilibrium with the fission rate and no physical explosion should be expected. However, above this initial value and depending on the value of the energy coefficient of reactivity, the maximum central temperatures and pressures are found to be in the neighborhood of the triple point and some portion of the core will vaporize and/or melt. The resulting high internal pressures (Figure 3) produce a more effective quenching mechanism leading to an asymmetry in the power spike. This effect produces a fission yield, initially somewhat less than that expected from an extension of the yield line from the lower reactivities. At still larger step inputs, the core expansion lags the energy release and the total fissions increase at a higher power of the initial reactivity.

The introduction of a high pressure gas can impart significant kinetic energy to the core and a physical explosion might be expected. These results from the RAC code are illustrated in Figures 4 and 5 as functions of the initial reactivity and the total fission energy release, respectively. The latter presentation removes some of the uncertainty in the value of the

temperature coefficient of reactivity. The kinetic energy (in units of pounds of high explosive equivalent) shows a distinct and sharp threshold at about 1.5 dollars or 1.5×10^{20} fissions; the knee of the curve near ~ 4 lbs. is associated with the liquifaction of graphite.

Because estimates of explosive energy are most uncertain (perhaps by a factor as large as ten) the energy used to create graphite vapor is also plotted in Figures 4 and 5 to serve as an upper limit to the possible kinetic energy.

The assumption of a homogeneous core now assumes more significance. In effect, the assumption is equivalent to the supposition that the vapor pressures shatter the graphite and plug the flow channels for a time at least of interest to the problem (of the order of milliseconds). If such gases could escape, the yield curve would be more nearly linear with excess reactivity (additional reactivity would still be lost as core material left the reactor or migrated to regions of lower worth) and explosive energies (from this source) would be much lower.

An assumption implicit in these calculations is that the graphite matrix contains no adsorbed gases. This situation is unlikely and when through auxiliary experiments (TREAT reactor, chemical analyses, etc.) the amount and nature of possible adsorbed gases are known some reasonable assumptions may be incorporated into the RAC code to allow for this. The effects will be similar to those from graphite vapor pressures, but will most likely occur at lower temperatures and fission energy densities. The magnitude of explosive energies will depend on the volume of adsorbed gases and the rate at which they are released.

Control Vane Transients

To calculate the maximum accident from control vane motion, the improbable and simultaneous failure of the servo-control system, the scram circuit and the safety springs of all vanes is assumed along with the appearance of a signal which forces all vanes to add reactivity at the maximum possible rate. Since vane speeds have not yet been set, three values are considered - $22\frac{1}{2}$, 45, and 90 degrees/sec with all vanes moving together.

For this study, the RTS code was used and results were normalized through special RAC problems. A maximum of five dollars over delayed critical was assumed to be available and, for the 45 deg/sec case, the input reactivity (in dollars) was forced by

$$\delta k_0(t) = 3.927 t - 0.177 t^2 - 0.26825 t^2 \quad (7)$$

which may be scaled for the other two speeds.

Figure 6 illustrates the power history of these three transients. The fission energy releases following the spikes are 3.1×10^{19} , 4.7×10^{19} , and 6.2×10^{19} , the larger value corresponding to the greater rate.

As was determined earlier, at least 1.5×10^{20} fissions are

necessary to bring the central portion of the core to vaporization temperatures. Even the extreme case of 90 deg/sec would reach this value only long after the initial power spike. Thus, a graphite gas explosion should not be expected, but some explosive force from the release of adsorbed gases could occur.

Liquid Hydrogen Accidents - An Upper Limit

The accident caused by the sudden flow of liquid hydrogen into the reactor system can be overestimated by making some grossly simplified assumptions. It is assumed that hydrogen in the core is worth about two dollars per pound and that the pump can start the flow of liquid hydrogen at the rate of seventy pounds per second with no time delay whatsoever. In addition, it is postulated that this flow is directed into a room temperature reactor (no cooldown) and no choking in the nozzle, reflector or core occurs.

With these assumptions, the energy release from a transient created by a steady insertion of 140 dollars/sec is calculated by the RAC code to be 2.8×10^{20} fissions. The kinetic energy (from Figure 5) is about 4 lbs. HE equivalent.

This energy release must be an overestimate for reasons cited above, but also because some exploratory calculations with the RAC code in which the axial fission density is highly peaked at one end of the core show a lower fission yield (compared to a cosine flux distribution) for the same insertion of reactivity. Such a peaked distribution tends to destroy one end of the core and quench the transient before the central part reaches destruction temperatures. Thus, the fission yield from such an accident is certainly less than 3×10^{20} fissions by some unknown factor; one guesses that the factor is no less than two and no greater than ten. The kinetic energy is more difficult to estimate. The effect of hydrogen gas in the core could appreciably increase this quantity relative to the fission yield.

Water Immersion Accidents

If a Kiwi-B-4 reactor were to fall into water, the immediate consequence would be a very rapid, near-step increase of reactivity. From Los Alamos critical experiments, end reflection of the core with polyethylene contributes 2.17 dollars and complete side reflection (outside the pressure shell) contributes 2.6 dollars. Thus, if the reactor were initially just critical, it could find itself some 3.77 dollars super prompt critical, creating an energy release of $\sim 3 \times 10^{20}$ fissions. However, it is unlikely that complete reflection could be accomplished quickly enough, and the excursion most likely would be of lower magnitude.

Another possible state of the reactor could be several dollars subcritical. In this case, the reflection might change the state of the core to near-delayed critical and water could penetrate the flow channels at a rate of several feet per second. Since 2 inches water penetration is worth about 2 dollars and 4 inches is about 5.5 dollars, it is clear that the reactor could not survive the subsequent power transient.

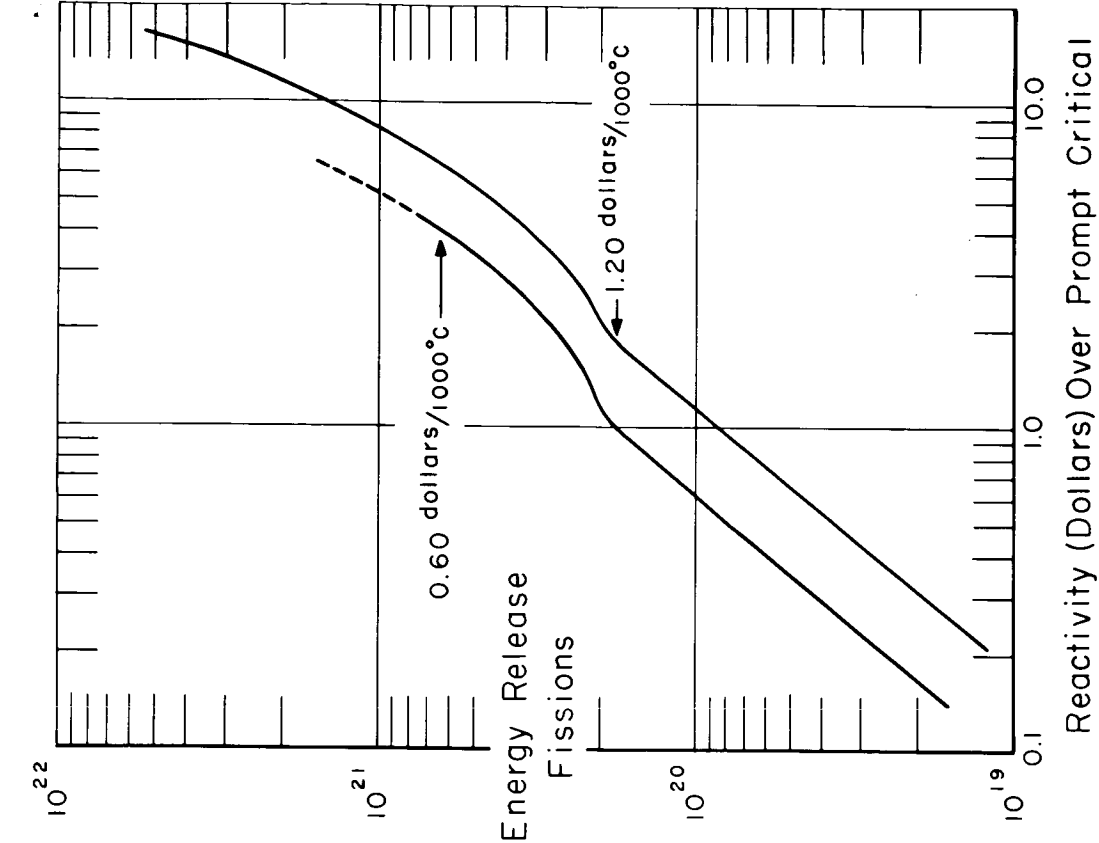


Figure 2. Fission energy release of Kiwi-B-4 reactors versus a step increase in reactivity relative to prompt critical.

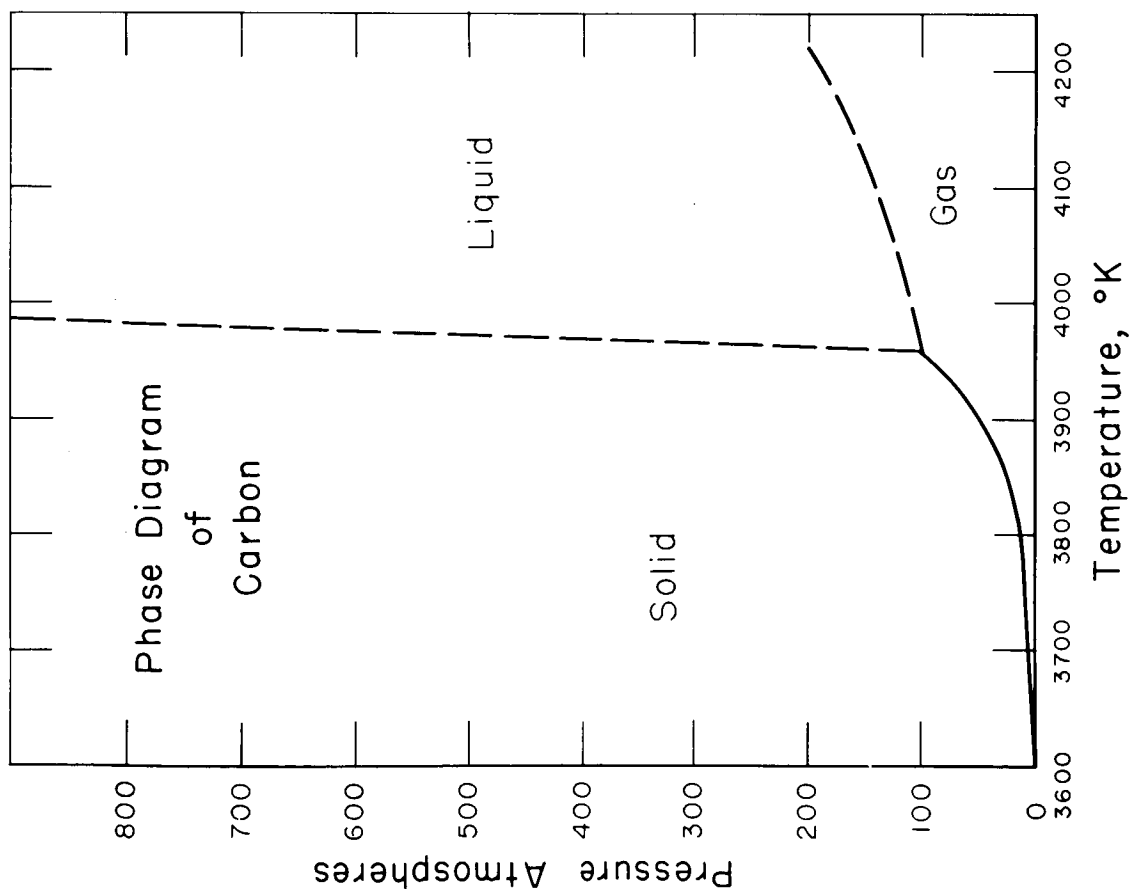


Figure 1. Assumed phase diagram of carbon in the neighborhood of the triple point. Triple point values are 100 atm and 3960 $^{\circ}\text{K}$.

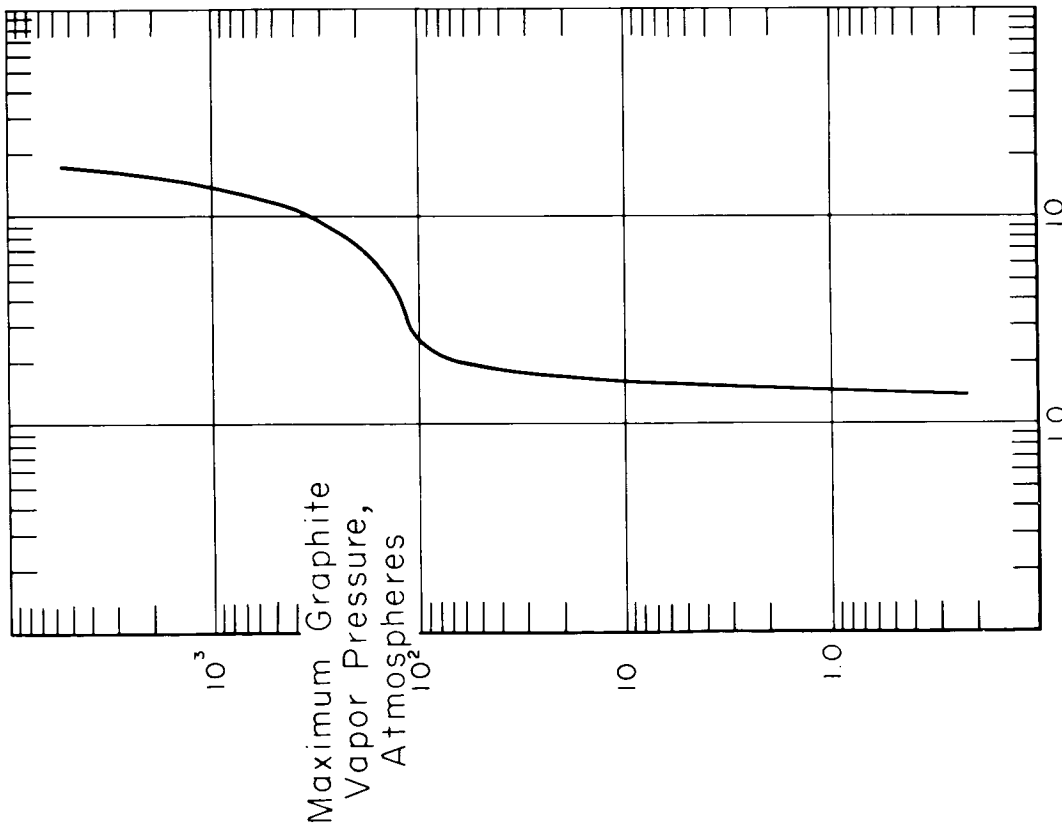


Figure 3. Maximum central graphite vapor pressures during power transients versus reactivity. Temperature coefficient of reactivity is 1.20 dollars/1000°C.

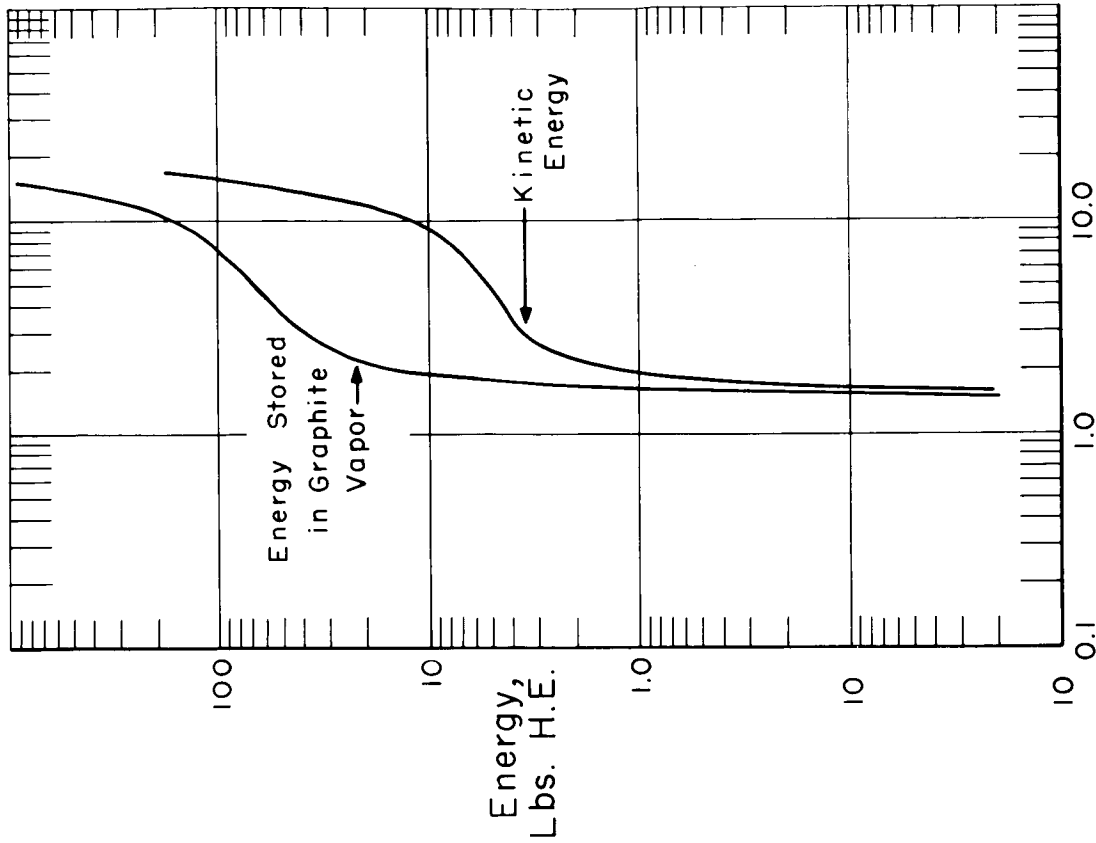


Figure 4. Explosive kinetic energy created during power transients versus reactivity. The energy stored in the graphite vapor is an upper limit.

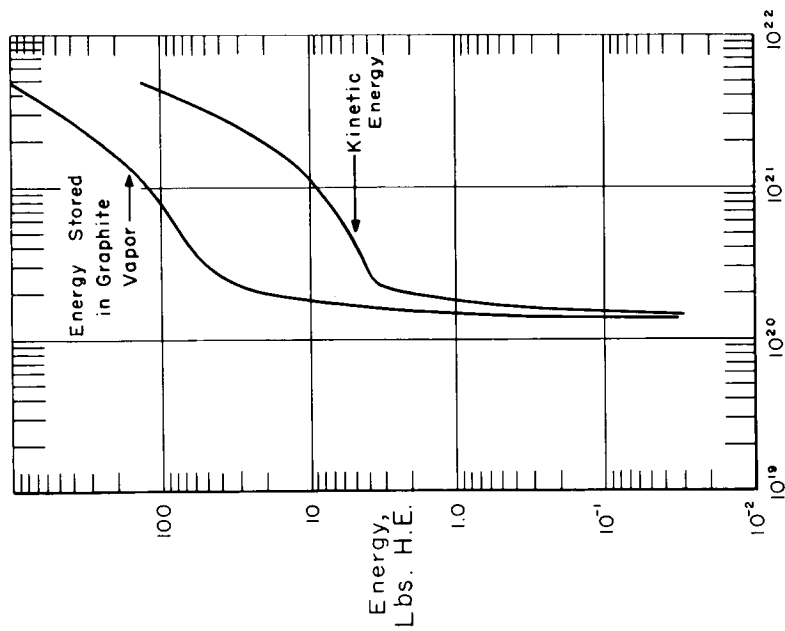


Figure 5. Explosive kinetic energy versus spike fission yield. The energy stored in the graphite vapor is an upper limit.

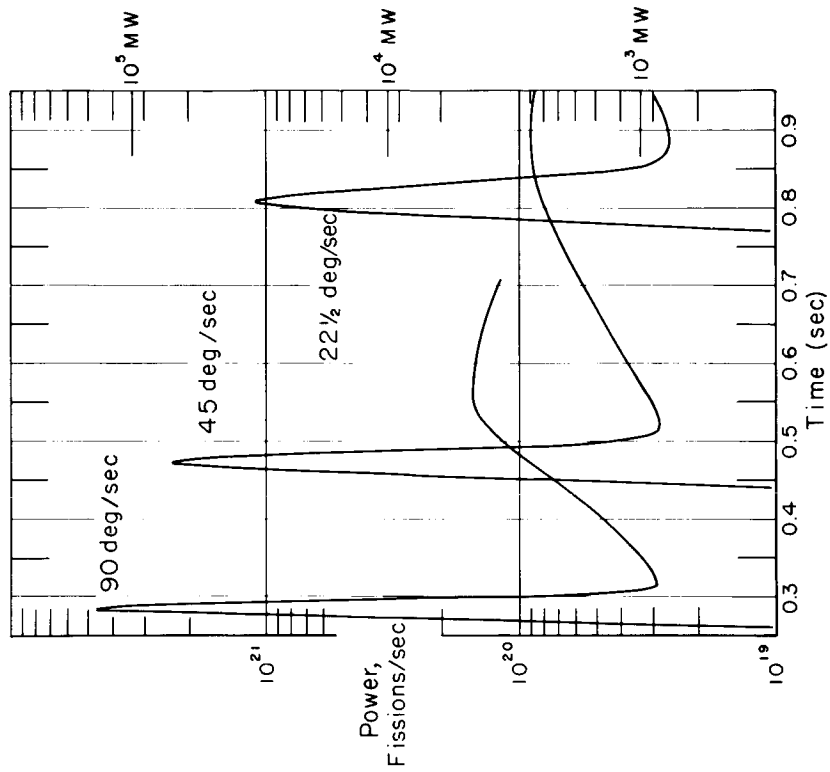


Figure 6. Reactor power for three control vane induced transients as a function of time. The spike integrals are 3.1×10^{19} , 4.7×10^{19} , and 6.2×10^{19} fissions.

X 66 50299

NUCLEAR ROCKETS - SAFETY PROBLEMS AND SAFETY PROGRAMS

George P. Dix, Space Nuclear Propulsion Office AEC/NASA

[U]

50299

This paper presents the potential safety problems associated with nuclear rockets, countermeasure philosophy, and the current safety program. Reference is made to causal non-nuclear accidents, which are defined as the event or series of events culminating in a nuclear incident. During the past two years the subject has been extensively studied^{1,2} so that both the causal accidents and potential nuclear incidents are sufficiently well known to proceed with the engineering of safety devices and the formulation of safety procedures to prevent, override, or minimize nuclear incidents. The philosophy adopted is to assume that certain credible causal accidents will occur and provide reliable countermeasure devices to assure nuclear safety.

CONF. R.D.

Author

↑

1. THE NUCLEAR ROCKET REACTOR - Since the nuclear rocket reactor is a uranium-graphite system designed to operate in the 2000°C. temperature range, it is inherently a large energy sink. Some fundamental estimates of its behavior can accrue from a comparison of its energy capacity and energy potential to various sources of energy that it can be exposed to over its operational history, as shown in Table I.

TABLE I

CORE ENERGY CAPACITY VERSUS SOURCES OF ENERGY (APPROXIMATE)

<u>CORE ENERGY CAPACITY</u>	<u>MWS</u>
Energy required to raise core from 0° C. to 4000° C.	6,800
Energy required to raise core from 2000° C. to 4000° C.	4,000
Heat of vaporization	72,000
Energy required to completely vaporize cold core	78,800
<u>CORE ENERGY SOURCES</u>	
Afterheat to 1/2 hour after shutdown	3,960 (1)
Nuclear Transients:	
1. Spherical collapse (Maximum Impossible Accident)	75,000 (1)
2. Extreme control drum failure (B-4)	1,500 (3)
3. Liquid hydrogen flooding (B-4)	900 - 9,000 (3)
4. Extreme water flooding (B-4)	16,000 (4)
5. Threshold range for carbided fuel destruction from TREAT	5,000 - 11,000 (5)

OTHER ENERGY SOURCES

MWS

Heat of combustion of core	40,000
Maximum kinetic energy of core at orbital reentry (25,000 fps)	33,000
Kinetic energy of core impacting at terminal velocity (500 fps)	13
Kinetic energy of 100 pounds of TNT to pulverize core	145
Maximum energy derived from Saturn (C-2) propellants under ideal stoichiometric mixing conditions	7,600,000 (6)

A number of nuclear transients have been cataloged in Table I. These range in magnitude from 1500 to 75,000 megawatt-seconds (MWS) depending upon the core model analyzed, the initial core conditions, the amount and rate of reactivity insertion, the method of analysis, and shutdown mechanism postulated. The upper limit or maximum incredible accident of 75,000 MWS¹ is derived from spherical collapse, removal of the core void volume, and reflection of the core and approximates the maximum thermal energy capacity of the core. Lesser energy releases are derived from more credible accidents recently analyzed by Stratton^{3,4}. Some preliminary empirical estimates of the fission energy required to break-up the fuel have been derived from the TREAT experiments.

Other energy sources include the exothermic heat liberated by complete combustion of the core and the kinetic energy of the core at reentry. When combined, these two sources approximate the energy capacity of the core. However, during actual reentry of a complete engine these combined sources of energy cannot be effectively coupled and fully applied to the core because of chemical reaction inefficiency and system heat loss, yielding the intuitive conclusion that reentry heating and oxidation alone will not completely consume the core. However, the detonation of 100 pounds of explosives, representing a comparatively small energy input, in the core prior to reentry would enhance the aerothermochemical reaction efficiency by exposing the fuel and creating more surface area. Also of interest is the theoretical upper limit energy inventory of Saturn propellants which over-shadows the potential nuclear energy releases of the nuclear rocket engine.⁶

2. RADIONUCLIDE INVENTORY - A relative measure of the magnitude of safety problems associated with nuclear rockets is the inventory history of fission products developed by the reactor, shown in Figure 1. Of note is the comparatively small contribution of a hypothetical terminal excursion occurring at impact in the deep ocean downrange to the inventory developed by normal full power operation. Depletion of the inventory by fission product diffusion is expected to be a few percent during full power operation, about 80% during typical afterheat conditions, and from 30-60% during excursions. Radioactive decay achieved by residence of the nuclear rocket in space and temporary retention of engine particulate debris in the upper atmosphere as fallout, and fission product boil-off, all serve to decrease the magnitude of the safety problems associated with operational nuclear spacecraft.

3. CHARACTERISTIC MISSIONS - Present planning for RIFT considers the testing of the nuclear rocket as an upper stage on four variant ballistic flights including the following: (1) a dummy engine test, (2) continuous application of thrust, (3) powered operation with one restart, and (4) powered operation with two restarts.⁷ The full power operation of the nuclear stage will occur at high altitudes downrange, where its instantaneous impact point will be in deep water downrange.

The following future nuclear stage modus operandi are envisioned: (1) pre-orbital startup, orbital parking, and restart to escape⁸, (2) pre-orbital

startup direct to escape, and (3) chemical injection into a parking orbit with orbital startup.

4. POTENTIAL SAFETY PROBLEMS - Potential safety problems associated with nuclear rockets can best be isolated in an orderly manner by discussing them within the chronology of conceptual operational phases. A parallel sequential discussion of safety countermeasures is also appropriate since they are designed to prevent nuclear and radiation incidents for a wide spectrum of assumed causal primary non-nuclear failures and accidents. Figures 2 and 3 show the relationship of conceptual operational phases, safety problems, and countermeasures during transport, ground handling, and flight.

A. DURING ENGINE TRANSPORT - Conceptually, the nuclear rocket reactor core will be transported to Cape Canaveral in a fully assembled condition, and the remaining engine components will be shipped separately. The core will be heavily poisoned to maintain it subcritical even when immersed in water, contained in a water-tight structure designed to withstand impulsive loads, and shipped in a preferential manner. At least three simultaneous failures must occur to cause a nuclear incident, as follows: (1) a catastrophic carrier accident, (2) structural or thermal failure of the shipping container, and (3) poison removal in an undetermined manner while still maintaining a critical geometry. Because of the infinitesimal probability of this event when countermeasures are used, safety analysis in this area has yielded to countermeasure engineering.

B. DURING GROUND HANDLING - Programmatic philosophy is to safe the reactor whenever possible by maintaining a dual poison capability by inserting poison wires in the core coolant channels and locking the control drums in the most sub-critical position during ground handling. Dual poison usage is effective since the core poison will override the reactivity available in the control drums even if they are rotated to the most critical position.

(1) NUCLEAR ENGINE AND STAGE ASSEMBLY - The reactor will be assembled in the Nuclear Assembly Building (NAB) following its arrival at Cape Canaveral. During assembly poison wires will remain in the core and the control drums will be locked. Dry criticality incidents during reactor assembly are not deemed credible when the reactor is thus poisoned.

Following reactor assembly the poison wires will be removed and the control drums unlocked preparatory to critical testing. The critical test constitutes the only discontinuity in poison usage during the ground handling phase and appears intuitively to be one of the more credible places, for a nuclear accident to occur, because the countermeasure devices are virtually negated. Should a nuclear incident occur, it's worst form would be a dry excursion due to excessive, but velocity-limited, drum rotation resulting in a maximum energy release of from 1000-2200 MWS estimated for similar excursions of Kiwi-B type reactors. However, up to May, 1962 some 953 similar tests⁹ had been run on Kiwi-B type reactors without incident and several thousand such tests will be run before the NERVA reactor is tested at the NAB. Hence, it is expected that a high degree of personnel competence and hardware reliability will be inherent in the NAB critical tests. During critical tests at the NAB, a personnel exclusion radius of one-half mile is tentatively planned even though the test cell will offer a high degree of aerosol containment and direct radiation attenuation.

Following critical testing, the poison wires will be reinserted and the control drums locked before the reactor is assembled with the remaining engine components. The nuclear rocket engine will then be mated to the nuclear stage and the stage moved to the Vertical Assembly Building (VAB). Movement of

the fully poisoned reactor on a velocity-limited carrier through a controlled area does not appear to constitute a significant potential nuclear safety problem.

(2) RIFT VEHICLE ASSEMBLY - Upon arrival at the VAB, the nuclear stage will be mated to the Saturn chemical stages to constitute the RIFT vehicle. Since the VAB is a "cold" area of high personnel density, the reactor will be doubly poisoned in the manner previously described. A conceivable, but unlikely, non-nuclear causal failure would be the inadvertent dropping of the nuclear stage from a height of more than 200 feet atop the Saturn booster as a result of human error or equipment malfunction. In this case, the free fall impact velocity would be about 110 feet per second, with a corresponding impact pressure of about 15,000 psi, and considerable distortion of the engine would be expected. However, hydrogenous materials would not be present in the VAB, and in order to induce a "dry" excursion critical geometry would have to be maintained while at the same time the poison would have to be removed from the core and the majority of the control drums rotated in the "poison-out" position by impact. Current analyses of the response of the reactor core, control systems, and poisons to impact loads will shed more light on the credibility of this incident. When the RIFT vehicle is completely assembled, it will be moved from the VAB to the launch position with the reactor remaining in a doubly poisoned condition.

(3) VEHICLE TRANSPORT AND PRE-LAUNCH PREPARATIONS - Conceptually, movement of the unfueled RIFT vehicle will be accomplished in a vertical position on a massive crawler-type Transporter-Launcher (T-L). The T-L will move from the VAB to the launch position via the arming tower, where pyrotechnics and certain ordnance equipment will be installed on the RIFT vehicle. When the T-L has reached the launch position, it will be stabilized as a launch platform.

One very unlikely non-nuclear causal failure during the vehicle transport phase appears to be the fallover of the complete RIFT vehicle or its nuclear stage from the Transporter-Launcher during transport or after stabilization at the launch position. Since the center of mass of the loaded T-L is quite low, it appears that departure of the RIFT vehicle from the T-L will be dependent upon the integrity of the vehicle lock-down mechanism. The T-L will be designed to support the vehicle during a line squall with maximum wind velocities of 60-65 knots. This accident is quite similar to the one described earlier for vehicle assembly in the VAB. The sole difference is whether or not water is present along or adjacent to the route of the T-L from the VAB to the launch position. Nuclear incidents as a result of fall over would be more likely when immersion of the reactor in water is possible. Because of the massive nature of the T-L it does not appear that it will cross bodies of water over bridge-type structures, rather if water must be traversed at all, earth fill roadways might be utilized.

C. DURING CHEMICAL BOOST - The chemical boost phase is arbitrarily defined as the time period beginning with the countdown and fueling of the vehicle and ending with nuclear stage start-up and booster separation. Potential nuclear incidents during this phase are clearly dependent upon: (1) the probability of causal failures of the vehicle and (2) the reliability of countermeasures utilized to preclude nuclear incidents in the event of vehicle failures.

The conceptual use of countermeasures during chemical boost warrants discussion. It is currently planned to maintain poison wires in the core and the control drums locked until the countdown. At this point the poison wires would be withdrawn and replaced by the Anti-Criticality Destruct System (ACDS) which in turn is connected to the vehicle destruct system. The ACDS is only operative during chemical boost and is designed to render the reactor

permanently subcritical with shaped charges, which cut the pressure vessel and fragment the core. Hence, if range safety destruct action is necessary during chemical boost, the vehicle tankage is disrupted, thrust is terminated, and the nuclear rocket reactor is neutralized without a nuclear incident.

(1) LIFT-OFF AND VERTICAL BOOST - An accident that has been observed in the past is the vehicle fallback accident or launch pad abort in which the vehicle fails on the launch pad or vertically above it during or after lift-off. The fallback area in which the vehicle can impact during its vertical flight can encompass an area a mile or more in radius from the launch position. In such an accident the ACDS would be fired by a command destruct signal from the ground. Reliability of the vehicle and engine destruct system would be quite high. Should the ACDS fail to function, the nuclear rocket engine would sustain appreciable impact damage and become involved in a major propellant conflagration and/or detonation.^o The probability of a nuclear excursion during this event is at best unknown, since it is not conducive to straightforward numerical analysis or experimentation. Another related problem is one of the possible chemical toxicity of beryllium that might be vaporized by the conflagration. Here it appears that only small fragments of beryllium could be vaporized by a sustained propellant fire, and propellant detonations with high kinetic energy yields would present an insufficient thermal pulse to vaporize any appreciable amount of beryllium. As a safety precaution an off-site exclusion radius of eight miles and an on-site personnel exclusion radius of three miles is planned around the launch position during launch.

(2) GRAVITY TILT PROGRAM - During the gravity tilt program, which is initiated ten seconds after launch, structural failure, thrust-cut-offs, and guidance malfunctions are credible vehicle failures. Should the vehicle deviate from its planned azimuth immediately downrange and cross the destruct limit line, destruct action involving the firing of the ACDS would be necessary. Again both the engine and vehicle destruct systems would have a high degree of reliability. However, should the ACDS fail to fire, the nuclear rocket reactor would impact in the ocean from one to 250 miles downrange where the water depths vary from several feet to 3600 feet respectively. If the critical geometry of the core is not destroyed by the impulsive load (about 17,000 psi), an amount of positive reactivity far above the negative reactivity available in the control system would be inserted as water entered the core, and a nuclear excursion (probably non-cyclic) and attendant release of fission products would result. This event does not appear to be serious as the impact point approaches the Blake Escarpment, but takes on somewhat serious temporary aspects early in the tilt program when the instantaneous impact point of the vehicle is in the shallow water zone from one to twenty miles downrange. However, a range safety zone would be established during chemical boost, exclusion from the impact point could be enforced, and monitoring of the area could be accomplished until the radioactive contaminants had been diluted by natural diffusion and advection.

(The previous treatment of potential nuclear rocket safety problems during engine transport, ground handling, and chemical boost applies equally to both RIFT missions and operational missions. The safety problems and counter-measures remain essentially the same during these phases for all types of missions. The subsequent discussion reflects the divergent nature of safety problems, during the nuclear stage operation and post-mission disposition phases, between RIFT ballistic missions and the more complex operational missions.)

D. DURING NUCLEAR STAGE OPERATION AND POST-MISSION DISPOSITION

(1) RIFT BALLISTIC MISSIONS - A ground rule for RIFT ballistic missions is that the nuclear stage does not come to full power until its

instantaneous impact point is beyond the Blake Escarpment which is approximately 250 miles downrange. Hence, once that the nuclear rocket has developed any appreciable fission product inventory, any subsequent in-flight failures would result in ballistic reentry over a zone where the average water depth is three miles. The final resting place of the nuclear rocket engine or its debris would be on the ocean floor beyond the active biosphere.

On RIFT there are two options for the disposition of the nuclear rocket engine, namely: (1) allow the reactor to reenter and impact in mid-ocean, or (2) proof test the Engine Destruct System (EDS) at or beyond apogee. Referring back to Figure 1, it has been shown that a terminal excursion at impact represents only a small contribution to the fission product inventory developed by the powered operation of the nuclear rocket, so that it is somewhat of an academic matter whether or not the reactor is allowed to impact in deep water. On the other hand, testing of the EDS on RIFT appears mandatory to qualify it for operational flights. The Engine Destruct System is operative during and after nuclear stage operation, and its ultimate purpose is to resolve the reactor core into small particles which will not survive the aerothermochemical environment of reentry. In summary the EDS is not required to make RIFT missions safe, but RIFT provides an ideal means for testing the EDS preparatory to operational flights.

(2) OPERATIONAL MISSIONS - The predominant safety problem posed by operational nuclear rockets is one of the random reentry of the reactor and its entrained fission products. In the case of suborbital start-up of the nuclear stage, velocity decrements short of orbit or escape could result from thrust cut-offs and guidance failures. Large decrements yielding velocities well below orbital velocity would result in ballistic reentry over the mid-ocean and relatively safe disposal of the radioactive engine debris in deep water. Small velocity decrements would yield a spectrum of cases ranging from prompt reentry downrange to a variety of poor orbits of varying lifetimes. Following orbital regression, the nuclear stage could reenter at random.

In the case of orbital start-up or orbital restart to escape, a somewhat different situation exists. D. B. Cross has examined a series of orbital start-up failures² assuming a number of thrust cut-offs and guidance failures. It was concluded that early thrust cut-offs of a nuclear rocket with proper guidance control would result in orbital lifetimes which are always greater than the lifetime of the parking orbit. In cases where the planned thrust is derived, the angle of thrust application can vary between approximately $\pm 40^\circ$ and -40° and still yield escape conditions. However, more acute guidance failures can yield elliptical orbits of varying lifetimes or hyperbolic and parabolic flight paths resulting in prompt random reentry. With adequate guidance control, early shutdown of the nuclear rocket will not significantly decrease its orbital lifetime but generally will increase it. Since only acute guidance failures can result in prompt random reentry with a full radionuclide inventory, a guidance-propulsion interlock to prevent or terminate thrust if attitude control fails would be an effective safety device.

The random reentry problem has stimulated the development of the Engine Destruct System previously mentioned. The requirements for this system are: (1) high reliability, (2) uniform and effective destruction of the reactor core into fragments that will be consumed aerothermochemically, and (3) fast response time. The engine destruct systems under investigation are described under the countermeasure development program in the next section. The relationship of the operational phases, safety problems, and countermeasures are summarized in Table II.

TABLE II - OPERATIONAL PHASES, POTENTIAL SAFETY PROBLEMS, AND COUNTERMEASURES

OPERATIONAL PHASE	CAUSAL FAILURE	SAFETY PROBLEM	COUNTERMEASURE
Engine Transport	Catastrophic carrier accident	Criticality incident (Crushing, fire, water immersion)	Shipping container Poison Preferential shipment
Ground Handling	Human error or equipment failure during critical test in NAB	Dry excursion	Containment Exclusion zone
	Human error or equipment during engine, stage, or vehicle assembly. (Drop accident.)	Dry excursion	Poison wires Control drum locks Special handling
	Vehicle fallover in transport	Excursion (dry or wet)	Poison wires Control drum locks Elimination of water traverse (if possible)
	Inadvertent firing of vehicle destruct system	Excursion (dry or wet)	Same as above
Chemical Boost	Vehicle fallback or launch pad abort	Excursion (dry or wet) Beryllium release	Anti-criticality destruct system Exclusion zone
	Vehicle failure during tilt program	Excursion in shallow water	Anti-criticality destruct system Marine exclusion zone
Nuclear Stage Operation and Post-Mission Disposition	RIFT BALLISTIC MISSIONS Nuclear stage failure (or successful mission)	Impact in deep water (minor problem)	Engine destruct system (if necessary)
	OPERATIONAL MISSIONS Velocity decrements due to thrust cut-offs or guidance failures	Random reentry of radioactive core (prompt or delayed)	Engine destruct system Propulsion-guidance interlocks Retro-systems

TABLE III - NUCLEAR ROCKET SAFETY PROGRAMS

PART A - COUNTERMEASURE DEVELOPMENT

TASK	PROGRAM TYPE	SUBTASKS	CONTRACTORS	TASK OBJECTIVES
ANTICRITICALITY DESTRUCT	R&D, THEORETICAL, EXPERIMENTAL, ENGINEERING	1. SYSTEM DESIGN 2. FEASIBILITY TEST 3. QUALIFICATION AND PROOF TEST	AEROJET (AGC) AGC AGC	TO PROVIDE ANTICRITICALITY SYSTEM TO RENDER REACTOR PERMANENTLY SUBCRITICAL FOR ALL POSSIBLE CHEMICAL BOOSTER FAILURES.
ENGINE DESTRUCT (ORDNANCE)	R&D, THEORETICAL, EXPERIMENTAL, ENGINEERING	1. SYSTEM DESIGN 2. EXPLOSIVES EFFECTIVENESS 3. ORDNANCE DELIVERY SYSTEMS 4. RADIATION SUSCEPTIBILITY 5. ENVIRONMENTAL SUSCEPTIBILITY	AGC LASL, AGC ABERDEEN PROVING GROUND, AGC PICATINNY ARSENAL, WESTING - HOUSE (WANL), AGC AGC, WANL	TO PROVIDE ENGINE DESTRUCT SYSTEM TO EFFECT SAFE DISPOSITION OF ENGINE FOR FAILURES OCCURRING DURING AND AFTER NUCLEAR STAGE OPERATION.
ENGINE DESTRUCT (THERMOCHEMICAL)	RESEARCH, THEORETICAL, EXPERIMENTAL	1. INTERCALATION REACTIONS 2. EFFECTS OF VARIOUS CHEMICAL REAGENTS 3. METALLURGICAL ADDITIVES	LASL LASL, WANL WANL	TO DEVELOP THERMOCHEMICAL DESTRUCT CONCEPT FUNCTIONING WITH AFTERHEAT AND/OR AEROTHERMOCHEMICAL ENVIRONMENTS.
ENGINE DESTRUCT (NUCLEAR)	RESEARCH, THEORETICAL, EXPERIMENTAL	1. DESTRUCTIVE NUCLEAR TRANSIENTS (TREAT) 2. BACK-REACTIONS TO LOWER THRESHOLD 3. FISSION PRODUCT BOIL-OFF	LASL, ANL, WANL LASL, WANL LASL, ANL, WANL	TO DEVELOP NUCLEAR DESTRUCT CONCEPT FUNCTIONING WITH REACTIVITY INSERTIONS WHICH INDUCE DESTRUCTIVE NUCLEAR TRANSIENTS.
INTEGRATION OF ENGINE AND VEHICLE DESTRUCT SYSTEMS	R&D, ENGINEERING	1. INTEGRATION OF ENGINE AND STAGE DESTRUCT SYSTEMS 2. INTEGRATION OF STAGE AND VEHICLE DESTRUCT SYSTEMS	MSFC, LOCKHEED (LASC) MSFC, LOC, LASC	TO INTEGRATE ENGINE AND VEHICLE DESTRUCT SYSTEMS AND RANGE SAFETY EQUIPMENT.
IN-FLIGHT TEST OF ENGINE DESTRUCT SYSTEM	PROOF TESTING	1. ANALYSIS OF FATE OF ENGINE DEBRIS 2. PROOF TEST ON RLFT	MSFC, LOC, LASC MSFC, LOC, LASC	TO PROOF TEST POST-OPERATIONAL ENGINE DESTRUCT SYSTEM ON RLFT TO QUALIFY IT FOR USE IN OPERATIONAL NUCLEAR SPACECRAFT.
REACTOR POISONS	R&D, THEORETICAL, ENGINEERING	1. SHIPPING POISONS 2. GROUND HANDLING POISONS 3. CONTROL DRUM LOCKS	WANL, LASL WANL WANL	TO PROVIDE POISON SYSTEMS FOR REACTOR FOR SHIPPING AND GROUND HANDLING OPERATIONS.
REACTOR SHIPPING CONTAINER	R&D, THEORETICAL, EXPERIMENTAL, ENGINEERING	1. CONTAINER DESIGN 2. CONTAINER TESTING	WANL WANL	TO PROVIDE SHIPPING CONTAINER TO WITHSTAND CREDIBLE SHIPPING ACCIDENTS.
CONTROLLED REENTRY	RESEARCH, THEORETICAL	1. RETRO SYSTEMS FOR INDUCING ORBITAL DEPARTURE 2. RETRO SYSTEMS FOR INDUCING DOWNRANGE IMPACT DURING LATE ABORTS 3. SURVEY OF MARINE DISPOSAL AREAS	MSFC, LEWIS LAB, LASC MSFC, LEWIS LAB, LASC ABC (ADNS)	TO DEVELOP A SYSTEM FOR DISPOSING OF SPENT NUCLEAR ROCKET ENGINES IN DEEP MARINE ENVIRONMENT.

#1

TABLE III - NUCLEAR ROCKET SAFETY PROGRAMS

PART B - SAFETY ANALYSIS

TASK	PROGRAM TYPE	SUBTASKS	CONTRACTORS	TASK OBJECTIVES
DEFINITION OF NUCLEAR TRANSIENTS	ANALYTICAL, THEORETICAL, EXPERIMENTAL	1. THEORETICAL STUDIES OF TRANSIENTS 2. CRITICAL MASS MEASUREMENTS 3. TREAT TESTS 4. SCALE TESTS OF WATER-FUEL SYSTEMS 5. NON-DESTRUCTIVE TRANSIENT TESTS 6. WATER FLOODING TEST	LASL, WANL LASL LASL, ANL, WANL LASL LASL LASL	TO DEFINE EFFECT OF VARIOUS REACTIVITY INSERTIONS, MAGNITUDE OF ENERGY RELEASE, FORM OF EFFLUENT MATERIALS, AND DISPERSION PATTERN.
AEROTHERMODYNAMIC AND AEROTHERMOCHEMICAL BEHAVIOR OF ENGINE	ANALYTICAL, THEORETICAL, EXPERIMENTAL	1. PRELIMINARY STUDIES ON FUEL 2. PRELIMINARY EXPERIMENTS IN PLASMA ARC 3. TRAJECTORY ANALYSIS 4. HEATING, ABLATION ANALYSIS OF ENGINE 5. FEASIBILITY STUDY OF REENTRY EXPERIMENTS 6. REENTRY EXPERIMENTS	MARTIN, WANL WANL-PLASMADYNE MSFC, LMSC	TO DETERMINE REENTRY EFFECTS ON ENGINE (OR ITS DEBRIS) FOR SPECTRUM OF REENTRY CONDITIONS FOR BOTH ABORTS AND SUCCESSFUL MISSIONS.
RESPONSE OF ENGINE TO SATURN PROPELLANT EXPLOSION AND FIRE	ANALYTICAL, THEORETICAL, EXPERIMENTAL	1. NATURE OF PROPELLANT ENERGY RELEASE 2. EFFECTS OF THERMAL AND KINETIC ENERGY ON ENGINE 3. RELEASE OF BERYLLIUM 4. BERYLLIUM-CARBON REACTIONS	A. D. LITTLE (ADL), APG ADL ADL, WANL	TO DETERMINE EFFECTS OF PROPELLANT ENERGY RELEASES ON ENGINE. TO ESTIMATE AMOUNT OF BERYLLIUM RELEASED AS AEROSOLS DURING LAUNCH PAD ABORT.
SOURCE TERM AND RADIONUCLIDE INVENTORY OF ENGINE	ANALYTICAL, THEORETICAL, EXPERIMENTAL	1. FISSION PRODUCT INVENTORY HISTORY 2. ACTIVATION PRODUCT INVENTORY HISTORY 3. FISSION PRODUCT LOSS FROM FUEL UNDER VARIOUS TEMPERATURE CYCLES 4. SOURCE TERM FOR REACTOR DEBRIS	WANL WANL WANL, LASL WANL	TO DEFINE SOURCE TERM HISTORY. TO DEFINE LOSS OF FISSION PRODUCTS UNDER VARIOUS TEMPERATURE CYCLES. (E.G., POWERED OPERATIONS, AFTERHEAT, ETC.)
EFFECTS OF IMPACT ON ENGINE	ANALYTICAL, THEORETICAL, EXPERIMENTAL	1. WATER RISE IN CORE 2. EFFECTS OF IMPULSIVE LOADS ON ENGINE	WANL WANL WANL	TO DEFINE CONDITION OF ENGINE AFTER IMPACT.
START-UP MODE	ANALYTICAL, THEORETICAL	1. STUDY OF GROUND START-UP SAFETY 2. STUDY OF IN-FLIGHT START-UP SAFETY 3. VEHICLE STAGING CONSIDERATIONS	WANL WANL LMSC	TO DEFINE SAFEST MODE OF START-UP COMPATIBLE WITH MISSION OBJECTIVES.
SAFETY ANALYSIS OF FLIGHT OPERATIONS	ANALYTICAL, THEORETICAL	1. VEHICLE FAILURE MODES 2. RANGE SAFETY 3. IMPACT POINTS 4. ORBITAL MECHANICS	MSFC, LMSC LOC, MSFC, LMSC MSFC, LMSC MSFC, LMSC	TO DEFINE FLIGHT MECHANICS FOR BOTH SUCCESSFUL AND ABORTED MISSIONS.
SAFETY ANALYSIS OF GROUND OPERATIONS	ANALYTICAL, THEORETICAL	1. FACILITY SAFETY PLANNING 2. GROUND HANDLING SAFETY 3. EMERGENCY PROCEDURES	LOC LOC LOC	TO PROVIDE SAFETY INPUT TO FACILITY PLANNING, GROUND HANDLING, AND POST-ACCIDENT PROCEDURES.
GENERAL OPERATIONAL SAFETY ANALYSIS	ANALYTICAL	1. ISOLATION OF SAFETY PROBLEMS 2. SAFETY PROGRAM MONITORING 3. SAFETY PROGRAM REVIEW	LASL, MARTIN, SNPO SNPO WITH MSFC, LOC	TO ASSURE THAT ALL SAFETY PROBLEMS ARE COVERED

TABLE III - NUCLEAR ROCKET SAFETY PROGRAMS

PART C - ENVIRONMENTAL SAFETY

TASK	PROGRAM TYPE	SUBTASKS	CONTRACTORS	TASK OBJECTIVES
1. METEOROLOGICAL PROGRAM METEOROLOGY OF AMR	ANALYTICAL, THEORETICAL, EXPERIMENTAL	1. COLLECTION OF CAPE CANAVERAL METEOROLOGICAL DATA 2. EXAMINATION OF SEA BREEZE DATA 3. UPPER ATMOSPHERE DATA 4. DOWN RANGE DATA	NUS, USWB, USAF USWB MSFC USWB	TO COLLECT AND INDEX METEOROLOGICAL DATA, DETERMINE ADEQUACY OF THESE DATA, AND COMPILE NEW DATA WHEN NECESSARY.
IN SITU METEOROLOGICAL EXPERIMENTS	ANALYTICAL, THEORETICAL, & EXPERIMENTAL	1. DIFFUSION EXPERIMENTS 2. CLOUD RISE EXPERIMENTS 3. EVALUATION OF EXISTING METEOROLOGICAL NETWORK 4. EXTENSION OF PRESENT NETWORK	USWB, MSFC, LOC USWB, MSFC, LOC USWB, MSFC, LOC USWB, MSFC, LOC	TO DETERMINE DIFFUSION AND ADVECTION OF EFFLUENTS FROM SATURN PROPELLANT FIRMS AND EXPAND METEOROLOGICAL NETWORK.
RESULTANT BIOLOGICAL DOSES FROM RELEASES OF TOXIC AND RADIOACTIVE MATERIALS	ANALYTICAL, THEORETICAL	1. DOSES FROM FISSION PRODUCTS (ABORT) 2. DOSES FROM BERYLLIUM (ABORT) 3. KIWI MEASUREMENTS AT MTS	NUS, USWB NUS, USWB LASL, USWB	TO DETERMINE ON- AND OFF-SITE DOSES FROM LAUNCH PAD ABORTS..
FALLOUT FROM ENGINE EFFLUENTS AND POST - OPERATIONAL DESTRUCT	ANALYTICAL, THEORETICAL	1. ENGINE EFFLUENTS FROM POWERED FLIGHT 2. REACTOR DEBRIS FROM POST- OPERATIONAL DESTRUCT	USWB USWB	TO DETERMINE GROUND CONCENTRATIONS OF RADIOACTIVE MATERIALS RELEASED AT HIGH ALTITUDES.
BIOLOGICAL HAZARD FROM ENGINE DEBRIS	ANALYTICAL, THEORETICAL	1. RADIOLOGICAL SIGNIFICANCE OF FUEL DEBRIS SURVIVING REENTRY	ORNL	TO RECOMMEND DESTRUCT SYSTEM CRITERIA.
2. OCEANOGRAPHIC PROGRAM MARINE LEACHING OF FUEL ELEMENTS AND ENGINE MATERIALS	ANALYTICAL, THEORETICAL, EXPERIMENTAL	1. LEACHING OF FISSION PRODUCTS DURING EXCURSIONS 2. QUIESCENT LEACHING OF FISSION PRODUCTS 3. LEACHING OF ACTIVATION PRODUCTS	LASL, AML, WANL LASL, NRD NRDL	TO DEFINE RELEASE OF RADIONUCLIDES IN MARINE ENVIRONMENT.
MARINE DIFFUSION AND ADVECTION	ANALYTICAL, THEORETICAL, EXPERIMENTAL	1. RIVERS 2. SHALLOW OCEAN 3. DEEP OCEAN	WHOI-CBI WHOI-CBI WHOI-CBI	TO DEFINE TRANSPORT OF CONTAMINANTS RELEASED AT AMR BY ABORTS.
CENSUS OF AMR BIOTA	FIELD SAMPLING	1. COMMERCIAL SPECIES 2. SPORTS SPECIES	USFWS USFWS	TO DEFINE BIOLOGICALLY SIGNIFICANT SPECIES IN FOOD-CHAIN.
BIOLOGICAL UPTAKE OF RADIONUCLIDES	ANALYTICAL, THEORETICAL, EXPERIMENTAL	1. STABLE ELEMENT ANALYSIS 2. SPECIFIC ACTIVITY ESTIMATES 3. UPTAKE EXPERIMENTS	MIT MIT USFWS	TO PREDICT UPTAKE GIVEN SOURCE AND RELEASE TERMS.
EMERGENCY PROCEDURES	ANALYTICAL, THEORETICAL, EXPERIMENTAL	1. POST-ACCIDENT MONITORING 2. ISOTOPIC DILUTION 3. SUBMARINE BURIAL OR ENVELOPMENT 4. EXCLUSION 5. CATCH MONITORING	ADNS ADNS ADNS ADNS USFWS	TO DEVELOP EFFECTIVE EMERGENCY PROCEDURES FOR MARINE IMPACT ACCIDENTS.
3. TERRESTRIAL PROGRAM GEOLOGICAL AND HYDROLOGICAL STUDIES	ANALYTICAL, THEORETICAL	1. GEOLOGICAL SURVEY 2. SURFACE AND SUBSURFACE HYDROLOGY	USGS USGS	TO PREDICT SURFACE AND SUBSURFACE DIFFUSION OF CONTAMINANTS.
ON-SITE BACKGROUND MONITORING	FIELD SAMPLING AND SURVEY	1. SAMPLING OF LAUNCH SITE 2. AIRBORNE RADIOMETRIC SURVEY	PBS DEM, USGS	TO ESTABLISH DATUM BACKGROUND LEVELS ON-SITE.
OFF-SITE BACKGROUND MONITORING	FIELD SAMPLING AND SURVEY	1. SAMPLING OF CAPE CANAVERAL AND ENVIRONS 2. AIRBORNE RADIOMETRIC SURVEY	PBS, STATE OF FLORIDA DEM, USGS	TO ESTABLISH DATUM BACKGROUND LEVELS OFF-SITE.
4. GENERAL ENVIRONMENTAL PROGRAM				
OVERALL EMERGENCY PROCEDURES	ANALYTICAL, THEORETICAL	1. EMERGENCY PROCEDURES FOR ABORTS 2. DECONTAMINATION PROCEDURES	LOC, ADNS ADNS	TO ESTABLISH EMERGENCY AND DECONTAMINATION PROCEDURES.
SITE SURVEY	ANALYTICAL, THEORETICAL	1. COLLECTION OF ENVIRONMENTAL DATA 2. FACILITY SITING	AFSNC LOC	TO ESTABLISH SITING CRITERIA.
GENERAL ENVIRONMENTAL	ANALYTICAL, THEORETICAL	1. ORGANIZATION OF ENVIRONMENTAL SAFETY PROGRAM 2. DATA REDUCTION	NUS, SIFO, ADNS NUS, SIFO, ADNS	TO PROVIDE OVERALL ENVIRONMENTAL SAFETY ANALYSIS.

5. SAFETY PROGRAMS - The safety program for the nuclear rocket shown in Table III consists of the following three parts: (A) Countermeasure Development, (B) Safety Analysis, and (C) Environmental Safety. This three-fold approach follows the philosophy of developing adequate countermeasures (safety engineering), continually refining the many safety analyses, and determining the effects of nuclear rocket flight operations on the environment for purposes of facility siting, operational planning, and establishing emergency procedures. A fourth program, often overlooked as routine, provides the important operational safety support of Kiwi reactor and NERVA engine development program activities such as critical testing, reactor transport, propellant handling, and reactor and engine testing in Nevada.

The countermeasure development program shown in Table III, Part A, is directed specifically at the major potential safety problems posed by transport and ground handling accidents, launch pad aborts, shallow water impact, and the post-mission disposition of the engine. The countermeasure tasks constitute the nucleus of the overall safety program and, without exception, are devoted to the prevention of potential nuclear or radiation incidents, assuming a variety of independent yet credible non-nuclear causal failures (e.g., rocket vehicle aborts, carrier accidents, human error).

The safety analysis program shown in Table III, Part B, defines the various safety problems by analyzing the safety neutronics of the system, the radiation source term, the response of the system to various physical forces, and spatial and temporal factors characteristic of its operational mode. This is envisioned as a continuous program with constant refinement.

The environmental safety program, shown in Table III, Part C, is four-fold including meteorological, oceanographic, and terrestrial sub-programs and a general sub-program to correlate the many diverse environmental tasks. This is a cooperative program between the USAF, AEC, and NASA with active support from a large number of specialized environmental organizations.

CONCLUSION

The analytical model, safety problems, and safety programs for the nuclear rocket have been presented in a macroscopic fashion in order to correlate and summarize the program. Closer examination of the work being done by the Los Alamos Scientific Laboratory, the Nuclear Vehicle Projects Office, the NASA Launch Operations Center, the Space Nuclear Propulsion Office, and their various contractors will reveal the depth of the safety program.

REFERENCES

1. Graves, G. A., Harris, P. S., Langham, W. H., Nuclear Safety Aspects of the Rover Program, LASL-2409, March, 1960.
2. C. Boehmer, C. Riggs, J. Watcher, R. Weiner, G. Dix, Final Report - Nuclear Rocket Safety Study, MND-2517, August 9, 1961.
3. LASL, Primary Radiological Safety Guide and Hazards Evaluation for Kiwi-B Reactors, LAMS,2710, June, 1962.
4. Stratton, W. R., Some Comments Apropos the Rover Water Hazard Problem, January, 1962. (Unpublished)
5. Boltax, A., Personal Communication, August 3, 1962.
6. Arthur D. Little, Inc., Effects of Liquid Rocket Propellant Explosions on Nuclear Rocket Engines, March 14, 1962.
7. Callaway, R. C. and Sullivan, E. L., Preliminary Trajectories for RIFT, MSFC, March 26, 1962.
8. Jordan, W. Y., et al, Mating Nuclear Propulsion with Saturn for the Lunar Mission, MSFC, March 22, 1962.
9. King, L. D. P., Personal Communication, April 27, 1962.

FISSION PRODUCT INVENTORY (NO LEAKAGE)

Figure 1 BALLISTIC NUCLEAR ROCKET MISSION

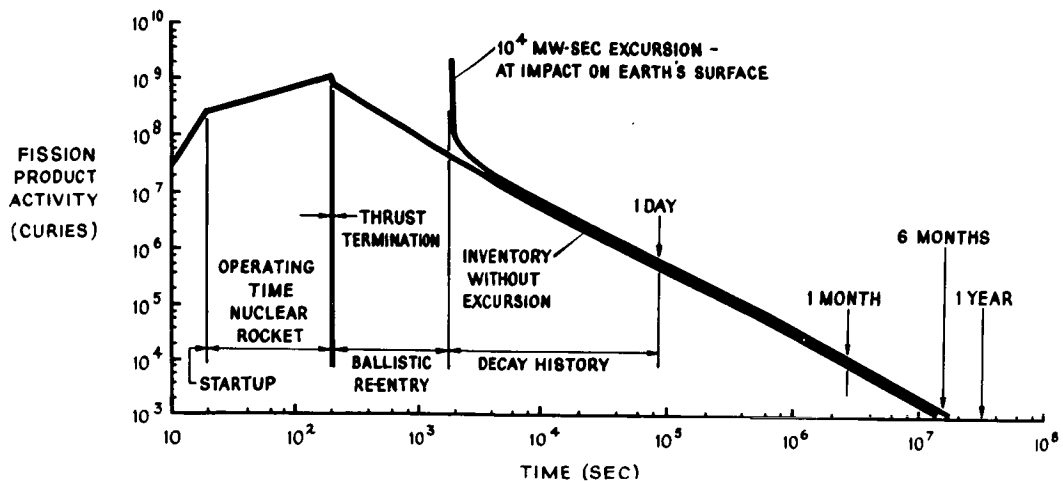
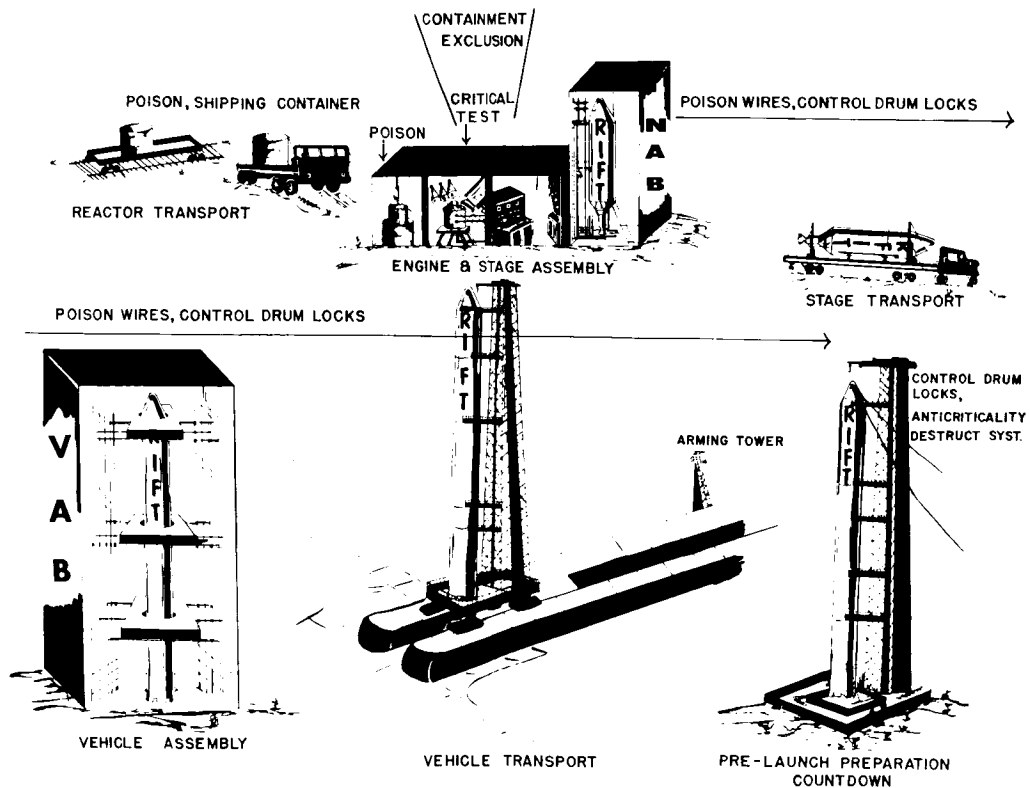


FIGURE-2 GROUND HANDLING CHRONOLOGY



FLIGHT OPERATION

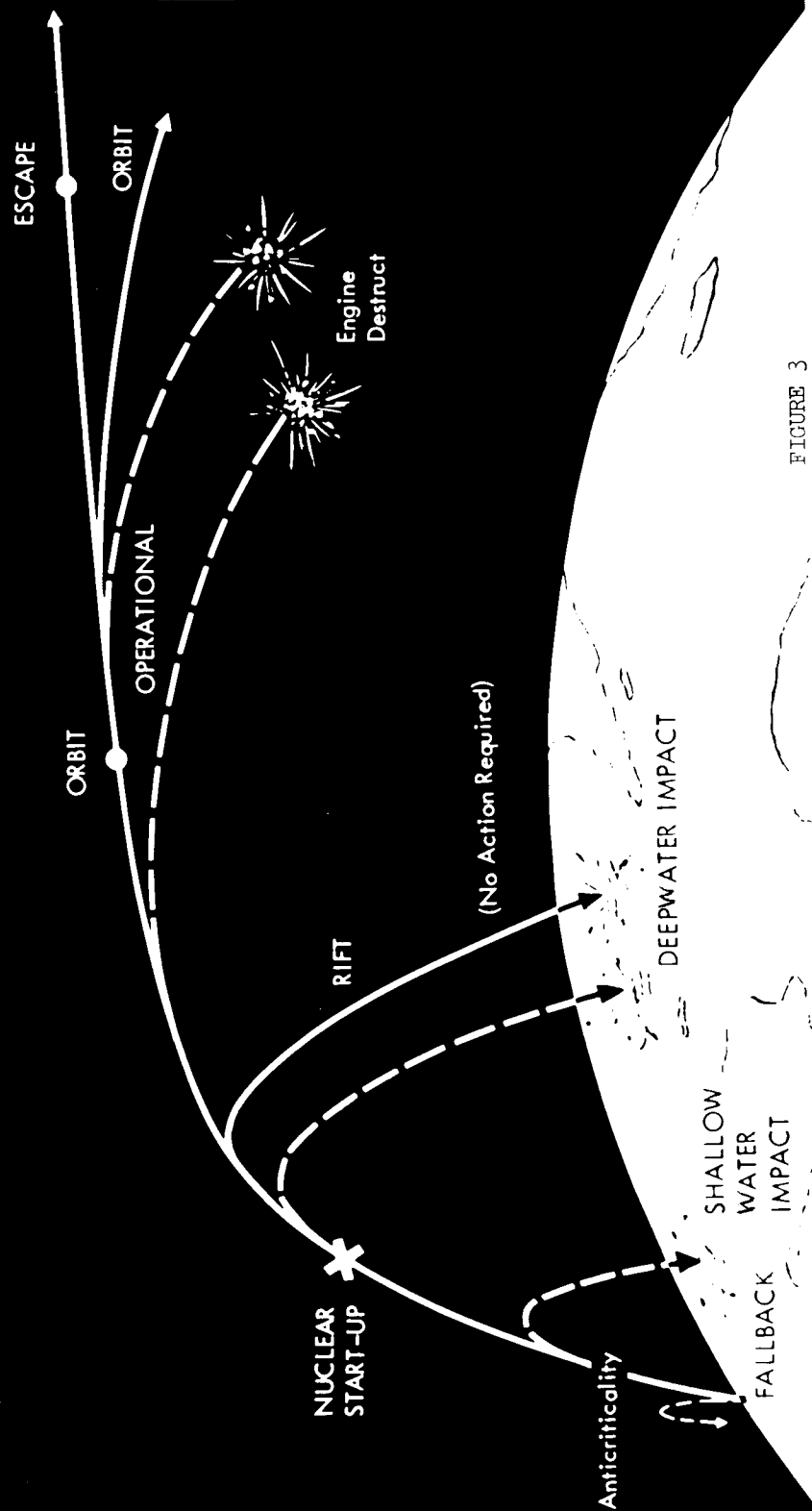


FIGURE 3

X 66 50300

NUCLEAR SAFETY AND HAZARDS
ASPECTS OF RIFT FLIGHT OPERATIONS

[U]

by

James Malcolm Rives*

ABSTRACT

50300

The nuclear safety and hazards considerations for RIFT static test operations at the Nuclear Rocket Development Station in Nevada, and RIFT flight tests at the Atlantic Missile Range, Cape Canaveral, Florida, are discussed in general terms. The RIFT vehicle system and facilities are briefly described with particular emphasis on the safety aspects. Since the RIFT Program has as one of its main objectives to demonstrate safe operation of the RIFT vehicle, the safety features and mechanisms incorporated into the system design and operation will be thoroughly evaluated. Safety analysis will be conducted to determine all conceivable hazards for all RIFT operations. An ambitious safety program is already underway by the KIWI, NERVA and RIFT Organizations. With safety successfully demonstrated in the RIFT Flight Program, a major preparatory step toward an operational nuclear vehicle for space flight missions would be achieved.

Conf. R.D.

Author

*Nuclear Vehicle Projects Office
George C. Marshall Space Flight Center
Huntsville, Alabama

I. Introduction

The RIFT (Reactor-In-Flight-Test) Project is one of the major projects now underway in the Nuclear Rocket Program. The basic objective of the RIFT Project is to advance the technologies necessary for development of an operational Nuclear Vehicle System for space flight missions. The other major projects are the Los Alamos Scientific Laboratory KIWI Reactor Development and NERVA Engine development by Aerojet General Corporation. The NERVA Engine will incorporate a KIWI type reactor. The RIFT Project will develop a complete vehicle stage by captive tests and flight operation using C-5 boosters. The RIFT research and design effort is with Lockheed Missiles and Space Company.

Design and development of the RIFT Nuclear Vehicle System will present problems that are typical and comparable to the problems experienced with chemical vehicles, except for the nuclear radiation environment and nuclear hazards which present new problems for resolution. With nuclear propulsion as a very desirable means of propelling upper stages of launch vehicles, much consideration will be given to the nuclear safety aspects of the RIFT Program from both technical requirements and public interest viewpoints. The purpose of the RIFT Nuclear Safety Program is to insure maximum human safety against all possible radiological and toxicity injury during the static and flight test operations of nuclear stages and vehicle systems. Emphasis is placed on nuclear safety by implementing an active safety program early in the design phase. The RIFT Program is designed to demonstrate nuclear safety in the static tests and particularly during flight test of the RIFT vehicle.

A ROVER Flight Safety Panel was organized in mid-1961 by the Space Nuclear Propulsion Office and is made up of members of the Space Nuclear Propulsion Office, Atomic Energy Commission - Assistant Director for Nuclear Safety, Los Alamos Scientific Laboratory, Lewis Research Center, Launch Operations Center, Atlantic Missile Range, and Marshall Space Flight Center, with participating contractors; Lockheed Missiles and Space Company, Aerojet General Corporation, and its subcontractor, Westinghouse Astronuclear Laboratory. The functions of this Panel are to identify hazards and determine means of countermeasures. Safety is defined such that it consists of two major parts, i.e. accident analysis and hazards analysis. The accident analysis involves analyzing potential accidents resulting from failure modes with consideration given to the conditions pertaining to each particular event in time and location. Hazards analysis involves defining the fission product release and toxic source terms as may result from an accident, tracing the transport of this material through the environments, and determining the results or consequences to man.

A Nuclear Safety and Hazards Working Group was established in mid-1962 by the Marshall Space Flight Center with membership from the various MSFC Divisions and Offices, Launch Operations Center, and Lockheed Missiles and Space Company. The objectives of this Group are to review and recommend safety features and techniques for vehicle system design, test operations, procedures and to integrate the safety aspects of the RIFT Program including these activities at the Nuclear Rocket Development Station (NRDS), Nevada, and the Atlantic Missile Range (AMR), Cape Canaveral, Florida.

II. RIFT Nuclear Vehicle Description

The RIFT nuclear vehicle configuration incorporates the S-1C booster stage, S-II dummy second stage, RIFT third stage, the instrument unit, and a nose fairing compartment which contains the payload components. Shown in Figure 1 is a comparison of the RIFT vehicle with a nuclear escape vehicle. For the RIFT vehicle, the S-1C booster stage is approximately 140 feet in length and incorporates five F-1 engines which utilize LOX and RP-1 as propellant producing 7.5 million pounds thrust. The propellant capacity of this stage is 4.5 million pounds of LOX and RP-1. The S-II stage is approximately 80 feet in length and will be used as a dummy stage for the RIFT flight tests; however, it would be a live stage for the nuclear escape vehicle. The RIFT stage incorporating the NERVA Engine has a length of 137 feet including the nose fairing section. The nuclear engine utilizes LH_2 as propellant and produces approximately 56 thousand pounds thrust with a burning time of about 20 minutes in a RIFT flight test. The propellant capacity of the RIFT Stage is approximately 156 thousand pounds of LH_2 . The total RIFT vehicle is 357 feet in length with the NERVA Engine located approximately 240 feet from the vehicle base. Shown in Figure 2 is an outline of the RIFT Stage with the NERVA Engine mated to the propellant tank.

Design of safety into the RIFT vehicle system and facilities will be accomplished to the maximum extent possible. In order for the RIFT Safety Program to be effective, recommended safety criteria will be implemented into design. Typical areas and activities where safety criteria is required for design are the following: (1) vehicle system designs, (2) NRDS facility designs, (3) AMR facility designs, (4) operating procedures, etc. RIFT design efforts are geared to incorporate the most advantageous safety techniques and mechanisms for total system safety. Typical safety features under consideration include: (1) pre-static test and prelaunch radiation monitoring systems, (2) radiation shielding, (3) reactor poison safety wires, (4) engine destruct system, (5) stage and vehicle destruct system, (6) nuclear safing and arming system, (7) emergency detection system, (8) reactivity checks, (9) checkout emergency procedures, etc. From the standpoint of design, other project inputs to the RIFT Safety Program is by reliability efforts on failure mode analysis and failure effect analysis, qualification testing in anticipated operating environments, and human engineering factors for reducing possible human errors. Shown in Figure 3 is an indication of the nuclear environmental problems imposed on the RIFT system affecting safety and reliability of operation during static and flight tests.

III. Ground Operations

The RIFT static tests will be conducted at the Nuclear Rocket Development Station, shown in Figure 4, to confirm the stage design and operation. These tests will begin in late 1965 with present plans for testing approximately five RIFT stages. Facilities for these tests will require safety criteria in design and operation in the following typical areas: (1) facility isolation, orientation and separation, (2) exhaust effluent and contamination control, (3) procedural and personnel control, etc. Shown in Figure 5 is the RIFT captive test stand concept to be utilized at NRDS. The stage would be positioned by lowering and assembling it to the firing silo during test runs and transported by means of a prime mover. The RIFT safety effort at NRDS will benefit from the previous

KIWI and NERVA tests; however, accident and hazards analysis peculiar only to RIFT stage operations will be necessary due to differences in design and operations. Accidents causing nuclear hazards could occur during the many test activities as: stage/engine mating, handling, transport, test and checkout, fueling, etc. Hazards from a normal static test firing include direct radiation, fission product releases, activation, etc., resulting in ground, air, stage, and facility contamination. More severe hazardous situations could result from abnormal events during the stage test operations. Initiation of accidents could be through various failure or malfunction modes of the system causing hazards of varying degrees. Hazards involved could affect personnel by direct exposure, inhalation, consumption, etc. A safety monitoring and control system, personnel exclusion requirements and procedures, and physical separation of nuclear activities from non-nuclear activities are safety considerations which assist in reducing possible injury to operating personnel. All nuclear testing at NRDS is remote from offsite populated areas and in addition, the test stand positions are located with due consideration given to the atmospheric environmental factors, site analysis, etc.

RIFT stages designated for flight tests will be transported to the Launch Operations Center by combination of land and water. Figure 6 shows the launch site area at Cape Canaveral indicating the general location of the C-5 Complex. The engine and reactor components would be shipped separately to the Launch Operations Center where they would be assembled and checked out in an engine configuration in the Engine Assembly Building. The engine then would be mated with the stage and checked out in the Stage Assembly and Checkout area. The RIFT stage would then be transferred to a Vertical Assembly Building for mating with the S-IC booster, S-II stage, instrument unit, etc., and overall system checkout. Shown in Figure 7 is an artist's concept of the launch platform and the launch umbilical tower for launching the C-5 vehicle. Nuclear safety during these activities, not only duplicates some of the potential problems at NRDS, but presents more severe problems which require much consideration for resolution. These potential problems are brought about by additional environmental and population factors. Typical of NRDS; however, a safety monitoring and control system, personnel control, radiation shielding, etc., would be necessary at AMR during certain engine, stage and vehicle operations. In addition, appropriate vehicle and pad safety procedures will be necessary during periods of preparation for launch. Ground operations also include problems in the disposal and storage control of radioactive materials. Before a RIFT vehicle is launched, sister stages will have been fully tested at NRDS with safety demonstrated. Also the stages allocated to the Launch Operations Center will have been thoroughly tested (less nuclear), thus eliminating radiation problems during ground operations at AMR. All conceivable classes of accidents at NRDS and AMR will be postulated and analyzed to determine potential hazards and also means of preventing or countering them.

IV. Flight Operations

A series of four RIFT flight tests are scheduled to be conducted at the Atlantic Missile Range beginning approximately 1967. Shown in Figure 8 is a typical RIFT flight trajectory. RIFT trajectory studies include three different test objectives regarding the engine burning periods as follows: (1) one continuous burning period, (2) one restart, and (3) two restarts. Figure 9 presents a plot of certain RIFT vehicle trajectory parameters for the two

restart case. For the three trajectory cases, the maximum altitude varies from 600 to 1200 kilometers. A flight azimuth of approximately 100° E. of N. was assumed with an initial consideration given to range safety. An optimum RIFT flight azimuth as typically shown in Figure 10 would be based on safety of the down range tracking stations, wind directions, and reliability of telemetry transmission and reception. Also considered in the trajectory optimization study for purposes of safety would be the trajectory profile, maximum range, impact location, etc. The flight trajectory analysis assumes that, if the RIFT stage fails to start up after cutoff and separation from the S-IC Booster, or if separation fails to occur, the stage and/or vehicle would impact in the Blake Escarpment area in the Atlantic, approximately 400 kilometers (250 miles) from the launch site. Start up of the nuclear engine would be after the S-IC Booster separation at an altitude of approximately 120 kilometers and at a range of 70 kilometers. Studies have indicated that particles falling from altitudes below 30 kilometers would travel predominately in an easterly direction during the months October through May; therefore, the optimum time of the year for launching nuclear vehicles may be during these months.

The AMR safety officer has the prerogative of destructing the vehicle, as necessary, for range safety; however, the conditions on which a decision would be made must be designed into the systems and incorporated in the procedures. As already mentioned, the flight safety mechanism includes the nuclear safing and arming system and command destruct system, etc. Many classes of accidents and failure situations can be postulated during the boost phase after liftoff from the launch pad and for each time interval during this flight period. Each case, flight period and situation, will require a thorough evaluation with regard to accidents and resulting hazards. The hazards associated here could result from nuclear vehicle, stage and/or engine being submerged in vehicle propellant, propellant fires and explosions, impacts on the beach areas and shallow waters or submerged in sand/water, etc. The final disposition of the RIFT stage after a normal flight would be in deep water of the Atlantic Ocean. A consideration would be to destruct the total nuclear stage just prior to impact. Regardless of the final disposition of the RIFT stage at impact, it may be desirable to maintain surveillance around the impact point for a period of time to obtain samples and collect informational data.

Another aspect of the nuclear flight safety program involves the nuclear escape vehicle and operational missions in which consideration would be given to problems as: random re-entry, orbital destruct, operational destruct system, random impact on earth land masses, etc. Also there would be the safety problems pertaining to space, lunar operations, etc.

V. Safety and Hazards Analysis

The RIFT ground and flight operations present certain safety and hazards problems which require evaluation prior to actual static and flight tests of the RIFT system. Several safety studies have been made by the KIWI, NERVA, and RIFT contractors and other study efforts are underway by other organizations. As the RIFT program progresses, pertinent theoretical and analytical safety studies will be required to define potential accidents and hazards during all RIFT operations at NRDS and AMR. At NRDS, the hazards could be direct radiation from normal operation or direct radiation from excursions with the atmosphere being the principal means of transport. At AMR; however, several

nuclear hazard situations are evident for analysis with sources being a wet or dry excursion, vehicle propellant fire and excursion, land or water impact, etc. The transport media for these could be by anyone or a combination of the following environmental conditions: (1) atmosphere (cloud, fallout, washout, etc.), (2) water (fresh and salt waters), (3) ground, (4) marine, animal, and plant life. The physical transport of the fission product releases, release models, diffusion parameters, and dispersion patterns on the ground and at altitudes along the flight path will require analytical development for environmental safety analysis and evaluations. Hazards analysis determines the consequences to human life as a result of body intake and exposure to radioactive and toxic materials from potential nuclear excursions. Countermeasures for the potential hazards include confinement, shielding, vehicle safety features, permissives, etc.

Prior to flight of the RIFT C-5 nuclear vehicle, appropriate RIFT safety presentations and reviews will be conducted to assure adequate nuclear flight safety and obtain approval for operation.

In conclusion, I wish to state that nuclear propelled vehicles are no more susceptible to operation failure than any other class of vehicles and that with an ambitious safety program, the nuclear safety problems will be resolved prior to operation of the RIFT vehicles.

TYPICAL NUCLEAR VEHICLES

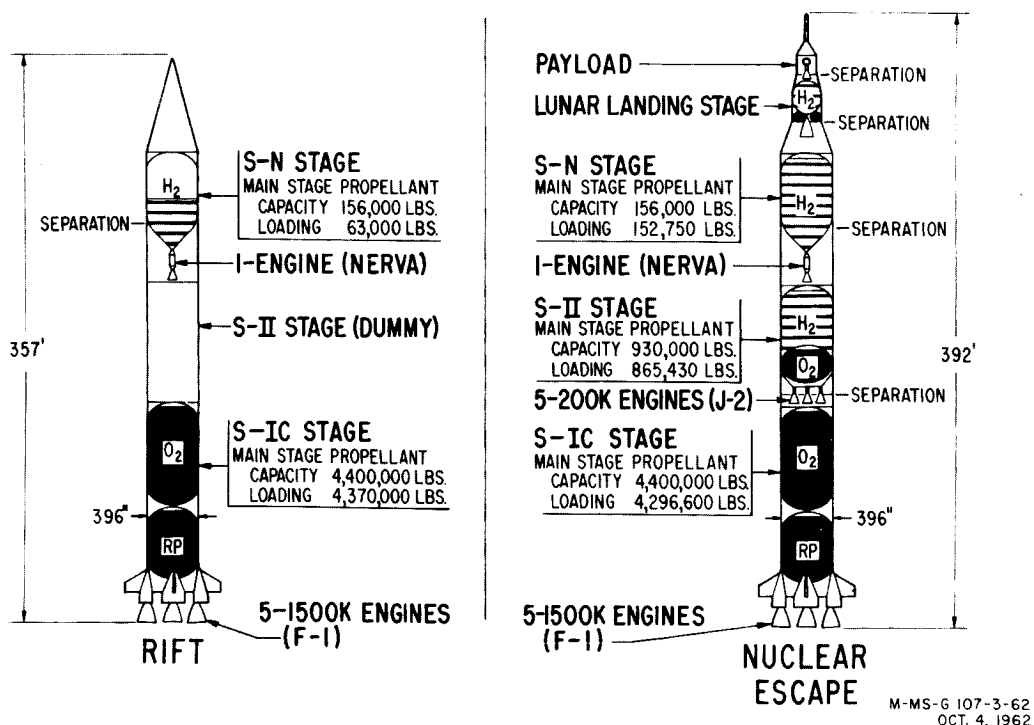
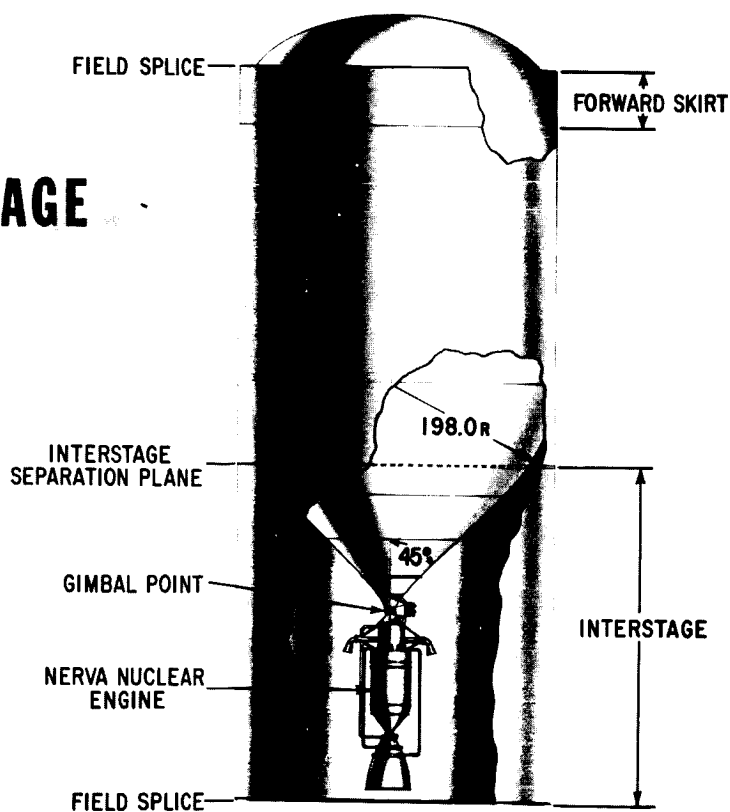


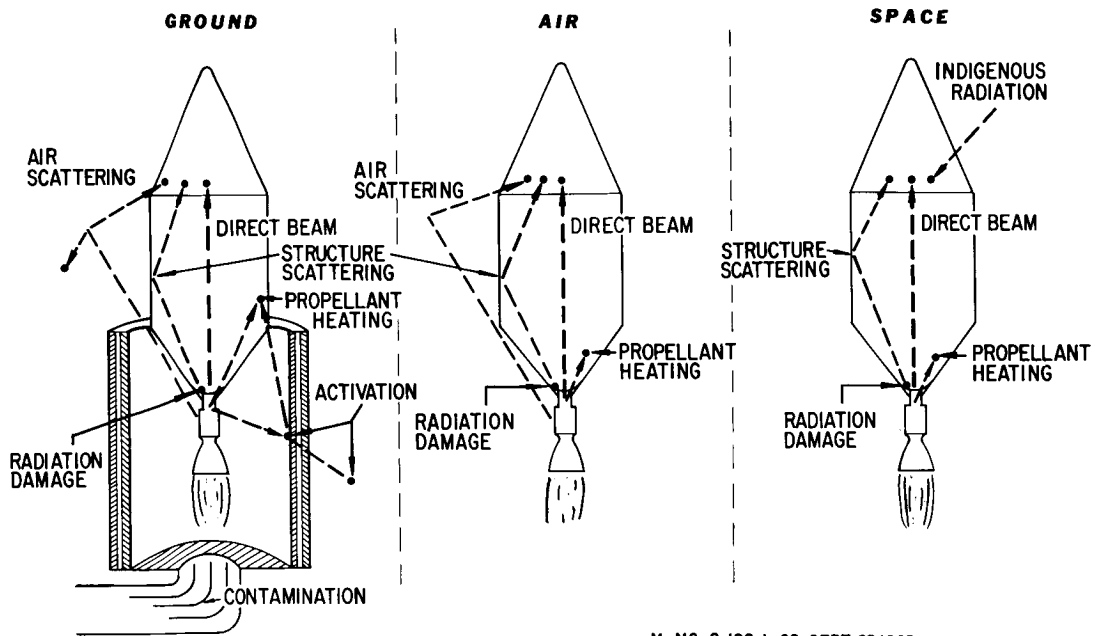
FIGURE 1 - TYPICAL NUCLEAR VEHICLES (Confidential)

S-N STAGE



M-MS-G56-2-62 REV A SEP 13, 1962

FIGURE 2 - S-N STAGE (Unclassified)



M-MS-G 100-I-62 SEPT. 25, 1962

FIGURE 3 - RADIATION CONSIDERATIONS FOR NUCLEAR VEHICLES (Uncl.)

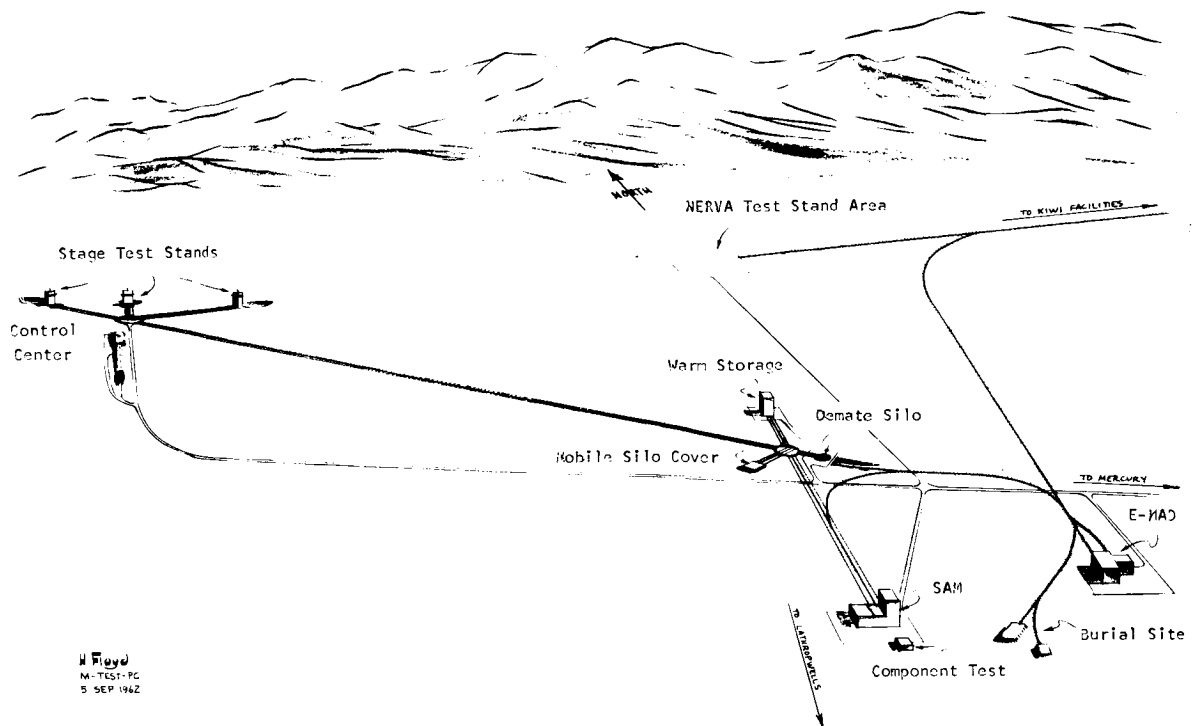


FIGURE 4 - NRDS RIFT STATIC TEST SITE CONCEPTS (Unclassified)

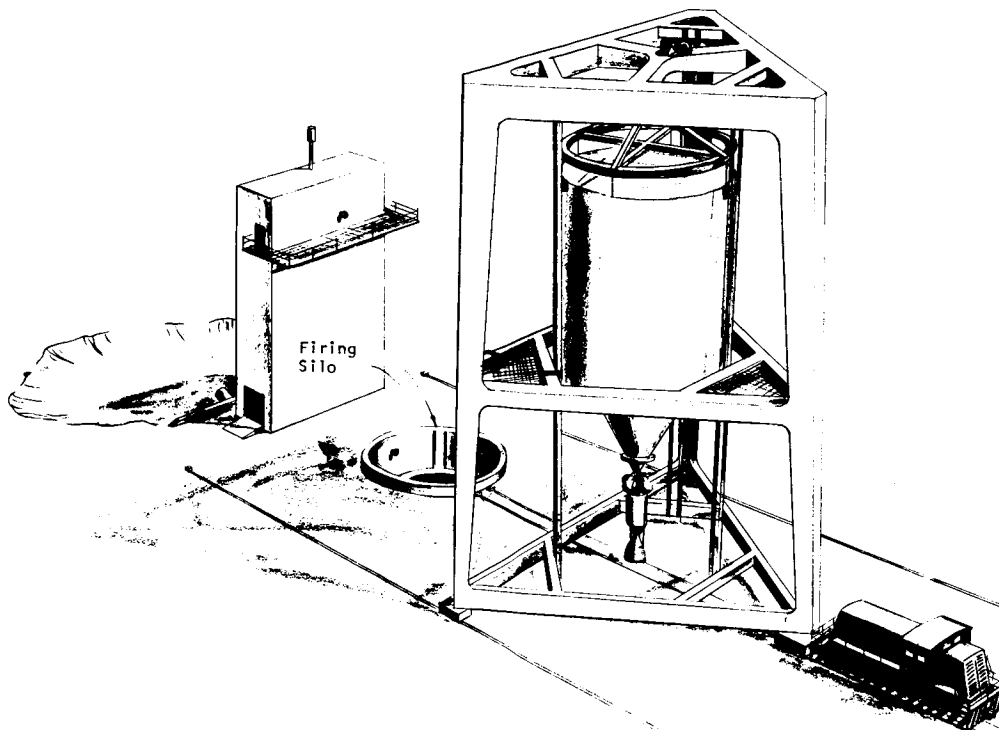


FIGURE 5 - VEHICLE TEST STAND, NRDS, NEVADA (Unclassified)

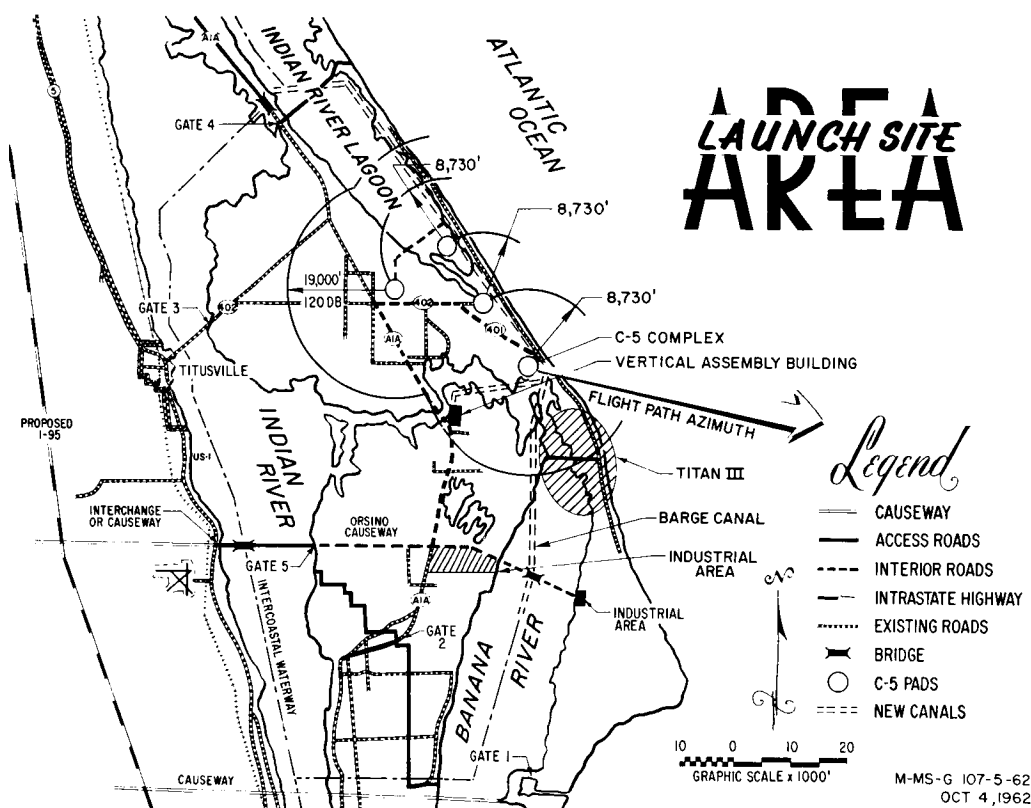
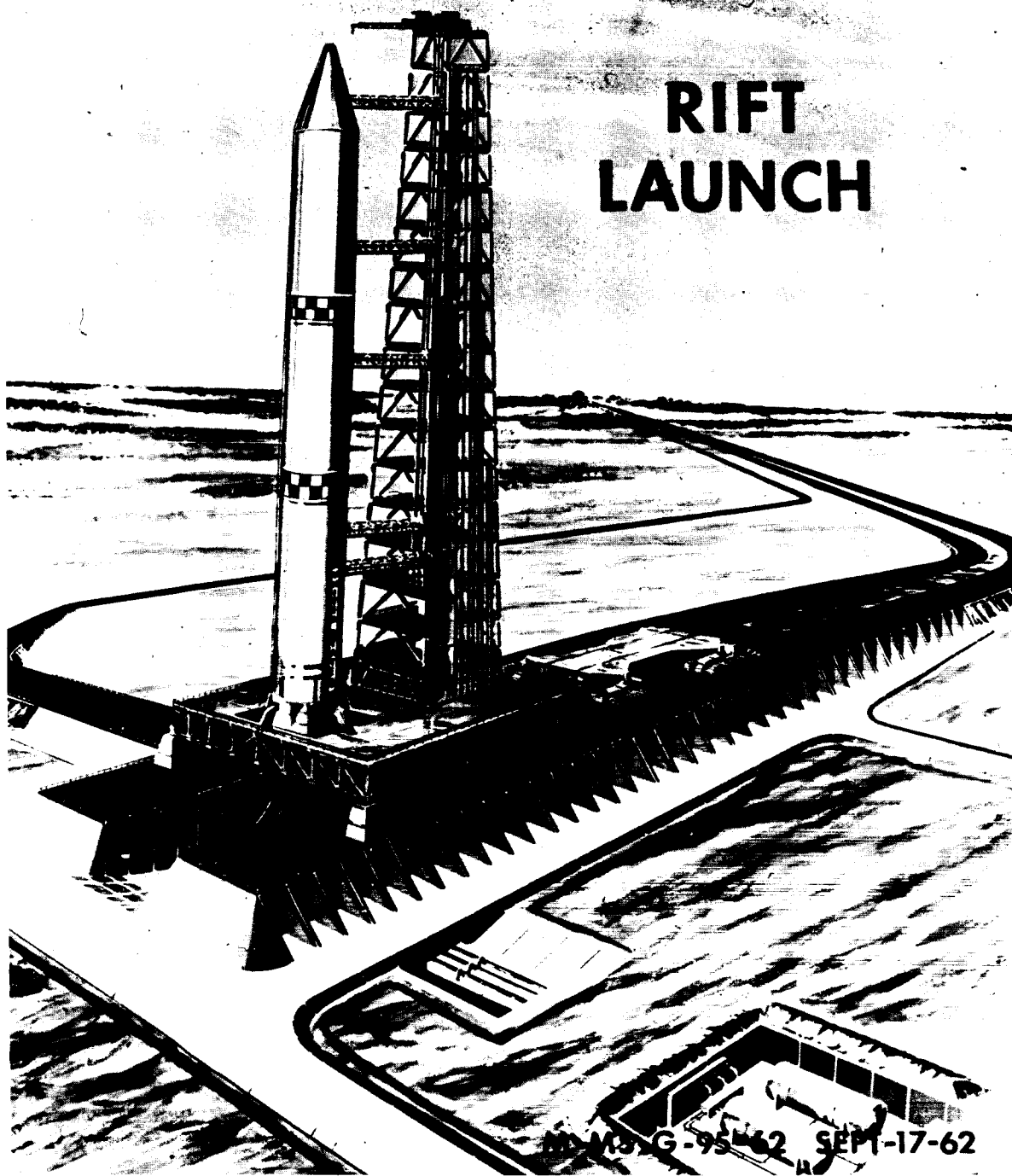


FIGURE 6 - LAUNCH SITE AREA (Unclassified)

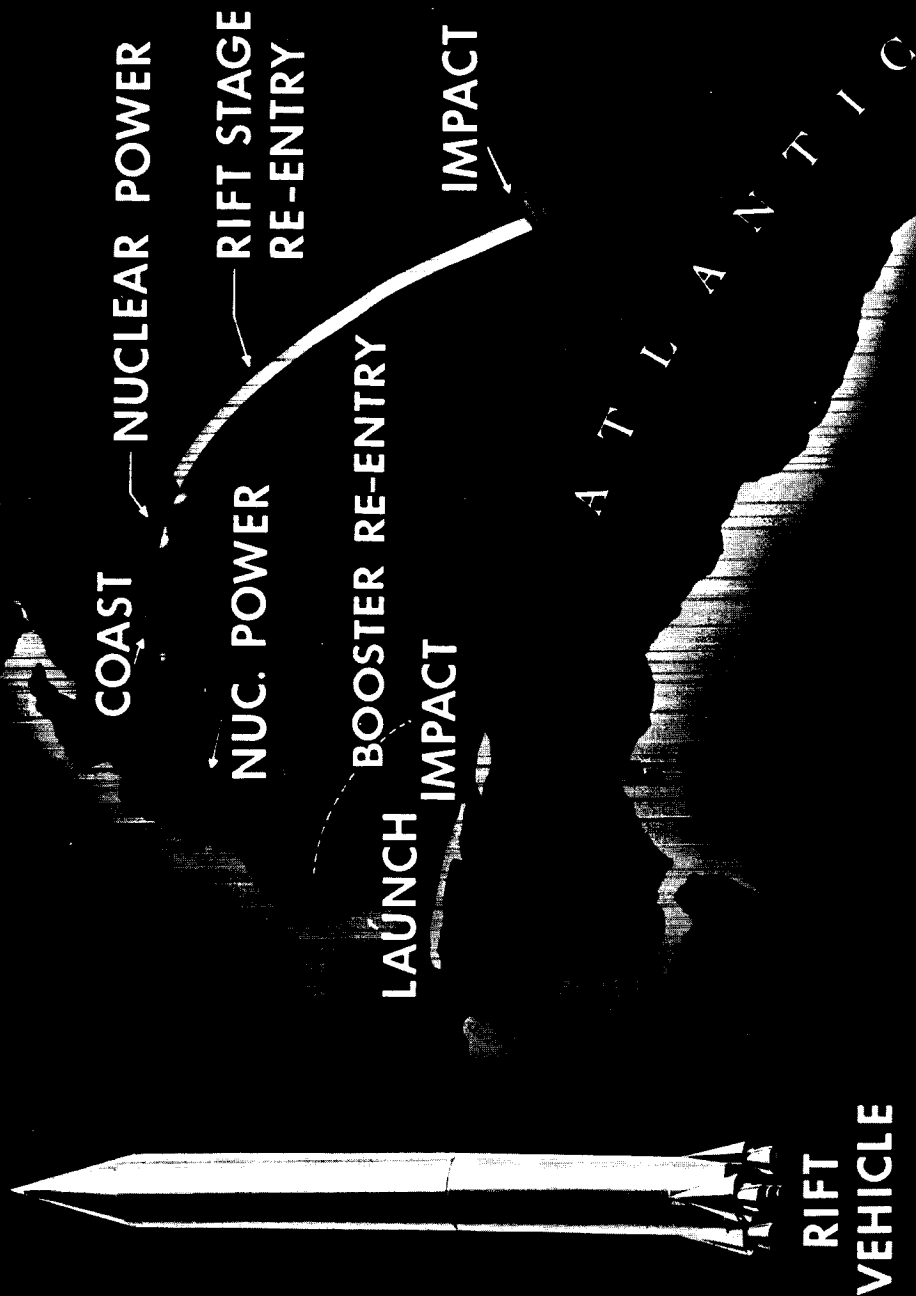
RIFT LAUNCH



NO. 15 G-95-62 SEPT-17-62

FIGURE 7- RIFT LAUNCH (Unclassified)

TYPICAL RIFT FLIGHT TRAJECTORY



RIFT
VEHICLE

M-MS-G 96-62 SEPT 17, 62

FIGURE 8 - TYPICAL RIFT FLIGHT TRAJECTORY (Unclassified)

RIFT VEHICLE TRAJECTORY PARAMETERS FOR THREE BURNING PERIODS OF S-N

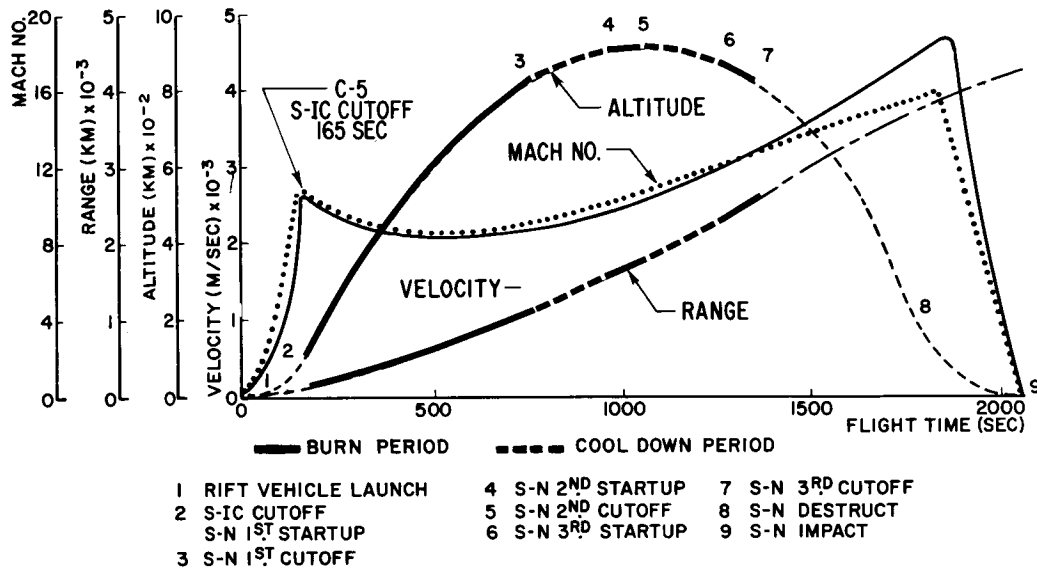


FIGURE 9

M-MS-G 107-2-62 OCT 4, 1962

RIFT VEHICLE TRAJECTORY IN GEOGRAPHIC COORDINATES FOR THREE BURNING PERIODS OF S-N

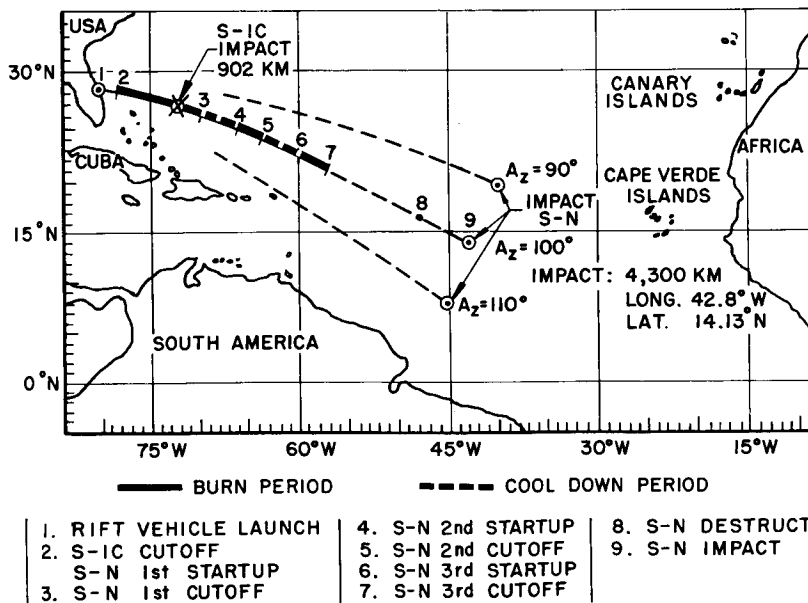


FIGURE 10

M-MS-G-107-4-62 OCT 4, 1962

X 66 50301

TRANSIENT REACTOR EXPERIMENTS ON NERVA FUEL MATERIAL

[U]

A. Boltax*, R. C. Liimatainen**, M. A. Vogel*, R. O. Ivins**, and P. H. Wilks*

Abstract

50301

This paper describes an experimental program to determine the feasibility of using a reactor transient to destroy the core of a nuclear rocket. The technical approach involves transient irradiation of unrestrained sections of NERVA (KIWI B-4 type) fuel elements in the TREAT reactor. Transient irradiation experiments were performed in helium, vacuum, and water environments on fueled graphite made with either UO_2 powder or pyrolytic carbon coated UC_2 particles. The data obtained include nuclear excursion data, fuel temperature, threshold energy values for fuel fragmentation, particle size of fuel fragments, and fission xenon release. The results indicate that fragmentation of the fueled graphite made from UO_2 powder will occur during TREAT excursions of 100 to 770 megawatt-seconds (MWS). The NERVA-equivalent fragmentation values range from 1,000 to 11,000 MWS. Preliminary results obtained on the fueled graphite containing the coated UC_2 particles indicate that it is more resistant to fragmentation than the fuel made with UO_2 powder.

Conf. R.D.

Author

Introduction

Consideration of the safety aspects of conducting orbital missions with a nuclear rocket indicates that one effective way to minimize hazards related to the possibility of an intact reactor falling on land is to physically destroy the reactor while still in flight. Various methods of reactor destruct have been considered. These involve the use of high explosives, thermochemical techniques, and reactor transients. Each of these reactor destruct methods have been examined theoretically and several experimental programs are under way to determine their feasibility. This paper is concerned with an experimental program to determine the feasibility of using a reactor transient to destroy the core of a nuclear rocket. In addition to this primary objective the transient experiments also provide:

- (a) Information on the nature of the shutdown mechanism to form a basis for estimating the maximum credible incident for the NERVA reactor.
- (b) Determination of fission product release during controlled reactor transients.
- (c) A study of reactions between NERVA fuel and water during a reactor transient occurring as a result of an intact reactor falling into water.

* Materials Department of the Westinghouse Astronuclear Laboratory.

**Chemical Engineering Division of the Argonne National Laboratory.

Experimental Technique

The experimental approach involves irradiation of encapsulated sections of the NERVA fuel in the TREAT (Transient Reactor Test Facility) reactor. The TREAT reactor is designed to produce large transient thermal fluxes ($\sim 3 \times 10^{15}$ nvt).⁽¹⁾ With appropriate control rod motion, an integrated power of up to 1000 megawatt-seconds (MWS) can be produced on a period of the order of 40 milliseconds. Some examples of heating rates obtained on NERVA fuel (fueled graphite containing 400 milligrams of 93% enriched uranium per cubic centimeter) are given in Table I.

A description of the various types of fueled graphite used in the program is given in Table II. The old type fuel was made from a dispersion of UO_2 powder (< 5 micron diameter) in graphite which converts to UC_2 during the graphitizing heat treatment. The new fuel is a dispersion of pyrolytic carbon coated particles of UC_2 (50-150 micron diameter particle with 25 micron coating) in graphite. The old type fuel was subject to hydrolysis which would cause reversion of some UC_2 to UO_2 . Samples of the old type fuel prepared with minimum contact with hydrolyzing environments following graphitization (at 2250°C) contained about 5 percent of the UC_2 reverted to UO_2 (completely carbided fuel). Fuel samples stored in air normally contain about 20 percent UO_2 (air stored fuel) and samples stored in moist air about 35 percent UO_2 (oxygen stored fuel). The coated particle fuel is resistant to hydrolysis following graphitization (at $\sim 1900^\circ\text{C}$). The size of the fuel sample used for most experiments was a 0.5 inch diameter by 0.75 inch long seven hole section of a KIWI B-4 element. Except where specifically noted, the fuel samples were unrestrained and did not have NbC liners on the coolant channels.

Transient experiments were carried out in high pressure autoclaves and in capsules which permitted photographing the fuel specimen during the transient.⁽²⁾ The autoclave tests included experiments in helium, vacuum, and water environments. Figure 1 shows the internal components of the high pressure autoclave used for experiments in either helium or vacuum. The autoclave instrumentation consisted of a thermocouple to measure the sample temperature, a thermocouple to detect specimen fragmentation, and a transducer to monitor the pressure developed in the autoclave. It may be noted that significant pressures (> 100 psia) were obtained only when fuel samples were pulsed in contact with water.

In general, two types of transient experiments were performed; a calibration experiment consisting of several transients on one sample to obtain data on peak sample temperature as a function of integrated power, or a single transient to determine the behavior of the fuel material. Examples of the results obtained from the calibration experiments are shown in Figure 2. The difference between the experimentally determined peak temperature and that calculated assuming adiabatic heating of the sample represents the heat loss from the samples.

Measurements following the transient irradiation include: particle size of fuel fragments (if any); composition of gases in the autoclave including fission products; fission products retained in the sample; and in the case of water experiments fission products in the water. The values of average particle size reported are the "Sauter" mean diameter which is defined as follows:

$$d_{sv} = \frac{\sum n_i d_i^3}{\sum n_i d_i^2}$$

and computed from the relationship:

$$d_{sv} = \frac{1}{\sum_{i=1}^N \frac{w_i}{d_i}}$$

where:

d_{sv} = Sauter mean (surface to volume) diameter

d_i = Average diameter of i^{th} size group

n_i = Number of particles in i^{th} size group

N = Number of size groups

w_i = Fraction by weight of particles in the i^{th} size group.

The Sauter mean diameter is a convenient quantity to use since it represents the diameter of spheres that would have the same ratio of surface area to volume as the total population of particles.

Results

Summaries of the results obtained on the various forms of old type fuel material are given in Table III and Figure 3. The results reveal that the threshold energy for fragmentation is lowest in the water tests (~ 100 MWS), intermediate for the air or oxygen-stored samples (~ 350 MWS) and highest for the completely carbided samples (~ 770 MWS).

Additional data obtained from the transients performed on fuel specimens in contact with water are given in Table IV. With regard to the experiments in water, the test performed at 800 MWS differed from the tests at lower energy in two principal ways. In the highest energy transient sea water was admitted to the autoclave 20 seconds prior to the transient. In the low energy tests the fuel samples were coated with Krylon and placed in the autoclave and in contact with distilled water for about one week prior to the transient. The Krylon coating was necessary to prevent chemical reaction of fuel and water during the storage period. Finally, samples of the gas contained in the autoclave after the high level transient were taken 5 minutes and one week after the transient. In the low energy tests gas samples were only taken one week after the test.

The results in Table IV show that a rather violent reaction occurred between fueled graphite and water during the transient at 800 MWS. The chemical reaction produced a 5000 psi pressure pulse of less than 0.1 second duration at about the same time as the attainment of the peak fuel temperature ($> 2500^{\circ}\text{C}$). The results also show that the xenon release during the transient is small compared to the xenon release during the week of contact between the fuel sample and water following the transient. Thus, it would appear that the major portion of the fission xenon release is due to a water leaching reaction. Further work is necessary to confirm this preliminary result.

The results obtained on air and oxygen-stored fuel samples show rather clear trends in particle size and xenon release as a function of transient energy. It is interesting to note the marked increase in xenon release which occurs when the samples fragment during the transient. The results obtained on the completely carbided samples also indicate the marked xenon release with sample fragmentation.

The high speed motion picture (4,000 frames per second) records obtained from the photographic series of experiments, using the specially designed TREAT capsule, provided qualitative information valuable to the interpretation of the results of the autoclave experiments. The results obtained from these experiments show:

- (1) The old type fuel heats uniformly during the transient. Preliminary studies on the first batch of coated particle fuel show evidence of non-uniform fuel particle distribution in these particular samples as indicated by non-uniform heating of the samples.
- (2) During fragmentation of air-stored samples a small fraction of the fragments have velocities as high as 8 feet per second.
- (3) Vaporization of considerable quantities of the fueled graphite samples (up to 20%) has been observed when sample temperatures exceed 3000°C .

Finally, preliminary transient experiments on the coated particle fuel indicate that it is more resistant to fragmentation than the air-stored or fully carbided material. An extensive series of transient experiments on the coated particle fuels are now in progress.

Discussion

A brief discussion of possible mechanisms of fuel fragmentation will be presented. The fragmentation threshold for transient experiments in water occurs at approximately 900°C . At this temperature the water-gas reaction (i.e. C plus H_2O forming CO , CO_2 and H_2) proceeds at an appreciable rate. It is suggested that fragmentation is due to the formation of steam and products of the water-gas reaction at the surface and within the pores of the fueled graphite.

The fragmentation threshold for air-stored material occurs at about 2100°C . At this temperature the back reaction between UO_2 and C proceeds at a rapid rate, resulting in the formation of CO or CO_2 gas. The proposed mechanism of fragmentation involves cracking of the graphite matrix by rapid build up of locally high pressures due to the formation of CO or CO_2 gas within the graphite body. This mechanism is consistent with the results of electrical heating experiments carried out at Los Alamos Scientific Laboratory. (3)

The mechanism of fragmentation of the completely carbided fuel is believed to be the same as that proposed for the air-stored material. It is presumed that the lower oxygen content of the completely carbided material is responsible for the high fragmentation threshold of 770 MWS (fuel temperature $> 3200^{\circ}\text{C}$). It may be noted that above 2800°C the mechanical strength of graphite decreases rapidly with increasing temperature. For example, at 3200°C the tensile strength of graphite has been reported to be about 100 psi. (4)

Table V summarizes the fragmentation threshold values obtained from the transient experiments on the old type fuel. Also given in Table V are the calculated values of the NERVA-equivalent nuclear transients which correspond to the experimental threshold values. For each threshold value a maximum and minimum NERVA-equivalent energy has been calculated. The minimum NERVA threshold was obtained by considering the neutron flux in the peak power regions of the reactor during a nuclear excursion and assuming no heat loss from the fuel. At the minimum value only a small portion of the reactor fuel elements would be expected to fragment. The maximum NERVA threshold

values were obtained by assuming a uniform power distribution in the core and values of heat loss similar to that obtained in the TREAT experimental program. At the maximum threshold value, most of the fuel elements would be expected to fragment.

The calculated NERVA-equivalent fragmentation threshold values for the various excursion conditions range from 1,000 to 11,000 MWS. If one assumes that the NERVA engine is capable of a programmed excursion of the order of 10,000 MWS, then it may be concluded that nuclear transients would be useful in fragmenting the core (made of old type fuel) or at a minimum weakening the core to enhance the effectiveness of an explosive or thermochemical destruct system. It should be noted that the preliminary information available on the coated particle fuel indicates that nuclear transients may be somewhat less effective in causing fuel fragmentation. However, theoretical analysis of the behavior of coated particle fuels during nuclear excursions indicate that faster excursions (periods ≤ 1 millisecond) may cause fuel fragmentation.⁶⁾ Experiments are being planned in the TRIGA Mark F reactor to evaluate the theoretical studies.

Acknowledgments

The experimental work described is the result of the efforts of a considerable number of people located at various sites throughout the country. The most active participants in this work included L. D. P. King, P. Wagner, W. Stratton, and E. Bryant of the Los Alamos Scientific Laboratory; L. Baker, E. Mouradian, and F. Testa of the Chemical Engineering Division, Argonne National Laboratory, J. Boland and S. Lawroski of the TREAT Reactor (Argonne National Laboratory); and W. H. Esselman, W. H. Arnold, A. B. Rothman, and E. Hemmerle of the Westinghouse Astronuclear Laboratory. The authors are grateful to S. Lawroski and R. C. Vogel of the Chemical Engineering Division, Argonne National Laboratory for permission to use their facilities for this program.

References

- (1) G. A. Freund, P. Elias, D. R. MacFarlane, J. D. Geier, and J. F. Boland, "Design Summary Report on the Transient Reactor Test Facility (TREAT)," ANL-6034, 1960.
- (2) For more details see the following reports:
 - (a) A. Boltax, "Transient Reactor Experiments on NERVA Fuel Material--Status Report," WANL-TNR-038, 1962 (CRD).
 - (b) R. C. Liimatainen, R. O. Ivins, M. A. Vogel, and F. J. Testa, "Status Report I on the Testing of Graphite-Type Nuclear Rocket (Rover) Fuel in a Pulsed Reactor (TREAT)," ANL-6522, 1962 (CRD).
- (3) Monthly Status Report for LASL NERVA Activities for Period Ending Nov. 20, 1961, LAMS-2645 (CRD).
- (4) C. Malmstrom, R. Keen, and L. Green, Jr., "Some Mechanical Properties of Graphite at Elevated Temperatures," Jnl. Appl. Phys. 22, 5, 1951.
- (5) Personal communication from W. Stratton, LASL, September, 1962.

Table I Maximum Heating Rates Obtained on KIWI B-4 Fuel Samples in TREAT

<u>Transient Energy MWS</u>	<u>Reactor Period (ms)</u>	<u>Maximum Fuel Temperature (°C)</u>	<u>Maximum Heating Rate (°C/sec)</u>
100	150	940	1150
375	75	2040	2500
550	50	> 2700	8500

Table II Description of Fuel Samples Used in the TREAT Program

		<u>Percent of UC₂ present as UO₂</u>	<u>Fuel Particle Size (microns)</u>
OLD	Completely Carbided	~ 5	< 5
	Air Stored	~ 20	< 5
	Oxygen Stored	~ 35	< 5
NEW	Coated Particle	< 1	50-150*

* UC₂ fuel particle coated with 25 microns of pyrolytic carbon.

Table III Summary of Selected Transient Experiments

	Reactor Energy (MWS)	Peak Power (MW)	Reactor Period (ms)	Maximum Sample Temp. (°C)	Xenon-133, microcuries		Particle Size d_{sv} (mils)
					Produced	Released	
Water Tests Air Stored Fuel	105	300	140	900	735	109	15
	360	1120	75	1710	2480	1680	68
	800	4470	40	> 2600	4470	--	--
Helium Tests Air Stored Fuel	255	700	95	1700	1300	30	2
	380	2430	54	2150	1940	1400	72
	645	3850	40	2900	3300	2100	64
	890	3850	40	> 3000	4550	2300	51
Helium Test Oxygen Stored Fuel	325	1120	81	1950	--	--	--
Helium Tests Completely Carbided Fuel	270	--	54	1740	1590	60	4
	770	3860	42	> 3000	3860	2150	56
	790	4730	40	> 3000	4340	320	7
Vacuum Test Completely Carbided Fuel	765	4140	40	> 3000	3930	1070	27
							66

* The results given were the last obtained in a series of transients used in a calibration experiment.

** The fuel sample holes were lined with NbC. Also, this sample was constrained by multiple layers of graphite cloth. Further experiments on the effects of constraint on fuel sample fragmentation are in preparation.

Table IV Detailed Comparison of Results Obtained from Water Tests

	Test Number		
	83	84	96
Reactor Energy, MWS	105	360	800
Particle size, d_{sv} (mils)	86	28	18
Peak fuel temperature, °C	900	1710	> 2600
Peak pressure during transient, psi	negligible	--	~ 5000
Xe ¹³³ Release, microcuries			
5 minutes after transient	--	--	20
1 week after transient	175	1660	> 470*
Gaseous Reaction Products, cc. at STP			
5 minutes after transient	--	--	2850
1 week after transient	450	1550	--*
Composition of Gases, mole % **			
H ₂	71.1	48.3	55.2
CO	20.0	42.7	35.0
CO ₂	0.5	5.4	8.4
Hydrocarbons	8.4	2.6	0.7
Extent of Fuel Reaction, weight %	17	25	33

* Gas leak in autoclave following transient prevented accurate determination.

** For tests 83 and 84 gas was collected one week after transient.
For test 96 gas was collected 5 minutes after transient.

Table V Fragmentation Thresholds for Nuclear Transients

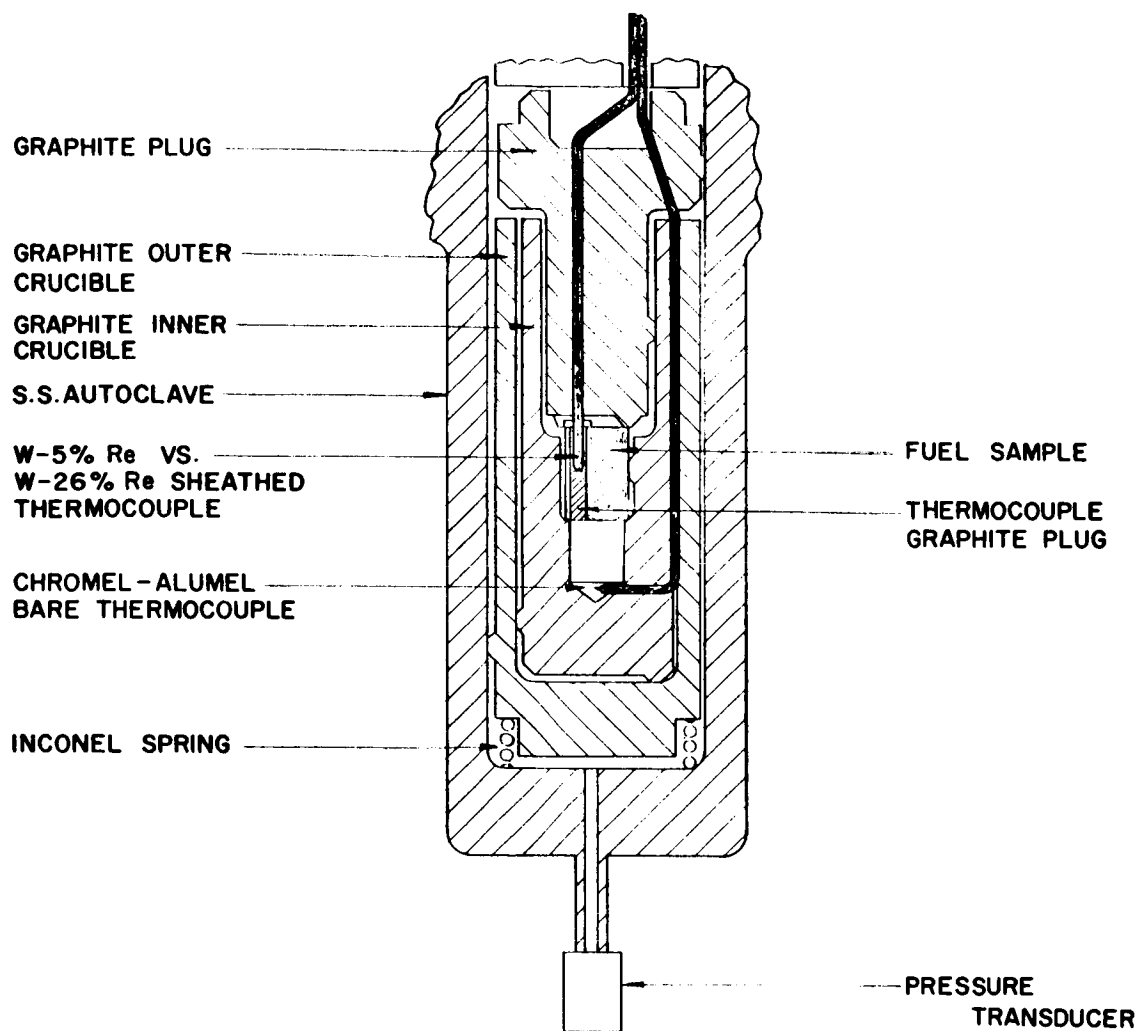
(Reactor periods of 40-150 milliseconds)

	TREAT	Energy of Transient (megawatt-seconds)	
		NERVA	
		Minimum*	Maximum**
Water Excursion	~100	1,000	2,000
Air Stored Fuel			
Dry Excursion	~350	3,000	6,000
Air Stored Fuel			
Dry Excursion	~770	5,000	11,000
Completely Carbided Fuel			

* At peak power positions.

** Assuming uniform power in core.

NOTE: A 10,000 megawatt-second NERVA transient will vaporize ~20% of the core (neglecting heat losses).

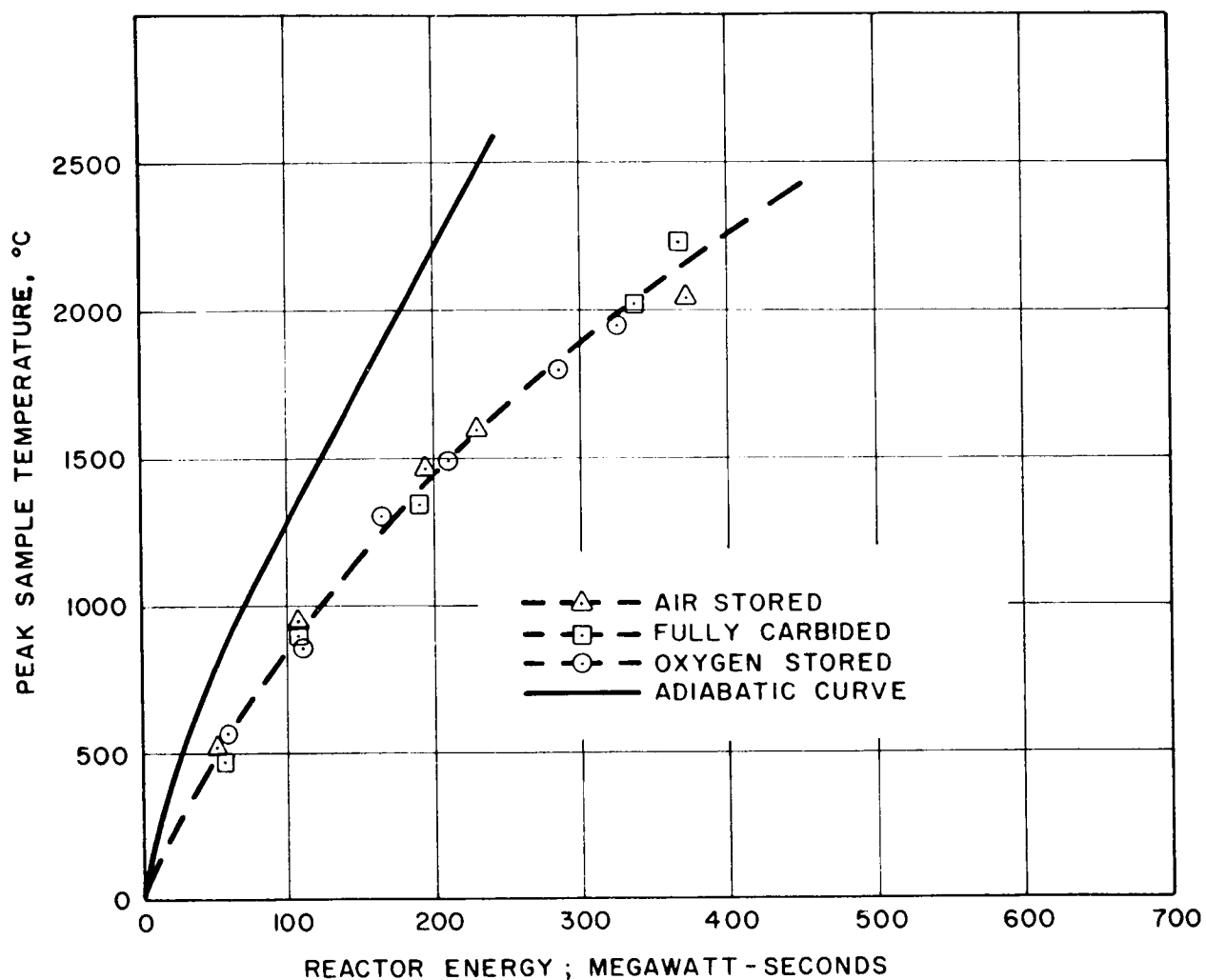


AUTOCLAVE ASSEMBLY CONTAINING FAILURE DETECTOR

FIG. 1



547133



PEAK SAMPLE TEMPERATURE VS. REACTOR ENERGY

FIG. 2

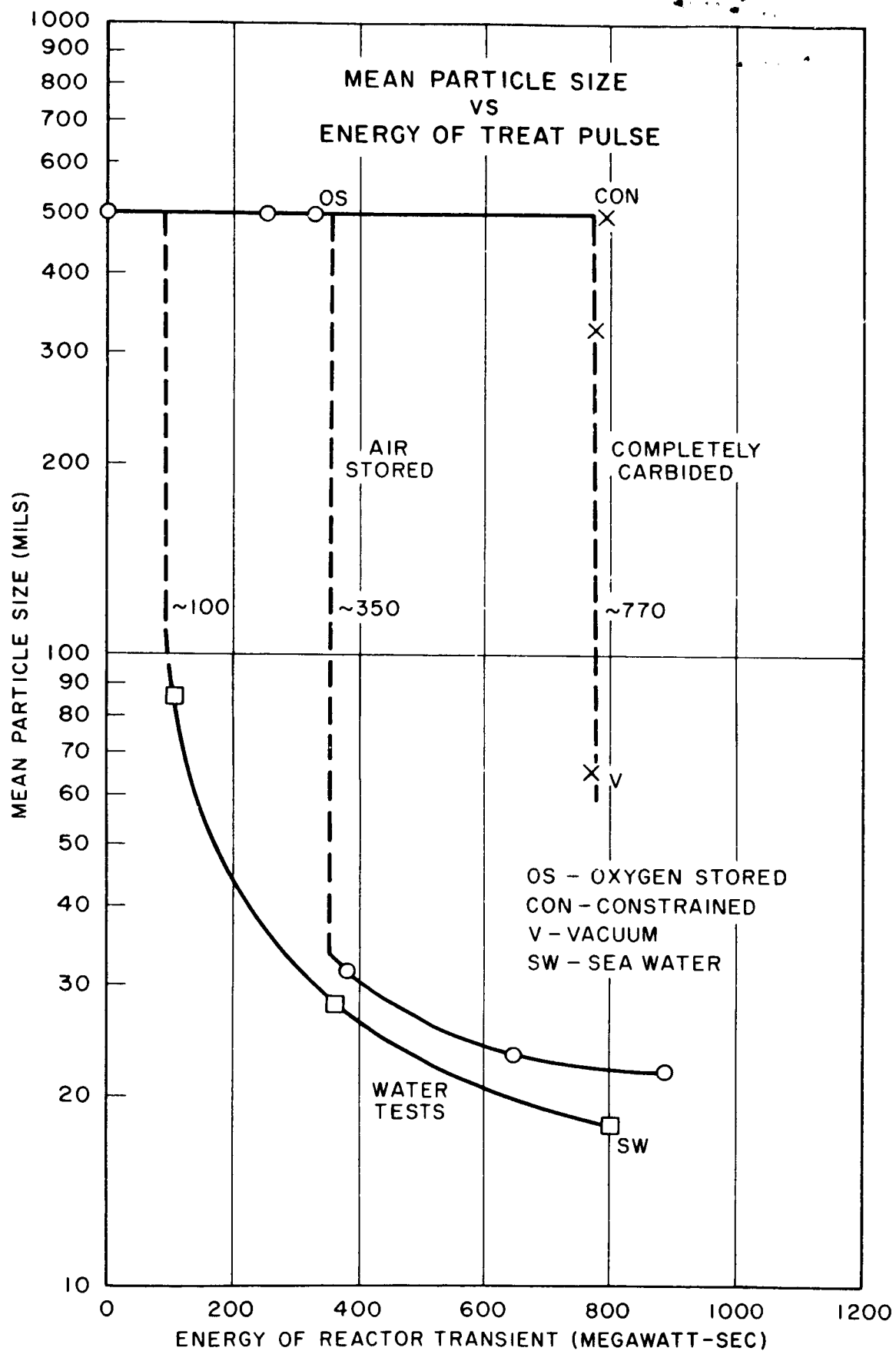


FIG. 3

66 50302

EFFECTS OF LIQUID PROPELLANT EXPLOSIONS

ON NUCLEAR ROCKET ENGINES¹

E. Karl Bastress
Arthur D. Little, Inc.
Cambridge, Massachusetts

50302

ABSTRACT

An experimental program was conducted to determine blast effects from explosions of liquid rocket propellants. One phase of the program was concerned with the internal characteristics of propellant explosions and their effects on nuclear rocket engines. The purpose of this phase of the work was to determine the hazards which might result from a failure at launch of a large liquid-propellant booster rocket with a nuclear powered upper stage.

A variety of instruments were used to measure peak-pressures and heat transfer rates within propellant explosions. In addition, observations were made during each test of the movements of the fireball and dust-cloud, and of the fragmentation and scattering of debris.

Measured characteristics of propellant explosions were utilized to predict their effects on nuclear rocket engines of the NERVA type, and to determine the hazards which might arise from distortion of the engine or vaporization of reactor components. Hazards considered were blast, radioactivity, dispersion of toxic materials, and scattering of reactor fragments. As a result of this analysis it was concluded that incorporation of a NERVA engine in a SATURN vehicle is not likely to create a hazard to personnel or property beyond safe distances required for propellant blast effects.

Conf. R. D. Author

¹This work was sponsored by George Marshall Space Flight Center, National Aeronautics and Space Administration, and Space Nuclear Propulsion Office, U. S. Atomic Energy Commission, under Contract No. NAS8-523.

I. Introduction

The projected use of nuclear powered rocket engines for space exploration has introduced a number of new problems in the form of hazards to personnel in the vicinity of the launch site and near the point of re-entry or impact. One of the problems arises from the fact that a typical nuclear reactor contains toxic materials such as radioactive fission products and metallic beryllium. Any mechanism by which these materials could be dispersed in finely divided form constitutes a serious hazard.

In early use, nuclear rockets will serve as upper stages in combination with chemically powered boosters. In this situation it is possible that toxic materials from the nuclear stage could be dispersed by a failure of the chemical booster, particularly at launch where the maximum quantities of propellants are present. In order to evaluate the possible hazards which will be created, the conditions to be expected in the failure of chemical boosters must be determined. The effects of these conditions on a nuclear powered engine can then be predicted.

Arthur D. Little, Inc. has recently completed a series of experimental tests to determine the blast effects which might result from a failure at launch of a SATURN rocket vehicle (1)². In brief, the tests involved intentional spilling of scaled quantities of SATURN propellants: RP-1, liquid hydrogen and liquid oxygen. These liquids were spilled on the ground and allowed to mix, and detonation of the mixture was initiated by a small explosive charge. The purpose of the tests was to determine the maximum blast which might be expected from a SATURN failure. Tests were conducted using propellant quantities equal to 1/10,000, 1/2000 and 1/25 that to be used in the C-2 configuration. The propellant containers used in the 1/25-scale tests are shown prior to spilling in Figure 1. Instrumentation was employed to determine the characteristics of the resulting blast waves over a range of distances from the test site. The tests were also observed by high-speed motion picture cameras to provide more information as to the nature of the detonations.

In order to obtain information which might aid in evaluating the hazards associated with a nuclear stage, additional instrumentation was provided in the largest scale tests to determine the characteristics within the region of the detonation and resulting fireball (2, 3). Instruments were devised which would indicate peak pressures and total heat flux at various locations. Also, photographic coverage was increased to include observations with a wide field of view to provide cloud travel information. Photographs of the fireball and dust-cloud from one of the tests are shown in Figure 2. Three 1/25-scale tests were conducted and each of these were instrumented in this manner. Difficulties were encountered in these large-scale tests in that ignition of the propellant mixtures occurred prematurely in each case. It was intended that ignition take place seven seconds after the start of the spilling process to provide an optimum time for mixing. However, ignition occurred spontaneously between three and five seconds from the start of the spill, so that mixing had proceeded to a different degree in each test. As a result, the characteristics of the detonations varied widely, and a greater range of conditions were obtained than had been intended.

Another program associated with these blast tests involved the exposure of samples of beryllium to the detonation and fireball. This work was performed under a subcontract with Westinghouse Electric Corporation (4).

²Numbers in parentheses indicate References at end of paper

II. Test Results

A. Pressure Conditions

The SATURN vehicle utilizes three liquid propellants: RP-1 (kerosene), liquid hydrogen and liquid oxygen. The C-5 configuration will contain approximately five million pounds of these propellants. Spilling and mixing of these propellants create a two-phase mixture - a gas phase consisting principally of hydrogen, oxygen and air; and a liquid phase (or liquid-solid mixture) containing RP-1, oxygen, and possibly a small percentage of hydrogen. Ignition of this mixture results in a violent detonation and a blast wave in the surrounding air similar to that produced by high explosive materials. A description of blast waves from liquid propellant explosions is contained in Reference 1. Within the detonating mixture the blast characteristics of the two phases are found to be quite different. Peak pressure measurements in the liquid phase have indicated pressures ranging from 7000 to over 90,000 psi. The wide variation results from the inhomogeneity of the mixture. The highest pressures were obtained in mixtures wherein the greatest degree of mixing had occurred. The maximum theoretical pressure attainable in these liquid propellant mixtures is approximately 150,000 psi. This value was calculated by assuming a constant volume reaction.

In the gas phase, peak pressures are of a lower magnitude than in the liquid. Gas phase pressure measurements ranged below 2000 psi in all instances with most measurements below 1200 psi. The gas phase pressures are caused by shock waves from the liquid reaction as well as reaction within the gaseous components. Therefore, peak pressures decrease rapidly with distance from the liquid body.

The dimensions of the zones of the detonation region are shown in Figure 3. A reduced distance coordinate is used in the form of $d/w^{1/3}$ where d is the radial distance in feet from the center of the detonation, and w is the weight in pounds of propellant which is spilled and mixed. Experimental results (1) indicate that only premixed propellants contribute to the blast and that the explosive yield³ is approximately 1.0 lb of TNT per pound of propellant mixture. In predicting the extent of the detonation region for failure of a given vehicle, it would be unrealistic to assume that all the propellant would participate. The actual amount which could become mixed prior to ignition can only be estimated.

The dimensions shown in Figure 3 are based on results of the experimental program. Liquid detonation zone dimensions were taken from crater measurements, and vapor cloud dimensions were taken from photographic records. The dimensions shown are those predicted for a symmetric collapse of the vehicle creating a pool of mixed propellants on the launching pad. This is an unrealistic model, but represents the worst case from the standpoint of blast level. Asymmetry in the mode of failure of the vehicle would reduce the concentration and mixing of the propellants and would probably result in lower blast pressures.

³ Explosive yield as used here is defined as the weight of TNT required to produce a blast wave of equal magnitude as that produced by the propellant mixture, divided by the propellant weight. The value of 1.0 pertains only to the SATURN propellant combination. Yields for other combinations of these propellants are contained in Reference 1.

Also shown in Figure 3 are the maximum peak pressures to be expected at ground level as a function of distance from the center of the blast. The distribution of peak pressures can be divided into three zones wherein the mechanisms producing the over-pressures are different. In Zone I, which is that area covered by a liquid propellant mixture, pressures up to 150,000 psi result from the detonation reaction within the liquid. In Zone II, pressures vary from 2000 psi near the inner edge of the zone to 100 psi at the outer edge. Peak pressures within this zone are generated by the combined effects of the shock wave emerging from Zone I, continuing chemical reaction in Zone I, and vapor phase chemical reactions in Zone II behind the shock wave. In Zone III peak pressures are below 100 psi and fall off rapidly with increasing distance from the center. Within this zone the shock wave is no longer supported by continuing chemical reaction, and its characteristics are similar to those of a wave produced by a point-source explosive.

B. Heat Flux Conditions

During the experimental blast tests, the following measurements and observations were made on the fireball produced in each test:

1. Internal heat flux measurements
2. External heat flux measurements (radiant)
3. High-speed motion picture recording
4. Spectrographic recording of external radiation

These observations were made on fireballs resulting from tests ranging in size from 1/10,000 to 1/25 of the SATURN C-2 propellant load. As a result, the characteristics and behavior of the fireball were well established and a basis was obtained for predicting the characteristics of the fireball which might be expected from a vehicle failure.

In the event of a failure of a SATURN C-5 wherein a major portion of its propellant load participated in the initial explosion, a fireball would be formed up to 2000 feet in diameter. The fireball diameter is less dependent upon propellant mixing than is blast level. Unmixed propellant can react quickly enough to contribute to the initial fireball. The average temperature of the fireball would be approximately 3000 F. The fireball would remain in contact with the ground for a period of 3 to 10 seconds and during this time its temperature would remain nearly constant (Radiant heat loss appears to be balanced by continuing energy release during this period). As the fireball began to rise from the ground, it would begin to cool, but would continue to glow visibly for 15 to 20 seconds after ignition. Heat transfer to objects within the fireball would be primarily by radiation, and would occur at an initial rate of approximately 0.5 Btu/sq in-sec. An object remaining on the ground with an absorptivity of 0.8 would receive a total heat input of 1 to 4 Btu/sq in. Material fragments carried upwards with the fireball might receive a greater heat input, but since the heat flux drops rapidly with temperature, the additional energy received would be small.

Quantities of fuel which were not consumed during the initial explosion would remain on the ground and burn in an air-fuel diffusion flame. Because of its volatility, liquid hydrogen could be expected to vaporize and burn quickly. However, an RP-1 flame might persist for several minutes depending upon the depths of the pools formed. Results of experimental studies of burning pools of kerosene have been analyzed to determine heat transfer characteristics of such flames (3). The analysis has indicated that surfaces within kerosene-air diffusion flames could not be expected to rise above 1100 F. This value is in agreement with results obtained from heat flux gages which were enveloped in flames from burning RP-1 during the SATURN blast tests. Maximum temperatures attained in these instances were between

800 and 1000 F. These temperatures correspond to a maximum heat transfer rate of approximately 0.02 Btu/sq in-sec.

Because of the complex structures of the SATURN vehicles and the many possible modes of failure, the manner in which the propellants were consumed could vary considerably from the conditions of the SATURN blast tests. However, in any event it is unlikely that heat transfer rates could be obtained greater than 0.5 Btu/sq in-sec which was the maximum rate observed with pre-mixed propellants.

C. Fireball and Dust Cloud Movement

Photographic records were utilized to determine the movement of the fireball and dust cloud resulting from each of the large-scale blast tests. This information was required to aid in predicting the hazards which could result from airborne materials released from a propellant explosion. The photographs shown in Figure 2 were taken at 4 and 30 seconds after initiation of a blast test. Cloud movements as determined from these records are shown in Figure 4. It is observed that the initial rate of rise is approximately 75 fps and that an altitude of 1000 feet is attained within 20 seconds. Beyond this altitude the movement is variable, but an ultimate height in excess of 2000 feet is indicated.

III. Hazards Analysis

A. General

There are a number of hazards associated with the launching of large liquid propellant rockets. Chief among these are:

1. Blast
2. Thermal effects
3. Acoustic effects
4. Toxic effects
5. Flying debris

For each vehicle the potential hazards must be estimated and protective measures taken to prevent injury to persons and property. The primary protective measure is the establishment of safe distances for personnel, equipment and property not associated with the launching operation. Additional protective measures are required for launching personnel and equipment.

In assessing the hazards that could result from launching of a combined nuclear-chemical vehicle, such as SATURN with a NERVA engine for upper stage propulsion, we are primarily interested in those aspects which might require protective measures beyond those normally provided for the launching of a chemically propelled vehicle of nominally the same size. The hazards which could result from damage to a nuclear engine are:

1. Blast
2. Radioactivity
3. Dispersion of Toxic Materials
4. Scattering of Reactor Fragments

B. Blast

The maximum blast potential of SATURN rocket vehicles has been well established (1). However, with a nuclear stage, a question arises as to

whether a launching failure could cause a power excursion of sufficient magnitude to increase significantly the potential blast effect of the vehicle. The energy content of NERVA engines will be comparable to the available chemical energy of the booster propellants. Therefore, the fraction of this energy which could be released accidentally is important in analyzing the blast hazard.

A number of studies have been made of accidents which could occur during various stages of flight of a nuclear rocket (5, 6). The "maximum credible accident" anticipated during launching would result from immersion of the reactor in water or other liquids, and the blast accompanying such an accident would be small. These analyses did not take into account the pressure levels occurring within propellant explosions. Recognizing that these conditions could conceivably cause a more extensive excursion than had been predicted previously, Arthur D. Little, Inc. studied the possible modes of failure of a nuclear-chemical vehicle (3). As a result of this study it was concluded that in theory propellant detonation pressures would be sufficient to compress the reactor and cause a serious power excursion. However, it would be unreasonable to expect that the conditions necessary to achieve this result could be encountered in an actual launching failure. Therefore, the maximum credible accident is still regarded as that due to immersion or its equivalent, and the blast hazard associated with a nuclear rocket is small in comparison to the chemical booster.

C. Radioactivity

Hazards analyses of nuclear rocket operations have established that release of fission products during launch pad accidents would not create hazardous conditions beyond the launching site. In the case of the maximum credible accident, release of 15 percent of the fission product inventory is predicted. In the event of a propellant explosion, the quantity of fission products created would not be increased, but the fraction released could exceed the 15 percent prediction. Fragmentation of the reactor and combustion of fuel elements could cause a greater release of these materials. The radioactivity levels in the vicinity of the launch area would be increased accordingly. However, from the analysis of fission product dispersion conducted by the Martin Company (6), it appears that even a 100 percent release would not create a hazard to personnel.

D. Dispersion of Toxic Materials

The current design of the NERVA engine includes a beryllium reflector weighing approximately 2200 pounds. Beryllium in the form of vapor or fine particles is extremely toxic, and as a result, exposure of the reflector to a propellant explosion could create a hazard. A review of experimental data on the vaporization of beryllium has shown that the metal must be raised to temperatures approaching its melting point (2340 F) before vaporization occurs at significant rates. Substantially higher temperatures are required to ignite beryllium particles. As mentioned in the previous section, the maximum heat flux rate observed within propellant explosions was 0.5 Btu/sq in-sec. In Figure 5 calculated surface temperatures are shown as a function of time for beryllium fragments of various shapes when exposed to this heat flux. The maximum expected exposure of ground objects to a fireball from a SATURN C-5 failure is 10 seconds. It is seen from the figure that only small particles of beryllium would reach temperatures above 2000 F in this time. Thus, it can be concluded that the quantity of beryllium vaporized in an explosion would be determined by the degree of fragmentation rather than the total quantity present. Since beryllium exhibits some ductility under stress, it would not be expected to shatter into tiny fragments. Only areas of stress concentration would be expected to be reduced to small particle sizes. An

analysis of the reflector element design, as shown in Figure 6, indicated that small fragments could be expected from the corners and from the webs formed by the control drum passages. The maximum quantity of beryllium which would be reduced to particles susceptible to vaporization has been estimated to be 110 pounds.

To determine the concentrations of airborne beryllium particles which would result from an instantaneous release of 110 pounds of beryllium, Sutton's equations for atmospheric dispersion were utilized. Conservative, but realistic, values of diffusion coefficients and release height were used. The results indicated that the maximum concentration occurring at ground level would be of the same order as the minimum allowable concentration for instantaneous exposure. Total exposures predicted would exceed maximum recommended levels only for wind velocities below 1 mph. Since all assumptions made in this analysis were conservative, it is concluded that there is little likelihood of a beryllium hazard arising from launching accidents involving NERVA reactors of the present design.

E. Scattering of Reactor Fragments

The positive impulse (overpressure-time integral) of blast waves increases with the mass of the explosive substance to the $1/3$ power. It is reasonable to expect that scattering of debris from a vehicle failure would vary similarly. Analyses of debris patterns and motion picture records from the SATURN blast tests confirmed this expectation. On this basis, it is predicted that debris scattering from a failure of a SATURN C-5 would extend to a radial distance of approximately 1-1/2 miles with isolated fragments traveling farther. The presence of a nuclear reactor would not increase the hazard from flying debris, but would result in the distribution of toxic and possibly radioactive material fragments in the vicinity of the launching area.

IV. Conclusions

During this analysis it was necessary to make assumptions or estimates regarding the extent of various processes. In each case an effort was made to assure that the assumption was conservative, but not unrealistic. As a result, the effects predicted for a nuclear-chemical vehicle failure are regarded as improbable but not impossible, or in terminology used in hazards analysis, the predicted effects are the "maximum credible" hazards which could result. After consideration of the various potential hazards and the mechanisms by which they could be generated, the most serious effects predicted are as follows:

1. The quantity of beryllium vaporized during a propellant explosion depends upon the design of the reflector elements rather than the total quantity present. Only small fragments of beryllium would be susceptible to vaporization.
2. In the case of a NERVA reactor, a release of beryllium vapor or particles could result within the fireball, but the maximum concentration occurring at ground level would not exceed the maximum allowable concentration for instantaneous exposure. Total exposures could exceed maximum recommended levels only if wind velocities were low (1 mph or below).
3. There is little likelihood of a propellant blast causing a nuclear power excursion of a greater magnitude than that described in Reference 5 as the "maximum credible accident".

4. Dispersion of fission products could exceed that predicted for an accidental power excursion prior to launching (5). The increased concentrations of radioactive materials would not exceed tolerable limits except possibly within the immediate vicinity of the vehicle failure.
5. Fragments of reactor material could be scattered around the launching area to distances of up to 1-1/2 miles.
6. Contamination of the launching area with beryllium particles and fission products could prevent further use of the area until radiation had subsided or until precautionary measures had been taken against beryllium poisoning.

From this description of possible effects it is apparent that the presence of a nuclear engine does not constitute a hazard to personnel or property beyond safe distances which would be required for propellant blast effects. However, the contamination of the launching area would be objectionable, and the release of airborne contaminants, though not harmful, could constitute a public relations problem.

References

1. "A Study of the Blast Effect of the SATURN Vehicle," Summary Report, Arthur D. Little, Inc., 13 December 1961, (C).
2. "Effects of Liquid Propellant Explosions on Nuclear Rocket Engines," Interim Report on Experimental Program, Arthur D. Little, Inc., 15 December 1961, (C).
3. "Effects of Liquid Propellant Explosions on Nuclear Rocket Engines," Final Report, Arthur D. Little, Inc., 14 March 1962, (S-RD).
4. "Study of the Safety Hazards Caused by the Addition of Beryllium to the SATURN Blast," Final Report, Arthur D. Little, Inc., 15 December 1961, (U).
5. "Nuclear Safety Aspects of the ROVER Program," Report No. LA-2409, Los Alamos Scientific Laboratory, March 1960, (S-RD).
6. "Nuclear Rocket Safety Study, Final Report," Report No. MND-2517, The Martin Company, 9 August 1961, (S-RD).

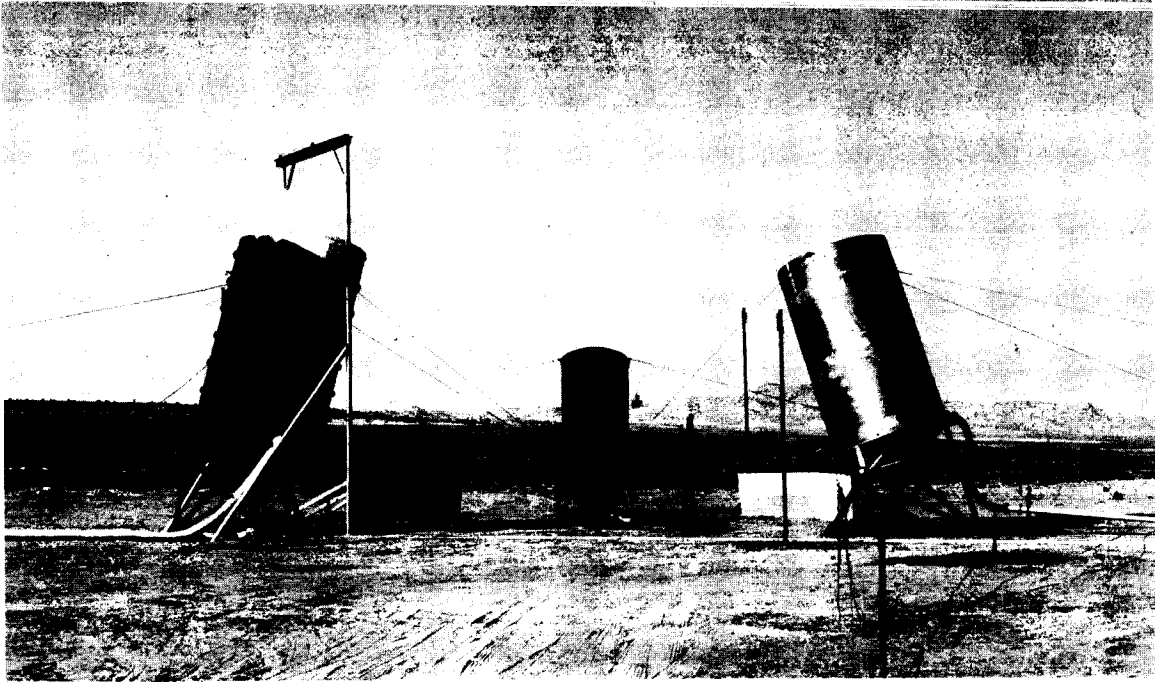


Figure 1 - Propellant Container Arrangement for Large-Scale SATURN Blast Test

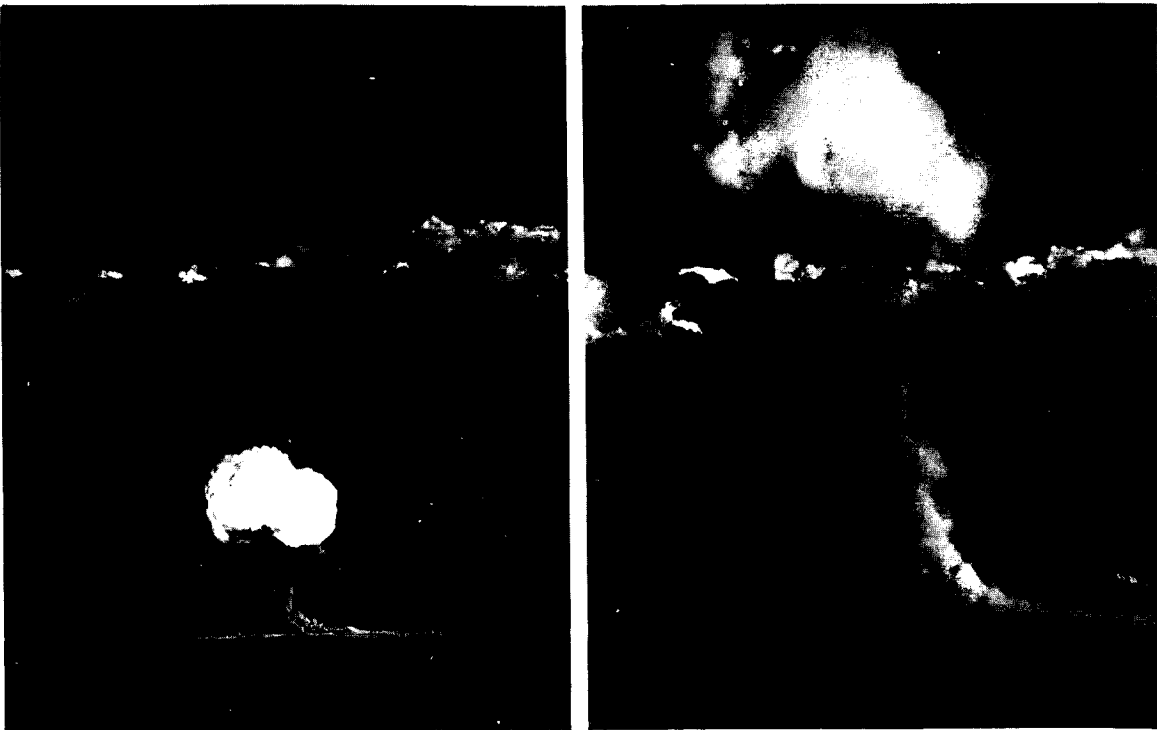


Figure 2 - Fireball and Dust Cloud from Large-Scale SATURN Blast Test

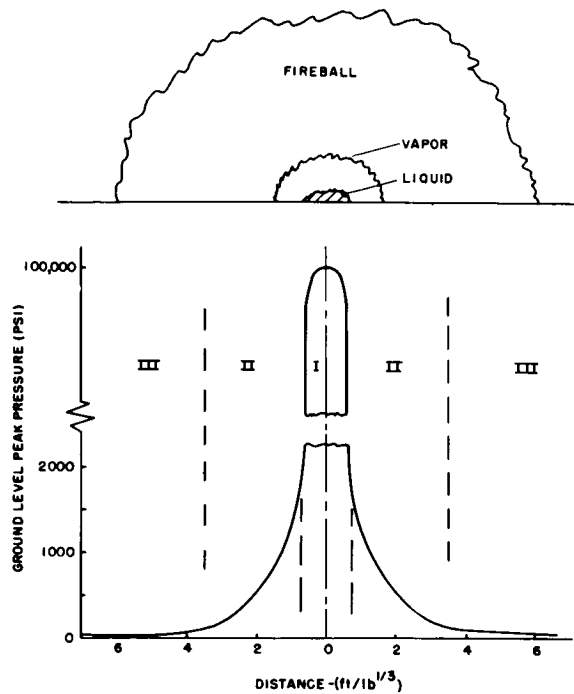


FIGURE 3 - PREDICTED GEOMETRY OF SYMMETRICAL SATURN PROPELLANT EXPLOSION AND DISTRIBUTION OF PEAK PRESSURES

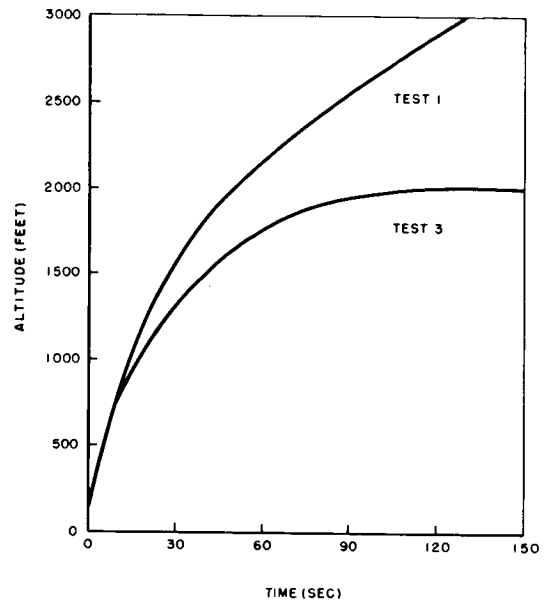


FIGURE 4 - VERTICAL MOVEMENT OF CLOUDS FROM BLAST TESTS

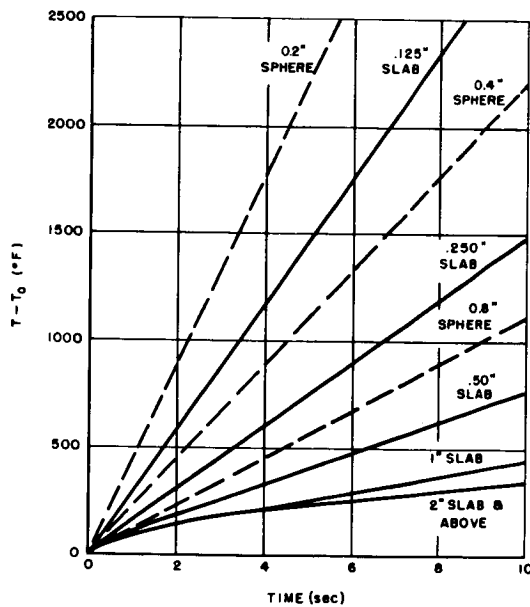


FIGURE 5 - SURFACE TEMPERATURE OF BERYLLIUM SHAPES WITH CONSTANT HEAT FLUX ON ALL SURFACES OF $0.5 \text{ BTU/IN}^2 - \text{SEC}$

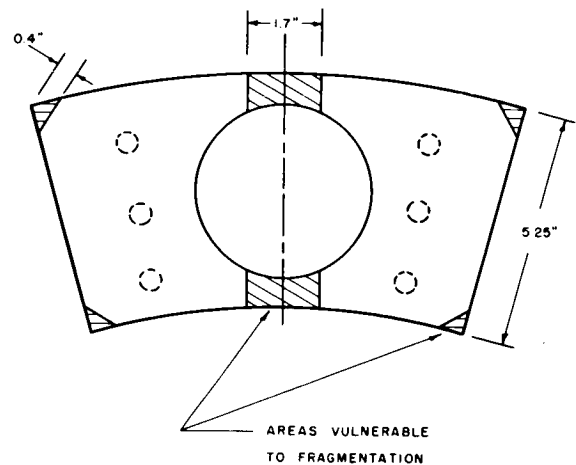


FIGURE 6 - CROSS-SECTION OF BERYLLIUM REFLECTOR SEGMENT

THE LOS ALAMOS SCIENTIFIC LABORATORY
ROVER FLIGHT SAFETY PROGRAM*

[4]

L. D. P. King

Los Alamos Scientific Laboratory, University of California
Los Alamos, New Mexico

About a year and a half ago an effort was made at Los Alamos to coordinate and expand the contributions the laboratory could make towards solving Rover Flight Safety problems. The responsibility for providing early technical data clearly lies with organizations capable of doing so. It was with this in mind that a Rover Flight Safety Office and committee were established at Los Alamos. Their aim was to evaluate potential problems, in particular those concerned with the reactor itself, and see that suitable experiments were undertaken.

It was becoming evident at this time that the demonstration of the feasibility of nuclear rockets was in itself not sufficient to make them useful. Of equal importance was that government agencies concerned, as well as the general public, are convinced that all Rover Flight Safety requirements can be met.

To assist in attaining this objective the documentary film you will now see was made. It illustrates that substantial work towards solving flight safety problems has already been performed at Los Alamos.**

*Submitted as a portion of the Rover Flight Safety Session of the Nuclear Propulsion Conference August 15 - 17, 1962 at Monterey, Calif.

**At this point a 25 minute color sound film was shown at the conference. The written material which follows covers the same material as presented in the movie. This documentary film is available on loan from the Los Alamos Report Library for any organization having a Sigma 16.2 clearance or equivalent.

At present, only very broad safety guidelines are available. Namely, radiation levels in all nuclear rocket work are not to exceed the values specified in the Federal Radiation Protection Guides, and nuclear rocket engines are not to be operated in any manner which would permit the reactor or any large part thereof to re-enter or impact on any of the earth's land masses. Laboratory effort has been directed towards seeing if these broad guidelines can be met under all test and operational conditions. The principal types of problems have been pointed out in a previous LASL report.¹

No difficulties are anticipated during normal launch pad operations where standard procedures using distance and shielding can be used. Abnormal behavior, however, does present a number of new potential hazards. A booster abort could place the reactor in an intense explosion or fire, break up the engine by impact on the launch pad, or flood the core with liquid hydrogen or water.

The beryllium reflector produces a potential toxic vapor problem if a fire from the liquid oxygen, hydrogen, and RP1 fuels can be shown to last an appreciable time. This problem and the possibility of a self sustaining high temperature beryllium water reaction is under investigation elsewhere. The LASL has performed calculations to study the relative merits of other reflector systems in case design changes are required.

Extensive calculations have been carried out and are in progress to determine the magnitude of an incident which might occur on the launch pad. The maximum energy release would be due to a rapid water insertion into the reactor. This is estimated to produce about 10^{21} fissions with a kinetic energy release of a few hundred pounds equivalent of high explosive. More probable types of incidents caused by accidental control rod motion

or hydrogen flooding are expected not to exceed 10^{19} - 10^{20} fissions with only a minor kinetic energy release.

Another type of accident which is receiving extensive calculational effort and experimentation is to determine the possibility that a core continue to operate in a semi-stable manner if it were slowly submerged in water. This requires some knowledge of heat transfer rates, water injection velocities, and fuel element life while the reactor is at high temperature. Present indications are that for water injection pressures which exceed about 6 psi the reactor will be disintegrated by a fuel vapor explosion. For low water additions rates the reactor might not be disrupted if the average power does not exceed its ability to dissipate heat, estimated to be 250 to 500 KW. Preliminary experiments on fuel element life indicate that the fuel itself has a good possibility of surviving a number of hours in the temperature range 1000° to 2000°C .

Estimates of reactivity effects which might be expected from water immersion have been performed using polyethylene in a reactor mockup. The total contributions from external reflection are about equivalent to the cold hold-down available from control rods. The addition of water into the reactor coolant channels is worth, reactivity wise, about \$2.6/kg of hydrogen for the first two inches of penetration and \$5.7/kg of H_2 for the next six inches.

Additional work is in progress to delineate the probability of continued reactor operation if submerged in water.

Experiments have been performed to determine the release of fission products to water. Results show that the extraction is slow and generally limited to a few percent. The maximum release from normal fuel has been obtained from fully carbided elements in boiling sea water; the minimum from partially

carbided "shelf" type fuel in room temperature distilled water. The release is highly specific in regard to which isotopes are more soluble. The iodine isotopes are the principle offenders and have given a maximum leaching rate of 2 to 3% of the initial activity in the first 24 hours. After one week the extraction rate is down an order of magnitude. Additional leaching information with fuel at high temperature is being obtained from in pile transient testing of water immersed samples.

How does one take care of reactor disposal after operation? Can one shatter the reactor into sufficiently small parts that will either burn up and be destroyed on reentry or reduce the radioactivity of any remaining fragments to harmless levels through induced escape of fission products and wide dispersal? A number of experiments have been undertaken at the LASL to obtain answers to the problem of safe reactor disposal. These include the use of nuclear explosives, chemical explosives, nuclear transients, after heat to boil off fission fragments and chemical additives to weaken, alter, or disintegrate the core.

The use of nuclear explosives is not desirable since it increases the total radiation hazard. Calculations indicate that megaton yields would be required to vaporize the entire reactor in a fire ball with the distances required to prevent damage to the bomb components from reactor radiation.

A series of experiments were undertaken to determine the feasibility of using chemical explosives for the dispersal of a Rover core. Forty-six 1/3 and smaller scale shots have been fired to study (1) the effect of varying the size and type of explosive charge (2) the applicable scaling laws (3) the effect of the physical and mechanical properties of the fuel material (4) the effect of the geometrical configuration of the fuel (5) the effect of the case and reflector.

Based on present information, it is estimated that a full scale core could be fragmented for 100% HE into pieces in which less than 10% would exceed a radius of 1 centimeter. This may not by itself produce fragments with a sufficiently low radio-activity.

The use of rapid core heating as a destruct mechanism is under investigation. Initial experiments consisted of rapid resistance heating of fuel samples. Results from these studies indicated the "shelf type" fuel in which the uranium carbide has partially back reacted to the oxide can be shattered. Fully carbided fuel on the other hand could not be fragmented with almost double the energy deposition.

These experiments were continued in the Argonne Laboratories' TREAT Reactor Facility at Arco, Idaho, to more nearly simulate heating during a reactor transient excursion, to extend the temperature range, and to test the feasibility of self destruction. Pressures, temperatures, and the characteristics of the TREAT reactor pulse are observed. Rover fuel samples could be heated by this means to the vaporization point at 3350°C with up to 10% vaporization of the sample. Transient periods as short as 40 milliseconds are obtainable. Such transient testing verified the electrical heating experiments. Partially oxidized fuel could be fragmented into small pieces 1/8" in diameter or less by transients producing sample temperatures of 2000°C or higher. On the other hand, fully carbided fuel could be broken into large pieces only if the sample was partially vaporized. The fragmentation in the "shelf type" fuel is believed to be caused by the rapid conversion of uranium oxide to carbide accompanied by rapid internal pressure rise due to the formation of carbon dioxide. Breakup of the fully carbided fuel appears

to be due to the formation of internal vapor pressure.

Experiments to test the maximum removal of fission products by the use of afterheat have been carried out up to a temperature of 3200°C. At this temperature a maximum of 80% of the fission products could be removed in 5 minutes with little further gain expected by extending the time.

The use of UF_6 as a post operational additive was found to be remarkably effective in crumbling and disintegrating the fuel in 1 or 2 minutes. This process is most effective at low temperatures, however, and stops at 400°C. Its use is therefore questionable since the core would have to be precooled. BrF_3 is another potentially destructive additive under present investigation. Explosive reactions at high temperatures have been obtained between finely dispersed graphite and this material.

The promising fragmentation results produced by a rapid nuclear transient with partially carbided fuel has lead to the investigation of means of rapidly converting a fully carbided fuel, which is expected in a reactor after operation, to a partially oxidized condition. Investigations using CO or water vapor as a post operational additive look promising for achieving this objective.

Safe core disposal after operation by the use of one or more of the above methods now appears possible. Another area of investigation is a determination of the release of fission products due to nuclear accidents. Measurements have been carried out at all of the Kiwi reactor tests in Nevada to determine the total radiation release and dose rate during and following normal tests.

Experimental measurements have been made on the gamma decay dose rate from Kiwi B 1A. Since the accumulated fissions, 9.2×10^{20} , were obtained in about 1.5 minutes, the analogy

to an accident is good. The initial dose rate measured at 60 ft was 5.4×10^5 rad/hour. The decay during the first 100 minutes followed the relation $y = kt^{-1}$ and for the next 7 hours a $y = kt^{-1.85}$ law. Residual ground and test cell activation after reactor removal decayed with a 15 hour half life indicative of Na^{24} .

The following table of normalized values for total dose obtained from the Kiwi B 1A operation is compared with theoretical predictions for 10^{20} fissions.

Position	Gamma rads		Neutron rads		Total rad	
	Exp.	Theor.	Exp.	Theor.	Exp.	Theor.
2" from pressure shell	1.3×10^6		1.2×10^6			
100 ft	700	980	500	320	1200	1300
200 ft	170	220	120	69	290	290
100 yds	70	90	50	26	120	116
200 yds	14	17	9	4.2	23	21
400 yds	1.8	2.4	1	.42	2.8	2.8
800 yds	0.12	0.19	0.053	0.017	0.17	.21

The experimental mean free paths for gammas and neutrons were determined at this Kiwi test to be 300 and 260 yds. respectively. The sea level values used in the calculations were 350 yds. and 220 yds.

The principal biological hazard associated with the effluent from normal reactor tests is the release of a number of Iodine isotopes. This would presumably also be true for accidents. The majority of the activity appears as very small particulate matter or gas. Instrumentation is available at each test to determine the transient pulse shape and to measure the dispersal and release of any fission products in case of an accident.

The material shown in the film covers the period through the first part of this year. Work since then which has been

completed or is in progress at Los Alamos includes

1. The determination of the expected fuel life as a function of temperature when immersed in sea water.
2. The escape of fission products from fuel fragmented in sea water by a fast nuclear transient.
3. Calculations on the expected transient behavior of the new type Rover fuel. Experiments on this fuel are now in progress in the TREAT reactor.
4. Detailed planning for several full scale reactor experiments are in progress to determine:
 - a. The reactor response and shut down mechanisms to abnormal controlled excursions.
 - b. The feasibility of self destruction of a reactor with a fast nuclear transient.
 - c. The fission product dispersal and explosive yield due to a maximum credible type incident produced by means of a "Simulated Water Entry Test".

In conclusion, a few brief remarks on the new type of Rover fuel and its effect on the Rover Flight Safety program. A decision was recently reached to alter the composition of the fuel for both the Kiwi and Nerva reactors. Fuel used in previous Rover tests has made use of a mixture of very small UC_2 particles uniformly distributed in a graphite matrix. These particles are only two or three microns in diameter. Unless protected from air or water vapor as much as 20 to 30% of the particles will be in the form of UO_2 . The new type of fuel makes use of much larger UC_2 beads. These are 100 to 150 microns in diameter and covered with an additional 25 micron thick pyrolytic carbon layer. This coating, furthermore, has less than one tenth the conductivity of normal graphite. About 90% of the fission product energy is

lost in the new fuel particles themselves and the remainder in the pyrocarbon layer. In the old type fuel, on the other hand, over 90% of the energy can escape the fuel particles and be uniformly deposited in the graphite matrix. Fission product energy is deposited in only 3% of the core material instead of as previously in 100% of the core material. It is evident that this can have a profound effect on the mode of breakup of the fuel when subjected to a fast nuclear transient. Large temperature differences can be created between the fuel beads and the graphite matrix. The faster the transient the greater the temperature gradients will be. Fuel may now fragment due to temperature stresses, differential expansions, or vapor pressure created in the fuel particle itself or the carbon jacket.

Extensive experiments and calculations are in progress to obtain a complete understanding of the transient behavior of the beaded fuel and its potential as a self destruct mechanism for the reactor.

1. LA 2409 "Nuclear Safety Aspects of the Rover Program"
March 1960, G.A. Graves, P.S. Harris and W. H. Langham

X 66 50304

[U]

A Destruct System For the NERVA Engine

K. N. Kreyenhagen, W. H. Thiel, and S. K. Yoder

Aerojet-General Corporation

Abstract

50304

High explosives represent a promising source of energy, both for reducing the NERVA reactor core to sub-critical masses in the event of booster malfunction, and for disposing of the reactor after operation so that contamination will be prevented. Several design concepts are possible for the pre-operation requirement, including the use of linear explosive charges and shaped charges for cutting open the pressure hull and dispersing the core rods. The post-operational requirement is more difficult, since the 3000-pound core must be broken up into fragments of approximately one mm major dimension. Various concepts are being explored, utilizing external charges of explosive as well as charges which are propelled into the reactor prior to detonation. The feasibility of accomplishing the required fragmentation with reasonable masses of explosive is currently being determined. Experiments are also being performed to assess the physical and chemical changes which will occur in explosives when they are subjected to the radiation environment around the NERVA reactor.

Conf. R.D.

Author ↑

1. Introduction

A probable mode for accomplishing the destruction requirements for the NERVA engine is through the use of conventional high explosives. The energy density in explosives would appear to make it possible to design a relatively light weight system or systems, and the high reliability and rapid response time of explosive system add desirability to their employment. As part of the NERVA engine development, a program is being conducted to initially evaluate the feasibility of a high explosive destruct system. Assuming that such feasibility is established and an explosive mode for destruction is chosen, subsequent applied research and development will be undertaken.

2. Destruct System Requirements

Two separate requirements exist for the NERVA engine destruct system. One is for a system to render the reactor harmless in the event of malfunction

of the booster system prior to operation of the reactor. The second requirement is for a system to adequately dispose of the core fission products in a manner which will not cause unacceptable contamination in the event of reentry to the earth's surface. These requirements differ quite distinctly, such that two separate systems appear to be indicated. We call these a pre-operational, or anti-criticality system, and a post-operational, or perhaps more descriptively, disposal system.

In the event of failure of the booster system prior to reactor operation, the reactor core should be broken into pieces which are sub-critical even when immersed in a highly moderating water, hydrocarbon, or liquid hydrogen environment. This means that the core must be broken into pieces and distributed such that no critical masses form. Assuming a uniform distribution, no more than 0.205 grams of U_{235} can be distributed per square centimeter of water surface. This is equivalent to an approximate total mass of 750 grams of uranium within a 27-in. dia circle.

During operation the reactor produces a large inventory of fission products. To prevent unacceptable contamination of the earth's surface, the core must therefore be fragmented into pieces which will ablate down to 25 micron size by the time they reach 100,000-ft. level. Current investigations suggest that the characteristic dimension of graphite particles which will meet this criteria is approximately 1 mm.

Since the post-operational fragmentation criteria certainly encompasses the pre-operational dispersion requirement, it is appropriate to consider whether or not a single system might satisfactorily do both jobs. While such a combination would be desirable from the standpoint of design simplicity and weight, it appears that a double system is more appropriate. This conclusion is reached based upon the desirability for using a minimum explosion to accomplish the pre-operational destruction, so as to minimize the attendant risks from detonating a large quantity of explosive in proximity to the large booster fuel and oxidizer tanks.

3. Pre-Operational Destruct Concepts

The achievement of the pre-reactor operation destruct requirements appears to be within the existing bounds of high explosive technology. There are available, indeed, a multiplicity of concepts for accomplishing this task. We are currently involved in experiments to demonstrate the efficiency of these concepts, thus providing data upon which to base selection of the best concept, and upon which to commence preliminary design work.

Figure 1 shows one pre-operational destruct concept, consisting of a girdling array of linear shaped charges. Upon command, these charges cut through the reactor casing and the reflector segments, delivering an impulse to the core modules, thus dislodging, freeing, and scattering these modules. This is a simple and reliable basic concept, readily adaptable to the reactor and engine design. The explosives in the linear shaped charges are, of course, unable to withstand the thermal and radiation environment during reactor operation. Hence provision must be made for dismounting or discarding of the array of charges during starting of the reactor.

Figure 2 shows a second pre-operational destruct concept, consisting in this case of a single conical explosive shaped charge to be fired up into the core from its mounting in the nozzle. A hypervelocity jet of metal is ejected by such a shaped charge, which will impact and penetrate the core. This impact and penetration process will introduce a strong shock in the core material, which, if it is sufficiently strong, will break and dislodge the rods and cause rupture of the reactor casing, thus permitting escape or dispersion of the rods. While this concept is extremely simple and reliable, we are uncertain as to whether the shock produced in the core will be strong enough to break open the casing and free the fuel modules. Full-scale testing will be required to verify this concept. Its major advantage is light weight. Upon startup of the engine, of course, the shaped charge is discarded.

The girdling array of linear cutting charges and the nozzle-mounted shaped charge can be combined as an additional design. The linear charges are reduced to the minimum required to cut through or substantially weaken the reactor casing, thus assuring that the nozzle-mounted shaped charge can achieve scattering of the fuel modules. We have subjected this concept to preliminary full-scale testing, and have found that it performs adequately. Figure 3 shows the reactor mockup which was used for this experiment. The important components of the reactor were simulated, i.e. the pressure vessel by a steel rocket casing, the reflector segments by magnesium bars, the fuel modules by 3/4 in. dia stacked graphite rods. A discarded Titan nozzle was attached to the aft closure which, while it is much shorter than the NERVA nozzle nevertheless provides a throat diameter for the shaped charge jet to pass through which is nearly the same as on NERVA. The network of explosive girdling charges is seen in this photo. These charges contained Composition C-4 high explosive with a cross-sectional area of 4.5 square inches. Total weight in the girdling charge was 125 pounds. These charges were simultaneously initiated at six separate points. The conical shaped charge is seen mounted in a location which corresponds to the exit plane of the NERVA nozzle. This entire mockup weighed approximately 9000 pounds.

Figure 4 shows the test arena shortly after the explosive charges were detonated. It is possible among the scattered remains of the reactor to identify pieces of the casing, reflector bars, graphite rods, and test stand. The graphite was very effectively broken up, primarily into pieces 3 - 4 inches long and shorter. The largest pieces were approximately 12 inches long.

We believe that this test demonstrates the ability of this type of explosive system to break the reactor core into small pieces. If anything, the fuel modules were broken up more than is necessary or desirable. We look forward in subsequent experiments to substantially reducing the quantity of explosive used in the girdling charges.

4. Post-Operational Destruct Concepts

The achievement of the post-operational destruction of the reactor constitutes an extremely difficult physical task. A 3000 pound core of fuel-enriched graphite must be broken up into pieces with a maximum characteristic dimension of the order of 1 mm. This core consists of extruded fuel rods (either stacked hexagonal rods or round rods inserted in a structural graphite matrix)

each containing numerous small axial holes for propellant passage. Typical graphite sections between holes are 1/10-inch thick. Figure 5 is a cross-sectional schematic of the reactor. The core assembly is surrounded by pyrolytic graphite tiles, support tiles, a lateral support system, graphite reflector barrel, steel barrel, shim rods, coolant channels, tie bolts, beryllium reflectors containing control rods, and the aluminum pressure hull.

Fragmentation of the reactor by use of an explosive charge detonated within the core has been the concept for post-operational destruct which has received the largest amount of attention to date. In the paper by L. D. P. King from Los Alamos, the work at that Laboratory with such a central burster concept has been described. The scaled-down equivalent of 100 pounds of explosive was detonated in scale models of reactors. Based upon extrapolations of data obtained, it was concluded that a significant portion of the graphite core will break up into fragments with a characteristic dimension of 1 cm or greater. One surmises, however, that through use of multiple charges and a larger total mass of explosive, satisfactory fragmentation of the core can be obtained.

It is not possible, of course, to include large cylinders of explosives within the reactor core design, primarily because explosives cannot withstand such an intense radiation environment. Consideration has therefore been given to techniques by which explosives can be quickly moved into the core and detonated there. Figure 7 shows one concept to which we are giving current attention. The explosive is stored in long projectiles located in launcher tubes situated around the engine compartment behind the shield. Upon command, the projectiles are simultaneously accelerated by propellant charges, penetrating the shield and the core of the reactor. When the bodies of the explosive charges are within the reactor, the explosive is detonated. Supporting experiments are being conducted at the Aberdeen Proving Ground to evaluate this general concept. In initial experiments, gun projectiles were fired into a stack of solid graphite bars to study if the projectile could completely enter the stack without causing premature disintegration in the process. At an impact velocity of 1000 feet per second, it was shown that adequate penetration can readily be achieved without immediate disruption of the core.

The second series of experiments at Aberdeen will consist of firing explosive-loaded projectiles into full-scale reactor mockups. Discarded uranium-enriched fuel rods will be utilized for some of these experiments. Three previously emplaced explosive charges will be simultaneously detonated along with the injected projectile. The experiment is expected to provide clear knowledge of the effectiveness of the internal explosive charge system in a full-scale geometry.

Providing that the multiple internal explosive charge system works satisfactorily, we are then faced with the problems of designing guns or launchers which are both lightweight and reliable, and with achieving the required degree of simultaneity with respect to the arrival time of the multiple projectiles at the position for detonation. Relatively heavy weight appears unavoidable with this projectile injection system. If we assume, for example, that four charges of 30 pounds of explosive each are required, the parasitic weight is estimated as follows:

metal parts in projectile	85 pounds each
launcher, or gun barrel	140 pounds each
supporting structure,	140 pounds each

A total weight of nearly 1500 pounds is therefore estimated for the system, and this does not include control and power source circuitry.

Because of the high parasitic weight penalty for the projectile insert concept, and also because its feasibility in accomplishing the total fragmentation of the core is still in doubt, we are also exploring alternate concepts. One of these is shown in Figure 8. Multiple shaped charges are fired through the reflector into the core from all sides. These shaped charges consist of cylinders of explosive with a conical cavity in one end, this cavity being lined with metal. This cavity collapses under the pressure of the explosive detonation, ejecting a portion of the liner as a jet of metal particles traveling at velocities in the range of 25,000 - 30,000 feet per second. The effect of many such jets around the reactor periphery will cause not only the direct penetration of the core at many points, but also since the penetration occurs at extremely high velocities, intense shock waves will be introduced, causing additional fracture of the fuel rods by interaction with the coolant passages. The extent of such shock-induced fracture is unknown at present, but it will be evaluated in future full-scale tests.

One means for incorporating such a multiple shaped charge concept into the reactor and engine design is suggested in Figure 8. The shaped charges are stored behind the shielding and are translated on tracks or by mechanical linkages to their firing positions around the waist of the reactor.

It is worth noting that, while the effect of a single shaped charge will probably be relatively small, multiple charges may be expected to produce amplifying interactions. For the same 1500-pounds that is envisioned for the projectile insert concept which was previously described, an array of perhaps 100 or more conical shaped charges plus inert components can be employed.

A third concept for fragmenting the core material is by use of external crushing charges. These consist of slabs of explosive surrounding the reactor which, when detonated, implode on the core. Preliminary experiments with this concept have produced promising results. As with the multiple shaped charge concept, the explosive would be stored behind the shielding during reactor operations, and would be moved into proper position just prior to firing.

5. Radiation Damage to Explosives

Providing that realistic weights of high explosives can achieve the degree of fragmentation required to meet the post-operational destruct criteria, a second question must then be answered: can the explosive withstand the radiation flux surrounding the reactor?

The radiation field around the NERVA reactor will vary from total dose rates of 10^5 rad/sec around the sides to $10^3 - 10^4$ rad/sec behind the shield. With reactor operation of 1200 seconds, the total dose will therefore vary from $10^6 - 10^8$ rads ($10^8 - 10^{10}$ ergs/gm).

When an explosive is subjected to such an environment, it will, just as any material, be heated due to gamma absorption and inelastic scattering processes. When explosives are heated by any means they reach a temperature where the exothermic decomposition reaction releases energy at a rate which exceeds the rate at which energy escapes from the explosive mass. Self-heating, and eventually spontaneous and rapid decomposition and perhaps deflagration follow. The temperature at which this occurs is of course dependent upon the mass of the explosive, but typical temperatures are in the range of 150 - 200°C.

In addition to the indirect effects of thermal heating, explosives all appear to be directly degraded by reactor radiation, due apparently to bond breaking in the explosive molecules.

The energy threshold at which most explosives appear to be seriously degraded is in the range from $10^9 - 10^{10}$ ergs/gm. ($10^7 - 10^8$ rad). This degradation consists of significant decomposition as evidenced by gas evolution and porosity, plus a 10% reduction in heat of explosion. Direct application of these threshold values to the NERVA environment suggests that, at least behind the shield, high explosives could be safely, and perhaps reliably, employed. These rough threshold values, however, have been established as a result of studies made with explosives in radiation fluxes which are several orders of magnitude lower than are anticipated even behind the shield of the NERVA reactor. At the higher NERVA fluxes, some cooling of the explosive will clearly be necessary to avoid unacceptable heating. In addition, we must perform experiments to find whether or not the direct radiation effects are independent of the flux level.

In association with J. V. R. Kaufman of Picatinny Arsenal, we are planning to conduct four series of experiments aimed at clarifying several of the questions which remain concerning explosives in the NERVA environment, and which will provide data upon which to base shielding and coolant designs for the explosive system.

As an initial exploratory experiment, impact sensitivity measurements will be made on explosive samples which have been irradiated at the highest flux levels which are available. This will probably be 5×10^{13} nvt. These sensitivity measurements will serve to indicate either an unsafe increase in sensitivity or, conversely, a serious degradation, such that initiation becomes unreliable. Several explosives will be studied, including TNT, DATB, PETN, HMX, and perhaps a propellant material.

The second experiment is of a somewhat more fundamental nature, consisting of monitoring the temperature rise occurring in relatively large samples of explosives during irradiation. As mentioned earlier, radiation has two apparent effects on explosives -- the indirect damage due to heating, and the direct effect on molecular bonds. By monitoring the temperature rise, and comparing this with the temperature increase which can be expected on the basis of calculated energy deposition and conduction, we obtain a quantitative measure of the energy released by the explosive, both from thermal decomposition and radiation-induced chemical reactions. We hope to obtain from this difficult experiment a better understanding of radiation damage mechanisms in explosives.

Some experimental evidence is available suggesting that radiation damage thresholds are increased by reducing the explosive temperature. This possibility is very attractive to us, since a coolant system would be far lighter than massive shielding. To evaluate the effect of reduced temperature on the explosive, we are preparing a cryogenic experiment in which 80 gm. spheres of explosive are irradiated while being continuously cooled in a specially-cooled Helium environment to 100°K. Temperature rise in the explosive spheres will be monitored and compared with results at higher temperatures. From these experiments, we will hopefully confirm that reduced temperatures improve the usefulness of explosives, and further, will establish design conditions for a coolant system.

The final experiments will involve measurements of any changes which may occur in the energy threshold required for reliable initiation of explosives during and immediately following irradiation. Again this is a difficult experiment, since it involves attempts to deliberately initiate explosives while they are in or near a reactor, which is certainly not a very popular idea. It is necessary for us, however, to obtain the results of these experiments so as to know whether or not the explosives are reliably useful during and after irradiation.

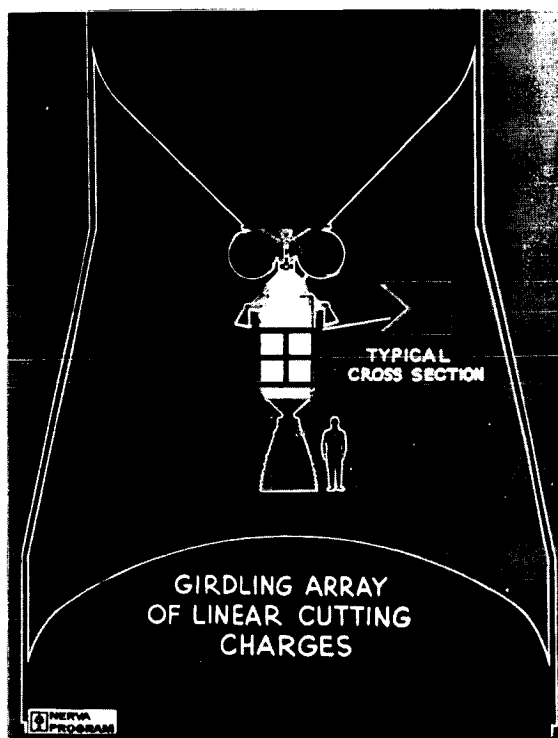


Figure 1

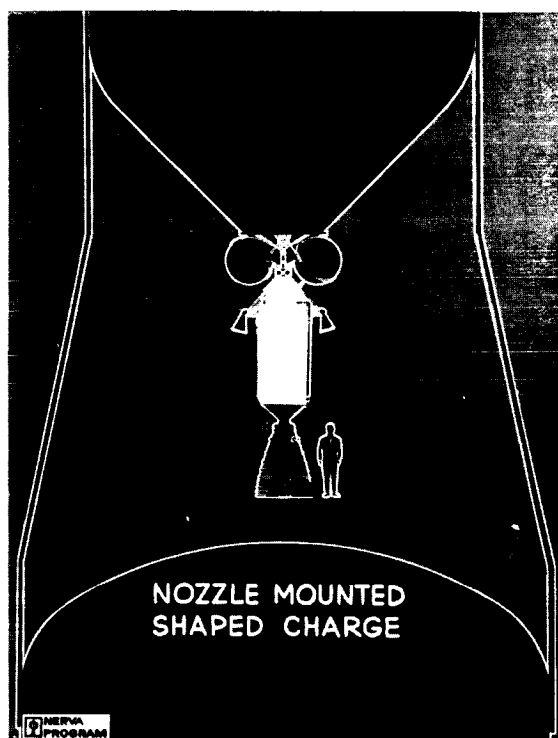


Figure 2

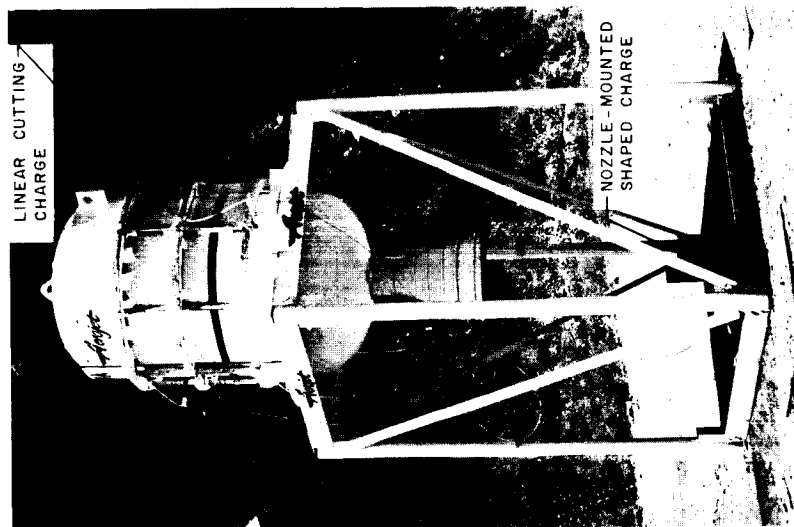


Figure 3. Simulated NERVA Reactor for Pre-Operational Destruct Concept Experiment.



Figure 4. Test Arena Following Experiment.

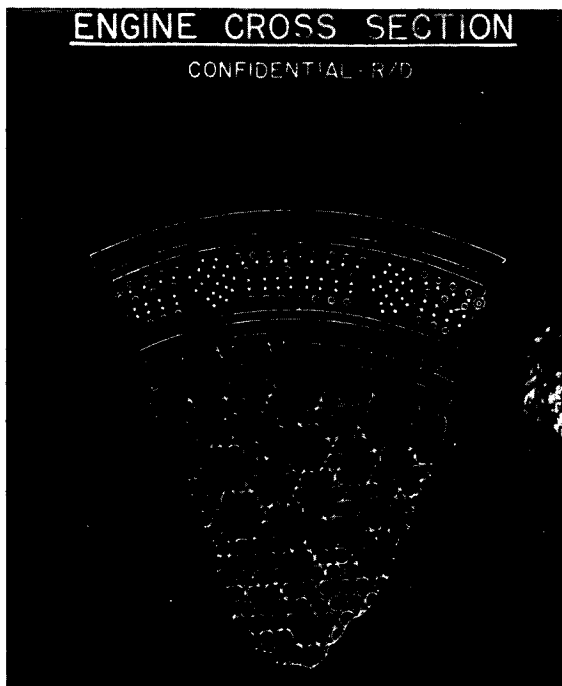


Figure 5

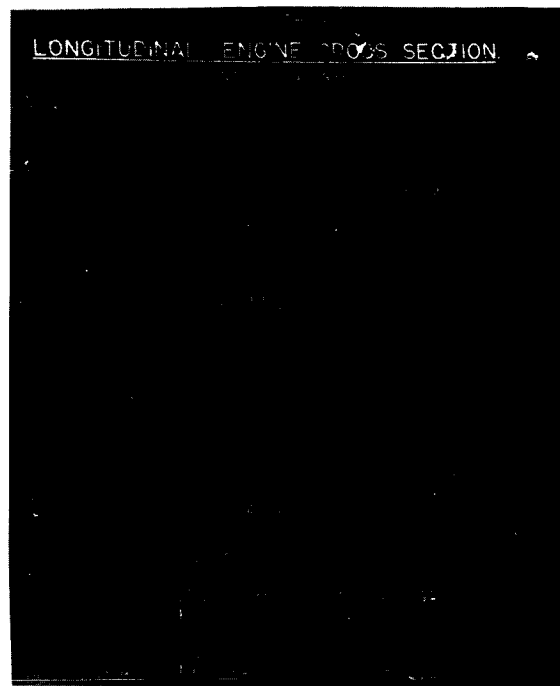


Figure 6

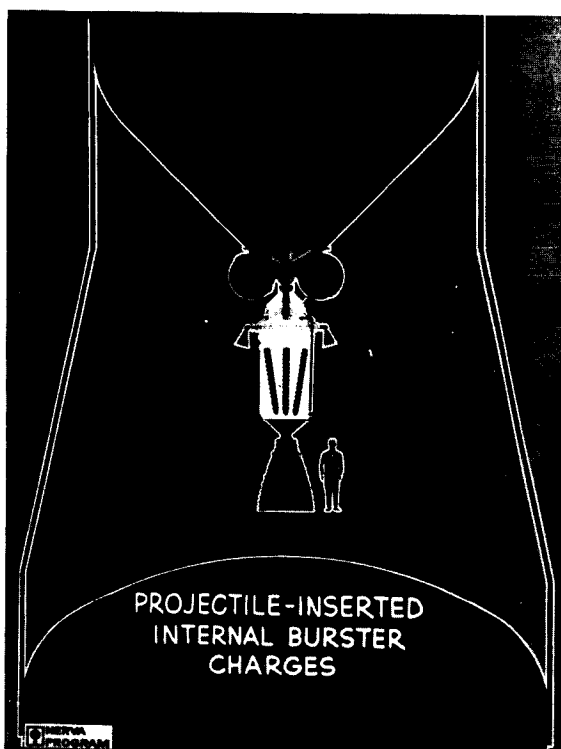


Figure 7

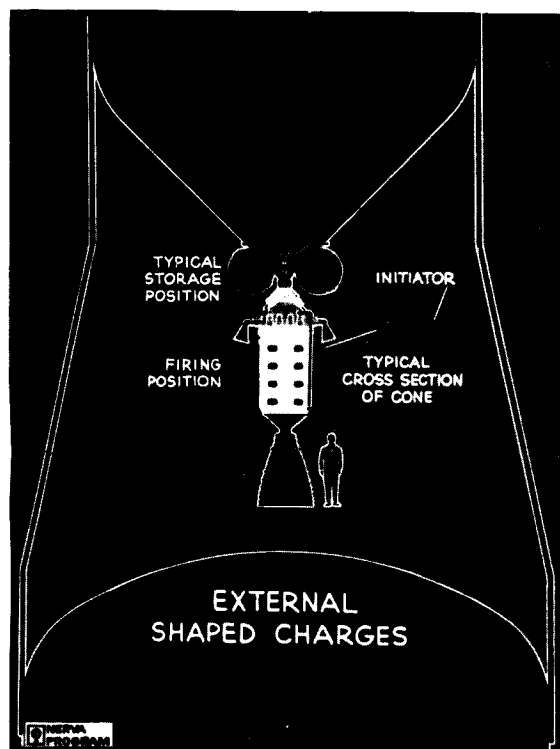


Figure 8

66 30305

E-MAD FACILITY DESIGN CONCEPT

[U]

Stanley K. Hellman
Vitro Engineering Co.

INTRODUCTION

The successful flight of a nuclear rocket requires test facilities to optimize engine and vehicle reliability and insure safety of the program. Paramount among the facilities in the static test complex is the nuclear rocket engine maintenance, assembly and disassembly (E-MAD) facility, which will be a part of the Nuclear Rocket Development Station (NRDS) at Jackass Flats (Fig. 1), an area within the Nevada Test Site. This facility (Fig. 2) will have the capability for assembly of new reactors and engines; disassembly of fired engines; maintenance of reactors and engines - before, after, or between firing sequences; and post mortem examination and testing of reactor and engine components.

It was obvious at the start that the development of criteria for this facility depended, to a large degree, on the definition of the NERVA engine, its configuration, and its handling characteristics. Since the engine program was in the initial development phase, close coordination with the NERVA engine industrial team was required. In addition, since much experience had been obtained at Los Alamos Scientific Laboratory in the testing and handling of the KIWI reactors and in the operation of the reactor (R-MAD) facility at NRDS, it was felt that the valuable technical information developed by LASL should be incorporated into Vitro's design. This permitted the development of initial facility concepts. After review of design criteria by all parties concerned, the facility concepts were presented by Vitro in a report.* This effort is being followed by detail design of the facility, an initial part of which has been completed. Construction work on this facility is presently underway, with partial occupancy expected during the latter part of 1963.

This presentation defines the design concept of the E-MAD Facility in terms of size, capability and operational characteristics.

DESIGN BASES AND FACILITY OPERATIONS

During the criteria development phase of the project, consideration was given to designing a facility capable of handling future generation engines, as well as the NERVA and Phoebus engines (the Phoebus engine is defined here as one that operates 4000 Mw with only a slight increase in size over NERVA). The largest engine originally contemplated for this facility was one which would operate at 16,000 Mw, being a scaleup in size from the NERVA-Phoebus unit. The resulting preliminary study indicated that to accommodate

*Engineering Study Report - "E-MAD Facility", KLX-1833 Vitro Eng. Co., Dec. 2, 1961

such a power level would result in a very high construction cost for this facility, not in line with the limited funds available. In addition, the study clearly indicated scaleup factors which were based on hypothesized data sufficiently indefinite to render the facility designed for the largest engine merely conjecture. In view of this, and on the basis that the Phoebus engine utilizes a reactor similar to NERVA, it was decided to limit the design of the E-MAD Facility to the size and power level of Phoebus.

In establishing the radiation levels for building design, it became obvious that a time interval between completion of firing (shutdown of engine) at the static test stand and return to the E-MAD hot bay would have to be established. Past studies on the engine had indicated that forced convection cooling for removal of decay heat is necessary up to 12 to 24 hr after firing to prevent overheating the engine. Consequently, it was assumed that after shutdown, the Phoebus engine would remain at the test stand 24 hr before being brought into the E-MAD Facility.

Studies of disassembly indicated a need for flexibility in facility design to accommodate the final procedures selected. Consequently it was felt that, with experience gained in operation, it might be desirable to bring the core through the hot bay to the core disassembly cell as soon as possible, although this could not be ascertained at the time the study was being made. Accordingly it was assumed that radiation levels throughout the hot bay portion of the building (up to and including the disassembly cells) could be based on the radiation level of the engine 24 hr after shutdown. Further, it was obvious that several days would be required to disassemble an engine. Therefore, it was reasonable to assume that small internal engine and core parts would reach the post mortem cells 2-1/2 days after shutdown. Thus ultimate storage of fuel modules in the fuel module storage area and of parts in the low level graveyard (outside of the E-MAD building) would not be accomplished for at least 5 days after shutdown. Consequently, radiation levels for subassemblies were derived with due consideration for these assumed decay periods.

Generally, the functions of the E-MAD Facility are to:

1. receive the completely assembled engine (minus the core) and critically safe complete core together with component engine parts and fuel modules
2. store unfired engines, cores and their components
3. inspect, checkout and assemble cores and engines with core
4. receive engines for maintenance and modification during test sequences or engines following test completion for disassembly, examination and disposal.

FACILITY DESCRIPTION

The NRDS is located within the northwest confines of the AEC Nevada Test Site (NTS), which is in a desert area, approximately 80 miles northwest of Las Vegas. This area of the NTS, designated as Jackass Flats, is reached via Road A and Road C (See Fig. 1).

The existing facilities, test cells A, C, R-MAD and CP Area, operated under the direction of LASL, are used for the development of reactors. The E-MAD Facility is directly west of the CP Area and south of Road H. It is

connected by railroad to the static engine test stands (Test Stands 1 and 2) which are almost directly north of E-MAD. Directly west of this area, toward 40 Mile Canyon, will be located a nuclear rocket stage static testing area which will eventually tie with E-MAD via a railroad track running east-west.

The components of the facility (Fig. 2) within the fenced area include: E-MAD building, the decontamination pad for the locomotive and rocket engine conveyor car, the warehouse, a substation, a water tank and stacks for heating and ventilation. The auxiliary facilities in the immediate vicinity (outside the fence) include the guard house, locomotive maintenance building, a sanitary waste tile field, low level burial site, fuel module storage area and a radioactive waste tile field. For the latter three auxiliaries, a sufficient exclusion area is fenced in for personnel protection. A new railroad Spur A runs from the E-MAD Facility to the existing Spur B which services the R-MAD area and test stands. In the vicinity of E-MAD, spur tracks from Spur A service the Locomotive Maintenance Building, the Cold Assembly Area, the Low Level Burial Site and Fuel Module Storage Area.

The E-MAD building is essentially a multistoried structure divided into six separated sections based on specific functions and personnel and material traffic flow. These sections (See Fig. 3) are as follows:

1. Hot Maintenance Assembly and Disassembly Area
2. Cold Assembly Area
3. High and Low Level Cells
4. Operating Galleries
5. Shop and Service Areas
6. Office Area

COLD ASSEMBLY AREA

The cold assembly area is divided by function into three sections, namely: the core and fuel module storage area, the engine receiving area, and the final engine assembly area. One of the basic premises in the design is that this area houses only cores and engines that have never been fired and are thus nonradioactive.

Fuel elements or whole cores enter the E-MAD Building via a door, in the south wall. It is anticipated that cores may be shipped assembled in sealed containers, adequately safeguarded to prevent criticality. Total floor space for this area is 84 ft by 72 ft, ample to provide storage space for the eventuality that fuel modules must be shipped individually or in groups, and then require core assembly in this area.

When cores are required for assembly in an engine, they are transferred to the final engine assembly area through a door on the north wall. This area is neutron monitored and provided with alarms to warn personnel of an incident.

The nonnuclear engine (engine minus core) enters on the east side of the E-MAD Building via the Engine Receiving Area. It is assumed that the engine is received in the horizontal position in a sealed container. The floor space, measuring 72 ft by 36 ft, is utilized for unpacking, and inspection, after the hardware has been unloaded onto a truck dock from a large trailer. Following uncrating and inspection, the engine is moved through a door in the north wall, into the final engine assembly area.

The engine is brought into the Final Engine Assembly Area and placed in the vertical position on a turntable. Depending on the final design of the engine and its assembly sequence, it can then be brought over to the other turntable (or the nozzle section removed and brought to this station) for installation of the core into the engine assembly. In order to provide flexibility for final assembly procedure (being developed at present by the engine contractor), adequate floor space (144 ft by 72 ft) is provided to accommodate jigs, fixtures, special tools, etc. In addition the clear bay height of the building is set at 53 ft to accommodate the engine in the vertical position, to allow passage of a 40 ton crane and to allow for a mockup station for final checkout before transfer to the test stand.

SHOP AREA

In order to assist in assembly operations, a machine shop and an instrumentation shop are located on the west side of the final engine assembly area (See Fig. 3). This layout permits easy access to the cold disassembly bay for minor hardware repairs, etc. In addition, access to the other side of the E-MAD Facility (operating gallery) is also provided in the event that cold parts must be modified and transported into the hot areas. Except for these passageways, normal access to Final Engine Assembly Area is through the Cold Change Room.

HOT MAINTENANCE, ASSEMBLY AND DISASSEMBLY AREA

The Hot Disassembly Area receives the radioactive engine after firing at the test stand. It consists of the Main Hot Bay, the Crane Maintenance Balcony, the Core and Engine Disassembly Cells and the Hot Hold and Transfer Tunnel. Normally, the locomotive backs the engine installation vehicle (with engine on it) into the Main Hot Bay where it can be either completely disassembled, or have a part replaced and transported back to the test stand for further static firing.

The main hot bay is a large shielded area approximately 66 ft wide, 146 ft long, and 77 ft high. The floor area permits dismantling engines through the use of jigs and fixtures utilizing the remote handling equipment, turntables and crane permanently installed in the bay. The railroad track, which permits easy transport of the engine and subassembly through the building is offset so as to permit the area on the west side of the track to be utilized as working area, and the area on the east side of the track to be utilized as lay-down area for major parts.

Among the major remote handling equipment in the bay is a newly developed overhead positioner and handling device capable of covering approximately all of the floor area and reaching a height of approximately 40 ft off the floor. This is a special development for this facility. In addition four specially developed side wall manipulators (two on the west wall and two on the east wall) together cover nearly all of the plan area in the bay. These units can reach a height of approximately 44 ft.

An operating gallery extends the entire length of both the east and west walls (and at higher levels) and partly around the south side and by the hold tunnel of the main bay. This gallery, which has numerous working stations (shielded viewing windows and master slave manipulators), provides the

flexibility for final disassembly sequences on the engine.

A completely shielded master control room is located, at the southwest corner of the main bay, above the first floor operating gallery. This room contains all of the instrumentation and communications necessary to direct operation of the complete facility including: 1) remote control and monitoring of the entire railroad layout, including the test stands; 2) override control of the major remote handling equipment, turntable, crane, etc. (operation of the equipment can be accomplished from selected working stations under permissive control from the master control room); 3) operation or override control of the main doors, such as the front door to the main bay through which the engine enters the building, the personnel access door on the northeast wall, the balcony doors and hold tunnel door for removal of the engine, core, or radioactive parts from the main bay; 4) monitoring and control of the facility air handling system; and 5) radiation instrumentation.

The balcony is located south of the main bay, with its floor at the third floor level and extends up to the top of the main bay elevation. Structurally it is contiguous with the main bay and extends across the entire south end. It extends in depth over approximately half the two disassembly cells and the hold tunnel. Its primary use is for maintenance of remote handling equipment, jigs and fixtures and for working on the core or other hot parts. Working stations with shielding windows and a master slave manipulator are located around the east, west, and south sides of the balcony.

South of the main bay is the hold tunnel, used primarily to store hot engines or to transfer hot cores and other hardware to the disassembly cells, on the east and west side of the tunnel. This transfer is accomplished through the assistance of an overhead crane, manipulator, turntable, and railroad tracks at grade level. Again, viewing windows in the cell provide work stations for remote work to be done in this area.

The two major disassembly cells are located south of the main bay on either side of the hold tunnel (east and west), and directly below the balcony. The west cell is defined as the core disassembly cell and is to be used primarily for disassembly and detailed examination of cores and modules through special equipment, including an overhead crane and manipulator, to be placed in the cell. In addition, numerous working stations at grade level (with shielding windows and master slave manipulators) are available to assist in accomplishing intricate operations. The east cell, engine disassembly cell, is used to perform close examination and further breakdown of the engine parts (non-fuel).

Directly to the south of the disassembly cells are the two banks of post mortem cells separated by an associated cell service area. These cells are utilized for detailed examination of small parts, radiography, small component testing, etc. In each bank, the cells are contiguous with common shield walls separating each cell. Steel doors are provided in the partition walls to permit passage from cell to cell and isolation of any particular cell.

The fuel module cells are directly south and adjacent to the core disassembly cell while the engine post mortem cells are directly south and adjacent to engine disassembly cell.

AUXILIARY SERVICE AREAS

There are auxiliary service areas in the basement and first floor. These areas accommodate the auxiliary electric power requirements, motor control and electric breaker center, waste handling tanks and pumping equipment, counting room, change room areas, etc. In addition two stacks (Fig. 2), approximately 115 ft high, are located outside and just north of the main bay. One stack handles the discharging air load from the main bay and balcony (actually the filter exhausts from the main bay below grade to the stack) while the second stack handles the cell area. Gamma monitors are located in the stack to detect high activity release due to possible filter failure.

SHIELDING CRITERIA

While the E-MAD facility will initially handle the NERVA engine, the shielding, in order to provide flexibility for future generation engines, has been designed for the Phoebus engine 24 hr after shutdown.

The shielding design of the facility is based on maintaining a dose rate which permits a man to work for 40 hr/wk, 8 hr/shift and receive no more than 100 mr in any weekly period.

The shielding design is based upon the criterion which assumes one engine test per week. It is assumed that the engine arrives at the E-MAD Building after its third successive full power run at its earliest possible time of arrival, 24 hr after shutdown. It is further assumed that a single individual is always in a position in a gallery which exposes him to the highest dose rate from the engine throughout a period of 40 hr week cited above.

Normal operating areas such as the galleries, the office and shop area, the cold bay, and outside the building are normally considered as unlimited access areas. However, at certain times personnel will be located in warm areas for less than 40 hr per week.

The shelter area is designed to protect personnel as the hot engine is transported from the test stand to the main disassembly area. The shielding for this area is designed to limit the maximum dose rate in the shelter to 25 mr/hr during the approach of an engine, at the moment when the dose rate in the shelter is greatest (just before the engine enters the main bay). This produces an integrated dose of 2 mr during the approach of an engine.

SOURCE DATA

The unshielded dose rate 10 ft from a bare Phoebus core, 24 hr after the third shutdown from a full power run is 124,547 r/hr. This dose rate includes the contributions from all energy groups and has been calculated from data supplied by the reactor subcontractor.

The engine consists of the core surrounded by a pressure vessel and reflector. There is a difference in the facility shielding required for handling the complete engine rather than the bare core because of the shielding effect of the pressure vessel, reflector and thermal shield. These engine parts serve to attenuate the radiation from the bare core by a factor of 3.8 if no other shielding is present. However, if in addition, a 5 ft concrete wall (biological shield) is interposed between the bare core and a dose point, the total

attenuation factor attributable to the reflector, thermal shield and pressure vessel is 2.9.

The radiation source level of the Phoebus engine 24 hr after shutdown as a function of distance from the engine has been calculated for 10 to 3,600 ft. The results, which include the effect of air attenuation, indicate that a distance of 3,500 ft is required to reduce the dose to 2.5 mr/hr.

In order to evaluate the integrated dose to meet the criteria that a man receive no more than 100 mr/wk in a series of five 8 hr shifts spaced 24 hr apart, the curves of gamma energy vs. time are integrated to determine the effect of the source strength decay.

This analysis shows that the dose through a 5 ft concrete wall is primarily due to the 1-2 mev and 2-3 mev groups. Based on the decay of these groups one can see that the radiation level drops by a factor of approximately 5, between 1 and 5 days post shutdown.

The dose in the control room is within unlimited access tolerance, because most of the front is protected by 5 ft thick concrete walls facing the inside of the main bay. A small section of 2 ft 6 in. thick wall facing the front of the building serves to extend the width of the control room. The west wall of this room is 18 in. thick; the rear wall is 1 ft thick. A 2 in. thick steel door is provided to attenuate the gammas streaming down the gallery, which might otherwise back-scatter into the control room.

In the gallery, the dose rate from the core through 5 ft of ordinary concrete at the centerplane of the core, is 48 mr/hr, with the core 10 ft from the dose point; through a 6 ft wall of ordinary concrete the instantaneous dose rate is 2.5 mr/hr. The ratio of the core dose rate to the engine dose rate, both shielded by a 5 ft concrete wall, without accounting for engine parts activation, is 2.9. Thus the dose rate due to the engine at 10 ft from the dose point through the 5 ft concrete wall 24 hr after shutdown is 16.5 mr/hr. The dose calculated by integrating the dose rate from the engine over a 40 hr week, is $16.5 \times 11 = 182$ mr/wk. However, because of the relative position of the engine, and its normal distance from the wall during disassembly sequences, an operator working in a gallery is exposed to a maximum of 100 mr/wk.

The sources from engine parts are due to the activation of aluminum and steel. When the core is in the engine, these parts then contribute to the total dose from the engine. It has been determined, by studying the various parts and their source spectrum, that the maximum contribution from the most radioactive part is 11.5 mr/wk.

The areas designed to shield (6 ft of concrete) an entire bare Phoebus core, 24 hr after shutdown include: the southwest portion of the main bay, the crane maintenance balcony, the core and engine disassembly cells and the engine hold tunnel.

The walls of the core and engine disassembly cells are also 6 ft thick. They attenuate the radiation from a Phoebus core, 24 hr after shutdown, to 2.5 mr/hr, with a core 4 ft from the inside surface of the cell walls.

The balcony is designed to hold a full core. Its walls are 6 ft thick from the floor to an upper elevation. Above this walls reduce in thickness up to the roof. The upper two wall thicknesses are reduced to 4 ft and 3 ft respectively to accommodate the crane rails. These thicknesses are adequate

because of the combined effects of slant penetration and distance attenuation, Fig. 4.

The total dose rate (direct and scatter) to a man in the gallery from a bare core in the balcony, 24 hr after shutdown, is approximately 5 mr/hr with the core 4 ft from a wall, and a maximum of 6 mr/hr with the core 22 ft from a wall.

RADIATION MONITORING

The philosophy used in radiation monitoring for the E-MAD Facility is to provide an adequate, integrated surveillance of the facility. The installed radiation monitoring for this building may be divided into three systems:

1. Neutron Monitoring System
2. Gamma Monitoring System for Process Areas
3. Gamma Monitoring System for Personnel Areas Adjacent to the Process Areas

Each core has a neutron monitor, which travels with the core as it moves about the facility. Remote record and alarm of the neutron count rate are provided. Fixed gamma detectors with remote readout are located in the process areas (main disassembly bay, crane maintenance balcony, hold tunnel, core disassembly cell and engine disassembly cell). Personnel areas adjacent to these process areas are provided with local gamma indication and alarm with individual remote alarm to indicate the trouble area to the health physics personnel. Portable gamma monitors are used to supplement the installed monitoring. Hand and foot counters are located at the personnel entrances to the process areas.

The health physics office is the center of all radiation monitoring operations for the E-MAD facility. For initial operations, this office has been temporarily located on the first floor of the east operating gallery, adjacent to the engine disassembly cell. In the final facility it will be relocated in the office area of the building. Instrument local panel Y1 is installed here. This panel contains the readout instrumentation for the neutron and gamma radiation monitoring systems, which consist of a 40-point annunciator assembly, a 20-channel gamma radiation recorder, the amplifiers for the process area detectors, two neutron recorders, and the patch panel for the neutron monitor connection boxes.

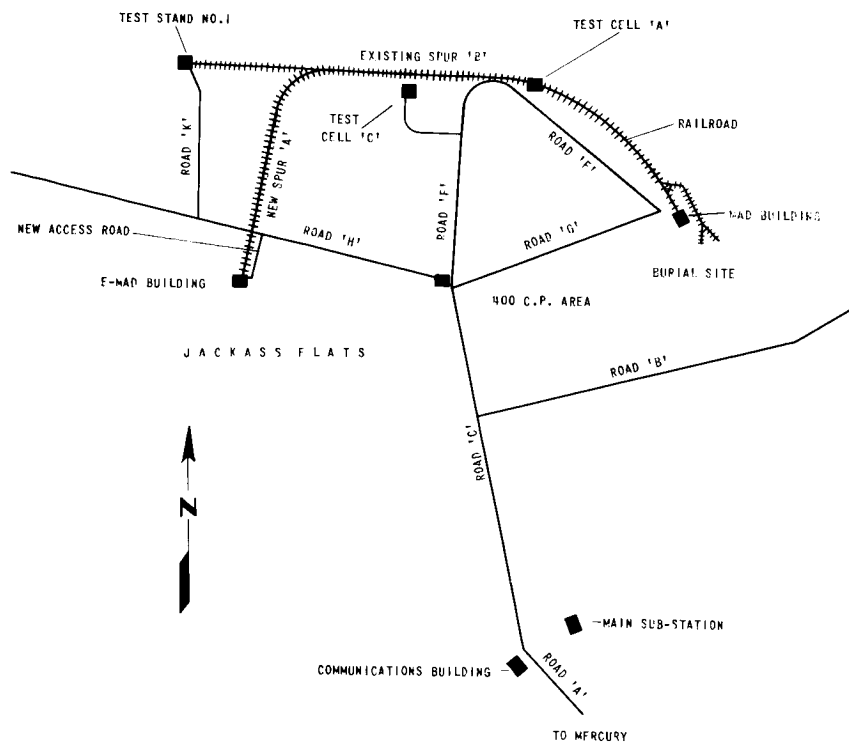


FIG. 1 E-MAD FACILITY AREA MAP

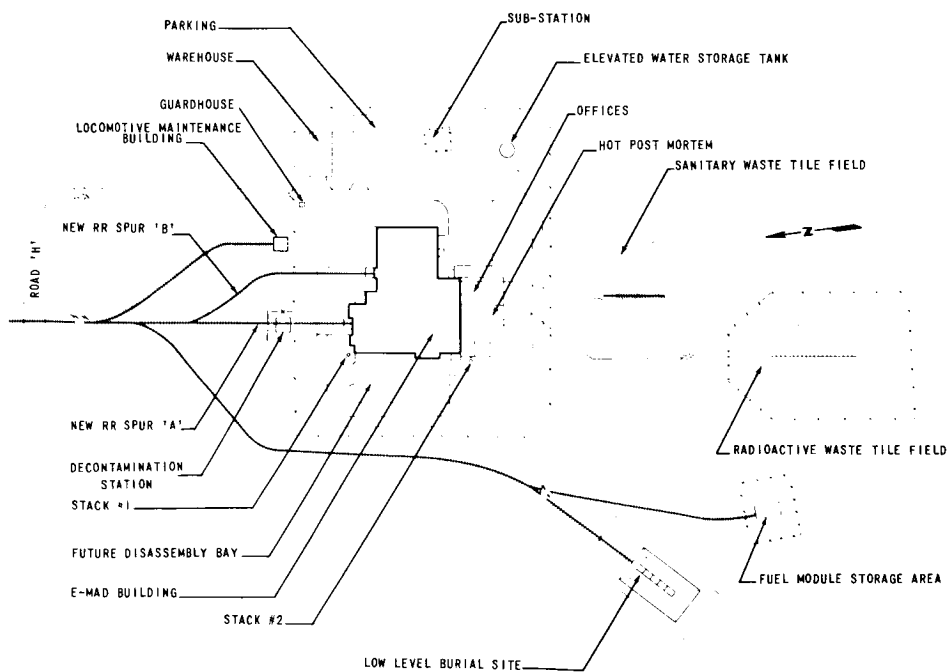


FIG. 2 E-MAD FACILITY PLOT PLAN

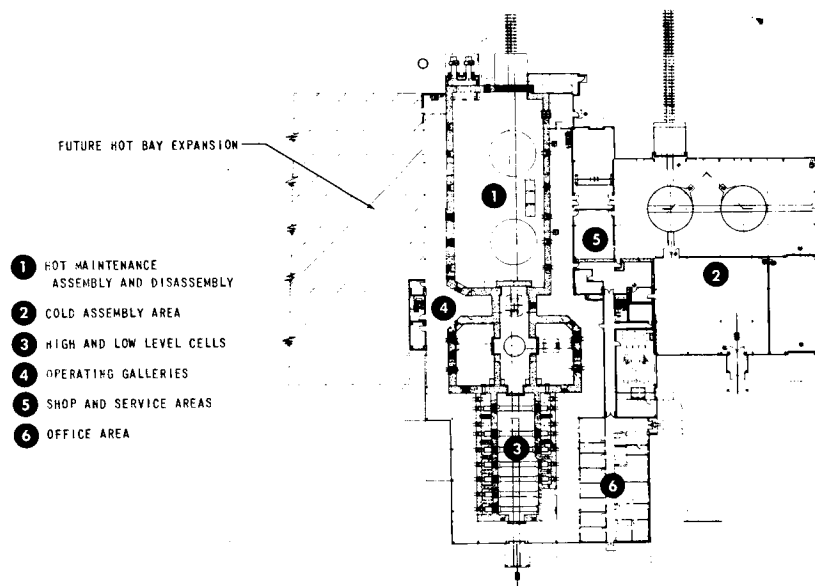


FIG. 3 E-MAD FACILITY FUNCTIONAL AREAS (1ST FLOOR PLAN VIEW)

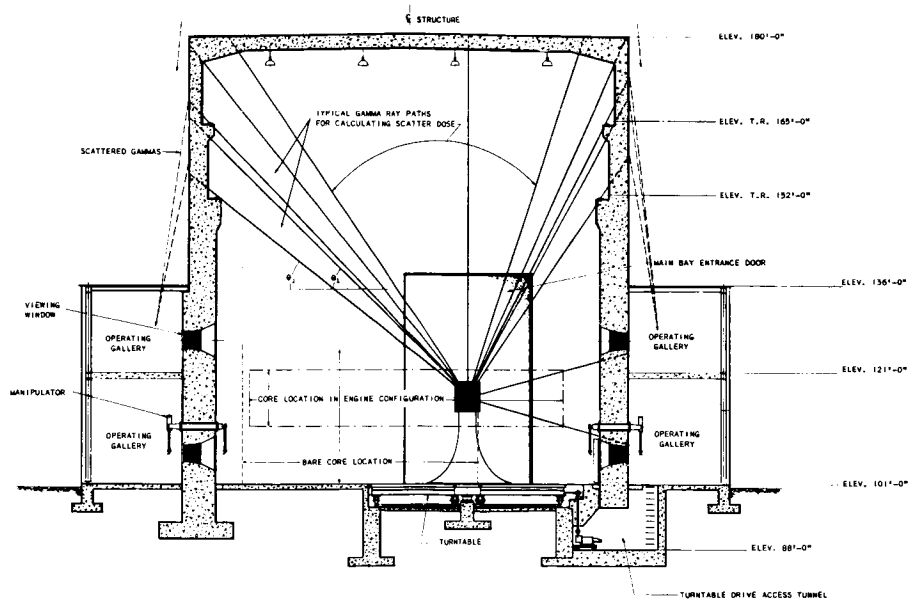


FIG. 4 TYPICAL PATHS OF DIRECT AND SCATTERED RADIATION

THE KIWI-B-1A FULL-POWER TEST*

D. W. Brown
University of California
Los Alamos Scientific Laboratory

and

S. Cerni
Westinghouse Electric Corporation
Astronuclear Laboratory

14
X 66 50306

Introduction

Kiwi-B-1A, the first in the Kiwi-B series of reactors to be designed and tested by the Los Alamos Scientific Laboratory as part of the Rover program, was operated at full power on December 7, 1961 at the Nevada Test Site. The test of this reactor, the only reactor in the Kiwi-B test series for which it is presently planned to use gaseous hydrogen as the coolant, was essentially a scaled-down version of subsequent reactor tests designed for liquid hydrogen operation.*

As originally planned, the reactor was to have been operated for 300 seconds at a nominal power level of 270 megawatts with a hydrogen flow rate of 20 lbs/second, the power level being automatically adjusted to maintain a core exit gas temperature of 4100°R. However, as a result of the intentional opening of the temperature control loop and a considerable calibration error in the linear neutronics system, the reactor only reached a power level of 225 megawatts with a measured flow rate of 20 lbs/second. Unfortunately, it was necessary to terminate the experiment soon after reaching the full-power plateau due to several large and potentially dangerous hydrogen fires near the nozzle flange area, the actual full power duration being only approximately 36 seconds.

Notwithstanding the brief duration of the full-power plateau at lower-than-design conditions, considerably more information was obtained from the Kiwi-B-1A test than from any previous Kiwi full-power test. Almost every core thermocouple functioned properly during the full-power run, providing information on the core thermal performance that had been previously all but unobtainable. The quality and amount of experimental information obtained from the highly-instrumented Kiwi-B-1A core would indicate that this experiment was quite successful, even though the test conditions were not fully achieved.

Description of Kiwi-B-1A

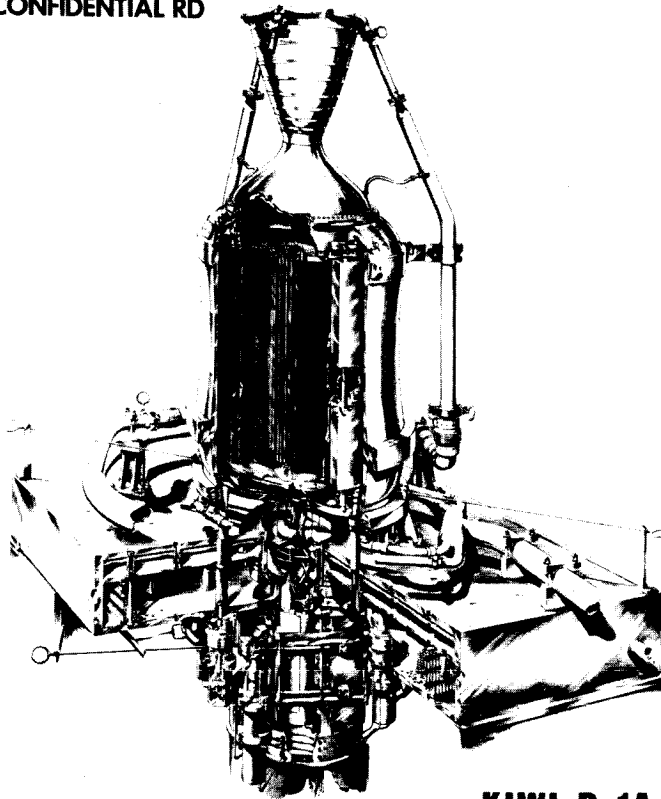
Figure 1 shows a sectioned view of the Kiwi-B-1A reactor. The hydrogen coolant, after entering a toroidal manifold around the base of the reactor, flowed up through three risers to the nozzle coolant inlet manifold (uppermost part of the drawing). The hydrogen then flowed down through the coolant passages of the tubular nozzle and the reflector system into the core inlet plenum. After reversing direction, the hydrogen flowed up through the core and was expelled through a conventionally-shaped rocket nozzle.

A cross-sectional view of the Kiwi-B-1A core and reflector system is shown in Figure 2. This core was of a cold-end-supported modular design with a length of 52.3 inches and a radius of 35.2 inches. The loaded graphite fuel elements were contained in modified hexagonal graphite modules which supported the fuel elements against the core pressure drop and provided additional moderation. The modules were in turn supported in tension from an aluminum plate at the inlet

*Work performed under AEC Contract W-7405-ENG 36 and AEC-NASA Contract SNP-1

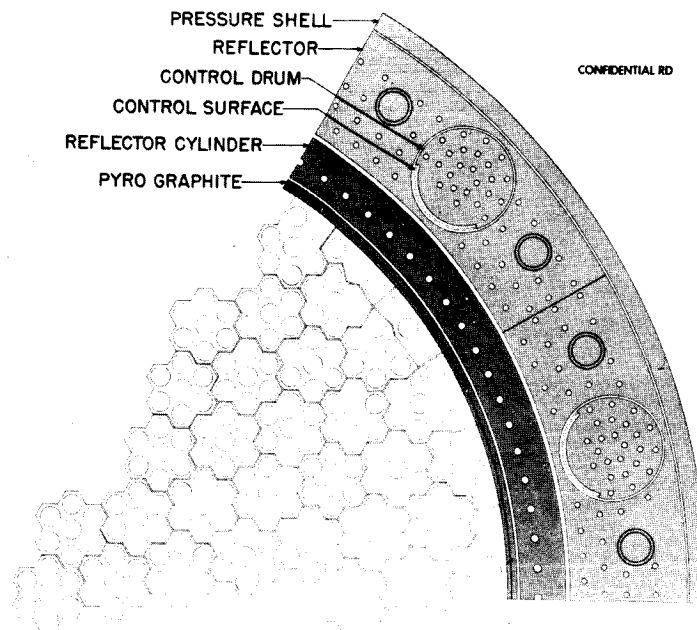
*For a more complete discussion, see LAMS-2708, "Final Report on the Kiwi-B-1A Full-Power Run", Donald W. Brown and Samuel Cerni, April 20, 1962.

CONFIDENTIAL RD



KIWI B-1A
CONFIDENTIAL RD

Figure 1. Sectioned View of Kiwi-B-1A



CONFIDENTIAL RD

Figure 2. Cross-Sectional View of Core and Reflector

end of the core. Each fuel element contained seven coolant passages (not shown) which were niobium carbide coated to prevent hydrogen corrosion.

The core was enclosed by the core sleeve assembly which separated and thermally insulated the core from the graphite reflector cylinder. The core sleeve assembly, comprised of an axially-segmented $\frac{1}{2}$ -inch-thick cylindrical ring of graphite surrounded by a 20-mil stainless steel wrapper, was held away from the core by rows of pyrographite tiles glued to the inner surface of the graphite ring. A thick concentric beryllium reflector, made up of twelve sectors, surrounded the graphite reflector. Each sector contained a rotary beryllium control drum with boral plates covering approximately one-third of the drum surface. The entire reactor was enclosed within a two-piece aluminum pressure shell.

Test Objectives and Abortive Runs

The primary objective of the Kiwi-B test series is to develop the basic reactor design for the NERVA nuclear rocket engine. As a result of this primary objective, the specific objectives of the Kiwi-B-1A full-power run were to obtain early design verifications on the following items:

1. The structural integrity of the cold-end-supported graphite modules.
2. Fuel element integrity.
3. Beryllium reflector and control vane system.
4. Graphite reflector system and pyrographite core insulation.
5. Regeneratively-cooled nozzle.
6. Closed-loop reactor control on measured exit gas temperature.
7. Core power and flow balancing.

In order to save several months in facility availability, it was decided to test Kiwi-B-1A with gaseous hydrogen rather than liquid hydrogen as originally planned, even though the reactor and nozzle had been designed for liquid hydrogen operation. Design studies indicated that the gaseous-cooled nozzle would perform adequately, but that the full-power level would have to be reduced from the design value of 1120 MW due to flow limitations arising both from flow choking in the nozzle coolant tubes and a limited test facility gas storage capacity.

The full-power test was originally scheduled for November 7, but was postponed after an unfortunate series of events during pre-test operations culminated in a hydrogen explosion within the shed covering the reactor. A subsequent reactor inspection revealed only minor damage to the core itself so after suitable repairs to the shed, the full-power run was again attempted on December 6. Soon after starting the full-power run, it was discovered that the majority of the core thermocouples were reversed, and in addition, the neutronic behavior of the reactor was in question. Therefore, the reactor was scrammed and the full-power run rescheduled for the next day.

The Kiwi-B-1A Full-Power Run

After the initial full power run conditions of 8 KW and a hydrogen flow rate of 1.7 lbs/second had been established, the reactor power was slowly increased to 10 MW in such a way as to increase the exit gas temperature at 25°R per second. With the low flow rate, this allowed the core to thermally expand against the core sleeve assembly, the integrity of which was in question as a result of the previous hydrogen explosion, particularly under large flow-induced pressure

differentials. Figures 3 and 4 on the following page show several of the major test parameters as measured during the Kiwi-B-1A full-power run. Soon after reaching the 100-second low-power hold, an error in demanded flow rate (specified flow rate was 2 lbs/second) in combination with the aforementioned neutronic power calibration error caused the temperature loop to reduce the power to 5 MW for the remainder of the hold. During the rise to the intermediate power hold of 165 MW and 15.9 lbs/second, one of the three exit gas temperature thermocouple channels became excessively noisy. Since the average of these three channels was used as an additional input to the power controller, the perturbation resulting from this noisy channel effected the control drum position demand signal, causing large control drum oscillations. An automatic rejection system had been specifically designed in anticipation of such a problem, but before the noise level of this thermocouple had increased enough to trip the reject circuitry, the temperature loop was opened to prevent further control drum oscillations and the resulting large power variations. From this point in the run, exit gas temperature became a dependent variable, being determined by the correctly-programmed flow rate and the pre-determined power profile, the latter being dependent on the 15 percent high neutronic power calibration in the absence of an overriding exit gas temperature feedback signal.

Following the 60-second intermediate-power hold, the power and flow rate were again increased to the full-power hold values of 225 MW and 20 lbs/second. The majority of the hydrogen fires first observed just prior to reaching this hold apparently resulted from hydrogen leaks at several circumferential locations around the nozzle flange area. These hydrogen leaks appear to have resulted from the combined effect of the differential-pressure-induced flexure of the pressure vessel at full flow, and the inability of the soft aluminum o-ring to seal the resulting gap between the nozzle and the pressure vessel. Twenty-four seconds after the full-power hold had been established, the reactor was shut down and flow switched to helium because of concern about the potential dangers of these hydrogen fires.

The average measured core exit gas temperature during the full-power hold was 3550°R, showing excellent agreement with the post-run computed value of 3530°R. The average computed hydrogen mass flow rate was 20 lbs/second, exactly as specified. On the basis of a reactor coolant heat balance, the average thermal power level during the full-power hold was 225 MW, only slightly greater than the post-run radiochemically-corrected neutronic power level of 220 MW (the best agreement ever obtained for a Kiwi reactor test). An essentially independent series of radiochemical power determinations produced an additional average full-power value of 225 MW. The ideal specific impulse during the full-power hold was 761 seconds as compared to a non-ideal value of 606 seconds, calculated on the basis of existing site conditions and using experimental data.

Core Temperature Distributions

The Kiwi-B-1A core was instrumented with approximately 280 thermocouples located at three axial stations: 8, 20 and 32 inches from the inlet end of the core. These thermocouples were not located in the fuel elements themselves but rather in the graphite modules. In addition, approximately 1000 thermal capsules were placed in longitudinal holes in the last 14 inches (exit end of the core) of selected modules. Post-run analysis of the reduced thermocouple data indicates that the core radial temperature distributions at the three above-mentioned axial stations were essentially uniform during the approximately steady-state operation at the intermediate- and full-power holds. Figure 5 is a plot of the core radial temperature profiles during the full-power hold.

However, two separate and distinct types of temperature irregularities were observed at or near the edge of the core. The first, and as yet unexplained temperature irregularity, existed near the edge of the core as measured by the station 8 thermocouples. In order to better understand the anomalous behavior

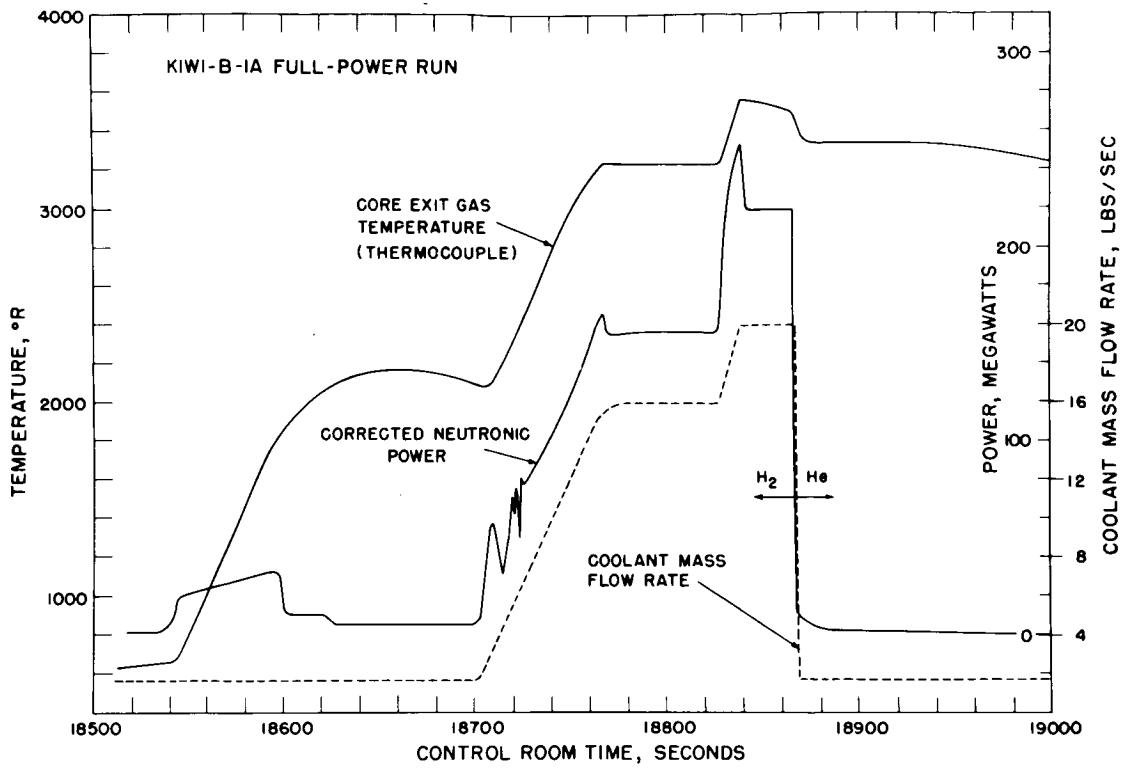


Figure 3

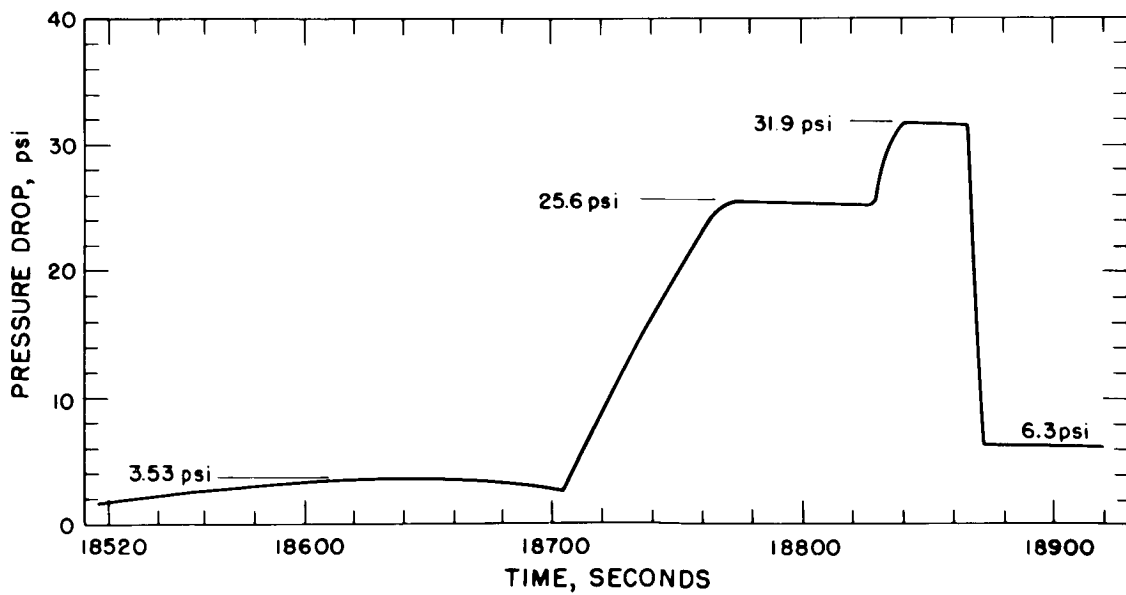


Figure 4. Core Pressure Drop

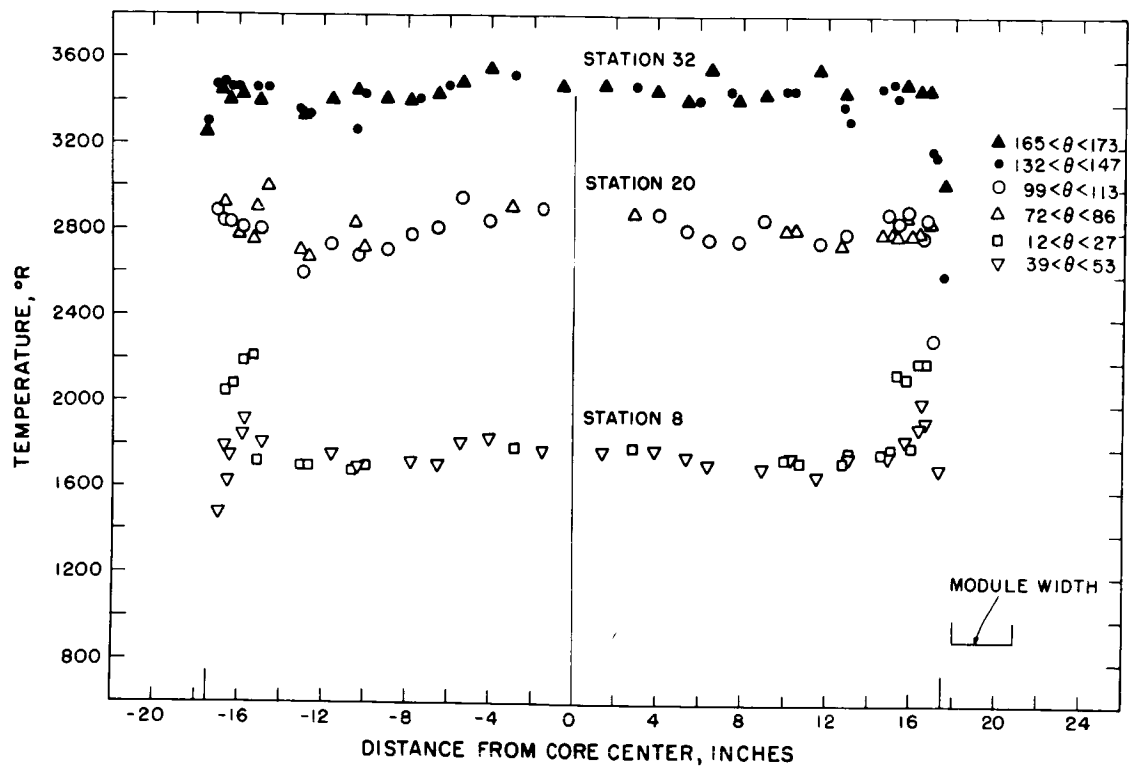


Figure 5. Radial Temperature Profiles During the Full-Power Hold

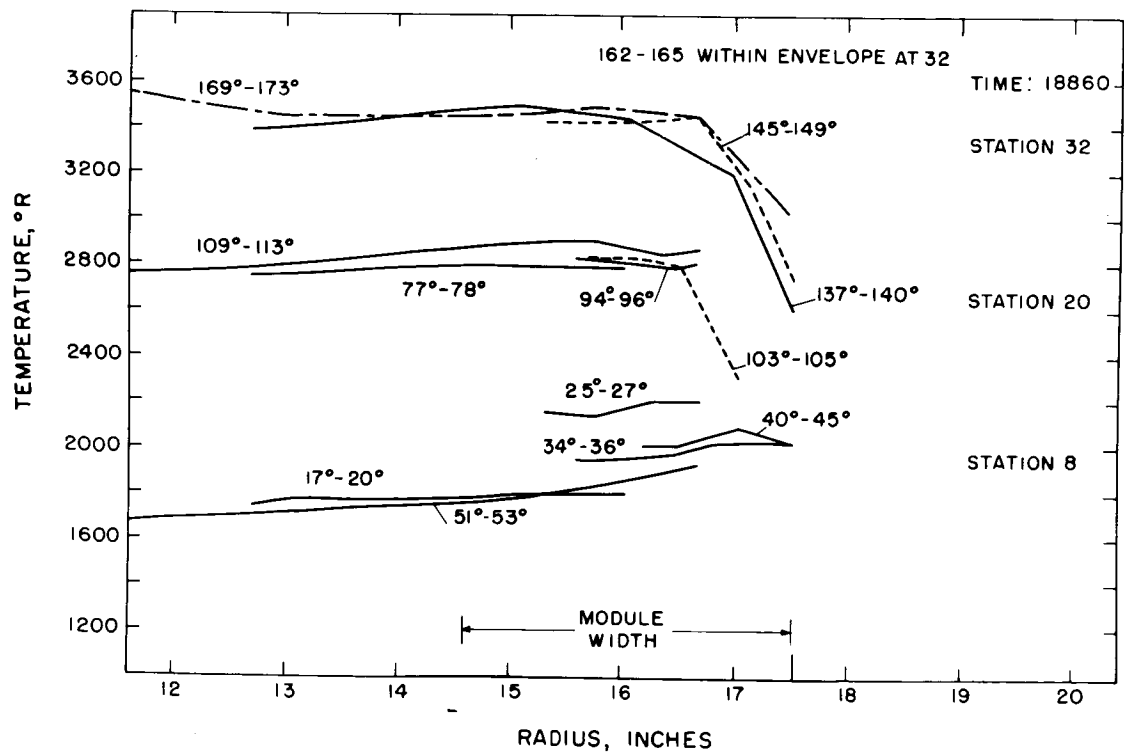


Figure 6. Radial Profiles for Different Azimuths and Stations During the Full-Power Hold

at station 8, the temperature distributions near the outer edge of the core are shown in considerable detail in Figure 6. In this figure, radial temperature profiles for each of the three core stations over a small angular band of less than 5 degrees, are shown at a time during the full-power hold. As can be seen, large temperature gradients ranging up to 400°R existed across several outer modules in an azimuthal direction. However, those large temperature gradients did not exist at either station 20 or station 32.

Bypass coolant flow at two nearby azimuthal locations between the core and the core sleeve assembly became pronounced during the rise to the intermediate-power hold, and persisted during the remainder of the full-power run. The existence of this bypass flow was verified, both by peripheral core thermocouple data at station 32 as shown in Figure 7, and by post-run core and core sleeve assembly visual inspection. During the rise to the intermediate-power hold, the hydrogen flow rate increased from 1.7 lbs/second to 15.9 lbs/second, with a resultant increase in the core pressure drop as shown in Figure 4. As the core pressure drop increased, so did the pressure difference between the outside and inside of the core sleeve assembly, tending to compress the core sleeve around the core. Because of restraints, perhaps caused by pyrographite tiles that had been dislodged and overlapped as a result of the hydrogen explosion mentioned earlier, the core sleeve assembly did not shrink uniformly around the core. Consequently, the bypass flow between the core and the core sleeve assembly preferentially channeled up a small portion of the core periphery, cooling this region of the core surface more markedly than the rest.

Axial temperature profiles at the center of the core were obtained for both the intermediate and full-power holds from core instrumentation at stations 8, 20, and 32 supplemented by thermal capsule temperature data beyond station 32 for the full-power hold. These data for the first time afforded a check on the model assumptions as well as the flow and heat transfer relationships incorporated in a LASL steady-state digital code. This code was used prior to core assembly to determine fuel element locations and flow orificing to produce an approximately uniform radial temperature distribution, as well as supplying axial and radial temperature distribution predictions for the full-power run. Since the test conditions were not achieved, the experimentally measured average mass flow rate, core pressure drop and coolant temperature rise for the intermediate and full-power holds were used as code inputs. The resulting computed axial temperature profiles show remarkable agreement with the experimentally determined profiles, providing a substantial verification of the analytical model. The computed profiles (solid and dashed lines) and the measured core axial temperatures are compared in Figure 8.

Kiwi-B-1A Post-Run Condition

The niobium-carbide-coated Kiwi-B-1A fuel elements all survived the full-power run with no blistering or other apparent damage except for one isolated pair which were found on post-run examination to have plugged center coolant passages. The anomalous behavior of these two fuel elements has been only partially explained, though it is evident that these two elements operated at a considerably higher temperature than neighboring fuel elements.

During post-run visual examination of the graphite core modules, all of which had experienced differential-pressure-induced tensile stresses during the full-power run, two large transverse cracks were discovered, one on each of two peripheral modules. In each case, the transverse crack extended almost half way around the module and was centered on the outermost module face (at the edge of the core). Axially, these two cracks were located at approximately station 41, corresponding to the hottest portion of the core during the full-power hold. Azimuthally, these two cracked peripheral modules were located on either side of the point of maximum bypass flow during the full-power hold and as a result,

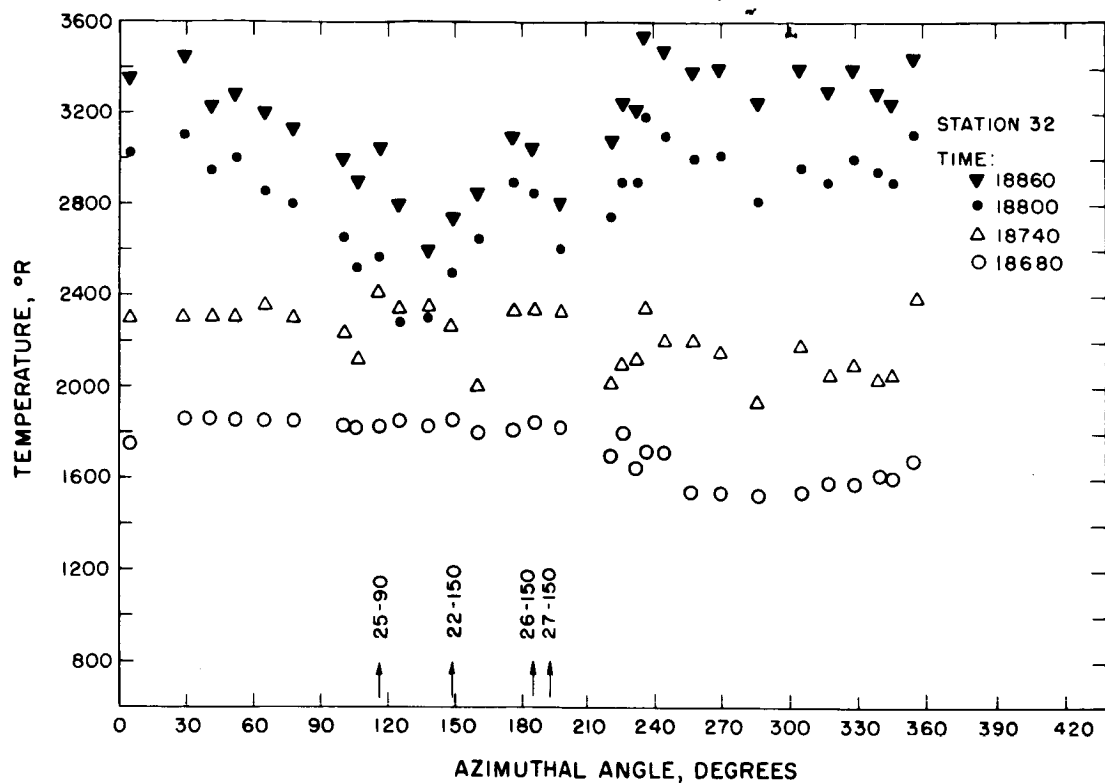


Figure 7. Peripheral Temperature Profiles at Several Times During the Full-Power Run

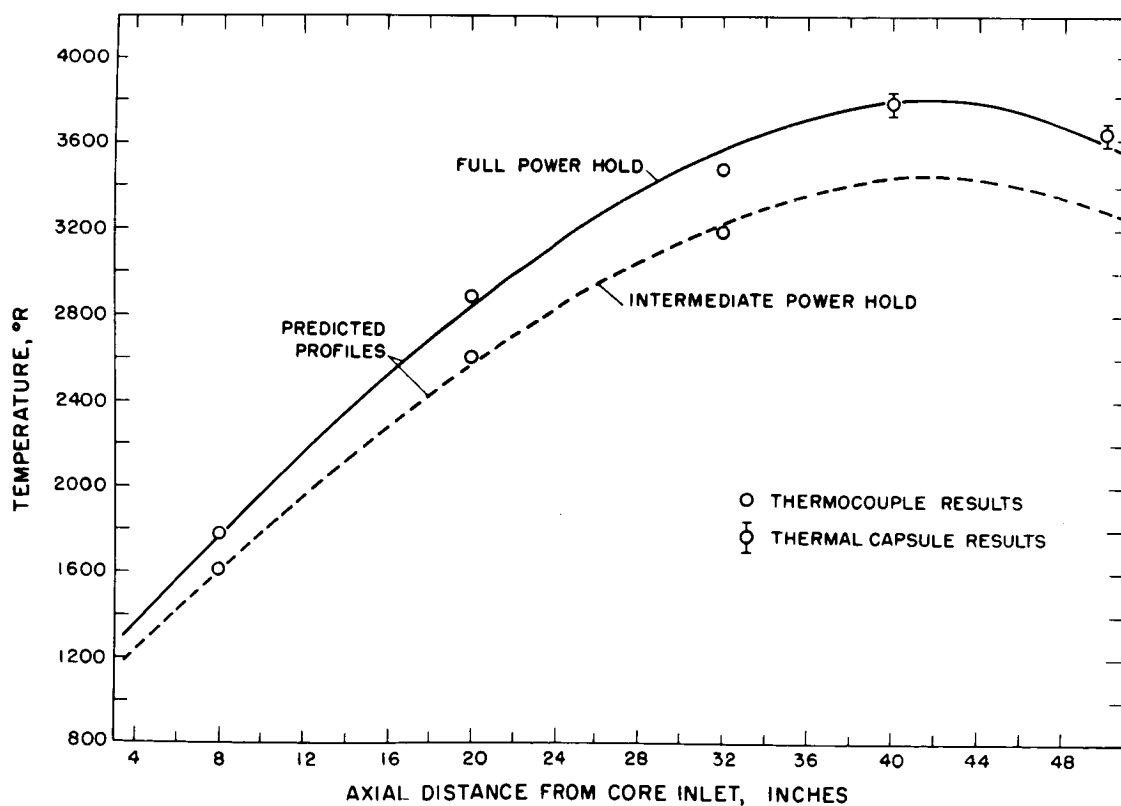


Figure 8. Axial Temperature Profiles for the Intermediate- and Full-Power Holds

exhibited quite large radial temperature gradients in excess of 1000°R . Figure 9 shows the transient temperature behavior of a peripheral module with coolant bypass flow. The upper curve shows the temperature behavior of the inner surface of this module. Two additional peripheral modules were found with large transverse cracks by post-run radiography. These two modules were located in the region of a smaller bypass flow. It has been concluded that these four modules were cracked by thermal stress due to the large radial temperature gradients which were the direct result of bypass flow.

Of all the reactor components, the core sleeve assembly sustained the most damage. Post-run examination of the sleeve showed many permanent longitudinal wrinkles in the stainless steel wrapper. In addition, evidence of overheating of this wrapper was found near the core exit end. The intermediate graphite section was very badly cracked to the extent that large pieces were completely severed. Approximately 50 pyrographite tiles which had been glued to the inner surface of the graphite to provide core thermal insulation were loose and about 10 tiles had been dislodged and were out of their proper locations during the run. It appears that the non-uniform circumferential shrinkage and wrinkling of the core sleeve assembly along with local restraint due to dislodged pyrographite tiles was responsible for the observed bypass flow.

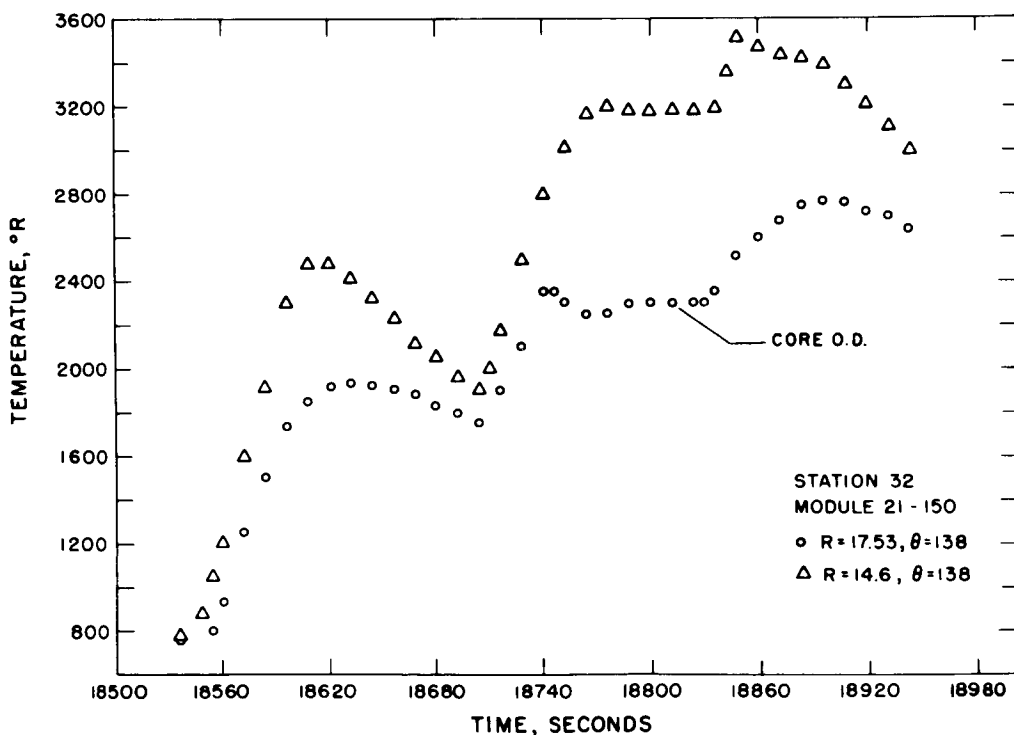


Figure 9. Transient Temperature Behavior of a Peripheral Module with Coolant Bypass Flow

X 66 50307

KIWI-B-1A TEMPERATURE-REACTIVITY EFFECTS* [U]

H. B. Demuth, C. E. Stiles and J. E. Perry, Jr.
Los Alamos Scientific Laboratory

I. INTRODUCTION

The nuclear propulsion reactor Kiwi-B-1A exhibited peculiar temperature-reactivity variations during its final runs in Nevada. An analysis of the unusual effects was made by reconstructing the runs on an analog computer model of the reactor system. The Nevada data on reactor power, hydrogen flow rate, control rod positions, and exit gas temperature were used as input data and the analog model was used to decompose reactivity into its various separable components.

This paper reviews the reactor phenomena, the methods of the investigation, and its results.

II. EXPERIMENTAL PHENOMENA

Various anomalous static and dynamic reactivity phenomena were observed in Kiwi-B-1A. When it was first assembled at Los Alamos, cold delayed critical operation was observed with the control rods extracted \$6.60. Upon reassembly at the Nevada Test Site, the reactor had gained about 80¢ in reactivity. It was conjectured that the core components were more closely packed, or that the fuel elements had adsorbed hydrogen as products of hydrolysis of UC_2 .

In the first low-power runs, when the core temperature rose only about 100° F, abnormally large control rod motions were required to overcome an apparently large negative temperature coefficient. Temperature data were meager, so that no definite conclusions could be reached.

In Experimental Plan 6, the first attempt at a full-power run, the control rods moved out about \$1 more than had been expected in raising the exit gas temperature from ambient to 2000° R. This unanticipated rod motion led to aborting the run. Subsequent cold critical operation showed that the reactor lost about \$1.70 of reactivity. In the post-mortem, it was decided that if things got no worse, it probably would be possible to achieve design power and temperature.

In the final full-power run, Experimental Plan 6A, design conditions were nearly reached. The exit gas temperature was 3550° R instead of the 4100° R desired, due to an error in neutronic power measurement. The control rods were 98.5% retracted, but otherwise had shown no untoward behavior. A subsequent cold critical check showed a nominal loss of 10¢ of reactivity during the run.

* Work performed under AEC Contract W-7405-ENG. 36.

III. TEMPERATURE-REACTIVITY INVESTIGATION

Because of the unusual reactivity effects noted above, it was decided to try to unscramble thermal reactivity effects during Experimental Plans 6 and 6A. This study would serve the dual purpose of possibly explaining the temperature effects and checking the validity of the analog computer model used prior to the run for the design of automatic control loops and power-flow-temperature profiles¹.

In the reactivity study, the following equation was used:

$$\delta k \text{ TEMP} = \delta k \text{ EXCESS} - \delta k \text{ RODS} - \delta k \text{ SHUTDOWN} - \delta k H_2 \quad (\text{Eq.1})$$

Here $\delta k \text{ EXCESS}$ is the reactivity required to produce the power profile observed during the run. It is the amount of reactivity by which the reactor is supercritical at any time. The $\delta k \text{ RODS}$ is the positive reactivity given to the reactor as the rods are withdrawn. It is defined to be \$0 when the rods are fully inserted. The $\delta k \text{ SHUTDOWN}$ is the rod worth extracted to achieve cold delayed critical operation at 40 kw in Experimental Plan 6. In all of what follows,

$$\delta k \text{ SHUTDOWN} = \$5.70.$$

The $\delta k H_2$ is the positive reactivity of the hydrogen coolant gas in the reactor. Finally, $\delta k \text{ TEMP}$, the quantity calculated in Eq. 1, is the reactivity presumed to be due to all effects caused by changes in core temperature.

Several temperature effects are possible: (1) core thermal expansion; (2) changes in neutron interaction cross sections; and (3) loss of adsorbed hydrogen from the core. From the outset it was clear that if two or more of the phenomena occurred simultaneously, it might not be possible to resolve their effects. However, it was felt that comparison of $\delta k \text{ TEMP}$ with other quantities measured during the run might produce useful insight into reactor behavior.

The various components of Eq. 1 were obtained as functions of time during the runs in the following ways:

A. $\delta k \text{ EXCESS}$

The measured power profiles were fed as a demand into a closed reactor power loop which included the reactor neutron kinetic equations. The analog computer then calculated that variation of reactivity required to produce the observed power profiles.

B. $\delta k \text{ RODS}$

Control rod positions were recorded during the experimental runs; and the rod reactivity was computed from the position data and from pre-run rod worth calibrations performed by LASL Group N-2.

C. $\delta k \text{ SHUTDOWN}$

As noted previously, this was determined directly in Experimental Plan 6.

D. $\delta k H_2$

This component was the smallest (maximum of 35¢), but involved the most detailed calculations. The observed profiles of power and hydrogen flow were fed into the analog computer, and slight adjustments made in power until

the observed experimental core and outlet gas temperature profiles were produced. Hydrogen density was calculated from average core temperature and gas pressures. The total hydrogen in the core was multiplied by reactivity weighting functions to yield hydrogen reactivity.

Certain facts should be noted before giving the results of the study. The δk EXCESS, as calculated here, agreed to within a few cents with that derived by two independent methods, one digital and one analog, used by T. E. Springer and J. D. Balcomb, respectively. The slight adjustments in power profile mentioned above did not influence δk EXCESS by more than about 2¢. Some small errors in the core heat transfer model were discovered during the study. When these were corrected, calculated core temperatures, both transient and steady state, agreed quite closely with thermocouple readings recorded during the runs, and with other values calculated digitally². Average core temperatures for Experimental Plans 6 and 6A were computed from the calculated temperature of the individual core segments in the analog model, and from their known masses. The average core temperature has an estimated standard error of 5% of the temperature rise above ambient. The quantity δk TEMP is derived through a multiple subtraction process; and it has an estimated standard error of about 20¢. It was possible to register curves to within ± 2 sec in time before performing the calculations required to obtain δk TEMP.

IV. RESULTS

The results of the study are given in Figs. 1, 2, and 3.

Figure 1 shows profiles of power, flow exit gas temperature, average core temperature, and the various reactivity components for Experimental Plan 6. The large discrepancy between a linear temperature reactivity, calculated from a constant $-65\text{¢}/1000^\circ\text{R}$,* and the actual temperature reactivity obtained in this study is especially interesting. Note also the permanent loss of about \$1.70 during the run.

Similar data for the final power run (Experimental Plan 6A) are presented in Fig. 2. The violent rod position and power fluctuations just after 8700 sec occurred when an exit gas thermocouple became noisy and gave poor feedback signals to the exit gas temperature control system. It is apparent from the figure that δk TEMP was relatively linear in Experimental Plan 6A. The smoothness of the δk TEMP curve indicates that the various profiles must have been registered in time to about ± 1 sec. Prior to Experimental Plans 6 and 6A, a temperature coefficient of $(-50\text{¢} \pm 25\text{¢})/1000^\circ\text{R}$ was used in the analog computations. The value $(-65\text{¢} \pm 10\text{¢})/1000^\circ\text{R}$ derived from Experimental Plan 6A data is within the anticipated range.

In Fig. 3, δk TEMP is plotted versus average core temperature for both experimental runs. Here, the over-all temperature-reactivity behavior of the core is shown directly. The progress of time during runs is indicated by arrow-heads. It is believed that the sharp variations in Fig. 3 are not caused by displacement in time of the various profiles. Possible explanations for these variations are being investigated³.

V. DISCUSSION

Several temperature effects appear to have contributed to the complex pattern shown in Fig. 3.

* All temperature-reactivities refer to reactivity changes due to changes in average core temperature.

The \$1.70 loss between the beginning and end of Plan 6 (points A and F) is attributed largely to the loss of hydrogen adsorbed in the reactor fuel⁴, but may be due in part to irreversible deformation of the core structure. Subsequent experiments** have shown that water vapor is adsorbed by uranium-graphite fuel, the amount of water being dependent on the humidity of the atmosphere in which the fuel is stored and the length of storage. Quantitative analyses have shown the presence of enough hydrogen in typical cases to create a reactivity of the order of \$1 to \$2. In the adsorption process UC_2 hydrolyzes to form UO_2 plus hydrocarbons. Additional controlled heating experiments have indicated that the temperature-time history of Plan 6 was sufficient to drive off essentially all of the hydrocarbons. Indeed, no further significant loss was noted in Plan 6A.

A recent attempt has been made to calculate the loss of reactivity caused by core expansion and the change of neutron cross sections with temperature in an unpoisoned Kiwi-B-1 reactor⁵. The result is a larger average coefficient ($-\$1.0 \pm \$0.2/1000^\circ R$) than that found in Plan 6A. The calculated curve is essentially linear, whereas the trend observed in Plan 6A between points F and J of Fig. 3 is generally concave downward. The presence of control drum absorber materials in the reflector may mean that the reactivity-temperature curve will be a function of control drum angle, an effect which may be investigated in the future.

VI. CONCLUSIONS

Despite the fact that it was not possible to separate the effects of core deformation from those of adsorbed hydrogen in Experimental Plan 6, and despite the fact that it is not now possible to explain all the detailed meanderings in Fig. 3, the general technique of decomposing reactivity into its separable components has provided considerable insight into the operation of Kiwi-B-1A.

It is planned to use similar analog computation techniques to study reactivity variations during the actual operation of future Kiwi-B reactors. In these reactors the use of liquid hydrogen will give rise to a large propellant reactivity. With this added complication direct interpretation of the reactivity decomposition results will become more difficult, but understanding of the runs will be virtually impossible without such a decomposition. It is hoped that an "on-line" reactivity computer will provide on-the-spot diagnostic information in the case of aborted runs or nuclear excursions.

ACKNOWLEDGEMENTS

We are indebted to D. W. Brown for supplying the best profiles of reactor power and flow rate, to T. E. Springer for devising a method of converting the original Nevada digital power data into usable analog form, and to Mrs. Shirley Cashwell for reducing and plotting test data and analog re-run data. We wish to thank J. D. Rogers for discussions of the hydrogen adsorption phenomena.

REFERENCES

1. Equations for the model are given in R. R. Mohler and J. E. Perry, Jr., Nucleonics 19, No. 4, 80(1961), and in C. E. Stiles, "Interaction of Liquid Hydrogen with the Kiwi-B Reactor", Los Alamos Scientific Laboratory report,

** The water adsorption and heating experiments were carried out by LASL Group N-1, while the quantitative analyses were performed by LASL Group CMB-1.

LAMS-2648, Confidential, Restricted Data, unpublished (1962). Use of the analog model is discussed in the paper, "Kiwi-B-1A Power and Temperature Control Systems", by E. A. Brown, H. B. Demuth, P. B. Erickson, R. R. Mohler, S. J. Singer, and C. E. Stiles, published in this compendium.

2. Steady-state digital temperature calculations were made by O. A. Farmer using the KIB code and by J. A. McClary using the BGT code. Transient digital temperature calculations were made with the HEX code by J. D. Balcomb. For a description of the HEX code, see "Startup Studies of a Nuclear Rocket Reactor, Part 1, Computational Procedures and Experimental Checks", by R. S. Thurston and R. Pollock, published in this compendium.
3. It may be that k^* or other reactor "constants" vary significantly with core temperature. This possibility is being investigated by C. B. Mills and E. A. Plassman, Los Alamos Scientific Laboratory.
4. Private communication from J. D. Rogers, Los Alamos Scientific Laboratory.
5. Private communication from A. W. Chermatz, Los Alamos Scientific Laboratory.

POSTSCRIPT

Kiwi-B-1B, the first liquid-hydrogen-cooled reactor, was operated successfully on September 1, 1962. Design hydrogen flow of 65 ± 5 lb/sec was achieved for some 75 seconds, and a reactor power of about 950 MW was held briefly. Loss of some core material forced the control rods to go fully out, after which power decreased and the reactor operated quite smoothly on a balance between hydrogen and temperature reactivities. Despite careful attempts to keep moist air away from the fuel elements, there appears to have been about \$1 of adsorbed hydrogen which was driven off during the run. A reactivity decomposition of the general type discussed in this paper is in progress, and is indeed providing much insight into the reactor operation. The "on-line" reactivity computer malfunctioned during part of the run (operational amplifiers were temporarily overloaded), but provided very interesting on-the-spot information during the rest of the run.

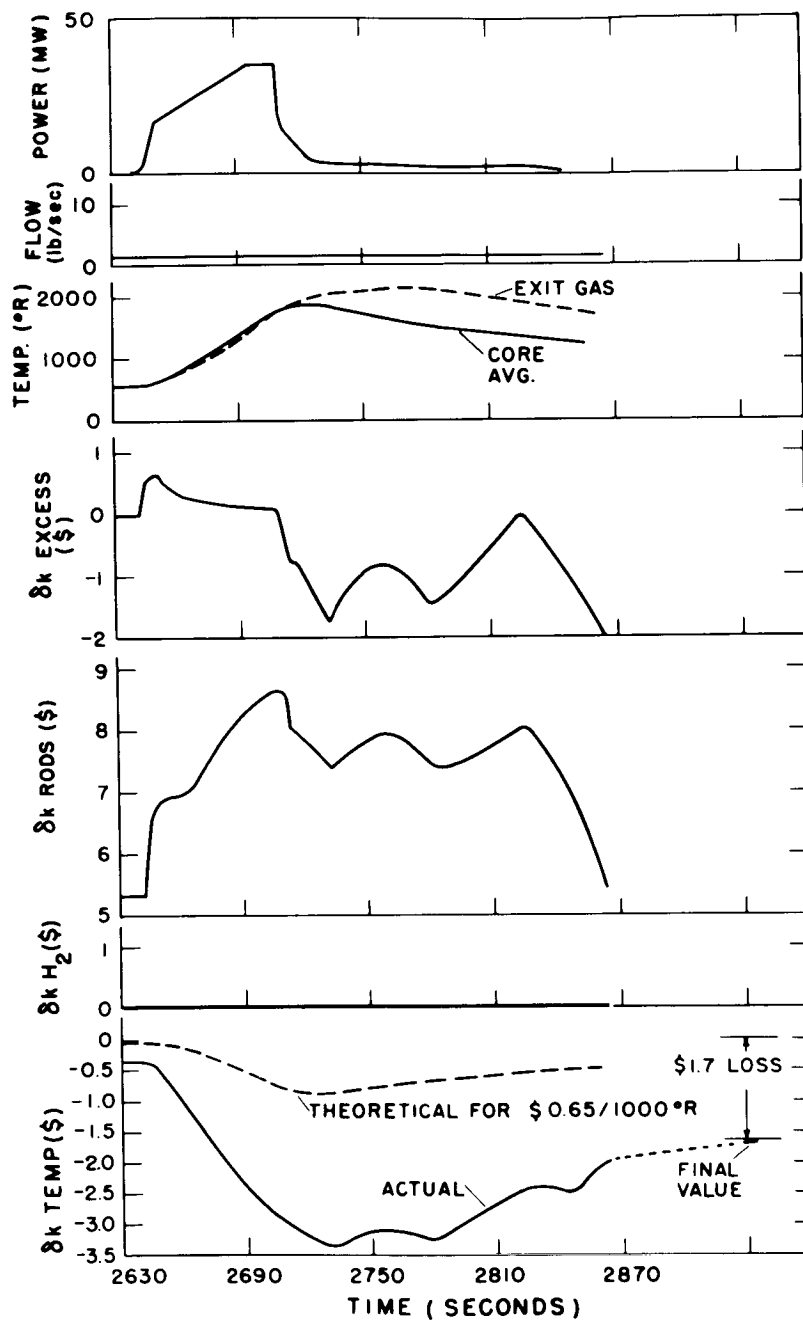


Figure 1 Temperature-Reactivity Data for Kiwi-B-1A, Experimental Plan 6

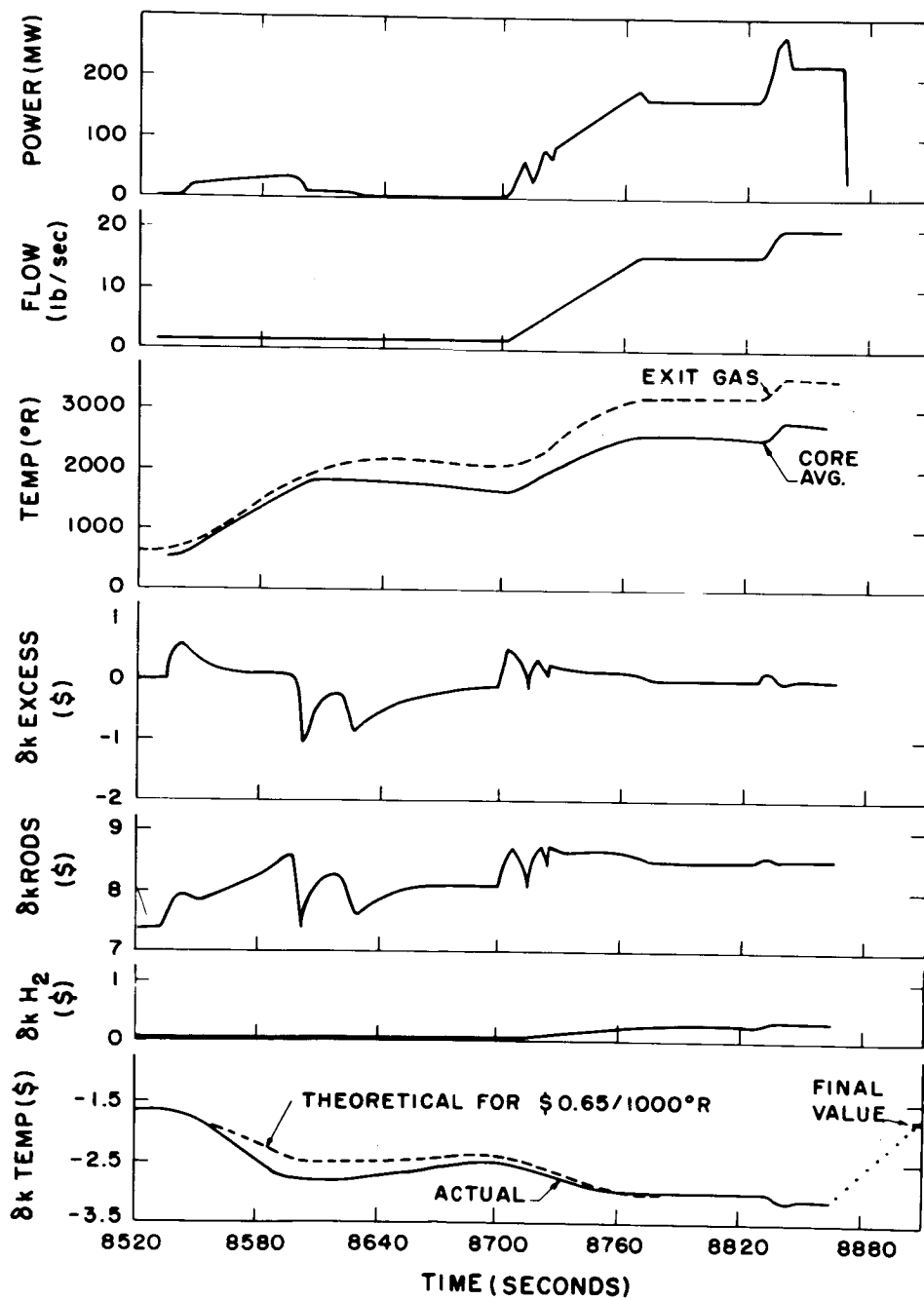


Figure 2 Temperature-Reactivity Data for Kiwi-B-1A, Experimental Plan 6A

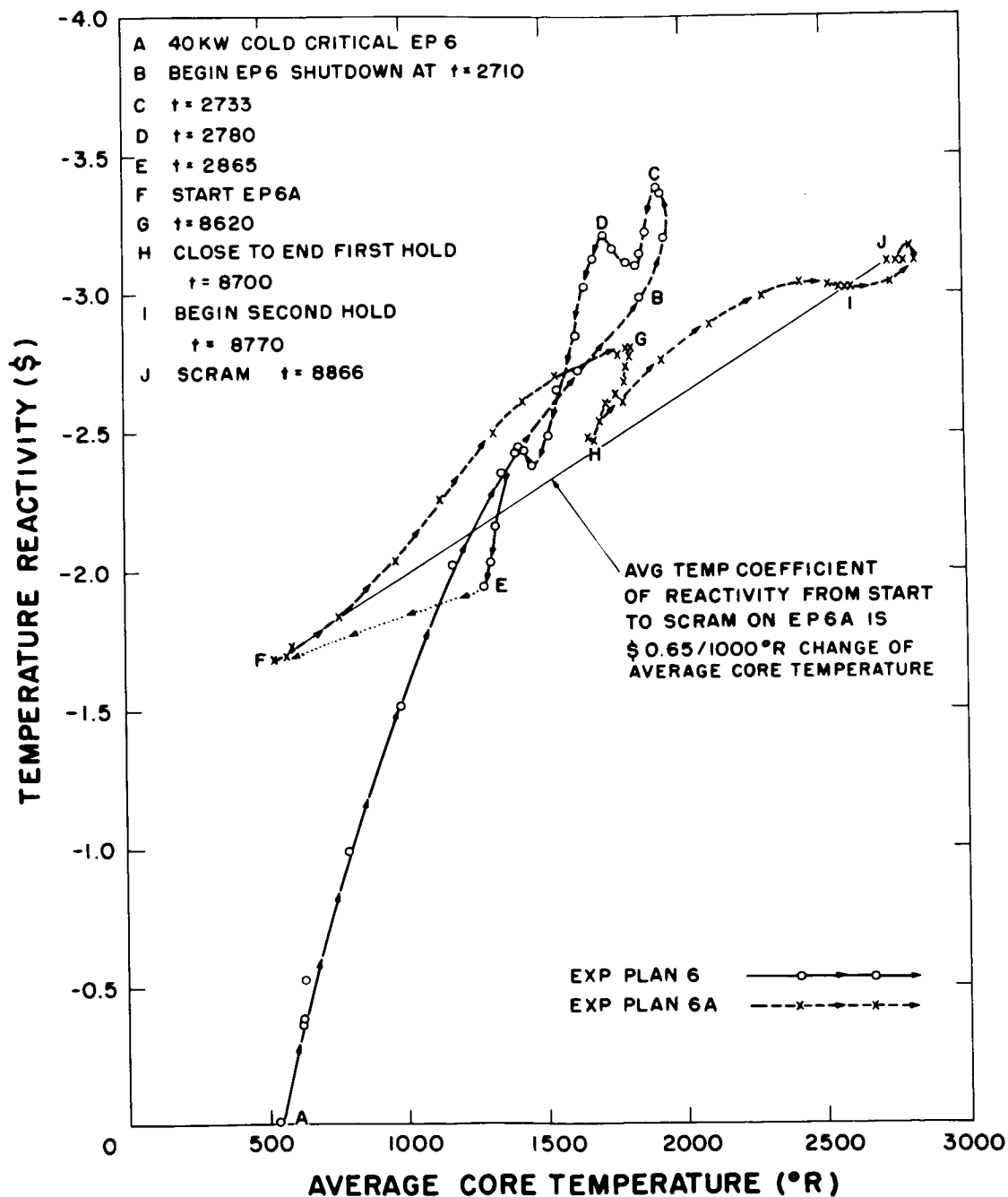


Figure 3 Temperature-Reactivity versus Average Core Temperature for Kiwi-B-1A.

KIWI-A PRIME DISASSEMBLY

[U]

Donald B. Anderson Everett B. Ramsey
Charles D. Montgomery Marvin N. Swink

INTRODUCTION

The KIWI-A Prime Nuclear Propulsion Reactor was the second engine in the Rover Program to be tested at Jackass Flats, Nevada. This engine was tested on July 8, 1960, and disassembly operations began on July 9, 1960. It was the first engine of the series to be disassembled entirely by remote methods. The assembly and disassembly of this reactor was performed by ACF for Los Alamos Scientific Laboratory. The over-all post-mortem requirements were supplied by the LASL reactor design groups and details of accomplishment were worked out with ACF.

Remote disassembly operations consisted of the following basic steps:

1. Recovery of the test car from the test cell.
2. Removal of the reactor from the test car.
3. Exposure of the core.
4. Disassembly of the core into its component parts.
5. Extraction of fuel elements.
6. Post-mortem examination.

The disassembly area of the Rover Program Maintenance, Assembly & Disassembly (MAD) Building, is divided into two (2) major sections composed of the upper bay and the lower bay with a separate hot cell section for post-mortem operations. However, portions of the post-mortem operations were performed in the upper bay. The lower bay was equipped with two (2) General Mills Model-300 side wall manipulators. Both the upper bay and the lower bay were served by a General Mills Model 700 overhead manipulator (O'Man) and a P & H 25-Ton crane with one (1) 5-Ton auxiliary hook. The upper bay contained two (2) pairs of master-slave manipulators. The hot cell area was served by a General Mills Model-300 overhead manipulator, a 2-Ton hoist and three (3) pairs of CRL Model-8 manipulators. TV equipment and binoculars were used as an aid in distant viewing.

C. D. Montgomery, Manager, MAD Building Operations, Los Alamos Scientific Laboratory,
Los Alamos, N. M.
D. B. Anderson, Project Engineer, ACF Industries, Inc., Albuquerque, N. M.
E. B. Ramsey, Senior Project Engineer, ACF Industries, Inc., Albuquerque, N. M.
M. N. Swink, Project Engineer, ACF Industries, Inc., Albuquerque, N. M.

RECOVERY OF THE TEST CAR FROM THE TEST CELL

The recovery of the test car from the test cell was initiated within twenty-four (24) hours after reactor shutdown. Technicians manually disconnected the control rod hydraulic lines in the test cell with sixty-five inches (65") of concrete protecting them from the highly radioactive engine. Remote operation began with the automatic positioning of the radio controlled locomotive. The locomotive was positioned so that when the test car was jacked away from the test cell, the two (2) would be coupled automatically.

After the locomotive was in place, the instrumentation plug of the test cell was remotely disconnected from the plug of the test car. Complete disconnect of the instrumentation plug was indicated by a light at the control point. At this time, the controls for the test cell jacks were actuated and the test car was moved away from the test cell to the locomotive. After the coupling of the test car to the locomotive and the jack was fully extended, the locomotive was started towards the MAD Building. The trip from the test cell to the MAD Building required approximately ninety (90) minutes.

REMOVAL OF THE REACTOR FROM THE TEST CAR

The test car was brought into the disassembly bay of the MAD Building by the locomotive, stopped automatically, and operations were started for transfer of the reactor from the test car.

The top of the core was viewed through the nozzle opening using television cameras, since it was suspected that three (3) modules with elements were lost during full power operation of the reactor. It was found that three (3) modules appeared to be missing. During the viewing of the core, radiation effects samples were removed from the test car and reactor using the side wall manipulator.

Removal of the reactor from the test car required the prior removal or disconnection of instrumentation, coolant piping, deuterium piping, propellant piping and tie down lugs and clamps. The main coolant, deuterium and propellant piping has specially designed flanges and clamps so that the joints could be separated without the use of special equipment. Instrumentation, stainless steel tubing and stainless steel flex hose were severed from the reactor using a remotely controlled heating torch.

The first problem of the operation was encountered when installation of the reactor lift bail was attempted. It was discovered that a section of pipe which had been changed at the last minute prior to the power run, interfered with the installation of the reactor lift bail. A heating torch was used to melt away enough pipe to allow the lift bail to be installed using the 25-Ton crane with assistance from the O'Man. A ten foot (10') lift was required to clear all obstacles on the test car. The reactor was transferred to the disassembly stand and was locked in place with tie down lugs, using the side wall manipulator and an impact wrench.

EXPOSURE OF THE CORE

The exposure of the core consisted of the removal of the center island, the nozzle - exit plenum liner - inlet section package, the clamp ring, and half of the reflector segments.

The bolts attaching the center island jacket to the pressure shell were removed using a 200-foot-pound electric impact wrench held by the O'Man. With the bolts removed, the reactor and upper part of the disassembly stand were withdrawn from the center island. This package was placed on the bay floor while visual inspections were made of the charred thermal paint protecting the center island.

The reactor was repositioned on the turntable. The four (4) clamp rings holding the pressure vessel halves together were removed after the attaching bolts were severed in two (2) locations with a cutting torch positioned by a manipulator.

Many pieces of instrumentation had to be severed with an oxy-acetylene heating torch before the pressure vessel halves could be separated. When all connections had been severed, the disassembly continued with the installation of the reactor lift bail. At this time, the fixture was used for removal of the nozzle package. The nozzle package was raised slowly. After about two feet (2') of movement, the package was suspended in this position while several additional pieces of instrumentation within the reactor were severed.

Disassembly operations continued with the removal of the reflector segments. Each reflector segment was removed by a fixture containing two (2) expanding screws. After removal, each reflector was placed on the flat car for transfer to the dump.

After removal of the first two (2) rows of reflector segments, the reflector cylinder surrounding the core could be removed. The cylinder was raised slowly off of the core to permit different length thermocouple leads to strip easily from the I.D. and O.D. With the reflector cylinder removed, the next step in the disassembly procedure was removal of the entire core.

The core was raised very cautiously to permit over eighty (80) thermocouples to strip from their locations. This stripping was required as all thermocouples exited the pressure vessel via pass-thrus located in the bottom of the pressure vessel and which were completely inaccessible.

After the core was withdrawn from the pressure vessel, numerous pictures were taken of its outside diameter. Imprints of carbon wool insulation (contained between the core O.D. and the reflector cylinder) and bypass gas flow were evident. The core was then inserted into the trunnion fixture.

The core was positioned in the trunnion fixture and the core handling fixture was withdrawn. Several attempts to install the can cover over the top of the core proved unsuccessful. It was determined that there was one-quarter inch (1/4") interference between the core I.D. and the can cover. This oversight caused four and one-half (4-1/2) hours delay in disassembly while modifications were made. The cover was removed from the bay, decontaminated and one-quarter inch (1/4") of stock was removed. The cover was easily installed after modification and was secured in place. The trunnion fixture was rotated 180° and the cover, now visible on top, was removed.

CORE DISASSEMBLY

The core disassembly consisted of the removal of the support tube nuts and the inlet reflector; the extraction of the loaded modules and the subsequent transfer of the modules to the upper disassembly bay for ejection of fuel elements.

Prior to removal of the inlet reflector, one hundred and twenty-six (126) each support tube nuts, washers, springs and spring covers had to be removed from the support tubes which projected from the inlet reflector. The nuts were removed from the support tubes using a side wall manipulator equipped with a special, electrically powered, nut removal tool. All but four (4) nuts were unscrewed with this tool. These nuts appeared to be jammed in place. The inlet reflector removal tool was attached to the inlet reflector by means of three (3) expanding lift screws similar to those used on the reflector segment removal tool. The inlet reflector was then lifted two inches (2") and spacers were inserted between the modules and inlet reflector. The offending nuts raised the modules attached to them. The fixture was removed and the support tubes were unscrewed from the modules using a conventional socket with the electric impact wrench. The freed modules slid back into place. The fixture was again attached to the inlet reflector and the part was removed and placed on the flat car.

With the removal of the inlet reflector accomplished, the extraction of modules began. The modules were pulled from the can of the trunnion fixture, one (1) at a time, utilizing the support tubes which were gripped by the manipulator. As each module was pulled, it was replaced by a dummy module made of wood. These dummy modules were installed to maintain the physical integrity of the core. Each module, as it was extracted, received a preliminary visual inspection for excessive erosion, discoloration and cracking. When the module viewing was completed, it was placed in a handling storage container.

The first three (3) modules removed were portions of those broken during the full power operation. These modules were placed in a special transfer container and taken to the hot cells for immediate examination and photography. All modules which contained radiation samples and radiochemical thermometers (RCT's) were then extracted and transferred to the upper bay for element ejection. Rapid recovery of these samples was imperative due to the decay of the radioactive isotopes contained within the samples which were to be used in the radiochemical analysis. The remaining modules were removed in a predetermined sequence and transferred to the upper bay for fuel element removal.

EXTRACTION OF FUEL ELEMENTS

As modules were transferred from the lower disassembly bay, the extraction of the fuel elements commenced. Approximately four thousand (4000) fuel elements were extracted and either packaged for storage or sent to the hot cell area for post-mortem examination.

The module transfer containers were placed in an inclined rack in front of one of the viewing windows in the upper disassembly bay. The master-slave manipulators, with special designed hands, were used to remove the modules from the containers and place them in the fuel element ejector.

The element ejector was an automatic, remote controlled, turret type tool, for ejecting the elements from the modules. The position of the turret of the ejector was determined by the number of holes contained in the module.

After clamping the module in place, the turret was positioned and the push rods of the ejector matching the hole pattern of the module were actuated. It was necessary to stop the push rods at different positions to allow the manipulator operator to remove the ejected elements and place them in a rack for transfer to another viewing window. As each element was handled, the serial number of the element was read and recorded.

Upon completion of the ejection of elements from the module, the elements were either transferred to storage containers or sent to the hot cell area and the module was replaced in its container. Certain modules, containing RCT's, were transferred to a remotely operated saw for post-mortem operations.

POST-MORTEM

The post-mortem effort on KIWI-A Prime was quite lengthy and, in fact, investigations of certain components are continuing to this date. Discussion of the post-mortem operations is separated in two (2) sections. The first will be modules, and the second, elements.

Certain modules in the core contained RCT's, which had to be removed by sectioning the modules. A specially designed, remotely operated saw was used to make a transverse cut across the module which produced a wafer. The wafer was positioned on the table of a modified drill press. A master-slave manipulator advanced a rotating end mill into the wafer and stopped just short of the RCT. The RCT was then shaken from the wafer. The RCT's were retrieved as soon as possible in the disassembly sequence and sent immediately to LASL for radiochemical analysis.

In addition to radiographic analysis of modules, many of the modules were sawed axially to expose the inner surfaces of the element holes. These exposed surfaces were inspected for indications of bypass gas flow and structural failures.

A few modules were weighed on a Metrogram balance for a pre- and post-operation comparison. This operation was discontinued after no trend in weight change appeared. Three (3) photographs were taken of each module, which were later correlated with the module visual inspection maps. These maps describe any cracks, punky porous regions, pits, etc., observed.

An important post-mortem investigation performed on the fuel elements was gamma counting. Information obtained was used to confirm core design parameters and to determine power output.

Each element received a cursory visual inspection of gas passage holes and outside diameters, and a portion of the elements were weighed to determine weight losses. Many elements were cut longitudinally to expose gas passage holes to permit more detailed examinations.

Numerous thermal capsules, which were small graphite capsules containing alloyed metals of different melting points, were removed from elements. The capsules were then crushed to reveal the condition of the contents.

Post-mortem investigations were not limited to core components. Many investigations were also performed on the nozzle, pressure vessel components, reflectors, graphite components and radiation effects samples.

CONCLUSIONS

Many things were learned from this operation and noted in detail for future reference and action during operations meetings. A few of the more general benefits noted for future progress were:

1. More reliable information is now available to provide a meaningful time study of operations, although a new appreciation for additional contingency time was realized.
2. The additional operational history allowed upgrading of routine maintenance schedules as more was learned about the manipulators and other equipment.
3. The use of several simple devices, such as extension handles on flange disconnect bolts, to expedite the remote disassembly, could be incorporated advantageously in future reactors and test cell assemblies.
4. The necessity of having all remote tooling and fixtures on hand well in advance of their planned use, in order to allow a detailed operational checkout was noted as imperative.

Looking back in retrospect after disassembly and post-mortem of subsequent reactors, it can be stated that this was a successful operation and much was learned which was very important to the design of reactors to follow KIWI-A Prime, as well as to the remote disassembly of them.

ACKNOWLEDGMENTS

This work was performed by ACF Industries, Inc., for Los Alamos Scientific Laboratory under Atomic Energy Commission Contract AT (29-1)-1352. The authors wish to thank Rex A. Prunty and James L. Burnham of ACF Industries, Inc., for their assistance in the preparation of this paper.

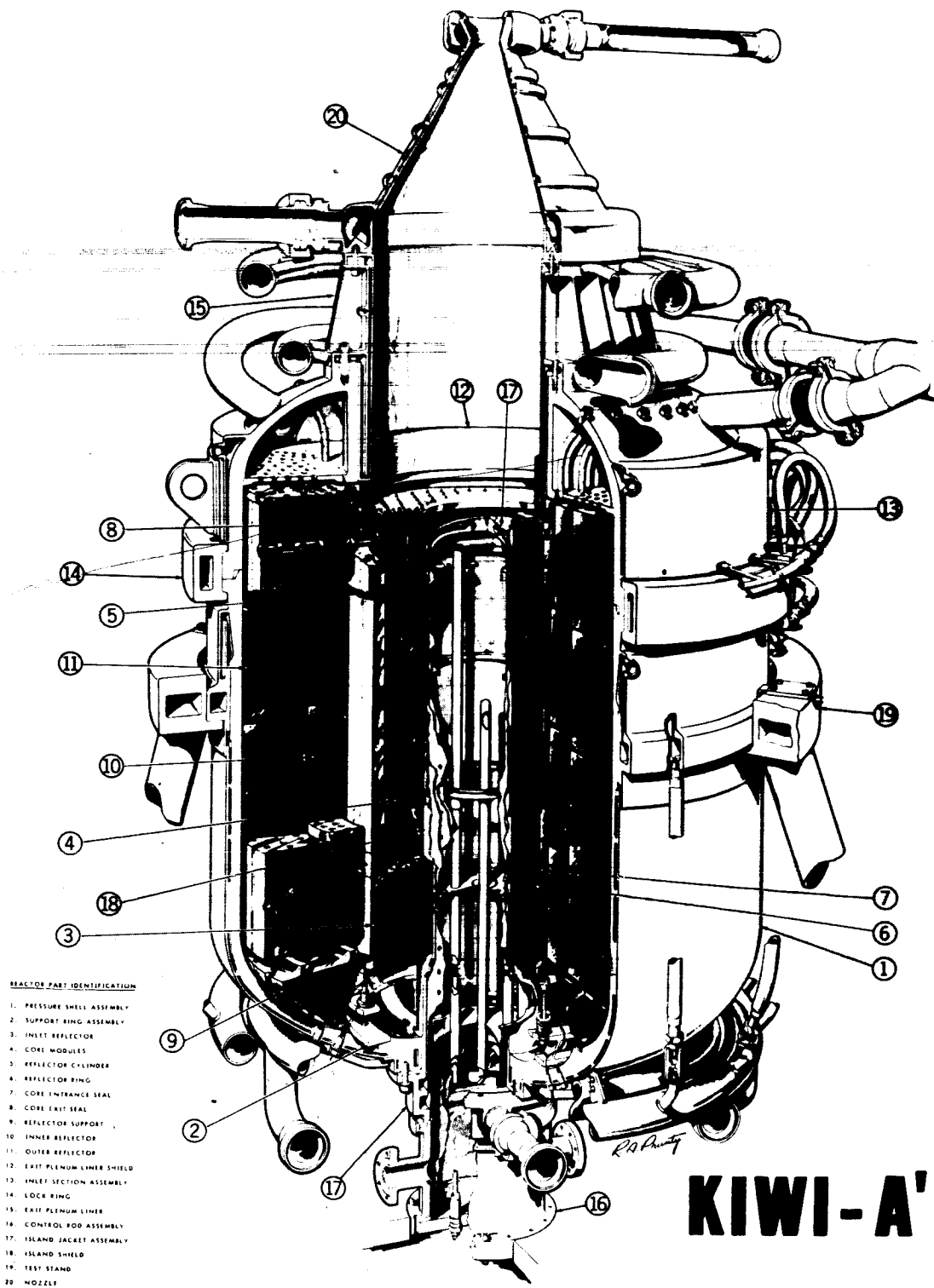


Figure I

KIWI-A Prime Reactor Cutaway



Figure II Test Car Recovery

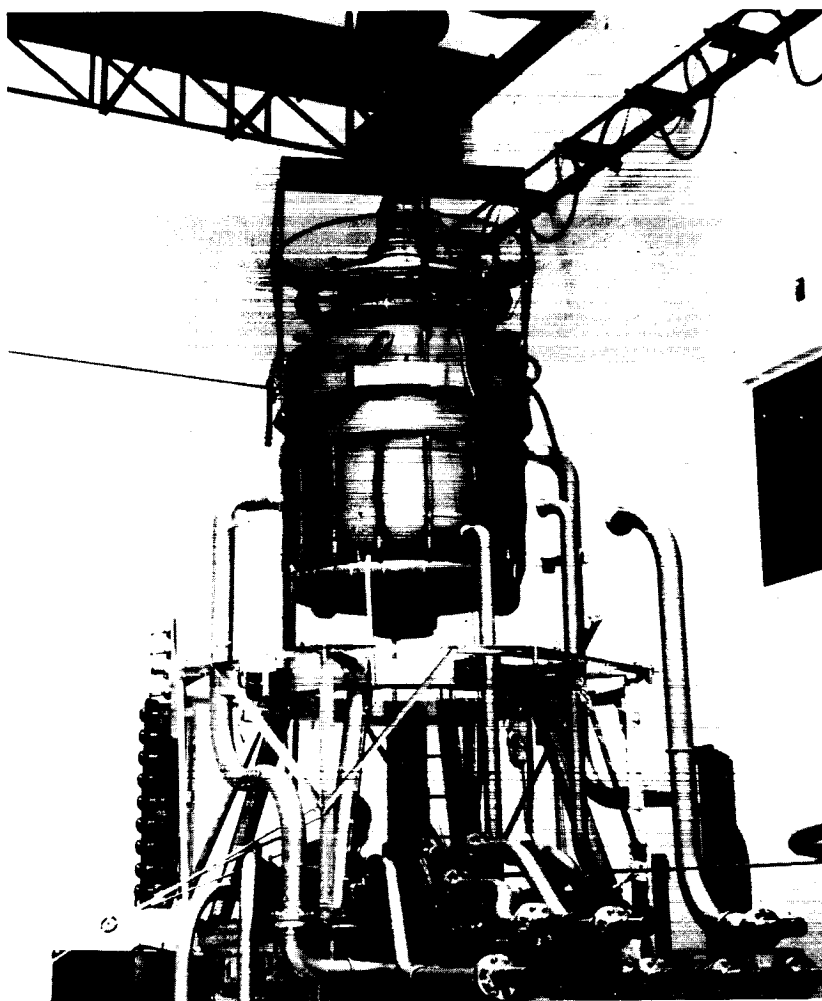


Figure III Separation of Reactor from the Test Car



Figure IV Cutting of Instrumentation

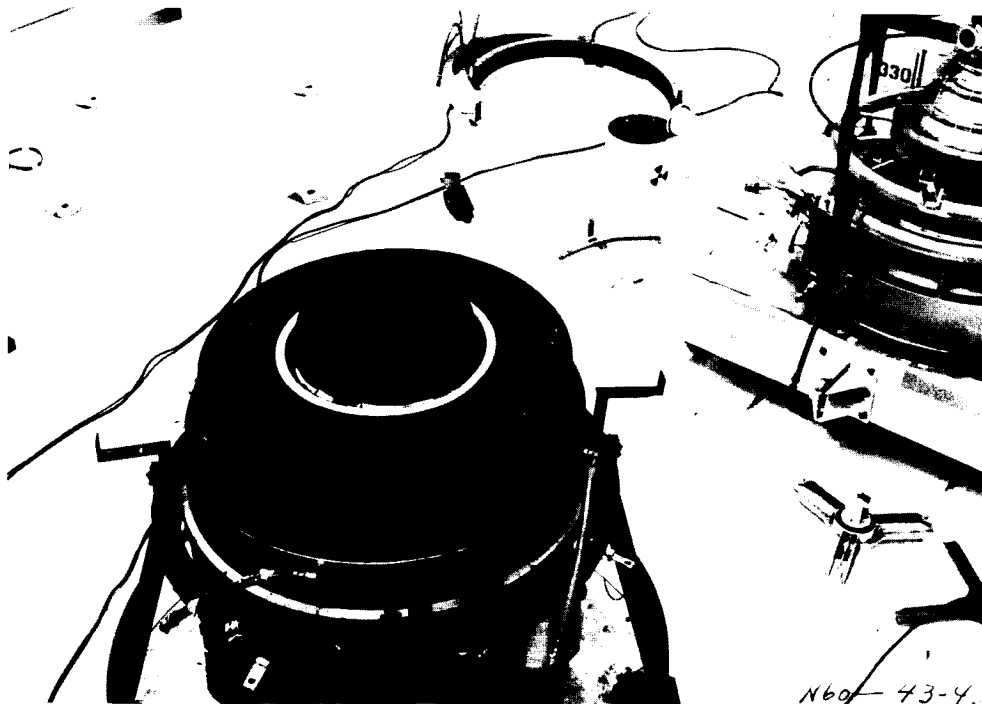


Figure V Exposure of Core and Reflector System

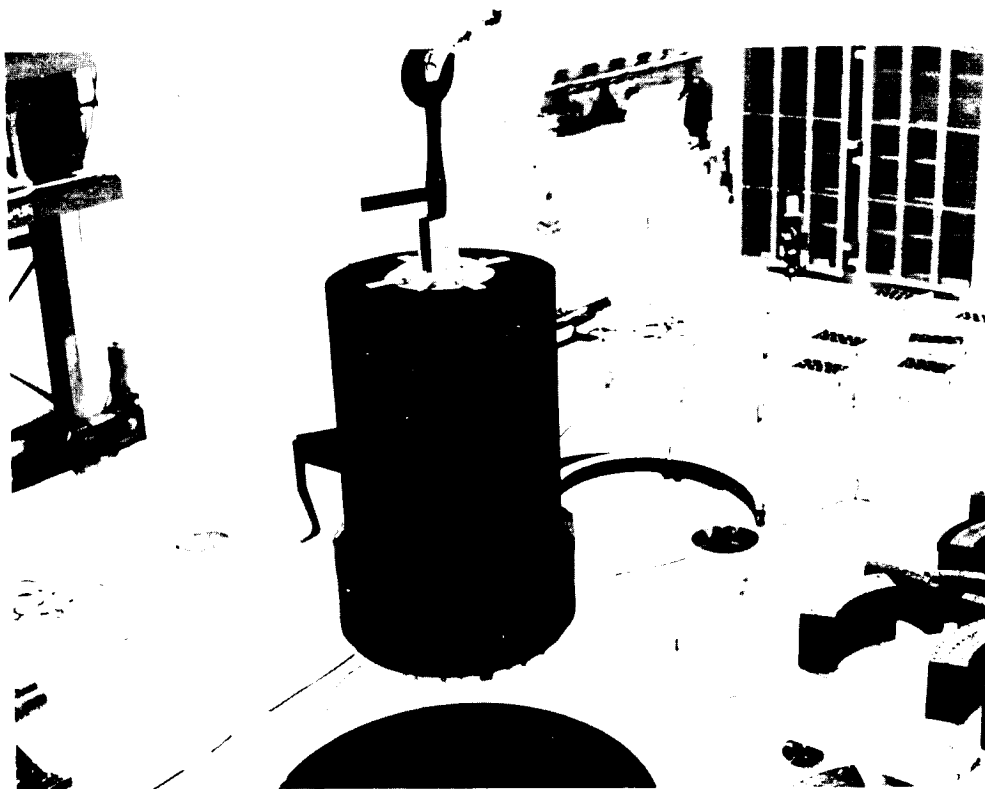


Figure VI Removal of Reactor Core

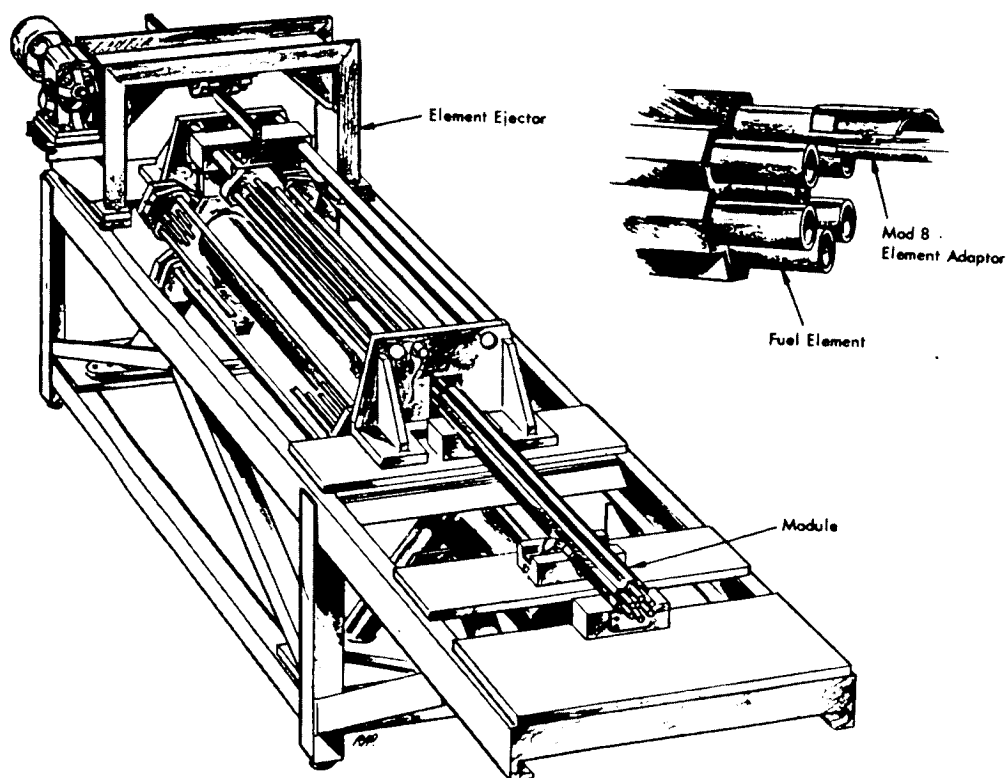


Figure VII Fuel Element Ejection

DESIGN CONSIDERATIONS IN THE DEVELOPMENT
OF THE LIQUID HYDROGEN FEEDSYSTEM FOR KIWI-B*

[U]

R. J. Bohl⁺, E. A. Brown, C. P. Milich, and M. J. Nutter

University of California
Los Alamos Scientific Laboratory
Los Alamos, New Mexico

INTRODUCTION

Kiwi-B-1B, which was tested in August of this year, was the first of a series of Rover and Nerva nuclear propulsion reactors to be cooled by liquid hydrogen. One of the major efforts leading to these tests was the development of a high-performance liquid hydrogen feedsystem capable of delivering 70 lbs/sec flow rate at a pressure of approximately 850 psi. The feedsystem dynamic characteristics and its operation with the remaining Kiwi-B control systems have been described briefly¹. The purpose of this paper is to present a more complete description of the feedsystem, the differential equations, the turbopump speed control system, and the specific speed control system.

The basic elements of the liquid hydrogen feedsystem are a Rocketdyne Mark IX pump driven by a Mark III turbine. The turbine is powered by ambient-temperature hydrogen gas which is stored in a tank farm. The turbopump speed is varied by positioning a throttle valve in the pipe between the tank farm and the turbine inlet nozzle. The valve has a linear relationship between stem position and effective area.

A block diagram of the feedsystem is shown in Fig. 1. It contains three closed servo loops which control turbopump speed, mass flow rate to the reactor, and specific speed. Reactor flow rate is measured with a venturi located a few feet down stream of the pump in the pipe leading to the reactor. This measured flow rate is compared to the demanded flow rate. The error voltage thus developed is operated upon by the flow rate controller, which changes the turbopump speed to bring the measured flow rate into correspondence with the demanded flow rate. The turbopump speed control system normally operates as a sub-loop in the flow rate control loop. It regulates speed to the value demanded by the flow rate controller by varying the position of the turbine throttle valve. The specific speed control system is an auxiliary safety system which protects the turbopump. If a flow blockage occurs in the main reactor flow pipe, the liquid hydrogen bypass valve is opened. This vents liquid hydrogen from the pump to the atmosphere, thus preventing the pump from stalling.

The reactor is some 100 feet down stream of the venturi which is used to measure reactor flow rate. Since flow rate is controlled at the venturi, the reactor

* Work performed under AEC Contract W-7405-ENG. 36.

+ Part of the work discussed herein was done by one of the authors (Bohl) at Rocketdyne, A Division of North American Aviation, Inc., Canoga Park, California.

flow rate is not actually controlled in the dynamic sense. An additional effect of the pipe is that it causes a frequency dependent gain and phase change between pump flow rate and discharge pressure. The pipe line dynamics are included in the digital and analog simulations of the system; however, they are not treated in this paper.

FEEDSYSTEM DIFFERENTIAL EQUATIONS

The differential equations which describe the feedsystem are given below. The symbols are identified in Fig. 1. Assuming choked flow through the turbine throttle valve and the inlet nozzle and a negligible time delay due to gas compressibility in the volume between them, one obtains the following relations:

$$\begin{aligned} A_{tv} &= \frac{C^* \dot{W}_t}{g P_s} \\ A_{tv} &= K_1 X_{tv} \\ P_{ti} &= \frac{C^* \dot{W}_t}{g A_{tn}} \\ \frac{dN}{dt} &= \frac{30}{1\pi} (L_t - L_p) \\ L_t &= \dot{W}_t (2050 - 0.0185N) \\ L_p &= -5.41(10)^{-6} N^2 + 5.61(10)^{-2} N \dot{W}_p - 10.33 \dot{W}_p^2 \\ P_{pe} &= -1.01(10)^{-6} N^2 + 2.63(10)^{-3} N \dot{W}_p - 0.591 \dot{W}_p^2 + P_{pi}. \end{aligned} \quad (1)$$

Assuming infinite pipe line bandwidth and a square law reactor load, then

$$\begin{aligned} P_{ri} &= P_{pe} - R_d \dot{W}_r^2, \\ \dot{W}_p &= \dot{W}_r + \dot{W}_{bp}, \\ \dot{W}_r &= \dot{W}_v, \text{ and} \\ P_{ri} &= R_r \dot{W}_r^2. \end{aligned}$$

Pump specific speed, which is a measure of the location of the pump operating point on the pump map, is defined as

$$N_s = \frac{N/Q}{n^{3/4}} = \frac{0.75N/\dot{W}_p}{(P_{pe} - P_{pi})^{3/4}}.$$

TURBOPUMP SPEED CONTROL

During the normal course of a reactor startup, the speed control system is called upon to regulate speed from approximately 1,000 to 24,000 rpm. The most critical region relative to starting a reactor on liquid hydrogen is generally above 6,000 rpm. For this reason it is desirable to have a speed control system which has reasonably constant dynamic characteristics above 6,000 rpm. Fortunately, the turbine inlet nozzle has choked flow above something like 4,000 to 5,000 rpm; therefore, this assumption was made in all of the system analysis work. Cold flow experiments were performed to make sure that the system would operate in a stable manner while traversing the region from 1,000 to 6,000 rpm.

The turbopump speed control system transfer functions for small perturbations are given below.

$$\frac{\delta E_5(s)}{\delta E_4(s)} = \frac{11(\frac{s}{8} + 1)(\frac{s}{40} + 1)}{s(\frac{s}{80} + 1)(\frac{s}{100} + 1)} \quad \frac{\text{Volts}}{\text{Volt}}$$

$$\begin{aligned} \frac{\delta X_{tv}(s)}{\delta E_5(s)} &= \frac{1.5 \text{ in.}}{100 \text{ volts}} \cdot \frac{\delta X_{tv}}{\delta X_{tvd}} \quad \frac{\text{in.}}{\text{in.}} \\ &= \frac{0.015}{(\frac{s}{63} + 1)(\frac{s^2}{282^2} + \frac{2(0.5)s}{282} + 1)} \quad \frac{\text{in.}}{\text{Volt}} \end{aligned}$$

$$\frac{\delta \dot{W}_{tv}(s)}{\delta X_{tv}(s)} = 0.813(10)^{-2} P_s \quad \frac{\text{lb/sec}}{\text{in.}}$$

If the pump operating point is kept on a constant specific speed line, pump torque can be represented by $L_p = K_p N^3$ rather than by equation (1). Assuming that $L_p = 2.03(10)^{-6} N^3$, then

$$\begin{aligned} \frac{\delta N(s)}{\delta \dot{W}_t(s)} &= \frac{2050 - 0.0185 N_0}{[4.06(10)^{-5} N_0 + 0.0185 \dot{W}_{to}] \left[\frac{4.51s}{1.22(10)^{-3} N_0 + 0.555 \dot{W}_{to}} + 1 \right]} \quad \frac{\text{rpm}}{\text{lb/sec}} \\ &= \frac{K_p}{(\frac{s}{W} + 1)} \end{aligned}$$

Some representative values of $\frac{\delta N(s)}{\delta \dot{W}_t(1)}$ are as follows:

N	$\frac{\delta N(s)}{\delta \dot{W}_t(s)}$
6,000	$\frac{2.3(10)^5}{(\frac{s}{1.6} + 1)}$
12,000	$\frac{9.9(10)^4}{(\frac{s}{3.5} + 1)}$
23,500	$\frac{4.3(10)^4}{(\frac{s}{7.2} + 1)}$

The speed transducer transfer function is

$$\frac{\delta E_5(s)}{\delta N(s)} = 3.33(10)^{-3} \quad \frac{\text{Volts}}{\text{rpm}}$$

The open loop transfer function of the speed control system at 23,500 rpm with $P_s = 3300$ psi is

$$G_N(s) = \frac{22(\frac{s}{8} + 1)(\frac{s}{40} + 1)}{s(\frac{s}{7.2} + 1)(\frac{s}{63} + 1)(\frac{s}{80} + 1)(\frac{s}{100} + 1)(\frac{s^2}{282^2} + \frac{2(0.5)s}{282} + 1)}$$

Nichols plots of the system characteristics for several speeds are shown in Fig. 2. The closed loop bandwidth is approximately 7 cps. The gain and phase margins are in the order of 12 db and 60°, respectively. As speed is decreased, closed loop bandwidth increases a small amount and stability margin decreases slightly.

SPECIFIC SPEED CONTROL

Care must be exercised in using a Mark IX liquid hydrogen pump to keep the pump pressure rise and flow rate within certain limits. If the pressure rise is allowed to get too high for a given flow rate, the pump goes into stall. This occurs when the velocity vector of the fluid relative to the blades shifts sufficiently to cause a sharp drop in pump pressure rise. Cavitation occurs when the fluid static pressure gets below the vapor pressure. Stall generally is more serious than cavitation because it can cause excessive turbopump speed and vibration. The pump in use at the Nevada Test Site has been driven into stall several times by momentary flow blockage in the pipe lines. This usually occurred because of the formation of a gas bubble in a pipe which was not thoroughly chilled before the turbopump was started.

The usable ranges of speed, turbine flow rate, pump flow rate, pump pressure rise, pump torque, and specific speed are shown on the pump map in Fig. 3. The specific speed at which stall and cavitation occur are approximately 750 and 1900, respectively.

The pump is prevented from going into stall by the specific speed control system shown in Fig. 1. This system senses when the pump specific speed falls below a pre-set value. When this happens, the liquid hydrogen bypass valve is opened, venting liquid hydrogen from the pump discharge to the atmosphere. The bypass valve automatically opens such that the correct amount of hydrogen is bypassed to increase the specific speed to the pre-set value. If the specific speed is above the value set into the system, the bypass valve remains shut.

Specific speed is sensed in the control system by comparing pump flow rate to a constant times speed. The pump flow rate is measured with a venturi located a short distance from the pump in the pump suction line. As can be seen in Fig. 3, both $(P_{pe} - P_{pi})/N^2$ and \dot{W}_p/N are equal to constants when the pump is operating on a constant specific speed line. The relationship \dot{W}_p/N was chosen as a measure of specific speed rather than $(P_{pe} - P_{pi})/N^2$ because the latter relationship is double valued when the pump goes into stall. This phenomenon is shown in Fig. 4, which is a plot of $(P_{pe} - P_{pi})/N^2$ vs \dot{W}_p/N for different operating levels. The specific speed at which the control system becomes active can be adjusted by changing the value of the constant.

The transfer function of the specific speed controller is

$$\frac{\delta E_b(s)}{\delta E_s(s)} = \frac{25(-\frac{s}{16} + 1)}{s(-\frac{s}{100} + 1)} .$$

The characteristics of the bypass valve for small perturbations can be approximated by

$$\frac{\delta X_{bp}(s)}{\delta X_{bpd}(s)} = \frac{1}{(-\frac{s}{32} + 1)(\frac{s^2}{160^2} + \frac{2(1.4)s}{160} + 1)}$$

The transfer functions of the remaining elements of the specific speed loop are heavily dependent upon the characteristics of the other feedsystem control sys-

tems and upon which other feedsystem loops are closed; therefore, the equations will not be listed in this paper. A representative Nichols plot of the specific speed loop characteristics is shown in Fig. 5. These data were obtained with the speed and flow rate control loops closed.

CONCLUSIONS

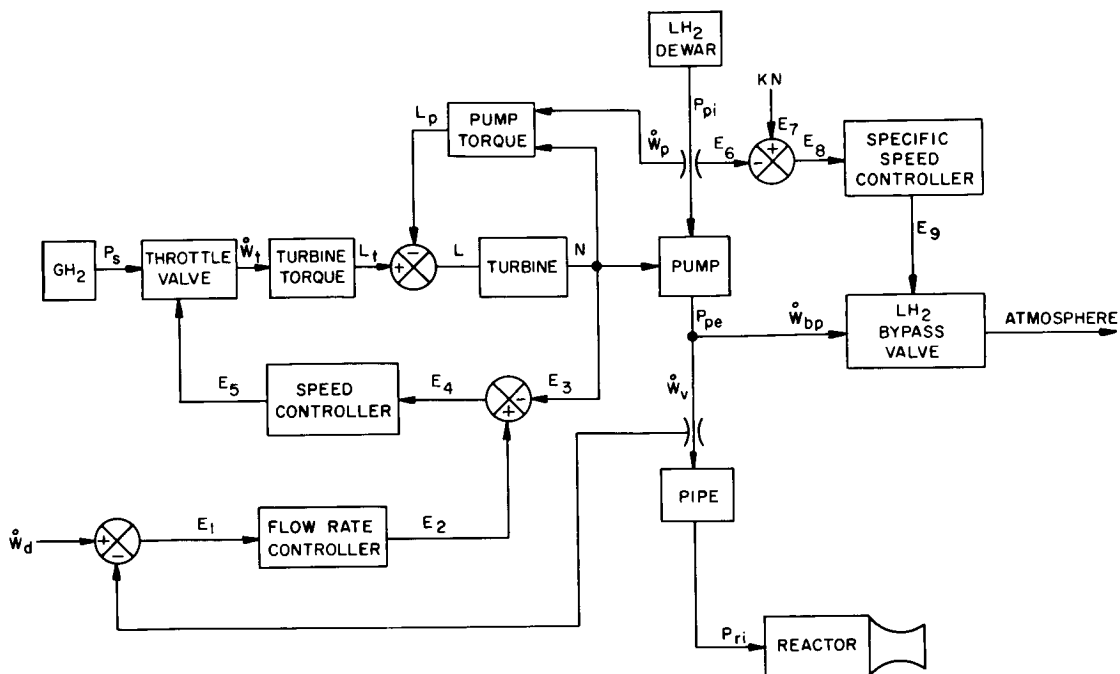
A liquid hydrogen feedsystem has been developed which is capable of meeting the cooling requirements of Kiwi-B and Nerva reactors. The flow rate and turbopump speed control systems operated well during the Kiwi-B-1B hot run despite large pipe line flow and pressure oscillations during most of the startup. The oscillations are believed due to an interaction between the specific speed control system and sections of two pipe lines which were not cooled sufficiently prior to starting the turbopump. The oscillations ceased as the pipes became chilled.

REFERENCE

1. P. J. Blake, R. J. Bohl, E. A. Brown, C. P. Milich, M. J. Nutter, C. E. Stiles, and B. G. Strait, "Control Systems for a Liquid-Hydrogen-Cooled Kiwi-B Reactor", Proceedings of the Nuclear Propulsion Conference, Monterey, August 1962.

ACKNOWLEDGMENTS

This paper would not have been written without either the encouragement of J. E. Perry, Jr. or the necessary support of Rocketdyne. The initial analytical design of the valve to produce a constant dynamic gain between pump speed and valve position was performed by R. Matulenko of Rocketdyne. Most of the frequency responses of the feedsystem were performed by O. Farmer of the Los Alamos Scientific Laboratory using a digital computer.



- A_{tv} = THROTTLE VALVE EFFECTIVE AREA, IN^2
 A_{tn} = EFFECTIVE TURBINE INLET AREA, IN^2
 C^* = CHARACTERISTIC TURBINE INLET VELOCITY, $6.33(10)^4 \text{ IN/SEC}$
 g = ACCELERATION DUE TO GRAVITY, 384 IN/SEC^2
 I = EFFECTIVE INERTIA, IN-LB-SEC^2
 L_t = TURBINE TORQUE, IN-LB
 L_p = PUMP TORQUE, IN-LB
 N = TURBO-PUMP SPEED, RPM
 P_{pe} = PUMP DISCHARGE PRESSURE, PSIA
 P_{pi} = PUMP SUCTION PRESSURE, PSIA
 P_s = GH_2 TANK FARM PRESSURE, PSIA
 P_{ri} = REACTOR INLET PRESSURE, PSIA
 R = GAS CONSTANT, $\text{IN-LB}^f/\text{R-LB}_m$
 R_d = PIPE LINE LOSS CONSTANT, $\text{PSI}/\text{LB}_2/\text{SEC}^2$
 R_r = REACTOR LOAD IMPEDANCE, $\text{PSI}/\text{LB}_2/\text{SEC}^2$
 T = TURBINE INLET GAS TEMPERATURE, $^{\circ}\text{R}$
 \dot{W}_r = REACTOR FLOW RATE, LB/SEC
 \dot{W}_t = TURBINE GAS FLOW RATE, LB/SEC
 \dot{W}_p = PUMP FLOW RATE, LB/SEC
 \dot{W}_{bp} = LH_2 BYPASS FLOW RATE, LB/SEC
 x_{tv} = TURBINE THROTTLE VALVE STEM POSITION, IN
 E = VOLTAGE
 P_{ti} = TURBINE INLET PRESSURE, PSI
 Q = PUMP FLOW RATE, GPM
 H = PUMP HEAD RISE, INCHES OF WATER
 SUBSCRIPT o = QUIESCENT VALUE OF VARIABLE
 K_i = CONSTANTS

FIGURE 1
 KIWI-B-1B PROPELLANT FEED SYSTEM

